



THERMODYNAMICS LABORATORY  
AEROSPACE AND MECHANICAL ENGINEERING DEPARTMENT

FACULTY OF APPLIED SCIENCES  
UNIVERSITY OF LIÈGE

---

# The role of residential micro-cogeneration fuel cells in the energy transition

*A case study in Belgium*

---

Author:  
Nicolas PAULUS

Supervisor:  
Pr. Vincent LEMORT

A THESIS SUBMITTED IN FULFILMENT OF THE REQUIREMENTS FOR THE DEGREE OF  
*Doctor of Applied Sciences*

Liège, September 2023

---

## **The role of residential micro-cogeneration fuel cells in the energy transition**

Copyright ©2023 by Nicolas Paulus. All rights reserved.

Thermodynamics Laboratory  
Aerospace and Mechanical Engineering Department  
Faculty of Applied Sciences - University of Liège  
Allée de la Découverte 17  
B-4000, Liège (BELGIUM)  
nicolas.paulus@uliege.be  
+32 475 49 90 65

### **Members of the Examination Committee:**

Pr. Dr. Ir. Vincent Lemort, *Supervisor*  
(University of Liège, Belgium)

Pr. Dr. Ir. Sylvain Quoilin  
(University of Liège, Belgium)

Pr. Dr. Ir. Nathalie Job  
(University of Liège, Belgium)

Doc. Dr. Ir. Jean-Baptiste Bouvenot  
(Nation institute of applied sciences of Strasbourg – INSA Strasbourg, France)

Pr. Dr. Ir. Steven Lecompte  
(Ghent University, Belgium)

# Abstract

Through theoretical, simulation, and experimental work, this thesis investigates the role of fuel cell micro-cogeneration systems in driving the energy transition. The thesis begins by defining the ‘decarbonization’ through the notion of carbon budgets, drawing insights from IPCC's latest work (AR6), which is then contextualized at both local and individual scales, with the examples of Belgium, Wallonia, and France serving as frequent case studies throughout this research. Considering imported emissions, the current commitments of those regions/countries is in fact not compatible with IPCC's +2°C recommendations. Also, since some greenhouse gases emissions could never be fully mitigated, 2050 carbon neutrality could only be reached by increasing carbon sinks to at least 1 tCO<sub>2eq</sub>/year per capita, which will be highly challenging for France or Wallonia as it represents +370% and +300% increases against respective current (natural) levels.

Introducing the concept of fuel cells, the thesis provides comprehensive descriptions of main existing fuel cell types and their respective characteristics. Furthermore, the future performance of micro-cogeneration fuel cells is reviewed according to their underlying technology. PEMFC (Polymer Electrolyte Membrane Fuel Cell) systems performance are not expected to be significantly increased. This is not the case for SOFC (Solid Oxide Fuel Cell) systems, that exhibit no Carnot limit and could offer theoretical electrical LHV (Low Heating Value) efficiency close to 100% (DC) for the dry electrochemical oxidation of biochar or methane, which can be a renewable hydrogen carrier. Maximum demonstrated LHV electrical efficiency (AC) of any commercially available fuel cell systems is already of 65%, for a utility scaled methane-fed SOFC system launched on the market in 2023.

The thesis then presents experimental and simulation work performed on two presently available fuel cell systems, namely (in this thesis) the BI\*\*\*G\*N SOFC and the P\*2 PEMFC. The experimental work encompasses both laboratory test campaigns and in-situ field-test monitoring in real applications, yielding dedicated performance models that can be integrated into building performance simulation or energy planning tools. The tested PEMC system exhibits a high-level of hybridization with a classical condensing boiler, which is assumed to prevent both sub-systems to operate as optimally and reliably as they would have as standalone units. Oppositely, the tested SOFC system exhibited no troubleshooting and a reliable electrical efficiency always close to 60% (LHV) at its nominal power outputs, which can also easily even be modulated in the 33-100% range.

Building on those experimental performance and anticipated advancements of fuel cell systems, the thesis demonstrates that their greenhouses gases mitigation potential over the average individual carbon footprint remains quite insignificant if their fuel is not decarbonized. Even so, their mitigation potential would still be way insufficient, and other actions, including behavioural changes, would still have to be implemented.

However, emerging technologies, such as Direct Carbon Solid Oxide Fuel Cells (DCSOFCs) or Direct Formic Acid Fuel Cells (DFAFCs) offer the capability of facilitating pure CO<sub>2</sub> capture at their anode exhaust and thus allow for potential negative emissions. With the case study of an average Belgian dwelling's electrical demand and the use of an electric car (for about 20000 km/year) provided by a DCSOFC with an electrical LHV efficiency of 80% fed by biomass, those negative emissions could be up to about 3 MtCO<sub>2eq</sub>/year. In view of the minimal carbon absorption level implied by the carbon neutrality target (reported above), which will unlikely rely only on natural sinks in densely populated western countries, the negative emissions potential of such fuel cell systems shall absolutely be further developed and implemented (in addition to the maximization of natural sinks).

## Résumé

Cette thèse examine le rôle des systèmes de micro-cogénération à piles à combustible dans la transition énergétique via un travail théorique et expérimental. La thèse commence par définir la 'décarbonisation' à travers la notion de budgets carbone, en s'appuyant sur les derniers travaux du GIEC (AR6), qui sont ensuite contextualisés à l'échelle locale et individuelle, avec les exemples de la Belgique, de la Wallonie et de la France. En tenant compte des émissions importées, les engagements actuels de ces régions/pays ne sont en fait pas compatibles avec les recommandations du GIEC visant à limiter le réchauffement à +2°C. De plus, étant donné que certaines émissions de gaz à effet de serre ne pourront jamais être complètement atténuées, la neutralité carbone en 2050 ne pourrait être atteinte qu'en augmentant les puits de carbone à au moins 1 tCO<sub>2eq</sub>/an par habitant, ce qui représenterait une augmentation de +370% et +300% par rapport aux niveaux actuels (naturels) respectifs pour la France et la Wallonie, ce qui sera extrêmement difficile.

La thèse fournit des descriptions complètes des principaux types de piles à combustible existantes et de leurs caractéristiques respectives. De plus, les performances futures des piles à combustible de micro-cogénération sont étudiées. Les performances des systèmes PEMFC ne devraient pas augmenter de manière significative. Ce n'est pas le cas des systèmes SOFC, qui pourraient offrir une efficacité électrique théorique (DC) de 100% (LHV) pour l'oxydation électrochimique de biochar ou du méthane, qui peut être un vecteur d'hydrogène renouvelable. Par ailleurs, l'efficacité électrique LHV maximale démontrée (AC) d'une SOFC disponible commercialement depuis 2023 est déjà de 65%.

Ensuite, la thèse présente des travaux expérimentaux et de simulation réalisés sur deux systèmes actuellement commercialisés, à savoir le SOFC BI\*\*\*G\*N et la PEMFC P\*2 (noms donnés dans ce manuscrit). Les travaux expérimentaux comprennent à la fois des campagnes de tests en laboratoire et un suivi des tests in situ, sur le terrain, dans des applications réelles, débouchant sur des modèles de performance qui peuvent spécifiquement être intégrés dans des outils de simulation de bâtiments ou de planification énergétique. Le système PEMC testé présente un niveau élevé d'hybridation avec une chaudière à condensation classique, ce qui est présumé empêcher un fonctionnement optimal et robuste de ces deux sous-systèmes. En revanche, le système SOFC testé est fiable et offre une efficacité électrique toujours proche de 60% (LHV) à sa puissance nominale, qui peut par ailleurs facilement être modulée dans la plage de 33% à 100%.

En s'appuyant sur ces performances expérimentales et sur les progrès anticipés des systèmes de piles à combustible, la thèse démontre que leur potentiel de réduction des gaz à effet de serre sur l'empreinte carbone individuelle moyenne reste relativement insignifiant si leur combustible n'est pas décarboné. Même dans ce cas, la réduction resterait insuffisante, et d'autres actions devraient encore être mises en œuvre.

Cependant, certaines piles, telles que les SOFC à 'Direct Carbon' (DCSOFC) ou les PEMFC à 'Direct Formic Acid' (DFAFC), offrent la possibilité de capturer du CO<sub>2</sub> pur à leur échappement anodique. Avec l'étude de cas de la demande électrique moyenne d'un logement belge et de l'utilisation d'une voiture électrique (pour environ 20000 km/an) fournie par une DCSOFC avec une efficacité électrique LHV de 80% alimenté en biomasse, ces émissions négatives pourraient atteindre environ 3 MtCO<sub>2eq</sub>/an. Vu le niveau minimal d'absorption de carbone requis par l'objectif de neutralité carbone (spécifié plus haut), le potentiel d'émissions négatives de ces systèmes de piles à combustible devra absolument être davantage développé et mis en œuvre en parallèle d'une augmentation significative des puits carbone naturels.

## Acknowledgments

I would like to express my sincere gratitude and appreciation to my wife, who has been by my side throughout this four-year journey. Her unwavering support and care for me and our family have made this accomplishment possible. I would also like to extend my thanks to both her parents and mine for taking excellent care of our two children during the countless extra hours I dedicated to this work.

Secondly, I would like to convey my heartfelt appreciation to Professor Vincent Lemort for his warm welcome, trust, and guidance over the years. Working under his supervision has allowed me to explore fascinating topics such as fuel cells, providing a unique balance of creative freedom and structured deliverables. Despite the personal challenges I encountered, this job has given me a sense of purpose like no other one I had before. I am truly grateful for Professor Lemort's knowledge, insights, valuable advice, and positive attitude that accompanied me throughout this journey.

Furthermore, I would like to acknowledge and thank the examination committee for their dedicated time and effort in reviewing and evaluating this manuscript.

I am deeply grateful to the *Gas.be* company for their substantial financial support and trust in the ULiege Thermodynamics Laboratory, as well as in me, for the field-tests and laboratory studies presented in this thesis. I extend my thanks to Olivier, their expert, for generously sharing technical information on gas-fed space heating appliances.

Undoubtedly, my appreciation goes to the entire ULiege Thermodynamics Laboratory community, including the academic staff, researchers, and especially the technicians involved in the laboratory activities: Bernard, Richard, and José. I would also like to express my gratitude to all my past and present colleagues who have served as teaching assistants. Their assistance in our academic duties has been invaluable. This is particularly the case with Alanis, whom I frequently sought help from and who was always available. It was a genuine honour to have the opportunity to know and collaborate with all of you.

I would also like to extend my special thanks to my colleague Camilà, who worked extensively with me on the *Gas.be* deliverables. I deeply admire her ability to handle those challenging assignments alongside her other responsibilities

Lastly, I would like to thank Professor Nathalie Job for spending a lot of time reviewing extensively some of my work. I truly learned a lot in a field that was new to me thanks to her judicious advices and comments.

It goes without saying that I would be delighted if my path was to cross again with the ULiege Thermodynamics Laboratory community in the future.



# Contents

<b>ABSTRACT</b> .....	<b>III</b>
<b>RÉSUMÉ</b> .....	<b>IV</b>
<b>ACKNOWLEDGMENTS</b> .....	<b>V</b>
<b>CONTENTS</b> .....	<b>VII</b>
<b>LIST OF FIGURES</b> .....	<b>XIII</b>
<b>LIST OF TABLES</b> .....	<b>XXI</b>
<b>LIST OF ABBREVIATIONS</b> .....	<b>XXV</b>
<b>LIST OF SYMBOLS</b> .....	<b>XXVII</b>
<b>CHAPTER 1 INTRODUCTION</b> .....	<b>1</b>
1.1 PERSONAL INTRODUCTION .....	1
1.2 TECHNICAL INTRODUCTION .....	2
1.3 THESIS OBJECTIVES .....	3
1.4 METHODOLOGY AND DETAILED MANUSCRIPT OVERVIEW .....	4
• <i>Chapter 1 – Introduction</i> .....	4
• <i>Chapter 2 – Collective and individual GHG mitigation pathways</i> .....	4
• <i>Chapter 3 – Fuel cell technologies and their residential applications</i> .....	4
• <i>Chapter 4 &amp; 5 – Study of the BI***G*N SOFC and of the P*2 PEMFC systems</i> .....	5
• <i>Chapter 6 – Residential fuel cells’ carbon footprint mitigation potential</i> .....	5
• <i>Chapter 7 – Perspectives</i> .....	5
• <i>Chapter 8 – Conclusions</i> .....	5
<b>CHAPTER 2 COLLECTIVE AND INDIVIDUAL GHG MITIGATION PATHWAYS</b> .....	<b>6</b>
2.1 CONFRONTING IPCC’S CARBON BUDGETS TO CLIMATE POLICIES .....	6
2.1.1 <i>Carbon budgets background information</i> .....	6
2.1.2 <i>Current France and Wallonia NDCs</i> .....	9
2.1.3 <i>Comparison methodology and data source</i> .....	13
2.1.4 <i>Comparison results</i> .....	14
2.1.5 <i>Discussion and perspectives about the section</i> .....	16
2.1.6 <i>Conclusions of the section</i> .....	17
2.2 ESTABLISHING INDIVIDUAL CARBON FOOTPRINT PATHWAYS BASED ON IPCC’S CARBON BUDGETS 19	
2.2.1 <i>Material and methods</i> .....	22
2.2.2 <i>Results for Wallonia : examples of sigmoidal GHG mitigation pathways</i> .....	29
2.2.3 <i>Results for France : missing data and example of sigmoidal GHG emission pathway</i> 30	
2.2.4 <i>Discussion and perspectives about the section</i> .....	33
2.2.5 <i>Conclusions of the section</i> .....	33
2.3 CURRENT EMISSIONS FACTORS FROM HEAT AND POWER GENERATION .....	36
2.3.1 <i>CO<sub>2</sub> and CO<sub>2eq</sub> emission factors</i> .....	36

2.3.2	<i>SO<sub>2</sub> and NO<sub>x</sub> emission factors</i> .....	39
2.3.3	<i>Methane slip in natural gas fed fuel cells</i> .....	42
2.4	CONCLUSIONS OF THE CHAPTER .....	43
<b>CHAPTER 3 FUEL CELL TECHNOLOGIES AND THEIR RESIDENTIAL APPLICATIONS</b> .....		<b>44</b>
3.1	GENERALITIES .....	44
3.1.1	<i>Fuel cell operations and main advantages</i> .....	44
3.1.2	<i>Fuel cell types and classification</i> .....	46
3.2	MICRO-COGENERATION FUEL CELLS SYSTEMS AND MARKETS .....	61
3.2.1	<i>Definitions and commercial fuel cell-based micro-CHP technologies</i> .....	61
3.2.2	<i>Status of commercialized HT-PEMFC-based micro-CHP systems</i> .....	63
3.2.3	<i>Main fuel cell-based micro-CHP markets</i> .....	65
3.2.4	<i>Focus on the European market and the available fuel cell-based micro-CHP systems</i> 67	
3.2.5	<i>Current and expected performance of micro-CHP systems based on a PEMFC or a SOFC</i> 69	
3.3	CONCLUSIONS OF THE CHAPTER .....	71
<b>CHAPTER 4 STUDY OF THE BL***G*N SOFC SYSTEM</b> .....		<b>73</b>
4.1	DESCRIPTION OF THE MACHINE .....	73
4.1.1	<i>Working principle</i> .....	73
4.1.2	<i>Applications and the different versions of the tested system</i> .....	74
4.1.3	<i>BL***G*N 2014+ - Manufacturer datasheet</i> .....	79
4.1.4	<i>Probable internal schemes</i> .....	79
4.1.5	<i>Conclusions of the section</i> .....	84
4.2	LABORATORY TESTS .....	85
4.2.1	<i>Description of the test bench</i> .....	85
4.2.2	<i>Measurement devices</i> .....	87
4.2.3	<i>Tests matrix</i> .....	90
4.2.4	<i>Test procedure</i> .....	91
4.2.5	<i>Experimental results and data analysis</i> .....	94
4.2.6	<i>Troubleshooting</i> .....	100
4.2.7	<i>Conclusions of the section</i> .....	100
4.3	IN-SITU MONITORING .....	102
4.3.1	<i>Description of the buildings</i> .....	102
4.3.2	<i>Measurement devices</i> .....	103
4.3.3	<i>Methodology</i> .....	105
4.3.4	<i>Results</i> .....	107
4.3.5	<i>Uncertainty analyses</i> .....	116
4.3.6	<i>Troubleshooting</i> .....	118
4.3.7	<i>Conclusions of the section</i> .....	118
4.4	MACHINE MODELLING .....	120
4.4.1	<i>LHV thermal efficiency modelling</i> .....	120
4.4.2	<i>LHV electrical efficiency modelling</i> .....	121
4.4.3	<i>Conclusions of the section</i> .....	122



4.5	COMPARISON OF LABORATORY AND IN-SITU MEASUREMENTS .....	123
4.6	NON-CO <sub>2</sub> POLLUTANT EMISSIONS.....	125
4.6.1	<i>Measurement devices</i> .....	125
4.6.2	<i>Measurements analysis</i> .....	126
4.7	CONCLUSIONS OF THE CHAPTER .....	131
<b>CHAPTER 5 STUDY OF THE P*2 PEMFC SYSTEM .....</b>		<b>132</b>
5.1	DESCRIPTION OF THE MACHINE .....	132
5.1.1	<i>Working principle</i> .....	132
5.1.2	<i>Applications and the different versions of the tested system</i> .....	136
5.1.3	<i>P*2 - Manufacturer datasheet</i> .....	140
5.1.4	<i>Probable internal schemes</i> .....	140
5.1.5	<i>Conclusions of the section</i> .....	145
5.2	LABORATORY TESTS .....	147
5.2.1	<i>Description of the test bench</i> .....	147
5.2.2	<i>Measurement devices</i> .....	148
5.2.3	<i>Test procedure</i> .....	150
5.2.4	<i>Test matrix</i> .....	150
5.2.5	<i>Experimental results and data analysis</i> .....	152
5.2.6	<i>Troubleshooting</i> .....	155
5.2.7	<i>Conclusions of the section</i> .....	155
5.3	IN-SITU MONITORING .....	157
5.3.1	<i>Description of the buildings</i> .....	157
5.3.2	<i>Measurement devices</i> .....	158
5.3.3	<i>Methodology</i> .....	160
5.3.4	<i>Results</i> .....	161
5.3.5	<i>Uncertainty analyses</i> .....	168
5.3.6	<i>Troubleshooting</i> .....	169
5.3.7	<i>Conclusions of the section</i> .....	170
5.4	MACHINE MODELLING .....	172
5.4.1	<i>Introduction</i> .....	172
5.4.2	<i>Material and Methods</i> .....	173
5.4.3	<i>Modelling</i> .....	175
5.4.4	<i>Modelling limitations &amp; further work</i> .....	186
5.4.5	<i>Conclusions of the section</i> .....	187
5.5	COMPARISON OF LABORATORY AND IN-SITU MEASUREMENTS .....	189
5.5.1	<i>Field-test chosen model</i> .....	189
5.5.2	<i>Steady-state laboratory results</i> .....	189
5.5.3	<i>Correlation</i> .....	189
5.5.4	<i>Results and conclusions of the section</i> .....	191
5.6	NON-CO <sub>2</sub> POLLUTANT EMISSIONS.....	193
5.6.1	<i>Measurement devices</i> .....	193
5.6.2	<i>Measurements analysis</i> .....	193
5.7	CONCLUSIONS OF THE CHAPTER .....	203

<b>CHAPTER 6 RESIDENTIAL FUEL CELLS' CARBON FOOTPRINT MITIGATION POTENTIAL</b>	<b>204</b>
6.1 CARBON FOOTPRINT CALCULATORS .....	204
6.2 INDIVIDUAL CARBON FOOTPRINT EXAMPLE WITHOUT ENERGY USES .....	205
6.3 CARBON FOOTPRINT OF ENERGY USES .....	207
6.4 CONCLUSION OF THE CHAPTER .....	211
<b>CHAPTER 7 PERSPECTIVES.....</b>	<b>213</b>
7.1 SUMMARY OF KEY FINDINGS AND CONTRIBUTIONS .....	213
7.1.1 Chapter 1 – Introduction.....	213
7.1.2 Chapter 2 – Collective and individual GHG mitigation pathways .....	213
7.1.3 Chapter 3 – Fuel cell technologies and residential applications.....	214
7.1.4 Chapter 4 – Study of the BL***G*N SOFC system .....	215
7.1.5 Chapter 5 – Study the P*2 PEMFC system.....	216
7.1.6 Chapter 6 – Residential fuel cells' carbon footprint mitigation potential .....	218
7.1.7 Chapter 7 – Perspectives and further works .....	218
7.1.8 Chapter 8 – Conclusions .....	219
7.1.9 Appendixes.....	219
7.2 DISCUSSION, LIMITATIONS & FURTHER WORKS .....	220
<b>CHAPTER 8 CONCLUSIONS .....</b>	<b>223</b>
<b>APPENDIX 1 : ENERGY CONTENT OF NATURAL GAS IN RESIDENTIAL APPLICATIONS</b>	<b>224</b>
INTRODUCTION .....	224
ESTABLISHING THE HHV OF THE CONSUMED GAS AT THE FIELD-TEST DELIVERY CONDITIONS .....	226
DISCUSSIONS AND CONCLUSIONS .....	229
<b>APPENDIX 2 : DOCUMENT PROPERTIES OF THE PREVIOUS BL***G*N MODEL INSTALLATION'S MANUAL .....</b>	<b>231</b>
<b>APPENDIX 3 : USER MANUAL OF THE TESTED BL***G*N SOFC SYSTEM.....</b>	<b>232</b>
<b>APPENDIX 4 : INSTALLATION MANUAL OF THE (TESTED) BL***G*N (FRONT PAGE AND DOCUMENT PROPERTIES).....</b>	<b>255</b>
<b>APPENDIX 5 : INSTALLATION MANUAL OF THE (TESTED) BL***G*N (REVERSE OSMOSIS PAGE).....</b>	<b>257</b>
<b>APPENDIX 6 : CALIBRATION PRINCIPLES OF THE SOFC TEST BENCH.....</b>	<b>258</b>
<b>APPENDIX 7 : SOFC LABORATORY MEASUREMENTS PROCEDURE .....</b>	<b>259</b>
<b>APPENDIX 8 : POLLUTANT TESTING (NOX, SO2 AND CO) OF COMMERCIALIZED MICRO-COMBINED HEAT AND POWER (MCHP) FUEL CELLS .....</b>	<b>261</b>
INTRODUCTION .....	261
MATERIAL AND METHODS .....	262
TESTED SYSTEMS .....	262
PEMFC hybridized to a gas condensing boiler.....	262
SOFC.....	263
Gas condensing boiler .....	264
Euro 6 diesel vehicle.....	264
MEASUREMENT DEVICE .....	265
CONVERSION OF PPM TO MG/KWH .....	265

TESTING PROCEDURE AND RESULTS .....	268
DISCUSSION AND CONCLUSION .....	271
<b>APPENDIX 9 : DETAILED SCHEMATICS OF THE MONITORING SENSORS CONFIGURATION OF THE P*2 FIELD-TEST SITES.....</b>	<b>273</b>
<b>APPENDIX 10 : P*2 BEHAVIOR AND HOW IT AFFECTS EFFICIENCY: ZOOMING ON REPRESENTATIVE DAYS.....</b>	<b>274</b>
<b>APPENDIX 11 : SATISFACTORY SURVEY OF THE HOUSE IN HUY .....</b>	<b>283</b>
<b>APPENDIX 12 : SATISFACTORY SURVEY OF THE HOUSE IN OOSTMALLE .....</b>	<b>288</b>
<b>APPENDIX 13 : P*2 – LABORATORY TROUBLESHOOTING DESCRIPTION .....</b>	<b>289</b>
MAY 2019 .....	289
OCTOBER 2020.....	290
NOVEMBER 2020. INTERVENTIONS SUMMARY AND PREVIOUS VISITS .....	290
JANUARY 2021 .....	291
<b>APPENDIX 14 : LITERATURE REVIEW ON PEMFC DEGRADATION MECHANISMS 293</b>	
REVERSIBLE AND IRREVERSIBLE DEGRADATION OF PEMFCs.....	293
GENERAL LITERATURE REVIEW OF PEMFC DEGRADATIONS AND CORRESPONDING RECOVERY PROCEDURES.....	294
<i>Lack of humidity and gas crossover</i> .....	295
<i>Water accumulation</i> .....	295
<i>Carbon monoxide poisoning</i> .....	296
<i>Oxidation, dissolution and sintering of the platinum catalysts</i> .....	299
<i>Sulfur contamination</i> .....	300
DEDICATED REVIEW OF SIMILAR COMMERCIALIZED APPLICATIONS BY PATENT RESEARCH .....	301
<i>Carbon deposition on the reforming catalyst</i> .....	301
<i>Ammonia poisoning of the oxidation catalyst of the carbon monoxide remover</i> .....	302
<b>REFERENCES .....</b>	<b>305</b>



## List of Figures

- Figure 1.** Short-term and long-term temperature response by component for a 1-year emission pulse. Emissions levels from 2008 except for black carbon (BC) and Carbon Monoxide (CO) for which their 2005 levels have been considered. Reproduced from reference [12]. 8
- Figure 2.** How non-CO<sub>2</sub> GHG are considered in IPCC's carbon budget expressed in CO<sub>2</sub>-only emissions. Reproduced from reference [8]. 9
- Figure 3.** Official carbon budgets adopted in April 2020 for France. Traduced reproduction of official revised France low carbon strategy [22]. 10
- Figure 4.** Historical evolution of France's individual carbon footprint between 1995 and 2018, which remains quite constant and around 11 tCO<sub>2eq</sub>/year per capita. Reproduced and traduced from reference [32]. 11
- Figure 5.** Historical evolution of GHG emissions in Wallonia. Traduced reproduction of legally adopted Wallonia 2030 strategy for air, energy and climate, originally requested by Regulation (EU) 2018/1999 of the European Parliament and of the Council of 11th December 2018 [24]. 12
- Figure 6.** Global GHG emissions scenarios reproduced from literature that follow inverted 'S-curve' theoretical pathways: (a) From IPCC's AR6 [10], (b) From Carbon Action Tracker [70] (c) From Rare organization [71]. 21
- Figure 7.** Schematic illustration of how global mean temperatures respond to different emissions trends in carbon dioxide (CO<sub>2</sub>) and methane (CH<sub>4</sub>). Reproduced from reference [72]. 21
- Figure 8.** Highlighted proportionality of the net warming impact of all anthropogenic forcings and the one CO<sub>2</sub>-only emissions. Dots represent multiple scenarios: they mark the peak warming and the lines end at the point of net-zero CO<sub>2</sub> emissions in each scenario. The larger spread of all anthropogenic forcings red dots relative to purple CO<sub>2</sub>-only dots is due to non-CO<sub>2</sub> emission scenarios that largely differ, which were all necessary to compute because of the great level of uncertainty in future non-CO<sub>2</sub> GHG emission pathways. TCRE means Transient Climate Response (to cumulative emissions). It is widely used for climate change characterization and basically corresponds to the temperature change compared to preindustrial levels. Reproduced and adapted from reference [77]. 24
- Figure 9.** Wallonia's historical and projected population from the database of Bureau du Plan [96], considering immigrants due to the Ukraine-Russia conflict started in 2022 [97]. 26
- Figure 10.** Two cases of proposed sigmoidal GHG mitigation pathways for Wallonia and their corresponding remaining carbon budget: **(a)** Safer case with the carbon budget never allowed to be overcome and early GHG mitigation starting in 2020, allowing for the slope of the mitigation effort not to be too steep, **(b)** Risky case with carbon budget allowed to be (slightly) overcome and delayed GHG mitigation that results in a quite steep slope of the mitigation effort. 30
- Figure 11.** Resulting yearly GHG emissions and territorial absorption of the two cases proposed in Figure 10: **(a)** Safer case with the carbon budget never allowed to be overcome and early GHG mitigation starting in 2020, allowing for the slope of the mitigation effort not to be too steep, **(b)** Risky case with carbon budget allowed to be (slightly) overcome and delayed GHG mitigation that results in a quite steep slope of the mitigation effort. 30

**Figure 12.** France's historical and projected population from the database of the Institut National de la Statistique et des Etudes Economiques [116,117], not considering immigrants due to the Ukraine-Russia conflict started in 2022 [97]. 31

**Figure 13.** Example of sigmoidal GHG mitigation pathways for France and the corresponding remaining carbon budget (case with the carbon budget never allowed to be overcome). 32

**Figure 14.** Schematic representation of a fuel cell core and definitions. GDL stands for Gas Diffusion Layer, which consists of porous and electrically conductive structures for gas and electrons transfer that have as main task to allow uniform access of gaseous reactants to the catalyst (abbreviated by Cat. on the figure) layer of both electrodes [202]. Reproduced from reference [201]. 45

**Figure 15.** Operation mode of ammonia solid-oxide fuel cells. Similar definitions ('Direct', 'Indirect', 'Internal' and 'External' 'Decomposition') can be applied to other fuel cell types, such as PEMFC [245] and/or other fuels, such as methane [246] or methanol [245], for which the 'Decomposition' term might be expressed as 'Conversion' or 'Reforming'. Reproduced from reference [244]. 48

**Figure 16.** Working principle of an (A)DBFC, i.e. an (Alkaline) Direct Borohydride Fuel Cell. Reproduced and adapted from reference [232]. 51

**Figure 17.** Working principle of the DASFC (Direct Alkaline Sulfide Fuel Cell). Similarly to the (A)DBFC case of Figure 16 and Equation (13) and Equation (14), an example of fuel compatible with such a DASFC is an alkaline sulfide solution composed of 1 mole of  $\text{Na}_2\text{S}$  and 3 moles of  $\text{NaOH}$  (in order to provide the  $\text{Na}^+$  charge carrier) [258]. Reproduced and adapted from reference [233]. 51

**Figure 18.** Identification key of fuel cell types. Some fuel cells types accronyms have been linked through their font color because they either share the same accronym and/or they use the same (or a derivative) fuel. Microbial and enzymatic fuel cells have not been represented so as fuel cell involving indirect internal or external decomposition of their primary fuel into a secondary fuel consumed at the anode of the stack, as described in Figure 15. 52

**Figure 19.** Main CHP technologies and their fields of applications. PV/T stands for photovoltaic hybrid technologies. Reproduced from reference [329]. 61

**Figure 20.** Cumulative number of residential micro-CHP systems installed (solid lines) and near-term projections (dotted lines) reported in 2015. Reproduced and adapted from reference [266] with 2020 data for Japan and Europe [335] and 2019 data for Korea [372,373]. 65

**Figure 21.** Status of the fuel cell micro-CHP European market in the countries involved in the PACE European Union project. That program aimed to demonstrate through field-test installations and monitoring in real applications the capability of fuel cell products to reach a commercial mass market [347]. Reproduced slide from the Final Conference of the PACE program (26<sup>th</sup> April 2023) [378]. 66

**Figure 22.** Fuel cell micro-CHP systems commercially available in Europe. The reported power output is the nominal electrical power output; the previous numeric row corresponds to the amount of units installed in Europe through the PACE supporting program. Reproduced slide from the Final Conference of the PACE European Union project (26 April 2023) [393], that aimed to demonstrate through field-test installations and monitoring in real applications the capability of fuel cell products to reach a commercial mass market [347]. 68

- Figure 23.** First part of the fuel cell micro-CHP systems commercially available in Europe and their main features. GCB stands for Gas Condensing Boiler. Reproduced and traduced from reference without modification [391]. 69
- Figure 24.** Second part of the fuel cell micro-CHP systems commercially available in Europe and their main features. Reproduced and traduced from reference without modification [391]. 69
- Figure 25.** Working principle of a O-SOFC. Reproduced and adapted from reference [428]. 74
- Figure 26.** First part of the design improvements implemented on the ‘BG-\*\*’ (declared by the OEM). Reproduced from reference [434]. 75
- Figure 27.** Second part of the design improvements implemented on the ‘BG-\*\*’ (declared by the OEM). Reproduced from reference [434]. 76
- Figure 28.** Photograph of the identification plate of the Bl\*\*\*G\*N tested in ULiege facilities (corresponding to the manual presented in *APPENDIX 3: User manual of the tested Bl\*\*\*G\*N SOFC system*). 76
- Figure 29.** Identification plate from the a previous similar Bl\*\*\*G\*N model reproduced from its installation manual, which document properties are presented in *APPENDIX 2: Document properties of the previous Bl\*\*\*G\*N model installation’s manual*. 77
- Figure 30.** Bl\*\*\*G\*N endurance behavior. A comparison between old and recent (2014+) installations. Reproduced from reference with original caption [425]. At least two versions of the Bl\*\*\*G\*N (prior to the BG\*\*) exists, demonstrating different ageing performance. 77
- Figure 31.** Most probable internal scheme of the tested Bl\*\*\*G\*N system. Main option, with a reverse osmosis filter that requires periodical purges as the second water outlet. Reproduced and adapted from reference [440]. 80
- Figure 32.** Photograph of the back of the system, with the two water excess evacuation pipes (and the water supply pipe). 81
- Figure 33.** Other possible internal scheme of the tested Bl\*\*\*G\*N system. Secondary option, with a pressure relief valve as the second water outlet. Reproduced and adapted from reference [440]. 82
- Figure 34.** Last possible internal scheme of the tested Bl\*\*\*G\*N system. Last option, with a water and CO<sub>2</sub> removal apparatus as the second water outlet. Reproduced and adapted from reference [440]. 83
- Figure 35.** CO<sub>2</sub> anode recirculation removal principles. Reproduced from reference [444]. 83
- Figure 36.** CO<sub>2</sub> anode recirculation removal with air feed and water recuperation through condensation in a knockout vessel KO-A1. Reproduced from reference [444]. 83
- Figure 37.** Bl\*\*\*G\*N laboratory test bench schematics. 85
- Figure 38.** Specific elements used in the presented test-tig. a) Thermostatic 3-way valve to control the return temperature (‘VTA 572’ by ESBE [450]). b) Variable speed circulator used in the laboratory test bench to control the space heating flow rate (‘Yonos Para 15/6’ by Wilo [451]). 86
- Figure 39.** Photographs of the Bl\*\*\*G\*N test bench. 87
- Figure 40.** BKG4T gas metering sensors of the test bench [452]. 88
- Figure 41.** Gas and electrical metering installations on the test bench. 88

- Figure 42.** Water and heat meter used in the heat rate measurement of the heat recovery system. a) Volumetric watermeter used to measure space heating flow rate ('DHV1300' by DH Metering Europe [456]). b) Ultrasonic heat meter included in the test-bench that allows for directly measuring space heating heat transfer ('Qalcosonic E1' by Axioma [455]). 89
- Figure 43.** Photograph of the separate PT-500 probe assembly required for the heat meter. 89
- Figure 44.** Thermocouple elbow immersion sleeve (without insulation features). 90
- Figure 45.** Empty laboratory test matrix sheet. The yellow parameter is the electrical power output set remotely by the manufacturer whereas the orange parameter is the flow rate controlled by the variable-speed circulator. The return temperature is controlled by the thermostatic 3-way valve (see test bench schematics on Figure 37). 91
- Figure 46.** System's responses to a big temperature step (about 20°C) in order to establish stabilization's time. 92
- Figure 47.** LHV thermal efficiency of the BI\*\*\*G\*N according to working temperature (and water flow rate) at 1500 W<sub>el</sub> of electrical power output. 97
- Figure 48.** LHV thermal efficiency of the BI\*\*\*G\*N according to working temperature (and water flow rate) at 1000 W<sub>el</sub> of electrical power output. 98
- Figure 49.** LHV thermal efficiency of the BI\*\*\*G\*N according to working temperature (and water flow rate) at 500 W<sub>el</sub> of electrical power output. 99
- Figure 50.** Laboratory results obtained in this work superposed on reproduced LHV efficiency results published in 2011 by the manufacturer for an older version of the BI\*\*\*G\*N [462]. 99
- Figure 51.** Market study on reported efficiencies for three different groups of micro-CHPs: Internal Combustion Engines (ICE), Fuel Cell based micro-CHPs and CHP based on Stirling principle. The efficiencies are put in perspective with a line (lower dotted one) representing the reference conventional power that the micro-CHPs must beat (i.e. the average grid efficiency for electrical generation and the gas condensing boiler for heat production). Average efficiency of the grid electrical mix is considered to be at 40 % HHV (as comparison, the one of UK in 2013 was about 38.6% LHV, i.e. 34.8% HHV [463]). Reference thermal efficiency of condensing gas boiler is considered to be at 90% HHV (as comparison, yearly HHV efficiency figure of field-tested gas condensing boiler have been reported in the 82-89% range [464] whereas the Walloon energy regulator in Belgium has stated, based upon field-test studies, that reference state-of-the-art gas condensing boilers have efficiencies of 90% LHV, i.e. 81.2 % HHV [127]). The maximum physically possible upper limit corresponding to total HHV efficiency of 100% is represented by the upper dotted line. Reproduced and adapted from reference [461]. The experimental results of this SOFC system at 30°C of return temperature reported in Figure 32 according to the output power setting have been added considering a 1.1085 HHV to LHV ratio [132]. The efficiency results over the upper line (total efficiency results over 100% HHV) are most likely due to measurement uncertainty, especially regarding how the HHV is accounted for [465]. 100
- Figure 52.** Location of the SOFC monitoring sites. 102
- Figure 53.** Monitored sensors configuration of the BI\*\*\*G\*N field-test sites The house in Duffel has an additional PV (photovoltaics) panels electrical production monitoring sensor. 103
- Figure 54.** LHV efficiency of both field-test SOFCs discretized per month for the year 2021. 108



- Figure 55.** Electrical energy and heat production of both field-test SOFCs discretized per month for the year 2021. 109
- Figure 56.** Daily electrical energy production of both field-test SOFCs for the year 2021. 109
- Figure 57.** Sensitivity study of the energy utilization economic balance according to energy prices. Positive economic balances mean that the SOFC system provides savings compared to the references (grid electricity consumption and gas condensing boiler). 113
- Figure 58.** The three recommended options to mount a temperature sensor in a pipe [489]  
 b) Example of the distribution of the temperature of the fluid within a pipe along with an example of multiple probes installation in order to study it [489]. 118
- Figure 59.** Model of the laboratory Bl\*\*\*G\*N LHV thermal efficiency according to return temperature of the heat recovery circuit and electrical output power. 121
- Figure 60.** Model of the laboratory Bl\*\*\*G\*N LHV electrical efficiency according electrical output power. 122
- Figure 61.** Correlation of the electrical efficiency between laboratory tests, field-tests and manufacturer expected performance. In the end of the year monitoring year 2021, the Duffel and Riemst systems had respectively already 30000 and 37000 operating hours. The underlying graph has been presented in Figure 30. 123
- Figure 62.** Reproduced figure from a 2011 publication of the manufacturer [462] on which the laboratory results have been superposed. Field-test results have not been superposed as the underlying graph is limited to 20000 of operating hours whereas the field-test systems had already been operating for more than 30000 hours. 123
- Figure 63.** Combustion and fine particulates devices. 126
- Figure 64.** Example of signal from the fine particulates sensor Afriso STM 225. 127
- Figure 65.** Pollutant measurement at minimal electrical output power (500 W<sub>el</sub>). The return temperature of the heat recovery circuit is changed after about 5 min of acquisition time from about 50°C to about 20°C. 129
- Figure 66.** Pollutant measurement at intermediate electrical output power (1000 W<sub>el</sub>). The return temperature of the heat recovery circuit is changed after about 10 min of acquisition time from about 20°C to about 50°C. 130
- Figure 67.** Working principle of a PEMFC (valid for LT and HT-PEMFCs). Reproduced and adapted from reference [497]. 133
- Figure 68.** Architecture of the P\*2 – High level of integration (through two heat exchangers, several 3-way valves and several pumps) of the PEMFC with the gas condensing boiler and the DHW tank. Reproduced and adapted from reference [521]. 136
- Figure 69.** Architecture of the 3\*\* – High level of integration (through two heat exchangers, several 3-way valves and several pumps) of the PEMFC with the gas condensing boiler and the tanks [500]. 137
- Figure 70.** Photograph of the PEMFC stack of the P\*2 (same as for the 3\*\* and the PA\*). Picture identical in the documentation of the three machines [522–524]. 137
- Figure 71.** OEM's declared performance of the PEMFC only (reproduced from reference [523,524]). PEMFC thermal efficiency is lower for the 3\*\* (no longer sold) [521]. 138
- Figure 72.** Internal photograph of the P\*2 system [523]. 140
- Figure 73.** (a) Hydraulic configuration of the system in DHW production; (b) Hydraulic configuration of the system in space heating production by the boiler; (c) Unlikely hydraulic configuration where the DHW tank acts as a heat storage for the space heating circuit. 142

- Figure 74.** Assumed basic scheme of the PEMFC module with its hydrogen processor. The water tank only consists of processed water (from the humid streams, such as the flue gases or the water produced by the stack and recuperated at the cathode exhaust) and should not be confused with the DHW tank illustrated in Figure 68. Several elements have not been illustrated : the scheme does not involve any pump or compressor to ensure flowing directions and appropriate pressure levels. It does not involve auxiliaries (such as safety valves, check valves, purging system, reactant filters, additional water recovery in humid streams such as at the anode outlet [509], potential natural gas desulfurizer, *etc.*). Mostly, it does not illustrate internal heat management : each component has its own operating temperature and multiple internal heat exchanges are implemented to optimize accordingly the inlet gaseous streams temperatures [267] (the heat recovered from the cathode exhaust dehumidification, i.e. from its water recovery, is not shown, for example). Potential anode off-gases recirculation (to the anode inlet, to increase fuel efficiency [538]) is not shown. The air bleed stream could also serve other purposes such as the main reforming process (if it involves the methane partial oxidation reaction) or the potential carbon monoxide mitigation (see *APPENDIX 14: Literature review on PEMFC degradation mechanisms* for more details). 143
- Figure 75.** Location of surface thermocouples (grey circles) in the P\*2 test bench. 147
- Figure 76.** P\*2 test bench scheme rear-view. 148
- Figure 77.** Thermocouples assembly configurations: surface, elbow and air thermocouples (in the system's chimney). 149
- Figure 78.** Gas and electrical installations. 149
- Figure 79.** Graphical representation of the thermocline in the buffer tank. 151
- Figure 80.** Daily tests 24-hour cycle evolution for fuel cell-only performance estimation. 152
- Figure 81.** Buffer tank temperatures definition for fuel cell efficiency estimation. 154
- Figure 82.** Location of the PEMFC monitoring sites. 157
- Figure 83.** Monitored sensors configuration of the P\*2 field-test sites (a more detailed schematics can be found in *APPENDIX 9: Detailed schematics of the monitoring sensors configuration of the P\*2 field-test sites*). 159
- Figure 84.** Monthly LHV efficiencies for monitored P\*2 dwellings for the year 2020. 162
- Figure 85.** Monthly heat and power production for both field-test P\*2 for the year 2020. 163
- Figure 86.** Daily Savings according to daily electrical production of the PEMFC machine (year 2020). 164
- Figure 87.** Sensitivity study of the energy utilization economic balance according to energy prices Positive economic balances mean that the PEMFC system provide savings compared to the references (grid electricity consumption and gas condensing boiler). 166
- Figure 88.** Linear fit of the field-test daily electrical efficiency according to the daily thermal efficiency. The 95% confidence interval is however quite large as it defines a  $\pm 10$  percentage points zone around the fit for the daily electrical efficiency. 176
- Figure 89.** Comparison between the monthly and the first daily model defined by Equation (47) and whose coefficients are given in Table 38. To allow the comparison, the daily heat demand from the first daily model has been multiplied by the average number of days contained within a month, i.e. 30. As deduced from *APPENDIX 11: Satisfactory Survey of the house in Huy*, in the summer, it is likely that the house in Huy has completely shut down its space heating (high temperature terminal units controlled manually on demand) and that its system was only used for DHW. These monthly data were separated

from the others monthly data to show that the models are relevant no matter if the system is used for DHW only or also for space heating. 177

**Figure 90.** Step by step improvement of the primary logarithmic empirical model defined by Equation (2) to account for key effects on thermal efficiency. 179

**Figure 91.** Flowchart of the daily models developed in this field-test study. 181

**Figure 92. (a)** Small decrease (considered linear) of thermal efficiency according to the operating temperature for identical total heat demands; **(b)** Small decrease (considered linear) of thermal efficiency according to the standard deviation of the return temperature for identical total heat demands. Six days have been highlighted per graph : X is either the 4-hour gliding average temperature or the daily standard deviation of the return temperature, Y is the total daily heat demand and Z is the LHV thermal efficiency. 182

**Figure 93.** Final two-variable models of this work. The first one includes the corrections made in the previous single-variable models (according to working temperatures and modulation smoothness) and provides a better fit. The data of the second one has not been postprocessed. 184

**Figure 94.** Field-test pollutant emissions in Huy - boiler only (part 1/3). 195

**Figure 95.** Field-test pollutant emissions in Huy - boiler only (part 2/3). 196

**Figure 96.** Field-test pollutant emissions in Huy - boiler only (part 3/3). 197

**Figure 97.** Field-test pollutant emissions in Huy - PEMFC only (part 1/3). 198

**Figure 98.** Field-test pollutant emissions in Huy - PEMFC only (part 2/3). 199

**Figure 99.** Field-test pollutant emissions in Huy - PEMFC only (part 3/3). 200

**Figure 100.** What happened on the monitored gas consumption during the field-test pollutant emissions (Huy). 201

**Figure 101.** Field-test pollutant emissions in Oostmalle. Test sequence has been detailed in the upper part of the figure. 202

**Figure 102.** Chosen example of individual carbon footprint without any energy uses considered for the dwelling (gas/electricity consumptions). The resulting total carbon footprint (without the energy uses of the dwelling) is close to 10 tCO<sub>2eq</sub>/year, way above of the 2050 individual target defined in *Chapter 2 - Collective and individual GHG mitigation pathways*. Implementing or not implementing a residential fuel cell (fed by natural gas, biogas or other climate neutral fuel) will not affect that remaining carbon footprint, so other actions should be taken to reach the 2050 carbon footprint target of 1 tCO<sub>2eq</sub>/year per capita established in *Chapter 2 - Collective and individual GHG mitigation pathways*. Indeed, for example, feeding habits and savings accounts have still have significant impacts that shall also be mitigated. 206

**Figure 103.** Impact of the implementation of the ideal fuel cell micro-CHP systems reported in Table 42 (for an average Belgian dwelling) on the individual carbon footprint pathways previously established in Figure 10 for Wallonia that allows for respecting IPCC's +2°C equity carbon budget. Only marginal emissions have been considered (Dataset 'A' from Table 42). Dataset 'E1' (also from Table 42) has not been used because there is no carbon footprint savings for natural gas fed fuel cells occur when average grid electricity is considered. The 'O' dot corresponds to the chosen example of initial carbon footprint, i.e. the addition of the carbon footprint without energy uses reported in Figure 102 with the carbon footprint of energy uses of the average Belgian dwelling established at the top of Table 42 divided by the number of adults occupants in the dwelling (i.e. two in this case). 210

**Figure 104.** PEMFC system's architecture, including two heat exchangers, several 3-way valves, several circulators, the gas condensing boiler and the DHW tank [15]. 263

- Figure 105.** Tested micro-CHP SOFC in the laboratory facilities of the University of Liege [447]. 264
- Figure 106.** ‘Multilyzer STx’ combustion analyser portable meter. 265
- Figure 107.** Pollutant measurements of the fuel cell (only) startup phase of the PEMFC-gas condensing boiler hybrid system (performed in a laboratory environment). 269
- Figure 108.** Indoor temperature in the Oostmalle house for the focus week. 275
- Figure 109.** Indoor temperature in the Huy house for the focus week. 275
- Figure 110.** DHW energy index in the Huy house for the focus week. Red circles are showing that the PEMFC starts when (sufficient) DHW is drawn. 276
- Figure 111.** Space heating thermal power in the Oostmalle house for the focus week. 277
- Figure 112.** Space heating thermal power in the Huy house for the focus week. 278
- Figure 113.** Space heating return temperature in the Huy house for the focus week. The red circle highlights the moment when the PEMFC is breaking its designed cycle (and is not shut down only for ‘regeneration’). 279
- Figure 114.** DHW energy index in the Oostmalle house for the focus week. Green circles are highlighting sufficient DHW draws for the PEMFC to keep running whereas the red circle is highlighting a probable insufficient DHW draw. 279
- Figure 115.** Detailed behavior of the system for Oostmalle on the focus week according to the space heating thermal power signal. 280
- Figure 116.** Space heating thermal power and space heating return temperature in the Huy house for the focus week. The red box highlights a possible heat dissipation of the PEMFC in the space heating circuits. 282
- Figure 117.** Fuel cell keyboard. 290
- Figure 118.** Boiler return line after removing the installed water meter. 291
- Figure 119.** January 2021 fault message. 291
- Figure 120.** Characterization of reversible and irreversible losses in PEMFCs. Since PEMFC operating conditions can vary with time, reversible degradation (voltage loss) might not occur at a constant rate. Therefore, irreversible losses are more relevantly established after the recovery procedures than before. Figure reproduced and adapted with permission [616]. 293

## List of Tables

<b>Table 1.</b> IPCC's AR6 remaining carbon budgets from January 1st 2020.	7
<b>Table 2.</b> Current NDCs for France and Wallonia compared to the European Green Deal.	10
<b>Table 3.</b> Equity +2°C carbon budgets from January 1 <sup>st</sup> 2020 against Wallonia and France current NDCs.	15
<b>Table 4.</b> Reference and values found in literature for CO <sub>2</sub> or CO <sub>2eq</sub> emission factors of heat and power generation systems or mix, mainly in Belgium (LHV based figures) [15].	37
<b>Table 5.</b> SO <sub>2</sub> emission level reported from Energie+ [180] (website developed by the University of Louvain-la-Neuve and the Energy department of the Wallon Region, in Belgium).	41
<b>Table 6.</b> NO <sub>x</sub> emission level reported from Energie+ [180] (website developed by the University of Louvain-la-Neuve and the Energy department of the Wallon Region, in Belgium) [121].	42
<b>Table 7.</b> Comparison between main fuel cell types characteristics. Not all the fuel cell types mentioned in Figure 18 are reported in this table. For one fuel cell type, several electrolytes and fuels can be mentioned, the first one being the most common. All the other characteristics (other columns), especially the electrical efficiency, refer only to the first electrolyte and to the first fuel reported (if not explicitly specified). Main parts of this table are reproduced, adapted or corrected (by the use of a strikethrough font) from reference [205]. Additional elements from other sources are directly referenced in the table.	60
<b>Table 8.</b> List of HT-PEMFC commercialized micro-CHP products and their current availability status.	64
<b>Table 9.</b> Panel Perspective on Cost and Technical Potential for 1–10 kW <sub>el</sub> CHP Stationary Fuel Cell Systems Operating on Natural Gas. Reproduced and adapted from reference [400].	70
<b>Table 10.</b> Main differences between BI***G*N known models.	78
<b>Table 11.</b> BI***G*N 2014+ expected targets, provided by the manufacturer.	79
<b>Table 12.</b> Resolution and accuracy levels of main sensors used to compute efficiency laboratory results.	94
<b>Table 13.</b> Average HHV and LHV figures on the day of the test sequence.	94
<b>Table 14.</b> Laboratory test campaign of the BI***G*N at 1500 W <sub>el</sub> (nominal electrical power output).	96
<b>Table 15.</b> Laboratory test campaign of the BI***G*N at 1000 W <sub>el</sub> (intermediate electrical power output).	97
<b>Table 16.</b> Laboratory test campaign of the BI***G*N at 500 W <sub>el</sub> (minimal electrical power output).	98
<b>Table 17.</b> Reference of the monitoring sensors and acquisition system for the BI***G*N field-test sites.	104
<b>Table 18.</b> Monitoring performance of the field-tested SOFCs for the whole year 2021. Utilization savings indicators consider a gas condensing boiler of 90% constant LHV efficiency as reference for heat production.	110

<b>Table 19.</b> Additional monitoring data of the field-tested SOFCs for the whole year 2021.	110
<b>Table 20.</b> CO <sub>2eq</sub> impact of avoided electrical network losses thanks to the decentralized electrical production of the SOFC system and impact of extra fugitive natural gas emissions due to additional gas consumption at decentralized dwellings.	115
<b>Table 21.</b> Parameters of the LHV thermal efficiency model of the SOFC of Equation (30) and Equation (31), valid between electrical power output $W_{el}$ of 500 and 1500 W <sub>el</sub> .	120
<b>Table 22.</b> Parameters of the LHV electrical efficiency model of the SOFC of Equation (32) and Equation (33).	122
<b>Table 23.</b> Emissions measurement devices.	126
<b>Table 24.</b> SO <sub>2</sub> /Nox/CO pollutant emissions measurements results on the studied SOFC Bl***G*N system.	128
<b>Table 25.</b> PEMFC gas boiler hybrid expected targets (according to the manufacturer) - Nominal performance of the P*2 [523].	140
<b>Table 26.</b> P*2 test measurement devices.	149
<b>Table 27.</b> P*2 performed test campaigns.	150
<b>Table 28.</b> Daily tests profiles description to estimate the fuel cell efficiency, morning and evening sessions.	151
<b>Table 29.</b> Experimental data collected through the test campaigns of the P*2 PEMFC system.	153
<b>Table 30.</b> Electrical, thermal and global efficiencies of the system for DHW tests.	153
<b>Table 31.</b> Electrical, thermal, and global efficiencies of the system for SH tests.	154
<b>Table 32.</b> Boiler efficiency results obtained during boiler-only operation.	154
<b>Table 33.</b> HHV efficiency estimation of the P*2 fuel cell from experimental results.	155
<b>Table 34.</b> Reference of the monitoring sensors and acquisition system for the P*2 field-test sites. The sensors are the same as in the corresponding SOFC study conducted in the previous chapter except for the fact that the P*2 field-test sites require an additional heat meter (of the same reference), as the system as not only one (as in the Bl***G*N SOFC system) but two thermal outputs (for space heating and DHW).	159
<b>Table 35.</b> 2020 field-test figures for both PEMFCs (1866 degree-days in 2020 [551], base 16.5°C [552]). Utilization savings indicators consider a gas condensing boiler of 90% constant LHV efficiency as reference for heat production.	161
<b>Table 36.</b> 2021 field-test figures for both PEMFCs (2286 degree-days in 2021 [554], base 16.5°C [552]). . Utilization savings indicators consider a gas condensing boiler of 90% constant LHV efficiency as reference for heat production.	162
<b>Table 37.</b> CO <sub>2eq</sub> impact of avoided electrical network losses thanks to the decentralized electrical production of the PEMFC system and impact of extra fugitive natural gas emissions due to additional gas consumption at decentralized dwellings.	168
<b>Table 38.</b> Values for the parameters of the logarithmic models and goodness of fit indicators.	179
<b>Table 39.</b> Values for the parameters of the two-variables models with and without adjusted data.	185
<b>Table 40:</b> Laboratory results [550] (with adjustments) for comparison to field-test model (based on adjusted heat demands with correction factor $\gamma_1$ and electrical production) – fully opened heat demand valves.	192

<b>Table 41.</b> Laboratory results [550] (with adjustments) for comparison to field-test model (based on adjusted heat demands with correction factor $\gamma_1$ and electrical production) – fully opened heat demand valves.	192
<b>Table 42.</b> Yearly carbon footprint calculations of several SOFC micro-CHP systems energy uses corresponding to an average Belgian dwelling of 17000 kWh <sub>th</sub> and 3500 kWh <sub>el</sub> of gas and electricity consumption. The different cases are based on current and expected/hoped performance of fuel cell micro-CHPs. Those calculations are related to an average dwelling and are not expressed ‘per capita’.	209
<b>Table 43.</b> Altitude of the field-test sites.	227
<b>Table 44.</b> Comparison between PEMFCs and SOFCs. Reproduced and adapted from reference [205].	262
<b>Table 45.</b> PEMFC gas boiler hybrid expected targets (data published by manufacturer) [523].	263
<b>Table 46.</b> Specifications of the ‘Multilyzer STx’ combustion analyser portable meter [494].	265
<b>Table 47.</b> Combustion only and Life Cycle Assessment (LCA) NO <sub>x</sub> emission level reported from Energie+ [180] (website developed by the University of Louvain-la-Neuve and the Energy department of the Walloon Region, in Belgium).	266
<b>Table 48.</b> Natural gas <i>F</i> coefficients for Equation (68) depending on the pollutant type [608].	267
<b>Table 49.</b> Pollutant emissions measurements results (in all tests, the sensor indicated 0 ppm of SO <sub>2</sub> emissions).	270
<b>Table 50.</b> Field-test data for a repeatable week (7 repeatable days) for the two monitored houses. Main differences have been highlighted.	274
<b>Table 51.</b> Display error description.	289





# List of Abbreviations

- (A)DBFC (Alkaline) Direct Borohydride Fuel Cell
- AEM Anion Exchange Membrane
- AEMFC Anion Exchange Membrane Fuel Cell
- AFC Alkaline Fuel Cell
- AR6 Sixth Assessment Report (of IPCC)
- BOP Balance Of Plant (supporting components and auxiliary systems of a power plant needed to deliver the energy)
- Cat. Catalyst
- CCGT Combined Cycle Gas Turbine
- CCS Carbon Capture and Storage
- CDR Carbon Dioxide Removal
- CEMFC Cation Exchange Membrane Fuel Cell
- CHP Combined Heat and Power ( $\mu$ CHP or mCHP : micro-CHP)
- CREG Commission de Régulation de l'Electricité et du Gaz
- CWaPE Commission wallonne pour l'Energie
- D-SOFC Dual ion-conducting (or mixed-ion conducting) Solid Oxide Fuel Cell
- DAC Direct Air Capture
- DAFC Direct Ammonia/Alcohol Fuel Cell (not equivalent : depending on the literature references)
- DASFC Direct Alkaline Sulfide Fuel Cell
- DASOFC Direct Alcohol Solid Oxide Fuel Cell
- DC-SOFC Direct Carbon Solid Oxide Fuel Cell
- DCFC Direct Carbon Fuel Cell
- DEFC Direct Ethanol Fuel Cell
- DEGFC Direct Ethylene Glycol Fuel Cell
- DFAFC Direct Formic Acid Fuel Cell
- DDFC Direct Formate Fuel Cell
- DHFC Direct Hydrazine Fuel Cell
- DHSFC Direct Hydrogen Sulfide Fuel Cell
- DHW Domestic Hot Water
- DMFC Direct Methanol Fuel Cell
- DMSOFC Direct Methanol Solid Oxide Fuel Cell
- EFC Enzymatic Fuel Cell
- GDL Gas Diffusion Layer
- GHG Greenhouse Gases
- GWP Global Warming Potential (GWP-100 : GWP over 100 years)
- H<sup>+</sup>-SOFC Solid Oxide Fuel Cell with Proton Conduction, same as P-SOFC
- H-SOFC Solid Oxide Fuel Cell with Proton Conduction, same as P-SOFC
- HAC High Ambition Coalition
- (H)CFCs (Hydro)chlorofluorocarbons

HHV High Heating Value  
HT-PEMFC High Temperature Proton Exchange Membrane Fuel Cell  
IPCC Intergovernmental Panel on Climate Change  
LHV Low Heating Value  
LT-PEMFC Low Temperature Proton Exchange Membrane Fuel Cell  
LULUCF Land Use, Land Use Change and Forestry  
MCDCFC Molten Carbonate Direct Carbon Fuel Cell  
MCFC Molten-Carbonate Fuel Cell  
MEF Marginal Emission Factor  
MFC Microbial Fuel Cell  
MHDCFC Molten Hydroxide Direct Carbon Fuel Cell  
NDC Nationally Determined Contribution  
O-SOFC or O<sup>2</sup>-SOFC Oxygen Ion-conducting Solid Oxide Fuel Cell, same as SOFC-O  
OEM Original Equipment Manufacturer  
P-SOFC Proton-conducting Solid Oxide Fuel Cell, same as SOFC-H  
PACE Pathway to a Competitive European Fuel Cell micro-CHP Market, i.e. public supporting EU program for fuel cell micro-CHPs, or Plan for Air, Climate and Energy, i.e. Wallonia climate strategy for 2030  
PAFC Phosphoric Acid Fuel Cell  
PBI Polybenzimidazole  
PC-SOFC Proton Conducting Solid Oxide Fuel Cell, same as SOFC-H  
PCFC Protonic Ceramic Fuel Cell, same as H-SOFC  
PEFC Polymer Electrolyte Fuel Cell, same as PEMFC  
PEMFC Proton Exchange Membrane Fuel Cell or Polymer Electrolyte Membrane Fuel Cell (same as PEFC)  
PM Particulate Matter  
PV(/T) Photovoltaics (hybrid technologies)  
RMSE Root Mean Square Error  
ROI Return On Investment  
SAFC Solid Alkaline Fuel Cells  
SCY Perovskite ceramic electrolyte materials based on strontium earth zirconate  
SH Space Heating  
SLCP Short-Lived Climate Pollutant  
SMP System Marginal Price  
SODCFC Solid Oxide Direct Carbon Fuel Cell  
SOFC Solid Oxide Fuel Cell  
SOFC+ Solid Oxide Fuel Cell with Proton Conduction, same as P-SOFC  
SOFC- Solid Oxide Fuel Cell with Oxygen Ion Conduction, same as O-SOFC  
SOFC-H or SOFC(H<sup>+</sup>) Solid Oxide Fuel Cell with Proton Conduction, same as P-SOFC  
SOFC-O or SOFC(O<sup>2-</sup>) Solid Oxide Fuel Cell with Oxygen Ion Conduction, same as O-SOFC  
TCRE Transient Climate Response (to cumulative emissions)  
VOC Volatile Organic Compounds  
WGS Water-Gas Shift  
YSZ Yttria-stabilized zirconia

## List of Symbols

- $\epsilon_e$  average billed electrical residential price per kWh, €/kWh  
 $\epsilon_g$  average billed gas residential price per kWh, €/kWh  
 $\epsilon_{inj}$  average injection residential price per kWh, €/kWh  
 $\epsilon_{savings}$  total energy utilization costs savings of the fuel cell micro-CHP instead of reference energy production systems (see  $\epsilon_{ref}$ ), €  
 $\epsilon_{SOFC}$  energy utilization costs of the SOFC, €  
 $\epsilon_{ref}$  energy utilization costs of reference energy production systems (i.e. gas condensing boiler for heat production and general grid for electrical production), €  
 $cp$  or  $cp_A$  or  $cp_w$  specific heat capacity of water, J/(kg · °C) or J/(kg · °K)  
 $\dot{m}$  water flow rate going through the space heating appliance, kg/s  
 $\dot{m}_A$  heat recovery water flow rate (for the SOFC laboratory tests), kg/s  
 $CF(y)$  yearly carbon footprint, kgCO<sub>2</sub>/year or kgCO<sub>2eq</sub>/year  
 $CF_i$  initial yearly carbon footprint, kgCO<sub>2</sub>/year or kgCO<sub>2eq</sub>/year  
 $CF_f$  targetted (final) yearly carbon footprint, kgCO<sub>2</sub>/year or kgCO<sub>2eq</sub>/year  
 $C_\gamma$  minimum value for the  $\gamma_1$  correction factor applicable to the dataset of laboratory results for field-test correlation, -  
 $Max_{\overline{T_{R,4h}}}$  maximum value of  $\overline{T_{R,4h}}$  for the whole monitoring dataset (applicable to the PEMFC model), -  
 $Max_{\sigma_{TR}}$  maximum value of  $\sigma_{TR}$  for the whole monitoring dataset (applicable to the PEMFC model), -  
 $T_D$  depart temperature of the heat recovery water, °C or K  
 $T_R$  return temperature of the heat recovery water, °C or K  
 $L_{FC}$  daily load factor of the micro-CHP, i.e. ratio between the daily energy produced and the maximum energy produced (similar to  $\lambda$ ), -  
 $Q_{DHW}$  Domestic Hot Water demand, Wh or kWh  
 $Q_{g,LHV}$  equivalent energy consumption of the system (based on LHV), same as  $W_{g,LHV}$ , Wh or kWh  
 $Q_{recovered}$  heat recovered from the micro-CHP, Wh or kWh  
 $Q_{SH}$  space heating demand, Wh or kWh  
 $\dot{Q}_A$  heat recovery thermal heat rate, W or kW  
 $\overline{T_{R,4h}}$  non-dimensionalized daily maximum 4h gliding average temperature of the return line (applicable to the PEMFC model), -  
 $V_{gas}$  or  $\int \dot{V}_{gas}$  volume of consumed gas (by the micro-CHP), m<sup>3</sup>  
 $V_w$  volume of the internal tank of the PEMFC system, m<sup>3</sup>  
 $W_{g,LHV}$  equivalent energy consumption of the system (based on LHV), same as  $Q_{g,LHV}$ , Wh or kWh  
 $W_{el,house,in}$  electrical energy consumed by the house from the grid, Wh or kWh

- $W_{el,house,net}$  total electrical energy demand of the house, Wh or kWh
- $W_{el,house,out}$  electrical energy rejected/injected by the house on the grid, Wh or kWh
- $\dot{W}_{el}$  electrical power output of the micro-CHP, W or W
- $W_{el}$  or  $W_{el,FC}$  electrical energy production of the micro-CHP, Wh or kWh
- $W_{el,FC,local}$  electrical energy production of the micro-CHP that is directly consumed locally by the dwelling, Wh or kWh
- $\gamma_{1,2}$  correction factors applied for the PEMFC model to account for working temperature levels (1) and unsmooth heat demands (2), -
- $\gamma_d$  demand cover factor, -
- $\gamma_s$  supply cover factor, -
- $\Delta T$  temperature difference between depart and return of space heating appliance, °C or K
- $\Delta T_{top,m}, \Delta T_{bottom,m}, \Delta T_{top,e}, \Delta T_{bottom,e}$  temperature difference of the top/bottom half of the internal tank of the PEMFC system in the morning/evening, °C or K
- $\eta_{el(av)}$  (average) LHV electrical efficiency of the micro-CHP, %
- $\eta_{el,model}$  modeled LHV electrical efficiency of the micro-CHP, %
- $\eta_{syst}$  total LHV electrical efficiency of the micro-CHP, %
- $\eta_{th(av)}$  (average) LHV thermal efficiency of the micro-CHP, %
- $\eta_{th,model}$  modeled LHV thermal efficiency of the micro-CHP, %
- $\eta_{th,cb}$  90 % of LHV thermal efficiency of a condensing gas boiler used as reference for heat production, -
- $\lambda$  instantaneous load factor of the micro-CHP, i.e. ratio between electrical output power  $\dot{W}_{el}$  and nominal electrical power (similar to  $L_{FC}$ ), -
- $\rho_w$  specific mass of water, kg/m<sup>3</sup>
- $\sigma_{TR}$  daily standard deviation of the monitored space heating return temperature (applicable to the PEMFC model)
- $\varphi_0$  primary energy penalty applied to laboratory testing to allow correlation with field-test model (for the PEMFC system), kWh



# CHAPTER 1 INTRODUCTION

Although the main focus of the manuscript is on fuel cell technologies, I believe a proper introduction is necessary to explain my involvement in the field of renewable energies and the ultimate objective of greener technologies, such as fuel cells, in the energy transition.

## 1.1 Personal introduction

As early as I can remember, I have always been enthusiastic regarding Nature and greatly concerned by global warming and Greenhouse Gases (GHG) emissions. This was even the subject I chose for a school project at the age of 12. Then, at the age of 14, in chemistry class, I have been introduced to water electrolysis, which formed hydrogen and oxygen. As the teacher burnt the created dihydrogen collected in a test tube, I thought that this potentially clean molecule could be extremely useful in the energy transition. Not knowing that it existed already, I thought at that point of the hydrogen internal combustion engine for the automotive sector. Concurrently, this, which for me was a discover, gave me purpose. I knew from that point that I would want to dedicate my professional career to try to develop or improve renewable technologies. This was the reason for me to become an engineer. At the time, the main pollutant sources I was facing every day came from the transportation sector. This led me to choose the field of mechanics as specialization and even performed a complementary master's degree in automotive. It later also led me to a five-year career in the research and development department of an aeronautical company. During that time, I worked towards improving the efficiency of cargo and passenger airplane engines. Unfortunately, at one point, I realized that the potential fuel reduction that I was working towards was negligible compared to the expected growth of the aeronautical sector. I felt that my work was mainly serving to increase the distance that the plane could travel or the weight it could carry ('rebound effect' [1]), increasing the value of the engine but not really decreasing its emissions. This was for me quite a conflict of values and I felt that I was not really contributing to the energy transition.

Therefore, in 2019, I quit both the private company and the aeronautical sector to join the thermodynamics laboratory of the University of Liege and work in the renewable energy field. This opportunity arose thanks to the successful contacts I had with Pr. Lemort, to whom I am very grateful, as stated in the *Acknowledgments*. Working for a university definitely allowed much freedom in my research so I could focus on the pure interest of science and on what it could bring to the society, without necessarily caring for financial aspects. Also, Pr. Lemort job offer involved working on fuel cells and hydrogen technologies, which, as stated earlier on this page, oriented my choice of studies back when I was only a teenager and constitutes another reason for thanking him again.

## 1.2 Technical introduction

Hydrogen and fuel cells represent significant hopes for energy decarbonization, and some applications are already commercialized, even at the residential scale, as micro-cogeneration systems for heat and power production. Through theoretical reviews, simulations and experimental work, the main goal of this thesis is to verify and investigate the potential role of such fuel cell micro-combined heat and power (micro-CHP) systems in the energy transition of the residential sector.

Initially, this thesis defines the energy transition in terms of GHG emissions and carbon budget from IPCC's latest work (AR6 from 2022). This much-needed decarbonization is then expressed locally and even translated to the individual scale, using examples like Belgium, Wallonia or France as case studies frequently referenced through this work. In order to later on evaluate the environmental performance of fuel cells, emission factors of energy productions technologies have also been reviewed.

The thesis then introduces the notion of fuel cell, providing descriptions of the main existing types and their characteristics. An innovative fuel cell types identification key is even proposed. Then, the fuel cell micro-CHP market is investigated and a focus is brought on residential fuel cells currently commercialized in Europe. Also, depending on its underlying technology, the expected future performance of micro-CHP fuel cells is investigated.

Subsequently, experimental and simulation work performed of two currently available fuel micro-CHP systems, i.e. one SOFC (Solid Oxide Fuel Cell) and the PEMFC (Polymer Electrolyte Membrane Fuel Cell), is presented. The experimental work is based both on laboratory test campaigns and in-situ field-test monitoring in real applications. This work leads to dedicated performance models suitable for integration into building performance simulation or energy planning tools.

Based on the demonstrated performance of fuel cell micro-CHP systems (and on their expected future performance), their carbon footprint mitigation potential is then investigated with the case study of the average Belgian dwelling/occupants.

Finally, this thesis reflects on its own limitations, explores potential perspectives for future research, and concludes with valuable insights gained throughout the investigation. By shedding light on the possibilities and challenges of integrating fuel cells into the residential energy sector, this work contributes to the ongoing pursuit of sustainable and environmentally friendly energy solutions.

### 1.3 Thesis objectives

As stated, the ultimate objective of the thesis is to investigate the potential role of fuel cell micro-CHP systems in the energy transition of the residential sector. In fact, amongst other contributions, it aims to help answering the following questions :

- What are the technologies and the performance of fuel cell micro-CHPs currently commercialized ?
- Are they sufficiently reliable in real applications ?
- Can fuel cell micro-CHP technologies currently commercialized help in the much-needed decarbonization and to what extent ?
- What about future technologies of fuel cell micro-CHP ?

Aside the biodiversity crisis, climate change is indeed likely to be the biggest challenge of the century for human kind. Humanity does not have the luxury of wasting time by making technical societal choices that would not lead to sufficient reductions in greenhouse gas emissions. This phenomenon is well-known and reported as a technological ‘locked-in’, preventing the adoption of potentially superior alternatives [2].

This is specifically critical concerning energy production technologies, such as fuel cells, and it is hoped that the studies conducted in this thesis will be of help regarding which technologies shall be prioritized.

The main contributions of this thesis are multiple, as summarized in the following and detailed in *Section 7.1 - Summary of key findings and contributions* (with direct refers to the relevant sections of the thesis they are related to).

Indeed, it offers a direct and **objective link** between the **current** and **expected carbon footprint performance** of the studied fuel cell **technologies** at the **scale of the household** and the remaining **global carbon budget** reported by IPCC in its latest assessment report (**AR6**).

Firstly, this required a new and innovative **method** to translate globalized **carbon budgets**, expressed in **CO<sub>2</sub>-only** emissions (long-lived climate pollutants), into **individual carbon footprint mitigation pathways**, expressed in all-GHG emissions (in **CO<sub>2eq</sub>**), including both short and long-lived climate pollutants. One of the advantages of this method is that individual **carbon footprint calculators can thus be used** to verify if one’s carbon footprint is correctly following the targeted pathway and, if necessary, to easily reset new compatible objective GHG mitigation pathways.

This also necessitated to study the performance and potential of commercially available fuel cell micro-CHPs through the correlation between experimental investigations conducted both in a laboratory environment and in real field-test applications. This led to innovative **performance models** of the systems (and **modelling methods**) that could be easily be used in **building performance simulation** or **energy planning tools**. This **correlation work** between laboratory ideal conditions and real applications also resulted in the reporting of key findings related to the reliability of the studied technologies, as it **demonstrated** that the **complexity of their integration** (or hybridization) with heating appliances **can prevent the sub-systems to operate as optimally** as they would as standalones units.

Additionally, an extensive literature review was required to explore the expected performance of different fuel cell technologies, which resulted in the development of a **novel identification key for fuel cell technologies**.



## 1.4 Methodology and detailed manuscript overview

- **Chapter 1 – Introduction**

This is the current chapter. It aims to introduce myself and explain ‘the reasons I am here’, i.e. the reasons that led me to conduct a thesis related to the renewable energies at the Thermodynamics Laboratory of the University of Liege. This chapter further introduces the subject of the thesis, i.e. the potential contribution of fuel cells systems for the energy transition of the residential sector, along with the thesis objectives, the methodology and the manuscript overview.

- **Chapter 2 – Collective and individual GHG mitigation pathways**

To really assess the potential of a renewable technology in the energy transition, it felt important to me to objectively understand the global GHG reduction targets and report it in individualized carbon footprint figures. In fact, I wanted to know what level of GHG mitigation should actually be reached to be able to quantify or to relate the beneficial aspects of the technologies I was studying. This is the purpose of *Chapter 2 - Collective and individual GHG mitigation pathways*. This chapter contextualizes the challenge of limiting the increase of temperature to +1.5°C or +2°C compared to pre-industrial levels, i.e. the targets adopted in the Paris Agreement in 2015, by explaining how the global, local and individual GHG emissions targets can be set relevantly to the recommendations of the Intergovernmental Panel on Climate Change (IPCC). First, with the examples of France and Wallonia, Nationally Determined Contributions (NDCs) are analysed and compared to the latest recommendations of IPCC in its Sixth Assessment Report (AR6) to evaluate their relevance with the Paris Agreement.

Then, as it is sometimes a difficulty for people to evaluate their own impacts in the collective climate targets, this chapter also aims to provide individual carbon footprints directly based on IPCC’s AR6. One challenge that was addressed by dedicated researches was to link individual carbon footprints, usually expressed for all GHG pollutants, in CO<sub>2eq</sub>, to IPCC’s carbon budgets recommendations, expressed in CO<sub>2</sub>-only as climate science can directly link the amount of long-lived CO<sub>2</sub> in the atmosphere to global temperature increase. Expressed otherwise, the difficulty lied on how the (collective or individual) short-lived climate pollutants (SLCPs) mitigation pathways shall be accounted for along with the (collective or individual) CO<sub>2</sub>-only mitigation pathways.

In the end of this chapter, pollutant emissions factors of electricity generation technologies are compared to facilitate the environmental balances of the studied technologies reported later on in the manuscript (in *Chapter 4 - Study of the Bl\*\*\*G\*N SOFC system* and *Chapter 5 - Study of the P\*2 PEMFC system*). CO<sub>2</sub>/CO<sub>2eq</sub> constitutes the main subject of focus but NO<sub>x</sub> and SO<sub>x</sub> pollutants emission factors are also investigated. In addition, their other harmful effects, on human health and on the environment, are also reviewed.

- **Chapter 3 – Fuel cell technologies and their residential applications**

This chapter introduces the notion of fuel cells. It also offers a new identification key to list and differentiate all the existing fuel cell types that have been reviewed. A comparative table of the main fuel cell types is also proposed. Then, the chapter introduces the fuel cell micro-CHP market, focusing on the systems available on the European market. At last, this chapter investigate future expected performance of fuel cell CHP technologies.

- **Chapter 4 & 5 – Study of the BI\*\*\*G\*N SOFC and of the P\*2 PEMFC systems**

The goal of this chapter is to study the most representative SOFC and PEMFC systems on the European micro-CHP market established in *Chapter 3 - Fuel cell technologies and their residential* applications verifying their robustness and their performance. First, their (most probable) internal schematics is described to better understand their working principle. Then correlated laboratory and field-test experimental investigations are reported. Performance models of those systems are also proposed for possible integration with building and/or energy planning tools. At last, those respective chapters end by reporting NO<sub>x</sub>, SO<sub>x</sub> (and CO) pollutant emission measurements, as those have been introduced in *Chapter 2 - Collective and individual GHG mitigation pathways*.

- **Chapter 6 – Residential fuel cells’ carbon footprint mitigation potential**

Based on the performance of the systems tested in *Chapter 4 - Study of the BI\*\*\*G\*N SOFC system* and *Chapter 5 - Study of the P\*2 PEMFC system*, but also based on the expected performance of future fuel cell technologies (investigated in *Chapter 3 - Fuel cell technologies and their residential* applications), this chapter aims to establish the potential role of fuel micro-CHP in the energy transition contextualized in *Chapter 2 - Collective and individual GHG mitigation pathways*, through the case study of the average Belgian dwelling. It therefore aims to help answering the main research questions of this thesis.

- **Chapter 7 – Perspectives**

N/A – Self-explanatory title chapter.

- **Chapter 8 – Conclusions**

N/A – Self-explanatory title chapter.

# CHAPTER 2 COLLECTIVE AND INDIVIDUAL GHG MITIGATION PATHWAYS

The content of the first section of this chapter (*Section 2.1 - Confronting IPCC's carbon budgets to climate policies*) was published almost as-is in the *Journal of Ecological Engineering* [3]. The aims of this section are to introduce the notion of carbon budget in the context of global warming and energy transition. It also aims to establish the 'equity' carbon budgets for the 2020-2050 period for Wallonia, directly based on IPCC's latest AR6 report, and to compare it to its current climate commitments, i.e. its Nationally Determined Contributions (NDCs). As it is territorially and culturally close, the case of France is similarly developed as a comparison purpose. At last, other limitations of current NDCs are discussed.

In *Section 2.2 - Establishing individual carbon footprint pathways based on IPCC's carbon budgets*, this chapter also offers a method of establishing individualized carbon footprint mitigation pathways compatible with IPCC's equity carbon budgets (established in the first section of this chapter) that aim to solve most of the reported limitations of most current NDCs.

At last, emission factors of energy production systems are studied and reported in *Section 2.3 - Current emissions factors from heat and power generation* for further comparison with the studied fuel cell technologies. CO<sub>2</sub>/CO<sub>2eq</sub> is the main subject of focus but SO<sub>x</sub> and NO<sub>x</sub> pollutants are also investigated.

## 2.1 Confronting IPCC's carbon budgets to climate policies

### 2.1.1 Carbon budgets background information

At the 2015 United Nations Climate Change Conference (COP21), worldwide countries have adopted what is called as the 'Paris Agreement', which consists in engaging themselves towards limiting global warming to 1.5°C above pre-industrial levels, the absolute maximum acceptable increase being +2°C [4]. The +1.5°C target has been confirmed by the HAC (High Ambition Coalition) at the 2022 United Nations Climate Change Conference, known as the COP26 [5] and was supported by 41 signatories at the time [6], including the European Union [5], therefore including France and Wallonia, concerned by this work.

In 2018, IPCC (Intergovernmental Panel on Climate Change) officially published a report establishing the maximum amount of carbon dioxide that humankind still can emit in the atmosphere to be confident enough to respect the +1.5°C or +2°C targets set in the 'Paris Agreement', i.e. reporting the notion of 'carbon budget' [7]. It does not matter whether these amounts of CO<sub>2</sub> are emitted today, tomorrow or in ten years and, the carbon budget being limited, it also trivially implies that humanity necessarily reaches zero net CO<sub>2</sub> emissions at some point. As illustrated later in , the remaining carbon budget is linked to the increased global temperature, called 'TCRE' or 'transient climate response to cumulative emissions' [8]. Actually, in its Sixth Assessment Report (AR6), IPCC's Working Group I (WGI) has updated the carbon budgets set in 2018. As presented in Table 1, IPCC WGI reports that if humanity does not exceed 1150 GtCO<sub>2</sub> of emissions from January 1st 2020, it will have 2 out of 3 chances of not exceeding the +2°C maximum limit set in the

'Paris Agreement' [9]. It is worth mentioning that even more recently, IPCC's Working Group III (WGIII) has reevaluated the non-CO<sub>2</sub> global warming contribution and has decreased the remaining 2020 budget from 1150 GtCO<sub>2</sub> to 890 GtCO<sub>2</sub> with updated modelling method and other non-CO<sub>2</sub> mitigation scenarios [10]. Indeed, the non-CO<sub>2</sub> mitigation scenarios previously considered in the WGI AR6 [9] are coming from the former IPCC report established back in 2018 [7]. This work focuses on both the +2°C IPCC's AR6 carbon budget values (Table 1) because the +1.5°C target is already considered as unrealistic since IPCC's has reported that 'global Greenhouse Gases (GHG) emissions in 2030 associated with the implementation of NDCs announced prior to COP26 would make it likely that such warming level will be exceeded during the 21st century' [10].

One of the biggest challenges that still needs to be performed is to establish how these carbon budgets should be splatted fairly. Developing countries argue that they have the right to pollute as occidental countries have been doing it for 200 years. Colder countries argue that they require more energy to satisfy their primary need of heating whereas warmer countries argue that they need more air-conditioning. If the carbon budget were to be splatted by population, which is saying that every human being has the same carbon budget ('equity' principle between humans), developed countries would argue that 'Third World' already achieve those emissions targets per capita and that it is impossible to make such tremendous and urgent changes in their well-established way of living [11]. Fortunately, many countries have still already set their own GHG reduction targets, called 'Nationally determined contributions' (NDCs), but the lack of consultation between each other is an important drawback.

Likelihood of limiting global warming to temperature limit	Temperature limit of interest compared to preindustrial levels	Estimated remaining carbon budget from the beginning of 2020 (GtCO <sub>2</sub> )
50%	+1.5°C	500 [9] / 510 [10]
67%	+2°C	1150 [9] / 890 [10]

**Table 1.** IPCC's AR6 remaining carbon budgets from January 1st 2020.

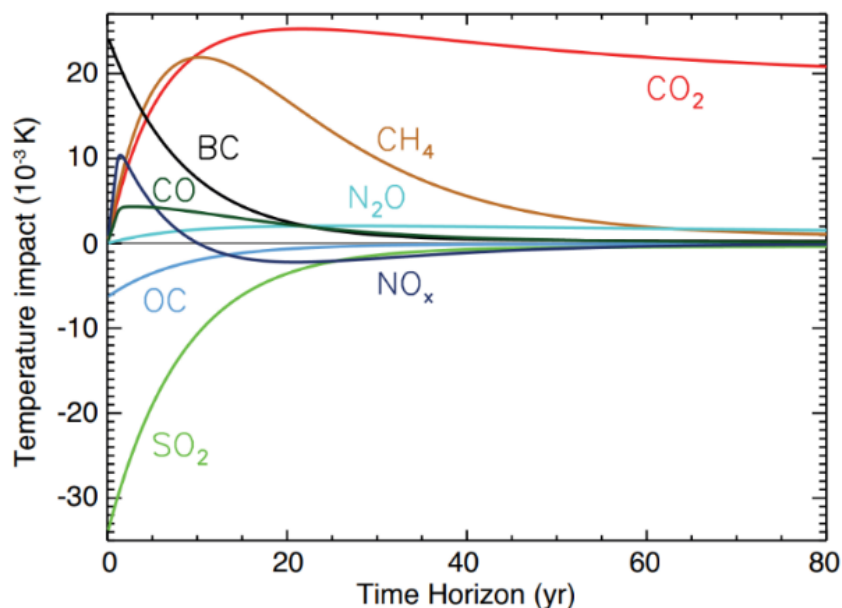
The significance of this work therefore relies in confronting (and showing the gap between) the NDCs that individual countries/regions are actually trying to implement regarding climate change and the original promises their representants have stated at the yearly Convention on Climate Change, such as the latest +1.5°C target supported by the HAC (which includes, amongst others, all European Union). The method used to highlight that gap, objectively based on IPCC's well accepted work, is also important as it could be easily reproduced by the many countries that are setting (or updating) their own NDCs, in order to hopefully respect IPCC's reported carbon budgets. Since most NDCs are expressed in terms of all-GHG emissions mitigation (CO<sub>2eq</sub>), their comparison with IPCC's carbon budgets expressed in terms of CO<sub>2</sub>-only is indeed not trivial. Therefore, this said method is explained and demonstrated in this work through the case of France and Wallonia (one of the main Belgian regions).

This work also reports other limitations of current climate targets and strategies of France and Wallonia (and by extension, of many other public authorities that have currently similar NDCs).

As reported in Table 1, carbon budgets are generally expressed in CO<sub>2</sub>-only and not in total GHG emissions (CO<sub>2eq</sub>). The main reason is that non-CO<sub>2</sub> GHG global warming potentials evolve in time differently accordingly to their own natural degradation or absorption rate. Similarly, their long-term behavior is very different to the one of CO<sub>2</sub>, as

illustrated in Figure 1 [12]. It is indeed well-established that, unlike for CO<sub>2</sub> (and N<sub>2</sub>O), the annual rate rather than the cumulative emissions of so-called short-lived climate pollutants (SLCPs) have the strongest effect on peak warming [13]. For example, it has been established that a 20-years delay in stringent methane mitigation has only an influence of 5 percentage points on the +2°C carbon budget compared to a stringent short-term methane mitigation [14], even though it has a 100-year global warming potential (GWP100) quite high, around 28 [15].

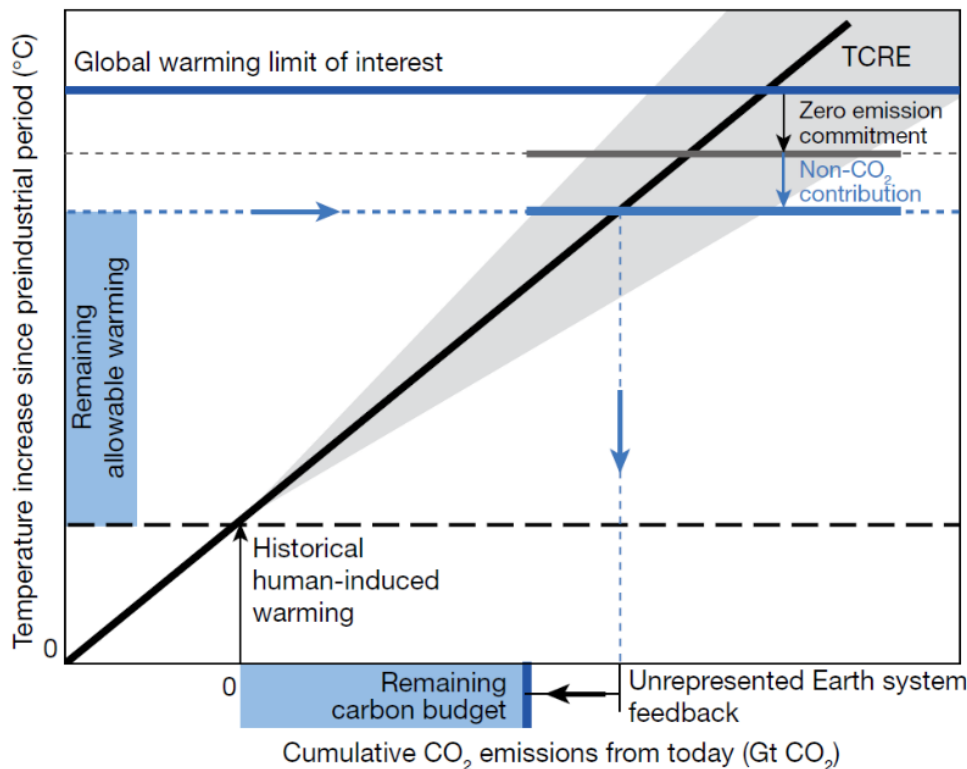
Since studies indicated that other GHG seem to have less mitigation potential than for CO<sub>2</sub> [16], their radiative forcing impact has been considered by implementing ‘an absolute security’ on the global warming temperature target, as illustrated in Figure 2 by the term called ‘Non-CO<sub>2</sub> contribution’ [8]. Therefore, respecting such carbon budgets and thus achieving zero carbon emission at some point will ensure respecting the temperature increase limit, even if the non-CO<sub>2</sub> GHG net emissions do not reach zero as well. This ‘absolute security’ on the global warming target has been estimated from the resulting radiative forcing of future non-CO<sub>2</sub> GHG emission at the moment at which global CO<sub>2</sub> emissions reach net zero [7]. This has been performed by computing different non-CO<sub>2</sub> mitigation scenarios always consistent with a carbon neutral future implied by IPCC's carbon budgets [8]. This means that IPCC's CO<sub>2</sub> budgets of Table 1 imply that other GHG shall be mitigated concurrently. Indeed, it would not be relevant to consider CO<sub>2</sub> mitigation scenarios along with constant SLCP emissions over time because some of them are emitted by common sources, such as in many combustion processes [14].



**Figure 1.** Short-term and long-term temperature response by component for a 1-year emission pulse. Emissions levels from 2008 except for black carbon (BC) and Carbon Monoxide (CO) for which their 2005 levels have been considered. Reproduced from reference [12].

IPCC's carbon budgets also consider the fact that global mean surface air temperature might still increase after cessation of net CO<sub>2</sub> emissions. For example, this could occur because of the effect of thermal equilibration that mainly results in the decline of ocean heat uptake [17]. To ensure that the maximum temperature target is not exceeded due to that ‘inertia’ effect, another ‘absolute security’ term, called ‘Zero emission commitment’, is considered. As it is shown in Figure 2 [8], this term is also applied to the global warming temperature target.

At last, IPCC's carbon budgets include an additional security adjustment called 'Unrepresented Earth system feedback', as presented in Figure 2 [8]. It is this time directly subtracted to the carbon budget (expressed in GtCO<sub>2</sub>) because it accounts for (often 'natural') additional uncontrolled 'direct' GHG emissions linked to anthropogenic global warming. Although a lot of potential Earth system feedbacks exists and have been listed, such as the increased frequency of wildfires [18], their associated level of uncertainty is so wide [19] that the main one that is typically accounted for in carbon budgets is the amount of GHG that could be released by thawing of the permafrost [8].



**Figure 2.** How non-CO<sub>2</sub> GHG are considered in IPCC's carbon budget expressed in CO<sub>2</sub>-only emissions. Reproduced from reference [8].

### 2.1.2 Current France and Wallonia NDCs

France and Wallonia, as well as the whole 27 countries of the European Union, are trivially supporting the European Green Deal initiated in 2019, which aims to a 55% minimum reduction of GHG compared to 1990 and a territorial carbon neutral objective for 2050 [20]. However, as it will be reported in Table 2, the European Green Deal objectives have not yet been (or only have just been) totally implemented in legally adopted NDCs of Wallonia and France.

In 2020, France legally adopted its carbon budget for the years to come corresponding to its official goal of carbon neutrality to be achieved by 2050 [21], as described in Figure 3. However, current France's law defines 'carbon neutrality' only territorially and there is no direct link with the notion of 'carbon footprint' [21]. That is unfortunately why Figure 3 only mentions territorial emissions and carbon sinks.

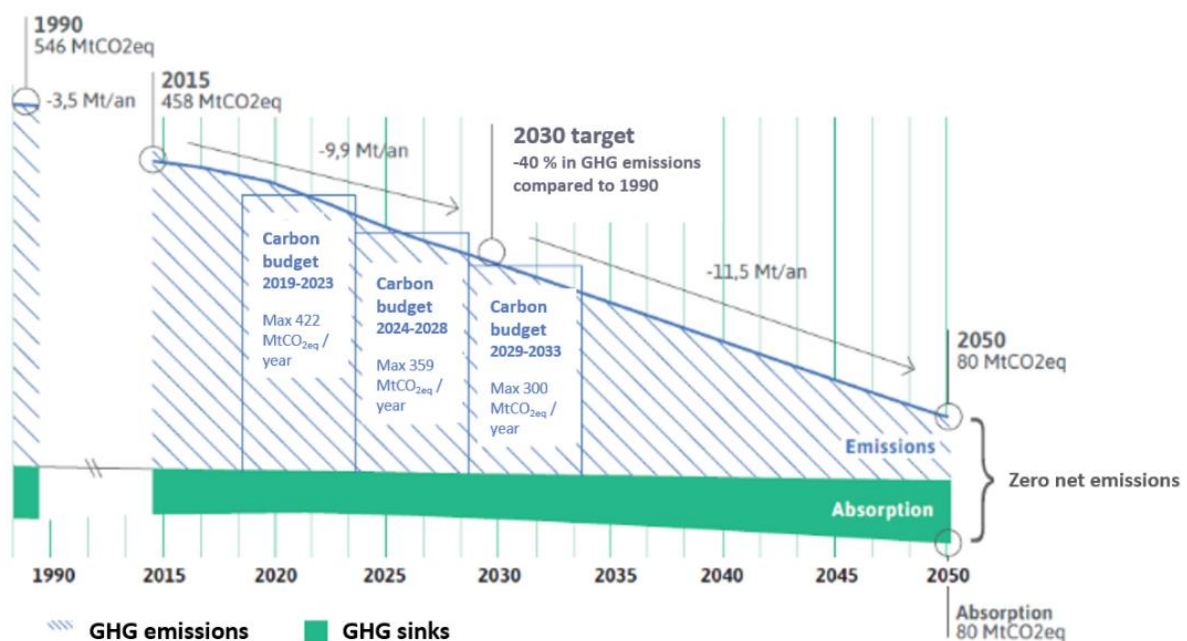
The trajectory to get to the 2050 target is considered linear from 2020 [22].

European Green Deal targets [20]	France	Wallonia
55% reduction of GHG emissions by 2030 compared to 1990	Not yet legally adopted Current target is -40% [21]	Both targets finally legally adopted in March 2023 [23]. Previous 2050 target was -95% [24].
Carbon neutrality by 2050	✓ Legally adopted [21]	

**Table 2.** Current NDCs for France and Wallonia compared to the European Green Deal.

In Wallonia, such a projective GHG emission reduction curve with time and its resulting carbon budgets no longer exist. Indeed, the proposed 2023 – 2027 carbon budget [25] should have been voted by 2017 but it is, as stated, not yet the case. Since March 2023, the legal current commitment of Wallonia in terms of GHG finally matches the European Green Deal [23] but there is no legally adopted path on how to get to the 2050 target even though linear reduction pathways can be assumed, even by Belgian experts [26] and

**Territorial GHG emissions and sinks between 1990 and 2050. CITEPA 2018 inventory and SNBC revised scenario (carbon neutral scenario)**



officials [27].

**Figure 3.** Official carbon budgets adopted in April 2020 for France. Traduced reproduction of official revised France low carbon strategy [22].

### 2.1.2.1 Main criticisms of France and Wallonia NDCs

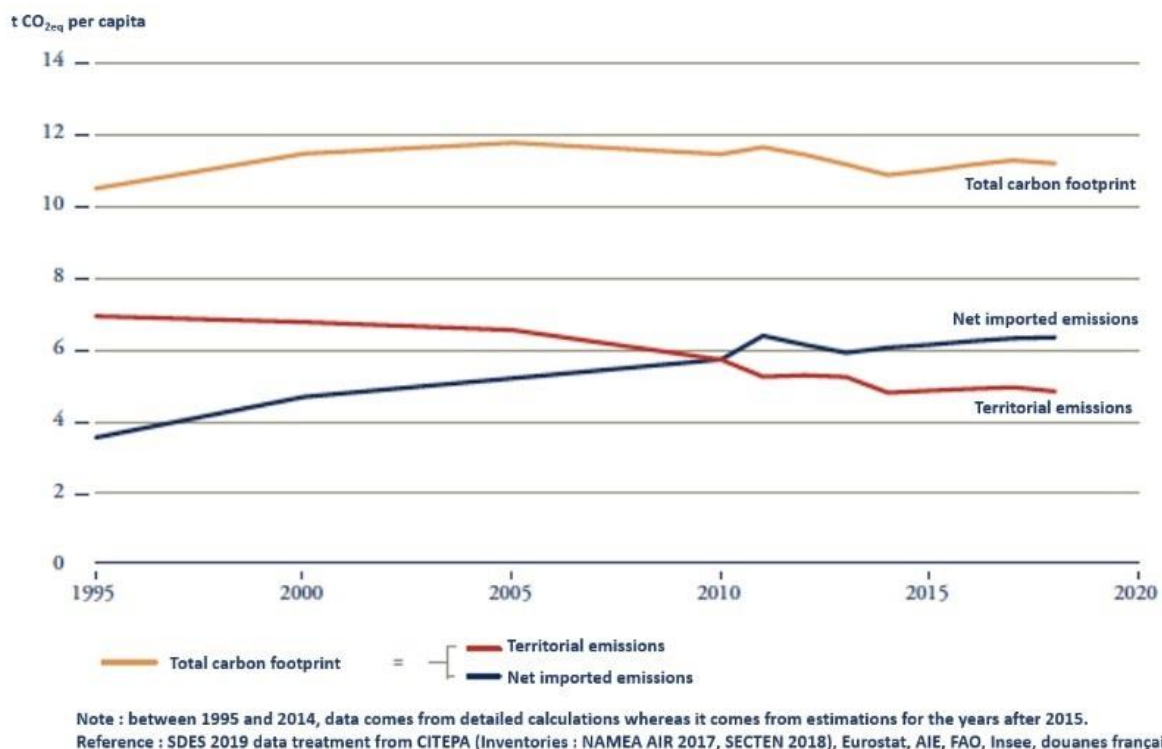
Firstly, Wallonia's NDCs main limitation comes from the fact that, other than the -55% goal in 2030 (Table 2), it has only set a long-term objective and no longer adopts short-term carbon budgets, as stated in the previous section. Without short-term objectives and monitoring, it is likely that reduction in CO<sub>2</sub> emissions will be delayed, which must absolutely be prevented to avoid emptying all the carbon budget in the few years to come. In addition, the either official (France) or unofficial (Wallonia) linear GHG reduction pathways could be discussed. Indeed, GHG mitigation has been known face barriers and

would likely to be better represented with an inverted 'S-curve' [28], with a reduced slope in the beginning (important mitigation projects take years to be implemented and to be efficient) and in the end (further CO<sub>2</sub> emission reduction will be harder close to the carbon neutrality goal as main mitigation projects will already be in place).

Unfortunately, those are not the only limitations of current France and Wallonia NDCs, as explained here below.

### 2.1.2.2 What about imported emissions and total carbon footprint?

What is common between the two studied public policies is that they only express targets based on territorial emissions. However, other GHG emissions accounting methods exist, such as the Consumption-Based System (CBS), which covers all emissions resulting from the consumption of local and imported goods and services [29]. Therefore, it is considered more comprehensive than production-based and territorial models [30], especially for European countries for which imported emissions represent the main part of the carbon footprint [31], as it is for example shown for France in Figure 4 [32].

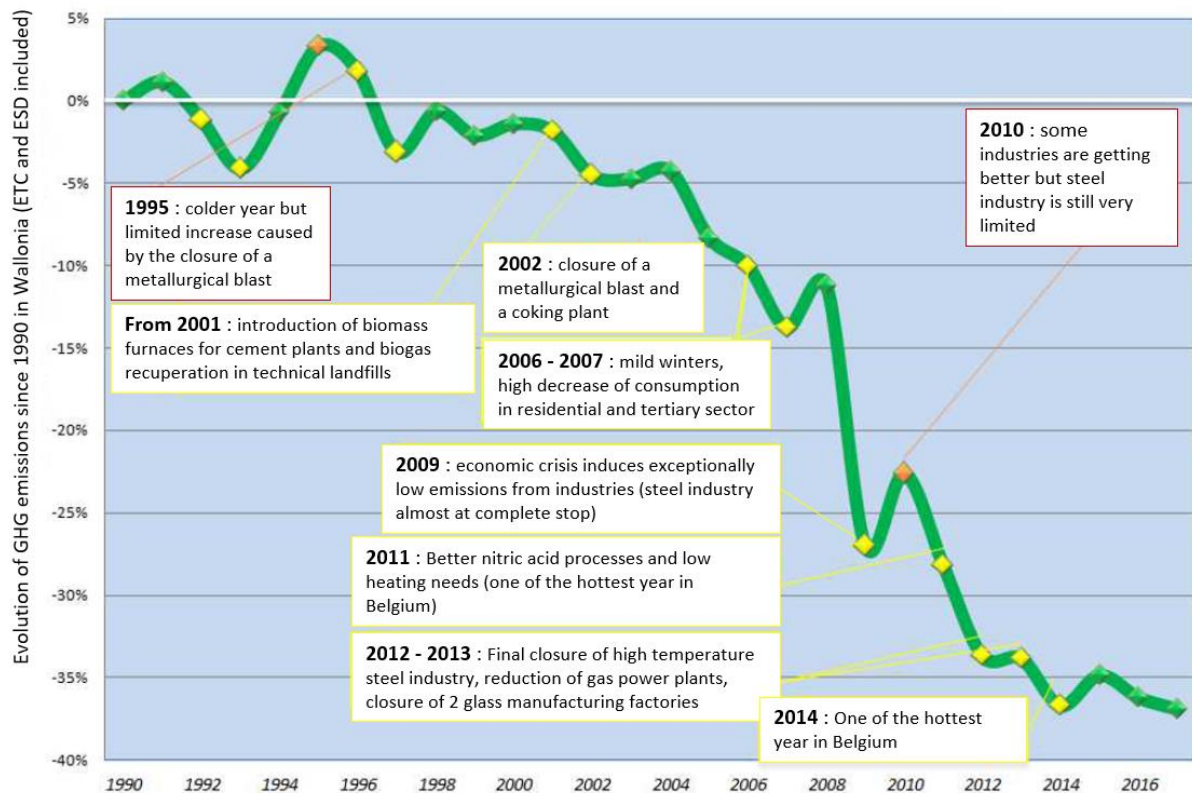


**Figure 4.** Historical evolution of France's individual carbon footprint between 1995 and 2018, which remains quite constant and around 11 tCO<sub>2eq</sub>/year per capita. Reproduced and traduced from reference [32].

This figure also demonstrates that even though territorial emissions are decreasing, imported emissions are greater and they are increasing up to a point that the resulting carbon footprint remains stable. This figure even finds its equivalent in France's official governmental documents: the French government establishes that their imported emissions were 1.8 times greater than territorial emissions in 2018 and it acknowledges that 'in the French situation, imports that substitute national production generally degrade the carbon footprint' [21]. This is because the imported goods might be produced in a region where the energy mix is more CO<sub>2</sub>-reliant, where climate strategies are less ambitious. Furthermore, transportation emissions increase with imported goods.



This problem is also implicitly shown in Wallonia's official governmental documents, as it is demonstrated in Figure 5. This curve is showing that historical territorial reductions of emissions are almost never resulting from measures taken in the context of GHG mitigation strategies. Indeed, they are mainly due to tremendous changes in the industry or in the economy that only occurred at the local scale. For example, the world steel industry has not been decreasing as in Wallonia and it has even been growing, like its resulting global CO<sub>2</sub> emissions [33].



**Figure 5.** Historical evolution of GHG emissions in Wallonia. Traduced reproduction of legally adopted Wallonia 2030 strategy for air, energy and climate, originally requested by Regulation (EU) 2018/1999 of the European Parliament and of the Council of 11th December 2018 [24].

Thus, one can expect that Wallonia (or Belgian) carbon footprint has also not been reduced during that time and that is what literature is showing for Belgium, at least up to 2007 [34] and even up to 2011 [35]. Those studies have evaluated Belgian's 2007 and 2011 carbon footprints respectively to 16 tCO<sub>2eq</sub>/year [34] and 15.4 tCO<sub>2eq</sub>/year [35] per capita, considering a Belgian population of about 11 million in 2011 [35]. This is consistent with other sources that evaluated Belgian's 2001 carbon footprint to 16.5 tCO<sub>2eq</sub>/year per capita [36]. Unfortunately, no Belgium carbon footprint figure has been found after 2011 but there is nothing that indicates that it has been significantly lowered if one looks at the French case stated here (Figure 4). Regrettably, to the knowledge of the authors, Wallonia's carbon footprint has only been established once in a detailed study to 15 tCO<sub>2eq</sub>/year per capita for the year 2011 [35].

It is worth mentioning that the imported emissions problem is already acknowledged by public authorities. On the one hand, France is recognizing in its legally adopted documents [21] the need to monitor carbon footprint as an indicator to evaluate the results of climate mitigation measures, the need to push people decrease their carbon footprint, the need to associate with economic partners that are also ambitious about emissions reduction. It even mentions, without any binding commitment, that the final 2100 objective should be between 1.6 and 2.8 tCO<sub>2</sub>/year per capita to limit global warming to maximum +2°C (CO<sub>2</sub>-

only, not the whole GHG footprint). However, it will be seen in the next section that it would be preferable, at least for France (and Wallonia), to consider a final carbon footprint target of 1 tCO<sub>2eq</sub>/year per capita (all GHG considered).

On the other hand, Wallonia is way behind because its legally adopted strategy only mentions the term 'carbon footprint' by stating the need to give a special attention to 'the carbon footprint of vehicles and their fuels' [24] or of 'numerical technologies' [23], for examples.

Since, in both cases, there is no unambiguous legally adopted carbon footprint target, no tangible method defined, those few recommendations regarding carbon footprint might be considered as simple 'wishful thinking'. Only considering territorial emissions and not the imported ones (thanks to tangible carbon footprint targets, for example) represents a wide opened door to all kind of populist oppositions to global warming mitigation measures. Firstly, this individualism behavior only tends to delocalized GHG emissions and not reduce them (as demonstrated in the last decades with Figure 4 for France and Figure 5 for Wallonia). Secondly, by having lower territorial emissions compared to the countries which goods are imported from, a sentiment of 'whataboutism' [37] could arise and even slow down further territorial emission reductions: 'Why should we decrease our territorial emissions even further because they only represent a small fraction of worldwide GHG emissions?'. For example, this sentiment could strengthen the already strong 'NIMBYsm' ('Not-In-My-Backyard') public resistance [38] and slow down renewable energy penetration.

### 2.1.2.3 How can people relate to territorial emissions targets only?

Furthermore, populations will hardly relate to territorial objectives, as they will rightly consider that those apply primarily to the public authorities and to private companies. Again, some kind of 'whataboutism' sentiment [37] is likely to occur. And it has already been stated that there is nothing that prevents those authorities and private companies from relocating their production even in less ambitious countries to cope with territorial GHG targets.

In fact, it is well-established that solving the climate crisis relies on changing human behavior [39] and, to achieve it without redhibitory resistance, applied policies and economics must meet people where they are, with 'audience-specific messaging and framing' [40]. Using carbon footprint targets, especially expressed per capita or per household, along with providing people with simple carbon footprint calculators for them to evaluate themselves and their actions, is one the first step for inducing those required behavior changes. Even though methods of calculating carbon footprint are far from a global consensus [41], they allow sensibilization of the public about the order of magnitude of its emissions (including the imported ones).

## 2.1.3 Comparison methodology and data source

As conducted in the following section, the methodology considered in this work computes the whole projected CO<sub>2</sub>-only emissions over the 2020-2050, based on current emission levels and on the mitigation pathways reported in the studied NDCs, so they can directly be compared to the relevant IPCC's 'equity' carbon budgets (expressed in CO<sub>2</sub>-only). Unfortunately, whereas current CO<sub>2</sub>-only emissions are easily obtained, studied NDCs consider all-GHG 2050 targets (expressed in CO<sub>2eq</sub>) and 2050 CO<sub>2</sub>-only targets are not officially reported. However, 2050 non-CO<sub>2</sub> emission levels, which cannot be fully mitigated and which occur in stabilized GHG emissions future, once CO<sub>2</sub> neutrality has managed to be reached [16], have been established by IPCC to 8 GtCO<sub>2eq</sub>/year [10]. This (worldwide) figure can also be allocated to countries following the 'equity' principle (according to population shares, that must therefore be considered). So, the 2050 CO<sub>2</sub>-only

emissions can be obtained by subtracting the allocated non-CO<sub>2</sub> 2050 projected emissions to the all-GHG target reported in the respective NDCs. The CO<sub>2</sub>-only emission pathways from 2020 to 2050 are assumed linear as it is the mitigation pathway assumed by both France [22] and Wallonia [26] officials.

## 2.1.4 Comparison results

### 2.1.4.1 Are the NDCs in line with IPCC's +2°C carbon budgets ?

With 2020 population data for Wallonia [42] and for the World [43], Wallonia currently accounts for 0.048% of the world's population. With IPCC's Sixth Assessment carbon budget of 1150 GtCO<sub>2</sub>, its carbon budget from January 1<sup>st</sup> 2020 can be established to 540 MtCO<sub>2</sub>.

However, one might consider that this 540 MtCO<sub>2</sub> budget is overestimated because it should not only take into account the demographics of a single year but of its evolution through time. Since the share of the European Union in the total population of the world will decline [44], the remaining budget of Wallonia can be considered lower. Indeed, for example, considering 2050 Wallonia [42] and world's [43] demographic projections, the share of Wallonia in the world's population will decrease down to 0.039%. That would account for a remaining 2020 budget of 449 MtCO<sub>2</sub>, 17% lower than the carbon budget based on population data of 2020.

It has been considered in this study that the actual remaining carbon budget shall simply be averaged between the carbon budgets calculated with 2020 and 2050 population data and projection, even though it would be more relevant to implement yearly updates based on updated population data and projections. The main reason is that having a constantly changing carbon budget would be confusing to the public that, as stated, needs to relate to the GHG mitigation objectives. Therefore, to compare Wallonia's commitment to the +2°C IPCC's Working Group I remaining budget of 1150 GtCO<sub>2</sub> [9] considered here, this study will consider a 2020 carbon budget of 494.5 MtCO<sub>2</sub>. With updated IPCC's Working Group III remaining budget of 890 GtCO<sub>2</sub> [10], Wallonia's 2020 carbon budget can be considered equal to 382.7 MtCO<sub>2</sub>. All those calculations have been reported in Table 3 (which also presents the case of France).

Table 3 also reports the projected CO<sub>2</sub> emissions from 2020 to the 2050 according to Wallonia and France's current NDCs to allow the comparison with those remaining IPCC 'equity' carbon budgets.

Based on territorial emissions only, it has been established from Table 3 that French current NDC indeed ensures IPCC's carbon budgets with a minimum margin of about 30% (about 2100 MtCO<sub>2</sub>) against the lower IPCC's AR6 carbon budget (the one of Working Group III, equal to 890 GtCO<sub>2</sub>).

On the other hand, Wallonia's projected CO<sub>2</sub> emissions are estimated just in between the carbon budgets of IPCC's Working Group I and IPCC's Working Group III (that have been established to 'likely' remain below the +2°C target). However, territorial absorption, expressed in CO<sub>2eq</sub> or in CO<sub>2</sub>-only as it is the main GHG naturally or technologically absorbed [45], has not been considered. Wallonia's natural CO<sub>2</sub> absorption capability is not well-known but has been estimated to 1 MtCO<sub>2</sub>/year [27], which could/should be increased by 2050 and fortunately decrease the accumulated CO<sub>2</sub> to potentially ensure both IPCC's carbon budget. It is worth mentioning that in a carbon neutral future, carbon sinks must not only compensate for CO<sub>2</sub>-only emissions, but also the unavoidable GHG emissions (see Table 3). Subsequently, the calculations of their beneficial aspects on CO<sub>2</sub> accumulation is not trivial. One method would consist in only considering the impact of non-CO<sub>2</sub> SLCPs for the 20 years prior to peak warming [46], which would mean that current natural CO<sub>2</sub> sinks could be fully considered at least in the 2020-2030 period.

Data and calculations	Wallonia	France
Projected GHG emissions in 2050 from NDCs (without LULUCF <sup>a</sup> )	2.8 MtCO <sub>2eq</sub> /year <sup>b</sup> [27]	80 MtCO <sub>2eq</sub> /year [22]
Population share in 2050	0.039% [42,43]	0.720% [43]
Share of the unavoidable non-CO <sub>2</sub> emission in 2050, i.e. 8 GtCO <sub>2eq</sub> /year [10]	3.12 MtCO <sub>2eq</sub> /year	57.6 MtCO <sub>2eq</sub> /year
Deduced resulting CO <sub>2</sub> -only emission in 2050 according to current NDCs	±0 MtCO <sub>2</sub> /year	22.4 MtCO <sub>2</sub> /year
2020 CO <sub>2</sub> -only emission data (without LULUCF <sup>a</sup> ) <sup>d</sup>	28.4 MtCO <sub>2</sub> /year [47]	289 MtCO <sub>2</sub> /year [48]
CO <sub>2</sub> -only emissions over the 2020-2050 period assuming linear decrease (without LULUCF <sup>a</sup> ) <sup>d</sup>	440.2 MtCO <sub>2</sub> <sup>c</sup>	4826.7 MtCO <sub>2</sub>
Population share in 2020	0.047% [42,43]	0.835% [43]
Average population share in the 2020-2050 period	0.043%	0.778%
Equity +2°C carbon budget from AR6 WGI total budget of 1150 GtCO <sub>2</sub> [9]	494.5 MtCO <sub>2</sub>	8947 MtCO <sub>2</sub>
Equity +2°C carbon budget from AR6 WGIII total budget of 890 GtCO <sub>2</sub> [10]	382.7 MtCO <sub>2</sub>	6924 MtCO <sub>2</sub>

<sup>a</sup> Land Use, Land Use Change and Forestry related net emissions, usually considered as a carbon sink in Europe [49]

<sup>b</sup> In March 2023, Wallonia has legally adopted his new Plan for Air, Climate and Energy named 'PACE 2030' to match the European Green Deal targets stated in Table 2 [23]. It confirms the 2050 target of Table 3 emitted in 2019, stating that 2050 neutrality will be achieved with technological and natural territorial absorption.

<sup>c</sup> This does not consider the 2030 -55% GHG emissions objective (Table 2). However, the linear pathway from 2020 to 2050 considered in Table 3 would lead in 2030 to a -66.6% reduction of GHG compared to 1990 levels, i.e. higher than the -55% legally adopted target. Therefore, the total CO<sub>2</sub>-only emissions projected for Wallonia over the 2020-2050 period in its latest NDC would even be higher than the one reported in Table 3. The problem is that the share of CO<sub>2</sub>-only and non-CO<sub>2</sub> emissions corresponding to the -55% GHG goal in 2030 is not known. However, it can be assumed that the projected non-CO<sub>2</sub> emissions would follow a linear pathway between their 2020 and 2050 levels, i.e. respectively 5.8 MtCO<sub>2eq</sub>/year [47] and 3.12 MtCO<sub>2eq</sub>/year (Table 3). This would lead to a 4.85 MtCO<sub>2eq</sub>/year non-CO<sub>2</sub> emissions level in 2030 to cope with the -55% GHG target, which would subsequently imply CO<sub>2</sub>-only emissions of 20.35 MtCO<sub>2eq</sub>/year. Again assuming linear pathways between 2020 and 2030 and then between 2030 and 2050, this would lead to 471.6 MtCO<sub>2</sub> over the 2020-2050, which is only slightly higher than 440.2 MtCO<sub>2</sub> figure reported in Table 3 and has no influence on any of the statements made in this work.

<sup>d</sup> This study considered the year 2020 for a direct comparison with IPCC's carbon budgets. However, the reported 2020 emissions levels might not be considered as sufficiently representative as it was the first year of the Covid-19 crisis which has decreased worldwide CO<sub>2</sub> emissions from about 7-8% compared to 2019 [50]. However, considering slightly higher emission levels for the year 2020 would not significantly affect any of the statements made in this work.

**Table 3.** Equity +2°C carbon budgets from January 1<sup>st</sup> 2020 against Wallonia and France current NDCs.

Wallonia, having no (or even negative) margin against IPCC's carbon budgets, must therefore closely monitor their GHG emissions and prevent any decrease in their territorial natural sinks. It would also be preferable to commit to more ambitious GHG reduction targets (especially short-term targets to avoid long-lived CO<sub>2</sub> accumulation) and to commit to natural sinks increase in parallel of investing in CCS, i.e. Carbon Capture and Storage [51] and/or DAC, i.e. Direct Air Capture [52] currently unmaturing technologies. In fact, it is worth mentioning that the potential carbon capture of some fuel cell technologies will be developed later on in *Chapter 6 - Residential fuel cells' carbon footprint mitigation potential*.

However, it must be stressed that this study considers that carbon technological sequestration and capture can only represent an uncertain opportunity that should be further developed before entering climate strategies, as CO<sub>2</sub> net emissions reduction must rely on tangible commitments and current proven technologies. Humanity cannot indeed afford to bet on uncertain technologies. Furthermore, if those technologies really happen to spread in the future, there is no guarantee that the economic and fiscal context will prevent the beneficial resulting CO<sub>2</sub> reduction not to be associated with an increase of consumption and a considerable 'rebound effect', as it has been demonstrated in the past with the introduction of energy efficient technologies [1].

#### *2.1.4.2 Are the +2°C carbon budgets still secured considering imported emissions?*

Figure 4 has shown that net imported emissions are even greater than territorial emissions in France. Another study only on CO<sub>2</sub> has shown that Belgium and France share of CO<sub>2</sub> emitted abroad in total CO<sub>2</sub> embodied in domestic final demand was equal to about 45% in 2015 [53]. This study also showed that the imported emission share has increased between 2005 and 2015 by about 2.5-3 percentage points, which partially correlates with Figure 4.

Therefore, for Wallonia, it is clear that IPCCs +2°C carbon budgets of Table 3 will be highly exceeded by considering the impact of imported emissions, as it has already no margin with the territorial emissions only. This means that it is vigorously advised that GHG emissions of imported goods shall be reduced even more than the territorial emissions (possibly both in quantity and in carbon intensity), in addition to the other GHG mitigation measures stated in the previous section.

For France, both equity carbon budget from IPCC's AR6 will be obviously exceeded if one considers the current fact that territorial GHG reduction is unfortunately compensated for in the carbon footprint by higher imported emissions (Figure 4). However, it will actually depend on the amount and of the carbon intensity of future imported goods. Indeed, lower equity carbon budget from IPCC's Working Group III will only slightly be exceeded considering a 45% constant share of CO<sub>2</sub> emitted abroad in total CO<sub>2</sub> embodied in domestic final demand (i.e. its current value [53]) whereas the upper equity carbon budget from IPCC's Working Group I will not be exceeded considering that same assumption. This basically means that the GHG reduction effort to be made on imported emissions must at least reach the same extent as the one projected on the territorial emissions.

Considering potential territorial absorption capacity will not change those statements except that for France, the projected absorption capacity of 80 MtCO<sub>2</sub>/year achieved in 2050 [22] will possibly secure the lower carbon budget of IPCC's Working Group III in addition of the one of Working Group I (Table 3), at least if the share of CO<sub>2</sub> emitted abroad in total CO<sub>2</sub> embodied in domestic final demand remains constant or even reduces. As expected, if Table 3 was considering the +1.5°C carbon budgets reported in Table 1, those would be significantly exceeded for both France and Wallonia's current NDCs, even with the territorial emissions only.

### **2.1.5 Discussion and perspectives about the section**

A small limitation of the method considered in this work to verify the relevance of NDCs against IPCC's carbon budgets is that it considers a linear evolution over time of the share of national population compared to the world's over time. It could consider the exact future population trend even though it will very unlikely change the statements made in this work.

At last, by lack of available data for 2021 and 2022, recent CO<sub>2</sub> emissions trends of Wallonia and France have not been verified, especially if they are following the assumed

reduction (linear) pathway projected in the respective NDCs. Indeed, if that was not the case and emissions were not reduced (enough) compared to 2020 levels, the equity carbon budgets should be updated and would be even lower than the one considered in this work. This is even emphasized as 2020 was the first year of the Covid-19 crisis which has decreased worldwide CO<sub>2</sub> emissions (only punctually) from about 7-8% compared to 2019 [50]. Projected and actual reduction pathway as well as remaining carbon budget shall thus be closely monitored and updated yearly.

### 2.1.6 Conclusions of the section

This work has identified some of the main limitations of current Nationally Determined Contributions (NDCs) for France and Wallonia climate strategies, which are likely to be applicable to similar NDCs of other countries:

- Wallonia, unlike France, has currently only a long-term mitigation commitment and has unfortunately abandoned establishing short-term carbon budgets, unlike France. Absence of short-term objectives constitutes a very likely risk of delaying CO<sub>2</sub> mitigation;
- Both current NDCs assume linear Greenhouse Gases (GHG) reduction trajectories whereas 'S-curve' pathways seem more realistic to account for the well-established inertia of major GHG mitigation projects;
- People, which must absolutely embark in the transition, can hardly relate to GHG objectives that are applicable to the scale of their public authority, as it is the case in both current NDCs.
- Current NDCs only treat territorial emissions, leaving the door open to GHG emissions delocalization, which has in fact been demonstrated for the last decades for France in Figure 4 (which shows that total carbon footprint does not decrease) and for Wallonia in Figure 5. GHG emissions are likely to be delocalized in countries less ambitious towards GHG mitigation or with more CO<sub>2</sub> reliant industries. Delocalization also often increases GHG emissions due to transportation. At last, only focusing on territorial emissions constitutes an individualistic behavior that leaves the main GHG mitigation effort on exporting countries. This could even lead to a 'whataboutism' [37] sentiment in importing countries and slow down the acceptance of GHG mitigation measures: 'Why should we decrease our territorial emissions even further because they only represent a small fraction of worldwide GHG emissions?'

On one hand, this work also demonstrated that if the emissions targets in France's NDCs are actually met, IPCC's +2°C AR6 2020 equity carbon budgets will likely be ensured (based on territorial emissions only). With imported emissions, it can be considered that there is no margin left in France's carbon budget when considering a 45% constant share of CO<sub>2</sub> emitted abroad in total CO<sub>2</sub> embodied in domestic final demand [53]. This basically means that the GHG reduction effort to be made on imported emissions must at least reach the same extent as the one projected on the territorial emissions.

On the other hand, for Wallonia, since it can be considered that there is no margin in the CO<sub>2</sub> budget even with territorial emissions only, the following recommendations have been made:

- Setting a more ambitious GHG reduction pathway (especially with short-term commitments to avoid CO<sub>2</sub> accumulation) to make room for imported emissions;
- Lowering the imported GHG emissions to an even quicker rate than territorial emissions (lowering the quantity of imported goods as well as their carbon intensity, for example by choosing economic partners that share ambitious GHG mitigation commitments);

- 
- Monitoring closely the projected CO<sub>2</sub> reduction pathway and updating it directly in case of delay in GHG mitigation. This constitutes a parallel opportunity to also monitor carbon footprint, as it has almost never been established in a detailed study for Wallonia;
  - Preserving and extending natural carbon sinks;
  - Potentially investing in Carbon Capture and Storage (CCS) and/or Direct Air Capture (DAC) technologies (only in order to possibly increase margin in the CO<sub>2</sub> budgets as those technologies are unmaturing). In fact, it is worth mentioning again that the potential carbon capture of some fuel cell technologies will be developed later on in *Chapter 6 - Residential fuel cells' carbon footprint mitigation potential*.

At last, although both France and Wallonia have confirmed the +1.5°C maximum global warming target [5], this work demonstrated that even the projected territorial emissions only will exceed IPCC +1.5°C AR6 2020 equity carbon budgets (according to their current NDCs).

The content of the second section of this chapter (*Section 2.2 - Establishing individual carbon footprint pathways based on IPCC's carbon budgets*) has been accepted almost as-is for publication in the *Renewable and Sustainable Energy Reviews* academic journal under the name '*Developing individual carbon footprint reduction pathways from carbon budgets: examples with Wallonia and France*' [54]. The previous section highlighted significant limitations of most NDCs, including the fact that climate strategies often establish long-term targets for emission rates while disregarding cumulative CO<sub>2</sub> emissions. These strategies often concentrate on territorial emissions, allowing countries to shift their economy to less climate-conscious nations. Furthermore, these strategies frequently assume unrealistic linear patterns that do not consider the inertia of major projects to be implemented on large scales and the exponential difficulty of reducing GHG emissions as they approach zero. Finally, individual citizens often find it challenging to relate to or engage with objectives set at the community or local level. The goal of this section is to address these issues by translating collective carbon budgets, such as the 'equity' carbon budgets that align with IPCC's +1.5°C or +2°C recommendations (as outlined in the previous section), into individual carbon footprint pathways based on inverted 'S-curve' patterns (assumed much more realistic). These personalized pathways, in addition to being directly linked to IPCC's carbon budgets and addressing the stated issues of common climate strategies, offer the possibility of being easily integrated into carbon footprint calculators [55], which will be performed in *Chapter 6 - Residential fuel cells' carbon footprint mitigation potential*. These calculators are often used by a broad public to assist in mitigating their own impact on global warming [55].

## 2.2 Establishing individual carbon footprint pathways based on IPCC's carbon budgets

In its Sixth Assessment Report (AR6), IPCC has established to 890 GtCO<sub>2</sub> the remaining carbon budget that humanity can emit from January 1<sup>st</sup> 2020 in order to limit global warming to +2°C compared to pre-industrial levels, with a likelihood of 67% [10] (see previous section).

Indeed, as it is observable in Figure 6(a) from IPCC, it is common to express as a percentage the likelihood of not exceeding a certain temperature of interest thanks to its corresponding cumulative carbon emissions limit, i.e. thanks to its matching carbon budget, expressed in CO<sub>2</sub>-only emissions [56–58].

Non-CO<sub>2</sub> contribution is usually related to short-lived climate pollutants (SLCPs), such as methane. As shown in Figure 7, it is well established that, unlike CO<sub>2</sub>, the annual rather than the cumulative emissions have the strongest effect on peak warming [13]. Therefore, as seen in the previous section, in IPCC's remaining carbon budget, the radiative forcing of SLCPs is considered through a 'security margin' [8] [3], estimating future non-CO<sub>2</sub> GHG emission at the moment at which global CO<sub>2</sub> emissions reach net zero [7] (necessary at some point with the carbon budget paradigm [59]). This has been performed by computing different non-CO<sub>2</sub> mitigation scenarios always consistent with a carbon neutral future implied by IPCC's carbon budgets [8]. This means that IPCC's CO<sub>2</sub> budgets infer that other non-CO<sub>2</sub> GHG must also be mitigated.

One acknowledged difficulty lies in the carbon budget allocation between countries [11]. For example, two well-known approaches are the 'grandfathering' principle (measures of 'inertia') and the 'equity' principle [60]. The 'grandfathering' principle considers that the carbon budget should be allocated to countries proportionally to their current emission levels whereas the 'equity' principle considers that it should be allocated proportionally to their population levels, i.e. that each human being has the same 'right to pollute'. The 'grandfathering' principle is much more criticized, mainly because it favours 'the

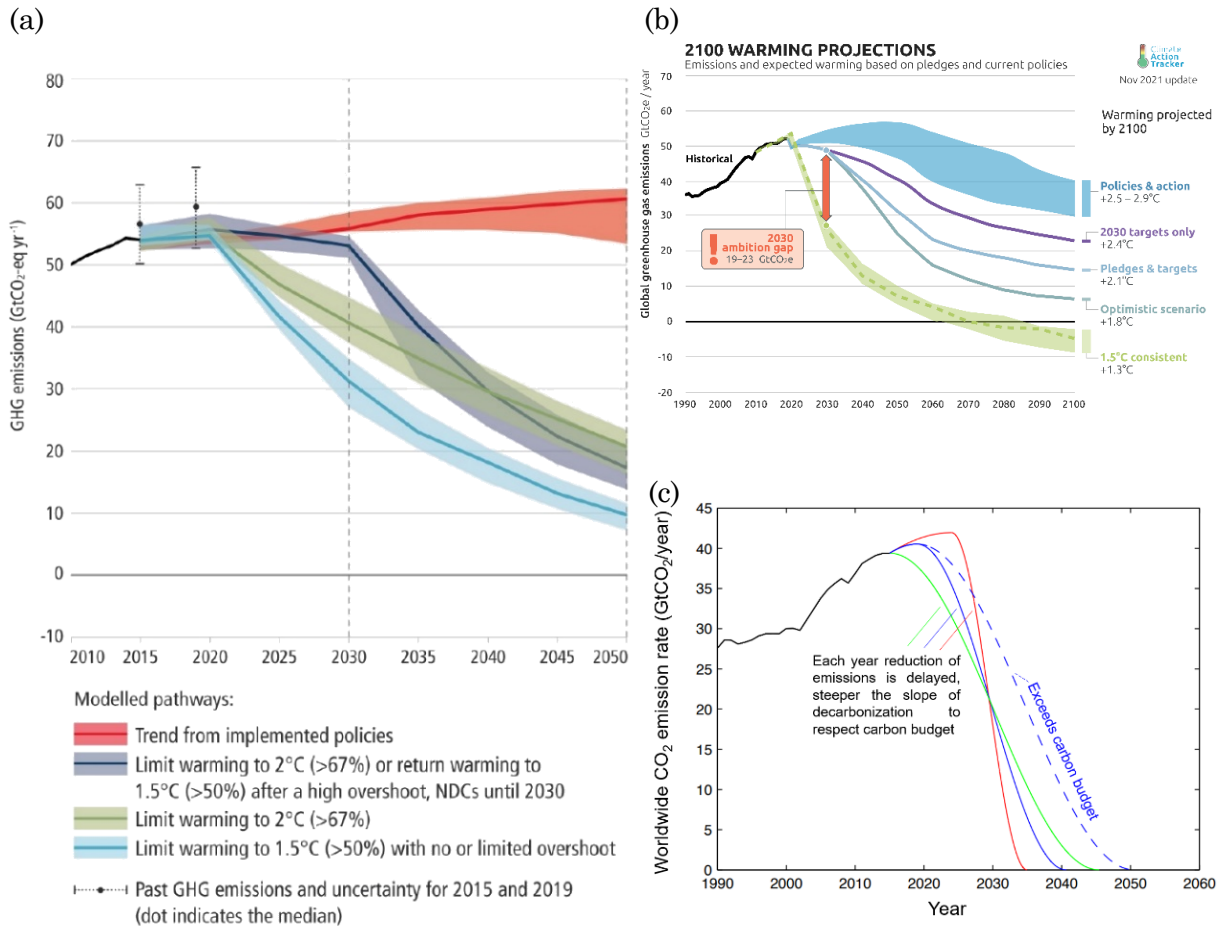


perpetuation of an unjust allocation of rights on the basis of the previous unjust allocation of the same rights' [61], meaning that is already unjust enough that historical emissions per capita have not been even between countries and they should not therefore be considered as references for further (unjust) carbon budget allocation. Thus, if countries are considering carbon budgets in their climate strategies as they should [62], they usually consider the 'equity' principle, as it is for example the case for France and Wallonia [3].

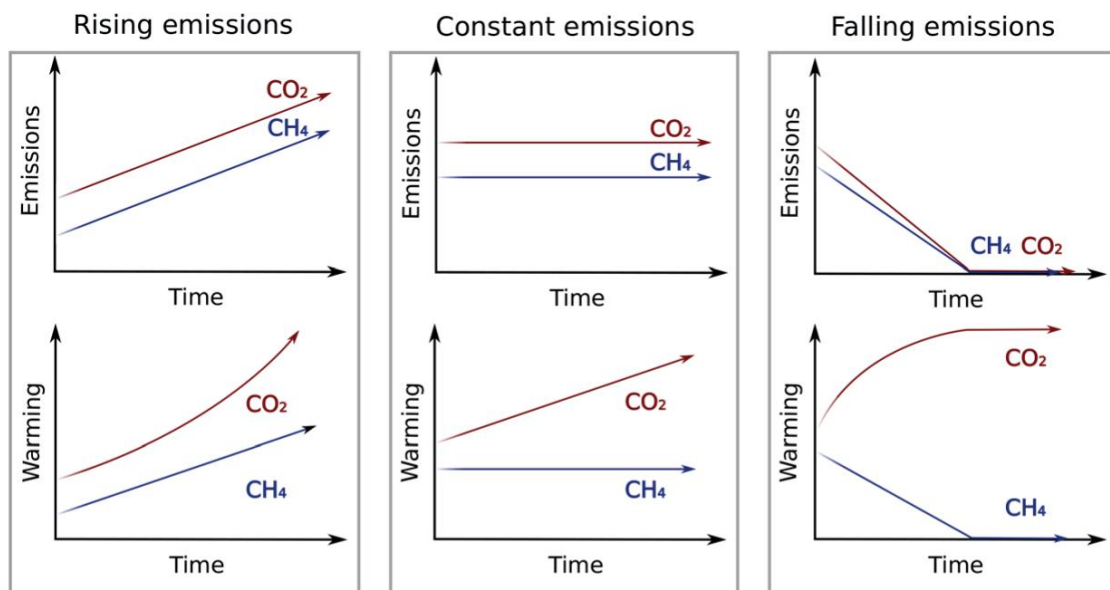
Unfortunately, those latter have only been committing on territorial emissions in their climate mitigation policies whereas it has been established in the previous section that the AR6 'equity' +2°C carbon budget will likely to be exceeded if emissions embodied in trade are considered and are not subjected to vigorous mitigation effort similar to territorial emissions [3].

The previous section has also identified other problems of most current NDCs, i.e. Nationally Determined Contributions [63]. They have been summed up here below :

- Long-term only emission rate commitment such as the carbon neutral 2050 promise does not allow for limiting the cumulative CO<sub>2</sub> emission below the carbon budget [64] and will unlikely be reached without short-term carbon budget targets [65], mainly because it would require even more stringent (and surely less realistic) policies in the long-term [66].
- NDCs usually assume linear emission mitigation pathways towards their long-term targets [3]. However, GHG mitigation has been known to face barriers and would likely to be better represented with an inverted 'S-curve' [28], with a reduced slope in the beginning (important mitigation projects take years to be implemented and to be efficient) and in the end (further CO<sub>2</sub> emission reduction will be harder close to the carbon neutrality goal as the main mitigation projects will already be in place). In fact, those (inverted) 'S-curves' or 'S-shaped' patterns constitute the commonly represented GHG emissions pathways in literature, at least for the realistic scenarios that ensure securing the +2°C carbon budget, as observable in Figure 6. Similar inverted 'S-shaped' emissions pathway curves have also been found in other studies [58,66–69]. It is worth mentioning that, at this point, only the +2°C carbon budget compatible scenarios are considered realistic because IPCC's AR6 has lately reported that 'global Greenhouse Gases (GHG) emissions in 2030 associated with the implementation of NDCs announced prior to COP26 would make it likely that such warming level will be exceeded during the 21<sup>st</sup> century' [10]. This can also be deduced from Figure 6, which by the way shows that the +2°C compatible scenarios are the ones that particularly exhibit proper inverted 'S-curve' patterns.
- Populations will hardly relate to territorial objectives, as they will rightly consider that those apply primarily to the public authorities and to private companies. Indeed, some kind of 'whataboutism' sentiment [37] is likely to occur: 'Why should I mitigate my emissions since my carbon footprint is only a small part of the national emissions?'. In fact, it is well-established that solving the climate crisis relies on changing human behavior [39] and, to achieve it without redhibitory resistance, applied policies and economics must meet people where they are, with 'audience-specific messaging and framing' [40].



**Figure 6.** Global GHG emissions scenarios reproduced from literature that follow inverted ‘S-curve’ theoretical pathways: (a) From IPCC's AR6 [10], (b) From Carbon Action Tracker [70] (c) From Rare organization [71].



**Figure 7.** Schematic illustration of how global mean temperatures respond to different emissions trends in carbon dioxide (CO<sub>2</sub>) and methane (CH<sub>4</sub>). Reproduced from reference [72].

Through examples for Wallonia and France, this section tries to offer a method of establishing IPCC's +2°C 'equity' carbon budget compatible GHG emission pathways, that aims to solve those usual limitations of current NDCs.

Thus, the conceived method remains simple enough for the population to relate with and is based on inverted 'S-curve' patterns. In addition, those proposed pathways have been designed to be adapted to different scales, even down to the simple household or down to the individual, in order for everyone to grasp their role in addressing the tremendous emission mitigation challenge that humanity is facing. This has notably been allowed by linking the global IPCC's +2°C 'equity' carbon budget to individual targets, that can be implemented as reference to carbon footprint calculators. Therefore, by (regularly) monitoring one's own emissions and the outcomes of one's personal mitigation efforts through such calculators, that would hopefully allow for each individual to set its own GHG reduction targets on both a short-term and a long-term basis.

## 2.2.1 Material and methods

### 2.2.1.1 General mathematical function for inverted 'S-curve' GHG emissions mitigation pathway

'S-curve' are used in this work because they are particularly relevant in case of GHG emissions mitigation. Indeed, they have been known to be used 'for ecological modelling' [73]. That same article reports that 'S-curve' are also used for 'projecting the performance of technologies', 'market penetration analyses' or 'diffusion mechanisms of technological and social inventions' which are all also relevant with GHG emissions mitigation because of its intrinsic link to renewable technologies penetration (both technologically and socially). For information, a 'S-curve' can also be known as a 'Verhulst-Pearl equation', a 'Pearl curve', a 'Growth curve', a 'Gompertz curve', a 'S-shaped pattern', a 'Saturation curve', a 'Foster's curve', a 'Bass model', or as considered in this work a 'logistic curve' or a 'sigmoid(al) function' [73].

Equation (1) is generally used to define a sigmoid (or a logistic) function between the [0;1] ordinate range [74] :

$$P(i) = \frac{1}{1 + e^{-(\alpha+\beta i)}} \quad (1)$$

$i$  and  $P(i)$  are respectively the abscissa and the ordinate of the sigmoid function, i.e. the horizontal and vertical coordinates, while  $\beta$  and  $\alpha$  are parameters that respectively control the slope, i.e. the rate [75] and the position on the horizontal axis of the 'S-shaped' pattern, i.e. the abscissa at which the curve is no longer on a quite constant path (and start to significantly increase or decrease).

Decreasing (inverted) 'S-shaped' function would require the 'inversion' of Equation (1). In addition, in carbon footprint yearly rate mitigation pathways applications, the range of the function is no longer [0;1] but it is starting at the current (initial) yearly carbon footprint (or GHG emissions) level, i.e.  $CF_i$ , and it is ending at the long-term (final) yearly carbon footprint (or GHG emissions) objective, i.e.  $CF_f$ . Those manipulations allows for obtaining Equation (2), for which the  $\alpha$  and  $\beta$  parameters have simply been renamed  $a$  and  $b$ . Also, the horizontal coordinate has been defined as  $y$  to account for yearly discretization of the carbon footprints, the yearly carbon footprint being expressed as  $CF(y)$ .

$$CF(y) = CF_i - \frac{CF_i - CF_f}{1 + e^{-(a+by)}} \quad (2)$$

One last manipulation of the formula relevant to make it more relevant for this application allows for highlighting the year  $c$  ( $= -ab^{-1}$ ) for which the ordinate achieves the 'center' of its scale. In other words,  $c$  is the moment at which the ordinate has reached 50% of its range between its initial and final ordinate value [76], i.e. the year at which the 'S-curve' reaches its maximum slope. This has been performed in Equation (3) :

$$CF(y) = CF_i - \frac{CF_i - CF_f}{1 + e^{-b(y-c)}} \quad (3)$$

### 2.2.1.2 From IPCC's 'equity' carbon budgets to individual carbon footprint

It is worth mentioning that carbon budgets usually consider territorial sinks through Land Use, Land Use Change and Forestry (LULUCF [49]), related net CO<sub>2</sub> emissions [77]. For simplicity reasons, this work however will consider separately the CO<sub>2</sub> emissions without LULUCF (positive) and the ones of territorial sinks (negative).

Equation (3) has directly been expressed in terms of carbon footprint (not only in terms of CO<sub>2</sub>-only emissions as used in IPCC's carbon budget).

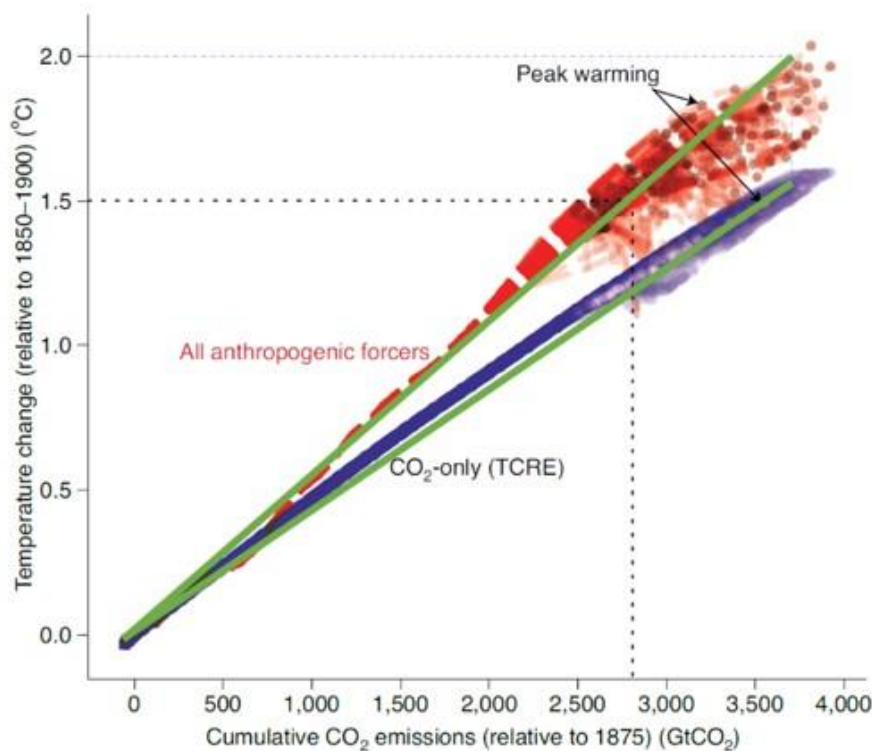
Unfortunately, linking carbon budget (expressed in CO<sub>2</sub>-only) to all GHG emissions and therefore to carbon footprint is not trivial. Indeed, the impact of non-CO<sub>2</sub> species, which, as stated, is considered at the time of net-zero CO<sub>2</sub> emissions through 'an absolute security margin' [3], represent the largest source of uncertainty in the remaining carbon budget [57]. This can be explained thanks to the following main reasons :

- The time-dependency of the warming impact of non-CO<sub>2</sub> GHG species (as illustrated in Figure 7), such as short-lived climate pollutants (SLCPs), explains why CO<sub>2</sub>-only carbon budget are preferentially used [3]. In addition, non-CO<sub>2</sub> GHG species also involve N<sub>2</sub>O and some long-lived (H)CFCs [78] which still have high long-term global warming potential (such as CO<sub>2</sub>). Establishing a non-CO<sub>2</sub> GHG budget by assimilating their short-term and long-term impacts on global warming to be combined with IPCC's CO<sub>2</sub>-only carbon budget is thus tricky. This is especially the case since future emission pathways of every non-CO<sub>2</sub> GHG species are intrinsically also associated to great uncertainty levels.
- Some SLCPs, mainly represented by anthropogenic aerosols co-emitted in fossil fuels combustions, have a negative radiative forcing [79]. That cooling effect tends to significantly mask (balance) the current global warming impact of non-CO<sub>2</sub> pollutants [80]. Indeed, non-CO<sub>2</sub> pollutants have been reported to presently account for about 50% of current positive radiative forcing and, 'thanks' to negative forcing aerosols, they only account for about 25% of current net forcing [81]. It is worth mentioning that one example of negative forcing aerosol is SO<sub>2</sub>, as it will be seen in the following section. Those negative forcing aerosols will decrease with necessary fossil fuel emissions reduction (and effective air quality policies), therefore unmasking some radiative forcing of remaining non-CO<sub>2</sub> pollutants [82]. This represents an additional difficulty in linking all-GHG emissions to CO<sub>2</sub>-only carbon budgets.

Nevertheless, as (positive radiative forcing) non-CO<sub>2</sub> GHG emissions must be mitigated as well as CO<sub>2</sub> to respect global warming targets [83], it is still common to consider that the share of the radiative forcing (i.e. the net warming) of non-CO<sub>2</sub> species is linearly proportional in time to the radiative forcing of CO<sub>2</sub>-only [84–88]. All those references report the non-CO<sub>2</sub> net warming impact to be between 22 and 30% of the one of CO<sub>2</sub>-only. This is also observable in Figure 8 [77], which has been established computing non-CO<sub>2</sub> GHG mitigation scenario compatible with a +2°C maximum temperature increase. In Figure 8, the slope of the all-anthropogenic forcers assimilated straight line is 26% higher than the one of CO<sub>2</sub>-only, consistent with the other literature references.

It must be stressed again that this proportionality between CO<sub>2</sub>-only and non-CO<sub>2</sub> radiative forcing through time is however valid as long as non-CO<sub>2</sub> pollutant are mitigated in +2°C compatible scenarios. And this shall be ensured thanks to specific structural policies (implemented by public authorities). For example, main N<sub>2</sub>O emissions come from agricultural sources [89] and it is unrealistic for such non-CO<sub>2</sub> GHG mitigation effort to rely on individual consumption choices. The only mitigation effort that can realistically rely on individuals is the commonly called 'sobriety', the necessary reduction of their carbon footprint through an overall reduction of their consumption levels and/or energy use. Individuals should not have to conduct intensive researches to consider the non-CO<sub>2</sub> GHG impact of the upstream processes involved in their specific consumption choices.

In addition, based on Global Warming Potential (GWP) over 100 years, it has been reported that non-CO<sub>2</sub> pollutant have accounted for 25.6% of the total GHG emissions in 2020 [90], which is a quite similar figure as the one established for the proportionality between CO<sub>2</sub> and non-CO<sub>2</sub> forcing (Figure 8). This work could have thus established an all-GHG budget (expressed based on GWP over 100 years) by increasing IPCC's 'equity' +2°C carbon budget by that common figure of about 26%. In that case, the study would have subtracted to this all-GHG budget the yearly (hopefully decreasing) carbon footprint, also based on GWPs over 100 years as it is generally the case [34]. Of course, doing so, one would have made sure that this all-GHG budget would never be overcome.



**Figure 8.** Highlighted proportionality of the net warming impact of all anthropogenic forceners and the one CO<sub>2</sub>-only emissions. Dots represent multiple scenarios: they mark the peak warming and the lines end at the point of net-zero CO<sub>2</sub> emissions in each scenario. The larger spread of all anthropogenic forceners red dots relative to purple CO<sub>2</sub>-only dots is due to non-CO<sub>2</sub> emission scenarios that largely differ, which were all necessary to compute because of the great level of uncertainty in future non-CO<sub>2</sub> GHG emission pathways. TCRE means Transient Climate Response (to cumulative emissions). It is widely used for climate change characterization and basically corresponds to the temperature change compared to preindustrial levels. Reproduced and adapted from reference [77].

However, in an expected net-zero CO<sub>2</sub> emissions future, the share of the non-CO<sub>2</sub> pollutant in the yearly total GHG emissions would no longer account for about 25% as it is today.

Since other GHG have less mitigation potential than for CO<sub>2</sub> [16], it would indeed trivially increase to 100%, even though their share in the total radiative forcing is still expected to remain to about 25% (because of cumulative emissions of long-lived CO<sub>2</sub>). Therefore, all-GHG budgets have no longer been considered in this study.

It is nevertheless worth mentioning that conducting such a method with an all-GHG budget is still possible, but it would require both the carbon footprint calculators and the all-GHG budget to be expressed based on approaches that would at least consider the variation of the radiative forcing of short-lived climate pollutants (SLCPs) over time (illustrated with Figure 7). To that end, literature indeed reports methods that evaluate the future radiative forcing of GHG based on their year of emission, usually through GWP alternatives metrics, denoted 'GWP\*' [46,91–94] or CO<sub>2-fe</sub>, i.e. CO<sub>2</sub>-forcing-equivalent [85]. Unfortunately, even in their simplest forms, those methods would complexify greatly the understanding of carbon footprint calculators for the public and could therefore slow down the much-needed individual carbon footprint mitigation (which simplification constitutes one of the aims of this work aims).

Therefore, it has been decided to keep IPCC's CO<sub>2</sub>-only carbon budget and establish in parallel CO<sub>2</sub>-only footprint from the all-GHG carbon footprint. For example, the 2020 CO<sub>2</sub>-only carbon footprint level can simply be established by subtracting the share of worldwide non-CO<sub>2</sub> emissions in 2020 all-GHG emissions, i.e. 25.6% [90].

This work assumes a completely decarbonized economy by 2050, as it is the year targeted by the European Green Deal [20]. Therefore, the final CO<sub>2</sub>-only carbon footprint is equal to 0 in 2050. It is worth mentioning that the European Green Deal unfortunately only commits to a 2050 territorial carbon neutral future but, in this work, it will be assumed that European Union will (hopefully) adopt trading policies that compel the imported emissions to also reach carbon neutrality by 2050. This could indeed be allowed if European Countries choose to only import from external countries that have also committed to a 2050 territorial carbon neutral future.

It is also worth mentioning that, at net-zero CO<sub>2</sub> emissions (assumed in 2050), IPCC has reported that all GHG could not be completely mitigated as well as CO<sub>2</sub>. A 8 GtCO<sub>2eq</sub> yearly footprint would indeed remain for humanity [10] (as seen in the previous section). Considering again the 'equity' principle and a world 2050 population of 7.735 billion people [95], this leads to an individual unmitigated 2050 footprint of about 1 tCO<sub>2eq</sub>/year per capita (represented only with non-CO<sub>2</sub> pollutants). The European Green Deal [20] carbon neutral future thus trivially implies that GHG absorption shall also reach this 1 tCO<sub>2eq</sub>/year per capita. Territorial absorption will in fact permanently reduce the accumulated CO<sub>2</sub> in the atmosphere, i.e. reduce its 'long-lived' radiative forcing rather than the 'short-lived' radiative forcing of unmitigated non-CO<sub>2</sub> GHG rate of emissions. In the upcoming years, carbon absorption will slightly slow down the CO<sub>2</sub>-budget decrease through time and, towards the net-zero CO<sub>2</sub> emissions future, this will even (slightly) continuously increase the carbon budget.

The 2020 carbon footprint and 2050 carbon footprint target that have just been discussed account for the  $CF_i$  and  $CF_f$  parameters of Equation (3).  $b$  and  $c$  parameters will be manually tuned later on, as explained in the following paragraphs.

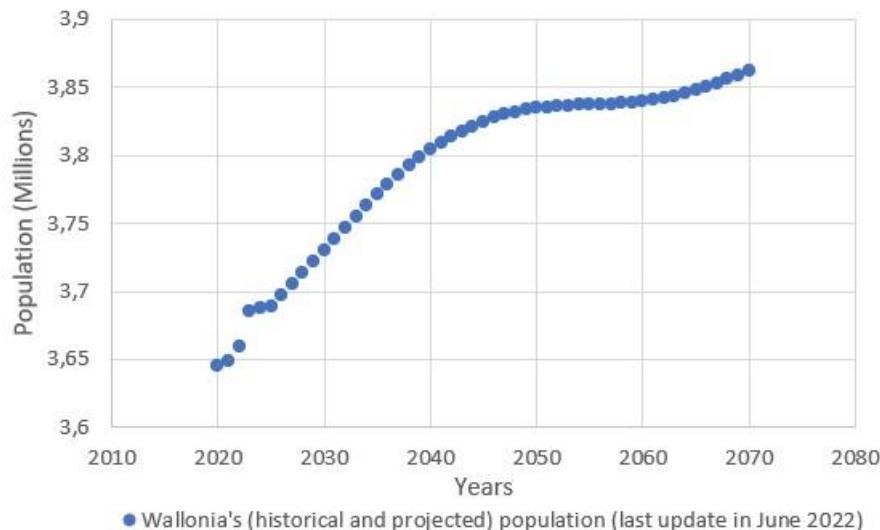
The sigmoidal decrease of all-GHG carbon footprint (compatible with carbon footprint calculator) does not directly allow for computing the CO<sub>2</sub>-only emission pathway that will be used to be subtracted to IPCC's CO<sub>2</sub>-only carbon budgets. Therefore, this work also assumes a sigmoidal mitigation of the non-CO<sub>2</sub> GHG individual carbon footprint between its initial and final values (that have already been established). Thus, Equation (3) is reused (with adapted values for the  $CF_i$  and  $CF_f$  parameters), but the  $b$  and  $c$  parameters

are assumed equal as the ones used for the sigmoidal decrease of the all-GHG carbon footprint. Indeed, this assumption seems quite relevant as reduction in fossil fuel combustion required for CO<sub>2</sub> emissions mitigation will simultaneously also reduced committed non-CO<sub>2</sub> GHG [14].

### 2.2.1.3 Slope, year of maximum mitigation rate (*b* and *c* parameters) and territorial absorption pathway

At last, the *b* and *c* parameter of Equation (3) are manually tuned in order for both the resulting all-GHG carbon footprint mitigation and non-CO<sub>2</sub> footprint pathways to be as realistic as possible (a decrease as smooth as possible is preferable). More importantly, the resulting individual carbon footprint mitigation pathway must ensure that the remaining all-GHG +2°C 'equity' carbon budget is not exceeded either on the whole 2020-2050 timeframe or, at least, that it has come back to positive values by 2050.

This is performed through the multiplication of the CO<sub>2</sub>-only yearly individual carbon footprint to the yearly population level (shown for Wallonia in Figure 9, for instance). Indeed, this allows for the yearly CO<sub>2</sub> emission (total CO<sub>2</sub> footprint of the population) to be obtained and subtracted yearly to its remaining CO<sub>2</sub> carbon budget (of the previous) year.



**Figure 9.** Wallonia's historical and projected population from the database of Bureau du Plan [96], considering immigrants due to the Ukraine-Russia conflict started in 2022 [97].

Yearly territorial absorption is considered with a linear pathway from the initial 2020 value to the 2050 final value. This latter has been stated to be equal to 1 tCO<sub>2eq</sub>/year per capita implied by GHG-neutral European Green Deal commitment [20], to match the unmitigated non-CO<sub>2</sub> GHG footprint in a net-zero CO<sub>2</sub> emissions future [10], as discussed in the previous section.

As stated, territorial absorption is simply added to the yearly CO<sub>2</sub> remaining budget. Territorial absorption indeed consists in Carbon Dioxide Removal (CDR) techniques [98], which can be nature-based [99] or technological [100]. CO<sub>2</sub> is indeed trivially the main GHG concerned by both natural, through photosynthesis, and technological CDR techniques, such as Direct Air Capture, i.e. DAC [52], or Carbon Capture and Storage, i.e. CCS [51].

However, those latter negative emissions technologies raise questions (mainly because of their unmaturation) and their scaling-up capabilities constitute an 'unjust gamble against the future' [101]. Facing the tremendous challenge of global warming, it has been indeed

advised for climate policies to rely on negative emissions only if they are mature enough [3], with lowered risks. This is why this work will later on verify that territorial absorption pathways are not unrealistically far from to the current level allowed only thanks to natural sinks. However, it will in fact later on be seen that the considered 1 tCO<sub>2eq</sub>/year per capita absorption level target is very challenging on land-use efforts alone and it is therefore advised to also develop negative emissions technologies (such as some particular types of fuel cells discussed in *Chapter 6 - Residential fuel cells' carbon footprint mitigation potential*).

#### 2.2.1.4 Wallonia's missing data

To sum up, the methodology section, applicable to any region or nation, has established that :

- Initial CO<sub>2</sub> budget to consider is IPCC's 'equity' +2°C carbon budget (established in the previous section).
- Remaining 'equity' CO<sub>2</sub> budget should at least be positive in 2050 and it is preferable that it stays positive over the whole 2020-2050 period.
- All-GHG carbon footprint is obtained by multiplying population levels (shown in Figure 9 for Wallonia) to average individual carbon footprint.
- The initial 2020 non-CO<sub>2</sub> footprint is established considering the all-GHG footprint (yet to be discussed for Wallonia) and the 25.6% share of non-GHG emission in the all-GHG footprint [90]. The remaining 74.4% of the GHG emissions account for the CO<sub>2</sub>-only initial 2020 footprint.
- The rest of the CO<sub>2</sub>-only footprint pathway is established similarly from the all-GHG footprint pathway and the non-CO<sub>2</sub> footprint pathway, which are assumed to follow inverted 'S-curve' patterns defined by Equation (3) between their initial 2020 and final 2050 values. Having defined the initial 2020 and 2050 values, b and c parameters (considered equal for both the all-GHG and the non-CO<sub>2</sub> sigmoidal pathways) are manually tuned to offer realistic patterns compatible with the +2°C 'equity' carbon budget.
- CO<sub>2</sub>-only final 2050 footprint is assumed to 0 (net-zero CO<sub>2</sub> emission future).
- As previously stated, this implies that the non-CO<sub>2</sub> final 2050 footprint is assumed to be equal to 1 tCO<sub>2eq</sub>/year per capita because of the unmitigated non-CO<sub>2</sub> GHG footprint in a net-zero CO<sub>2</sub> emissions future [10].
- Yearly territorial absorption is simply added to the yearly remaining carbon budget. A carbon absorption linear pathway is considered from the initial 2020 value (yet to be discussed for Wallonia) to the 2050 final value, which has also been stated to be equal to 1 tCO<sub>2eq</sub>/year per capita (implied by the GHG-neutral European Green Deal commitment [20] to match the unmitigated non-CO<sub>2</sub> GHG footprint in a net-zero CO<sub>2</sub> emissions future [10]).

Therefore, some data specific to Wallonia is still need to be discussed, as aimed in the following sub-sections.

#### • **Territorial absorption (expressed equivalently in CO<sub>2eq</sub> or CO<sub>2</sub>)**

Current level of Wallonia's territorial carbon sinks has been reported to about 1 MtCO<sub>2</sub>/year [3], figure considered in this work or, with another source, to about 1,8 MtCO<sub>2</sub>/year [102]. Given Wallonia's future population (Figure 9), the 2050 absorption level shall reach about 4 MtCO<sub>2eq</sub>/year for GHG neutrality. Therefore, Wallonia's carbon yearly uptake need to be increased by about 3 MtCO<sub>2eq</sub>/year (+300%). Although very challenging, especially considering only natural sinks, this does not seem unrealistic considering the following reasons :



- It has been reported that agroecological methods that rebuild organic components in soil such as permaculture can increase carbon uptake to 8.23 tCO<sub>2eq</sub>/ha per year [103], whereas the average European harvested crop absorbs 1.96 tC/ha per year [104], which accounts for 7.2 tCO<sub>2eq</sub>/ha per year [105]. Zero-tillage agriculture or conversion to permanent crops and perennial grasses have also respectively been reported to increase carbon sequestration by up to 1.47 tCO<sub>2eq</sub>/ha per year and 2.2 tCO<sub>2eq</sub>/ha [106]. Another study confirms those figures as it has reported that improved grazing management, introduction of legumes and improved grass species, irrigation, and the conversion of croplands into pasture lands can increase soil carbon sequestration by more than 1 tC/ha per year [107], i.e. 3.67 tCO<sub>2eq</sub>/ha per year [105]. Given the 762120ha devoted to agriculture in Wallonia [108], and an average increase of carbon sequestration of 1 tCO<sub>2eq</sub>/ha per year through alternative agricultural techniques, territorial absorption of agriculture lands could be increased by about 0.76 MtCO<sub>2</sub>/year.
- Also, lawns and green roofs have been reported to minimum carbon uptakes of 2.7 tCO<sub>2eq</sub>/ha per year (which can go up to 10.2 tCO<sub>2eq</sub>/ha per year for green roofs) [109]. Given the 225 900 ha of urbanized lands in Wallonia (residential lawns not considered) [110], and average increase of carbon sequestration of 5 tCO<sub>2eq</sub>/ha per year through intensive urban vegetation, territorial absorption could again be increased by about 1.95 MtCO<sub>2</sub>/year.

In addition, private lawns have also the capability to significantly absorb more carbon since their carbon uptake has been reported in a range from 3 to 11 tCO<sub>2eq</sub>/ha per year [111].

It has just been demonstrated that the implementation of alternative agriculture techniques and intensive urban vegetation (potentially with more intensive vegetalization of private laws) may significantly increase the current territorial absorption of Wallonia. However, the targetted absorption level of 4 MtCO<sub>2eq</sub>/year that will balance the unmitigated non-CO<sub>2</sub> GHG emissions rate in a net-zero CO<sub>2</sub> emissions future [10] is so high that pretty much every single area of the territory must 'be designed' to maximize carbon absorption, depending on chosen land-use.

It is worth mentioning that positive carbon sequestration feedbacks with global warming have not been considered, such as increased wildfire risks [112] or the potential reduction of carbon uptake through vegetation increased respiration [113].

It should be pointed out that Wallonia has only a +32% increase of nature-based carbon sinks in its current NDC (versus current levels) [23] instead of the +300% objective reported here. Thus, even if Wallonia states that the lack nature-based carbon sinks will be compensated with potential technological carbon absorption methods to ensure carbon neutrality [27], this commitment is extremely low and relies on risky unproven technologies.

- **Initial 2020 carbon budget**

It was reported in the previous section that IPCC's +2°C 'equity' carbon budget for Wallonia (from Working Group III's contribution to AR6, which is the most recent carbon budget estimation) starting from January 1<sup>st</sup> 2020 was 382.7 MtCO<sub>2</sub>.

- **Initial 2020 individual (all-GHG) carbon footprint**

Unfortunately, there is a lack of recent studies on Wallonia's carbon footprint. This work has considered that its individual 2020 carbon footprint is equal to the 2007 average one of Belgium [3], i.e. 16 tCO<sub>2eq</sub>/year per capita [34]. By comparison, Belgian carbon footprint was reported in another study to 16.5 tCO<sub>2eq</sub>/year per capita back in 2001 [36]. It should be noted that very recently, a new study has evaluated Wallonia's carbon footprint a little

bit lower to 15 tCO<sub>2eq</sub>/year per capita in 2011 [35], but this has no impact on the statements made in this work. Since Belgium's carbon footprint (or by extension, Wallonia's) has not significantly decreased in ten years (between 2001 and 2011) [3], there is no tangible reason to think that Wallonia's 2020 carbon footprint is significantly lower than the 2007 value considered in this work.

### 2.2.2 Results for Wallonia : examples of sigmoidal GHG mitigation pathways

Two cases have been established. Firstly, the nominal one never allows for the remaining CO<sub>2</sub> budget to be overcome. Secondly, an auxiliary case has also been computed for which very risky and challenging technical carbon absorption allows for the CO<sub>2</sub> budget to slightly go into negative values, as long as it comes back to positive values by 2050.

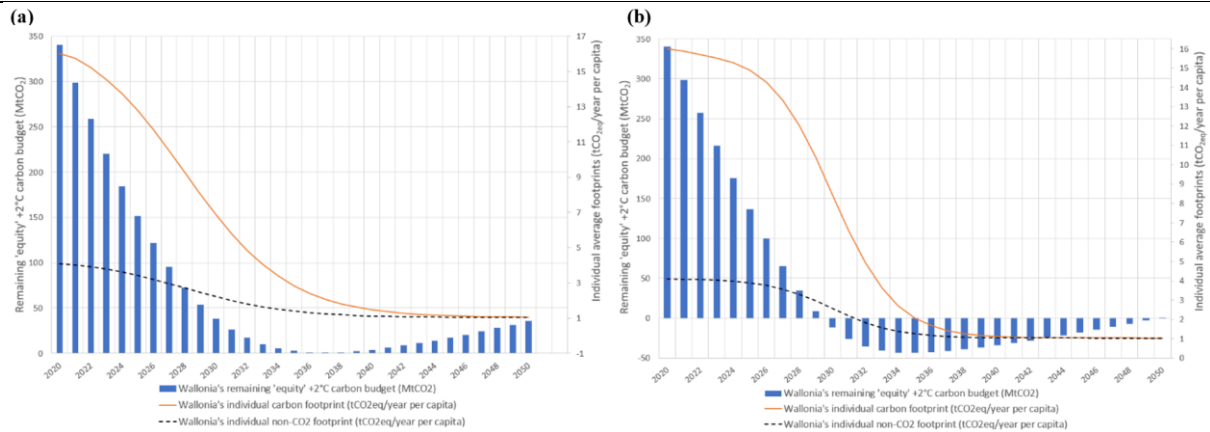
#### 2.2.2.1 CO<sub>2</sub> budget never overcome – nominal case

This case is presented on Figure 10(a) and Figure 11(a). *b* (slope) parameter has been set to 0.3 while *c* parameter has been set to 2028. This case pretty much implies that carbon neutrality will almost be reached by 2040, i.e. 10 years before the Green Deal commitment [20], for the 'equity' carbon budget not to be overcome. This is the safer case because it intrinsically leaves some carbon budget margin in 2050, but also because it implies early GHG mitigation (actually starting directly back in 2020), whose benefits in terms of accumulated CO<sub>2</sub> avoided allows for the slope of the mitigation efforts not to be too steep.

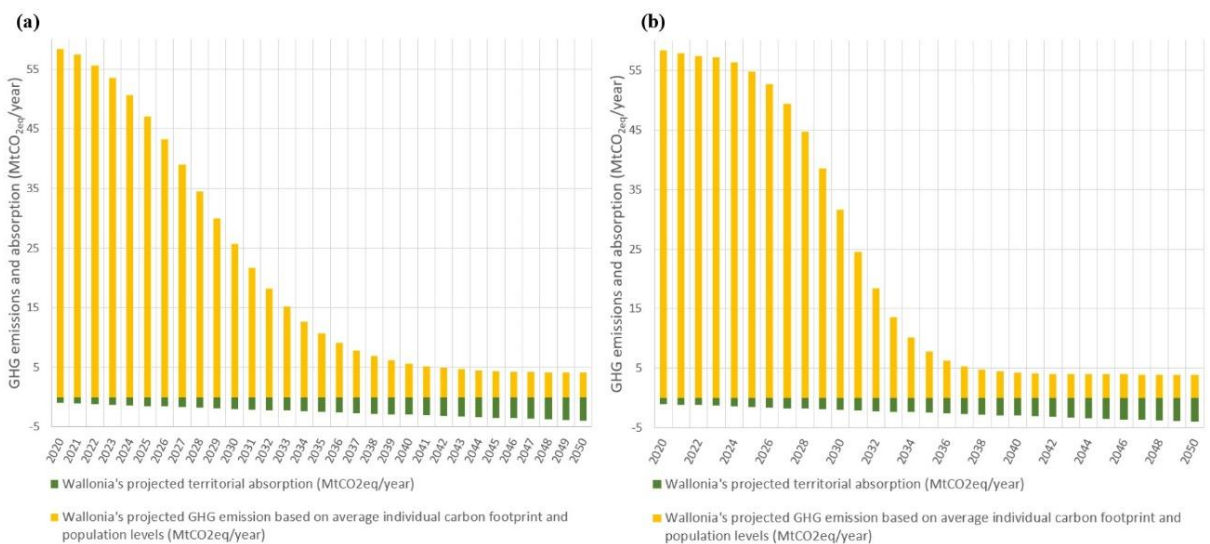
#### 2.2.2.2 CO<sub>2</sub> budget just comes back to positive values in 2050

This case is presented on Figure 10(b) and Figure 11(b). *b* (slope) parameter has been set to 0.52 while *c* parameter has been set to 2030. This case even implies that carbon neutrality will almost be reached by 2038, i.e. 12 years before the Green Deal commitment [20], for the 'equity' carbon budget to be positive in 2050.

This case is risky as it absolutely requires negative emissions (that can be ethically questionable [101]) for the carbon budget to come back to positive values, but also because of the very steep mitigation effort that would have to be performed due to delayed GHG reduction. Indeed, delayed mitigation of only 2 years (represented by the *c* parameter) compared to the nominal case require dangerously steeper GHG emission pathways and a carbon neutrality to be achieved approximately 2 years earlier than in the nominal case.



**Figure 10.** Two cases of proposed sigmoidal GHG mitigation pathways for Wallonia and their corresponding remaining carbon budget: **(a)** Safer case with the carbon budget never allowed to be overcome and early GHG mitigation starting in 2020, allowing for the slope of the mitigation effort not to be too steep, **(b)** Risky case with carbon budget allowed to be (slightly) overcome and delayed GHG mitigation that results in a quite steep slope of the mitigation effort.



**Figure 11.** Resulting yearly GHG emissions and territorial absorption of the two cases proposed in Figure 10: **(a)** Safer case with the carbon budget never allowed to be overcome and early GHG mitigation starting in 2020, allowing for the slope of the mitigation effort not to be too steep, **(b)** Risky case with carbon budget allowed to be (slightly) overcome and delayed GHG mitigation that results in a quite steep slope of the mitigation effort.

### 2.2.3 Results for France : missing data and example of sigmoidal GHG emission pathway

The same method conducted for France requires some data to be adapted.

#### 2.2.3.1 France's missing data

- **Territorial absorption (expressed equivalently in CO2eq or CO2)**

Unlike Wallonia, France has implemented a territorial absorption objective pathway up to 2050 in its climate strategy [3]. It assumes a linear increase from the current level to the 2050 target of 80 MtCO<sub>2eq</sub>/year [3], represented by 66 MtCO<sub>2eq</sub>/year of nature-based carbon sinks [114]. The current level of absorption considered in France's current climate strategy is 38 MtCO<sub>2eq</sub>/year but it has recently been calculated 63% lower, to 14 MtCO<sub>2eq</sub>/year [114]. Related to superficies, this carbon uptake level is close (although a

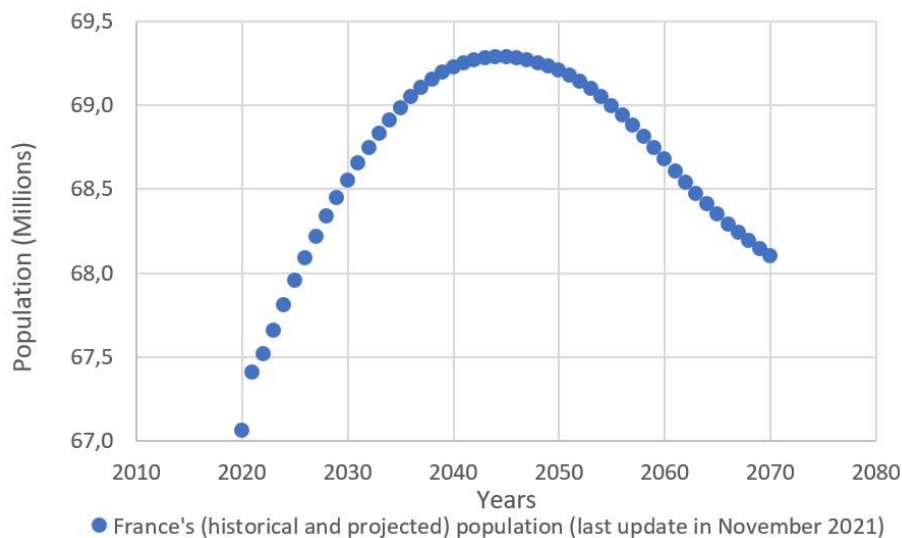
litter lower) to the one considered for Wallonia, i.e. 1 MtCO<sub>2eq</sub>/year. Therefore, this initial carbon uptake figure of 14 MtCO<sub>2eq</sub>/year has been considered for France in this work along with the 2050 target of 66 MtCO<sub>2eq</sub>/year of nature-based carbon sinks and the linear pathway between the two. Technological carbon sinks are again considered immature so the full 80 MtCO<sub>2eq</sub>/year absorption level is not considered in this work.

This would mean that territorial carbon uptake would require a +370% increase compared to current levels, probably explaining why the 2050 target of 66 MtCO<sub>2eq</sub>/year of nature-based carbon sinks has recently been considered unrealistic in a particular study [114]. However, this same reference also indicates historical 2005 level of nature-based carbon uptake of nearly 50 MtCO<sub>2eq</sub>/year, which represented already 75% of the final 2050 target considered in this work (which is thus not that unrealistic, although still very challenging).

In addition, again comparing superficies with Wallonia, this figure of 66 MtCO<sub>2eq</sub>/year of French nature-based carbon sinks in 2050 is quite similar to the 4 MtCO<sub>2eq</sub>/year of carbon uptake assumed for Wallonia in 2050, which was demonstrated to be realistic with alternative agricultural techniques and intensive urban vegetation (although, again challenging).

Also, considering France's 2050 projected population (which is presented in Figure 12), this 66 MtCO<sub>2eq</sub>/year target level of absorption coincides with the absorption target of 1 tCO<sub>2eq</sub>/year per capita implied by the Green Deal [20] to match the 'equity' unmitigated non-CO<sub>2</sub> GHG footprint in a net-zero CO<sub>2</sub> emissions future [10].

It is worth mentioning that, although it has been stated that 2050 individual carbon footprint shall cap between 1 and 2 tCO<sub>2</sub>/year per capita [115], 2 tCO<sub>2</sub>/year per capita is the target generally considered, for example with carbon footprint calculators [55]. However, this work has just highlighted that the individual carbon footprint shall preferably be lowered to about 1 tCO<sub>2</sub>/year per capita in order for GHG neutrality to be reached at the French level (as it was also the case earlier for Wallonia).



**Figure 12.** France's historical and projected population from the database of the Institut National de la Statistique et des Etudes Economiques [116,117], not considering immigrants due to the Ukraine-Russia conflict started in 2022 [97].

• **Initial 2020 carbon budget**

It was reported in the previous section that IPCC's +2°C 'equity' carbon budget for France (from Working Group III's contribution to AR6, which is the most recent carbon budget estimation) starting from January 1<sup>st</sup> 2020 was 6924 MtCO<sub>2</sub> [3].

• **Initial 2020 individual (all-GHG) carbon footprint**

Between 1995 and 2018, French individual carbon footprint has been reported to remain quite constant and around 11 tCO<sub>2eq</sub>/year per capita [3] (see Figure 4). However, the methodology has been very recently revised (especially regarding how imported CH<sub>4</sub> emissions are accounted for), which has actually slightly decreased the French individual carbon footprint figure [114]. The 2020 French carbon footprint projection has therefore been reported to 8.2 tCO<sub>2eq</sub>/year per capita, but it is only a provisional unverified figure [114]. In addition, that particularly low figure considers the COVID-19 (temporary) sanitary crisis impact on carbon (and other pollutant) emissions, which was significant in the case of France with about two months of complete lock-down [118].

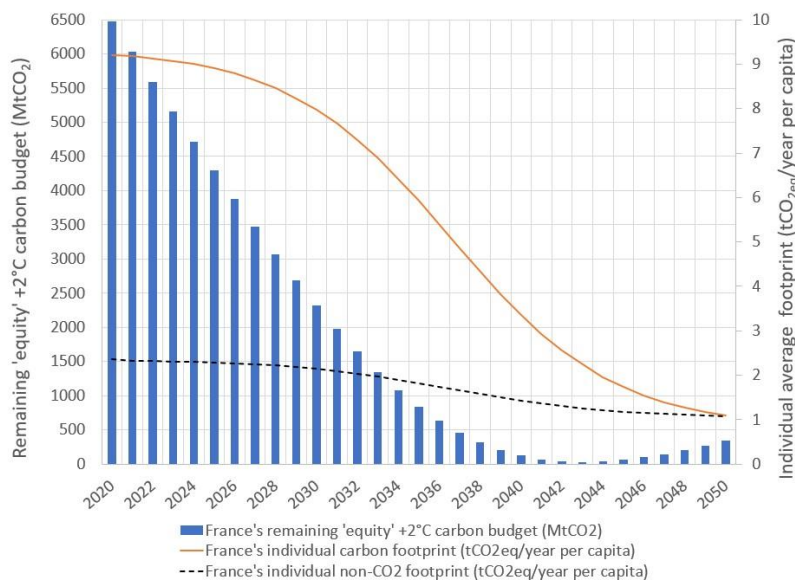
Therefore, this work will consider the last verified calculation of French carbon footprint, which has been reported to 9.2 tCO<sub>2eq</sub>/year per capita for the year 2018 [119].

• **Population projected pathway**

France's historical and projected population is shown in Figure 12. Demographic assumptions up to 2050 are quite similar as the ones of Wallonia (Figure 9). It is worth mentioning that, after 2050, Wallonia's population still increases whereas France's population decreases, according to the respective national institutes that compute the demographic data.

2.2.3.2 Example of sigmoidal GHG emission pathway for France

Similarly to Figure 10(a), the nominal case for which the +2°C 'equity' carbon budget has been computed and reported in Figure 13. Since starting individual carbon footprint is about two times lower in France than the assumption made for Wallonia, early GHG mitigation is not as critical.



**Figure 13.** Example of sigmoidal GHG mitigation pathways for France and the corresponding remaining carbon budget (case with the carbon budget never allowed to be overcome).

Therefore, the year of maximum mitigation rate, i.e. *c* parameter of Equation (3) has been set to 2036 whereas the slope parameter, i.e. *b* parameter of Equation (3) has been set to 0.25.

There is no significant interest in reporting the second case for France, as it was done in Figure 10(b) for Wallonia. Indeed, delaying GHG mitigation (and allowing the 'equity' carbon budget to temporarily go into negative values), requires once again steeper GHG

mitigation rate, which was already inferred with Wallonia's case. It is worth mentioning that, as for Wallonia, the slope of the GHG decreasing emissions would need to be about twice steeper, i.e. with an almost doubled  $c$  parameter in Equation (3).

#### 2.2.4 Discussion and perspectives about the section

It is worth mentioning that the cases computed in Figure 10 (or Figure 13 for France) are examples of GHG pathways that are 'just-compatible' with IPCC's +2°C 'equity' carbon budget. Those scenarios are yet considered 'extreme' in terms of  $b$  and  $c$  parameters (slope and year of maximum mitigation rate) and other intermediate 'just-compatible' scenarios could be similarly computed, with intermediate  $b$  and  $c$  values. However, those would not change the inferences established in the previous sections.

Also, those 'just-compatible' scenarios must not prevent GHG policies to aim earlier or steeper GHG mitigation.

It has already been established in the methodology section that, in carbon budget and carbon footprint calculations, the use of GHG forcing-equivalent potential varying over time (to consider the future warming impact of short-lived climate pollutants, i.e. SLCPs) instead of traditional 'absolute' GWP would be more relevant [85]. However, it is considered that conversion of common carbon footprint figures, established simply for example thanks to largely-used individual carbon footprint calculators [55], was not in the scope of this work and could directly be implemented at the calculator level.

Another limitation of the proposed method is that it assumes a carbon absorption target of 1 tCO<sub>2eq</sub>/year per capita (mainly through natural sinks). Although it has been established relevant (but challenging) for Wallonia and France, it would most likely be unrealistic for regions and nations with higher population density. Those might therefore require international collaboration in order to 'share' carbon sinks (and/or even 'share' initial 'equity' carbon budget).

Even if the proposed method is not perfect, mainly because one's capability of mitigating its GHG emissions can be quite different to one another's and because there is no scientific consensus on the method of calculating carbon footprint [120], one of the aims of this work is for everyone to relate to the order of magnitude that individual carbon footprint shall reach both on short-term and long-term basis.

At last, the method developed in this work to link IPCC's carbon budget to individual carbon footprint is fully reproducible with other GHG pathways than the sigmoidal ones preconized in this work (such as exponential decays, for example).

#### 2.2.5 Conclusions of the section

The method developed in this section allows for linking IPCC's 'equity' carbon budgets [3] to individual carbon footprints and is therefore compatible with existing individual carbon footprint calculators [55]. Thus, considering population levels, it can be used in climate policies to establish GHG mitigation pathways compatible with those carbon budgets, which is not guaranteed with usual existing policies, mainly because of the lack mitigation objectives set on imported emissions [3].

In addition to the consideration of imported emissions through total carbon footprints (and not only territorial emissions), the method proposed in this work offers other advantages to most current climate policies :

- By committing to GHG mitigation pathways (over the 2020-2050 period) and not only to a late emission rate target [3], carbon budget can be more easily secured, at least if those GHG pathways are respected. Indeed, essential short-term GHG mitigation targets are quite easily established with this method.

- Even if those initial pathways are not respected from one year to the next (less mitigation than expected), yearly updates can easily be established once again using the same method. The slope of mitigation efforts to come will thus be increased (as inferred by Figure 10). This requires carbon footprints to be monitored yearly and compared to the carbon budget compatible GHG emissions pathways.
- The proposed GHG mitigation pathways follow inverted 'S-shape' patterns thanks to Equation (3) that, even though quite theoretical, are more realistic [73] than linear trends assumed in most climate policies [3]. This is mainly because 'S-curves' consider 'inertia' and 'asymptotic' effects in the implementation of (renewable) technologies. Also, this method has been stated to be reproducible with other realistic GHG mitigation patterns (such as exponential decays).
- More importantly, this method has been scaled down to the individual carbon footprint and could be reproduced easily on other levels (household, district, region, continent). As stated, the individual level allows for everyone to set its own yearly GHG mitigation targets and monitoring thanks to the intrinsic compatibility with largely used carbon footprint calculators [55]. People can therefore relate more easily to climate policies set by public authorities and public resistance to climate policies can be reduced thanks to an 'audience-specific messaging and framing' [40]. In that matter, individuals shall also be encouraged to regularly compute and compare their individual carbon footprint with the targeted one (and maybe also their cumulative historical emissions). In addition, the proposed method has the advantage to intrinsically consider projected population levels through its multiplication with the average individual carbon footprint.

It is worth mentioning that developing this method over the chosen case studies has led to the following general inferences :

- Since, at net-zero CO<sub>2</sub> emissions levels, some non-CO<sub>2</sub> GHG will not be completely mitigated [10] and will account for about 1 tCO<sub>2eq</sub>/year per capita, this work has highlighted that it is preferable to consider this figure as the 2050 individual carbon footprint target rather than the 2 tCO<sub>2eq</sub>/year per capita usually reported, for example, in well-known carbon footprint calculators [55].
- Through the Green Deal 2050 GHG-neutral commitment in Europe [20], those unmitigated non-CO<sub>2</sub> GHG emissions are assumed to be absorbed territorially. This could either be performed through nature-based, i.e. natural sinks [99], or technological methods [100]. However, those latter are still unmaturing: they can be judged too risky [3] and ethically questionable [101] for climate policies to rely on them, even though their development is still highly needed in the context of risk mitigation.

At last, this work has led to the following conclusions specific to France and Wallonia's case studies (that may be relevant to other public policies):

- Wallonia should follow France's example: it needs to conduct (and finance) studies on individual and/or total carbon footprint (considering imported emissions). To the knowledge of the author, last carbon footprint available data has been established for the year 2011 [35].
- (Strong) GHG mitigation, especially in Wallonia, is required to be implemented as soon as possible for suggested pathways to be compatible with IPCC's 'equity' carbon budget. Unlike France, both 'just-compatible' computed scenarios for Wallonia, that either demonstrate delayed steep mitigation or early and milder mitigation efforts, show that the initial carbon footprint is so high that carbon neutrality would have to be reached at least 10 years before the 2050 climate-neutral European Green Deal commitment [20].

- 
- Considering technological carbon absorption methods too risky, both Wallonia and France need to maximize their natural carbon sinks to match as closely as possible the unmitigated 'equity' non-CO<sub>2</sub> GHG footprint in a net-zero CO<sub>2</sub> future [10] and ensure the GHG neutral commitment of the Green Deal [20]. As stated, that accounts for 1 tCO<sub>2eq</sub>/year per capita and this respectively represents a +300% and a +370% increase compared to the estimated current levels of Wallonia and France's territorial carbon absorptions. This could be performed by rethinking land-use in every single area of the territory. Carbon uptake can still be maximized without changing land affectation, especially for agricultural lands, through alternative agricultural techniques such as permaculture [103], or for urbanized area, through intensive urban vegetation such as green roofs [109]. Residential lawns have also a good increase potential in carbon uptake [111] if specific encouraging policies were to be implemented. However, this will be very challenging on land-use efforts alone and it is therefore still advised to also develop negative emissions technologies (such as some particular types of fuel cells discussed in *Chapter 6 - Residential fuel cells' carbon footprint mitigation potential*).

At last, it must be stressed that, even though CO<sub>2</sub>-only emissions mitigation may partly rely on the individuals, through reduction of their consumption levels for example, non-CO<sub>2</sub> GHG emissions mitigation according to +2°C compatible scenarios must rather be ensured structurally with specific compulsory or incentive policies (implemented by the relevant public authorities).



The residential fuel cells that will be the focus of this thesis are used as micro-cogeneration units (to provide power and heat). In order to evaluate their potential environmental benefits and their place in the GHG mitigation contextualized in the two previous sections, a dedicated literature review on emission factors for heat and power generation from several widely known organizations has first been conducted and reported in *Section 2.3 - Current emissions factors from heat and power generation*. Main focus is brought on GHG emissions, i.e. expressed in CO<sub>2</sub>-only or CO<sub>2eq</sub> emissions, but other pollutants are also investigated, such as SO<sub>2</sub> and NO<sub>x</sub> emissions. Further sections of this thesis (*Section 4.3 - In-situ monitoring* and *Section 5.3 - In-situ monitoring*) will indeed directly be based on the emission factors reported in this section. Most of the content the section has been published in the *proceedings of the 35<sup>th</sup> International Conference On Efficiency, Cost, Optimization, Simulation and Environmental Impact of Energy Systems (ECOS2022)* [15] for the CO<sub>2</sub> emissions factors or in the *proceedings of the 36<sup>th</sup> International Conference On Efficiency, Cost, Optimization, Simulation and Environmental Impact of Energy Systems (ECOS2023)* [121] for the other pollutants emissions factors, which are also presented in *APPENDIX 8: Pollutant testing (NO<sub>x</sub>, SO<sub>2</sub> and CO) of commercialized micro-combined heat and power (mCHP) fuel cells* and accepted for publication in the *Journal of Environmental Management* [122].

## 2.3 Current emissions factors from heat and power generation

### 2.3.1 CO<sub>2</sub> and CO<sub>2eq</sub> emission factors

The main ecological indicators that will be computed in this work (for the studied SOFC in *Section 4.3 - In-situ monitoring* and for the studied PEMFC in *Section 5.3 - In-situ monitoring*) consist of absolute CO<sub>2</sub> or CO<sub>2eq</sub> (equivalent) utilization savings, depending whether all Greenhouse Gases (GHG) are considered or not. Those indicators could also be called 'CO<sub>2</sub> or CO<sub>2eq</sub> balances'. The fuel cell systems will be compared to reference energy production appliances (for heat and power).

In order for those indicators to be computed, one must establish emission factors for natural gas combustion (heat production) or consumption as well as for the electrical production (or consumption). Several set of assumptions, from several widely known organizations, have been reported in Table 4 in order to enable sensitive studies on the ecological balances of the studied systems in case one particular emission factor is disputed.

Even if natural gas combustion (or consumption in a fuel cell) emission factor is quite stable in time, it is not the case for the electrical mix (mainly thanks to increased yearly penetration of renewables). Therefore, one should look for the date considered for the establishment of the emission factors (and preferably consider the most recent ones).

One must also pay attention that the electricity mix considered for Belgium can either be relevant for the territorial production or for the territorial consumption. The difference relies on the exportation/importation of electricity with neighbouring countries. Consumption mix might be more relevant as it is the one that is really used by the houses monitored in this work (see *Chapter 4 - Study of the Bl\*\*\*G\*N SOFC system* and *Chapter 5 - Study of the P\*2 PEMFC system*) but its variation is way greater with time. From one day to the other, Belgium could import low-carboned electricity from France and the day after, it could import quite high-carboned electricity originated from Poland. The only emission factor that would account for that is the consumption one.

In addition to CO<sub>2</sub> only or CO<sub>2eq</sub> specification, one must pay attention if the emission factor provides non-LCA or LCA values for the energy uses, which implies that emissions of the

whole cycle of energy or fuel production are included. However, even if the utilization ecological balances that consider LCA emission factors for energy uses (such as the emissions involved in the production of the fuel), it does not include the whole LCA of the end user system that consumes this fuel (to provide decentralized heat and/or power). For example, this means that the emissions linked to the manufacturing or the disposal of systems such as gas condensing boilers or micro-cogeneration fuel cells are not accounted.

Organization	Emission factor of natural gas combustion and consumption	Emission factor for electricity production from natural gas power plant	Emission factor for Belgian electricity consumption	Emission factor for Belgian electricity production
Internal Energy Agency (combustion only) [123,124]	202 gCO <sub>2</sub> /kWh (2013 but relevant) <sup>B</sup>	400 gCO <sub>2</sub> /kWh <sub>el</sub> (2013)	Unavailable	160 gCO <sub>2</sub> /kWh <sub>el</sub> (2020) <sup>B</sup>
IPCC 2014 (combustion only) [125]	202 gCO <sub>2eq</sub> /kWh	370 gCO <sub>2eq</sub> /kWh <sub>el</sub>	Unavailable	Unavailable
IPCC 2014 (LCA) [125]	Unavailable <sup>a</sup>	490 gCO <sub>2eq</sub> /kWh <sub>el</sub>	Unavailable	Unavailable
European Commission CoM <sup>b</sup> [126]	240 gCO <sub>2eq</sub> /kWh (LCA) <sup>C</sup>	543 gCO <sub>2eq</sub> /kWh <sub>el</sub> (LCA)	239 gCO <sub>2eq</sub> /kWh <sub>el</sub> (LCA) – (2013) <sup>C</sup>	Unavailable
Walloon energy regulator – CWaPE <sup>c</sup> [127]	251 gCO <sub>2eq</sub> /kWh (LCA)	456 gCO <sub>2eq</sub> /kWh <sub>el</sub> (LCA) <sup>A</sup>	Unavailable	Unavailable
Electricitymap.org (yearly average) <sup>d</sup>	Unavailable <sup>a</sup>	490 gCO <sub>2eq</sub> /kWh <sub>el</sub> (LCA)	162 / 167 gCO <sub>2eq</sub> /kWh <sub>el</sub> (LCA) (2020 / 2021) <sup>D1</sup>	148 / 145 gCO <sub>2eq</sub> /kWh <sub>el</sub> (LCA) (2020 / 2021) <sup>D2</sup>
Electricitymap.org <sup>e</sup> (hourly discretization)	Unavailable <sup>a</sup>	490 gCO <sub>2eq</sub> /kWh <sub>el</sub> (LCA)	Hourly discretization (LCA) <sup>d</sup> <sup>E1</sup>	Hourly discretization (LCA) <sup>d</sup> <sup>E2</sup>

<sup>a</sup> Can be estimated between 241 gCO<sub>2eq</sub>/kWh and 254 gCO<sub>2eq</sub>/kWh. Those figures have been established from the 202 gCO<sub>2eq</sub>/kWh base value [125] with an additional 0.52 gCH<sub>4</sub>/MJ<sub>LHV</sub> [125] of methane leakage in fuel supply (main contributor of indirect emissions [125]). Methane GWP100 has been considered as recommended [125], which can be assumed equal to 21 according to 1995 IPCC assumptions [128], 28 according to 2013 IPCC assumptions [12] and 27.9 according to 2021 IPCC assumptions [129]. It is worth observing that the resulting values come close other LCA set of assumptions A and C (see the corresponding boxes in Table 4). 254 gCO<sub>2eq</sub>/kWh will be considered in this study as it involves the most recent consideration of methane GWP100.

<sup>b</sup> Reference considers the reported emission factors valid for the period 2008-2015 [126].

<sup>c</sup> Reference has established these emission factors in 2005 but they are still used [127]. This is mainly because there has neither been any game changer regarding the efficiency of the reference systems for energy production nor regarding natural gas production and importation.

<sup>d</sup> Yearly average from hourly discretized emission factors provided by Electricitymap.org.

<sup>d</sup> Hourly discretized emission factors provided by Electricitymap.org will directly be integrated in (hourly) computation when establishing yearly CO<sub>2</sub> balance of the systems (see Section 4.3.3.2 - *Economical and ecological performance*).

<sup>d,e</sup> They consider the IPCC 2014 (LCA) emission factors for individual electricity generation systems [125].

**Table 4.** Reference and values found in literature for CO<sub>2</sub> or CO<sub>2eq</sub> emission factors of heat and power generation systems or mix, mainly in Belgium (LHV based figures) [15].

At last, to the understanding of the author, grid transportation and distribution electrical losses (which can reach about 6-7% in EU [130]) have not been considered in any of the electrical emission factors.

To sum up:

- Dataset 'A' represents the CO<sub>2eq</sub> LCA savings considered by the Walloon regulator for CHP systems. This latter wants to promote CHP based on European Parliament directives [131] and they especially consider an overestimated emission factor for the electricity mix of 456gCO<sub>2eq</sub>/kWh (LCA) [132]. It assumes that all the electricity produced by the CHP system replaces electricity generation from a Combined Cycle Gas Turbine (CCGT) plant of 55% LHV efficiency [127]. The regulator indeed divides its natural gas combustion emission factor by 0.55.

With CHP systems not electrically drive that are supposed to run as long as possible (which is particularly the case for the PEMFC tested in this work, as explained in *Chapter 5 - Study of the P\*2 PEMFC system*), this may not be considered as accurate compared to set of assumptions considering the average (or hourly) actual electrical mix (actually represented by a great fraction of nuclear energy that is often assumed to be 'low-carboned' [133]). However, it would still be relevant for electrically driven technologies (such as the SOFC tested in this work, as explained in *Chapter 4 - Study of the Bl\*\*\*G\*N SOFC system*) that could only produce just before or when CCGT plants are turned on. Actually, the electrical market and electrical prices (at least in the EU) relies on the System Marginal Price (SMP) [134] and it means that they are defined by the last power plants that have to be launched to meet the demand. Those are generally the CCGT plants for flexibility, ecological and economic reasons.

In fact, according to the hourly data provided by Electricitymap.org for both year 2020 and 2021 (that have been used for Dataset 'D' and 'E'), there was always some electrical production that came from natural gas power plants. Therefore, through the SMP principle, the Marginal Emission Factor (MEF), which 'reflects the emissions intensities of the marginal generators in the system, i.e. the last generators needed to meet demand at a given time' [135], can be considered always equal to the 'emission factor for electricity production from natural gas power plant' as reported in Table 4. For example, marginal emissions of CHP systems can thus be studied by simply using 'Dataset A' of Table 4 (for the year 2020 and 2021 in Belgium). Furthermore, this will supposedly be the case for a long time in Belgium considering the fact that its government is currently supporting the construction of new CCGTs to phase-out old nuclear plants [136,137].

- Dataset 'B' considers savings only for CO<sub>2</sub> emissions (not all GHG) but the main issue is that the complete LCA is not considered (only combustion is considered). Combustion only emission factors (especially expressed in CO<sub>2</sub> only) do not evolve in time as they are mainly related to the carbon content of the fuels and to the intrinsic efficiency of the power plant technologies. However, the electrical mix evolves (mainly due to renewable penetration). This is therefore probably the most accurate dataset due to the recent information on the Belgian electrical mix and the constant carbon content of natural gas through time. However, this might not be the most relevant one as it considers the electrical production mix (whereas the consumption one would have been preferred) but mainly because it does neither consider all GHG nor the full LCA.
- Dataset 'C' considers CO<sub>2eq</sub> (all GHG) LCA savings. This could be considered as relevant but the consumption mix considered is the one of 2013 and is therefore quite obsolete. In fact, according to the International Energy Agency [123], the Belgian production mix emissions per kWh (CO<sub>2</sub> only) have been reduced by 15.2% between the year 2013 and the year 2020. Therefore, if one was to consider the same reduction

in the LCA CO<sub>2eq</sub> emissions, one would be at about 203gCO<sub>2eq</sub>/kWh instead of the 239gCO<sub>2eq</sub>/kWh of the dataset. Nevertheless, this LCA consumption of 203gCO<sub>2eq</sub>/kWh does not account for an officially recognized value and has not been computed.

- Dataset 'D' and 'E' considers CO<sub>2eq</sub> LCA savings similarly but the emission factors are built thanks to Electricitymap.org database that has been granted for Belgium for this academic work. This database collects real-time data from electricity generation and imports/exports around the world [138]. It calculates the resulting (hourly) emission factor according to the real-time mix. It is mainly based according to IPCC 2014 (LCA) emission factors for electricity generation power plants [125]. It provides both the emission factors for the production and for the consumption. Dataset 'D' considers the statistical average emission factors for the whole given year (between the population of unweighted hourly emission factors) whereas Dataset 'E' has discretized the study down to the hour. This allows for individually considering and computing each provided real-time emission factors. Dataset 'E1' (consumption electrical mix) is very likely to be the most relevant set of assumptions. In fact, the IPCC 2014 based emission factors for electricity production means can still be considered as valid as they have still been used in IPCC Sixth Assessment Report published in April 2022.

### 2.3.2 SO<sub>2</sub> and NO<sub>x</sub> emission factors

Table 4 will be used to address GHG emissions of the studied fuel cell systems (see *Section 4.3 - In-situ monitoring* and *Section 5.3 - In-situ monitoring*) and therefore their relevance in the global warming issue contextualized in *Chapter 2 - Collective and individual GHG mitigation pathways*, but another key element in assessing the environmental impacts of those technologies lies in the other common air pollutants : the emissions of nitrogen oxides, i.e. NO<sub>x</sub>, sulphur dioxide, i.e. SO<sub>2</sub>, and carbon monoxide, i.e. CO emissions.

Nitrogen oxides (NO<sub>x</sub>) in the ambient air consist primarily of nitric oxide (NO) and the much more harmful nitrogen dioxide (NO<sub>2</sub>) [139] that NO readily turns into (in the presence of volatile organic compounds, i.e. VOCs [140]) in the atmosphere [139]. NO<sub>2</sub> indeed irritates lungs and promotes respiratory infections [141]. The two forms of gaseous nitrogen oxides are not only considered as pollutants of the lower atmosphere but they also can have significant impact on the upper atmosphere. Indeed, NO<sub>2</sub> have been reported to contribute to acid rain [139], which subsequently, in addition to endanger vegetation, ecosystems and freshwater [139] or increase human exposure to nitrate/nitrite consumption [142], enhance the soil nitrous oxide (N<sub>2</sub>O) emissions [143,144]. In fact, this strong GHG pollutant, with a global warming potential over 100 years that is evaluated about 300 times greater than CO<sub>2</sub> [145], is also responsible for most of the stratospheric ozone depletion [146]. It is worth mentioning that, through the subsequent formation of N<sub>2</sub>O, the global warming potential over 100 years of NO<sub>x</sub> is estimated between 7 and 10 [147].

In the lower atmosphere, in addition of being again a precursor of acid precipitation, it is also a precursor of fine particulate matters [148], which can penetrate deep into vitals systems, causing cardiovascular and respiratory diseases [149] as bad as lung cancers [150], increasing morbidity and mortality [151]. Nitrogen dioxide is also precursor of tropospheric ozone (O<sub>3</sub>) formation [139]. And O<sub>3</sub> is a poison even more harmful than NO<sub>2</sub> [141]. Indeed, it damages vegetation, irritates lung tissues and it can lead to smog, even more harmful to respiratory functions than ozone (and can even cause deaths) [139], as it can coarse many other pollutants of different toxicities (such as particulate matters). Indeed, smog primarily consists of ozone and 'secondary' pollutants that are produced through photochemical reactions of directly emitted species (mainly consisting once again of VOCs [152]), in processes that are driven by sunlight and accelerated by warm

temperatures [153]. The chemical composition of smog can vary according to meteorological conditions (mainly temperature, humidity and radiation) and to the concentration of other atmospheric species (especially the other pollutants, not only the VOCs) [154]. For example, the effect of smog is even aggravated when it contains fine particulate matter [155] but it can also contain peroxyacyl nitrates (PAN), aldehydes, CO, SO<sub>2</sub>, NO<sub>x</sub> [154] (or their sulphate/nitrate derivatives [156]), or lead [157], and therefore also induce the health problems of those species.

Similarly to NO<sub>2</sub>, SO<sub>2</sub> is a major precursor of acid rains and fine particulate matters [158] (and thus can be associated with their environmental and health issues). Another similarity is that it is an irritating gas that leads to respiratory illnesses [139] and it has been reported that it can aggravate existing heart (and pulmonary) diseases [159]. Oppositely to NO<sub>x</sub>, SO<sub>2</sub> has a negative contribution to global warming (with a GWP100 estimated between -18 and -25 [160]) because of the sulphate or sulfuric acid aerosols it is a precursor of [141]. Also, it is not a direct precursor of ozone although it has been reported that sulphur compounds initiated by SO<sub>2</sub> emissions can play the role of VOCs in the ozone formation cycle (by re-oxidizing NO into NO<sub>2</sub> once NO<sub>2</sub> has reacted with O<sub>2</sub> and formed O<sub>3</sub> and NO) [161]. At last, it can aggravate smog toxicity (either directly [157], through its sulphate derivatives [156], or through the fine particulate matters it can coarse into [154,158]).

CO is a well-known major atmospheric pollutant as it is also known as the 'silent killer' (invisible and odourless): at a concentration of 12000 ppm, it kills in two to three breaths as it blocks the ability of hemoglobin to transport oxygen to the cells of the body [162]. However, at lower concentration, it also has many impacts on human health: impaired vision, reduced brain function [159], coma, seizures, heart and respiratory diseases, physical weakness [141], tissue damages [163]. It is also considered as a minor ozone precursor in urban areas as it can play the role of VOCs in the ozone formation cycle [164]. At last, even though the lifetime of CO in the atmosphere is quite short (a few months) [165], its GWP100 is still estimated at 5 because of its interaction with methane [165]. Indeed, this is mainly due to the fact that the main removal process of both CO and CH<sub>4</sub> includes the reaction with hydroxyl radicals [166]. CO emissions reduce the hydroxyl radicals concentration for methane removal, which has a quite high GWP100 of about 28 [15], thus leading to a significant indirect impact of CO emissions on global warming.

SO<sub>x</sub> and NO<sub>x</sub> emission factors of typical space heating appliances have respectively been reported in Table 5 and Table 6. The data required to feed such a comparative table relative to CO emission factors of typical space heating appliances could not (yet) be computed with the literature review conducted through this thesis.

Space-heating appliance	SO <sub>2</sub> (source from 2007 : Fondation Rurale de Wallonie - combustion only) mg/kWh <sub>th</sub>	SO <sub>2</sub> (source accessed in 2007: Gemis 4.5 - complete LCA cycle) mg/kWh <sub>th</sub>
Oil-fired boiler	504	600
Gas condensing boiler	0 <sup>a</sup>	111
Electrical radiators (Joule heating)	Unavailable	392 <sup>b</sup>
Old log wood boiler	36	Unavailable
Modern log wood boiler	36	320
Wood chip boiler (wood chips)	36	Unavailable
Condensing wood boiler (pellets)	Unavailable	472

<sup>a</sup> Combustion only SO<sub>2</sub> emissions of natural gas combustion are definitely low as most natural gas markets require less than 4 ppm of (all) sulfur-containing compounds in the gas [167]. Indeed, decentralized desulfurization is implemented in natural gas processing [168]. However, the SO<sub>2</sub> combustion only emissions of gas condensing boilers are not completely nil as other studies have reported about 2 mg/kWh<sub>th</sub> [169] or between 3.5 and 4 mg/kWh<sub>th</sub> [170] (the latter study considers a residential domestic hot water demand of 300 L a day at 45°C [170] and this has been considered to correspond to 12.3 kWh<sub>th</sub> a day [171]).

<sup>b</sup> The power plant type has a strong influence on the SO<sub>2</sub> emissions. As a comparison, in 2012 in the US, coal-fired and Combined Cycle Gas Turbine (CCGT) power plants were reported to have average SO<sub>2</sub> emission intensities respectively of about 1200 mg/kWh<sub>el</sub> and about 2.4 mg/kWh<sub>el</sub> (combustion only) [172]. Another study reported (in 2013) the following SO<sub>2</sub> LCA emission intensities : 10-320 mg/kWh<sub>el</sub> range for natural gas power plants (of all kinds, not only the most efficient ones, i.e. the CCGTs), 30-6700 mg/kWh<sub>el</sub> range for coal-fired power plants, 3-38 mg/kWh<sub>el</sub> range for nuclear power plants [173]. At the time when Table 5 was computed (in 2007), coal-fired power plants (of high SO<sub>2</sub> emission intensity) were still in use for electricity generation. In fact, for example, Belgium closed its last coal-fired power plant in 2016 and was the seventh EU country to completely remove coal from their electrical mix [174]. Therefore, SO<sub>2</sub> emissions of electrical radiators can be considered much lower than reported in this table. For example, considering the 2022 Belgian electrical mix [175] and the maximum SO<sub>2</sub> emission factors for electricity generation reported by the European Topic Centre on Air and Climate Change [176] (except for nuclear electricity for which the French emission factor has been considered), the LCA SO<sub>2</sub> intensity of the 2022 Belgian electrical mix can be considered to only 77 mg/kWh<sub>el</sub>, i.e. five times lower than the value reported in Table 5. In this calculation, the assumption that the 3.2 TWh electrical production referred as 'Other' in the Belgian electrical mix [175] entirely corresponds to incineration of municipal waste with a SO<sub>2</sub> emission factor of 1220 mg/kWh<sub>el</sub>, coming from the most SO<sub>2</sub> emitting waste incineration technology reported in literature (2010 study for China power plants) [177]. This is a safe assumption (providing the worst SO<sub>2</sub> intensity for the Belgian electrical mix) as municipal waste incineration in Belgium corresponded only to 1 TWh per year in 2014 [178] or 1.5 TWh in more recent years [179] while other power plant technologies (hydropower, geothermal, solar-thermal, and solid biomass) are much cleaner, or are at worst similar (liquid biofuels) in terms of SO<sub>2</sub> emissions [176].

**Table 5.** SO<sub>2</sub> emission level reported from Energie+ [180] (website developed by the University of Louvain-la-Neuve and the Energy department of the Wallon Region, in Belgium).

Space-heating appliance	NOx range (source from 1998 : Electrabel-SPE – combustion only) mg/kWh <sub>LHV</sub>	NOx (source from 2007 : Fondation Rurale de Wallonie - combustion only) mg/kWh <sub>th</sub>	NOx (source accessed in 2007: Gemis 4.5 - complete LCA cycle) mg/kWh <sub>th</sub>
Old oil-fired boiler	up to 200	Unavailable	Unavailable
Non-low NOx oil-fired boiler	150 – 180	144	244
Low NOx oil-fired boiler	90 – 120	Unavailable	Unavailable
Old gas boiler	150 – 200	Unavailable	Unavailable
Atmospheric gas boiler	100 – 180	Unavailable	Unavailable
Modulating gas condensing boiler	20 – 90	144	140
Electrical radiators (Joule heating)	420 <sup>a</sup>	Unavailable	459
Old log wood boiler	Unavailable	180	Unavailable
Modern log wood boiler	Unavailable	151	235
Wood chip boiler (wood chips)	Unavailable	162	Unavailable
Condensing wood boiler (pellets)	Unavailable	Unavailable	344

<sup>a</sup> Considering the average Belgian electricity generation efficiency of 38% in 1998. With the same methodology (and references) as conducted in Table 5 to establish the SO<sub>2</sub> intensity of the current Belgian electrical mix, the LCA NOx intensity of the current Belgian electrical mix can be considered to only 90 mg/kWh<sub>el</sub> or less, i.e. also about five times lower than reported in Table 6.

**Table 6.** NOx emission level reported from Energie+ [180] (website developed by the University of Louvain-la-Neuve and the Energy department of the Wallon Region, in Belgium) [121].

### 2.3.3 Methane slip in natural gas fed fuel cells

It should be mentioned that methane slip (or slippage), i.e. ‘unburnt’ methane is sometimes mentioned in fuel cell literature. However, this term is usually rather used not for the methane content in the flue gases but for the methane slipping from the reformer to the stack (to the anode of the fuel cell stack) if the fuel cell is not directly fed by hydrogen but by natural gas (or other hydrocarbons) [181–183].

Regarding Solid Oxide Fuel Cells (SOFCs), their high operating temperature fuel flexibility allows them to directly use methane (and other hydrocarbons) as fuel onto the stack anode, as it will be seen in *Section 3.1.2 - Fuel cell types and classification*. In addition, in the case of commercialized micro-CHP SOFC systems (in fact, even in the case of the SOFC system that will be tested later on in *Chapter 4 - Study of the BI\*\*\*G\*N SOFC system*), existing studies of exhaust gases reported in literature have shown that there is no or negligible methane slip [184]. It has been reported that the ‘operation of the stack’ is at a temperature between 700 and 800°C, which ‘enables the internal reforming to proceed with negligible methane slip’, which maximizes the amount of fuel available for

the electrochemical process [184]. Increased internal SOFC temperatures have indeed been reported to significantly reduce methane slip/emissions in exhaust gases [185]. Furthermore, specific SOFC literature confirms that when operated on natural gas, SOFC do not have problems of methane slip in exhaust gases [186,187].

Regarding Proton Exchange Membrane Fuel Cells (PEMFCs), their stack relies high purity H<sub>2</sub> fuel [188], which implies reforming processes if the fuel cell is fed by natural gas (or other hydrocarbons) [189,190], as it will be seen in *Chapter 3 - Fuel cell technologies and their residential applications*. In fact, CH<sub>4</sub> concentration up to 20 ppm downstream of the fuel processor and upstream of the fuel cell stack (anode) have been reported not affect the power-generation performance [191]. However, as it will be seen in *Section 5.1 - Description of the machine* (and Figure 74) for the PEMFC micro-CHP tested in this work, an afterburner is usually implemented with PEMFC systems fed by natural gas in order to ensure the (complete) utilization of the unreacted fuel (mainly CH<sub>4</sub> and H<sub>2</sub>) [190,192], simultaneously providing the necessary heat to the reforming processes [190].

For those reasons and also because of the unavailability of dedicated CH<sub>4</sub> sensors to place in the exhausts of the systems in the experimental studies performed in this thesis, potential unlikely methane emissions of fuel cell micro-CHP systems have not been considered from here onwards.

## 2.4 Conclusions of the chapter

Conclusions related to *Section 2.1 - Confronting IPCC's carbon budgets to climate policies* and *Section 2.2 - Establishing individual carbon footprint pathways based on IPCC's carbon budgets* have been reported for each section in specific explicit 'Conclusions of the section' paragraphs.

In addition, the key contributions and findings of *Section 2.3 - Current emissions factors from heat and power generation* have been summarized here below :

- A literature review on emissions factors for energy consumption has also been reported (for CO<sub>2</sub>, CO<sub>2eq</sub>, NO<sub>x</sub>, SO<sub>x</sub>), mainly applicable for Belgium.
- It has been reported that methane slip (methane emissions) from PEMFCs and SOFCs fed by natural gas can be considered nil.
- CO, NO<sub>x</sub> and SO<sub>x</sub> harmful effects on human health and environments have also been reported from a review of literature.



# CHAPTER 3 FUEL CELL TECHNOLOGIES

## AND THEIR RESIDENTIAL APPLICATIONS

The aim of the first section of this chapter is to introduce the notion of fuel cell and to describe its main features. Then, as many fuel cell types exist, a literature review has been conducted and a new fuel cell classification and identification key is offered, depending primarily on the fuel cell charge carrier. At last, the key characteristics of the main fuel cell types existing in literature and reported in the fuel cell identification key are presented, including performance, advantages and disadvantages. This section is currently under review almost as-is in the *Journal of Power Sources* [193].

*Section 3.2 - Micro-cogeneration fuel cells systems and markets* then focuses on the heat and power cogeneration market (CHP). First, the notion of micro-CHP is defined and the fuel cell types currently considered on CHP markets are introduced, with an emphasis on the residential market, which is later on described regionally. This section then investigates why the only fuel cell technology available on the micro-CHP market are O-SOFC and LT-PEMFC (Low Temperature PEMFC), i.e. why HT-PEMFCs (High Temperature PEMFCs) applications have never been successful on the micro-CHP market. A focus is then brought on the systems currently available on the European market. At last, the latest most remarkable achievements regarding the industries of PEMFC and SOFC-based CHP have been reported as well as the expected and hoped performance that those systems could offer in a mid-term future.

### 3.1 Generalities

#### 3.1.1 Fuel cell operations and main advantages

A fuel cell is a galvanic cell that transforms directly the energy from a fuel (typically hydrogen, sometimes other hydrocarbons, alcohols [194], ammonia [195], hydrazine [196], hydrogen sulfide [197] or borohydride [198]) and an oxidizing agent (usually oxygen or air, sometimes hydrogen peroxide [199] or chlorine dioxide [194]) into electrical energy [200] and heat [201]. In electrochemical converter such as galvanic cells, the production of electricity relies on an oxidation-reduction reaction (redox reaction) as its underlying process [202]: the electrons transferred during the redox reaction move through an external circuit, exiting from the anode (negative electrode) after oxidation, and entering into the cathode (positive electrode) for reduction [202]. The complete redox process is thus split into two half-reactions that happen on those two distinct electrodes [202], which are separated by an electrolyte [203]. The electrolyte consists of a conductive liquid or solid phase able to transfer ionic species (cations or anions) and thus permitting the closing of the electric circuit [202].

As shown in Figure 14, fuel cells are thus built around the unit cell, i.e. its core, which includes both electrodes and the electrolyte. The cell is responsible for converting chemical energy to electrical energy [204].

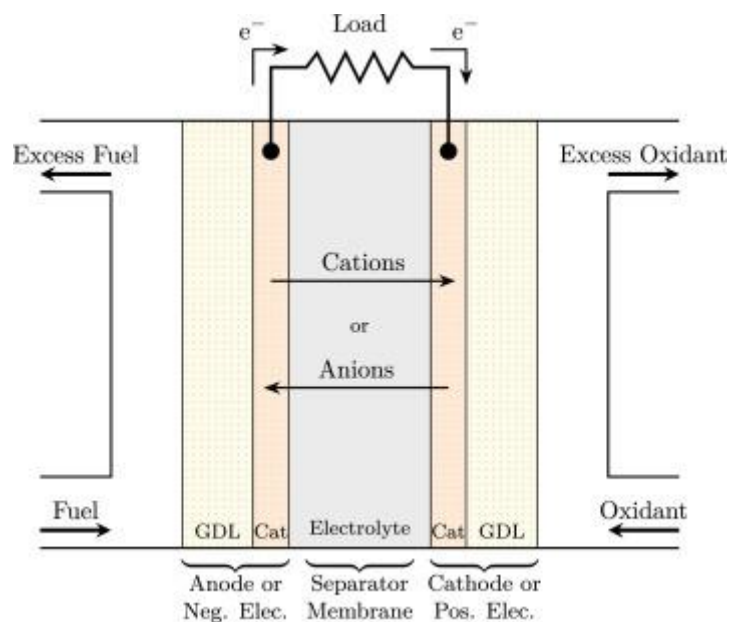
The most common redox reaction in a fuel cell is the oxygen-hydrogen reaction defined by Equation (4) [203]:



It generates water and heat as byproducts that must be continuously removed in order to maintain continuous isothermal operation for ideal electric power generation [205]. In fact, the intrinsic heat and electricity generation of fuel cells make them well suited for CHP (Combined Heat and Power) applications [206].

However, if the type of oxidizing agent or fuel (used directly at the anode and not converted into hydrogen in upstream processes) is changed, this redox overall reaction can be altered. For example, this is especially the case with the quite common use of methanol as fuel in DMFCs (Direct Methanol Fuel Cells) [207] and/or with the use of hydrogen peroxide as oxidant [199,208]. Likewise, as another example, fuel cell that involves borohydride as fuel usually have another similar overall reaction as Equation (4) [198], which will be later on given by Equation (15). However, it is worth mentioning that fuel cells using sodium borohydride only as hydrogen source, processed internally to generate hydrogen upstream of the stack, have also been reported [209]).

The overall redox reaction of Equation (4) is identical to the combustion of hydrogen with oxygen [210], which is considered as a chemical reaction rather than an electrochemical reaction [201]. The main difference lies in the fact that both oxidation and reduction reactions involved in a chemical reaction takes place at the same place whereas they are performed via an external circuit in electrochemical reactions [201]. It is also reported that chemical reactions can be performed in the bulk whereas electrochemical reactions generally occur at the surface of a solid catalyst [201] (heterogeneous catalysis). However, this can be disputed as fuel cells with homogenous (not solid) catalysts [211] or catalytic hydrogen combustion [212] (occurring at the catalytic surface and not in the bulk) nowadays exist.



**Figure 14.** Schematic representation of a fuel cell core and definitions. GDL stands for Gas Diffusion Layer, which consists of porous and electrically conductive structures for gas and electrons transfer that have as main task to allow uniform access of gaseous reactants to the catalyst (abbreviated by Cat. on the figure) layer of both electrodes [202]. Reproduced from reference [201].

This direct process of converting chemical energy to electrical energy in one step in a fuel cell is opposed to the multi-step process involved in combustion-based heat engines [201] and includes a higher efficiency rate that can range from 40% to 60% [200], and even higher, up to 75% or more, as it will be discussed in *Section 3.2.5 - Current and expected performance of micro-CHP systems based on a PEMFC or a SOFC*. From this perspective, fuel cells are essentially the same as traditional electrochemical batteries, with one key

distinction. Batteries have a limited amount of available energy, determined by the quantity of active mass contained within them [205]. In contrast, fuel cells do not store any energy on their own. As long as fuel and an oxidizing agent are provided to the fuel cell from external supplies, it will produce DC electricity, like a reactor [205].

Most current energy generation technologies that rely on combustion are highly detrimental to the environment, contributing to a range of global concerns such as climate change, ozone layer depletion, and acid rain, as well as causing a consistent reduction in vegetation cover [201] (see *Section 2.3.2 - SO<sub>2</sub> and NO<sub>x</sub> emission factors*). Additionally, these technologies are mostly reliant on finite and diminishing supplies of fossil fuels [201]. In contrast, fuel cells are compatible with renewable sources and modern energy carriers, such as hydrogen, which promote sustainable development and energy security [205]. In addition, due to their static nature, fuel cells operate quietly without producing noise or vibration [205]. Furthermore, by connecting single cells in series and/or parallel within a stack, i.e. the power module [213], they are also modular, allowing for easy construction and versatile application in portable, stationary, and transportation power generation [205]. In summary, fuel cell technologies represent one of the most promising solutions for the efficient, eco-friendly, and potentially versatile conversion of chemical energy into electrical energy, positioning them as key technologies in the much-needed energy transition contextualized in the first two chapters of this work.

### 3.1.2 Fuel cell types and classification

Fuel cells are usually categorized based on the type of electrolyte and fuel they use [204], but it is sometimes reported that the electrolyte only usually suffices to identify the fuel cell type (its operating temperature, the required catalysts, its fuel and its electrochemical reaction) [214].

As it can be perceived from the list of main fuel cell types reported here below [214], this classification is generally explicitly mentioned in the acronym of the fuel cell type:

- PEMFC, i.e. Polymer Electrolyte Membrane Fuel Cell (sometimes referred as ‘Proton Exchange Membrane Fuel Cell’). Its main identifiable characteristic is its solid polymer membrane as electrolyte.
- PAFC, i.e. Phosphoric Acid Fuel Cell. Its electrolyte is a liquid solution of phosphoric acid.
- SOFC, i.e. Solid Oxide Fuel Cell. Its electrolyte, usually a (solid) ceramic, includes oxides.
- AFC, i.e. Alkaline Fuel Cell. Traditional AFC involve a liquid alkaline solution (usually KOH) as electrolyte. As explained a little further in section, this AFC group of fuel cells now includes the SAFC (Solid Alkaline Fuel Cell), which are also known as AEMFC, i.e. Anion Exchange Membrane Fuel Cell, which include as electrolyte a solid alkaline membrane capable of transferring anions.
- MCFC, i.e. Molten-Carbonate Fuel Cell. MCFCs are using an electrolyte composed of a molten carbonate salt mixture suspended in a ceramic matrix solid electrolyte which is chemically inert and porous [215].

That same reference [214], as many others, also cites DMFC (Direct Methanol Fuel Cell) as a main fuel cell type. Although DMFC are widely known and use, they belong to the PEMFC family [216], with the same kind of electrolyte [217], but they use methanol as the fuel instead of hydrogen or hydrogen-rich gas. As stated, this change of fuel (and the ‘Direct’ appellation in the acronym, as it will be explained later on in this section) implies another electrochemical reaction than in hydrogen-fed PEMFC [216]. Therefore, a fuel cell classification only based on the electrolyte type is not sufficient.

In addition, the reference [214] does not mention biofuel cells, which use the ability of microorganisms to extract energy from a range of chemical substrates [216]. Like other fuel cells, they contain porous electrodes to support the fuel transport to the catalyst reaction sites and a polymer electrolyte membrane or a salt bridge to separate the electrodes. Biofuel cells are however a category of fuel cells that employs biocatalysts such as microorganisms, for Microbial Fuel Cells (MFC), or enzymes, for Enzymatic Fuel Cells (EFC). Those fuel cells are thus identified based on their catalysts and not on their electrolyte.

Thus, except for biofuel cells (EFC and MFC) that are very specific (bio)technologies, another classification (which is novel, to the knowledge of the author) is proposed in this work, according to the charge carrier [218] (see Figure 18). Indeed, the charge carrier flows through the electrolyte from one electrode to the other and directly impacts the nature of the half-reactions involved in the redox process. Firstly, PEMFC (Proton exchange membrane fuel cell) [219], PAFC (Phosphoric Acid Fuel Cell) [213], MFC (Microbial Fuel Cell) [220], EFC (Enzymatic Fuel Cell) [221], the main type of DAFC (Direct Alcohol Fuel Cell) [222], DFAFC (Direct Formic Acid Fuel Cell) [205] and SOFC+ [223], also called SOFC-H [195] (Solid Oxide Fuel Cells with Proton Conduction), SOFC(H<sup>+</sup>) [224], H-SOFC [225], PCFC (Protonic Ceramic Fuel Cell) [226], PC-SOFC [227], P-SOFC [228] or H<sup>+</sup>-SOFC [229] all use hydrogen ions (protons) as charge carriers.

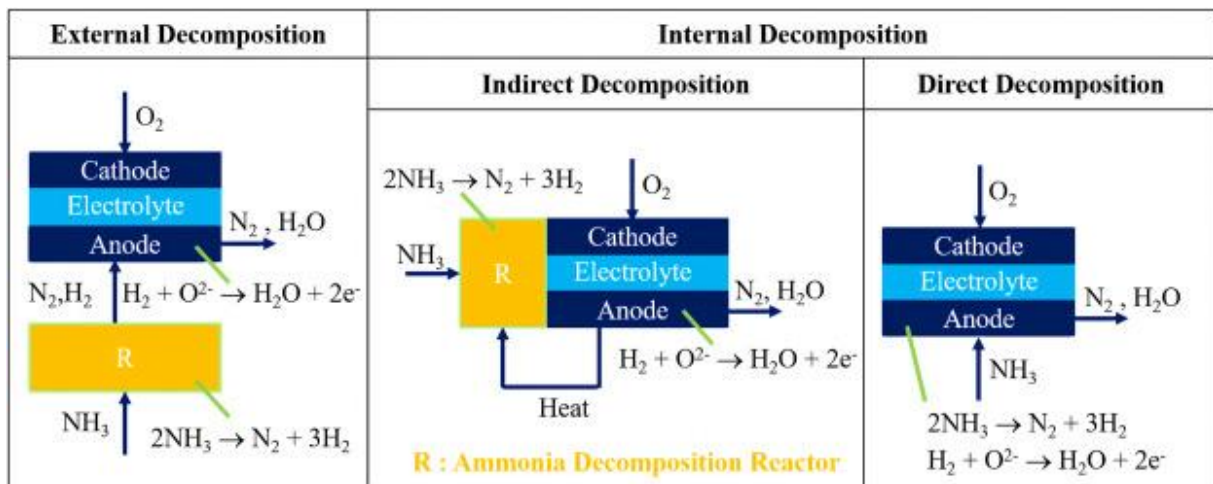
Secondly, SOFC- [223], also called SOFC-O [195] (Solid Oxide Fuel Cells with Oxygen Ion Conduction), SOFC(O<sup>2-</sup>) [224], O-SOFC [225] or O<sup>2-</sup>-SOFC [229] trivially use oxygen anions (O<sup>2-</sup>) as charge carriers such as (SO)DCFC (Solid Oxide Direct Carbon Fuel Cell) [230]. Thirdly, MCFC (Molten-Carbonate Fuel Cell) [205] and (MC)DCFC (Molten-Carbonate Direct Carbon Fuel Cell) [230] use carbonate anions (CO<sub>3</sub><sup>2-</sup>) as charge carriers. Lastly, (MH)DCFC (Molten-Hydroxide Direct Carbon Fuel Cell) [230] and AFC (Alkaline Fuel Cell) [213], which involve several fuel cell sub-types including the other main type of DAFC (Direct Alcohol Fuel Cell) [222], use hydroxide anions (OH<sup>-</sup>) as charge carriers.

It is noteworthy that DMFC (Direct Methanol Fuel Cell), DEFC (Direct Ethanol Fuel Cell) and DEGFC (Direct Ethylene Glycol Fuel Cell) are classified as DAFC (Direct Alcohol Fuel Cell), therefore including either H<sup>+</sup> or OH<sup>-</sup> as charge carriers (depending on their electrolyte configuration) [222].

As seen in Figure 18, it is worth mentioning that fuel cells with Na<sup>+</sup> (or even other ions, such as K<sup>+</sup> [231]) as charge carriers exist for the (A)DBFC, i.e. the (Alkaline) Direct Borohydride Fuel Cell, i.e. the DBFC that involves a cation exchange membrane [232]. Likewise, the DASFC, i.e. the Direct Alkaline Sulfide Fuel Cell, also use Na<sup>+</sup> as charge carrier [233]. The working principles of both those fuel cells will be later on developed (see the explanations relevant with Figure 16 and Figure 17).

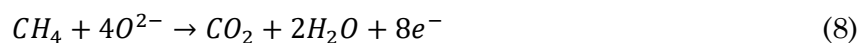
Since those sodium cations can also be used as charge carriers in fuel cell configuration close to the usual PEMFCs [234], those can sometimes more generally be reported as CEMFCs (Cation Exchange Membrane Fuel Cells), as opposed to AEMFCs (Anion Exchange Membrane Fuel Cell) [235], which are classified as the more recent type of AFCs, with a dedicated selective membrane similar to PEMFCs instead of the traditional liquid alkaline solution (generally potassium hydroxide) used as electrolyte [236,237]. As stated, AEMFCs are also known as SAFCs (Solid Alkaline Fuel Cells) [238,239]. As demonstrated in Figure 18, most CEMFC types also exist with their AEMFC version. However, although ammonium ions (NH<sub>4</sub><sup>+</sup>) have once been reported as a charge carrier for a particular type of CEMFC (not shown in Figure 18) [240], there is no reference about Direct Ammonia Fuel Cell (DAFC) involving a proton exchange membrane (with H<sup>+</sup> as charge carrier) as it exists as an AEMFC [195]. Also not shown in Figure 18 because there is no dedicated acronym for it (to the knowledge of the author), AEMFCs can simply be fed with hydrogen as fuel as in PEMFCs [241].

Depending on the fuel cell technology, the fuel can either participate directly as a reactant of the redox reaction at the anode or it can be used as an energy carrier, as ‘primary fuel’ [242], which is generally processed upstream of the stack and transformed into a what will be called a secondary fuel, usually hydrogen [243], that will participate in the anode reaction. This ‘secondary fuel’ (often hydrogen) generation can even occur directly at the anode catalyst and not necessarily in a dedicated upstream fuel processor (either internal or external to the fuel cell embodiment). For example, in ammonia-fed AFCs, which overall reaction is defined by Equation (5), ammonia directly reacts at the anode with the hydroxide ions that flowed through the membrane, while in ammonia-fed SOFCs, the fuel is usually thermally dissociated into hydrogen in the presence of a catalyst directly at the anode [195] and the overall fuel cell reaction is the same as Equation (4). As shown in Figure 15, this latter operation mode is called ‘direct’ and, thanks to the use of a specific multifunctional anode [244], does not require any ammonia decomposition reactor, whereas fuel cells with dedicated (external or internal) ‘indirect’ ammonia processors (hydrogen generators) also exist. The main difference between internal and external fuel processing reactors lies in the proximity of internal reactor with the fuel cell stack, conveniently allowing the exothermic fuel cell reaction to provide heat to the endothermic reactor, which makes for a simpler design and greater thermodynamic efficiency [244].



**Figure 15.** Operation mode of ammonia solid-oxide fuel cells. Similar definitions (‘Direct’, ‘Indirect’, ‘Internal’ and ‘External’ ‘Decomposition’) can be applied to other fuel cell types, such as PEMFC [245] and/or other fuels, such as methane [246] or methanol [245], for which the ‘Decomposition’ term might be expressed as ‘Conversion’ or ‘Reforming’. Reproduced from reference [244].

It is also possible for the fuel cell fuel to be simultaneously used as both a primary and a secondary fuel. For example, in direct-methane SOFCs, temperature at the anode is sufficient to crack the methane into hydrogen and carbon (direct decomposition), which can then be oxidized in the stack according to Equation (6) and Equation (7), but it can also be directly oxidized by the stack according to the ‘dry oxidation of methane’ defined by Equation (8) [247].



In addition, it is worth mentioning that the oxidation products ( $H_2O$  and  $CO_2$ ) from Equation (8) will also react directly at the anode with methane following the ‘steam reforming reaction’ described by Equation (9) and the ‘dry reforming reaction’ described Equation (10) [246].



Those reactions, also reported as ‘direct internal reforming’ [248], generate hydrogen and carbon monoxide (called in this work ‘secondary fuels’), which can also be oxidized in the stack (and ‘provide electricity’) according to Equation (11) [247].



It is noteworthy that steam reaction defined by Equation (9) can also be completed to a low extent by Equation (12), called the ‘Water-Gas Shift’ (WGS) reaction (which is not an electrochemical oxidation that occurs on the anode stack and provide electrons) [249]:



Furthermore, since maintaining the required temperature gradients to achieve 100% of direct internal reforming is difficult with large SOFC stacks, a partial external pre-reforming stage can be used simultaneously with internal reforming [248], as it will be seen with the studied SOFC system in *Section 4.1.4 - Probable internal schemes*. Fuel cell – fuel processor [250] configuration possibilities as illustrated in Figure 15 are therefore numerous and can even be combined.

Thus, in the above definition and in all this work, the ‘primary fuel’ is the ‘chemical energy source’ that is provided externally to the fuel cell (or to the fuel cell system, i.e. the fuel cell – fuel processor embodiment [250]) and converted either into a secondary fuel or directly into electricity [251]. It must not be mistaken with by the term of ‘primary energy source’, which qualifies a natural resource (found ‘as-is’ in nature) [252].

Also, it should be highlighted that a ‘direct’ use of a fuel (in the fuel cell type acronym) can mean that it is used as a primary fuel and is involved in the overall fuel cell redox reaction, but it can also mean that it is decomposed ‘directly’ and internally at the anode (into secondary fuels) as illustrated in Figure 15. Indeed, for example, DAFCs (Direct Ammonia Fuel Cells) can either refer to the already mentioned ammonia-fed AFCs with direct involvement of ammonia in the overall fuel cell reaction [253] or to the ammonia-fed SOFC, shown in Figure 15, that directly and internally decompose the ammonia into hydrogen at the anode [223].

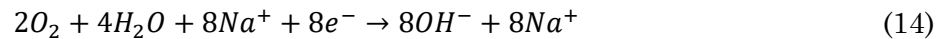
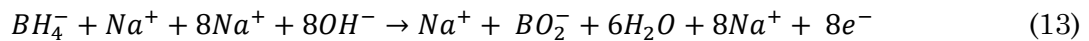
In the fuel cell types identification key of Figure 18, fuel cells that involve indirect or external decomposition of their primary fuel have not been presented. Only direct decomposition or direct electrochemical utilization possibilities are represented. Due to the plethora literature on fuel cells, it is likely that some types and/or other fuel cell types acronyms (which are listed in the *List of Abbreviations* at the beginning of this work) have been omitted in Figure 18.

Table 7 has been established to highlight (and compare) the characteristics the main fuel cell types usually reported in literature, also only including direct decomposition or direct electrochemical utilization of the specified fuel. Most of those types have been reported in Figure 18 but Table 7 also shows the characteristic of Microbial and Enzymatic Fuel Cells, i.e. EFCs and MFCs introduced earlier. One other crucial difference with the main reference [205] use to compute Table 7 is that it only considered the SOFC-O type of SOFCs and this work has added the SOFC-H type in the comparison.

It is noteworthy that another type of solid oxide fuel cell (SOFC) not reported in Figure 18 or in Table 7, known as a dual ion-conducting SOFC (D-SOFC) [228] or mixed-ion conducting SOFC [254], has gained significant interest recently. In this particular fuel cell, the electrolyte allows for the simultaneous diffusion of both oxygen ions and protons (and water is produced at both electrodes). These fuel cells have the potential to combine some advantages of both oxygen-ion conducting SOFCs (O-SOFCs) and proton-conducting SOFCs (P-SOFCs) [228]. SOFC are also sometimes segregated according to their working temperature levels without any explicit link to the fuel cell type and charge carrier, unlike for LT-PEMFC and HT-PEMFC, as shown in Table 7. Furthermore, there is no consensus about it as the working temperature of LT-SOFCs (Low Temperature Solid Oxide Fuel Cell) can either be reported in 200-400°C [255] or in the 400-600°C [256] whereas the working temperature of IT-SOFCs is either reported in the 400-600°C [255] or in the 600-800°C range [256]. This SOFC temperature classification will thus not be used in this work.

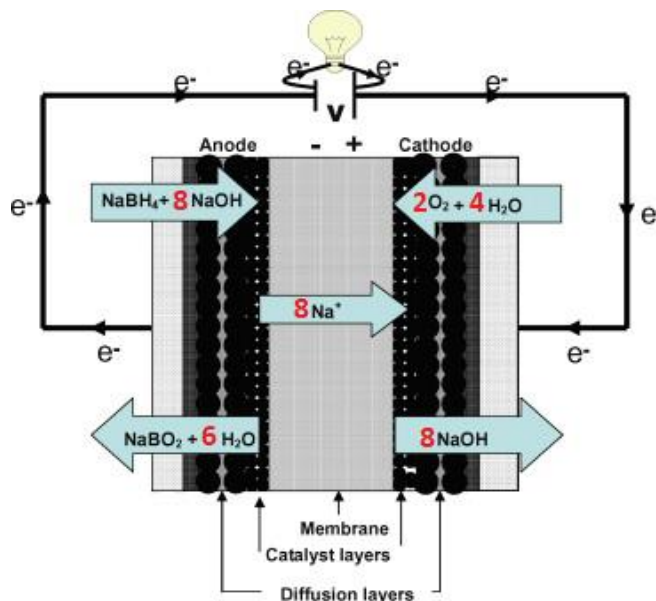
One fuel cell type that is neither reported in Table 7 nor in Figure 18 is the Metal-Air Fuel Cell, which is not exactly a fuel cell as it consumes its metallic anode (such as zinc, aluminium, or lithium) as a chemical energy storage, i.e. as a battery [201]. The active material of the anode being limited, the fuel cell stops when it is totally consumed. Other than this, Metal-Air Fuel Cell have the configuration of a regular fuel cell with traditional materials and use for the electrolyte and the cathode [201].

In all the fuel cell types reported in Figure 18, the DASFC and the (A)DBFC (with a cation exchange membrane) are quite interesting as they are the only type of fuel cell for which the charge carrier is directly involved in the electrochemical reaction at the electrode of the stack. Indeed, contrary to the other fuel cell types, the charge carrier (often  $\text{Na}^+$ ) is indeed neither produced onto the anode or onto the cathode. For example, for the (A)DBFC presented in Figure 16, the anode and cathode reaction are given respectively in Equation (13) and Equation (14):



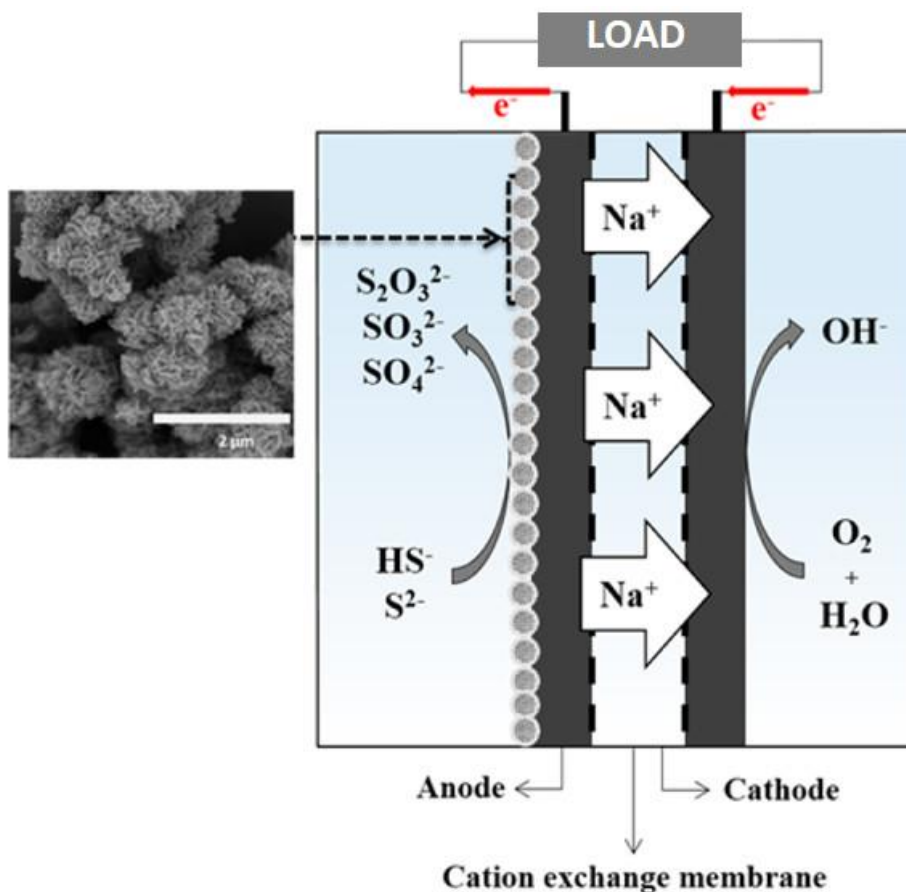
Indeed, in the overall fuel cell reaction defined by Equation (15) [257], the  $\text{Na}^+$  charge carrier does not appear (as it can be simplified, occurring at both sides of the equation) :





**Figure 16.** Working principle of an (A)DBFC, i.e. an (Alkaline) Direct Borohydride Fuel Cell. Reproduced and adapted from reference [232].

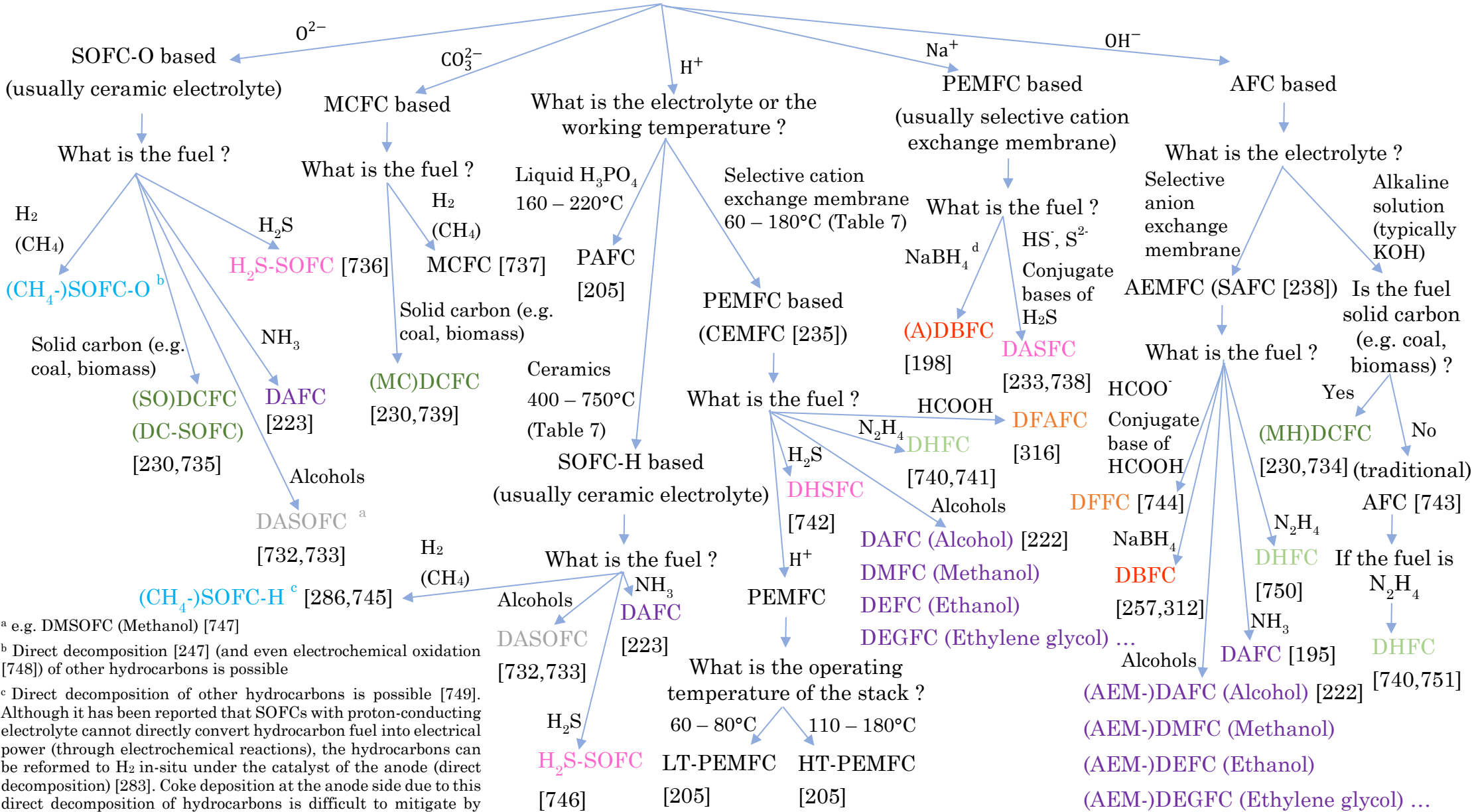
For information, the example of the DASFC is shown in Figure 17.



**Figure 17.** Working principle of the DASFC (Direct Alkaline Sulfide Fuel Cell). Similarly to the (A)DBFC case of Figure 16 and Equation (13) and Equation (14), an example of fuel compatible with such a DASFC is an alkaline sulfide solution composed of 1 mole of  $\text{Na}_2\text{S}$  and 3 moles of  $\text{NaOH}$  (in order to provide the  $\text{Na}^+$  charge carrier) [258]. Reproduced and adapted from reference [233].



### What is the charge carrier?



<sup>a</sup> e.g. DMSOFC (Methanol) [747]  
<sup>b</sup> Direct decomposition [247] (and even electrochemical oxidation [748]) of other hydrocarbons is possible  
<sup>c</sup> Direct decomposition of other hydrocarbons is possible [749]. Although it has been reported that SOFCs with proton-conducting electrolyte cannot directly convert hydrocarbon fuel into electrical power (through electrochemical reactions), the hydrocarbons can be reformed to H<sub>2</sub> in-situ under the catalyst of the anode (direct decomposition) [283]. Coke deposition at the anode side due to this direct decomposition of hydrocarbons is difficult to mitigate by oxidation since O<sup>2-</sup> is generally only supplied at the cathode side [282]. This is probably why no DC-SOFC with proton conducting electrolyte has been found in literature.

<sup>d</sup> Also exists with KBH<sub>4</sub> [231] (K<sup>+</sup> being the charge carrier)

**Figure 18.** Identification key of fuel cell types. Some fuel cells types acronyms have been linked through their font color because they either share the same acronym and/or they use the same (or a derivative) fuel. Microbial and enzymatic fuel cells have not been represented so as fuel cell involving indirect internal or external decomposition of their primary fuel into a secondary fuel consumed at the anode of the stack, as described in Figure 15.

Fuel cell type	Typical electrolyte <sup>a</sup>	Typical fuel	Typical catalysts <sup>b</sup>	Charge carrier	Major contaminants	Operation temperature (°C)	Specific advantages	Specific disadvantages	LHV Electrical efficiency (%)	Technological maturity (1-5) & Research activity (L-M-H) <sup>c</sup>
LT-PEMFC	Solid Nafion®, a polymer	H <sub>2</sub>	Anode: Platinum supported on carbon Cathode: Platinum supported on carbon	H <sup>+</sup>	Carbon monoxide (CO) <sup>d</sup> Hydrogen sulfide (H <sub>2</sub> S) <sup>d</sup>	60–80	Highly modular for most applications. High power density. Compact structure. Rapid start-up due to low temperature operations. Excellent dynamic response.	Complex water and thermal management <sup>d</sup> . Low-grade heat. High sensitivity to contaminants <sup>e</sup> and requires a CO remover in the (optional) hydrocarbons fuel processing [259]. Expensive catalyst. Expensive Nafion® membrane [260].	40-60 (with H <sub>2</sub> ) (Currently limited to 38.5 with CH <sub>4</sub> as some fuel needs to be burned to provide heat to a methane reformer [259])	A → changed from main reference [205] to 5 as commercial products are available [261] & H
HT-PEMFC	Polybenzimidazole, i.e. PBI, a polymer [262], doped in phosphoric acid (Main reference also mentioned Solid composite Nafion® [205]. Although other occurrences of that electrolyte type have been found [263], the most common one for HT-PEMFCs is PBI-based [264])	H <sub>2</sub>	Anode: Platinum–Ruthenium supported on carbon Cathode: Platinum–Ruthenium supported on carbon	H <sup>+</sup>	Carbon monoxide (CO) <sup>d</sup> Hydrogen sulfide (H <sub>2</sub> S) [265] <sup>d</sup>	110–180	Simpler water management (no need to humidify the phosphoric acid membrane to ensure its conductivity and therefore no need for reactant humidifiers as in LT-PEMFC [259,266], no liquid water to handle at those working temperatures [266]). Simpler thermal management. Accelerated reaction kinetics. High-grade heat. Higher tolerance to contaminants.  PBI membrane allows for 50% of cost reduction compared to Nafion® [260]. Does not require a CO remover in the (optional) hydrocarbons fuel processing as in LT-PEMFC [259].	Accelerated stack degradation (and short lifetime [267]). Humidification issues. Higher catalyst loading required [260] so even more expensive catalyst than LT-PEMFCs.	50–60 (Currently limited to 45 with CH <sub>4</sub> , as explained in <i>Section 3.2.5 - Current and expected performance of micro-CHP systems based on a PEMFC or a SOFC</i> . Requires a fuel reformer as in LT-PEMFCs)	3 (still big challenges to overcome before successful commercialization such as the thermal instability of the catalyst, for example [268]). See Table 8 for an history commercialization attempts of HT-PEMFC. & M

Fuel cell type	Typical electrolyte <sup>a</sup>	Typical fuel	Typical catalysts <sup>b</sup>	Charge carrier	Major contaminants	Operation temperature (°C)	Specific advantages	Specific disadvantages	LHV Electrical efficiency (%)	Technological maturity (1-5) & Research activity (L-M-H) <sup>c</sup>
MCFC	Liquid alkali carbonate (Li <sub>2</sub> CO <sub>3</sub> , Na <sub>2</sub> CO <sub>3</sub> , K <sub>2</sub> CO <sub>3</sub> ) in Lithium aluminate (LiAlO <sub>2</sub> )	CH <sub>4</sub>	Anode: Nickel Chromium (NiCr) Cathode: Lithiated nickel oxide (NiO)	CO <sub>3</sub> <sup>2-</sup>	Sulfides Halides	600–700	High electrical efficiencies. High-grade heat. High tolerance to contaminants. Possibility of internal reforming. Less strict material requirements than SOFC-O (allowed by lower working temperatures). Fuel flexibility. Inexpensive catalyst.	Slow start-up. Low power density. Electrolyte corrosion and evaporative losses. Corrosion of metallic parts. Air crossover <sup>e</sup> . Catalyst dissolution in electrolyte. Cathode carbon dioxide (CO <sub>2</sub> ) injection requirement (for the electrochemical reaction [269]).	55-65	4 & H
SOFC-O	Solid yttria-stabilized zirconia, i.e. YSZ, a ceramic	Hydrocarbons such as CH <sub>4</sub> [225,261]	Anode: Nickel–YSZ composite Cathode: Strontium-doped lanthanum manganite (LSM)	O <sup>2-</sup>	Sulfides (although SOFC fed by H <sub>2</sub> S exist with specific tolerant anode material [270])	800-1000 LT-SOFC-O are currently under study with co-doped (instead of single doped) ceria to enable the oxygen ion conductivity of the electrolyte at low-temperature range (300–600 °C) [271,272].	High electrical efficiencies. High-grade heat. High tolerance to contaminants. Possibility of internal reforming. Fuel flexibility. Inexpensive catalyst. Eliminated electrolyte issues (reference [205] probably meant simpler water management because SOFC can work at a perfect drying state whereas PEMFC electrolyte requires humidification [273,274]).	Slow start-up Low power density Strict material requirements High thermal stresses Sealing issues Durability issues High manufacturing costs (complexity of fabrication [275])	55-65 (Up to 74% gross DC electrical stack efficiency have already been measured, as explained in Section 3.2.5 - Current and expected performance of micro-CHP systems based on a PEMFC or a SOFC)	β → changed from main reference [205] to 5 as commercial products are available [261] & H

Fuel cell type	Typical electrolyte <sup>a</sup>	Typical fuel	Typical catalysts <sup>b</sup>	Charge carrier	Major contaminants	Operation temperature (°C)	Specific advantages	Specific disadvantages	LHV Electrical efficiency (%)	Technological maturity (1-5) & Research activity (L-M-H) <sup>c</sup>
SOFC-H	Perovskite ceramic electrolyte materials based on alkaline earth zirconate (BaZrO <sub>3</sub> , SrZrO <sub>3</sub> ) or alkaline earth cerate (BaCeO <sub>3</sub> , SrCeO <sub>3</sub> ) [229] SrCeO <sub>3</sub> , i.e. SCY, is reported as the most common [276]	Hydrocarbons such as CH <sub>4</sub> [225]	Various electrodes materials depending on electrolyte type [229,277]. Typically platinum electrodes are used for SCY electrolyte [276]	H <sup>+</sup>	Depends on the electrode's materials. Typically CO <sub>2</sub> and H <sub>2</sub> O for all the electrolytes reported in this table [278]. In addition to those contaminants, H <sub>2</sub> S poisoning of SOFC-H with similar electrolytes has been reported [279].	400-750 [275,278]. The ionic conductivity of the electrolyte of SOFC-H is indeed higher than for SOFC-O at those temperature levels [275].	Basically the same as SOFC-O [280] except that for SOFC-O, ionic conductivity comes from the oxide ions intrinsic to the electrolyte, whereas for SOFC-H, the electrolytes do not have structural protons [280] and their conductivity only appear after an 'hydration process' [281]. SOFC-H are thus not operated at a drying state. Also, the fuel flexibility is lowered as internal reforming is questionable [275] (coke formation from direct decomposition of hydrocarbons is a challenge [282] and their direct electro-chemical oxidation is unfeasible [283]). Water is formed at cathode rather than at the anode (as in SOFC-O), which avoids fuel dilution (higher fuel efficiency and less complex fuel recycling/recirculation, if implemented) [229].	Basically the same as SOFC-O but lower working temperatures, so quicker start-up, fewer thermal stresses, sealing issues, material requirements (cheaper interconnects, for example) [284], increased durability [275]. Complexity of fabrication remains high [275,285]. Low power density [286]: similar to SOFC-O (at least with CH <sub>4</sub> or H <sub>2</sub> ) [287,288]. Slightly lower in same operating conditions (above 800°C, with CH <sub>4</sub> ) [287] and theoretically slightly higher at low stack temperatures (i.e. 750°C) and low current densities (with H <sub>2</sub> ) [288]. Poor chemical stability of electrolyte in the presence of CO <sub>2</sub> and H <sub>2</sub> O [229]. Poor cathode activity (+ high cost and thermal expansion of Cobalt-containing cathodes) [289].	Theoretically 10-15 percentage points above corresponding SOFC-O in same operating conditions, whatever if the fuel is H <sub>2</sub> , NH <sub>3</sub> , CH <sub>4</sub> , methanol, ethanol [224,290–293]. However, many studies actually report it lower than SOFC-O considering irreversible losses (higher ohmic losses) [294]. For example, it was reported that the electrical efficiency of a SOFC-H was about 7 percentage points lower its corresponding SOFC-O with methane as fuel, i.e. respectively ±51% and ±58% [287].	2 & H

Fuel cell type	Typical electrolyte <sup>a</sup>	Typical fuel	Typical catalysts <sup>b</sup>	Charge carrier	Major contaminants	Operation temperature (°C)	Specific advantages	Specific disadvantages	LHV Electrical efficiency (%)	Technological maturity (1-5) & Research activity (L-M-H) <sup>c</sup>
PAFC	Concentrated liquid phosphoric acid (H <sub>3</sub> PO <sub>4</sub> ) in silicon carbide (SiC)	H <sub>2</sub>	Anode: Platinum supported on carbon Cathode: Platinum supported on carbon	H <sup>+</sup>	Carbon Monoxide (CO) Siloxane Hydrogen sulfide (H <sub>2</sub> S)	160–220	Technologically mature and reliable. Simple water management. Good tolerance to CO compared to PEMFC (>1% instead of a few ppm <sup>d</sup> , which does not require a CO remover in the hydrocarbons fuel processing) [295–297]. High-grade heat.	Relatively slow start-up. Low power density. High sensitivity to contaminants (other than CO [295–297]). <del>Expensive auxiliary systems</del> (no other occurrence of this element other than in the main reference [205] was found). Low electrical efficiencies. Relatively large system size. Electrolyte acid loss. Expensive catalyst. High cost.	36–45	5 & M
AFC	Potassium hydroxide (KOH) water solution  (Anion exchange membrane, i.e. AEM, a polymer [236])	H <sub>2</sub>	Anode: Nickel Cathode: Silver supported on carbon	OH <sup>-</sup>	Carbon dioxide (CO <sub>2</sub> )	Below zero–230	High electric efficiency due to fast reduction reaction kinetics. Wide range of operation temperature and pressure Inexpensive catalyst. <del>Catalyst flexibility</del> (no other occurrence of this element other than in the main reference [205] was found). Relatively low cost.	Extremely high sensitivity to CO <sub>2</sub> that consumes the electrolyte [298]. Pure oxygen (and hydrogen) are required for operation. Low power density. Highly corrosive electrolyte leads to sealing issues. Complex and expensive electrolyte management, especially for mobile applications (circulation of the liquid electrolyte required [299]).	60–70	5 & L
DMFC	Solid Nafion®, a polymer  (Anion exchange membrane, i.e. AEM, a polymer [222,236])	Liquid methanol–water solution	Anode: Platinum–Ruthenium supported on carbon Cathode: Platinum supported on carbon	H <sup>+</sup>	Carbon monoxide (CO)	Ambient-110	Compact size (small-scale systems possible). High fuel volumetric energy density. Easy fuel storage and delivery. Simple thermal management.	Low cell voltage and efficiency due to poor anode kinetics & Low power density. Lack of efficient catalysts for direct oxidation. Fuel and water crossover <sup>e</sup> . Complex water management. High catalyst loading & High cost. CO <sub>2</sub> removal system (produced CO <sub>2</sub> bubbles at the anode, reducing efficiency [300,301]). Fuel toxicity.  Fuel crossover <sup>e</sup> [302].	35–60	3 & H

Fuel cell type	Typical electrolyte <sup>a</sup>	Typical fuel	Typical catalysts <sup>b</sup>	Charge carrier	Major contaminants	Operation temperature (°C)	Specific advantages	Specific disadvantages	LHV Electrical efficiency (%)	Technological maturity (1-5) & Research activity (L-M-H) <sup>c</sup>
DEFC	Solid Nafion®, a polymer (Anion exchange membrane, i.e. AEM, a polymer [222,236])	Liquid ethanol–water solution	Anode: Platinum–Ruthenium supported on carbon Cathode: Platinum supported on carbon	H <sup>+</sup>	Carbon monoxide (CO)	Ambient-120	Compact size (small-scale systems possible). High fuel volumetric energy density. Easy fuel storage and delivery. Simple thermal management. Common biofuel. Relatively low fuel toxicity. Slightly higher gravimetric energy density than methanol.	Low cell voltage and efficiency due to poor anode kinetics. Low power density. Lack of efficient catalysts for direct oxidation of ethanol. Fuel and water crossover <sup>e</sup> . High sensitivity to carbon monoxide (CO). High cost. CO <sub>2</sub> removal system (produced CO <sub>2</sub> bubbles at the anode, reducing efficiency [301]).	20-40	2 & L
DEGFC	Solid Nafion®, a polymer (Anion exchange membrane, i.e. AEM, a polymer [222,236])	Liquid ethylene glycol	Anode: Platinum supported on carbon Cathode: Platinum supported on carbon	H <sup>+</sup>	Carbon monoxide (CO)	Ambient-130	Compact size. High fuel volumetric energy density. Easy fuel storage and delivery. Simple thermal management. Simple water management. Low volatility due to low vapor pressure and high boiling point. Existence of distribution infrastructure.	Low power density. Low cell voltage and efficiency due to poor anode kinetics. Lack of efficient catalysts for direct oxidation of ethylene glycol. Low fuel gravimetric energy density. Durability issues. High cost. Fuel crossover <sup>e</sup> . CO <sub>2</sub> removal system (produced CO <sub>2</sub> bubbles at the anode, reducing efficiency [301]).	20-40	2 & L

Fuel cell type	Typical electrolyte <sup>a</sup>	Typical fuel	Typical catalysts <sup>b</sup>	Charge carrier	Major contaminants	Operation temperature (°C)	Specific advantages	Specific disadvantages	LHV Electrical efficiency (%)	Technological maturity (1-5) & Research activity (L-M-H) <sup>c</sup>
MFC	Proton exchange membrane such as Nafion® [303], a polymer	Any organic matter (e.g., glucose, acetate, wastewater)	Anode: Biocatalyst (enzyme-based catalyst produced by microorganisms [304]) supported on carbon Cathode: Platinum supported on carbon	H <sup>+</sup>	Bacterial contamination of cathode (since bacteria are generally required for the anode reaction [303])	20-60	Fuel flexibility. <del>Biocatalyst flexibility</del> [205] → Potential use of biocatalysts (bacteria) [304]. No need for enzymatic catalysts isolation (from poisoning elements), extraction, and preparation as in enzymatic fuel cells [304]. Relatively higher lifetime for biocatalysts (than enzymatic catalysts [304]). Self-regeneration capacity of biocatalysts [305]. Ability to run (and treat) on wastes and wastewater (bioelectricity generation and pollutant removal) [303,305].	Direct electron transfer from the microorganisms to the anode is inefficient [306] and the inclusion of a mediator <sup>f</sup> can be required [307]. Relatively low energy density (microorganisms include living functions). Low columbic efficiency <sup>g</sup> . Very low power density. Inflexible operation conditions.	Coulombic efficiency: 15–65 <sup>g</sup>	1 & M
EFC	Membrane-less	Organic matters (e.g., glucose)	Anode: Biocatalyst (enzyme-based catalyst occurring as isolated proteins [304]) supported on carbon Cathode: Biocatalyst supported on carbon	H <sup>+</sup>	Foreign physical and/or chemical exposure to enzymatic catalyst	20-40	Capacity for miniaturization (e.g., for implantable medical micro-scale sensors and devices). Structural simplicity. High response time. Although EFC fuel flexibility is lower than MCF, currently glucose and alcohols (a single enzyme is not able to catalyze all the steps necessary for the complete conversion of some hydrocarbons [304]), some applications of bioelectricity generation through organic wastes treatment are starting to be reported [308].	Rapid decay of enzymatic catalyst due to operation in foreign environment. High susceptibility to enzymatic poisoning. Direct electron transfer from the protein matrix of the enzymes to the anode is not easy and the inclusion of a mediator <sup>f</sup> can be required [309]. Immobilizing the enzymes is problematic. Low power density. Very low columbic efficiency <sup>g</sup> . Inflexible operation conditions.	Coulombic efficiency: 30 <sup>g</sup>	1 & M

Fuel cell type	Typical electrolyte <sup>a</sup>	Typical fuel	Typical catalysts <sup>b</sup>	Charge carrier	Major contaminants	Operation temperature (°C)	Specific advantages	Specific disadvantages	LHV Electrical efficiency (%)	Technological maturity (1-5) & Research activity (L-M-H) <sup>c</sup>
DCFC	Solid yttria-stabilized zirconia, i.e. YSZ, a ceramic  (Molten carbonate)  (Molten hydroxide)	Solid carbon (e.g., coal, coke, biomass)	Anode: Graphite or carbon-based material Cathode: Strontium-doped lanthanum manganite (LSM)	O <sup>2-</sup>	Ash Sulfur	600–1000	High electrical efficiency. High volumetric energy density. Fuel flexibility. No PM, NO <sub>x</sub> , or SO <sub>x</sub> emissions (that would have occurred in the combustion of solid carbon fuel). Structural simplicity. High capacity for carbon capture (SDFCs produce almost pure CO <sub>2</sub> at the anode without including a CO <sub>2</sub> separation process [310]).	<del>Carbon dioxide (CO<sub>2</sub>) emissions</del> (as in the other fuel cell types that use fossil fuels). Rapid material corrosion and degradation. Durability issues. Sensitivity to fuel impurities. Low power density.	70–90	2 & L
DBFC	Solid Nafion®, a polymer  (Anion exchange membrane, i.e. AEM, a polymer [311,312])	Liquid sodium borohydride (NaBH <sub>4</sub> )	Anode: Gold, silver, nickel, or platinum supported on carbon Cathode: Platinum supported on carbon	OH <sup>-</sup>	N/A	20-85	Compact size. High fuel utilization efficiency. High fuel gravimetric hydrogen content. <del>No carbon dioxide (CO<sub>2</sub>) emissions</del> (as in other fuel cell types that use renewable fuels). Low fuel toxicity.	Fuel crossover <sup>e</sup> . High cost. Low power density. Lack of analytical modelling techniques due to unprecise (quite complex) reaction mechanisms [313] <sup>h</sup> . Expensive catalyst. Chemical instability of membrane and catalyst. Inefficient cathodic reduction reaction. Inefficient anodic oxidation reaction due to the unwanted hydrolysis parallel reaction of borohydride anions into hydrogen at the anode (reducing efficiency and power density) [313]. This hydrolysis reaction consumes the borohydride fuel without liberating electrons.	40–50	2 & M



Fuel cell type	Typical electrolyte <sup>a</sup>	Typical fuel	Typical catalysts <sup>b</sup>	Charge carrier	Major contaminants	Operation temperature (°C)	Specific advantages	Specific disadvantages	LHV Electrical efficiency (%)	Technological maturity (1-5) & Research activity (L-M-H) <sup>c</sup>
DF AFC	Solid Nafion®, a polymer	Liquid formic acid (HCOOH)	Anode: Palladium or platinum supported on carbon Cathode: platinum supported on carbon	H <sup>+</sup>	Carbon monoxide (CO)	30–60	High fuel utilization efficiency and higher conversion efficiency than DMFC, DEFC and DEGFC [314]. Limited fuel crossover <sup>e</sup> . Easy fuel storage and delivery (+ non-flammability of the fuel [315]). High power density. No water is neither required for the anodic nor for the cathodic reaction [316] (unlike direct alcohol fuel cells such as DMFC, DEFC, DEGFC, <i>etc</i> [222]). Compact size and structural simplicity.  Higher electromotive force than PEMFC [218], DMFC, DEFC and DEGFC [314].  High capacity for carbon capture (CO <sub>2</sub> is normally the only product of the reaction in the off-anode gases of DF A FCs, which offer the potential for a carbon-neutral cycle where CO <sub>2</sub> is transformed back into formic acid through an electrolyser [317]).	Fuel toxicity Components corrosion issues. Low fuel gravimetric and volumetric energy density. High fuel cost. <del>Low temperature operation</del> (Low-grade heat).  Poor anode kinetics [318] but still higher than DMFC [318,319].  CO <sub>2</sub> removal system (produced CO <sub>2</sub> bubbles at the anode, reducing efficiency [320]).	30–50	1 & L

<sup>a</sup> Nafion® was developed by E.I. DuPont de Nemours and Company in the 1960s as a solution to the need for a stronger cation exchange membrane for the electrochemical production of chlorine and sodium hydroxide. Nafion®s became the preferred membrane for both PEMFCs and DMFCs in the 1990s. Its chemical stability was greatly enhanced by the perfluorination of its polymer backbone [321].

<sup>b</sup> Supported catalysts are created for various reasons, such as reducing the amounts of precious metals required for the same catalytic activity. Catalytic activity (or selectivity) may even be enhanced by the metal dispersion on the support and the interaction between the two. Additionally, supported catalysts may be more stable than bulk catalysts, as they tend to sinter at a slower rate (due to altered solid-state chemistry, i.e. its crystal or non-crystal configuration) and may be less susceptible to poisoning [322].

<sup>c</sup> 1 and 5 are respectively the lowest and highest level of technological maturity. L, M, H respectively mean Low, Medium and High level of research activity.

<sup>d</sup> PEMFC contaminants, heat and water management have been discussed in *Section 5.1.4.2 - PEMFC module internal configuration* and in *APPENDIX 14: Literature review on PEMFC degradation mechanisms*

<sup>e</sup> Gas (Air, fuel, water, *etc*) crossover is related to the passing of some of the specified molecules through the electrolyte without participating in the electrochemical reaction, which can instead lead to direct (exothermic) combustion of the fuel, which then reduces the efficiency and endangers the fuel cell by generating local hot spots [296,323]. Gas crossover (for PEMFCs) will be discussed in more details in *APPENDIX 14: Literature review on PEMFC degradation mechanisms*.

<sup>f</sup> In mediator MFC, some mediators (added artificially or naturally secreted [324]) are used to transfer electrons from the microorganisms to the anode electrode. Examples of such mediators are thionine, methyl blue, neutral red, humic acid, and methyl viologen [303]. The purpose of the (also optional) mediator in EFC is the same as the one stated here above for mediator MFC<sup>f</sup>. Hydroquinone, benzoquinone, and ferricyanide salt are typical EFC mediators [309].

<sup>g</sup> Coulombic efficiency is defined as the efficiency of the charge/electrons transfer, at the electrode [325], not to be confused with the overall energy efficiency, which includes other losses, such as heat dissipation) [326,327].

<sup>h</sup> Cation borohydride fuel cells complex working principles is illustrated in Figure 16.

**Table 7.** Comparison between main fuel cell types characteristics. Not all the fuel cell types mentioned in Figure 18 are reported in this table. For one fuel cell type, several electrolytes and fuels can be mentioned, the first one being the most common. All the other characteristics (other columns), especially the electrical efficiency, refer only to the first electrolyte and to the first fuel reported (if not explicitly specified). Main parts of this table are reproduced, adapted or corrected (by the use of a strikethrough font) from reference [205]. Additional elements from other sources are directly referenced in the table.

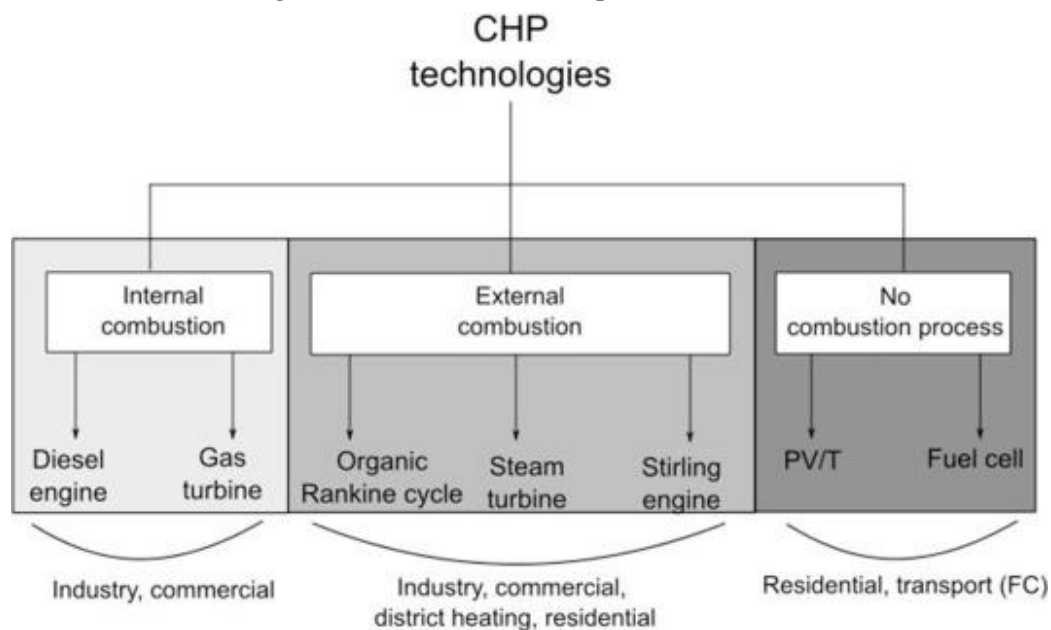
Now that the notion of fuel cell has been presented and that the fuel cell types have been described, the aim of the following section is to focus on the heat and power cogeneration market (CHP). First, the notion of micro-CHP is defined and the fuel cell types currently considered on CHP markets are introduced, with an emphasis on the residential market, which is later on described regionally. This section then investigates why the only fuel cell technology available on the micro-CHP market are O-SOFC and LT-PEMFC (Low Temperature PEMFC), i.e. why HT-PEMFCs (High Temperature PEMFCs) applications have never been successful on the micro-CHP market. A focus is then brought on the systems currently available on the European market. At last, the latest most remarkable achievements regarding the industries of PEMFC and SOFC-based CHP have been reported as well as the expected and hoped performance that those systems could offer in a mid-term future. Most of the content of this section is currently under review in the *Progress in Energy* journal [328].

## 3.2 Micro-cogeneration fuel cells systems and markets

### 3.2.1 Definitions and commercial fuel cell-based micro-CHP technologies

First of all, according to the Directive 2012/27/EU of the European Parliament, cogeneration (CHP) systems can be classified in three categories depending on their maximum electrical capacities, namely ‘micro-cogeneration’ (micro-CHP or  $\mu$ CHP) if fewer than 50 kW<sub>el</sub>, ‘small scale (or mini) cogeneration’ if ranging from 50 kW<sub>el</sub> to 1 MW<sub>el</sub>, and ‘cogeneration’ if higher than 1 MW<sub>el</sub> [329]. However, there is no consensus about those definition and academic literature sometimes limits the range of micro-CHP to a single dwelling, i.e. approximately 10 kW<sub>el</sub> [330], or even lower to 5 kW<sub>el</sub> [331,332], and the mini-CHP to a group of dwellings or a commercial site, i.e. 100 kW<sub>el</sub> [330], or even lower to 15 kW<sub>el</sub>, the mid-scale CHP and small-scale cogeneration being defined respectively on the 15-50 kW<sub>el</sub> and the 50-2000 kW<sub>el</sub> ranges [332].

An overview of the main existing CHP technologies is provided in Figure 19, the fuel cells being integrated in the ‘No combustion process’ segment of the classification and being the only one of those technologies suited for the transportation sector.



**Figure 19.** Main CHP technologies and their fields of applications. PV/T stands for photovoltaic hybrid technologies. Reproduced from reference [329].

Indeed, the interest for fuel cell technology in vehicle powertrains for a variety of transportation vehicles is growing, such as for boats, submarines, cars, buses, wheelchairs, airport vehicles, pallet trucks, forklifts, lawn maintenance vehicles, small military or unmanned vehicles, small aircraft, and other modes of transport [200]. However, the most significant fuel cell applications today are in building and off-grid power supply, as measured by the number of devices installed [200]. Fuel cells for stationary applications such as micro-cogeneration have been commercially available for more than 20 years, and can function as a backup power generator or as a standalone system that requires an alternate energy source during peak times (such as batteries, supercapacitors or a combination of both, for example) [200]. Fuel cells can also be connected to photovoltaics, batteries, capacitors, or wind turbines in hybrid energy systems [200].

As demonstrated in the previous section, numerous fuel cell technologies are currently being researched and developed for various applications, but only a few are suitable for micro-CHP systems. In order to be viable for this purpose, the fuel cell stack must be capable of being manufactured at a low cost and have a long operating lifetime, even in less-than-optimal conditions, particularly when dealing with impurities in the hydrogen fuel [206]. Safety, practicality, and cost-effectiveness are also important considerations, favoring technologies that are well-established, commercially demonstrated, and offer high operating efficiency [206].

Four fuel cell technologies, namely polymer electrolyte membrane (PEFC), i.e. PEMFC (both LT-PEMFC and HT-PEMFC), oxygen-ion solid oxide fuel cells (SOFC-O), phosphoric acid fuel cells (PAFC), and alkaline fuel cells (AFC), are or have been considered for micro-CHP applications [329]. Proton-conducting SOFC (SOFC-H) and more generally IT-SOFC (Intermediate Temperature Solid Oxide Fuel Cell) they are usually considered to be part of [286], are still under study and not currently considered in this work as a mature CHP technology. Indeed, their electrolyte, anode and cathode materials need to be developed to obtain good power density and make their commercialization viable [286]. Their commercialization is particularly limited by their cathode as it traditionally exhibits poor activity or high thermal expansion (and high cost) [289]. Furthermore, SOFC-H are reported to imply high manufacturing costs and scaling-up difficulties that also impede their commercialization [285].

Despite being developed earlier than PEMFC and SOFC, PAFCs and AFCs, have not attracted substantial commercial interest due to high manufacturing costs and low lifetimes, respectively [206]. Although no notable products have been developed for the domestic CHP market using these technologies, they possess many desired characteristics (sometimes with even better performance than PEMFC CHP systems [333]) and have been demonstrated or modelled at the 1-10 kW<sub>el</sub> scale (with hydrogen) as CHP units in previous studies [333,334]. It is noteworthy that PAFCs have been installed in large commercial and industrial applications for decades [335–337]. For instance, one commercial example as an electrical power output in the 100-400 kW<sub>el</sub> range [336]. This is not the case of AFCs [335,337], probably because of their CO<sub>2</sub> intolerance and their required pure oxygen feed (Table 7), although cost effective removal apparatus could and can be achieved [337].

Therefore, the only fuel cell technologies currently commercialized as micro-CHP (residential cogeneration) are PEMFC (mostly LT-PEMFC) and SOFC-O. In fact, as it will be demonstrated here below, to the knowledge of the author, no HT-PEMFC system for residential micro-CHP applications is currently available on the market and only a few of those have ever been (or close to be) commercialized (see Table 8). Indeed, micro-CHP HT-PEMFC systems (based on PBI electrolyte as reported in Table 7) have been reported to be commercially available in the near-term, their short lifetime being its main issue [267]. Also, a few of the remaining challenges that hinder HT-PEMFC commercialization have been detailed in a recent publication (such as the thermal instability of the catalyst) [268].

### 3.2.2 Status of commercialized HT-PEMFC-based micro-CHP systems

One of those HT-PEMFC CHP system is denominated as 'Enerfuel' (natural gas fed, 3 kW<sub>el</sub> of power output and 3 kW<sub>th</sub> of heat rate output) [338]. Three other commercial models manufactured by this 'Enerfuel' company, based in Florida [339], were reported without mentioning any heat rate output (nor explicit mention of a CHP application). The first one is also denominated 'Enerfuel' (natural gas fed and 9 kW<sub>el</sub> of power output [340]). The other two are denominated 'Flexsys 036' (power output of 1.3 kW<sub>el</sub> on hydrogen and 1 kW<sub>el</sub> on reformat) and 'Flexsys 132' (power output of 4.5 kW<sub>el</sub> on hydrogen and 3 kW<sub>el</sub> on reformat) [341]. Although a few other references of that HT-PEMFC manufacturing company have been found [339,342], the website sources they are reporting (and the one of the 'Enerfuel' company) are no longer available and no product datasheet has been found. However, no reference of that company being liquidated or renamed has been found either. In addition, this company seems to be more active developing HT-PEMFCs for the transportation sector [339,341,343,344].

Another HT-PEMFC CHP system, from the German company named 'Elcore' [345], is denominated as 'Elcore (Nex 2400)' or 'Elcore 2400' (0.3 kW<sub>el</sub> of power output and 0.6 kW<sub>th</sub>) [338,345,346]. This HT-PEMFC CHP system was involved in the 'ene.field' European Union project that aimed to demonstrate through field-test installations and monitoring in real applications the capability of fuel cell products to reach a commercial mass market [347]. However, the company has been liquidated in 2017 [348] and is no longer part of the 'PACE' (Pathway to a Competitive European Fuel Cell micro-CHP Market) project [261], the EU successor of 'ene.field' [347]. The Elcore company was finally taken over by the 'Freudenberg Group', which initially committed to keep selling the 'Elcore 2400' micro-CHP [348]. However, it is no longer the case. Indeed, the only fuel cell products the 'Freudenberg Group' is manufacturing are destined to the heavy-duty transportation sector (<https://www.fst.com/fuel-cell>). This is confirmed by the fact that the Freudenberg Group indicated in their 2019 annual report regarding the acquisition of 'Elcore' that the 'goal is the market launch of electric and fuel cell drive systems for heavy-duty vehicles, buses, trains and ships', without mention of stationary CHP applications [349]. In addition, according to a German forum website, the 'Elcore 2400' product was taken out of the market because of many flows : stack core to be changed between 2 and 4 times a year, reduced performance over time, sealing issues, *etc* [350]. The 'Elcore' systems were apparently sold for parts in public auctions sometimes for less than 350 € [350].

There is a few references of a HT-PEMFC CHP system named 'PureCell Model 5' or 'ClearEdge5' (5 kW<sub>el</sub> power output and approximately 5.9 kW<sub>th</sub> of heat rate output [343]) by the 'ClearEdge Power' company (formerly UTC Power [351]) in California [266,341,343]. Clearedge however declared bankruptcy in 2013 and was then bought by 'Doosan' (Korea) [351]. According to their website (<https://www.doosanfuelcell.com/en>), Doosan seems to only sell large-scale CHPs based on a PAFC fed by natural gas, i.e. the 'PureCell Model 400' (400 kW<sub>el</sub> power output) [352]. That system was even initially launched on the market by the predecessor of 'ClearEdge', i.e. UTC Power [353]. It was however reported that micro-CHP systems based on HT-PEMFC are still under development at the 'Doosan' company [354].

One reference was found about an HT-PEMFC CHP system named 'JxEneos' [266], but it is probably a mistake since it is reported as a SOFC by other sources [355,356]. Furthermore, it has been reported that JX Eneos (and Kyocera, another fuel cell manufacturer) concluded that the future of fuel cells in domestic built environment applications lies with SOFCs, and have therefore stopped PEMFC development [356].

Many references mentioned the 'Gensys Blue' (sometimes just referred as 'Gensys') HT-PEMFC CHP system, developed by the 'Plug Power' company in the US, with different reported power outputs (up to 3 kW<sub>el</sub> [356] or up to 8 kW<sub>el</sub> [266]). The most trusted sources

report however a power output in the 0.5-5 kW<sub>el</sub> range [338,343,344,357–360], with a heat rate output close to 9 kW<sub>th</sub> [338,359]. Although ‘Plug Power’ sold many stationary LT-PEMFC systems under the named ‘Gensys’ [361] mainly for off-grid power sources applications [359,362] (with a capability of working as a CHP unit and delivering heat [363]), the HT-PEMFC ‘Gensys Blue’ system was only under field trials between the years 2009 and 2012 [344,357,360] but never made it to the market as ‘Plug Power’ gave a ‘No-Go’ to the project back in 2012 [357].

It worth mentioning that a study reported that the ‘Dantherm’ Danish company was still developing a micro-CHP system based on a HT-PEMFC [364] with no indication about its potential commercialization.

Also, one study [343] reported that the ‘Serenus 166 air C v2.5’ and the ‘Serenus 390 air C v2.5’ were HT-PEMFC CHP units nominally producing 1 and 3.5 kW<sub>el</sub>, respectively. Their Original Equipment Manufacturer (OEM) was called ‘Serenergy’, a Danish company that merged in 2021 with others and is now named ‘Advent Technologies’, which is based in the US [365]. However, those units are just fuel cell stack modules, not commercialized directly as CHP units and must be integrated with other features since they require a pure hydrogen fuel (i.e. a fuel processor) and since they are simply air cooled (no dedicated heat recovery system) [344,366]. Furthermore, OEM (Original Equipment Manufacturer) integrators mostly use those systems in transportation applications [344]. According to their website (<https://serene.advent.energy>), the company no longer commercializes those systems but now sells methanol fed HT-PEMFC systems, not for CHP but for transportation or backup power applications [341,367].

That information have been summed up in see Table 8.

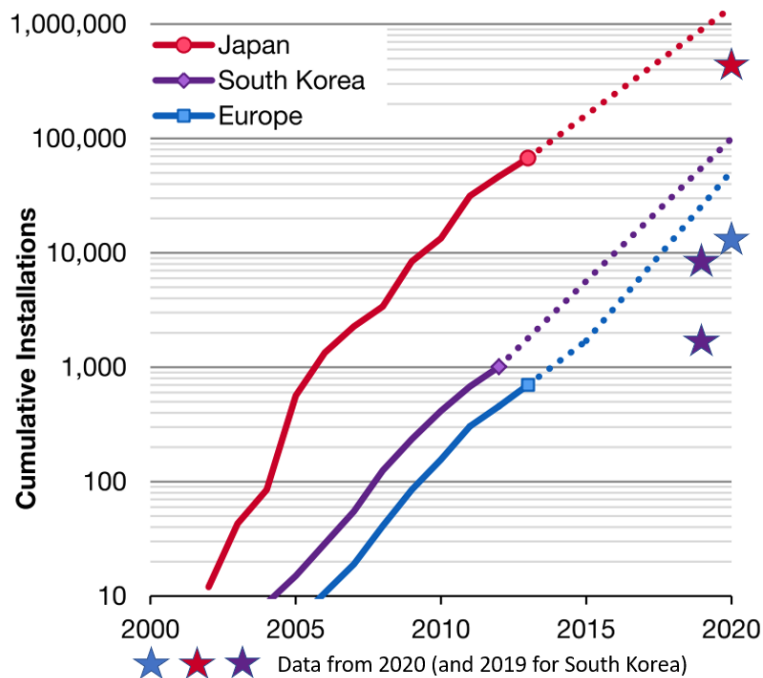
<b>Name of the HT-PEMFC CHP system commercial attempt</b>	<b>Current status of the product or of its manufacturing company</b>
Enerfuel by Enerfuel	Websites not available (even the one of the manufacturing company). Seems that the Enerfuel company focuses on the transportation sector.
Elcore by Elcore	Elcore company declared bankruptcy in 2017. The Freudenberg company that has taken over stopped the commercialization of HT-PEMFC CHP products (probably because many flows have been reported on the Internet about the product).
PureCell by ClearEdge	ClearEdge company declared bankruptcy in 2013. The Doosan company that has taken over stopped the commercialization of HT-PEMFC CHP products (only sells industrial-scale PAFC CHP systems).
Gensys Blue by Plug Power	Only field trials, never made it to the market. Plug Power gave a No-Go on the project back in 2012.

**Table 8.** List of HT-PEMFC commercialized micro-CHP products and their current availability status.

### 3.2.3 Main fuel cell-based micro-CHP markets

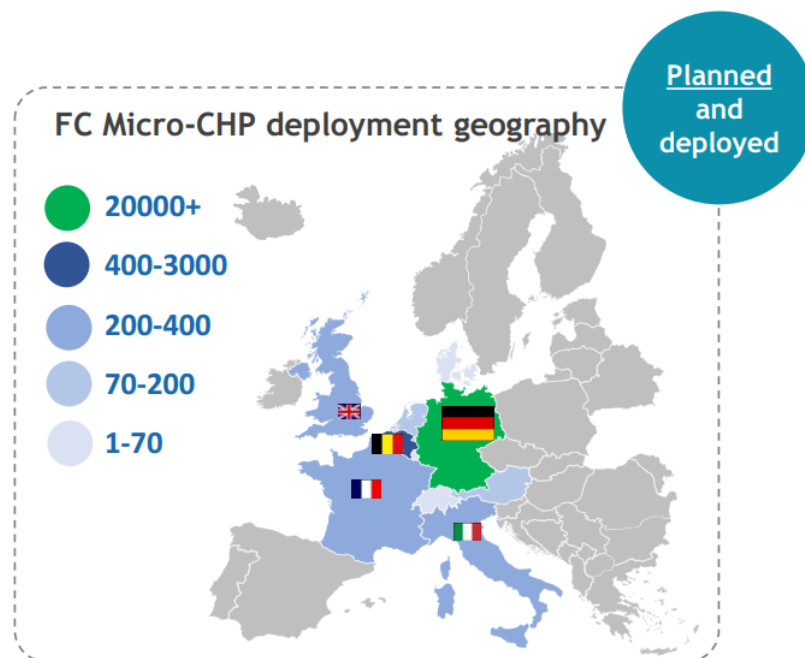
For the residential micro-CHP applications, Europe and Japan are leading the market, thanks to ad hoc-aimed subsidies and programs [335]. In fact, as it can be seen in Figure 20, Japan is the main leader in fuel cell-based micro-CHP unit installations, thanks to the financial support of the ‘ene.farm’ public program. The overall installations can be counted for 360000 units in 2020; almost 62% of them are PEMFCs and 38% are SOFCs [335]. That repartition can be questioned as another reference mentioned that only about 7% of Japan’s systems were SOFC in 2016 [368]. As comparison, about 10000 units have been installed at the time in Europe (in 2020) [335], mostly in Germany [369] (as it also shown in Figure 21).

South Korea is also a significant market for residential micro-CHP through large-scale field trials [206,370]. Indeed, about 1000 micro-CHP PEMFC-based systems were already installed back in 2011 [355,368]. As it is also indicated in Figure 20, it has been reported in 2013 that the South-Korean government had initially set a target of 100000 micro-CHP systems by 2020 [371]. However, the stationary fuel cell market in Korea is actually rather dominated by utility-scale units [369,372] (mainly with PAFCs and MCFCs [335]). That target was also too ambitious as it has been reported that ‘the residential and commercial fuel cell markets in Korea have not been so successful and stand in contrast to Japan’s success in these sections of the market’ [372]. According to a survey conducted by the Korea Energy Agency in 2019, the consumer satisfaction rate of residential and commercial fuel cell systems was only of 10.6% because of quality concerns, but mainly because of high city gas utility prices [372]. Therefore, in 2019, only 1.6 MW<sub>el</sub> of stationary fuel cell in the residential sector has been reported [372] while this number is sometimes considered at 7.1 MW<sub>el</sub> for ‘fuel cell for domestic buildings’ in general (and not only residential micro-CHP) [372,373], therefore probably including also commercial buildings and even exportations [372–374]. Those two boundary figures explains the two ‘stars’ attributed in Figure 20 for the 2019 data for South Korea, considering an average power output of 1 kW<sub>el</sub> for those fuel cell power generation units (which corresponds to the 2011 power output average of single units [355,368]).



**Figure 20.** Cumulative number of residential micro-CHP systems installed (solid lines) and near-term projections (dotted lines) reported in 2015. Reproduced and adapted from reference [266] with 2020 data for Japan and Europe [335] and 2019 data for Korea [372,373].

Figure 20 illustrates a consistent trend of market sizes approximately doubling annually [370]. However, around 2012, there was a noticeable deviation from this trend. Effective installations, while still exhibiting significant market growth, fell marginally short of projected expectations, particularly in the South Korean market. In response, it is worth mentioning that the Korean government has decided to offer a separate price for natural gas used in all power generation fuel cells (with a 6.5% reduction) [372]. Indeed, South Korea has still extremely high targets regarding power generation fuel cells: 2.1 GW<sub>el</sub> to achieve by 2040 for ‘fuel cell for domestic buildings’ in general and 15 GW<sub>el</sub> for utility fuel cell power plants, including exportations, while those figures were respectively reported to 7.1 and 370 MW<sub>el</sub> in 2019 [372–374]. Likewise, Japan remains ambitious as well as it has as goal to install 5.3 million of fuel cell micro-CHP systems by 2030, covering 10% of Japanese homes [371]. At last, it has been reported that Europe aims to reach a capacity of 10000 systems per year by 2021 [371,375], then to achieve (and stabilize), in its ‘expected scenario’, a capacity of about 3 million of micro-CHP installation in the residential sector in 2030 [376]. Those micro-CHPs would be mostly represented by fuel cells to meet the ‘EU Energy Goals 2030’ [377] and would correspond to a cumulative amount of about 15 million of installations by 2030 [376].



**Figure 21.** Status of the fuel cell micro-CHP European market in the countries involved in the PACE European Union project. That program aimed to demonstrate through field-test installations and monitoring in real applications the capability of fuel cell products to reach a commercial mass market [347]. Reproduced slide from the Final Conference of the PACE program (26<sup>th</sup> April 2023) [378].

Despite all this, it is often reported that the role of stationary fuel cell systems using natural gas will remain marginal and only rely on government support unless there is significant improvement on affordability [379]. Indeed, Europe for example is targeting a decrease of fuel-based micro-CHP systems investment costs from around 17 k€/kW down to 3.5 k€/kW in 2030 [380]. Japan on the other hand no longer gives subsidies for PEMFC-based micro-CHPs [371] while they have reached a cost of about 6.3-8.5 k€/kW [335,381], which corresponds to payback periods of 7–8 years, thanks to a learning rate of 16% (between 2004 and 2012), a typical value for new energy technologies [382].

More importantly, regarding the costs of such decentralized cogeneration technologies, it is crucial to consider the fact that they tend to be more economically competitive in regions

with high spark spreads, i.e. the difference between the grid electricity (€/MWh) and the cost of natural gas required to produce one MWh of electricity [347,375,381]. Those prices are unfortunately volatile and difficult to predict.

Regarding the US market, CHP stationary fuel cells are mainly represented by large-scale SOFC installations [335,369]. Indeed, in 2010, only 25 to 40 units of the micro-CHP system called ‘ClearEdge Power CE5’ or ‘ClearEdge5’ [343] were installed [383]. In addition, as stated in *Section 3.2.2 - Status of commercialized HT-PEMFC-based micro-CHP systems*, this system is no longer commercialized. Since then, no information has been found regarding other commercialized fuel cell-based micro-CHP systems in the US.

### 3.2.4 Focus on the European market and the available fuel cell-based micro-CHP systems

As explained, only SOFC-O and LT-PEMFC-based micro-CHP systems exist on the market. The most common systems commercialized on the European market are part of the European Union program named ‘PACE’ (that aimed to demonstrate through field-test installations and monitoring in real applications the capability of fuel cell products to reach a commercial mass market [347]). They are shown in Figure 22.

Amongst those systems, ‘Buderus’, a brand of the ‘Bosch’ company (Germany) [384], no longer commercializes its own ‘FC10’ system. Indeed, the ‘Buderus System Logaplust’ is simply a combination of the ‘Bl\*\*\*G\*N BG\*\*’ system with traditional heating systems from the ‘Buderus’ catalogue, such as classical gas condensing boilers [261,384]. According to their website, the ‘Bl\*\*\*G\*N’ system presented in Figure 22 and studied in *Chapter 4 - Study of the Bl\*\*\*G\*N SOFC system* is no longer commercialized and has been replaced by its successor, the ‘Bl\*\*\*G\*N BG\*\*’ (see *Chapter 4 - Study of the Bl\*\*\*G\*N SOFC system* for more details on ‘Bl\*\*\*G\*N’ system versions).

The ‘3\*\*P’ is no longer commercialized as it is the previous version of the ‘P\*2’ (which should have been mentioned in Figure 22) [385]. Both ‘3\*\*P’ and ‘P\*2’ are systems that involve a classical gas condensing boiler and a Domestic Hot Water (DHW) tank hybridized to a PEMFC module, as it will be discussed in *Section 5.1 - Description of the machine*. The PEMFC module of the ‘P\*2’, system studied in *Chapter 5 - Study of the P\*2 PEMFC system*, is also currently commercialized as a standalone module under the name ‘PA\*’ [386]. Contrary to what could be perceived from Figure 22, the manufacturer of the Vi\*ov\*\*r systems does not develop SOFC-based systems on its own, especially since 2020, when they sold to the ‘mPower’ company the parts from the Swiss-German SOFC developer named ‘HEXIS’ (that they had acquired in 2012) [387,388]. However, it is worth mentioning that the manufacturer of the Vi\*ov\*\*r systems has ensured that the ‘mPower’ purchase agreement includes the possibility of future cooperation of HEXIS for the supply of SOFC modules, if they wanted to integrate HEXIS SOFC products into their own energy systems [387,389]. In fact, this is actually the case as one occurrence of the ‘S\*2’ has been found in literature, reporting it as the ‘integrated system that includes the HEXIS latest generation of SOFC-unit, named ‘Leonardo’ [389]. This reference was published back in 2020 and the ‘S\*2’ was reported in field-test and ‘finalization’ stage at the time [389]. However, no additional information about the ‘S\*2’ commercialization (or its discontinuation) has been found since then, while it has been reported on the company website (<http://www.hexis.com>) that HEXIS has introduced the micro-CHP SOFC ‘Leonardo’ system [390] on the market on its own (via its ‘HEXIS Premium Partners’). Although its ‘Leonardo’ product was not ready to be properly integrated to the European PACE program (as the other fuel cell manufacturers reported in Figure 22), it is noteworthy that the ‘HEXIS’ company still received some PACE fundings through the PACE program [390].









The main features of the PACE systems shown in Figure 22 are also reported in Figure 23 and Figure 24, which has been translated from a reference in German [391] and represent, to the knowledge of the author, the most exhaustive comparative tables related to the fuel cell-based micro-CHP systems currently available on the European market. Indeed, they include systems that are not directly part of the PACE program, such as the already mentioned ‘Leonardo’ system from ‘HEXIS’ [390], but also such as the ‘Inhouse5000+’ system by ‘inhouse engineering’ (Germany) [392], on the market after 2020 and therefore also too late to be involved in the PACE program.








**Figure 22.** Fuel cell micro-CHP systems commercially available in Europe. The reported power output is the nominal electrical power output; the previous numeric row corresponds to the amount of units installed in Europe through the PACE supporting program. Reproduced slide from the Final Conference of the PACE European Union project (26 April 2023) [393], that aimed to demonstrate through field-test installations and monitoring in real applications the capability of fuel cell products to reach a commercial mass market [347].

The ‘I-1000’ system from the ‘ReliOn’ company (US) should not however be a part of Figure 24 as it runs only on hydrogen (and not on natural gas), as it is only air-cooled, as it has been commercialized as a back-up power unit for telecom applications (not as a CHP) [394], and as it has been discontinued since the integration of the ‘ReliOn’ company into the ‘Plug Power’ company [395], which, as already stated, develops the ‘Gensys’ LT-PEMFC system for off-grid back up applications [359,362]. Likewise, the ‘Convion’ CHP system (from the ‘Convion’ company in Finland) should not have been reported in Figure 24 as its electrical power output, which is now established at 60 kW<sub>el</sub> [396], is too high to be relevant with micro-CHP applications, as stated in the beginning of this section.

At last, the ‘Vaillant’ company is sometimes reported as a micro-CHP manufacturer [397]. However, it only integrated SOFC modules developed by its partner, the ‘Sunfire’ company (see Figure 22). In addition, Vaillant even paused its CHP activities in 2017 after having transferred its expertise to Sunfire [398,399].

Product	 SenerTec Dachs 0.8	 Remeha eLecta 300	 Sunfire- Home 750	 Vitovalor PT2	 Buderus GCB + BlueGEN	 BlueGEN
OEM	BDR Thermea	BDR Thermea	Sunfire	Viessmann	Bosch, Buderus	SOLIDpower
Fuel Cell type	PEMFC	PEMFC	SOFC	PEMFC	SOFC	SOFC
Electrical output power	0,75 kW	0,75 kW	0,375 – 0,75 kW	0,75 kW	0,5 – 1,5 kW	0,5 – 1,5 kW
Heat rate	1,1 kW	1,1 kW	0,65 – 1,25 kW	1,1 kW	Up to 0,85 kW (BlueGen only)	Up to 0,85 kW
LHV Electrical efficiency	38 %	38 %	36 % / 38 %	37 % / 38 %	Up to 57 %	Up to 57 %
LHV overall efficiency	92 %	92 % / 95 %	88 % / 90 %	92 %	Up to 89 % (BlueGen only)	Up to 89 %
Stack lifetime	80.000 h	80.000 h	40.000 h	80.000 h	Up to 60.000 h	40.000 h
Approximative cost	20 k€ (VAT excluded)	23 k€ (VAT excluded)	23 k€ (VAT included)	20 - 25 k€ (VAT included)	31 k€ (VAT included)	25 k€ (VAT excluded)
Fuel	Natural gas, H <sub>2</sub>	Natural gas, H <sub>2</sub>	Natural gas, LPG, H <sub>2</sub>	Natural gas, H <sub>2</sub> content up to 5 %	Natural gas	Natural gas, H <sub>2</sub> content up to 20 %
Heat storage	300 L	300 L	Not included	220 L (Domestic Hot Water)	Not included	Not included

**Figure 23.** First part of the fuel cell micro-CHP systems commercially available in Europe and their main features. GCB stands for Gas Condensing Boiler. Reproduced and traduced from reference without modification [391].

Product	 Vitovalor PA2	 Leonardo	 I-1000	 Inhouse5000+	 Convion
OEM	Viessmann	Hexis	ReliOn	inhouse- engineering	Convion
Fuel Cell type	PEMFC	SOFC	PEMFC	PEMFC	SOFC
Electrical output power	0,75 kW	0,5 – 1,5 kW	1 kW	1,68 – 4,2 kW	50 kW
Heat rate	1,1 kW	0,6 – 2 kW	N/A	3 – 7,5 kW	25 kW
LHV Electrical efficiency	38 %	40 %	38,4 – 40,6 %	34 %	> 55 %
LHV overall efficiency	92 %	95 %	N/A	92 %	82 %
Stack lifetime	80.000 h	5 – 7 years	22.000 h	?	> 4.000 h
Approximative cost	15 k€ (2021 Viessman Belgium catalogue)	?	?	60 k€ (VAT excluded)	?
Fuel	Natural gas, H <sub>2</sub> content up to 5 %	Natural gas, H <sub>2</sub> content up to 23 %	H <sub>2</sub>	Natural gas, exists with pure H <sub>2</sub>	Natural gas
Heat storage	Not included	Not included	N/A	Not included	Not included

**Figure 24.** Second part of the fuel cell micro-CHP systems commercially available in Europe and their main features. Reproduced and traduced from reference without modification [391].

### 3.2.5 Current and expected performance of micro-CHP systems based on a PEMFC or a SOFC

Back in 2010, the U.S. Department of Energy Hydrogen and Fuel Cells Program provided the expected performance of micro-CHP systems according to the fuel cell types (reproduced in Table 8) [400].

The maximum LHV electrical efficiency for LT-PEMFC systems fed by natural gas is reported at 40%. As seen in *Section 3.2.3 - Main fuel cell-based micro-CHP markets*, commercial systems are already close to that figure. Although some studies with major

technical improvements on the fuel reforming processor indicates that LHV electrical efficiency of LT-PEMFC micro-CHP could reach up to 45 % [267,401,402], it is usually considered that considered that electrical efficiency target of 45% (or more) are likely to be achievable with HT-PEMFCs and SOFCs only and unlikely to be achieved by LT-PEMFC [266].

Actually, regarding the LHV electrical efficiency of HT-PEMFC micro-CHP fed by natural gas, many studies reports a maximum around 45% [266,267,400,403,404], hereby confirming the figure given in Table 9.

	2012			2015			2020		
	LT-PEMFC	HT-PEMFC	SOFC	LT-PEMFC	HT-PEMFC	SOFC	LT-PEMFC	HT-PEMFC	SOFC
<b>LHV Electrical efficiency (%)</b>	38	42	40	40	42	45	40	45	60
<b>LHV CHP efficiency (%)</b>	85	85	85	87	87	90	87	87	90
<b>Operating lifetime<sup>a</sup> (h)</b>	30000	30000	30000	40000	40000	35000	40000	40000	40000
<b>System availability (%)</b>	97	97	97	98	98	98	99	99	99
<b>Factory cost<sup>b</sup> (\$/kWh)</b>	1000-1500	1000-2000	1300-4500	750-1200	550-1500	1000-3000	450-750	450-750	1000-2000

<sup>a</sup> Time until > 20% net power degradation.

<sup>b</sup> Cost defined at 50,000 unit/year production. The basic unit includes all processing necessary for conversion of natural gas to unregulated DC power; i.e. the basic unit does not include power conditioning.

**Table 9.** Panel Perspective on Cost and Technical Potential for 1–10 kW<sub>el</sub> CHP Stationary Fuel Cell Systems Operating on Natural Gas. Reproduced and adapted from reference [400].

Similarly to Table 9, both Europe and the International Energy Agency set the 2030 LHV electrical efficiency target of micro-CHP fuel cells (fed by natural gas or biogas) up to 65% [380,405], which seems only achievable with SOFC technologies [335,406–409]. It is worth mentioning that the ‘Bloom Energy’ company (in the US) is already commercializing a SOFC-based CHP unit, fed by natural gas (or biogas), of 330 kW<sub>el</sub> of power output (so, higher than the micro-CHP range) and of 65% of net LHV electrical efficiency (AC) [410–412].

In fact, without parasitic losses, the theoretical LHV electrical efficiency of a SOFC is close to 100% for the electrochemical direct oxidation of dry methane (therefore featuring no Carnot limit) [413], similar to the one reported for carbon fueled SOFC (DC-SOFCs) [414]. With hydrogen or carbon monoxide, the theoretical efficiency is still around 70% (LHV) [413]. That high 70% figure is in fact sometimes already reported as the current upper electrical efficiency limit for SOFCs with internal reforming [415,416]. It is noteworthy that the expected electrical LHV efficiency of proton-conducting SOFC (SOFC-H) used in CHP systems is also close to that figure (reported up to 68%) [417].

Regarding the other recent achievements in the (SOFC) industry, ‘Ceres Power’ (United Kingdom) announced a 65% LHV electrical efficiency for 5 kW<sub>el</sub> stack operating on

methane (gross DC efficiency) [413,418]. Lately, the ‘Robert Bosch’ company (Germany) announced a 10 kW<sub>el</sub> demonstrator of 70% of gross LHV DC electrical efficiency [419]. At last, both those companies, within the frame of a collaboration, announced having pushed this gross DC efficiency up to 72.4%, based on the LHV on methane, for a 150 W<sub>el</sub> stack [420]. Similarly, the ‘Elcogen’ company (Estonia) is commercializing SOFC stacks for micro-CHP OEMs with an announced gross DC LHV electrical efficiency of 74% [411,421,422], also measured at 72% [423] and announced at 75% on their website (<https://elcogen.com>). It has been reported that a 74% DC LHV efficiency performance was also already achieved by the ‘SolidPower’ (founded in Italy and renamed ‘SolydEra’) back in 2013 [422,424]. This OEM is in fact commercializing the micro-CHP product named ‘Bl\*\*\*G\*N’ of net LHV electrical efficiency (AC) of 60% [425], mentioned in *Section 3.2.4 - Focus on the European market and the available fuel cell-based micro-CHP systems*.

It is noteworthy that this (still significant) difference between gross DC and net AC efficiency might be explained by the fact that DC gross electrical efficiency do not consider the parasitic power losses (in the current collection), the DC-AC power conversion losses and the consumption of auxiliaries such as the air blower power consumption (oxidizing agent supply at the cathode) [426]. However, those gross efficiency figures are so promising that it is not unrealistic to hope for SOFC-based micro-CHP systems with LHV electrical efficiencies of 70%-80% or even more in a mid-term future.

### 3.3 Conclusions of the chapter

- Fuel cells do not necessarily require hydrogen as fuel. Indeed, another fuel type can be used as hydrogen carrier, which is decomposed either directly (onto the anode of the stack) or indirectly (in an indirect fuel processing reactor located internally or even externally to the fuel cell embodiment). This is also because the electrochemical oxidation of other species (fuels other than hydrogen) can occur in certain fuel cell types, such as carbon in DC-SOFCs, CH<sub>4</sub> and/or CO in methane-fed SOFC, ammonia in DAFCs, *etc...*
- The ‘Direct’ appellation in the fuel cell acronym means a ‘direct’ utilization of the fuel at the anode of the stack. This fuel can either participate directly in the electrochemical oxidation occurring in the fuel cell or it can also be decomposed onto the anode in another fuel type (that participates in the fuel cell electrochemical reaction).
- A tremendous amount of fuel cell types exists and most of the ‘direct’ utilizations (as defined here above) have been reported in an innovative identification key established in this work (Figure 18), which is based on the charge carrier.
- Main fuel cell types and their characteristics have been reported in Table 7.
- Four fuel cell technologies, namely polymer electrolyte membrane (PEFC), i.e. PEMFC (both LT-PEMFC and HT-PEMFC), oxygen-ion solid oxide fuel cells (SOFC-O), phosphoric acid fuel cells (PAFC), and alkaline fuel cells (AFC), are or have been considered for micro-CHP applications. Proton conducting SOFCs (SOFC-H), as well as other types of SOFCs, are not mature enough technologies to be considered suitable for the CHP markets.
- Although attempts have been numerous, there is still no successful commercial HT-PEMFC micro-CHP systems on the market. PAFCs and AFCs, have not attracted substantial commercial interest as micro-CHP due to high manufacturing costs and low lifetimes, respectively. Also, the complexity of AFCs is increased as they require pure oxygen feed as reactant.
- Fuel cell micro-CHP market have been and are mainly supported through public funding programs, mainly because of high investment costs. However, PEMFC systems are no longer subsidized in Japan as they have reached a cost that corresponds to payback periods of 7-8 years.

- 
- Maximum expected LHV electrical efficiency of methane-fed LT-PEMFCs and HT-PEMFCs and SOFCs is respectively about 40% and 45%, which are quite close figures compared to current performance.
  - Methane-fed SOFC already exists with up to and 65% LHV electrical efficiency (AC) or 75% LHV electrical gross efficiency (DC). Theoretical electrochemical oxidation of methane or carbon in a SOFC is close to 100% so is not unrealistic to hope for SOFC-based micro-CHP systems with LHV electrical efficiencies of 70%-80% or even more in a mid-term future
  - DC-SOFCs and DFAFCs are fuel cell types that exhibit a potential pure CO<sub>2</sub> off-anode stream that could facilitate CO<sub>2</sub> capture and offer the possibility of negative emissions (if fed by carbon neutral fuels).

# CHAPTER 4 STUDY OF THE BL\*\*\*G\*N SOFC SYSTEM

In the fuel cell micro-CHP market study conducted in the previous chapter, it has been established that only two fuel cell technologies are currently mature enough to be available as micro-CHP systems, i.e. the (O-)SOFC and the (LT-)PEMFC. At the European level, two fuel cell micro-CHP manufacturers are leading the market, as demonstrated by their higher number of installations (through the supporting PACE program) shown in Figure 22 : the SOFC BL\*\*\*G\*N system and the Vi\*ov\*\*r systems. Those have in fact been deeply studied during this thesis, respectively in *Chapter 4 - Study of the BL\*\*\*G\*N SOFC system* and *Chapter 5 - Study of the P\*2 PEMFC system*. Those studies mainly rely on experimental investigations conducted in ULiege laboratory facilities and on in-situ monitoring installations of real applications (in ‘real’ Belgian households). For the SOFC, in addition to the BL\*\*\*G\*N system in ULiege laboratory, two field-test systems were in fact studied, located in Riemst and Duffel.

The purpose of the study presented in this chapter is to assess the energy and environmental performance of the micro-CHP BL\*\*\*G\*N SOFC (1.5 kW<sub>el</sub> of nominal power output). Energy performance is analysed in terms of natural gas consumption, net electricity production, as well as thermal and electrical efficiencies of the system. Environmental performance is assessed in terms of pollutants emissions, including CO<sub>2</sub>, CO, SO<sub>x</sub>, NO<sub>x</sub> and particle matters. This chapter is organized as follows. After a description of the machine conducted in *Section 4.1- Description of the machine*, the tests carried out in ULiege laboratory are presented and analyzed in *Section 4.2 - Laboratory tests*. Then, *Section 4.3 - In-situ monitoring* investigates the monitoring of the two units installed in the two different residential buildings, including their CO<sub>2</sub> utilization performance. Based on those two latter sections, *Section 4.4 - Machine modelling* proposes empirical models of the system suitable for simulation of such micro-CHP SOFC installed in buildings. *Section 4.5 - Comparison of laboratory and in-situ measurements* draws conclusions from the comparison between in-situ performance and laboratory performance (and investigates the correlation between all the tested systems). Environmental performance in terms of non-CO<sub>2</sub> pollutants is finally analysed in *Section 4.6 - Non-CO<sub>2</sub> pollutant emissions* (CO<sub>2</sub> utilization performance of those systems being already investigated in *Section 4.3 - In-situ monitoring*).

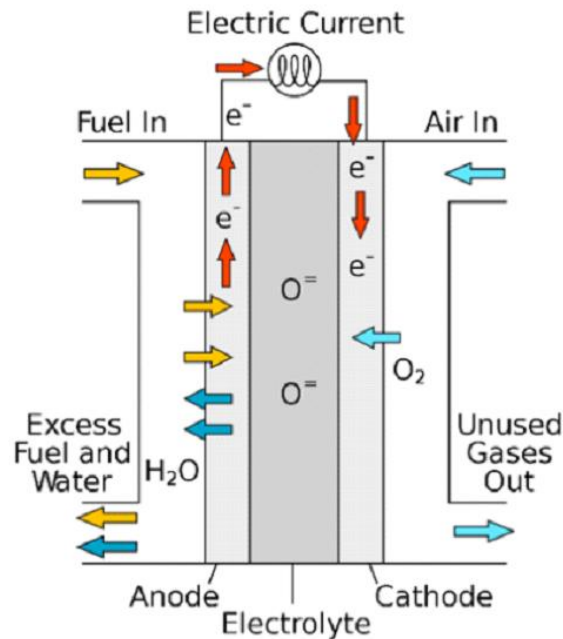
Several academic publications have been established in relation to several sections of this chapter. All of those have been specified in the introduction of each section they are related to. In fact, the assumed internal schematics of Figure 31 (and its description) included in the first section of this chapter, i.e. *Section 4.1- Description of the machine*, have been published in the *proceedings of the 7<sup>th</sup> International High Performance Buildings Conference at Purdue (Herrick 2022)* [427].

## 4.1 Description of the machine

### 4.1.1 Working principle

The fuel cell technology concerned by this chapter is the O-SOFC (Oxygen ion-conducting Solid Oxide Fuel Cell, i.e. oxygen ions as charge carriers), introduced in *Section 3.1.2 - Fuel cell types and classification* and in Table 7. As stated in that same section, a SOFC is

characterized by its electrolyte, usually a (solid) ceramic that includes oxides and its working principle is reminded in Figure 25 [428].



**Figure 25.** Working principle of a O-SOFC. Reproduced and adapted from reference [428].

As established in Table 7, although its high operating temperature could be seen as a drawback (increased complexity, strict materials requirements, long start-up time and durability issues), it brings remarkable advantages compared to other fuel cell technologies, which most important ones are reminded here below :

- High fuel flexibility [429]. As stated in *Section 3.1.2 - Fuel cell types and classification*, practically all hydrocarbons (or other fuels, such as ammonia) can be used with SOFCs either thanks to direct electrochemical oxidation (fuel used in the fuel cell reaction), direct decomposition on the anode, or internal indirect decomposition (reforming prior to the fuel cell stack) allowed by the tremendously high temperatures.
- High tolerance to contaminants. The main example is carbon monoxide. It is a common by-product of hydrocarbon reforming processes and can be used directly as fuel in SOFCs, in the electrochemical fuel cell reaction (while only a few ppm of CO suffice to poison LT-PEMFCs, which require an additional CO remover in the fuel processing, as it will be explained in details in *Section 5.1.1.2 - Hydrogen processor and reforming processes* and *APPENDIX 14: Literature review on PEMFC degradation mechanisms*) [430]. However, sulphur compounds are still absolute poison for SOFC and fuel desulphurization is often required when the system is not fed with pure hydrogen [431].
- High electrical efficiency (the BI\*\*\*G\*N tested in this chapter is expected to achieve 60% LHV, as it can be observed in Table 11).
- No necessary use of platinum, rhodium and other precious metals as catalysts [432].

#### 4.1.2 Applications and the different versions of the tested system

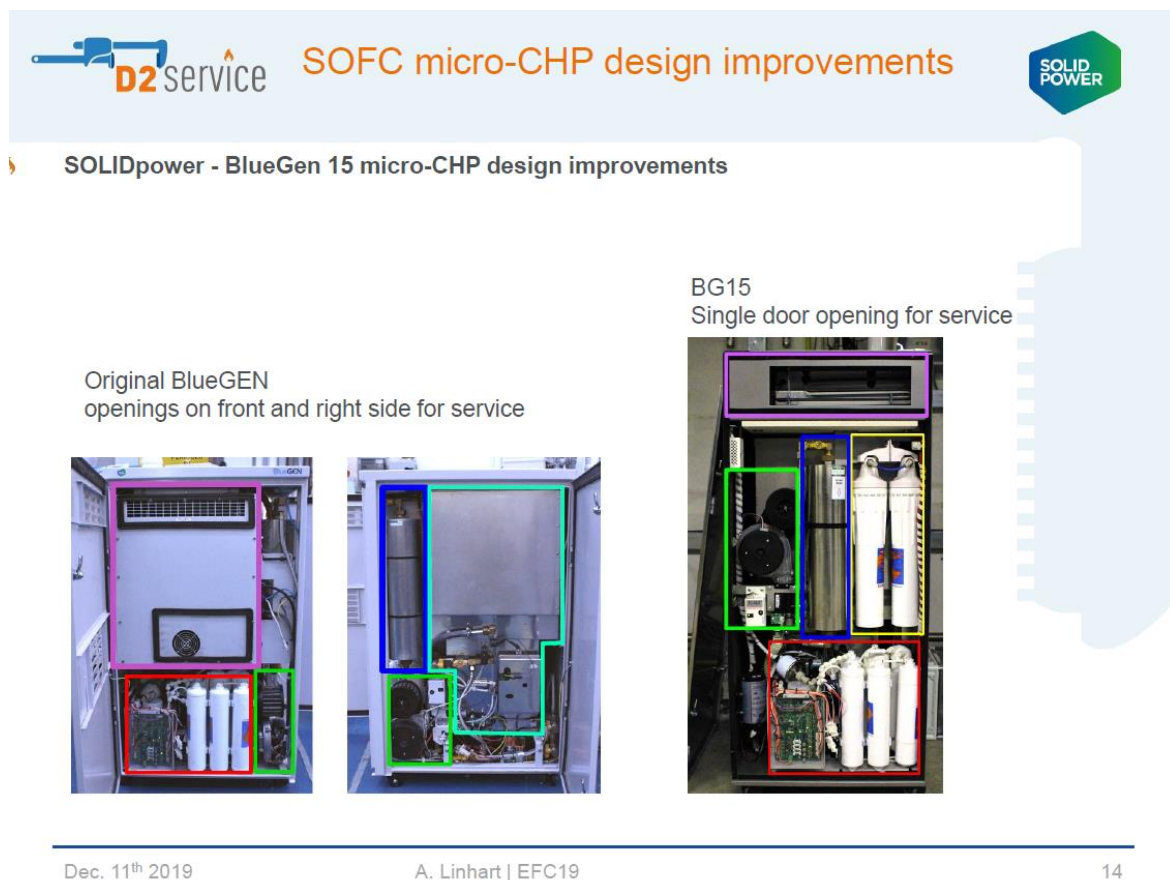
As it will be seen, the version of the studied SOFC system is not be confused with other versions released by the same OEM (Original Equipment Manufacturer). This subsection aims to introduce all those similar versions and describe their differences with the studied system (the 'BI\*\*\*G\*N 2014+').

The BI\*\*\*G\*N 2014+ system is electrically driven as the power output is set by the OEM itself over network connections (via a dedicated Ethernet port on the system). To do so, the owner cannot interact with its system himself and he has to contact the OEM by phone or by email to change the power output of its system. It is worth mentioning that in the following generation of the 'BI\*\*\*G\*N 2014+', i.e. the 'BI\*\*\*G\*N BG\*\*' [433], presented in Figure 22, the OEM has developed a smartphone application that allows for the user to monitor its performance but mostly to control its scheduled output power over the week and to better match its electrical demand.

For information, the OEM has declared some design improvements implemented to the 'BG-\*\*' at a European Fuel Cell conference (EFC 2019) [434], the relevant slides of which are presented in Figure 26 and Figure 27.


The fuel cell, even in its latest 'BG-\*\*' version, is not supposed to be cycled ON and OFF. It is optimized for a 1.5 kW<sub>el</sub> production but it can be modulated down to 0.5 kW<sub>el</sub> as well as any output power in between. It might be found in the given user manual (presented in APPENDIX 3: *User manual of the tested BI\*\*\*G\*N SOFC system*) that the system can be modulated to 0 kW<sub>el</sub> but that has been found to be incorrect (after verification with the OEM).

Indeed, the thermal cycles that would be induced would imply too intense temperature gradients, which are known to contribute to degradation by opening micro-cracks and delaminations (failure mode for which materials fracture into layers)[435]. It is known that start-up and shut-down procedures require appropriate control to ensure fuel cell durability [436] and it is believed that in this case, this is the reason why start-up operations last several dozens of hours (up to 30 hours, as stated in APPENDIX 4: *User manual of the tested BI\*\*\*G\*N*).




**Figure 26.** First part of the design improvements implemented on the 'BG-\*\*' (declared by the OEM). Reproduced from reference [434].


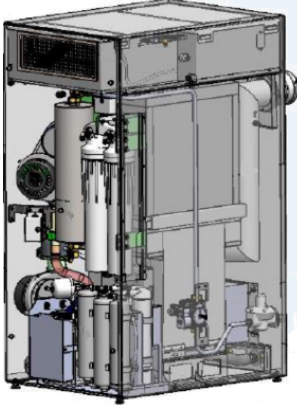




## SOFC micro-CHP design improvements



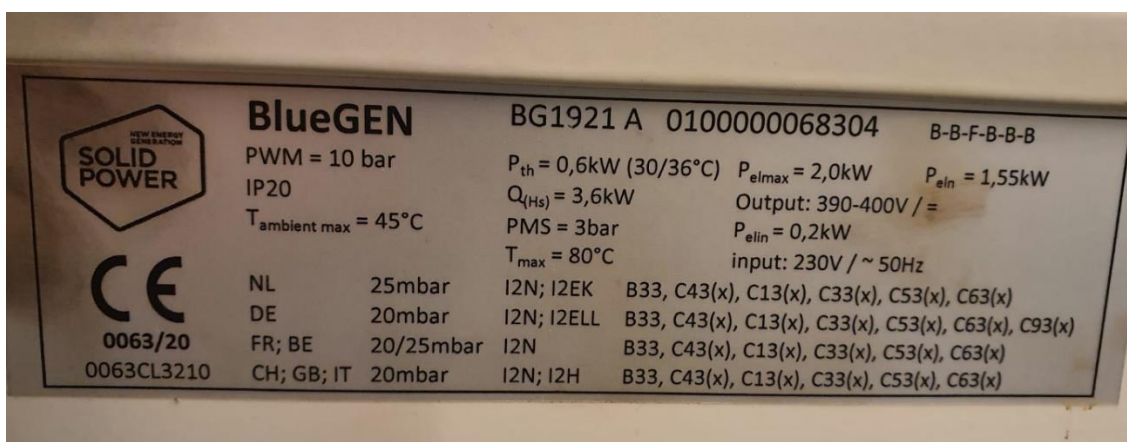
Objective	Starting point	Improvements
<b>BOP accessibility</b>	Difficult removal of heavy lateral panels.	Front panel light and easily removable with four cam locks.
<b>Stack</b>	Stack integrated in Hot BoP. Removal requires special tools; can only be performed at SP facilities.	Stack connected to Hot BoP by a flat manifold and integrated into BoP. Stack replacement only at SP facilities; whole BoP is replaced in case of stack failure.
<b>Hot BoP</b>	Hot BoP is part of frame and cannot be replaced outside SP facilities.	Hot BoP including stack can be easily replaced in the installation site with a dedicated tool by one single operator.
<b>Cold BoP</b>	Placed below Hot BoP; layout affected by Hot BoP complexity; difficult to reach certain components.	Cold BoP is placed before Hot BoP; components easily replaceable. Hydraulic and electrical connections are fool proof.
<b>Water treatment system</b>	Simple mixed resin cartridge surrounded by many pipes; difficult to move. Fixed to frame with 4 screws.	Very complex but effective and reliable; contains also a pump to feed the process water and related control board. Easy to remove and mount without tools. Fool proof hydraulic and electrical connections.
<b>Air Filter</b>	Two air filters, one for blower, not easy to handle because surrounded by pipes and cables.	Air filter fixed by a wingnut can be removed and installed without interferences with other devices.
<b>Desulphuriser</b>	Consists of two cartridges; not easily reachable because of cabling and piping; difficult to tighten some connections.	One single cartridge, very easy to replace. Apart from gas connections, the cartridge is fixed with cable ties.




Dec. 11<sup>th</sup> 2019
A. Linhart | EFC19
15

**Figure 27.** Second part of the design improvements implemented on the ‘BG-\*\*’ (declared by the OEM). Reproduced from reference [434].

In addition to the latest ‘BG-\*\*’ version, which is quite identifiable compared to the machine tested in this work because the packaging has significantly changed (the latest model is black, the model studied here is white), it is worth mentioning that there was also a previous BI\*\*\*G\*N version quite similar to the one tested here. Indeed, it is important to differentiate the two as some major characteristics are different. For example, the identification plate of the tested system is presented in Figure 28 whereas the identification plate of the previous similar version is presented in Figure 29. The main differences are the nominal and maximal power outputs.

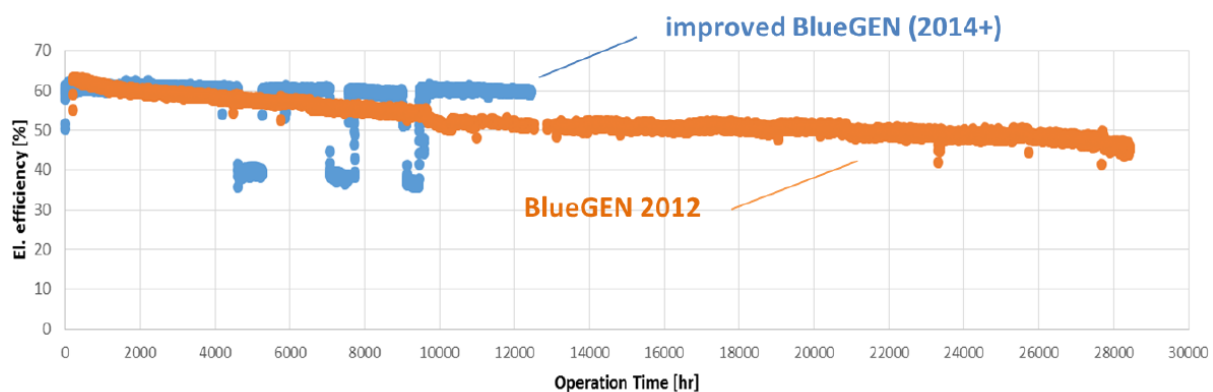


**Figure 28.** Photograph of the identification plate of the BI\*\*\*G\*N tested in ULiege facilities (corresponding to the manual presented in APPENDIX 3: User manual of the tested BI\*\*\*G\*N SOFC system).

 supplied by SOLIDpower GmbH		 0063	
Modèle:	<b>BlueGEN</b>	Identification produit:	0063 CL 3210
N° de Serie:		Désignation:	
Pays de Destination:	BE	Date de fabrication:	
<b>Circuit Electrique</b>		<b>Gaz</b>	
ALIMENTATION	230V~50Hz IP20 Nominal 200W	CATEGORIE GAZ	I2E+ / I2N
PUISSANCE ÉLECTRIQUE EXPORTÉE	Max PeI 2,5kW Nominal 2,0kW	TYPE DE GAZ	Gaz Naturel
<b>Circuit de Chaleur</b>		PRESSION D'ALIMENTATION	9 to 20 / 25 mbar
PUISSANCE CALORIFIQUE PRODUITE	Pth = 1,2kW	VOLUME DE LA CHAMBRE DE COMBUSTION	0,26L
DEBIT D'EAU	Nominal 2 L/min	DEBIT D'AIR	0,09m <sup>3</sup> /min
PRESSION	PMS = 3bar	DEBIT CALORIFIQUE ENFOURNÉ	H <sub>1</sub> = 3,3kW H <sub>2</sub> = 3,6kW
TEMPÉRATURE	Max 80°C	TYPE	B23, C13, C33, C53, C43 (Cascade)
		<b>Eau</b>	
		PRESSION D'ALIMENTATION	1 - 10 bar
		CONSOMMATION MAXIMALE	40 l/jour
 <p>LIRE LA NOTICE TECHNIQUE AVANT D'INSTALLER L'APPAREIL A GAZ PRODUISANT DE LA CHALEUR AU MOYEN D'UNE PILE A COMBUSTIBLE</p> <p>LIRE LA NOTICE UTILISATEUR AVANT LE PREMIER DEMARRAGE DE L'APPAREIL A GAZ PRODUISANT DE LA CHALEUR AU MOYEN D'UNE PILE A COMBUSTIBLE</p> <p>DANS LE CAS D'UNE INSTALLATION DE TYPE B23: IL EST NÉCESSAIRE D'ASSURER UNE VENTILATION SUFFISANTE AU BLUEGEN ET IL DOIT ÊTRE INSTALLÉ EN ACCORD AVEC LES RÉGLEMENTATIONS LOCALES EN VIGUER</p>			

**Figure 29.** Identification plate from the a previous similar Bl\*\*\*G\*N model reproduced from its installation manual, which document properties are presented in *APPENDIX 2: Document properties of the previous Bl\*\*\*G\*N model installation's manual.*

In another work [425], the OEM has presented the graph reproduced in Figure 30, which was also indicating back in 2016 (before the BG\*\*), the existence of two Bl\*\*\*G\*N versions, demonstrating different aging performance. It has been confirmed in an email with the OEM that the three machines studied in this work (the one in ULiege laboratory facilities, the field-tested one in Duffel and the field-tested one in Riemst) belong to the category referred in Figure 30 as 'Bl\*\*\*G\*N (2014+)'. Therefore, in this work, the studied system's will be associated either to the full name 'Bl\*\*\*G\*N 2014+' or to the simpler form 'Bl\*\*\*G\*N'. This explains the title of this chapter, even if 'Bl\*\*\*G\*N 2014+' is not an official name attributed to the system by the OEM on the system's ID plates.



**Figure 30.** Bl\*\*\*G\*N endurance behavior. A comparison between old and recent (2014+) installations. Reproduced from reference with original caption [425]. At least two versions of the Bl\*\*\*G\*N (prior to the BG\*\*) exists, demonstrating different ageing performance.

As reported in Table 10, it is worth mentioning that there are still some minor differences between the three units studied in this work according to the OEM (via an email discussion). The field-test units in Duffel and Riemst are of the same type/model and are equipped with the latest stack BI\*\*\*G\*N (2014+) generation. The one in the laboratory has the same stack generation installed and is very similar to the other ones except the inverter and control boards that are more recent (without noticeable further durability or efficiency improvement).

None of the BI\*\*\*G\*N systems include a DC/AC inverter, that must thus be added for residential applications.

BI***G*N known models	Main difference from previous version
‘BI***G*N 2012’ – not studied in this thesis	N/A
‘Improved BI***G*N (2014+)’ – studied in the field-test	Lower degradation rate. Slightly lower maximum and nominal electric power output (see Figure 28 and Figure 29).
‘Improved BI***G*N (2014+)’ – studied in the Laboratory	More recent inverter and control boards
‘BG***’ – not studied in this thesis	See Figure 26 and Figure 27. In addition, electrical output power setting can be controlled directly by the user (thanks to a smartphone application).

Table 10. Main differences between BI\*\*\*G\*N known models.

One main advantage of all Bl\*\*\*G\*N products reported in Table 10 is that the heat recovery system is designed to be purely optional and it can be shut down, removed or added as desired, even if the machine is producing electricity. The systems are therefore quite robust and well-suited for residential applications, for example if interventions are required on the heating system hydraulics of the household.

### 4.1.3 Bl\*\*\*G\*N 2014+ - Manufacturer datasheet

The performance announced by the manufacturer is listed in Table 11.

Type	Technical specifications
Operation mode	Power-led, continuous (approx. 8,700 h per year)
Fuel type	Natural gas, bio-methane
Fuel consumption (LHV)	2.51 kW
Electrical LHV efficiency <sup>a</sup> (output)	Up to 60 % (1.5 kW)
Thermal LHV efficiency <sup>a,b</sup> (output)	Up to 25 % (0.6 kW)
Electrical energy generated per year	~ 13,000 kWh <sub>el</sub>
Heat generated per year	~ 5,220 kWh <sub>th</sub>
Control	Remote monitoring and control via Internet
Weight, Dimensions (H x W x D)	195 kg, 1010 x 600 x 660 mm
Noise level	< 47 db (A)
Service interval <sup>c</sup>	12 months

<sup>a</sup> At maximum electrical efficiency, nominal output of 1.5 kW

<sup>b</sup> The manufacturer has not stated the return temperature condition for those thermal efficiency results

<sup>c</sup> Replacement of filters depending on local water, air and gas quality

**Table 11.** Bl\*\*\*G\*N 2014+ expected targets, provided by the manufacturer.

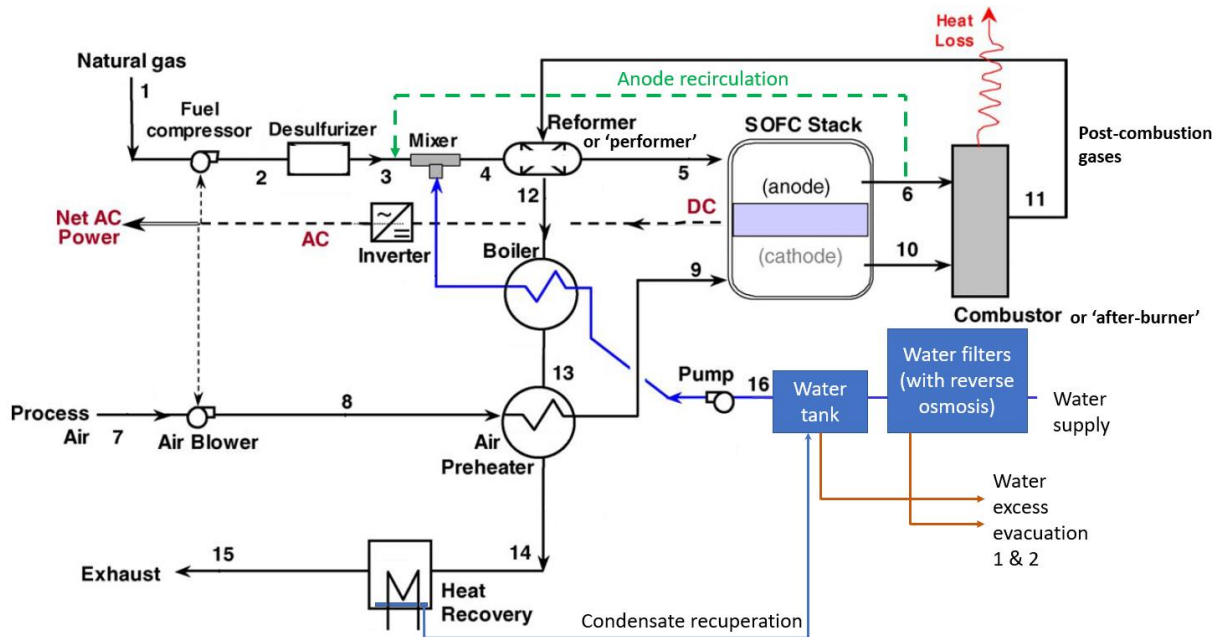
As stated, it is worth mentioning that the SOFC provides DC current at 400 V (see Figure 28). It is therefore necessary to use an inverter. The one chosen for the laboratory study has been advised and provided by the SOFC manufacturer. It is an inverter typically used for photovoltaics residential applications [437]. Other similar inverters can be used but it is preferable to follow the manufacturer recommendations.

### 4.1.4 Probable internal schemes

Unfortunately, the precise internal scheme is not available for intellectual property laws so the working principle could not be defined with certainty. However, base principle is quite common. As described in *Chapter 3 - Fuel cell technologies*, such as any fuel cell, this system provides electricity through redox reactions between a hydrocarbon fuel (here, natural gas) and an oxidizing agent (here, as often, the oxygen from the outdoor air). Since those redox reactions have combustion-like resulting equations [438], there are thus exothermic by nature [439] and release heat in addition of the produced electricity. Cogeneration is thus possible.

Specific literature review on micro-CHP SOFCs combined with little reverse engineering performed by observing the system with its protective cover unmounted (as performed in Figure 26) has nevertheless allowed for assuming the most probable internal scheme of the system, which is presented in Figure 31. This scheme's lay-out is strongly inspired from literature [440], cross-checked against a specific study conducted along with this particular SOFC's manufacturer (but not necessarily on these Bl\*\*\*G\*N systems) [441]. Adjustments to the literature scheme have been performed for relevance with the physical observations of the system without its covers (indeed, for example, the system involves two water outlets periodically actioned, as shown in Figure 32). It is assumed that those

adjustments constitutes (minor) improvements implemented in the commercialized version compared to the schemes that were previously published in research and development work with the collaboration of the manufacturer [441].



**Figure 31.** Most probable internal scheme of the tested BI\*\*\*G\*N system. Main option, with a reverse osmosis filter that requires periodical purges as the second water outlet. Reproduced and adapted from reference [440].

Important elements are presented in the base configuration of Figure 31 :

- Natural gas fuel supply is desulfurized as sulphur compounds have already been established as known SOFC poisons [431] (see Table 7).
- Natural gas is mixed with water vapor in order for steam reforming to take place, as defined by Equation (9) and, to a lower extent, to enable the subsequent water-gas shift (WGS) reaction of Equation (12). A reformer is implemented before the stack, sometimes also called 'preformer' [442] for this reason. Therefore, the reforming/decomposition process is partially 'external' and in not only 'internal' (onto the stack), as defined in Section 3.1.2 - Fuel cell types and classification and Figure 15. As already reported in that same section, such partial external pre-reforming stage are typical with SOFCs [248], in addition to the direct reactions of the fuel on the anode. As explained, those direct anode reactions involve : direct dry oxidation (electrochemical) of methane defined by Equation (8), direct (thermal) decomposition (cracking) of methane into hydrogen and carbon, and of course, direct electrochemical oxidation of reforming/cracking products such as C, H<sub>2</sub>, and CO as defined respectively by Equation (6), Equation (7) and Equation (11).
- Some of the fuel, i.e. methane and reforming products such as H<sub>2</sub> or CO from Equation (9), Equation (10) and, to a lower extent, Equation (12), is not directly consumed by the stack. It is rather consumed in an 'afterburner' [442] in order to generate heat required for steam generation (for the reformer).
- The post-combustion gases are then used to provide heat to the 'preformer', to the boiler (as explained) and at last, before the exhaust, to the external heat recovery circuit (offering the CHP capability of the system).
- Figure 31 does not show that the exhaust gases are providing their remaining heat to the inlet air thanks to a 'double walled chimney' [443], in addition to the probable 'air preheater'.

- Anode recirculation is most likely implemented to increase fuel utilization [444]. Indeed, the gases at the outlet of the anode can still contain  $H_2$ ,  $CO$ , i.e. products of reforming Equation (9), Equation (10) and, to a lower extent, Equation (12). Similarly, exhaust gases might still contain unused  $CH_4$ . All those products can still react and provide power, but they also contain  $H_2O$  usable for the required steam reforming upstream of the stack. Maybe cathode recirculation has also been implemented but this is not the strongest assumption one could make because it complexifies greatly the system. It is unknown to the author if cathode recirculation already exists in commercialized units whereas this SOFC's manufacturer is known to implement anode recirculation in its products [441].
- The system requires a connection to water mains for steam reforming purposes (in the 'preformer'). It has been observed that the system periodically draws water from the main, processes it and stores it in a tank. It is indeed reported in *APPENDIX 2: Document properties of the previous Bl\*\*\*G\*N model installation's manual* that the water consumption from the grid (for steam reforming purposes) is periodical and not continuous (thanks to a processed storage water tank at the bottom of the unit). However, if heat recovery is in fact implemented (which is actually, as mentioned, optional with this system, that can function as an electrical generator only), water can be recuperated from the condensation of the flue gases. This reduces the grid water consumption. Potential excess of water in the tank can be evacuated through one specific water outlet.
- Water impurities are processed through several filters involving reverse osmosis [445]. It is believed that, at a certain point, the water impurities concentration in the periodical inlet water volume becomes too high compared to the pressure used for the reverse osmosis. Thus, the remaining inlet water (with high levels of impurities) has to be thrown away for another periodical grid fresh water inlet to take place (and to be submitted to the reverse osmosis filter).

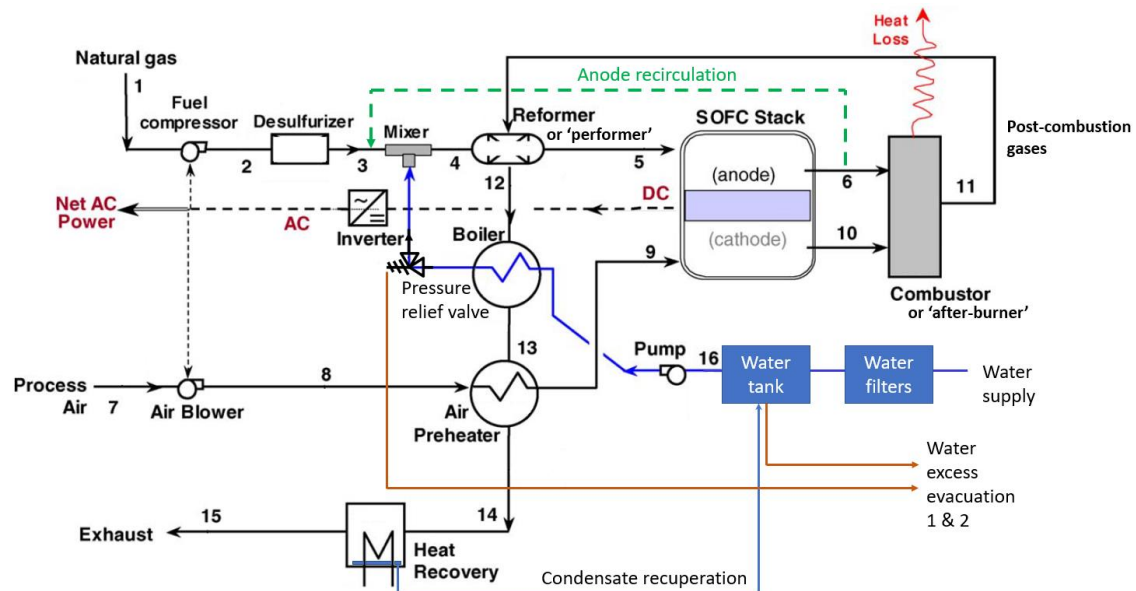


**Figure 32.** Photograph of the back of the system, with the two water excess evacuation pipes (and the water supply pipe).

It is worth mentioning that Figure 31 is not the only possible internal scheme that can be imagined from the information gathered. Indeed, Figure 33 or Figure 34 also constitutes potential schemes for the studied SOFC product. The only difference between the three lies in the second water outlet source (Figure 32).

In Figure 31, this second water output is used for the reverse osmosis filter [445], supposedly required to provide clean water to the ‘performer’ (prior to the stack).

The second possibility, presented in Figure 33 has again been established by looking at the unit without its front and side panels (Figure 26). Such reverse engineering highlighted the presence of a pressure relief valve in the water inlet. It might be because the water vapor pressure can become too excessive so a water discharge might be sometimes required. Indeed, too much steam dilutes the fuel concentration participating in the electrochemical reaction, resulting in a decline in the fuel cell performance [446].

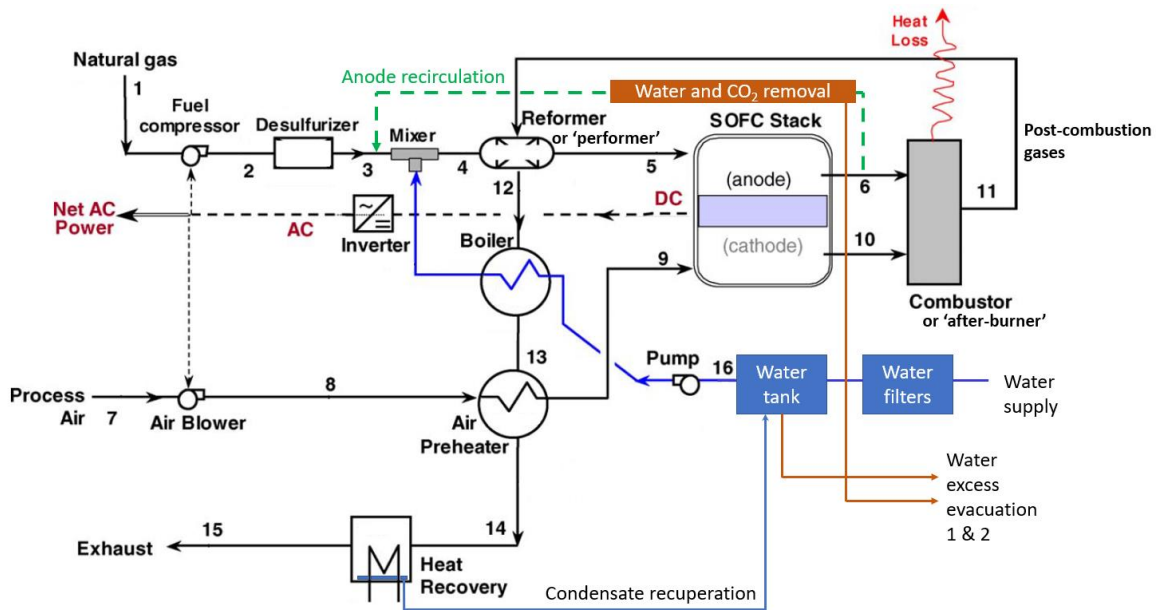


**Figure 33.** Other possible internal scheme of the tested BI\*\*\*G\*N system. Secondary option, with a pressure relief valve as the second water outlet. Reproduced and adapted from reference [440].

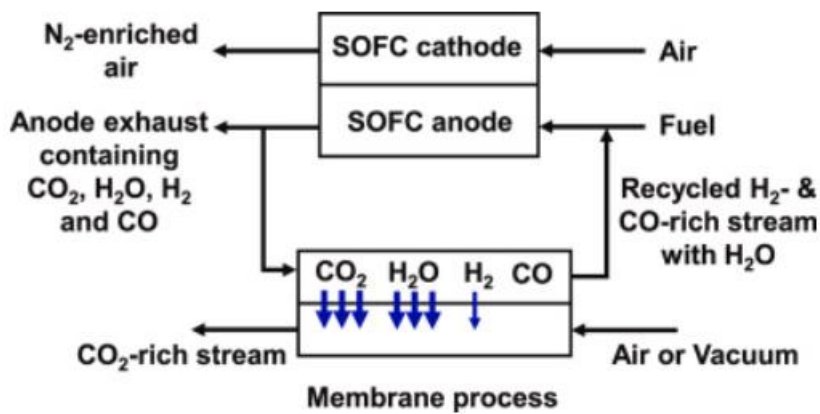
Last possibility has been presented in Figure 34 and is only useful in case of anode recirculation. Indeed, the anode recycled stream also contains  $\text{CO}_2$  from the oxidation of the fuel (natural gas). If the unreactive  $\text{CO}_2$  is not removed from the recirculated stream, it has been reported to dilute the concentration of reactants (i.e. to dilute the fuel) at the stack inlet, lowering the performance [444]. As presented in Figure 35,  $\text{CO}_2$  removal also implies water removal (and unfortunately a little unavoidable  $\text{H}_2$  removal). Indeed, in such  $\text{CO}_2$  removal apparatus, membrane  $\text{CO}_2/\text{H}_2$  selectivity is above 100 (which means that it is still letting through a little  $\text{H}_2$ ) whereas membrane  $\text{CO}_2/\text{H}_2\text{O}$  selectivity is typically around 1 [444].

As presented in Figure 36, which is a more detailed version of Figure 35, it is clear that water and  $\text{CO}_2$  removed from the anode recirculation feed are separated. With this option, it could be assumed that the water from the anode recirculation and condensed in the knockout vessel ‘KO-A1’ is sent to one of the water outlets of the system whereas the low-purity  $\text{CO}_2$  (also recuperated from the anode recirculation) is sent to through the chimney with the main flue gases.

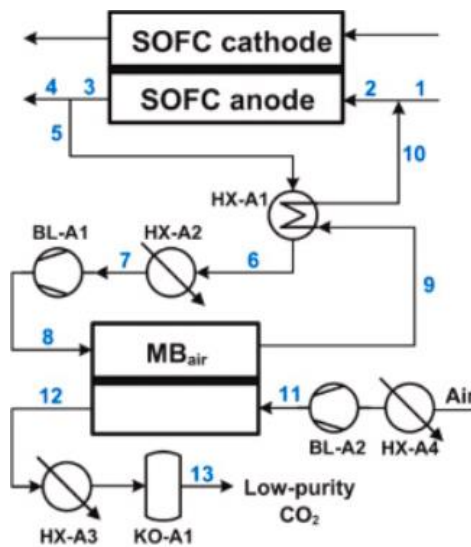
It is not excluded that the BI\*\*\*G\*N actually involves all three (or two out of the three) options presented in Figure 31, Figure 33 and Figure 34. Indeed, those probable water outlet sources could be internally connected.



**Figure 34.** Last possible internal scheme of the tested Bl\*\*\*G\*N system. Last option, with a water and CO<sub>2</sub> removal apparatus as the second water outlet. Reproduced and adapted from reference [440].



**Figure 35.** CO<sub>2</sub> anode recirculation removal principles. Reproduced from reference [444].



**Figure 36.** CO<sub>2</sub> anode recirculation removal with air feed and water recuperation through condensation in a knockout vessel KO-A1. Reproduced from reference [444].



### 4.1.5 Conclusions of the section

- Several versions of the Bl\*\*\*G\*N SOFC system exist and existed. The latest one, i.e. the 'BG\*\*', i.e. the successor of the version tested in this work, has been improved in a way that the electrical output power setting can be now controlled directly by the user thanks to a smartphone application (instead of by emailing the OEM). It is also slightly smaller.
- The tested system works as a standalone unit. It offers an electrical power output that can be modulated as wanted in the 33-100% range. Its announced LHV electrical efficiency is 60% at nominal electrical output power (1500 W<sub>el</sub>). The heat recovery is optional and is announced with a thermal LHV efficiency up to 25% (at nominal output power).
- A DC/AC inverter must be added in residential applications.
- Several potential internal schematics have been provided, the most probable one including the features listed here below.
- Natural gas fuel supply is desulfurized within the system as sulphur compounds have already been established as known SOFC poisons [431].
- The reforming/decomposition process of natural gas is likely to partially 'external' (through a steam reformer prior to the stack) and in not only 'internal' (onto the stack).
- Some of the fuel, i.e. methane and reforming products, is not likely directly consumed by the stack. It is likely rather consumed in an 'afterburner' [442] in order to generate heat required for steam generation (for the reformer).
- Anode recirculation is most likely implemented to increase fuel utilization. Maybe cathode recirculation has also been implemented but this is not the strongest assumption one could make because it complexifies greatly the system.
- The system requires a connection to water mains for steam reforming purposes. It has been observed that the system periodically draws water from the main, processes it and stores it in an internal tank. Potential excess of water in the tank can be evacuated through one (first) specific water outlet.
- The external optional heat recovery circuit (offering the CHP capability of the system) is placed just before the exhaust gases output and allows for recovering water from condensation of the flue gases (for steam reforming purposes). This reduces the grid water consumption.
- Water impurities are processed through several filters involving reverse osmosis [445]. It is believed that, at a certain point, the water impurities concentration in the periodical inlet water volume becomes too high compared to the pressure used for the reverse osmosis. Thus, the remaining inlet water (with high levels of impurities) has to be thrown away through the second and last specific water outlet, for another periodical grid fresh water inlet to take place (and to be submitted to the reverse osmosis filter).

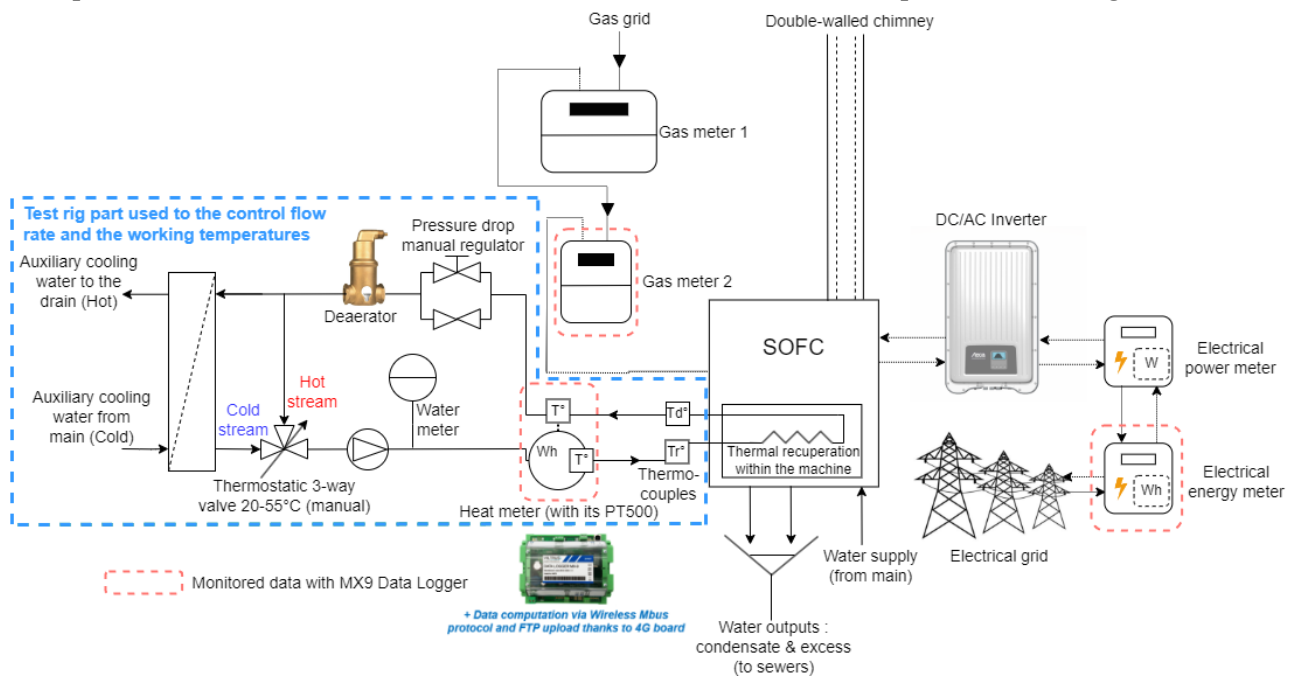
The content of *Section 4.2 - Laboratory tests* was published in two main publications. The first one has been published in the *proceedings of the 8<sup>th</sup> Conference of the Sustainable Solutions for Energy and Environment (EENVIRO 2022)* [447]. It includes additional information that have not been reported in this thesis such as cost estimates of main test bench components. The second one, published in the *proceedings of the 36<sup>th</sup> International Conference On Efficiency, Cost, Optimization, Simulation and Environmental Impact of Energy Systems (ECOS2023)*, aimed to describe the results that were obtained [448] (which is also currently under review in the *Entropy* journal [449]).

The main objectives of the laboratory test campaigns were to investigate the electrical and thermal performance of the system considering several electrical power output settings along with several working temperatures of the heat recovery circuit.

## 4.2 Laboratory tests

### 4.2.1 Description of the test bench

For warranty reasons, no sensors were placed within the system. Only the inputs and outputs of the SOFC were studied. The test bench schematics is presented in Figure 37.



**Figure 37.** BL\*\*\*G\*N laboratory test bench schematics.

The purpose of the laboratory study is to evaluate the heat recovery capacity of the system, as well as establishing electrical and thermal efficiencies, according to the power output setting of the system (set remotely by the manufacturer). In practice, the heat recovery capacity is mainly affected by the efficiency of the internal heat exchanger (that recovers heat from the flue gases to the optional recovery heat circuit). This internal exchanger is shown in Figure 37 but was also shown in the working principle of Figure 31. Therefore, the idea behind the laboratory test campaign was to evaluate this internal heat exchanger performance (for several SOFC electrical output powers). Considering that the heat-transfer fluid of the heat recovery circuit does not change (in all applications, it is always water), the heat transfer is affected by the flow rate  $\dot{m}_A$  and the working temperatures (depart temperature  $T_D$  and return temperature  $T_R$ ). Indeed, the rate of recovered heat  $\dot{Q}_A$  (expressed as a power) is established through Equation (16), corresponding to the application of the first thermodynamics law.

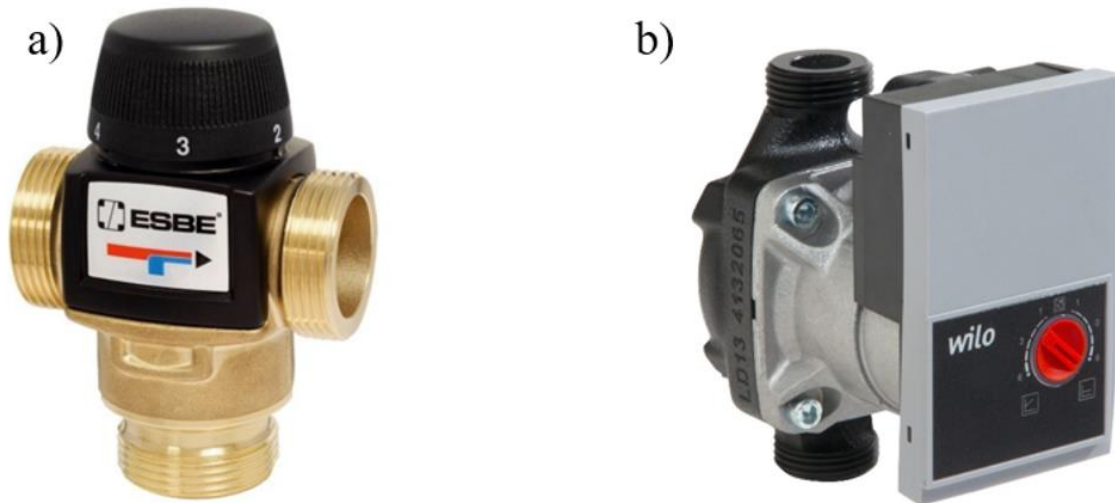
$$\dot{Q}_A = \dot{m}_A c_{p_A} (T_D - T_R) \quad (16)$$

Where  $c_{p_A}$  is the specific heat capacity of the recovery water.

The heat recovered must be dissipated for steady-state operating conditions to occur. This is performed thanks to an auxiliary heat exchanger that ‘cools’ down the recovery circuit with fresh water from the grid (left of Figure 37). This auxiliary water is thus heated up before being directed to the sewers.

Water flow rate  $\dot{m}_A$  of Equation (16) is simply controlled by adjusting manually the heat recovery variable-speed circulator (presented in Figure 38).

It should be stressed that Figure 37 shows a ‘Pressure drop manual regulator’ apparatus that aims to offer a finer control of the water flow rate in the heat recovery circuit (than the one allowed with the variable speed circulator).



**Figure 38.** Specific elements used in the presented test-tig. a) Thermostatic 3-way valve to control the return temperature (‘VTA 572’ by ESBE [450]). b) Variable speed circulator used in the laboratory test bench to control the space heating flow rate (‘Yonos Para 15/6’ by Wilo [451]).

Working temperatures are however set by bypassing the auxiliary heat exchanger thanks to a 3-way thermostatics valve (manual). This is a robust solution if the flow rate and/or the temperature of the auxiliary fresh water happen to change. Indeed, one must simply ensure that the cooling down capacity of the auxiliary water is higher than the thermal recovery output of the SOFC. The 3-way thermostatic valve (presented in Figure 38) will automatically mix the hot flow rate (at the depart temperature out of the SOFC) with the cooled down water coming out of the auxiliary heat exchanger.

It is worth mentioning that the depart temperature is not ‘controlled’; only the return temperature is. Indeed, the depart temperature cannot be controlled in this configuration because it is the consequence of the thermal exchange within the SOFC (at a given flow rate, a given return temperature and a given SOFC electrical output power).

The facilities of the test bench are shown in Figure 39.



Figure 39. Photographs of the BI\*\*\*G\*N test bench.

#### 4.2.2 Measurement devices

Sensors used in the test bench have two origins (see Figure 37) :

- First, sensors that were already there in ULiege facilities.
- Second, sensors identical to the one used in the field-test study (see *Section 4.3.2 - Measurement devices* and particularly Table 17 for sensor properties) that were added to the test bench.

The purpose of adding the same sensors as in the field-test study was to correlate the measurements and subsequently validate the field-test sensors used in the SOFC and the PEMFC studies reported in this work respectively in *Section 4.3 - In-situ monitoring* and in *Section 5.3 - In-situ monitoring*.

Calibration principles for all those sensors has been presented in a parallel internal presentation, the relevant slide of which is reproduced in *APPENDIX 6: Calibration principles of the SOFC test bench*).

##### 4.2.2.1 Gas metering sensors

Both gas metering diaphragm sensors (from the laboratory and the added one for correlation similar to the field-test study) are BKG4T (temperature compensation implemented) [452]. As mentioned, this exact reference is also used in the field-test study. Accuracy is presented in Table 12 and is below 0.5%. The photograph of the ULiege facilities gas meter is presented in Figure 41.



**Figure 40.** BKG4T gas metering sensors of the test bench [452].

#### 4.2.2.2 Electrical output sensors

The field-test electricity meter used for correlation (also used in the laboratory test campaigns) is a Iskraemeco MT174 [453], the specifications of which are presented in Table 12. It computes two indexes of electrical energy (for production and consumption). Electrical power is not directly provided and must be calculated by establishing the derivative of the energy index.

The ULiege usual electrical power meter is an A2000 bidirectional multifunctional meter that shows both the net electrical power consumed and generated [454]. A photograph of this sensor on the test bench is presented in Figure 41. As a power meter, its accuracy is  $\pm 0.5\%$ .

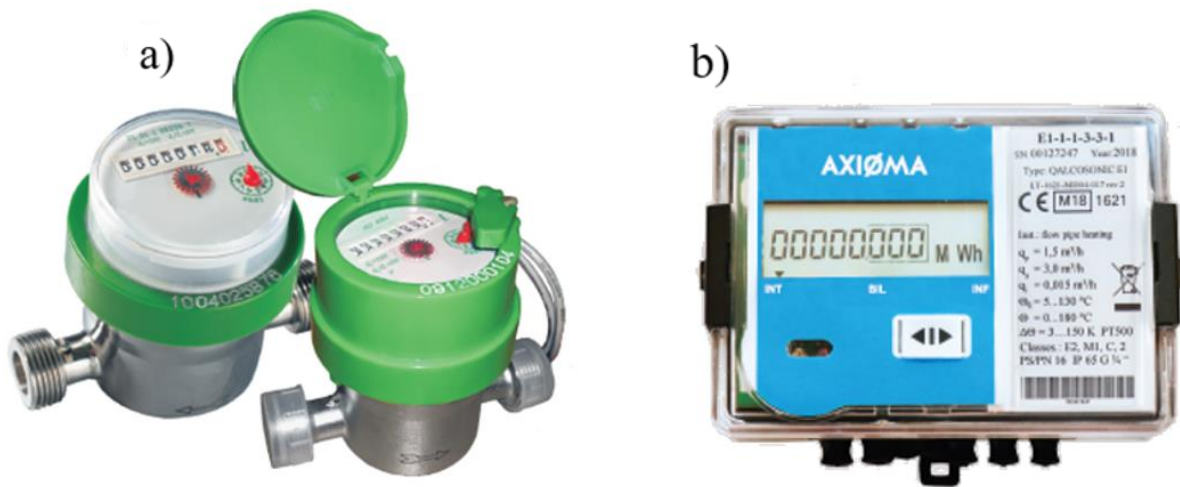
It is important to mention that the generated power exported to the grid is reduced by the power consumed by the operation of the  $Bl^{***}G*N$  itself. In electrical production mode (which occurs for all the test conducted in the laboratory), no electrical consumption is measured: the system provides for its own auxiliaries, except for the circulator of the heat recovery circuit, that is external to the SOFC and could be sized and chosen independently. For information, the power consumption in start-up mode and stand-by mode has been reported between 100-150  $W_{el}$  in the document referred in *APPENDIX 2: Document properties of the previous  $Bl^{***}G*N$  model installation's manual* (circulator of the heat recovery system not included, as it is optional). This figure, insignificant compared to the electrical net power output, has been verified in the field-test in the very few periods for which the systems were not producing. This will be later on observed in Figure 56.



**Figure 41.** Gas and electrical metering installations on the test bench.

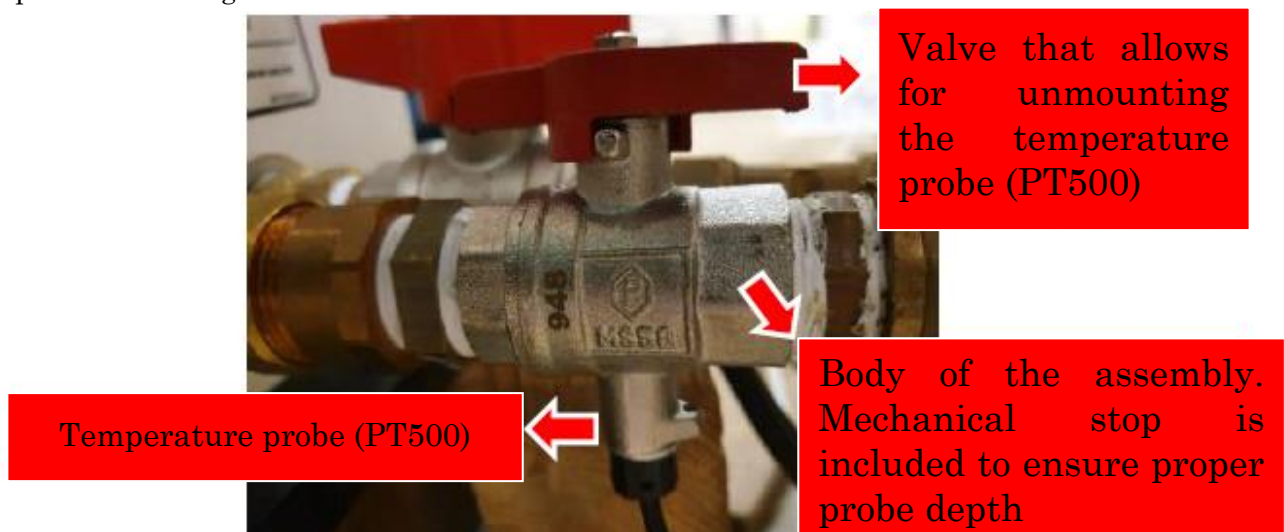
### 4.2.2.3 Heat recovery sensors

The field-test heat meter sensor (also used in the laboratory test campaigns for correlation) is a Qalcosonic E1 (see Figure 42), the specifications of which are presented in Table 12 [455].



**Figure 42.** Water and heat meter used in the heat rate measurement of the heat recovery system. a) Volumetric watermeter used to measure space heating flow rate ('DHV1300' by DH Metering Europe [456]). b) Ultrasonic heat meter included in the test-bench that allows for directly measuring space heating heat transfer ('Qalcosonic E1' by Axioma [455]).

It is preferably placed on the return line (as close as possible to the heating appliance, as it will be explained in *Section 4.3.2 - Measurement devices*). It is composed of a flow rate ultrasonic sensor combined with two PT-500 temperature probes to implement heat rate calculations according to the first thermodynamics law as defined by Equation (16). One of those probes is included in the main body part of the sensor (where the flow rate measurement occurs) whereas the other probe has to be mounted in a separate valve body (to place on the depart line as close as possible to the heating appliance), as shown in Figure 37. A commented photograph of this separate temperature probe assembly is presented in Figure 43.



**Figure 43.** Photograph of the separate PT-500 probe assembly required for the heat meter.

The sensor also provides the flow rate and temperature it measures. It also computes an energy index (by integration of the heat rate measurement).

This sensor is correlated to a specific combination of independent flow rate and temperature measurements. On the one hand, thermocouples are placed in specifically manufactured immersion sleeves (as shown in Figure 44). Those are located at the recovery circuit return and depart (close to the PT-500 probes of the Qalcosonic E1 heat meter). The thermocouples have been insulated to reduce thermal losses and to avoid the influence of radiation or convection with other sources.



**Figure 44.** Thermocouple elbow immersion sleeve (without insulation features).

On the other hand, the water flow rate of the heat recovery circuit is measured thanks to a DHV 1300 water meter [456] (see Figure 42). It computes the volume of water that is passing through the sensor (thanks to the displacement of a rotating piston). However, it also provides 10 pulses every litre so a frequency meter can be implemented. A specific calibration process allows for converting the given frequency into the desired flow rate measurement.

### 4.2.3 Tests matrix

As explained, the purpose of the laboratory test campaigns is to evaluate the heat recovery performance according to the electrical power output of the SOFC (set remotely by the manufacturer), according to the controlled flow rate and working temperatures (only the return temperature is required to be controlled).

It has been chosen to discretize the net electrical output range into three: nominal (maximum) power (1500 W<sub>el</sub>), minimal power (500 W<sub>el</sub>) and an intermediate power setting (1000 W<sub>el</sub>).

The flow rate range is also discretized into three. The chosen discretized flow rates are about 230 L/h, about 160 L/h and about 90 L/h. They correspond to the '1,2,3' position of the variable-speed circulator, as shown in Figure 38 (therefore considering the minimal and maximal flow rates that the circulator can provide, as well as an intermediate value).

The minimal return temperature that could be obtained depends on the auxiliary heat exchanger efficiency (and the temperature of the external water supply, i.e. the water mains). At the time of the test campaign (September 2021), it was not possible to go lower than about 18°C of return temperature. Maximum temperature of the return line is obtained by bypassing the auxiliary heat exchanger completely and depends on the thermal losses of the pipes to the air of the room. At the time of the test campaigns, it was difficult to obtain return temperature higher than 47°C (about 50°C of depart/supply temperature, as it can be deduced from the results given in Table 14, Table 15 and Table 16), especially for low output power settings. It was then chosen to conduct the tests with

8 additional intermediate temperature levels: each intermediate temperature step is of about 3 or 4 K.

All this can be summed up in an empty test matrix sheet, i.e. a form, to be progressively filled in tests after tests. This empty matrix example is presented in Figure 45. It is worth mentioning that in practice, the desired operating conditions for the flow rate and return temperature could only be achieved approximately. Therefore, as it will be seen in *Section 4.2.5 - Experimental results and data analysis*, the exact flow rate and temperature conditions shall be mentioned along with the measured heat transfer rate provided by the SOFC in its recovery heat circuit.

	1500W			1000W			500W		
Return Temperature	230L/h	160L/h	90L/h	230L/h	160L/h	90L/h	230L/h	160L/h	90L/h
18 °C									
21 °C									
24 °C									
27 °C									
30 °C									
34 °C									
37 °C									
40 °C									
43 °C									
47 °C									

**Figure 45.** Empty laboratory test matrix sheet. The yellow parameter is the electrical power output set remotely by the manufacturer whereas the orange parameter is the flow rate controlled by the variable-speed circulator. The return temperature is controlled by the thermostatic 3-way valve (see test bench schematics on Figure 37).

## 4.2.4 Test procedure

### 4.2.4.1 System's time constant (stabilization time)

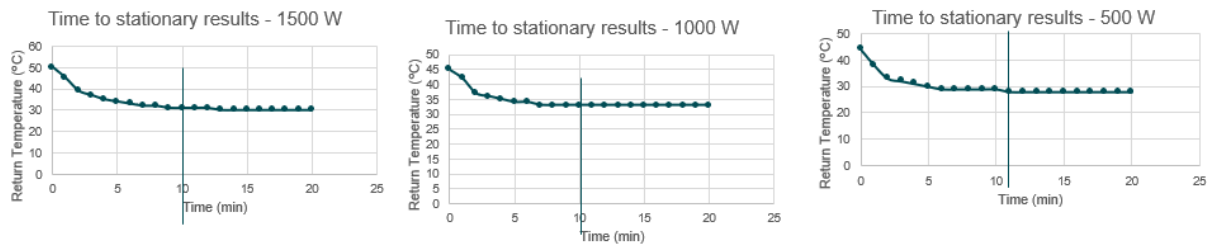
The first test that has been performed had as purpose to estimate the time constant of the system and therefore deduce the amount of time required to reach steady-state stable conditions after having operated a temperature step (by manually operating the thermostatic 3-way valve).

This has been performed for each of the three chosen electrical power setting by imposing a big temperature step to the system (from the maximal operating temperature to about 20 K lower).

The results are presented in Figure 46. The return temperature can be considered stabilized in about 10 minutes. Therefore, in the actual test campaigns, it has been chosen to wait 15 minutes after each temperature step to take and report the measurements in order to ensure that steady-state can absolutely be assumed.

Furthermore, the changes in working temperature operated in the actual test campaigns between two sets of operating conditions are much lower in intensity than the 20 K ones operated in Figure 46 to identify the system's time constant. Indeed, as explained and shown in Figure 45, the temperature change between two stabilized operating conditions is about 3 to 4 K. Therefore, the error implied by assuming that steady-state is surely reached after 15 minutes (or more) for each set of operating conditions is completely negligible.





**Figure 46.** System's responses to a big temperature step (about 20°C) in order to establish stabilization's time.

It is worth mentioning that it was observed that the system's time constant for positive temperature steps is larger than the one obtained here for negative temperature steps. This means that each temperature test sequence (defined by the flow rate and the chosen electrical output setting) shall preferably be operated from the maximum to the minimum temperature. Operating positive temperature steps could be performed by considering the extra waiting time required to achieve steady states conditions (compared to the 15 minutes considered here for negative temperature steps).

For information, gas consumption and electrical output have been found not to be altered by such temperature steps at all whereas the supply/depart temperature varies similarly with the return temperature (same time constants).

The reason for larger time constants with positive temperatures steps is that ambient thermal losses are slowing the warming up of all the masses of the system (pipes, auxiliaries such as the circulator). On the other hand, ambient thermal losses help the masses to cool down to stable conditions.

#### 4.2.4.2 Measurements sequence

First, the manufacturer was contacted over emails to set the electrical power output of the system (to 500, 1000 or 1500 W<sub>el</sub>). The '1,2 or 3' position of the heat recovery circulator (Figure 38) is also set to obtain the desired flow rate.

Then, the 'test sequence' consists in varying the return temperature for the given water flow rate and the given output power. Another flow rate or electrical output power means another test sequence.

As explained, one must start the test sequence with the highest temperature (achieved with the system having run over night to ensure steady-state conditions). Within the test sequence, the return temperature is decreased step by step by opening the valve of the auxiliary cooling water and adjusting the thermostatic 3-way valve. Each time, as explained, one shall wait at least 15 minutes before taking measurements to guarantee acceptable stationary conditions.

The measurements have each time been taken according to the procedure given in *APPENDIX 7: SOFC laboratory measurements procedure*. Within that procedure, successive and not completely synchronous measurements can be performed thanks to the ensured steady-state conditions obtained for each test.

#### 4.2.4.3 Laboratory conditions

For information, all the laboratory test campaigns were conducted in September 2021. There was no heat wave that month and the test bench was not built underneath any window (neither solar gain nor local overheating around the SOFC). Inside the laboratory, a thermostat ensures that the temperature is pretty much constant all day long (about 20°C). Internal humidity inside the laboratory has not been monitored but there was only

one person at a time in all the laboratory (which is about 3000m<sup>3</sup>), so it could also be considered quite constant as well.

Therefore, radiation and convective losses from the SOFC and its recovery heat circuit could be considered constant for all the laboratory tests.

At the time, since early field-test efficiency figures that were already available were not showing any influence of external weather (temperature and humidity of outdoor air, which is supplied to the stack through the SOFC's double walled chimney, as explained in *Section 4.1.4 - Probable internal schemes*), it was decided not to monitor the external temperature and humidity during the test campaigns. Looking at the results shown in *Section 4.2.5 - Experimental results and data analysis*, there is not any unexpected results that is significant enough to be related to any weather variation that would have occurred during the test campaigns. Therefore, with such a SOFC system (with tremendously high internal temperatures around 800°C), it could be considered that moderate external temperature and humidity variations (typical of Western Europe's climate) have no significant influence on the efficiencies of the system.

#### 4.2.4.4 Water consumption

As explained in *Section 4.1 - Description of the machine*, the SOFC consumes water (discontinuously, a few times a day) from the mains in order to (filter and) store water that could later on help providing steam for methane reforming purposes. Even though a water meter was placed on the test-bench (at the water mains connection), in such steady-state tests, the water consumption can hardly be related to the operating conditions as water withdrawn are only executed periodically (a few times a day). Indeed, no water consumption was generally observable while conducting the above test procedure for one given set of operating conditions (and the water withdrawal occurred a couple hours later, while conducting the test for other operating conditions).

In addition to this difficulty, it was already known at the time that the SOFC water consumption was considered 'quite low' : indeed, for example, the water brine (from the most probable reverse osmosis filter described in Figure 31) has been stated in *APPENDIX 5: Installation manual of the (tested) Bl\*\*\*G\*N* (reverse osmosis page) to reach 27 L per day at its maximum (at nominal output electrical power). This information comes from the installation manual of the system installed in the laboratory facilities (see *APPENDIX 4: Installation manual of the (tested) Bl\*\*\*G\*N* (front page and document properties) for details on this particular document). However, these 27 L per day only accounts for the brine water and not the water consumed for steam generation. It could thus be considered that the real water consumption is a little higher, also considering that the system is able to recover the water condensate in the flue gases (which limits the water consumption). Unfortunately, the information on the real water consumption from the mains has not been provided in any official document from the manufacturer (nor in any retrieved technical literature).

For comparison purposes, from 20<sup>th</sup> September 2021 to 16<sup>th</sup> February 2022, the SOFC has provided (continuously, mostly at its nominal power output) in the test bench facilities 5048 kWh<sub>el</sub> of electrical energy and 1434 kWh<sub>th</sub> of heat. During that time, the system consumed 6274 L of water from the grid. All indexes have been taken manually for both dates. This accounts for a water consumption of 1.24 L/kWh<sub>el</sub>. On the other hand, at nominal power, the maximum rejected brine water of 27 L per day gives 0.75 L/kWh<sub>el</sub> of brine water. Considering that the brine water is only part of the water consumption (used for the reverse osmosis filter) and not for the steam generation, both figures lie in the same order of magnitude and are therefore relevant.

The obtained water consumption of 1.24 L/kWh<sub>el</sub> can be considered as in the upper range because, in the laboratory facilities, the heat recovery circuit was turned off most of the time (except during the actual test campaigns). Therefore, the return temperature was generally not cooled down and water in the flue gases was less likely to condensate and to be fed back to the internal tank (as inferred by Figure 31), which would have reduced the water consumption from the mains.

#### 4.2.5 Experimental results and data analysis

First of all, it should be stressed that all the laboratory and the field-test sensors (as described in *Section 4.2.2 – Measurement devices*) correlated as expected, according to the method reported in *Section 4.2.4.2 – Measurements sequence*. This thus constitutes a partial validation of the sensors used for the field-test study described in *Section 4.3 - In-situ monitoring*. Then, resolution and accuracy levels of main sensors described in *Section 4.2.2 – Measurement devices* have been reported in Table 12.

LHV (Low Heating Value) equivalent energy of the consumed gas is established thanks to the HHV (High Heating Value) given by the gas provider, which was averaged for the whole day on which the test sequence has been performed (and which is presented in Table 13). It is worth mentioning that all the laboratory tests were conducted in three separate days over two weeks in September 2021, allowing the electrical power output to be changed between each day.

Sensors	Reference	Resolution	Accuracy
Recovery heat rate	Qalcosonic E1 Qn2,5 qi=0.025m <sup>3</sup> /h   L=130mm	1 W <sub>th</sub>	<5% Accuracy Class 2 [457]
Flow rate	Qalcosonic E1 Qn2,5 qi=0.025m <sup>3</sup> /h   L=130mm	1 L/h	<5% Accuracy Class 2 [457]
Paired [458] depart and return temperature (PT500). Assumed from Class B [459], highest tolerance figure for most common PT500	Qalcosonic E1 Qn2,5 qi=0.025m <sup>3</sup> /h   L=130mm	0,1 K	<0,04 K at 293 K <0,04 K at 333 K [459]
Electrical power	A2000	1 W	<0.5%
Gas volume counter	BK-G4T DN25 Qmax 6 m <sup>3</sup> /h	10 L	<0.5%

**Table 12.** Resolution and accuracy levels of main sensors used to compute efficiency laboratory results.

AC Electrical power output of the test sequences	1500 W <sub>el</sub>	1000 W <sub>el</sub>	500 W <sub>el</sub>
HHV (given by the gas provider)	11,58 kWh/m <sup>3</sup>	11,59 kWh/m <sup>3</sup>	11,61 kWh/m <sup>3</sup>
LHV (assuming HHV/LHV ratio of 1.1085 [132])	10,44 kWh/m <sup>3</sup>	10,45 kWh/m <sup>3</sup>	10,48 kWh/m <sup>3</sup>

**Table 13.** Average HHV and LHV figures on the day of the test sequence.

It must be stated that the HHV figures of Table 13 have been measured by the gas provider in reference conditions (1 atm and 0°C), which are different from the gas delivery conditions. Therefore, the metered gas volume must be corrected to be applied to those HHV or LHV figures. This is performed according to *APPENDIX 1: Energy content of natural gas in residential applications*. Regarding Equation (60), since the atmospheric pressure was not measured at the laboratory facility, it has been computed considering an assumed pressure at sea level of 101325 Pa and an ambient temperature of 15°C. See *APPENDIX 1: Energy content of natural gas in residential applications* for more details.

The uncertainty levels of the HHV-LHV figures of Table 13 have not been given by the gas provider. Therefore, ULiege facilities receiving type 'H' natural gas, the uncertainty level of those heating values can be assumed equal to  $\pm 105 \text{ Wh/m}^3$ , i.e. the same uncertainty level that will be considered for the field-test site that also receives type 'H' gas, as specified in detail later on in *Section 4.3.5 – Uncertainty analyses*.

The results of the laboratory test campaigns are presented in Table 14, Table 15 and Table 16, depending on the electrical power output setting. It is worth mentioning that at nominal power (Table 14), the measured gas consumption is extremely repetitive. Also, the electrical power fluctuated slightly around the output power setting ( $\pm 3 \text{ W}$ ). Since those power variations were balanced around the output power setting, the electrical power was supposed constant in all the test campaign, and exactly equal to the output power setting. Furthermore, the amplitude of the fluctuations was well below the uncertainty of the power meter, which is  $\pm 7.5 \text{ W}$  at nominal power with the  $\pm 0.5 \%$  accuracy range given in Table 12.

Even at lower electrical output power (1000  $W_{el}$  in Table 15 and 500  $W_{el}$  in Table 16), gas consumption is still tremendously repeatable. In addition to the constant output power, this leads to very stable electrical efficiencies. This means that the system is quite robust and insensitive to temperature changes (or flow rate changes) in the heat recovery system.

Therefore, only the thermal efficiency has significantly varied in all the laboratory test campaigns. Thus, Figure 47, Figure 48, Figure 49 are presented in this work to study its variation according to the working temperatures and of the flow rate (of the heat recovery circuit). It is clear that the flow rate, in the tested range, has never any significant influence on the thermal efficiency. Oppositely, the thermal efficiency decrease according to increased working temperatures is always noticeable and quite linear. It even increases (exponentially) as the electrical output power setting is lowered. Indeed, over similar tested working temperature range (of about 30°C each time), at 1500  $W_{el}$ , the decrease in thermal efficiency is about 26 percentage points; at 1000  $W_{el}$ , it is about 28 percentage points and at 500  $W_{el}$ , it is about 35 percentage points. This exponential trend can be explained by the exponential relation between thermal efficiency and electrical output power, observable in Figure 50. This graph is comparing these laboratory results to previous results presented in a fuel cell conference by the manufacturer. It is worth mentioning that those previous results have been presented in 2011 and might be relevant for a previous version of the BI\*\*\*G\*N, as it has been seen in *Section 4.1.1 – Working principle* that several versions of the BI\*\*\*G\*N have existed.

As shown in Figure 50, total LHV efficiency is always about or above 80%. Figure 50 also shows in laboratory conditions that the efficiency variations between nominal electrical output power and 1000  $W_{el}$  of output power is not significant. On the other hand, working at minimal power brings a significant total efficiency decrease (explained by the 17 percentage points decrease in electrical efficiency, which is not balanced by the slightly higher thermal efficiency). It is quite trivial that partial load functioning leads to lower electrical and total efficiencies (mainly due to higher heat losses than at design operating conditions while the internal temperature of the stack must be kept constant [460]). Therefore, it is also quite normal than, as electrical efficiency increases, thermal efficiency

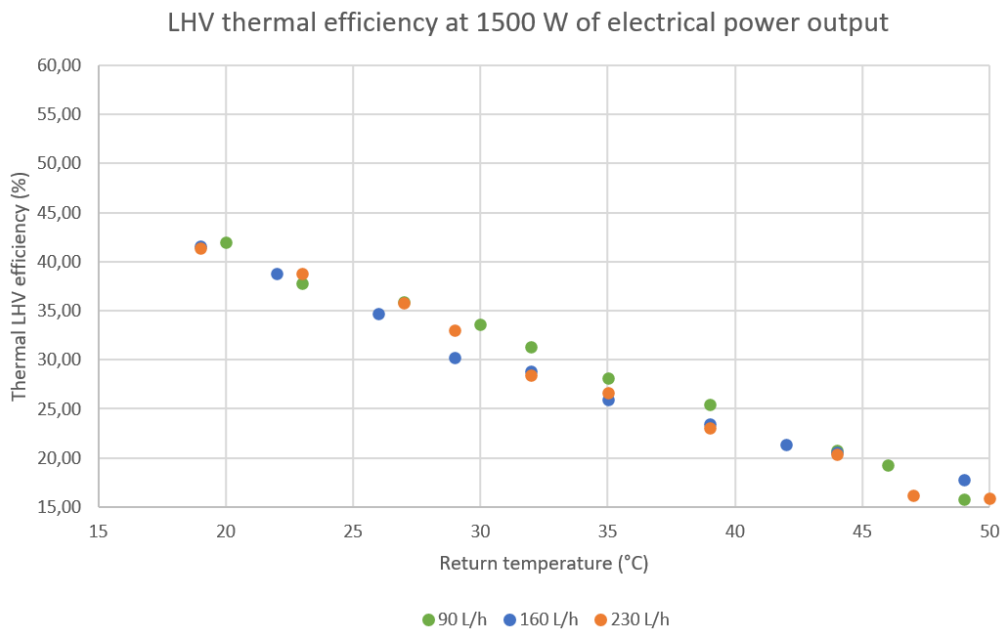
decreases. This has been verified in literature for many CHP systems [461], as demonstrated with Figure 51, for which the experimental results of the BI\*\*\*G\*N system reported in Figure 50 have been added for comparison.

LHV electrical efficiency at nominal power is about 3 percentage points below the manufacturer target (one has obtained 57 % and not 60 % as announced in Table 11). Still, it is quite close to it. As it will be seen in *Section 4.5 - Comparison of laboratory and in-situ measurements* and especially in Figure 62, this could be explained by the intrinsic statistical difference between production units and/or simply by the ordinary ageing of the stack. At lower electrical power (1000 W<sub>el</sub> and 500 W<sub>el</sub>), the laboratory electrical efficiency results seem to be relevant with the 2011 results of Figure 50. On the other hand, it seems that heat recovery has been significantly improved since then.

By deduction of Figure 47, the 25 % LHV thermal efficiency announced by the manufacturer in Table 11 is relevant with a return temperature of 40°C, which is sufficient in some DHW production applications as well as if the SOFC was directly connected to low-temperature terminal units (in older dwellings, for example).

Return temperature (°C)	Time for 0,01m <sup>3</sup> of gas consumption (s)	Water flow rate (L/h)	Thermal power (W)	LHV equivalent power of the gas (W)	Thermal LHV efficiency (%)	Electrical LHV efficiency (%)	Total LHV efficiency (%)
49	134	98	416	2640	15,76	56,82	72,57
46	134	98	508	2640	19,24	56,82	76,06
44	134	98	548	2640	20,76	56,82	77,57
39	134	96	672	2640	25,45	56,82	82,27
35	134	94	742	2640	28,10	56,82	84,92
32	134	93	826	2640	31,29	56,82	88,10
30	134	93	888	2640	33,63	56,82	90,45
27	134	92	949	2640	35,95	56,82	92,76
23	134	90	999	2640	37,84	56,82	94,65
20	134	89	1108	2640	41,97	56,82	98,78
50	134	232	420	2640	15,91	56,82	72,72
47	134	231	427	2640	16,17	56,82	72,99
44	134	231	538	2640	20,38	56,82	77,19
39	134	233	610	2640	23,10	56,82	79,92
35	134	230	704	2640	26,67	56,82	83,48
32	134	230	751	2640	28,45	56,82	85,26
29	134	233	872	2640	33,03	56,82	89,84
27	134	232	944	2640	35,76	56,82	92,57
23	134	229	1024	2640	38,79	56,82	95,60
19	134	235	1093	2640	41,40	56,82	98,21
49	134	157	469	2640	17,76	56,82	74,58
44	134	171	542	2640	20,53	56,82	77,34
42	134	169	565	2640	21,40	56,82	78,22
39	134	170	620	2640	23,48	56,82	80,30
35	134	169	686	2640	25,98	56,82	82,80
32	134	168	760	2640	28,79	56,82	85,60
29	134	157	798	2640	30,23	56,82	87,04
26	134	166	916	2640	34,70	56,82	91,51
22	134	163	1025	2640	38,82	56,82	95,64
19	134	163	1099	2640	41,63	56,82	98,44

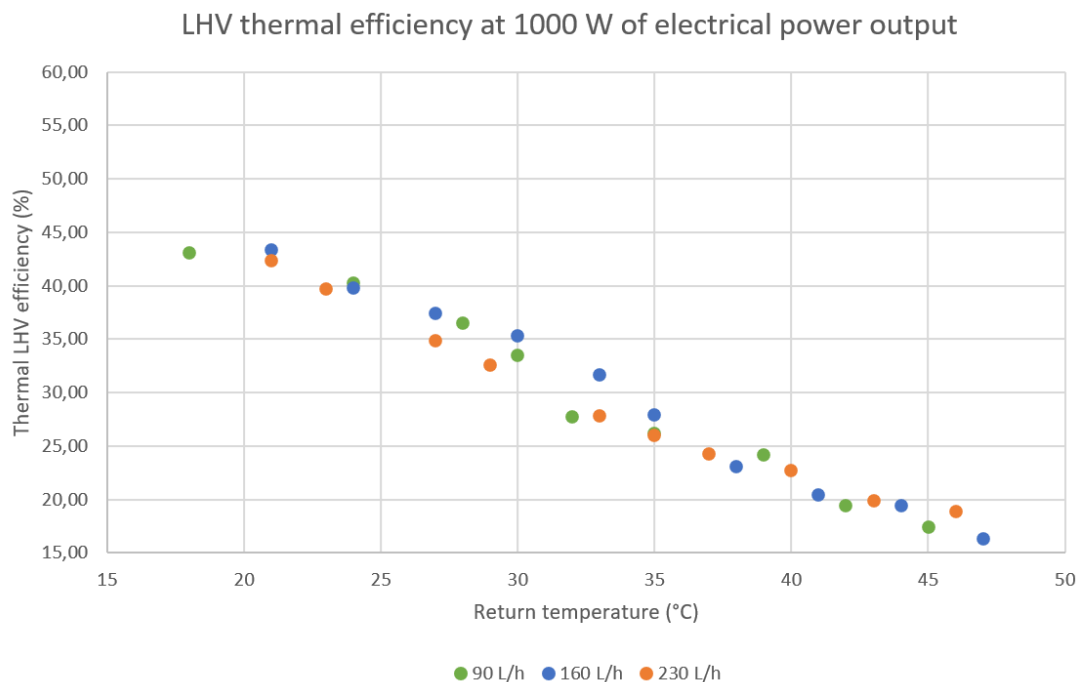
**Table 14.** Laboratory test campaign of the BI\*\*\*G\*N at 1500 W<sub>el</sub> (nominal electrical power output).



**Figure 47.** LHV thermal efficiency of the BI\*\*\*G\*N according to working temperature (and water flow rate) at 1500 W<sub>el</sub> of electrical power output.

Return temperature (°C)	Time for 0,01m <sup>3</sup> of gas consumption (s)	Water flow rate (L/h)	Thermal power (W)	LHV equivalent power of the gas (W)	Thermal LHV efficiency (%)	Electrical LHV efficiency (%)	Total LHV efficiency (%)
48	194	94	266	1826	14,57	54,78	69,35
45	195	94	316	1816	17,40	55,06	72,46
42	194	94	355	1826	19,45	54,78	74,22
39	195	94	438	1816	24,12	55,06	79,18
35	195	92	476	1816	26,21	55,06	81,27
32	196	91	501	1807	27,73	55,34	83,07
30	195	91	608	1816	33,48	55,06	88,54
28	195	91	663	1816	36,51	55,06	91,57
24	194	88	734	1826	40,21	54,78	94,99
18	195	86	782	1816	43,06	55,06	98,12
46	195	225	342	1816	18,83	55,06	73,89
43	194	227	363	1826	19,88	54,78	74,66
40	194	228	414	1826	22,68	54,78	77,46
37	195	228	440	1816	24,23	55,06	79,29
35	196	227	470	1807	26,01	55,34	81,35
33	195	226	505	1816	27,81	55,06	82,87
29	195	226	592	1816	32,60	55,06	87,66
27	194	226	636	1826	34,84	54,78	89,62
23	195	226	721	1816	39,70	55,06	94,76
21	196	229	765	1807	42,34	55,34	97,68
47	196	165	295	1807	16,33	55,34	71,67
44	196	165	351	1807	19,43	55,34	74,77
41	195	164	371	1816	20,43	55,06	75,49
38	194	163	421	1826	23,06	54,78	77,84
35	196	162	504	1807	27,89	55,34	83,24
33	195	161	574	1816	31,60	55,06	86,67
30	196	160	638	1807	35,31	55,34	90,65
27	195	159	680	1816	37,44	55,06	92,50
24	195	157	722	1816	39,75	55,06	94,81
21	194	155	791	1826	43,33	54,78	98,11

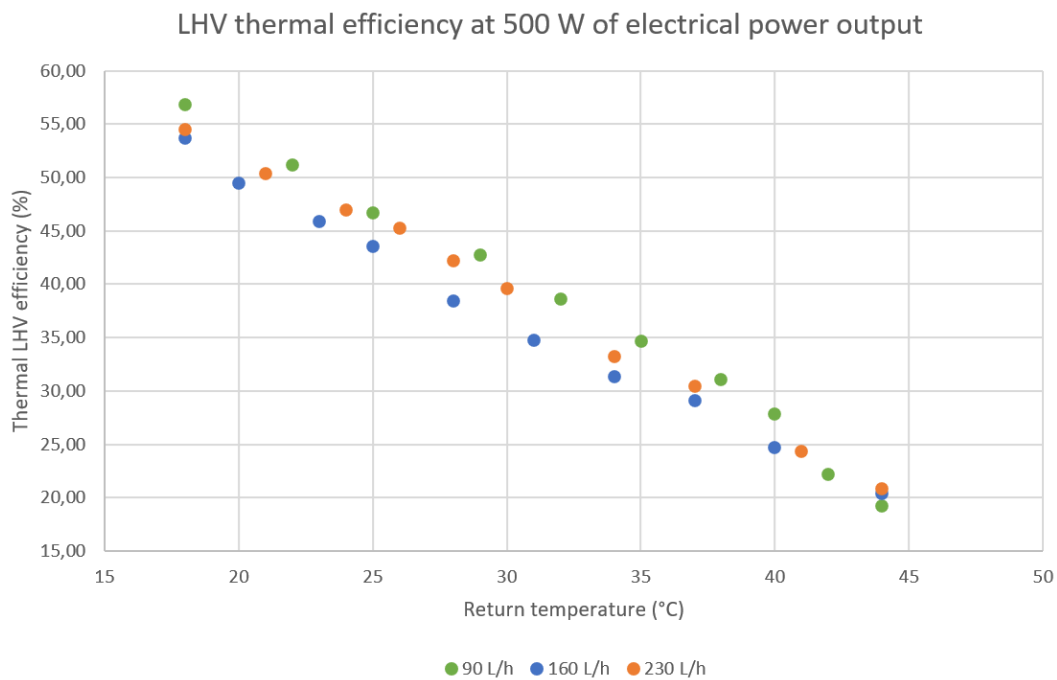
**Table 15.** Laboratory test campaign of the BI\*\*\*G\*N at 1000 W<sub>el</sub> (intermediate electrical power output).



**Figure 48.** LHV thermal efficiency of the BI\*\*\*G\*N according to working temperature (and water flow rate) at 1000 W<sub>el</sub> of electrical power output.

Return temperature (°C)	Time for 0,01m <sup>3</sup> of gas consumption (s)	Water flow rate (L/h)	Thermal power (W)	LHV equivalent power of the gas (W)	Thermal LHV efficiency (%)	Electrical LHV efficiency (%)	Total LHV efficiency (%)
44	279	84	245	1272	19,26	39,31	58,57
42	280	83	281	1268	22,17	39,45	61,62
40	278	83	356	1277	27,89	39,16	67,05
38	277	82	398	1281	31,06	39,02	70,09
35	279	81	441	1272	34,67	39,31	73,97
32	282	81	486	1259	38,62	39,73	78,34
29	279	80	544	1272	42,76	39,31	82,07
25	277	79	598	1281	46,67	39,02	85,70
22	277	78	656	1281	51,20	39,02	90,22
18	280	78	720	1268	56,80	39,45	96,25
44	283	225	261	1254	20,81	39,87	60,68
41	282	223	306	1259	24,31	39,73	64,04
37	281	223	384	1263	30,40	39,59	69,99
34	279	223	423	1272	33,25	39,31	72,56
30	278	220	505	1277	39,56	39,16	78,72
28	280	219	535	1268	42,21	39,45	81,65
26	277	219	580	1281	45,27	39,02	84,29
24	280	217	595	1268	46,94	39,45	86,39
21	279	216	641	1272	50,39	39,31	89,70
18	280	206	691	1268	54,52	39,45	93,96
44	280	166	258	1268	20,35	39,45	59,80
40	280	165	313	1268	24,69	39,45	64,14
37	280	164	369	1268	29,11	39,45	68,56
34	280	163	397	1268	31,32	39,45	70,77
31	279	162	442	1272	34,75	39,31	74,05
28	278	161	491	1277	38,46	39,16	77,62
25	280	160	552	1268	43,55	39,45	83,00
23	279	159	583	1272	45,83	39,31	85,14
20	278	157	632	1277	49,50	39,16	88,67
18	279	155	683	1272	53,69	39,31	93,00

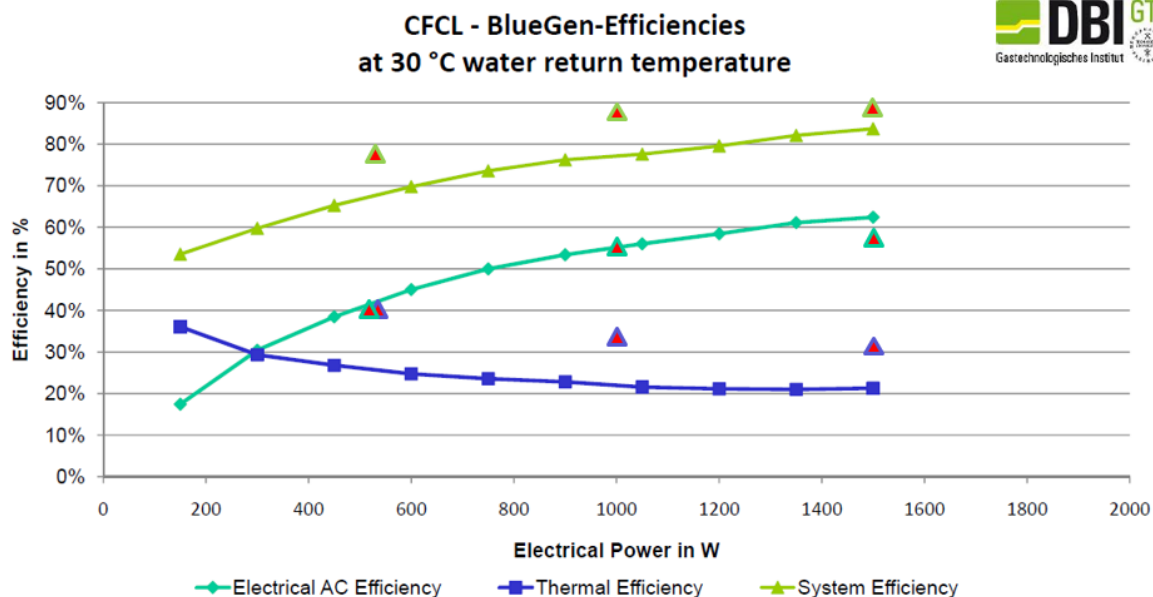
**Table 16.** Laboratory test campaign of the BI\*\*\*G\*N at 500 W<sub>el</sub> (minimal electrical power output).



**Figure 49.** LHV thermal efficiency of the BI\*\*\*G\*N according to working temperature (and water flow rate) at 500 W<sub>el</sub> of electrical power output.

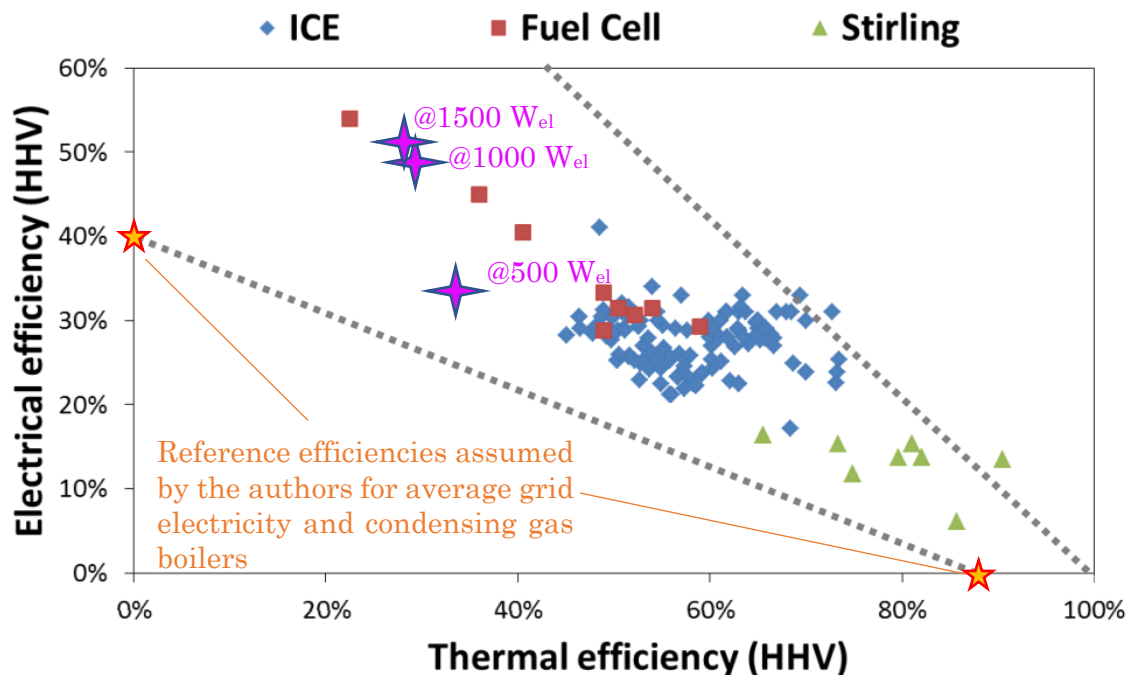


ULiege laboratory results



**Figure 50.** Laboratory results obtained in this work superposed on reproduced LHV efficiency results published in 2011 by the manufacturer for an older version of the BI\*\*\*G\*N [462].





**Figure 51.** Market study on reported efficiencies for three different groups of micro-CHPs: Internal Combustion Engines (ICE), Fuel Cell based micro-CHPs and CHP based on Stirling principle. The efficiencies are put in perspective with a line (lower dotted one) representing the reference conventional power that the micro-CHPs must beat (i.e. the average grid efficiency for electrical generation and the gas condensing boiler for heat production). Average efficiency of the grid electrical mix is considered to be at 40 % HHV (as comparison, the one of UK in 2013 was about 38.6% LHV, i.e. 34.8% HHV [463]). Reference thermal efficiency of condensing gas boiler is considered to be at 90% HHV (as comparison, yearly HHV efficiency figure of field-tested gas condensing boiler have been reported in the 82-89% range [464] whereas the Walloon energy regulator in Belgium has stated, based upon field-test studies, that reference state-of-the-art gas condensing boilers have efficiencies of 90% LHV, i.e. 81.2 % HHV [127]). The maximum physically possible upper limit corresponding to total HHV efficiency of 100% is represented by the upper dotted line. Reproduced and adapted from reference [461]. The experimental results of this SOFC system at 30°C of return temperature reported in Figure 32 according to the output power setting have been added considering a 1.1085 HHV to LHV ratio [132]. The efficiency results over the upper line (total efficiency results over 100% HHV) are most likely due to measurement uncertainty, especially regarding how the HHV is accounted for [465].

#### 4.2.6 Troubleshooting

No break-down were reported nor noticed during the laboratory study timeframe.

#### 4.2.7 Conclusions of the section

The electrical power output is tremendously stable and corresponds to the output power setting. This leads to very stable electrical efficiencies.

The electrical efficiency (and power output) is not altered at all by changes in working temperature of the heat recovery circuit (nor by change in heat recovery flow rate).

Thermal efficiency is almost not altered by the heat recovery flow rate in the tested range.

Thermal efficiency is linearly affected by the working temperature of the heat recovery circuit. Thermal efficiency decreases as working temperature increases. The slope of that linear decrease increases exponentially as electrical power output decreases. At nominal electrical power output (1500 W<sub>el</sub>), the thermal efficiency decrease between about 20°C and 50°C of return temperature is about 26 percent points. Over a similar temperature

range at minimal electrical output power (500  $W_{el}$ ), the thermal efficiency decrease reaches 35 percentage points.

At nominal electrical power output (1500  $W_{el}$ ), highest LHV thermal efficiency is about 42% (about 98% of total LHV efficiency) whereas it increases up to about 55% at minimal electrical power output (500  $W_{el}$ ) and at the lowest working temperatures (around 20°C).

The efficiency results at 1000  $W_{el}$  of electrical power output are really close to the one obtained at 1500  $W_{el}$  of electrical power output (for both electrical and total efficiency). However, lowering the electrical power output down to 500  $W_{el}$  reduces mainly the electrical efficiency, which is not balanced by the increase of the thermal efficiency, meaning that the total efficiency is decreased. Total LHV efficiency is indeed about 78% at 500  $W_{el}$  of electrical power output whereas it comes close to 90 % at 1000  $W_{el}$  and 1500  $W_{el}$  of electrical power output.

The announced LHV thermal efficiency of 25 % at nominal electrical output power of 1500  $W_{el}$  (Table 11) seems to correspond to a return of 40°C, which is relevant for some DHW applications. This corresponds to about 600 W of heat recovered (as announced by the manufacturer, see Table 11). As explained, lowering the return temperature even increases the amount of heat recovered (and the thermal efficiency of the system).

The content of *Section 4.3 - In-situ monitoring*, which mainly aims to report the energy performance of the field-tested systems in terms of natural gas consumption, net electricity production, as well as in terms of thermal and electrical efficiencies, was published almost as-is in the *proceedings of the 7<sup>th</sup> International High Performance Buildings Conference at Purdue (Herrick 2022)* [427]. This section (and its related publication) also reports an assessment of the environmental performance in terms of utilization CO<sub>2</sub> emissions, which methodology has been published (for another micro-CHP fuel cell system) in the *proceedings of the 35<sup>th</sup> International Conference On Efficiency, Cost, Optimization, Simulation and Environmental Impact of Energy Systems (ECOS2022)* [15].

## 4.3 In-situ monitoring

### 4.3.1 Description of the buildings

As stated in the introduction of this chapter, the first house is located in Riemst (East Belgium) whereas the other one is located in Duffel (North of Belgium). From a climatic point of view, one can state that the two houses are located in the same region. The location of the monitoring sites has been presented in Figure 52.



**Figure 52.** Location of the SOFC monitoring sites.

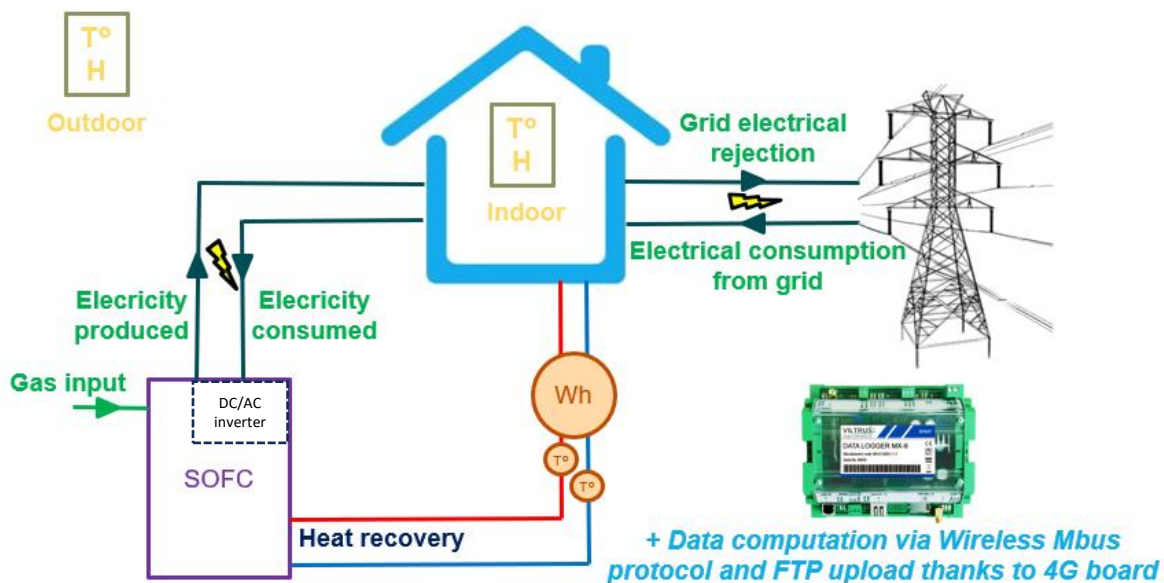
Both houses include a gas condensing boiler as the main space heating appliance. However, the house in Duffel has also invested in air-to-air heat pumps to increase its electrical consumption (produced by the SOFC). Unfortunately, none of the space heating appliances have been monitored because focus was intended towards the electrically driven SOFC only. Nevertheless, the houses and their occupants can still be briefly discussed.

The first monitored building (Riemst) is a full detached house from early 2000s. The family consists of a young active couple with two children under the age of 12. The household owns an electric car.

The second monitored building (Duffel) is a terraced house of three floors from the 70s but significant renovation has been conducted. The family consists of a middle-aged couple with two nearly adult children that mostly do not live in the house. The household owns an electric car, solar panels (that have been monitored) and, as explained, air-to-air heat pumps for both cooling and heating purposes (not monitored).

### 4.3.2 Measurement devices

Both houses are equally monitored. Sensors are identical and are placed at the same spots, according to the simplified scheme of Figure 53. Sensor reference, precision and resolution of the acquired data are presented in Table 17. Most of those sensors have been partially validated by correlation with the corresponding laboratory sensors (in a laboratory environment) as mentioned in Section 4.2.5 - *Experimental results and data analysis*.



**Figure 53.** Monitored sensors configuration of the BI\*\*\*G\*N field-test sites The house in Duffel has an additional PV (photovoltaics) panels electrical production monitoring sensor.

For economic reasons, it has been chosen not to monitor the water consumption from the mains by the SOFC (for the reverse osmosis filters and steam generation, used for methane reforming purposes, as shown in Figure 31). It is assumed that both machines induce similar water consumptions as observed in the laboratory (Section 4.2.4.4 - *Water consumption*).

Last very important parameter not shown in Table 17 is the sampling rate, the frequency of the acquisition, of the measurements. It has been set to a 5-minute time step for both houses. Reducing even more the time step requires extra power supply for the sensors (not possible only with the internal batteries of the sensors), which was not possible to provide for both houses. Furthermore, for such thermal monitoring applications especially with a SOFC working constantly at its nominal power output), a time step of 5 minutes is way enough for the majority of the analyses that are needed.

In any case, with this data logger and its ‘T2’ communication mode [466], it is impossible to set a time step smaller than 2 minutes due to the fact that it must establish a successful Wireless M-bus (Meter-bus) connection with every sensor, one after the other, and that takes time (a few seconds for each connection) [466].

This latter statement implies that the field-test monitoring measurements are not completely synchronous and this tends to impede transient behaviour analysis of the

systems. Through those monitoring signals, systems performance are thus preferably analysed over enlarged timeframes, typically 24 hours or more.

Sensors	Reference	Resolution (data logger included)	Accuracy
Outdoor temperature and <u>humidity</u>	Weptech Munia [467]	0,1 K   0,1 %	$\pm 0,3$ K   $\pm 2$ %
Indoor temperature and <u>humidity</u>	Weptech Munia [467]	0,1 K   0,1 %	$\pm 0,3$ K   $\pm 2$ %
Heat recovery heat counter	Qalcosonic E1 Qn2,5 $q_i=0.025\text{m}^3/\text{h}$   L=130mm [455]	1 kWh   1 L   0,1 K	Accuracy Class 2 [457]
Machine 2-ways electrical energy counter	Iskraemeco MT174-D2A42- V12G22-M3K0 [453]	10 Wh	Accuracy Class 1 [468]
House 2-ways electrical energy counter	Iskraemeco MT174-D2A42- V12G22-M3K0 [453]	10 Wh	Accuracy Class 1 [468]
Gas volume counter	BK-G4T DN25 $Q_{\text{max}} 6 \text{ m}^3/\text{h}$ [452]	10 L	<0.5%
Data logger (cloud connection)	Viltrus MX-9 [469]	NA	NA

**Table 17.** Reference of the monitoring sensors and acquisition system for the Bl\*\*\*G\*N field-test sites.

Except for temperatures and humidity, all of those meters are computing energy index values (always increasing).

It is interesting to note that the heat meters (ultrasonic technology) have a higher resolution (1 Wh) on their physical LCD (Liquid Crystal Display) screen but they are not able to provide that information through the wireless M-bus (Meter-bus [466]) communication protocol that is used. Also, as all heat meters, they base their energy index on the integration of their flow rate measurement, combined to (in-pipes) temperature probes on both depart and return lines of the machine (separate PT-500 temperature measures). One of those temperature probes is internally embodied with the ultrasonic flow rate sensor (and with the display) while the other one is placed at the other hydraulic output of the system being monitored with a dedicated valve assembly (already shown in Figure 43 in *Section 4.2 - Laboratory tests*). Heat meters are simply following the 1<sup>st</sup> thermodynamics principle, as defined by Equation (16), based on pre-programmed enthalpy laws (internal correlation with temperature is implemented). Sensor pre-programming thus depends on the heat transfer fluid (which is simple water in both houses). It also depends on the flow meter position (flow or return circuit) as this will impact the flow meter operating temperature, along with the properties of the fluid being measured. Heat meters are preferably placed on the pipe returning to the machine, as the temperature is lower and more stable. The life of the components is thus extended [470] and both sites considered in this study indeed follow this best practice.

Both electrical energy meters are measuring flows both ways: they are able to provide two indexes of energy, one for each flow. However, at one particular moment, only the net flow is seen and only one of the two indexes can be increasing, following the current direction at that moment. Actually, the machine cannot at the same time consume and produce electrical energy. Since the current always uses the shortest path, in electrical production mode, the machine provides the electricity for its own auxiliaries so no consumption on the meter can be measured. Thus, the lowered net electrical production can only be seen, because the power requested by the auxiliaries is taken directly from the gross production of the SOFC. Same goes for the ‘grid electrical meter’ that measures the net flows exchanged between the house and the grid. To compute the total electrical demand of the house  $W_{el,house,net}$ , one must use Equation (17):

$$W_{el,house,net} = W_{el,FC} - W_{el,house,out} + W_{el,house,in} \quad (17)$$

Where  $W_{el,FC}$  is the monitored electrical energy produced by the machine,  $W_{el,house,out}$  is the monitored electrical energy rejected/injected by the house on the grid and  $W_{el,house,in}$  is the monitored electrical energy consumed by the house from the grid. Those electrical

flows correspond to what is indicated in Figure 53. As explained, there will always be one or several of their corresponding indexes that will remain constant.

Also, the values of the High Heating Value (HHV) of the natural gas mix of both sites have been provided hourly for the whole monitoring period by the gas provider. This information allows for achieving a better accuracy of the analyses, since no assumption on the calorific values of the gas mix has to be made. The method for establishing the LHV or HHV equivalent energy of the consumed gas has been fully developed in *APPENDIX 1: Energy content of natural gas in residential applications* (considering a HHV to LHV ratio of 1.1085 [132]).

### 4.3.3 Methodology

This monitoring section is based on data collected during the whole year 2021. The year 2022 has not been extensively studied for those systems as it has been observed that the systems had behaved exactly as reported for the year 2021.

#### 4.3.3.1 Energetical performance

Electrical efficiencies have been computed without considering the monitored electrical consumption of the system. Only the equivalent energy of the consumed gas has been considered at the denominator of the efficiency calculations. As stated, it is worth mentioning that a consumption signal at the system's output can only be seen if the machine is not producing electricity. Indeed, the system provides electricity to its own auxiliaries in running mode and only the net electrical production is measured. Since the system is supposed to be ran constantly, its remaining measured electrical consumption is not relevant in the efficiency calculations. Due to budget constraints, the electrical consumption of the circulator of the heat recovery circuits have not been monitored and therefore not included in the energetical performance analysis. The electrical consumption of this feature, which depends on the speed setting and the pressure drops on the circuit, is however quite insignificant compared to the 1500 W<sub>el</sub> nominal electrical output power of the SOFC. It can indeed be estimated to only 3 to 45 W<sub>el</sub> [451].

#### 4.3.3.2 Economical and ecological performance

The chosen methodology for establishing performance indicators is similar to what the European Parliament recommends for calculation of primary energy savings of CHP [471]. Their directive recommends to study the performance of a cogeneration by comparison to state-of-the-art separate heat and electrical energy productions. Based on this European directive, the Walloon energy regulator (in Belgium) has stated that the reference state-of-the-art system for heat production is a gas condensing boiler of constant 90% LHV efficiency [127].

Reference electrical state-of-the-art production system will consider the actual electrical Belgian mix in most cases or, as considered by the Walloon energy regulator [127], following European directives [471], a Combined Cycle Gas Turbine (CCGT) plant of constant 55% LHV efficiency [127]. This assumption is only considered once, for one single ecological indicator (Dataset 'A' in *Section 2.3.1 - CO<sub>2</sub> and CO<sub>2eq</sub> emission factors*). The CCGT plants considered in this work as reference electrical production systems are never assumed to be used as CHP, as it is still not that common for large power plants.

Each indicator of this work has been established by considering the actual pricing or ecological performance in the field-test (computed with given pricing or emission factor assumptions) subtracted to the assumed performance that would be achieved by reference machines based on the same field-test heat demands (and local electrical production). Positive indicators imply better performance than reference machines.

Economical indicator subsequently consists in energy utilization cost savings (€ saved/year) compared to the reference machine, which is, as stated, a classical gas condensing boiler. In this work, one has neither taken into account the investment costs of the machine nor the one of its installation (or its removal). The pricing assumptions for this economical indicator have been provided by the Belgian energy regulator, named CREG (*Commission de Régulation de l'Électricité et du Gaz*), that oversees the whole energy market and parties. The federal regulator is providing those energy pricing based on the average Belgian household energy bills [15]. For 2021, only the second semester average prices have been considered and applied to the whole monitoring data of the year, in order to partially consider the impact of the energy crisis [472] on the economical performance of the machine. The energy prices, considered constant for the whole year, are thus 0.333€/kWh<sub>el</sub> for electrical energy and 0.093€/kWh<sub>HHV</sub> for natural gas [473]. It must be pointed out that European natural gas prices even rose by almost 70% after Russia invaded Ukraine in February 2022 [474] but that is not considered at this point.

Other important pricing assumption is that the electrical energy transport and distribution costs are rounded to 0.15€/kWh<sub>el</sub> (0.1€/kWh<sub>el</sub> for distributions and 0.05€/kWh<sub>el</sub> for transport) as considered by the Walloon regulator (named CWaPE) in its tariffication plans [475]. This means that rejected/injected energy on the grid will not be bought back to the residential customer at the same kWh price mentioned earlier. This is because the customer uses the grid to sell its extra energy and it must pay for its infrastructures. The selling price of the rejected/injected electrical energy is thus equal to the electrical price mentioned earlier minus the 0.15€/kWh<sub>el</sub> to account for transport and distribution costs.

As stated, the environmental indicators are based on the same method of comparison with reference systems. The pricing assumptions are simply replaced by emission factors (see *Section 2.3.1 - CO<sub>2</sub> and CO<sub>2eq</sub> emission factors* and Table 4). Two sets of assumptions are considered in this work. The first one is used by the Walloon energy regulator [127] to promote CHP (called Dataset 'A' in Table 4). It overestimates on purpose the reference electrical emission factor by considering that the local electrical production allowed by the system replaces CCGT power plants (of 55% LHV efficiency). As stated in *Section 2.3.1 - CO<sub>2</sub> and CO<sub>2eq</sub> emission factors*, this is still a relevant assumption as at least one of those natural gas power plants have always been turned on in 2020 and 2021 in Belgium (Dataset 'A' in Table 4 is indeed perfectly relevant for marginal emissions [135] studies). However, the actual average Belgian mix is far more decarbonated, as it involves renewables and a significant part of nuclear energy considered as 'low carbon' [133]. In fact, Belgian CHP investors can benefit from public grants depending on those CO<sub>2</sub> savings.

The second ecological indicator, called Dataset 'E1' in Table 4, considers the hourly emission factor for the Belgian consumption electrical mix (data provided for the whole year 2021 by [www.Electricitymap.org](http://www.Electricitymap.org) for academic purposes). Therefore, the first indicator implies a constant electrical emission factor of 456 gCO<sub>2eq</sub>/kWh<sub>el</sub> whereas the second evolves hourly. For information, the statistical average electrical emission factor for the whole 8760 hours of 2021 is 167 gCO<sub>2eq</sub>/kWh<sub>el</sub> [15], well below the assumption of the first indicator.

Regarding the emission factor for natural gas consumption/combustion, it is quite close between the two sets of assumptions : 251 gCO<sub>2eq</sub>/kWh for the first indicator as used again by the Walloon regulator [127] and, for the second one, relevant with the [www.Electricitymap.org](http://www.Electricitymap.org) data, 254 gCO<sub>2eq</sub>/kWh, [15].

It is worth mentioning that the ecological indicator used in this section accounts for all greenhouse gases (expressed in CO<sub>2eq</sub> and not in CO<sub>2</sub> only). Also, even if the first dataset has been established in 2005, it is still valid and used as there has neither been any game changer regarding the efficiency of the reference systems for energy production (nor

regarding natural gas production and importation). Actually, the only emission factor that is likely to become obsolete in the few years to come is the electrical one considered in the second set of assumption (from the [www.Electricitymap.org](http://www.Electricitymap.org) data). This is because electrical mix evolves constantly, especially with increased penetration of renewables.

At last, as stated, to the understanding of the author, grid transportation and distribution electrical losses, which can reach about 6-7% in EU [130], have not been considered in any of the electrical emission factors. However, this is for the moment assumed not to be significant and also partially compensated by the fact that it could also be considered that the extra gas consumption for the decentralized SOFC electrical production is subjected to fugitive methane emissions (with high GWP) on longer gas network distances. It can indeed be considered that this gas no longer goes to the nearest CCGT power plant but is transported to the dwelling. For information, fugitive losses can be estimated to  $5.4 \times 10^{-6}$  kg for the transport of 1 kg of natural gas for a distance of 1 km [476]. In fact, this balance between avoided electrical network losses and extra fugitive methane emissions in the gas network will even be illustrated later on in Table 20.

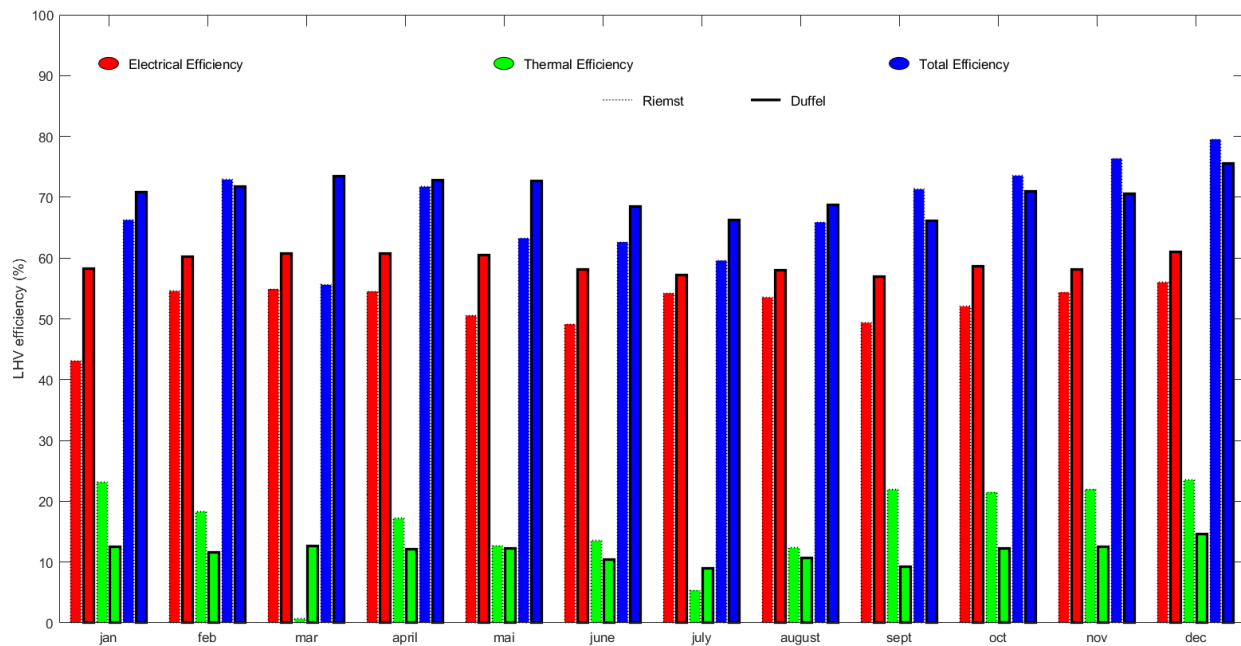
Further explanations on the method used to establish economical and ecological indicators have been published in a parallel study for a different fuel cell system [15], i.e. the PEMFC micro-CHP, discussed later on in *Chapter 5 - Study of the P\*2 PEMFC system*. That same study also involves the detailed explanations on emission factors, which have also been reported earlier in *Section 2.3.1 - CO<sub>2</sub> and CO<sub>2eq</sub> emission factors*.

#### 4.3.4 Results

Performance results are presented in Table 18. Overall, performance of both field-test machines are quite similar.

The first observation is that the Duffel system is really close to the expected electrical efficiency of 60% LHV (Table 11) whereas the Riemst system is a little below. The main reason is that the Riemst system's power output has been modulated down for some significant amounts of time through the year (for the vacation of the occupants, as it can be seen in Figure 54, Figure 55 and Figure 56) whereas the system in Duffel was running at nominal power the whole year. This can be perceived by the lower yearly electrical production (Table 18). Indeed, partial electrical load induces a reduction in electrical efficiency, as it has been seen for the laboratory tests in Figure 50. Second possible explanation is the probable intrinsic statistical efficiency difference between produced units. Indeed, the difference between percentile 0.9 and percentile 0.1 can account for a 2.5 percentage points efficiency difference for this system at nominal output power [462]. This has already been mentioned as a possible explanation to the electrical performance obtained in laboratory test campaigns, and this will be shown again in Figure 62 in *Section 4.5 - Comparison of laboratory and in-situ measurements*.

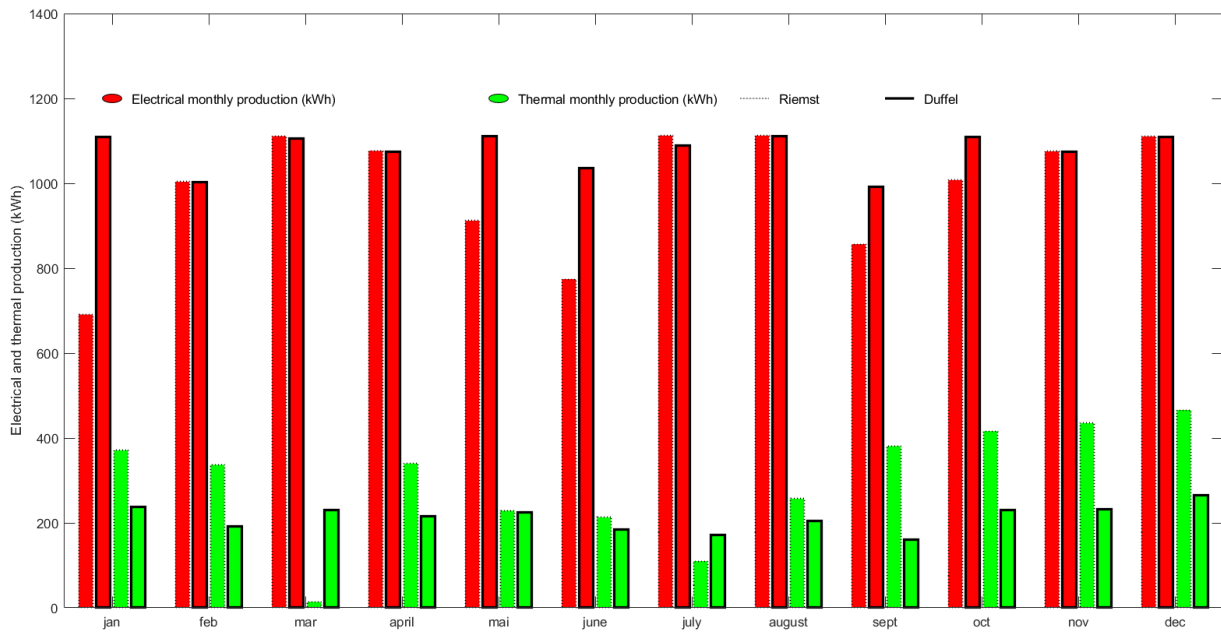




**Figure 54.** LHV efficiency of both field-test SOFCs discretized per month for the year 2021.

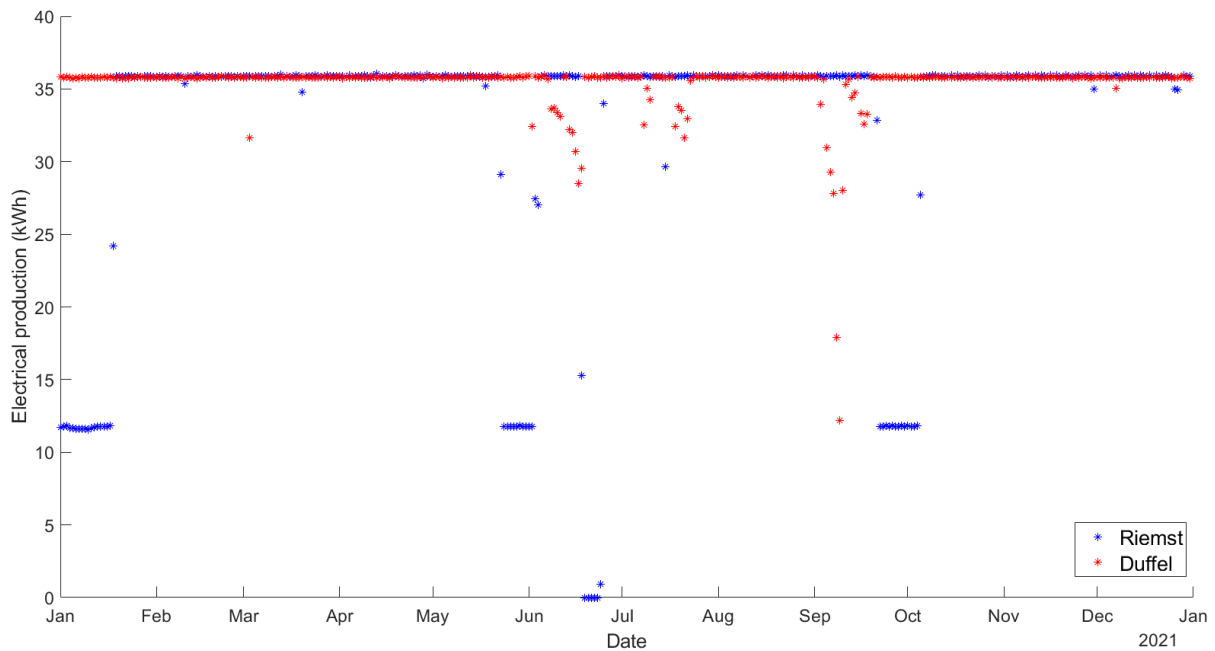
Second observation is that thermal efficiency (and heat recovered) is higher for Riemst. This is mainly again because of the fact that the SOFC electrical output power in Riemst was modulated down to the minimal value ( $500 \text{ W}_{\text{el}}$ ) during the vacation time of the owner. Indeed, the lower the electrical output, the higher the thermal recuperation, as it has been seen for the laboratory tests in Figure 50. In both cases, by looking only at the absolute yearly amount of heat recovered (and not the daily profiles nor the working temperatures), the heat recovered with this system is greater than the amount required by the 'M' DHW profile from the European Standard EN 16147:2011 [171]. It is also greater than the average household's DHW consumption of a lot countries, such as the USA, the UK, Finland Spain or Portugal [171]. The fact that this system might be able to provide all the DHW demand of the household might allow significant capital savings as it simplifies the DHW production system. For example, there would be no need for a dedicated heat pump water heater or extra investments for the gas condensing boiler or the heat pump to be able to provide DHW in addition to its space heating function. It seems however preferable to at least include a backup heating resistance in the upper part of the DHW tank in order to ensure minimum DHW delivery temperature. Especially if the household DHW demand occasionally peaks, the system's DHW capability might not suffice.

Because of the intrinsic correlation between efficiencies and load factor, the monthly discretized efficiencies of Figure 54 shall be looked at considering monthly electrical production of Figure 55. For a month of 31 days, the maximum electrical energy production would be equal to 31 (days) times 24 (hours) times  $1.5 \text{ (kW}_{\text{el}})$  of nominal output power). Thus, it can indeed be observed that the Duffel system indeed runs all year long at nominal power (maximized load factor), which is also confirmed by Figure 56.



**Figure 55.** Electrical energy and heat production of both field-test SOFCs discretized per month for the year 2021.

Figure 56 indicates that the Riemst system has even been turned down for a few days in the summer. It is worth mentioning that there were a few monitoring signal losses in Duffel (which led to daily electrical productions indicated below 35 kWh), but this had no effect on the established efficiencies (it was each time a loss of all signals at the same time, including electrical energy meter, heat counter and gas meter).



**Figure 56.** Daily electrical energy production of both field-test SOFCs for the year 2021.

Monitoring performance	Riemst	Duffel	Monitoring performance	Riemst	Duffel
HHV energy consumed by the SOFC (kWh)	25031	24273	LHV Electrical efficiency (%)	52,4	59,0
Electrical production of the SOFC (kWh)	11843	12922	LHV Thermal efficiency (%)	15,8	11,6
Electrical consumption of the SOFC (kWh)	11	0	LHV Total efficiency (%)	68,2	70,6
Heat recovered (kWh)	3569	2549	Utilization CO <sub>2eq</sub> savings (marginal emissions) – 1 <sup>st</sup> dataset (kgCO <sub>2eq</sub> ) <sup>b</sup>	723	1107
Energy utilization cost savings (€) <sup>a</sup>	1429	1308	Utilization CO <sub>2eq</sub> savings – 2 <sup>nd</sup> dataset (kgCO <sub>2eq</sub> ) <sup>c</sup>	-3013	-2969

<sup>a</sup> - Electrical price: 0.333€/kWh<sub>el</sub>. Gas price 0.093€/kWh<sub>HHV</sub>.

<sup>b</sup> - 1<sup>st</sup> dataset emission factors : 251 gCO<sub>2eq</sub>/kWh for gas and 456 gCO<sub>2eq</sub>/kWh<sub>el</sub> for electricity (see Dataset 'A' from Table 4).

<sup>c</sup> - 2<sup>nd</sup> dataset emission factors : 254 gCO<sub>2eq</sub>/kWh for gas and hourly data from Belgian electrical consumption mix from [www.Electricitymap.org](http://www.Electricitymap.org) for electricity (see Dataset 'E1' from Table 4).

**Table 18.** Monitoring performance of the field-tested SOFCs for the whole year 2021. Utilization savings indicators consider a gas condensing boiler of 90% constant LHV efficiency as reference for heat production.

Monitoring performance	Riemst	Duffel	Monitoring performance	Riemst	Duffel
Total electrical energy consumption of the household	11077	10608	Other local electrical production than the SOFC, i.e. PV panels for the Duffel house (kWh)	0	2549
Total electrical energy rejected/injected on the grid	3947	6861	Remaining electrical consumption from the household on the grid (kWh)	3188	1998

**Table 19.** Additional monitoring data of the field-tested SOFCs for the whole year 2021.

It is worth mentioning that energy utilization cost savings depend greatly on the ability of the household to consume the electricity the system is producing while it is producing (as it is financially not that interesting to reject electricity on the grid with such fixed electrical tariffication assumptions). Therefore, cost savings of Table 18 are strongly case-dependent: both households involve an electric car that largely helps increasing the 'self-consumption' of the electricity produced, also called 'supply cover factor' [477], to about 60% over the monitored year of 2021. This improves the economical indicator. In addition to local spark spread [478] and household supply cover factor, energy utilization cost savings should be looked at considering the capital costs of the system, as they will define the Return On Investment (ROI). For instance, with those results, if an investor wanted to ensure reaching ROI before 10 years, the maximum capital costs of the system should not reach more than about 13-14 k€, which shall include a reasonable margin for any potential maintenance costs (this is considering that the owner already has a gas condensing boiler as main space heating appliance and this is not considering the additional capital savings of the already stated simplified DHW production). This example is also directly applicable to households that do not need space heating at all (passive houses). If one particular household needed to invest in a space heating appliance such as a gas condensing boiler and was also considering this SOFC, that example shall not directly be considered as valid. Indeed, that household's choice would therefore lie between

a single gas condensing boiler (also able to provide DHW) against the combination of the SOFC system and a gas condensing boiler (or another space heating appliance). For the 10-years ROI to be reached, the addition of both appliances shall not exceed the stated 13-14 k€, which is thus more restrictive than the previous case (that considered such a similar figure but for the capital costs of the SOFC only).

Although this SOFC's capital costs are unknown to the author, it is interesting to point out that back in 2015, residential SOFC technology cost (with auxiliaries) was estimated to about 10 k€/kW [479]. This would mean that this 1,5 kW<sub>el</sub> system would cost about 15 k€, slightly above the 10-year energy utilization savings stated earlier. It is possible that current and future SOFC technology costs have been reduced and will continue to be reduced (with higher technology penetration and prices learning curve).

As stated, potential maintenance costs have not been considered in those economical analyses. Maintenance costs of fuel cell based micro-CHPs have been estimated around 0,04€/kWh<sub>el</sub> for the year 2024 [335]. Considering those costs as valid for the current period of time, yearly maintenance costs of the BI\*\*\*G\*N systems can be estimated about 500-600 € per year (based on yearly monitored electrical production of Table 18). With those assumptions, the figure of 13-14 k€ 10-year ROI maximum costs would significantly be reduced to 7-9 k€ of maximum capital costs (considering maintenance costs).

Considering LHV thermal and electrical efficiencies of the SOFC as constant all year long, energy utilization savings  $\epsilon_{savings}$  can be transcribed analytically as follows. First, as mentioned, they are defined by the difference between energy utilization costs of reference systems for energy production (heat and power), i.e.  $\epsilon_{ref}$ , and the energy utilization costs of the SOFC  $\epsilon_{SOFC}$  :

$$\epsilon_{savings} = \epsilon_{ref} - \epsilon_{SOFC} \quad (18)$$

Costs of reference systems for energy production (heat and power) are defined as follows. Indeed, it can be considered that the heat recovered from the SOFC, i.e.  $Q_{recovered}$ , would have been produced by a gas condensing boiler (with a LHV efficiency of  $\eta_{th,cb}$ , generally considered at 90 % (as already stated in this work). 1.1085 [132] is the typical HHV to LHV ratio of natural gas, as already discussed in this work, and  $\epsilon_g$  is the average billing price of natural gas (per kWh). With reference systems, the electrical net demand of the dwelling  $W_{el,house,net}$  is drawn from the grid at an average billing price of  $\epsilon_e$ .

$$\epsilon_{ref} = \frac{Q_{recovered}}{\eta_{th,cb}} \times 1.1085 \times \epsilon_g + W_{el,house,net} \times \epsilon_e \quad (19)$$

By definition of LHV thermal efficiency  $\eta_{th,av}$ , the heat recovered  $Q_{recovered}$  can be established according to the equivalent LHV energy contained in the gas consumed by the SOFC  $W_{g,LHV}$  :

$$Q_{recovered} = W_{g,LHV} \times \eta_{th,av} \quad (20)$$

The equivalent LHV energy contained in the gas consumed  $W_{g,LHV}$  can also be linked to the electrical production of the SOFC  $W_{el,FC}$  through the definition of the LHV electrical efficiency  $\eta_{el,av}$  :

$$W_{g,LHV} = \frac{W_{el,FC}}{\eta_{el,av}} \quad (21)$$

The total electric demand of the dwelling  $W_{el,house,net}$  can be linked to the electrical production of the SOFC that is directly consumed locally by dwelling thanks to the definition of the demand cover factor  $\gamma_d$  [477]:

$$W_{el,house,net} = \frac{W_{el,FC,local}}{\gamma_d} \quad (22)$$

The electrical production of the SOFC that is directly consumed locally by dwelling  $W_{el,FC,local}$  can be linked to the gross electrical production of the SOFC  $W_{el,FC}$  thanks to the definition of the supply cover factor  $\gamma_s$  [477]:

$$W_{el,FC,local} = W_{el,FC} \times \gamma_s \quad (23)$$

Energy utilization costs of the SOFC  $\epsilon_{SOFC}$  are trivially defined by the gas consumed by the system  $W_{g,LHV}$ , the remaining electrical energy consumed by the dwelling on the grid  $W_{el,house,in}$ , to which is subtracted the electrical energy produced by the SOFC not consumed by the dwelling and injected/rejected on the grid  $W_{el,house,out}$  (valued at an average injection price per kWh of  $\epsilon_{inj}$ ):

$$\epsilon_{SOFC} = W_{g,LHV} \times \epsilon_g + W_{el,house,in} \times \epsilon_e - W_{el,house,out} \times \epsilon_{inj} \quad (24)$$

By definition, the remaining electrical energy consumed by the dwelling on the grid  $W_{el,house,in}$  is equal to the total demand of the dwelling  $W_{el,house,net}$  minus the electrical production of the SOFC that is directly consumed locally by dwelling  $W_{el,FC,local}$ :

$$W_{el,house,in} = W_{el,house,net} - W_{el,FC,local} \quad (25)$$

Similarly, the electrical energy produced by the SOFC not consumed by the dwelling and injected/rejected on the grid  $W_{el,house,out}$  is defined by the difference between the gross electrical production of the SOFC  $W_{el,FC}$  and the electrical production that is directly consumed locally by the dwelling  $W_{el,FC,local}$ :

$$W_{el,house,out} = W_{el,FC} - W_{el,FC,local} \quad (26)$$

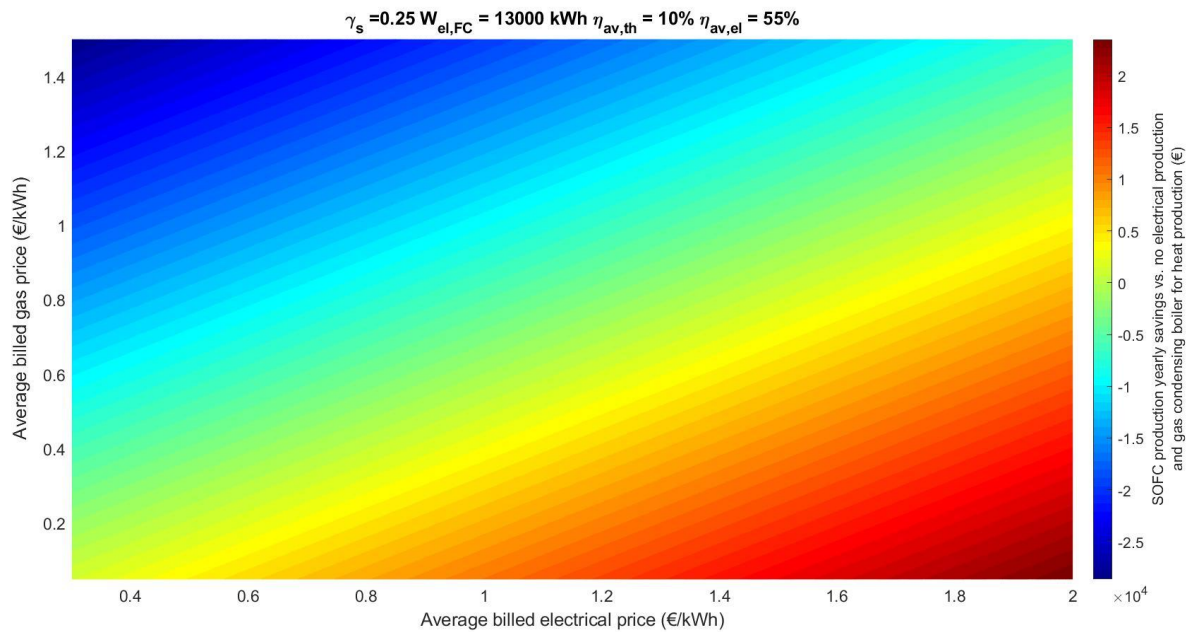
Thus, Equation (18) to Equation (26) give the following analytical formula for the energy utilization costs savings of using the SOFC:

$$\epsilon_{savings} = \epsilon_g \times \frac{W_{el,FC}}{\eta_{el,av}} \left( \frac{\eta_{th,av}}{\eta_{th,cb}} \times 1.1085 - 1 \right) + W_{el,FC} \times \gamma_s \left( \epsilon_e - \epsilon_{inj} + \frac{\epsilon_{inj}}{\gamma_s} \right) \quad (27)$$

Therefore, energy utilization costs savings do not directly depend on the demand cover factor  $\gamma_d$ . Indirectly, it should be pointed out that, for example, increasing the local production capacity (adding SOFCs for example) will affect both cover factors. So, if  $\gamma_d$  is changed in such a way,  $\gamma_s$  will also vary and affect the energy utilization savings. Reducing the total electrical demand of the dwelling is also likely to affect both cover factors if the reduction on the demand is not only associated to a reduction in the remaining energy withdrawn from the grid  $W_{el,house,in}$  (so the indirect link between  $\epsilon_{savings}$  and  $\gamma_d$  is again highlighted).

It is worth mentioning that in Equation (27), the electrical power output (expressed in terms of energy)  $W_{el,FC}$  as well as its depending SOFC LHV thermal and electrical efficiencies could also be considered as varying through time in a more complex expression. This could be performed by the use of the efficiency models that will be presented later on in Equation (30) and Equation (32) in *Section 4.4 - Machine modelling*.

As an example, for a relatively low average supply cover factor  $\gamma_s$  of 25%, an annual electrical production of the SOFC  $W_{el,FC}$  of 13000 kWh<sub>el</sub>, thermal  $\eta_{th,av}$  and electrical  $\eta_{el,av}$  LHV efficiencies respectively of 55% and 10% (in order to consider the least promising figures seen in the field-test, as shown in Table 18), Equation (27) leads to Figure 57. It is worth mentioning that those inputs parameters are relevant with the SOFC functioning at its nominal output power (all year long). The Riemst SOFC has indeed an electrical efficiency slightly lower than 55% LHV (Table 18) but that would not have been the case if it had been set at nominal output power all year long (see Figure 59), as in the simulated case of Figure 57. Figure 57 implies injection costs  $\epsilon_{inj}$  of the electricity not consumed by the dwelling and rejected on the grid equal to average billed electrical price  $\epsilon_e$  minus 0.15 €/kWh to account for transport and distribution costs, as explained in Section 4.3.3.2 - *Economical and ecological performance* (assumption currently valid for Wallonia). It can be pointed out that in Flanders, injection prices can be much less beneficial, as low as 0.035 €/kWh as reported in a study published in 2022 [480].



**Figure 57.** Sensitivity study of the energy utilization economic balance according to energy prices. Positive economic balances mean that the SOFC system provides savings compared to the references (grid electricity consumption and gas condensing boiler).

Figure 57 and Equation (27) indicate independent linear relation between the resulting savings and energy prices. It can be observed that about 5 k€ of savings (way enough to guarantee ROI under 10 years, maintenance costs included) should be reached if energy prices respect Equation (28), also expressed as Equation (29), which have been established graphically:

$$\epsilon_g \leq \epsilon_e \times \frac{0.9}{1.43} - 0.3 \text{ [€/kWh]} \quad (28)$$

$$\epsilon_e \geq (\epsilon_g + 0.3 \text{ [€/kWh]}) \times \frac{1.43}{0.9} \quad (29)$$

This is particularly interesting to consider with the current energy price crisis emphasized by the Ukraine-Russia conflict started in February 2022 [474].

For example, for the first semester of 2023, the difference between Belgian electricity and gas prices is still not sufficient for Equation (28) to be respected as electric and gas prices can respectively be considered equal to 0.425 €/kWh and 0.112 €/kWh [481]. However, the

yearly savings would be yet around 3 k€ (deduced from Figure 57), which is still likely of offer a ROI under 10 years.

At last, from an environmental point of view, the emission factors assumptions have significant influences. The ecological balances can either be considered as positive or negative. On one hand, the fact that the first dataset (marginal emissions [135]) gives positive CO<sub>2eq</sub> savings means that these decentralized electrical production systems are more environmentally friendly than centralized CCGT plants. On the other hand, the fact that the second dataset (average emissions) gives negative CO<sub>2eq</sub> savings means that these systems are ecologically worse than the average local electrical mix (with its renewables and its nuclear energy). As these systems are currently used with constant output power, the second emission factor dataset with the resulting negative CO<sub>2eq</sub> balances might be considered as more relevant. However, even if the Marginal Emission Factor (MEF) of Belgium was not always the one of natural gas power plants (Dataset 'A'), as it was the case in 2020 and 2021 (see *Section 2.3.1 - CO<sub>2</sub> and CO<sub>2eq</sub> emission factors*), these SOFC systems have the ability to only be powered up to replace CCGT electrical production (since remote control is already possible), validating the use of the emission factors from Dataset 'A'. Since this SOFC shall not be completely stopped (see *Section 4.1.2 – Applications and the different versions of the tested system*), its flexibility ability is yet limited (from the minimal output power to the maximum output power, or to every output power in between).

It is worth mentioning that those latter statements rely on the fact that the BI\*\*\*G\*N demonstrated 60% of LHV efficiency, which is intrinsically greater than the considered CCGT reference system for electrical production with a LHV efficiency of 55%. However, it is sometimes considered in literature that, in the near-to-medium term, CCGT power plants with similar 60% of LHV efficiency will be feasible [482]. Therefore, if that were the case, the electrical efficiency of near-to-medium SOFC systems should also increase in order to stay ahead of CCGTs. This should not be problematic as it has been shown in *Section 3.2.5 - Current and expected performance of micro-CHP systems based on a PEMFC or a SOFC* that commercial SOFCs already exist with 65% net AC LHV electrical efficiency or that the theoretical electrical efficiency of the direct electrochemical oxidation of methane in a SOFC is close to 100%.

In addition, with potential dynamic electrical production contracts, for example based on day-ahead hourly prices [483], this SOFC potential flexibility service could lead to higher rejection prices for the household and subsequent quicker ROI.

As mentioned in *Section 4.3.3.2 – Economical and ecological performance*, established CO<sub>2</sub> balances do not consider the beneficial impact of avoided electrical network electrical losses thanks to decentralized production (estimated to 6-7% in EU [130]) and they do not as well consider the negative impact of fugitive natural gas emissions over longer gas network distance up to the field-test dwellings. Indeed, the distance travelled by the consumed gas of a centralized CCGT is assumed to be shorter as such power plants are assumed to be placed on the main pipelines of the gas network. Table 20 aims to provide information on both those unconsidered features relevant to the SOFC studied in this work.

For information, fugitive natural gas losses (with high GWP) can be estimated to  $5.4 \times 10^{-6}$  kg for the transport of 1kg of natural gas for a distance of 1km [476], as reported in Table 20.

As the extra gas network distance up to the dwellings induced by the extra gas consumption related to the SOFC onsite electrical production is not available, the comparison has been expressed another way around. Indeed, the comparison reported in in Table 20 highlights the extra gas network distance that would result in extra CO<sub>2eq</sub> due

to natural gas fugitive emissions that match the avoided CO<sub>2eq</sub> emissions of electrical network losses thanks to the decentralized electrical production of the BI\*\*\*G\*N system. Since the obtained equivalent extra gas network distance is expressed in several hundreds of km (even with lowered SOFC efficiencies of 55% LHV electrical and 10% LHV thermal along with only 6% of electrical network losses), it can be assumed that it always will be greater than any Belgian gas pipeline length. This means that the avoided CO<sub>2eq</sub> emissions associated to the avoided electrical network losses allowed by decentralized electrical production can always be considered greater than the GHG emissions related to fugitive methane emissions associated to the extra local gas consumption required for the decentralized SOFC electrical production (with the SOFC at nominal power and enabled heat recovery).

Yearly electrical production of the SOFC - average of field-test figures of Table 18 [kWh <sub>el</sub> ]	'Ideal' electrical LHV efficiency of the SOFC based on field-test figures of Table 18 [-]	Equivalent LHV energy contained in the gas consumed by the SOFC [kWh]	'Ideal' thermal LHV efficiency of the SOFC based on field-test figures of Table 18 [-]	'Ideal' yearly heat recovered by the SOFC considering the 'ideal' thermal efficiency of this Table [kWh <sub>th</sub> ]	Equivalent LHV energy contained in the gas that would have been consumed by a condensing boiler of 90% of LHV efficiency [127] to match the heat recovered by the SOFC [kWh]
12383	0,6	20638	0,16	3302	3669
Equivalent LHV energy contained in the gas consumed by the SOFC for electrical production only, not considering the gas that would have been consumed for SOFC heat production with a gas condensing boiler of 90% LHV efficiency [127] [kWh]	Average LHV of natural gas based on average 2021 field-test figures and a HHV to LHV ratio of 1.1085 [132] [kWh/m <sup>3</sup> ] <sup>a</sup>	Equivalent gas volume consumed by the SOFC for electrical production only, not considering the gas that would have been consumed for SOFC heat production with a gas condensing boiler of 90% LHV efficiency [127] [m <sup>3</sup> ]	Equivalent gas (CH <sub>4</sub> ) mass consumed by the SOFC for electrical production only, not considering the gas that would have been consumed for SOFC heat production with a gas condensing boiler of 90% LHV efficiency [127] <sup>b</sup> [kg]	Average CH <sub>4</sub> fugitive emissions in gas network [476] [kg CH <sub>4,fugitive</sub> / (km * kg CH <sub>4,consumed</sub> )]	Extra fugitive CH <sub>4</sub> emissions associated to the local electrical production only of the SOFC [kg CH <sub>4,fugitive</sub> / km]
16969	9,86	1721	1446	5,40E-06	8,E-03
GWP-100 of CH <sub>4</sub> [15]. IPCC recommends the use of GWP-100 in CO <sub>2eq</sub> accounting of methane emissions [484].	CO <sub>2eq</sub> emissions related to the extra fugitive CH <sub>4</sub> emissions associated to the local electrical production only of the SOFC [kg CO <sub>2eq</sub> / km]	Average emission factor of consumption electrical mix of Belgium in 2021 - data provided by <a href="http://Electricitymap.org">Electricitymap.org</a> [gCO <sub>2eq</sub> /kWh <sub>el</sub> ]	Average electrical energy network losses [130] [-]	CO <sub>2eq</sub> emissions avoided considering the local electrical production of the SOFC, the average Belgian consumption emission factor of 2021 and the network losses [kg CO <sub>2eq</sub> ]	Maximum extra gas network distance that would lead to CO <sub>2eq</sub> emissions of fugitive natural gas that match the CO <sub>2eq</sub> saved from the avoided 7% electrical network losses thanks to decentralized power production [km]
28	0,219	167,7	0,07	145	665

<sup>a</sup> Average HHV for Riemst = 11.52 kWh/m<sup>3</sup>. Average HHV for Duffel = 10.34 kWh/m<sup>3</sup>. Figures given hourly by the gas provider.

<sup>b</sup> Natural gas density = 0,84 kg/m<sup>3</sup>[485].

**Table 20.** CO<sub>2eq</sub> impact of avoided electrical network losses thanks to the decentralized electrical production of the SOFC system and impact of extra fugitive natural gas emissions due to additional gas consumption at decentralized dwellings.



A relevant extra gas network distance up to the dwellings could be considered in the 0.1-50 km range, given Belgian urbanization levels. This would still mean that the avoided GHG emissions allowed by the local electrical production of the SOFC would at least be about ten times greater than the additional fugitive emissions. Therefore, the ecological balances of Table 18, i.e. the utilization CO<sub>2eq</sub> savings could be considered enhanced by about 110-145 kgCO<sub>2eq</sub>, considering the figures reported in Table 20. The upper limit directly comes from Table 20 and the lower limits considers 50 km of extra gas network distance (with SOFC LHV electrical and thermal efficiencies respectively of 55% and 10% as well as 6% of electrical network losses). Those kinds of corrections are not at all significant enough to change any of the statements made in this section. With these assumptions, fugitive methane emissions in natural gas transportation is only considered at the local level (the extra distance considered is basically the one from the nearest CCGT power plant to the dwelling). Therefore, the extra fugitive methane emissions from international transportation from production sites is not considered, which is only a valid assumption when SOFC's electrical production replaces the electrical production of CCGTs, as it is currently the case in Belgium as some CCGTs have always been on in 2020 and 2021 (see *Section 2.3.1 - CO<sub>2</sub> and CO<sub>2eq</sub> emission factors*). Furthermore, as stated, this is supposedly be the case for a long time considering the fact that Belgian government is currently supporting the construction of new CCGTs to phase-out old nuclear plants [136,137].

#### 4.3.5 Uncertainty analyses

The method used for uncertainty propagations in this work is the one advised by the National Institute of Standards and Technology [486] and to do so, the EES (Equation Engineering Solver) software has been used.

In order to compute the propagation of uncertainties, one must establish it for every variable. For each monitored sensor, it comes directly from Table 17 and its referenced standards. However, the uncertainty has not been established for the hourly HHV figures given by the gas provider for each field-test site. Therefore, it is assumed that it is directly linked to the variance of all the given HHV figures: the uncertainty has been set to thrice the standard deviation of the given HHV figures for the whole monitored year (actually, the standard deviation has been calculated from the population of the hourly HHV figures provided for two whole years, i.e. 2020 and 2021). According to statistical theory, fictively assuming that the actual HHV is constant all year long and that the values given by the gas provider follow a normal distribution around it, this would mean that the obtained uncertainty window accounts for 99.7% of the given HHV figures, which is, as often considered in statistics, sufficient. In reality, the actual HHV is not constant and slightly varies all year long but one can assume that the uncertainty window established here remains valid around the evolving actual value.

This gives an uncertainty on HHV figures of approximately  $\pm 234$  Wh/m<sup>3</sup> for Riemst and  $\pm 105$  Wh/m<sup>3</sup> for Duffel. There is a need for separate uncertainty analyses between the sites because the gas type provided to the machine by the grid is different: according to the gas provider, Duffel has still been provided with lean gas (called 'type L' in Belgium, as explained in *APPENDIX 1: Energy content of natural gas in residential applications*) whereas Riemst already has a rich gas supply (called 'type H' in Belgium, as explained in *APPENDIX 1: Energy content of natural gas in residential applications*). There is about a 10% difference in the given HHV figures between the two types of gas. Such a difference in the chemistry of the gas could indeed have a significant impact on the accuracy of the method used by the gas provider to establish HHV figures.

Thanks to the uncertainty on the HVV figures and the accuracy of the gas meter (about  $\pm 0.5\%$  according to Table 17), one can propagate the uncertainties to the daily HHV energy

consumed and then to the total yearly HHV energy consumed presented in Table 18 (which corresponds to 8760 observations of hourly HHV equivalent energy consumption). Thanks to the accuracy of the energy meters deduced from Table 17 ( $\pm 5\%$  for heat meters and  $\pm 1\%$  for electrical energy meters), one obtains, for the site of Riemst, uncertainties of about  $\pm 0.5$  percentage points for the electrical efficiency,  $\pm 0.8$  percentage points for the thermal efficiency and  $\pm 1$  percentage points for the total efficiency. For the site of Duffel, one obtains respectively  $\pm 0.6$ ,  $\pm 0.6$  and  $\pm 0.8$  percentage points for the electrical, thermal and total efficiency.

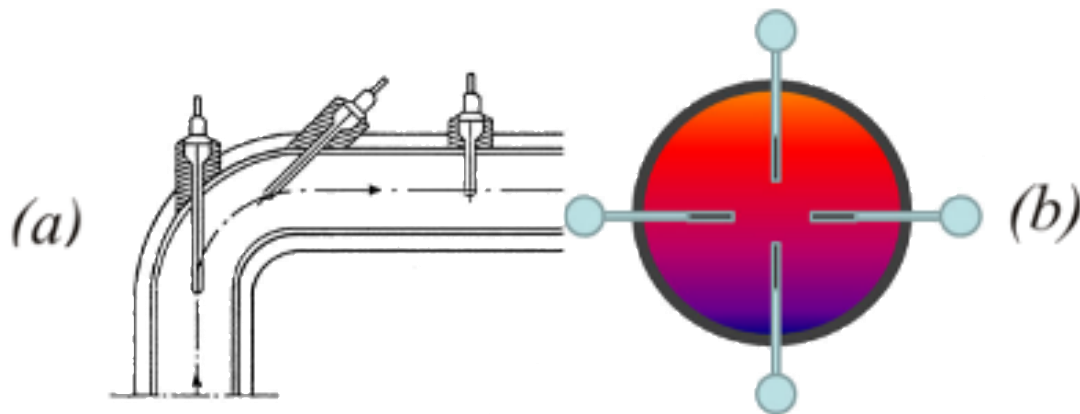
One limitation of those uncertainty calculations is that they have not considered the accuracy of the correction factor that must be applied to the metered volume to convert it in the reference conditions used by the gas provider in its HHV definition [465]. According to this study, the metered volume has to be multiplied by a correction factor established from the real gases equation of state, as explained in *APPENDIX 1: Energy content of natural gas in residential applications*. This correction factor, close to one, involves thus pressure ratio, temperature ratio and compression ratio between standard conditions and delivery conditions. Only the delivery conditions account for uncertainties. Delivery temperature uncertainty can be neglected as the gas meter used in the field-test (BK-G4T, as stated in Table 17) implements temperature compensation. According to the values given in ISO 13443:1996 [487], it is unlikely that the compression factor ratio would have an uncertainty greater than  $\pm 0.0002$  (absolute). At last, delivery pressure depends on the setting of the pressure regulator upstream of the system and on the atmospheric pressure at the field-test site. The pressure regulator setting is either 21 or 25 mbar depending on the gas type in Belgium [465], so a relevant maximum uncertainty can realistically be assumed to about  $\pm 2$  mbar. Regarding the atmospheric pressure, it comes from hourly measurement from Royal Meteorological Institute (in Belgium). The real uncertainty of those pressure measurements is unknown, especially since the pressure measurement are not performed at the field-test sites but at a meteorologic station nearby. Therefore, it has been assumed that the uncertainty of each pressure measurement is again equal to thrice the standard deviation of all the hourly pressure measurements that have been provided (again for two years: 2020 and 2021). This leads to an uncertainty of about  $\pm 3000$  Pa. The propagated uncertainty on the correction factor is thus equal to  $\pm 0.028$ . This is actually too small to have an influence on the propagated uncertainties on the efficiencies stated before.

The emission factor and pricing assumptions are not assumed to be subjected to any uncertainty (uncertainty only propagated on monitored measures and HVV figures). Since the economical and ecological balances are resulting mainly from the efficiencies of the system, it can be assumed that the maximum relative efficiency stated earlier can be considered for all the economical and ecological balances of this work. Actually, the relative uncertainty on thermal efficiencies is of about  $\pm 5\%$  for both field-test system.

In conclusion, it is safe to consider that the propagated uncertainties for all the results of this chapter are at a maximum of  $\pm 5\%$ .

Of course, this is only based on the measured values and the intrinsic accuracy of the sensors. There is no estimation of the uncertainty induced by potential unoptimized installations of the sensors or unoptimized fluidic conditions, especially for the temperature probes of the heat flow meter. Indeed, literature usually finds it is better to mount the probe within the pipe in an elbow to allow it to be parallel to the incoming flow [488]. However, that is not the case for the monitored sites, where probes are mounted perpendicularly to the pipe-wall (easier installation as they are commercialized monitoring sensors and not quite laboratory equipment). This probe configuration is still accepted in literature. Indeed, those two possibilities of mounting temperature probes on a hydraulic pipe (along with a third angular one) are shown in Figure 58 (a) [489].

Also, as the temperature probes are singularly placed in the pipe, the assumption is made that the single in-pipe temperature point accounts for all the fluid on the measured section of the pipe. As shown in Figure 58 (b) [489], this might not be the case as wall effects as well as temperature gradients may happen. Therefore, there might be a temperature distribution along the section of the pipe that one single temperature measurement might not reliably represent. This is another example of a source of uncertainty due to the quality of the installation and of the monitoring equipment that is neglected in this work uncertainty studies. At last, literature has established the need for the depth of the probe in the pipe to be set precisely (down to 45 to 50% of the pipe diameter) [490]. This time, this is likely to be ensured for the monitored sites, as the probes are sold with the corresponding portion of pipe that they are supposed to be screwed in. A mechanical stop is also involved within this probe-pipe assembly, for which a picture is shown on Figure 43. So, an unoptimized depth could only come from the unlikely improper mounting of the technician that may not have screwed the probe all the way to its mechanical stop. Unfortunately, this could still happen and there is no way of knowing for sure remotely without visiting the installations. Still, as best practices and sensor mounting manufacturer recommendations have been followed, these kinds of eventual misplacements can be neglected.



**Figure 58.** The three recommended options to mount a temperature sensor in a pipe [489] b) Example of the distribution of the temperature of the fluid within a pipe along with an example of multiple probes installation in order to study it [489].

#### 4.3.6 Troubleshooting

No break-down were reported nor noticed during the monitoring timeframe.

#### 4.3.7 Conclusions of the section

The strongest limitation of the work reported in this section is that the resulting economical indicators are strongly case dependent and that considering only two machines does not allow for drawing statistical conclusions on the system's performance (especially the economical ones that are affected by the household supply cover factor). The results developed here shall thus be considered as case studies. However, the ecological balances are unlikely to change much from one household to another as they have been established without considering supply cover factors. Indeed, the system is mainly used with a constant (and quite low) nominal power output that, if rejected on the grid, is likely to be consumed in the direct neighbouring dwellings rather than be transported on longer distances (with transport and distribution losses). It is noteworthy that it might be relevant to consider supply cover factors in ecological balances for technologies that exhibit simultaneous uncontrolled production such as with PV panels.

This 2021 field-test monitoring study has demonstrated in a real application the 60% LHV electrical efficiency of this residential SOFC micro-CHP system announced by the OEM (reported in Table 11), at least for one of the two SOFCs. The other SOFC system performance is close to that figure, although a little below it. This is probably because of the intrinsic variance between manufactured products (as it will be seen later on in Figure 62) but mostly because it has been functioning at partial load with a lower electrical efficiency on the studied timeframe (as it will also be seen in *Section 4.2.5 - Experimental results and data analysis*).

Demonstrated LHV thermal efficiency is not higher than 12-15%, mainly because the heat recovery is mostly used for DHW production (at high delivery temperature). However, the amount of heat still recovered has been proven to be quite significant and sufficient, for example, to cover the DHW demand of the average USA household [171] (backup heating appliance is still advice to ensure sufficient delivery temperature at all times).

Yearly resulting energy utilization costs savings (not considering the impact of the Ukraine-Russia conflict on the energy prices) are significant and at about 1.3 - 1.4 k€/year (for 2021 Belgian energy prices assumptions). This figure has been achieved thanks to a quite high monitored supply cover factor of about 60% for each household (mainly allowed thanks to an electric car). Potential dynamic day-ahead tariffication could even improve those energy utilization cost savings.

From an environmental point of view, two considerations could be made: compared to the actual Belgian consumption mix that involved renewables to a certain extent, the CO<sub>2eq</sub> balance is way negative because of the intrinsic use of natural gas (that remains a carbonated fossil fuel). However, the system has better efficiencies than CCGT power plants and its power output can be modulated from distance. Therefore, it can partially be considered that this system allows for decreasing the electrical demand on centralized CCGT power plants. This consideration, which corresponds to marginal emissions balance, changes totally the CO<sub>2eq</sub> performance that become quite beneficial.

It is worth mentioning that those latter statements lie on the fact that the BI\*\*\*G\*N demonstrated 60% of LHV efficiency, which is indeed intrinsically greater than the considered CCGT reference system for electrical production with a LHV efficiency of 55%. However, it is sometimes considered in literature that in the near-to-medium term, CCGT power plants with similar 60% of LHV efficiency will be feasible [482]. Therefore, if that were the case, the electrical efficiency of near-to-medium SOFC systems should also increase in order to stay ahead of CCGTs. This should not be problematic as it has been shown in *Section 3.2.5 - Current and expected performance of micro-CHP systems based on a PEMFC or a SOFC* that commercial SOFCs already exist with a 65% net AC LHV electrical efficiency or that the theoretical electrical efficiency of the direct electrochemical oxidation of methane in a SOFC is close to 100%.

The content of *Section 4.4 - Machine modelling*, which aims to offer empirical models of the system suitable for simulation of such micro-CHP SOFC installed in buildings, was published almost as-is in the *proceedings of the 36<sup>th</sup> International Conference On Efficiency, Cost, Optimization, Simulation and Environmental Impact of Energy Systems (ECOS2023)* [448].

## 4.4 Machine modelling

The machine has been modelled based on the laboratory results of Table 14, Table 15 and Table 16 with the *Matlab* software. The machine has been modelled in two main steps, starting with the thermal efficiency and finishing with the electrical efficiency.

### 4.4.1 LHV thermal efficiency modelling

As stated with the laboratory results (see *Section 4.2.5 - Experimental results and data analysis*), the thermal efficiency of the system does not depend on the water flow rate of the heat recovery circuit. Therefore, the only influencing parameters for the thermal efficiency are the electrical output power  $\dot{W}_{el}$  and the working temperature of the heat recovery circuit (which influence has been studied through its return temperature  $T_R$ ). The resulting LHV thermal efficiency model (with its more than satisfying goodness of fit) is presented in Figure 59. It consists of a polynomial regression of the second order on both axes of all the data of Table 14, Table 15 and Table 16 independently of the water flow rate of the heat recovery circuit. Between electrical power output  $\dot{W}_{el}$  of 500 and 1500  $W_{el}$ , this LHV thermal efficiency  $\eta_{th,model}$  model is defined by Equation (30), whose parameters are provided in Table 21. Equation (30) has been non-dimensionalized in Equation (31), which can be relevant for similar SOFC systems with other nominal power outputs (or combination of such systems). Equation (31) is therefore expressed in terms of load factor  $\lambda = \dot{W}_{el}/1500W_{el}$ , i.e. the ratio between the electrical output power and the nominal power, equal to 1500  $W_{el}$  in this case ( $\lambda = \dot{W}_{el}/1500 W_{el}$ ).

$$\eta_{th,model}(\%) = f(\dot{W}_{el}, T_R) = p_{00} + p_{10}\dot{W}_{el} + p_{01}T_R + p_{20}\dot{W}_{el}^2 + p_{11}\dot{W}_{el}T_R + p_{02}T_R^2 \quad (30)$$

$$\eta_{th,model}(\%) = f(\lambda, T_R) = p_{00} + 1500p_{10}\lambda + p_{01}T_R + 1500^2p_{20}\lambda^2 + 1500p_{11}\lambda T_R + p_{02}T_R^2 \quad (31)$$

Thermal LHV efficiency model parameters	$p_{00}$	$p_{10}$	$p_{01}$	$p_{20}$	$p_{11}$	$p_{02}$
Values	97.52	-0.03938	-1.699	9.855e-6	4.257e-4	3.249e-3

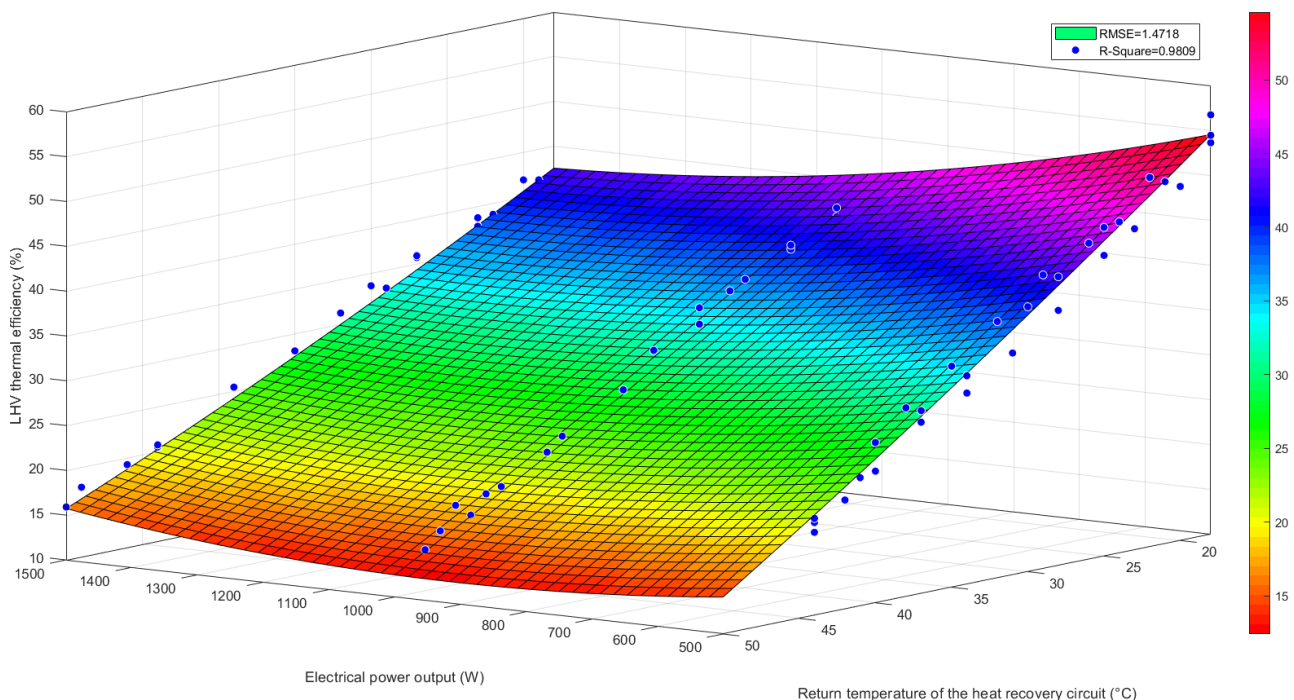
**Table 21.** Parameters of the LHV thermal efficiency model of the SOFC of Equation (30) and Equation (31), valid between electrical power output  $\dot{W}_{el}$  of 500 and 1500  $W_{el}$ .

It must be stressed that this thermal efficiency model is valid on the tested heat recovery water flow rate. It is likely that higher heat recovery flow rate will not affect the model (because the efficiency of the thermal exchange within the system seems to have reached its maximum asymptote). However, extremely low heat recovery flow rate will trivially reduce the efficiency of the exchange within the machine. It would therefore be considered as good practice to ensure at least 90 L/h of water flow rate in the recovery heat circuit (or ensure that lower flow rates will not affect the thermal efficiency of the system). The model is likely to be valid in real applications since the 90 L/h of water flow rate has been obtained at the 'lowest position' of the variable speed circulator of the heat recovery circuit

(‘position 1’, as explained in *Section 4.2.3 - Tests matrix*). Lower water flow rates will only occur with unlikely great pressure losses on the heat recovery circuit.

It is worth mentioning that the goodness of fit can be studied easily with the *Matlab* software thanks to RMSE (Root Mean Square Error) and R-square values. The following explanations have been provided by the *Matlab* software support regarding those fitting variables [491] :

- **R-square:** This statistic measures how successful the fit is in explaining the variation of the data. Put another way, R-square is the square of the correlation between the response values and the predicted response values. R-square can take on any value between 0 and 1, with a value closer to 1 indicating that a greater proportion of variance is accounted for by the model.
- **RMSE:** This statistic is also known as the fit standard error and the standard error of the regression. It is an estimate of the standard deviation of the random component in the data. RMSE value closer to 0 indicates a fit that is more useful for prediction.



**Figure 59.** Model of the laboratory Bl\*\*\*G\*N LHV thermal efficiency according to return temperature of the heat recovery circuit and electrical output power.

#### 4.4.2 LHV electrical efficiency modelling

Modelling the LHV electrical efficiency is simpler as it does not depend on the return temperature of the heat recovery circuit (nor on its flow rate, as it was already the case with the thermal efficiency).

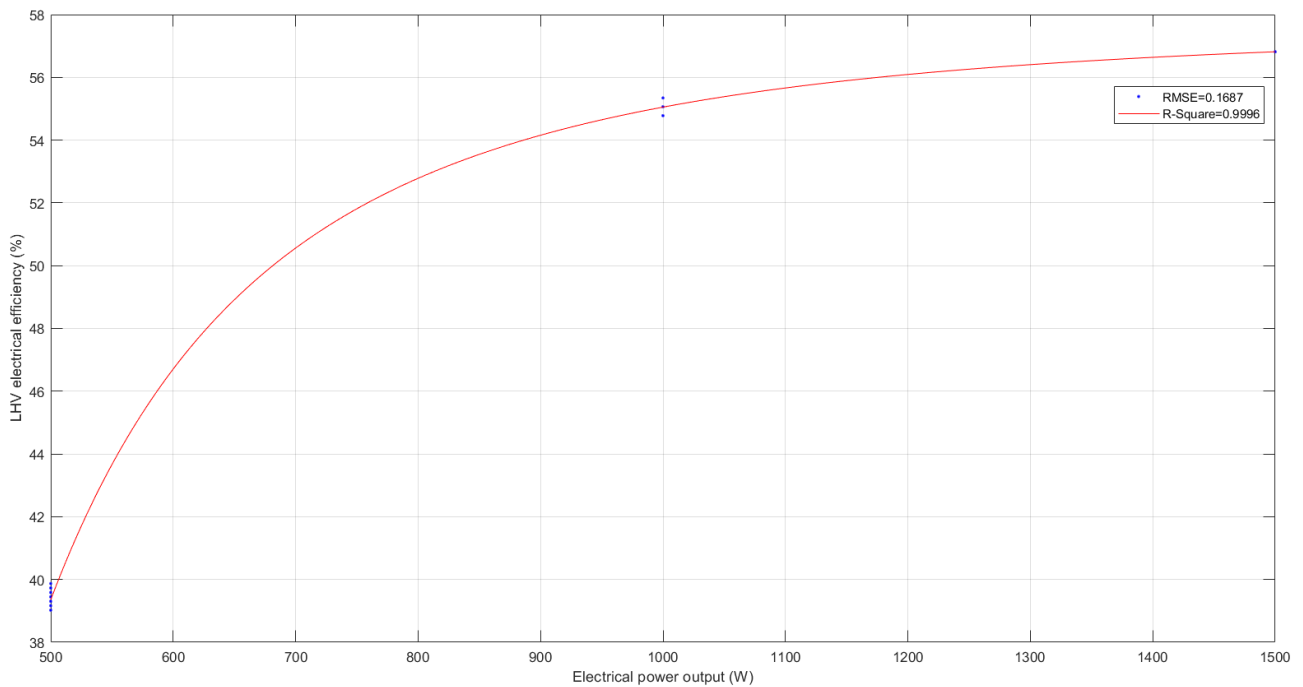
Again, the *Matlab* software has been used on whole the data of Table 14, Table 15 and Table 16. The resulting model is defined by the exponential Equation (32), which has also been non-dimensionalized in Equation (33). Equation (33) is therefore expressed in terms of load factor  $\lambda = \dot{W}_{el}/1500W_{el}$ , i.e. the ratio between the electrical output power and the nominal power, equal to 1500  $W_{el}$  in this case ( $\lambda = \dot{W}_{el}/1500 W_{el}$ ). Model parameters are given in Table 22. Its graphical representation and its (tremendous) goodness of fit are presented in Figure 60.

$$\eta_{el,model}(\%) = f(\dot{W}_{el}) = a \times \dot{W}_{el}^b + c \quad (32)$$

$$\eta_{el,model}(\%) = f(\lambda) = a \times 1500\lambda^b + c \quad (33)$$

Electrical LHV efficiency model parameters	<i>a</i>	<i>b</i>	<i>c</i>
Values	7.491e8	-2.82	57.64

**Table 22.** Parameters of the LHV electrical efficiency model of the SOFC of Equation (32) and Equation (33).



**Figure 60.** Model of the laboratory Bl\*\*\*G\*N LHV electrical efficiency according electrical output power.

#### 4.4.3 Conclusions of the section

The machine LHV thermal and electrical efficiencies have been modelled separately based on the laboratory results (all performed on a single machine) of Table 14, Table 15 and Table 16. In the tested range, the heat recovery water flow rate does not influence the efficiency results so it will not be considered in the models.

Modelled LHV thermal efficiency depends on electrical output power and return temperature of the heat recovery circuit. It is defined by Equation (30), which is a polynomial regression of the second order on both axes.

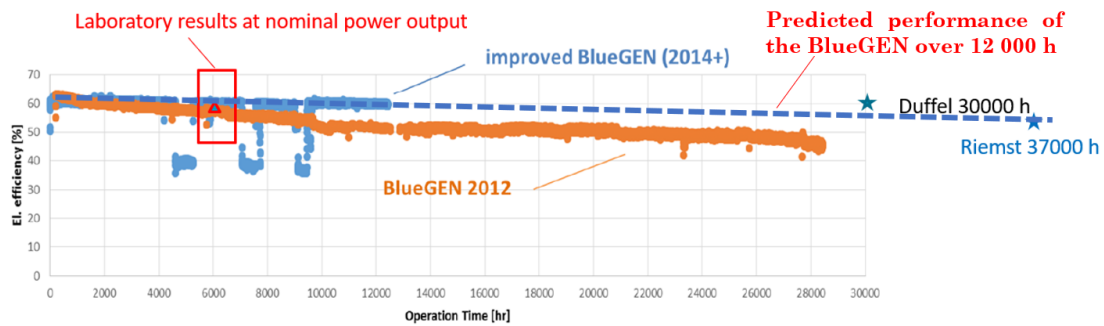
Modelled LHV electrical efficiency depends only the electrical output power. It consists in the exponential relation defined by Equation (32).

Both models have shown tremendous goodness of fit, expressed in terms of RMSE and R-square values.

The content of Section 4.5 - Comparison of laboratory and in-situ measurements, which aims to verify the correlation between the laboratory tests and the field-test study respectively performed in Section 4.2 – Laboratory tests and Section 4.3 - In-situ monitoring, has been partially published (at least for Figure 62) in the proceedings of the 36<sup>th</sup> International Conference On Efficiency, Cost, Optimization, Simulation and Environmental Impact of Energy Systems (ECOS2023) [448].

### 4.5 Comparison of laboratory and in-situ measurements

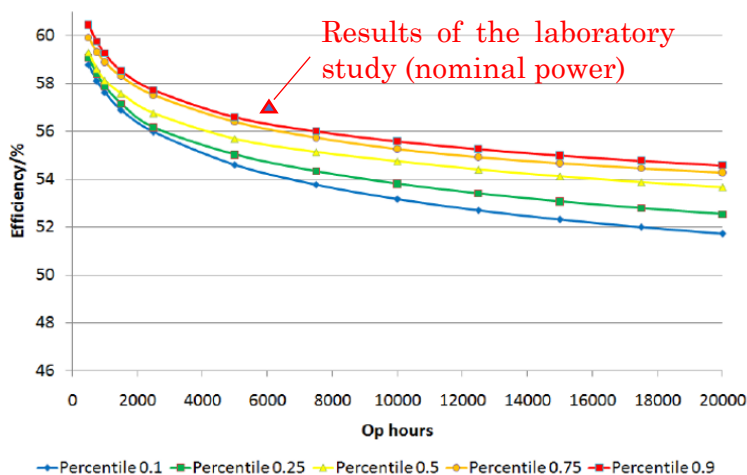
Correlation between laboratory and field-test in-situ measurements is quite facilitated by manipulation of Figure 30, which has been presented by the manufacturer in a past conference [425]. Both laboratory tests and field-test performance can be superposed to that graph to evaluate their correlation. This has been performed in Figure 61.



**Figure 61.** Correlation of the electrical efficiency between laboratory tests, field-tests and manufacturer expected performance. In the end of the year monitoring year 2021, the Duffel and Riemst systems had respectively already 30000 and 37000 operating hours. The underlying graph has been presented in Figure 30.

Even if the underlying graph does not provide information above 12 000 hours of functioning, it is clear that the predictive trend of the BlueGEN (2014+), i.e. the same model as in the laboratory and the field-test sites (as explained in Section 4.1 - Description of the machine), fits quite sufficiently the field-test results. The laboratory results are however very slightly under the targeted efficiency but this could be explained by the intrinsic difference between production units [462], as it can be seen in Figure 62.

#### Statistical Analysis of Current Production Systems



**Figure 62.** Reproduced figure from a 2011 publication of the manufacturer [462] on which the laboratory results have been superposed. Field-test results have not been superposed as the



underlying graph is limited to 20000 of operating hours whereas the field-test systems had already been operating for more than 30000 hours.

As a conclusion of this small section, it can therefore be assumed that all the results of the laboratory and field-test studies performed in this work are consistent with the manufacturer announced targets and that they all correlate.

This allows for assuming that even in real field-test applications, the system is robust and behave as intended. This is likely to be explained by the constant remote control and monitoring of the SOFC by the manufacturer, as explained in *Section 4.1 - Description of the machine*.

As illustrated by Figure 61 and Figure 62, ageing and intrinsic statistical efficiency difference between production units could explain the few differences in efficiencies that could be perceived between the studied systems.

Besides the energy performance, it is important to assess the environmental performance of the system in terms of non-CO<sub>2</sub> pollutants, as introduced in *Section 2.3 - Current emissions factors from heat and power generation* (CO<sub>2</sub> utilization performance of those systems being already investigated in *Section 4.3 - In-situ monitoring*). Thus, CO, NO<sub>x</sub> and SO<sub>2</sub> are the pollutants specifically studied in *Section 4.6 - Non-CO<sub>2</sub> pollutant emissions*. An attempt of evaluating the emitted particular matter (PM) is also performed in this section.

Most of the content of this section has been published in the *proceedings of the 36<sup>th</sup> International Conference On Efficiency, Cost, Optimization, Simulation and Environmental Impact of Energy Systems (ECOS2023)* [121] and accepted for publication in the *Journal of Environmental Management* [122]. These publications have the advantage of directly offering meaningful comparison of the studied SOFC system with other space heating appliances such as the PEMFC micro-CHP system studied in whole other chapter later on, a classical gas condensing boilers or even other typical appliances involving combustion of hydrocarbons, such as a Euro 6 diesel car engine (all tested with the same sensors). In fact, these publications investigate several systems and involves a more generalized and summarized content that has not been judged fit to this chapter, which shall mainly focus on the studied SOFC system. Since their content is still very relevant with the work conducted in this thesis, these publications have been fully reproduced in *APPENDIX 8: Pollutant testing (NO<sub>x</sub>, SO<sub>2</sub> and CO) of commercialized micro-combined heat and power (mCHP) fuel cells*.

Although the reported publications of *APPENDIX 8: Pollutant testing (NO<sub>x</sub>, SO<sub>2</sub> and CO) of commercialized micro-combined heat and power (mCHP) fuel cells* report the main results of this section, this latter has the main advantage of containing meaningful graphs and figures related to the pollutant emissions of the studied SOFC system that have not yet been published.

It is worth mentioning that the SO<sub>x</sub> and NO<sub>x</sub> emissions measurements from this section, in ppm, can be compared to the other space heating appliances SO<sub>x</sub> and NO<sub>x</sub> results from literature introduced in Table 5 and Table 6, through the conversion Equation (68) and Equation (67) specifically published and reported in details in *APPENDIX 8: Pollutant testing (NO<sub>x</sub>, SO<sub>2</sub> and CO) of commercialized micro-combined heat and power (mCHP) fuel cells*.

At last, potential methane emissions (methane slip) have already been considered negligible and have therefore not been measured, as explained in *Section 2.3.3 - Methane slip in natural gas fed fuel cells*.

## 4.6 Non-CO<sub>2</sub> pollutant emissions

### 4.6.1 Measurement devices

First of all, the Bl\*\*\*G\*N system (at least for the BG-\*\*, the successor of the tested system as described in *Section 4.1.2 - Applications and the different versions of the tested system*) is stated to belong to class 6 in terms of NO<sub>x</sub> [492] (according to EN 15502-1 [493]), but its exact emission levels have not been reported.

To realize the pollutants emissions analysis of the system, two different devices were available. The first one is the Multilyzer STx [494], dedicated to combustion analysis while the second one, the Afriso STM 225 [495] is meant to be used for fine particulates. The devices and their characteristics are shown in Figure 63 and Table 23. Additional features of the Multilyzer STx can be found in *APPENDIX 8: Pollutant testing (NO<sub>x</sub>, SO<sub>2</sub> and CO) of commercialized micro-combined heat and power (mCHP) fuel cells*.

It is worth mentioning that the sensor used for fine particulates measurements has a parameter to be set according to the type of fuel used. Natural gas as fuel is however not within the options. So by recommendation of *Gas.be*, the ULiege industrial partner that initiated and supported the project that led to most of the content of this thesis (as stated in the *Acknowledgments*), ‘Wood’ has been selected to carry out the tests. *Gas.be* technicians have indeed some experience (which they kindly and thankfully shared) with pollutants emissions sensors similar to the ones stated here above.



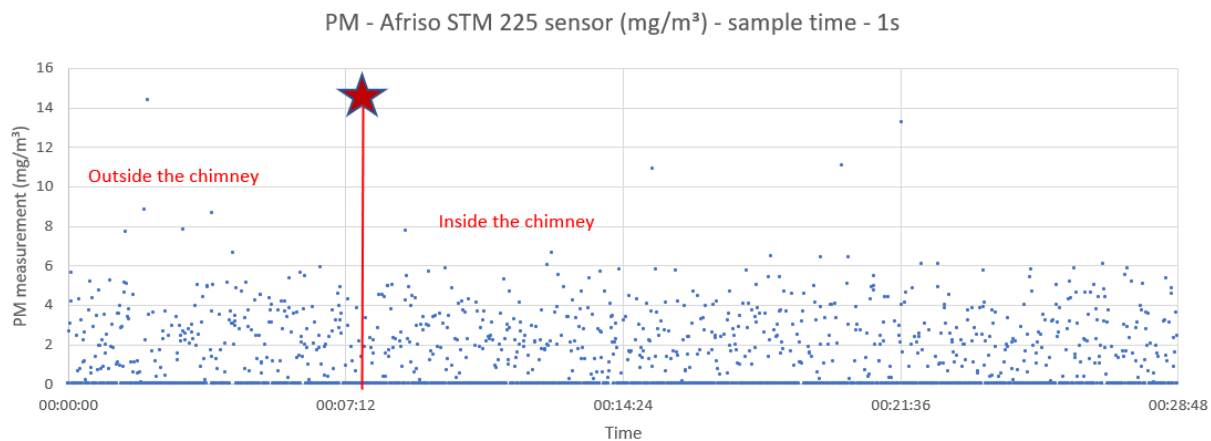
**Figure 63.** Combustion and fine particulates devices.

	Multilyzer STx	Afriso STM 225
Use	Combustion analysis	Fine particulates measurements
Sample frequency	5 seconds	1 second
Measure	CO, NO, NO <sub>2</sub> , SO <sub>2</sub> CO <sub>2</sub>	Mass concentration of particulate matter
Unit	ppm % vol	mg/m <sup>3</sup>

**Table 23.** Emissions measurement devices.

#### 4.6.2 Measurements analysis

Unfortunately, as expected because of the ‘Wood’ option (see *Section 4.6.1 - Measurement devices*) the fine particulates Afriso STM 225 sensor was not relevant for these kind of natural gas applications. Indeed, Figure 64 shows an example of an acquisition signal for the SOFC studied in ULiege laboratory facilities (see *Section 4.2 - Laboratory tests*) at its nominal output electrical power (1500 W<sub>el</sub>). It is clear that there is no difference when the probe is located in ambient air and when it is placed at the output of the SOFC’s chimney. It is believed that the sensor is not sensitive enough to measures natural gas appliances flue gases. Therefore, the rest of this work will only focus on the signal acquired from the Multilyzer STx pollutant sensor.



**Figure 64.** Example of signal from the fine particulates sensor Afriso STM 225.

Also, since it has been demonstrated in *Section 4.5 - Comparison of laboratory and in-situ measurements* that all the tested SOFCs behave quite similarly and since the only interaction with the machines are directly performed by the manufacturer remotely, it has been chosen to mainly conduct the pollutant emission tests in ULiege laboratory facilities. This offers the possibility to study the sensitivity of the pollutants emissions regarding the amount of heat recovered (by imposing temperature steps to the system thanks to the manual thermostatic valve implemented to the laboratory test bench, as explained in *Section 4.2.4 - Test procedure*).

Two pollutant test sequences have been conducted on the SOFC tested in ULiege laboratory facilities.

The first one has been performed at the minimal electrical output power of the SOFC (500 W<sub>el</sub>). Its results are shown in Figure 65. It is worth mentioning that the temperature step imposed in the heat recovery circuit after about 5 minutes of acquisition time is negative. Indeed, the return temperature of the heat recovery circuit is cooled down from about 50°C to about 20°C.

The second one has been performed at the intermediate electrical output power of the SOFC (1000 W<sub>el</sub>). Its results are shown in Figure 66. It should be stressed that the temperature step imposed in the heat recovery circuit after about 10 minutes of acquisition time is positive. Indeed, the auxiliary heat exchanger has been completely bypassed (see Figure 37) so the return temperature of the heat recovery circuit varied from about 20°C to about 50°C.

Both pollutant test sequences conducted on the SOFC tested in ULiege laboratory facilities have been summarized in the two first rows of Table 24.

It is worth mentioning that the pollutant testing at 1500 W<sub>el</sub> of electrical output power (nominal output) has been conducted in ULiege laboratory facilities but the acquisition data was unfortunately corrupted. However, SO<sub>2</sub>/NO<sub>x</sub>/CO pollutant emissions of the studied SOFC at its nominal electrical output power (1500 W<sub>el</sub>) have still been performed, but rather on one of the field-tested machines, i.e. the one in Riemst (see *Section 4.3.1 - Description of the buildings*). That particular test, which results have also been reported in Table 24, however did not benefit of the laboratory test-bench features described in *Section 4.2 - Laboratory tests* and therefore could not imply the sensitivity study of the heat recovery circuit recovery working temperatures (as for the other tested output electrical powers of 500 W<sub>el</sub> and 1000 W<sub>el</sub> reported in Figure 65 and Figure 66).

In all test sequences, no NO, NO<sub>2</sub> or SO<sub>2</sub> pollutants have been measured. Only little CO emissions have been measured: around 5 ppm for 500 W<sub>el</sub> of electrical output, around 11 ppm for 1000 W<sub>el</sub> of electrical output and around 8 ppm for 1500 W<sub>el</sub> of electrical power

output. Therefore, the CO pollutants are not linearly proportional to the output power of the system and, in terms of CO emissions intensity, it seems from Table 24 that it is preferable to operate the system at its nominal power output (of 1500 W<sub>el</sub>).

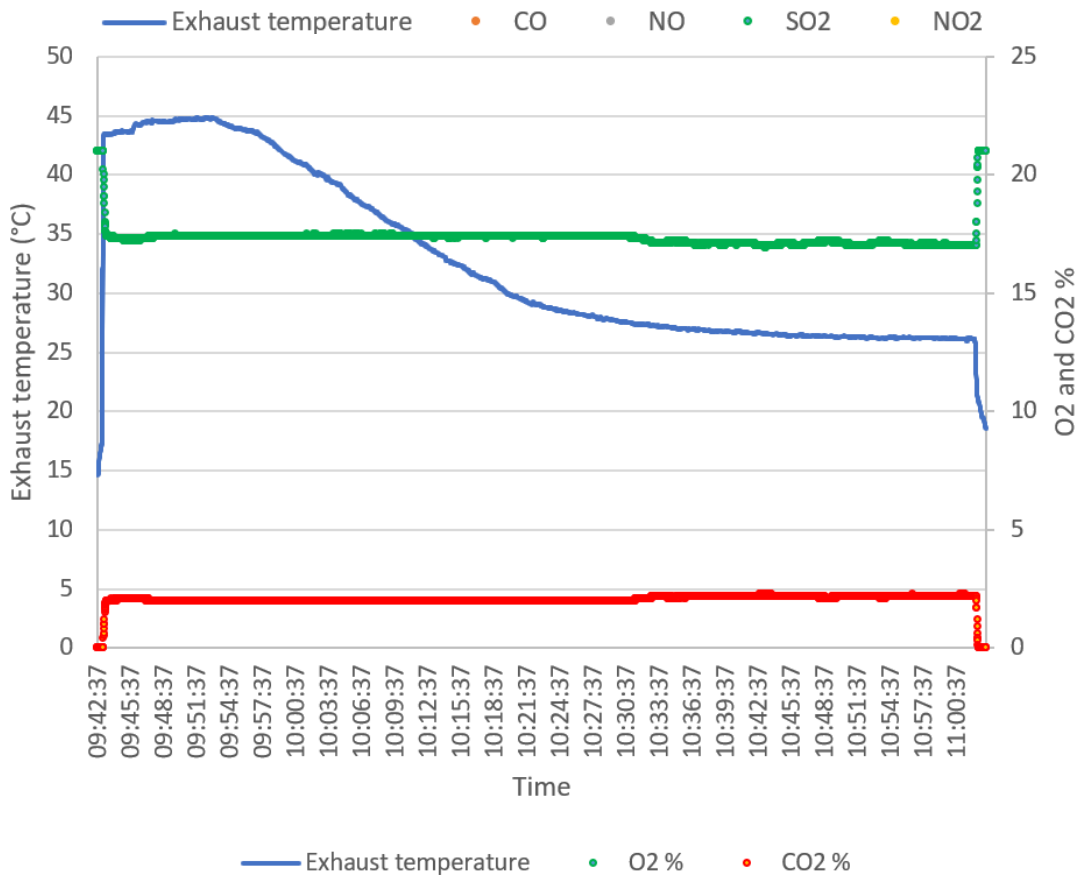
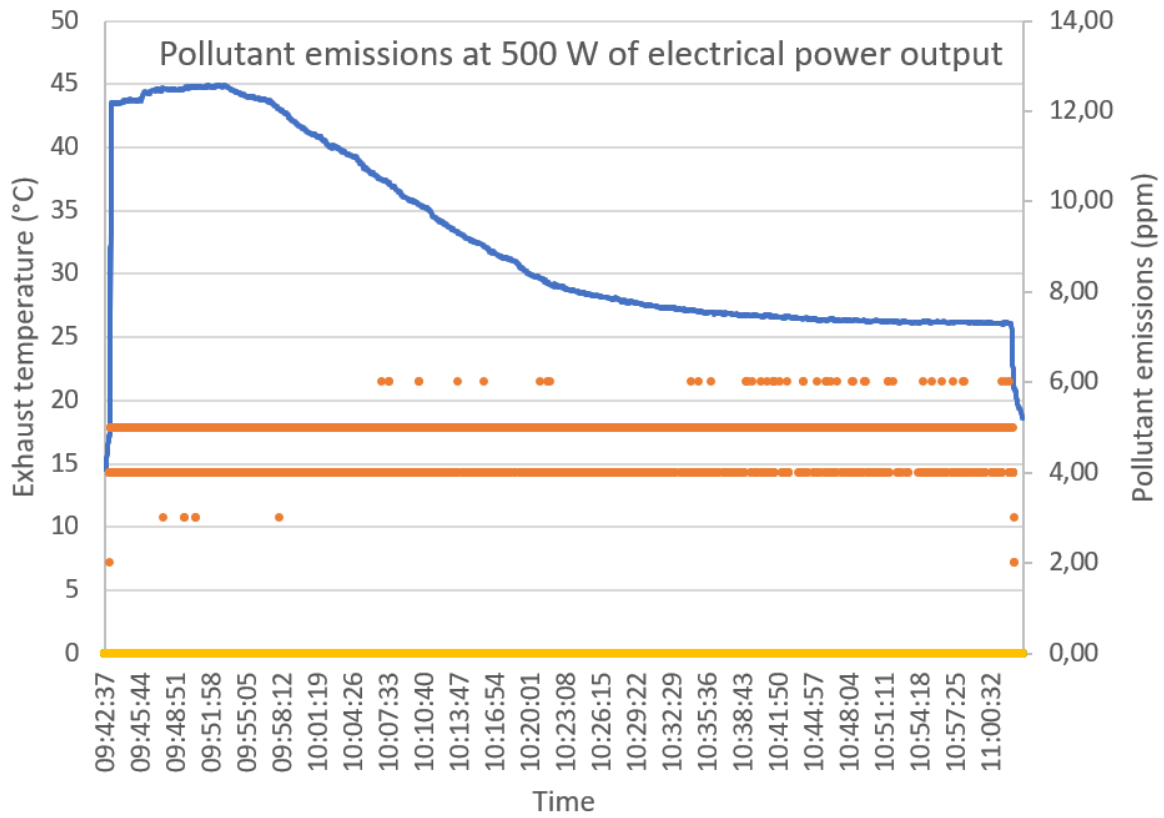
That remaining CO could have been oxidized in the SOFC stack and that would have increased the electrical efficiency of the system. Indeed, as already stated in *Section 3.1.2 - Fuel cell types and classification*, CO can act as a fuel for SOFC [441].

It is clearly visible on Figure 65 and Figure 66 that the heat recovery working temperature has no influence on the measured pollutant emissions.

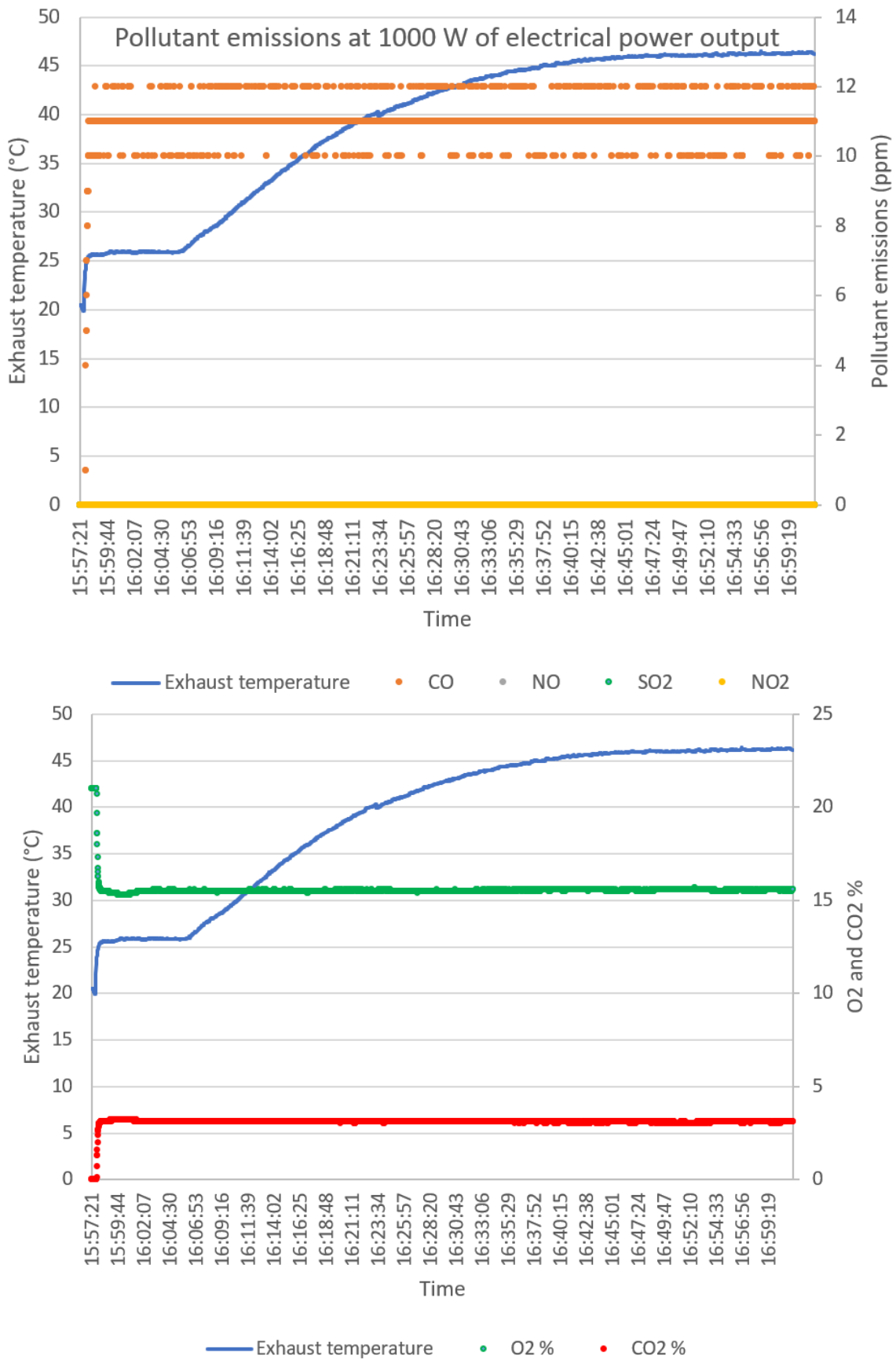
Test and conditions	SO <sub>2</sub>	NO <sup>a</sup>	NO <sub>2</sub> <sup>a</sup>	CO <sup>a</sup>	Remarks
SOFC – 500 W <sub>el</sub> output Tested in laboratory with different heat recovery temperatures, i.e. different exhaust gases temperature (from 45°C to 25°C) Deduced from Figure 65.	0	0	0	5 ppm, i.e. 28.3 mg/kWh	- Return temperature of the heat recovery circuit has no influence on the pollutant measurements - Only steady state data (the system is supposed to be turned on continuously and the startup test was not conducted)
SOFC – 1000 W <sub>el</sub> output Tested in laboratory with different heat recovery temperatures, i.e. different exhaust gases temperature (from 45°C to 25°C) Deduced from Figure 66.	0	0	0	11 ppm, i.e. 41.5 mg/kWh	- Return temperature of the heat recovery circuit has no influence on the pollutant measurements - Only steady state data (the system is supposed to be turned on continuously and the startup test was not conducted)
SOFC - 1500 W <sub>el</sub> output Measured on the field-test site in Riemst with only one heat recovery temperature corresponding to 60°C of exhaust gases temperature.	0	0	0	8 ppm, i.e. 17.0 mg/kWh	- Same SOFC reference as in the reported laboratory tests but a different machine (see differences in Table 10) - Only steady state data (the system is supposed to be turned on continuously and the startup test was not conducted)

<sup>a</sup> Equation (68) (from *APPENDIX 8: Pollutant testing (NO<sub>x</sub>, SO<sub>2</sub> and CO) of commercialized micro-combined heat and power (mCHP) fuel cells*) has been used to convert ppm measurement into mg/kWh (of natural gas appliances). The pollutant emission intensity (in mg/kWh) is not to be considered related to the electrical output energy (or power) of the SOFC system. Conversion Equation (68) (from *APPENDIX 8: Pollutant testing (NO<sub>x</sub>, SO<sub>2</sub> and CO) of commercialized micro-combined heat and power (mCHP) fuel cells*) is used in literature for natural gas combustion (and not exactly its use in a fuel cell) and should only be considered for comparison purposes.

**Table 24.** SO<sub>2</sub>/Nox/CO pollutant emissions measurements results on the studied SOFC BI\*\*\*G\*N system.



**Figure 65.** Pollutant measurement at minimal electrical output power (500 W<sub>el</sub>). The return temperature of the heat recovery circuit is changed after about 5 min of acquisition time from about 50°C to about 20°C.



**Figure 66.** Pollutant measurement at intermediate electrical output power (1000 W<sub>el</sub>). The return temperature of the heat recovery circuit is changed after about 10 min of acquisition time from about 20°C to about 50°C.

At last, it can be seen on Figure 65 and Figure 66 that the electrical power output of the SOFC has an effect on the O<sub>2</sub> of the flue gases (and subsequently, with air as oxidizing agent supplied to the system, on its CO<sub>2</sub> percentage). O<sub>2</sub> measured percentage was around 17 % at 500 W<sub>el</sub> and 15.6 % at 1000 W<sub>el</sub>. This decreasing trend is confirmed by the test at nominal electrical output power (1500 W<sub>el</sub>) conducted on the Riemst field-test system as O<sub>2</sub> measured percentage was around 11 %. Indeed, as expected, CO<sub>2</sub> percentage increases and O<sub>2</sub> percentage decreases with increased output power and increased natural gas consumption (with the combustion-like reaction in the SOFC stack [438]).

As it will be seen in *Chapter 5 - Study of the P\*2 PEMFC system* and more specifically in *Section 5.6 - Non-CO2 pollutant emissions*, similar non-CO<sub>2</sub> pollutant tests were also performed on the studied PEMFC micro-CHP system, i.e. on the other tested fuel cell technology. As it will be shown, no NO<sub>x</sub> and SO<sub>2</sub> were measured as with this SOFC system. While a few CO emissions have been measured for the tested SOFC system, the only main difference with the tested PEMFC system is that its results also not demonstrated any (steady-state) CO emissions. This is probably due to the fact that the tested PEMFC, unlike SOFCs, was likely to involve a CO removing apparatus upstream of the fuel cell stack in the natural gas processing system (to avoid critical CO poisoning of PEMFC) [496], as already introduced explained in *Chapter 3 - Fuel cell technologies and their residential applications* (Table 7).

## 4.7 Conclusions of the chapter

Conclusions related to *Section 4.1 - Description of the machine*, *Section 4.2 - Laboratory tests*, *Section 4.3 - In-situ monitoring* and *Section 4.4 - Machine modelling* have been reported for each section in specific explicit ‘*Conclusions of the section*’ paragraphs.

Also, the key contributions and findings of *Section 4.5 - Comparison of laboratory and in-situ measurements* have been summarized here below :

- All the results of the laboratory and field-test studies performed in this work are consistent with the manufacturer announced targets and correlate.
- This allows for assuming that even in real field-test applications, the system is robust and behave as intended. This is likely to be explained by the constant remote control and monitoring of the SOFC by the manufacturer, as explained in *Section 4.1 - Description of the machine*.
- Ageing and intrinsic statistical efficiency difference between production units could explain the few differences in efficiencies that could be perceived between the studied systems.

In addition, the key contributions and findings of *Section 4.6 - Non-CO2 pollutant emissions* have been summarized here below :

- CO, NO, NO<sub>2</sub> or SO<sub>2</sub> pollutants have been tested with the available sensors (see *Section 4.6.1 - Measurement devices*). CO is the only pollutant that could be measured. It has been found that the maximum CO concentration is obtained at intermediate output electrical power (1000 W<sub>el</sub>) and is about 11 ppm.
- Since CO can act as a fuel for SOFC [441], this fact even leaves room for improvement of the electrical efficiency of the system, which could thus hopefully become significantly higher than the one of CCGT power plants and improve the CO<sub>2</sub> environmental balance of the SOFC micro-CHP systems performed in *Section 4.3 - In-situ monitoring*. This system might therefore get closer to the expected performance of SOFC technologies reported in *Section 3.2.5 - Current and expected performance of micro-CHP systems based on a PEMFC or a SOFC*.
- At last, the heat recovery circuit (and its working temperature) has no influence on the pollutant emissions.



# CHAPTER 5 STUDY OF THE P\*2 PEMFC SYSTEM

Besides the SOFC studied in the previous chapter, *Chapter 3 - Fuel cell technologies* stated that Vi\*ov\*\*r systems also leads the market of fuel cell micro-CHPs with the P\*2 (0.75 kW<sub>el</sub> of nominal power output), studied in this chapter. This chapter mainly rely on experimental investigations conducted in ULiege laboratory facilities and on in-situ monitoring installations of real applications (in 'real' Belgian households). In addition to the P\*2 system in ULiege laboratory, two field-test systems were studied, located in Oostmalle and Huy. The purpose of this chapter is to assess the energy and environmental performance of the system in terms of natural gas consumption, net electricity production, efficiencies, pollutants emissions (including CO<sub>2</sub>, CO, SO<sub>2</sub>, NO<sub>x</sub>).

This chapter is organized as follows. After a description of the machine, the tests carried out in ULiege laboratory are presented and analyzed. Then, *Section 4.3 - In-situ monitoring* investigates the monitoring of the two units installed in the two different residential buildings, including their CO<sub>2</sub> utilization performance. Based on those two latter sections, *Section 5.4 - Machine modelling* proposes empirical models of the system suitable for simulation of such micro-CHP PEMFCs installed in buildings. *Section 4.5 - Comparison of laboratory and in-situ measurements* draws conclusions from the comparison between in-situ performance and laboratory performance (and investigates the correlation between all the tested systems). Environmental performance in terms of non-CO<sub>2</sub> pollutants is finally analysed in *Section 5.6 - Non-CO2 pollutant emissions* (CO<sub>2</sub> utilization performance of those systems being already investigated in *Section 4.3 - In-situ monitoring*). As it can be perceived, this chapter is organized as similarly as possible as the one on the micro-CHP SOFC system for comparison purposes. However, both investigated fuel cell systems are completely different and have their own particularities that sometimes necessitated a specific approach in their study and documentation.

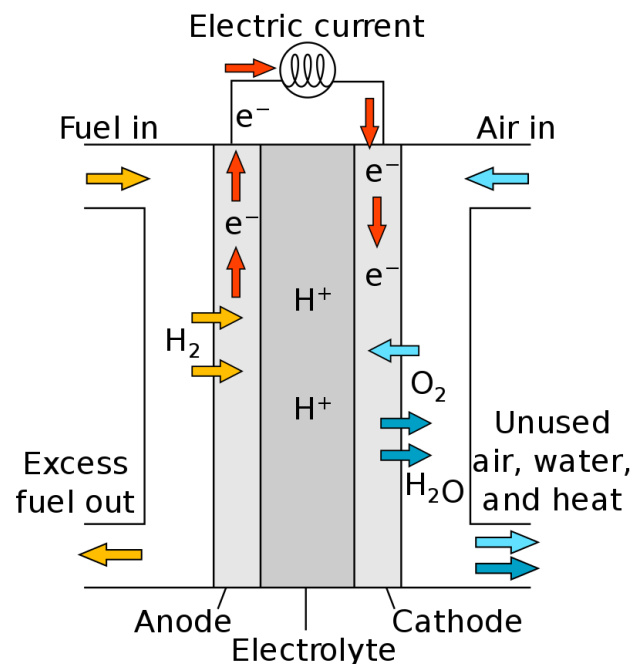
Several academic publications have been established in relation to the sections of this chapter. All of those have been specified in the introduction of each section they are related to. In fact, the assumed internal schematics of Figure 74 (and its description) included in the first section of this chapter, i.e. *Section 5.1 - Description of the machine*, have been included in a particular paper, which additional content is partially presented in *APPENDIX 14: Literature review on PEMFC degradation mechanisms*. It is intended to be submitted to the *Journal of Power Sources* (already reviewed by co-authors).

## 5.1 Description of the machine

### 5.1.1 Working principle

#### 5.1.1.1 PEMFC main features

The fuel cell technology concerned by this chapter is the (LT-)PEMFC, introduced in *Section 3.1.2 - Fuel cell types and classification* and in Table 7. As stated in *Chapter 3 - Fuel cell technologies*, a PEMFC is characterized by its electrolyte, a (solid) polymer that is permeable to protons (hydrogen cations) and its working principle is reminded in Figure 67 [497].



**Figure 67.** Working principle of a PEMFC (valid for LT and HT-PEMFCs). Reproduced and adapted from reference [497].

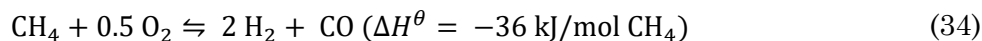
As established in Table 7, compared to SOFCs such as the one studied in the previous chapter, PEMFCs imply much lower working temperature, which lead to less strict material requirements, reduced start-up time and thermal stresses. On the other hand, they exhibit lower fuel flexibility and a much higher sensitivity to contaminants. Therefore, when fed by hydrocarbons, in order to provide high-purity hydrogen to the stack, a dedicated fuel processing system (a reformer) is embodied to the PEMFC system. In fact, reforming processes require heat to operate [259]. This heat is provided through the combustion of some of the fuel, which therefore lowers the electrical efficiency [259] as opposed to hydrogen-fed PEMFCs (or most SOFC systems, even if fed by hydrocarbons).

CO being a major contaminant of PEMFCs, as stated in Table 7 and, in more details, in *APPENDIX 14: Literature review on PEMFC degradation mechanisms*, the fuel processing systems of PEMFCs usually involves a CO remover unit prior to the stack [259]. However, as also seen in Table 7, the main difference between HT-PEMFCs and LT-PEMFCs is that the higher stack operating temperatures of the former increase the CO tolerance of the stack, which no longer requires the CO remover unit embodied in the hydrocarbons fuel processor (as in LT-PEMFCs) [259]. Unfortunately, as stated in *Chapter 3 - Fuel cell technologies*, some major technical issues (such as their short lifetime [267]) still remain with micro-CHP HT-PEMFCs and they have not yet been successfully commercialized (see *Section 3.2.2 - Status of commercialized HT-PEMFC-based micro-CHP systems*).

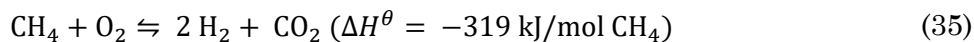
#### 5.1.1.2 Hydrogen processor and reforming processes

As mentioned, the system, fed by natural gas (high methane proportion), involves an upstream external reformer before the PEMFC stack. Indeed, the temperature within the stack is not sufficiently high for direct internal reforming at the electrode [498], as it is frequent for solid oxide fuel cells [440] (see Table 7). The hydrogen production is instantaneous so the system is not subjected to the highly constraining safety issues regarding hydrogen storage such as the ICPE (Installation Classée pour la Protection de l'Environnement) authorization in France or similar other legal barriers on EU markets [499]. Reforming technology has not been officially disclosed but the OEM states that it processes natural gas thanks to oxygen without mentioning steam or even water [500],

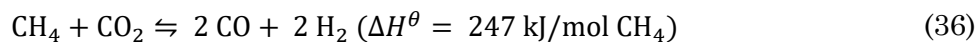
which allows for assuming that hydrogen might be produced by partial oxidation of methane [249], which chemical reaction is presented in Equation (34) :



This reaction may be non-catalytic for temperatures above 1300 K but it is well-known that catalysts have helped lowering the temperature to about 1000 K, still achieving excellent yields [501]. At those high temperatures, the reaction is affected by the oxidation equilibrium of carbon monoxide into carbon dioxide [502]. So, it is generally considered that partial oxidation implies also the reaction presented in Equation (35) [503].



Nevertheless, with partial oxidation reforming processes, which, in comparison, have not been reported in the tested SOFC fuel processing (see *Section 4.1.4 - Probable internal schemes*), air is usually fed to the system (for its oxygen content). Therefore, in addition to the carbon dioxide produced by Equation (35), the occurrence of the dry reforming of methane, which reaction is presented in Equation (36) [504], cannot be excluded. In comparison, this reaction has already also been introduced in Equation (10) as potentially occurring in the hydrocarbons processing of SOFCs.



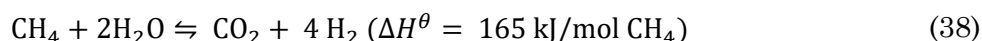
Indeed, dry reforming of methane has been reported to occur at pressure as low as 1 bar and temperatures as low as 925 K, which are even lower than for the partial oxidation of methane [505] presented in Equation (34). This is emphasized by the fact that partial oxidation reactions (potentially occurring with this PEMFC) are exothermic and are usually combined with endothermic reactions such as the dry reforming of methane of Equation (36) [504]. Both partial oxidation and dry reforming of methane can even occur with the same catalyst [506].

If that were to be confirmed, it would be called 'CRPOM' (Carbon dioxide Reforming with Partial Oxidation of Methane), said to be thermoneutral [507]. It is worth mentioning that 'tri-reforming' would require the occurrence of steam reforming (as an endothermic reaction) in addition to the partial oxidation and dry reforming reactions [504]. To be exhaustive, if methane reforming only consists in the combination of partial oxidation and steam reforming reactions (without dry reforming), it would be called 'autothermal reforming' [503].

It should be mentioned that, for the PEMFC studied in this chapter, the only external connection to water mains is used for DHW production, as it will later on be shown in Figure 68, when the user draws hot water in its household. However, even though there is no external water feed to the PEMFC module and its hydrogen processor, the very frequent methane steam reforming reaction cannot be excluded as well. Indeed, it has been reported that water obtained from the PEMFC stack reaction between oxygen and hydrogen can be sufficient to supply steam [508,509] or autothermal [509] reforming processes. As a reminder, the steam reforming reaction of methane is [503] :



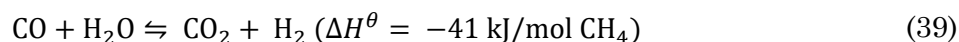
Equation (37) is generally completed to a lesser extent by the water-gas shift (WGS) of Equation (12), also given later in Equation (39) [249], to give Equation (12) :



In comparison, Equation (37) and the WGS reaction have already also been introduced respectively in Equation (9) and Equation (12) as potentially occurring in the hydrocarbons processing of SOFCs.

Steam reforming has been reported to occur in the 975-1300 K temperature range [249], i.e. similar to the one reported here above for the partial oxidation reforming [501].

A lot of applications tend to require better hydrogen yields and purity (primarily by getting rid of the remaining carbon monoxide content) and it has already been stated (Table 7) that it is the case for (LT-)PEMFCs, such as the studied in this chapter. Indeed, carbon monoxide is a well-known example of PEMFC pollutant that can severely poison both (platinum) electrodes of the stack and significantly affect the fuel cell performance [510] (see *APPENDIX 14: Literature review on PEMFC degradation mechanisms*). Furthermore, diluted hydrogen reduces fuel cell current density [511] and also even reduces the carbon monoxide tolerance of the stack [512]. Therefore, reforming apparatus in PEMFC industrial applications generally involve dedicated water gas shift (WGS) reactor(s) downstream of the main reforming process [513,514] (which, as stated, can be based on partial oxidation and/or steam reforming processes). Depending on the reformer type, operating conditions and fuel, carbon monoxide concentration in the outlet stream from the main reforming process is in the 3–10% range (molar) [498] and it can be reduced to the 0.5-1% range (molar) downstream of a WGS reactor, no matter the main reforming process [509]. This WGS reactor has its own catalyst and forms more hydrogen and carbon dioxide from the remaining carbon monoxide content of the reformat [515]. This reaction, already introduced in Equation (12) as potentially occurring in some SOFC fuel processing, is given again in Equation (39) [503] and is indeed quite simple to implement if steam is already required in the main reforming process (for steam, tri- or autothermal reformers).



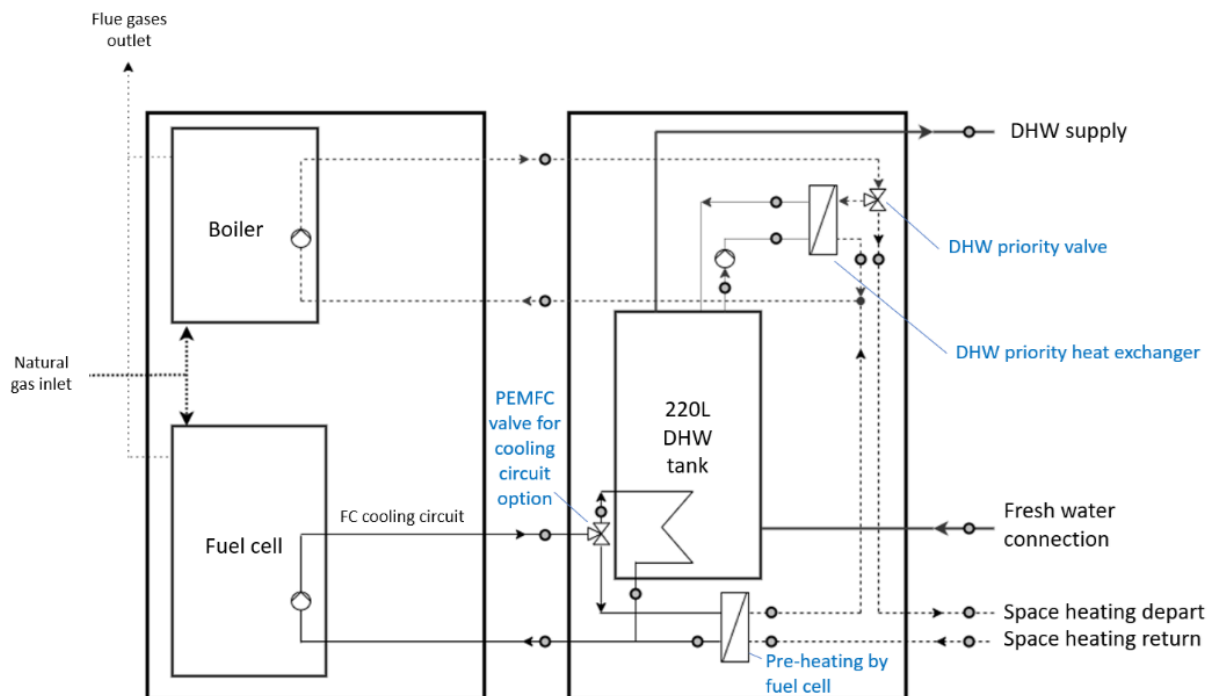
Even trace amounts of carbon monoxide can be harmful to the (LT-)PEMFC stack [516] and the acceptable carbon monoxide content in the stack, i.e. its carbon monoxide tolerance, is indeed very low. Concentration levels around or below 5 ppm are generally necessary [517] and are known to be particularly efficient to mitigate carbon monoxide poisoning, at least for low current densities [518].

As mentioned (in Table 7), to help reaching similar concentration levels, it seems that industrialists implement a carbon monoxide remover [514], also called a ‘carbon monoxide selective oxidizing unit’ [513]. This process relies on the selective (also called ‘preferential’ [509]) catalytic oxidation of carbon monoxide into carbon dioxide; it is called ‘selective’ because the chosen oxidation catalyst also needs to prevent the oxidation of hydrogen into water [519]. Preferential oxidation of carbon monoxide requires oxygen [520], which, as for the potential partial oxidation reforming process stated earlier, can conveniently be fed through ambient air (required as oxidizing reactant agent at the fuel cell cathode). This air bleed rate must be finely controlled. Indeed, if a large amount of oxygen is fed into the preferential oxidation reactor, carbon monoxide conversion will be enhanced, but the unavoidable hydrogen loss (due to the hydrogen oxidation reaction) will increase as well [520].

It is worth mentioning that the carbon monoxide remover can also consist of a carbon monoxide selective methanation reactor [509], where carbon monoxide reacts with hydrogen to form methane (so no additional reactant such as oxygen shall be fed at the fuel side [520]). However, the direct hydrogen loss from that reaction is much higher than for the preferential oxidation reaction so selective methanation is not usually applied in (LT-)PEMFC hydrogen production processes [520].

### 5.1.2 Applications and the different versions of the tested system

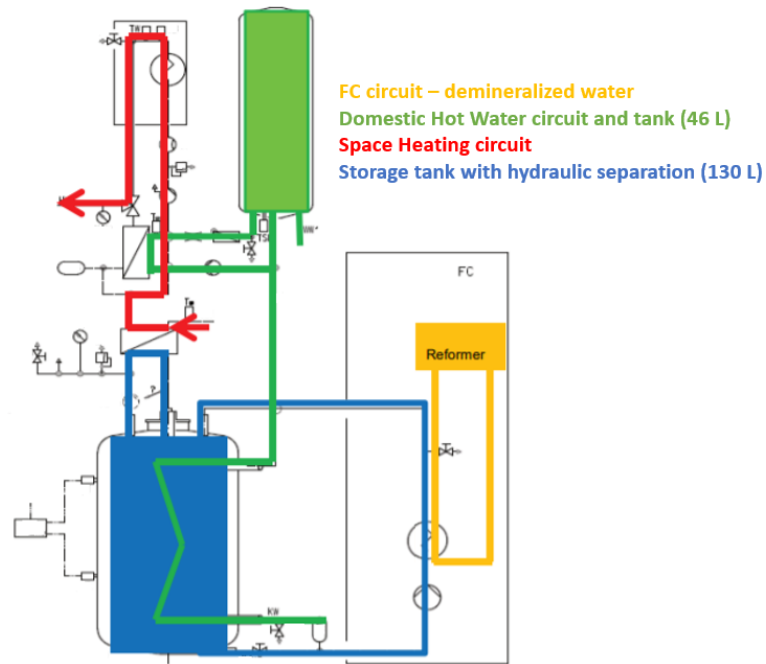
The machine is designed to provide all the heat demands (including DHW) of residential houses and to participate locally in the electrical production. This particular system (named 'P\*2'), exists in several versions, all based upon the same PEMFC module of nominal constant power of  $0.75 \text{ kW}_{\text{el}}$  and  $1.1 \text{ kW}_{\text{th}}$ , and all based upon the same 220 L DHW tank. The only module that may vary is the gas boiler that is supposed to ensure peak heat demands. Indeed, it exists in four rated power versions, from 11.4 to  $30.8 \text{ kW}_{\text{th}}$ , depending on the building and the resident's needs [521]. The hybrid architecture of the P\*2 system is presented in Figure 68 [521].



**Figure 68.** Architecture of the P\*2 – High level of integration (through two heat exchangers, several 3-way valves and several pumps) of the PEMFC with the gas condensing boiler and the DHW tank. Reproduced and adapted from reference [521].

As discussed in *Section 3.2.4 - Focus on the European market and the available fuel cell-based micro-CHP systems*, the previous version of the 'P\*2' was named '3\*\*' or '3\*\*-P' [385]. Also, the PEMFC fuel cell of the 'P\*2' system now exists as a standalone product, named the 'PA\*'. The fuel cell is assumed to be the same for all PEMFC products from that manufacturer. Indeed, as also mentioned in *Section 3.2.4 - Focus on the European market and the available fuel cell-based micro-CHP systems*, all those systems present the same power output fuel cell ( $0.75 \text{ kW}_{\text{el}}$ ) and the same photograph of the stack is presented in their respective datasheets (see Figure 70). The '3\*\*' (or '3\*\*-P') is assumed to be close to the P\*2 studied in this section and the only acknowledged differences are:

- The 3\*\* exhibits a smaller thermal efficiency (and thus thermal power) of the stack probably due to its less efficient hydraulic integration of the fuel cell. Indeed, thermal output of the 3\*\* is equal to  $1 \text{ kW}_{\text{th}}$  and not  $1.1 \text{ kW}_{\text{th}}$  as in the P\*2 [500]. Also, the 3\*\* has a tank of only 176 L as opposed to the 220 L of the P\*2 [500]. For comparison purposes, the 3\*\* architecture is presented in Figure 68.
- The 3\*\* only exists with two types of gas boiler (of  $19 \text{ kW}_{\text{th}}$  and  $25 \text{ kW}_{\text{th}}$  rated powers) [522], whereas, as stated, the P\*2 offers four options of boilers.

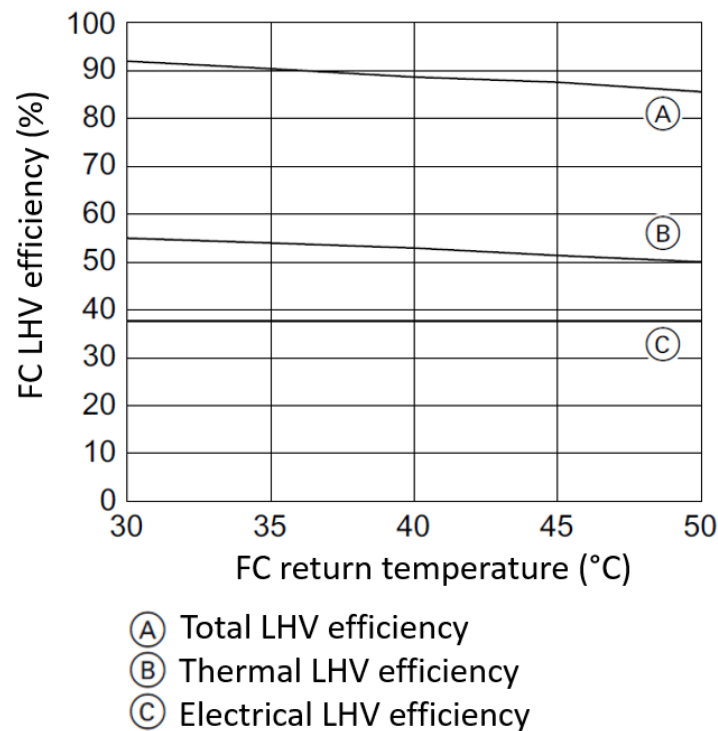


**Figure 69.** Architecture of the 3\*\* – High level of integration (through two heat exchangers, several 3-way valves and several pumps) of the PEMFC with the gas condensing boiler and the tanks [500]. For information, a photograph of the Panasonic PEMFC stack, supposedly the same for the 3\*\*, the P\*2 and the PA\* is presented in Figure 70.



**Figure 70.** Photograph of the PEMFC stack of the P\*2 (same as for the 3\*\* and the PA\*). Picture identical in the documentation of the three machines [522–524].

OEM's information provides the expected performance of the PEMFC on its own, as presented in Figure 71. It also states that the maximum return temperature for the PEMFC is 50°C [523,524], which is already, in addition to what Figure 71 shows, an indication that these systems perform worse as working temperature increases. For example, they are expected to perform better with floor heating than with high temperatures terminal units (such as cast-iron radiators).



**Figure 71.** OEM's declared performance of the PEMFC only (reproduced from reference [523,524]). PEMFC thermal efficiency is lower for the 3\*\* (no longer sold) [521].

As opposed to the micro-CHP SOFC system studied in the previous chapter, that could be parametrized with pre-programmed electrical load profiles in its 500-1500  $W_{el}$  range (and for which, as mentioned, the heat recovery circuit was completely optional), the behavior of PEMFC systems from the same manufacturer is purely heat driven. Indeed, their PEMFC has not been designed to be driven by the electrical demand; it can neither be turned on 'manually' (without any heat demand) nor modulated, and one might find in literature the following explanations for that:

- Electrical driven fuel cells are more complex and expensive units (high capital costs) [267] whereas it is obvious that, for the residential market, price is a main driver and the technology must remain affordable.
- One cannot assume that an electrically-led PEMFC alone would be able to reach any electrical demand profile, which could be particularly erratic at a residential level, as the residents come and go and as their daily activities can vary greatly. Indeed, since current PEMFC technologies need a certain time to adapt their output power to steep load changes [525] that occur very frequently in single residential buildings, PEMFC manufacturers usually do not market fully electrically driven micro-CHP applications.
- Following exactly the local electrical energy demand would require many start-up/shut-down cycles. However, the duration of warm up time for PEMFCs can vary greatly, even with external heat, from about 5 to 1000 minutes for the example of a 120°C PEMFC stack [526], which is way insufficient to meet typical electrical demand profiles in residential applications. In addition, many start-ups and shut-downs induce thermal cycling, which reduces already uncertain stack lifetime in such recent residential micro-CHP applications [527]. However, the electrical demand profile could still be followed to some extent (and the start-up/shut-down cycles problem would not be problematic) if the PEMFC system was able to (at least partially, not necessarily to a complete shutdown) modulate its electrical power in a given range, as for the micro-CHP SOFC system studied in the previous chapter.

- Thermal management is one of the biggest challenges of PEMFC technologies as temperature changes greatly influence lifetime [528] and performance [267]. With a thermal management already stated in Table 7 as complex for (LT-)PEMFCs, it is trivial that it would even be more difficult to implement and control with electric power output modulation.

One might also have thought that the electrical efficiency of the PEMFC technologies would lower as one spreads off the design operating conditions and that would constitute another reason for the system not to modulate and not to be electrically driven. However, the opposite is in fact usually reported in literature [529–531] (rated power is therefore not the one that provides the best efficiency but in fact constitutes an optimum between efficiency and power density).

Actually, even if this PEMFC has a constant output power, the duration for which it stays 'ON' is affected by several possible operating modes. In the 'economy' operating mode, the maximum operating time of the fuel cell is chosen so as to obtain a self-produced current consumption as high as possible [523] (increased supply cover factor). To do so, the OEM only discloses the fact that the system is taking into account '*data related to the power consumption, the temperature in the integrated buffer tank and the depart temperature of the heating circuits*' [523]. It also states in the user manual that energy costs (gas consumption, electricity consumption and production) must be parametrized and that a specific electrical energy meter is advised to correctly establish the building's electrical demand [532]. Without this meter (connected to the system), a demand profile 'by default' has been established as a factory setting [532]. In the 'ecological' operating mode, the fuel cell is said to operate in a way as to achieve maximum emission reduction of CO<sub>2</sub> (again, no further information provided by the OEM, especially regarding the emissions factors they are considering). In this mode of operation, the cost savings can sometimes be smaller than those that would have been obtained with the 'economy' mode. The last mode is the 'thermoregulated' one: the fuel cell module starts '*according exclusively to the temperature of the DHW tank and the depart temperature of the heating circuits*' [523,532]. In practice, it is said that, whatever the operating mode, the PEMFC can only produce electricity if heat dissipation is possible towards the DWH tank or the heating circuits [532]. One can also assume that it will produce electricity as soon as heat dissipation becomes possible unless, if such a mode is activated, it is established that it is not economically or ecologically favorable.

Even with those modes activated, it is likely that the parameterized values (energy costs or emissions factors) have been set to increase PEMFC use. Indeed, the OEM declares that the fuel cell is designed to operate in a 48-hour cycle: continuous electrical production for a maximum of 45.5 hours (if heat dissipation is sufficient) followed by a 2.5-hour regeneration phase for which the PEMFC is shut down [523]. In addition, it also states that the '*P\*2 is optimized for long durations of use*' [523]. Also, because relevant cost parameters can be tricky to establish (for non-specialists) and because relevant emissions factors can be quite political (as seen in *Section 2.3 - Current emissions factors from heat and power generation*), it is assumed that the ecological and economical modes mainly exist for specific technically aware customers that intend to have a strong interaction with their machine so they can modify the parameters as they desire.

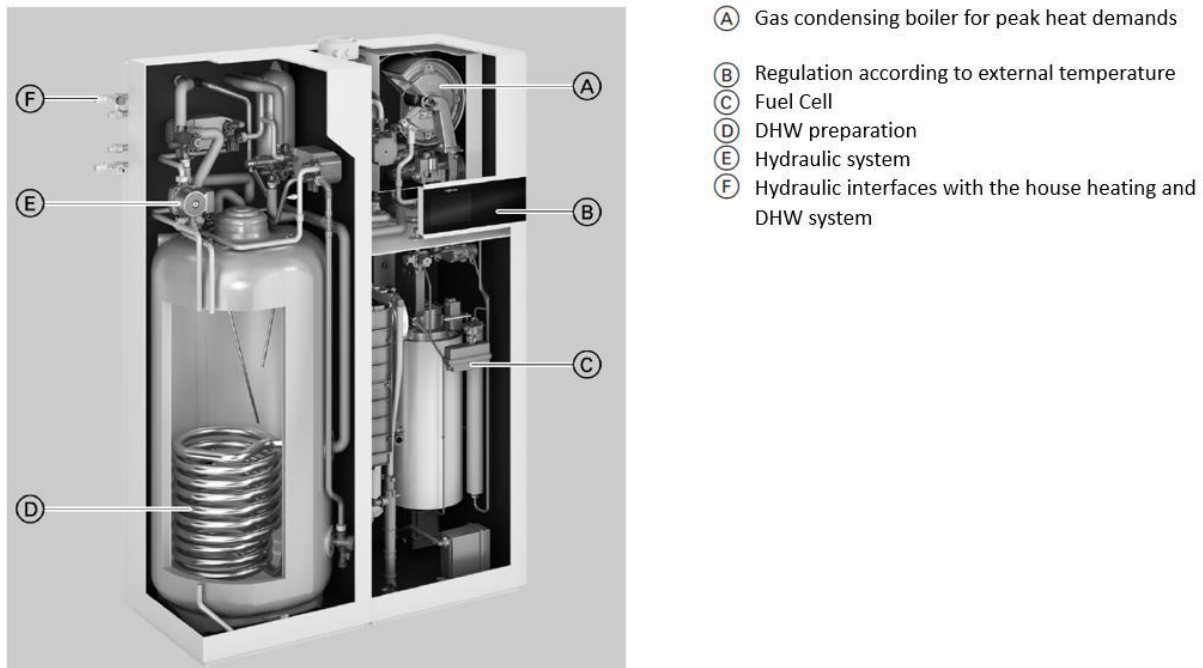
All the P\*2 machines studied in this work use the 'heat driven' operating mode (which is, as stated, named the 'thermoregulated' mode). Indeed, on one hand, this mode was deliberately chosen in the laboratory test campaigns and, on the other hand, the monitored dwellings do not have the required electrical meter connected to the system that is able to establish the building's electrical demand (see *Section 5.3.1 - Description of the buildings*).

In comparison with the SOFC system studied in the previous chapter, all the PEMFC systems from the studied manufacturer do include a DC/AC inverter in their embodiment.



### 5.1.3 P\*2 - Manufacturer datasheet

An internal photograph of the P\*2 (of which architecture has been presented in Figure 68) is shown in Figure 72 and the main performance announced by the manufacturer are listed in Table 11.



**Figure 72.** Internal photograph of the P\*2 system [523].

The system's overall dimensions are 600x1200x1800 mm (without the exhaust duct) and it weighs 326 kg.

Datasheet figures	Values
Maximum electrical production a day	17 kWh <sub>el</sub>
Maximum electrical production a year	6200 kWh <sub>el</sub>
Fuel cell rated electrical power	0.75 kW <sub>el</sub>
Fuel cell rated thermal power	1.1 kW <sub>th</sub>
Electrical fuel cell efficiency	37% (LHV)
Max global Fuel cell efficiency	92 % (LHV)
Max boiler efficiency (at rated power)	108.6 % (LHV) <sup>a</sup>
Max 'CO <sub>2</sub> savings' <sup>b</sup>	-50%

<sup>a</sup> Considering High Heating Value (HHV) to Low Heating Value (LHV) ratio of 1.1085 [132].

<sup>b</sup> Calculation method not specified in the datasheet.

**Table 25.** PEMFC gas boiler hybrid expected targets (according to the manufacturer) - Nominal performance of the P\*2 [523].

### 5.1.4 Probable internal schemes

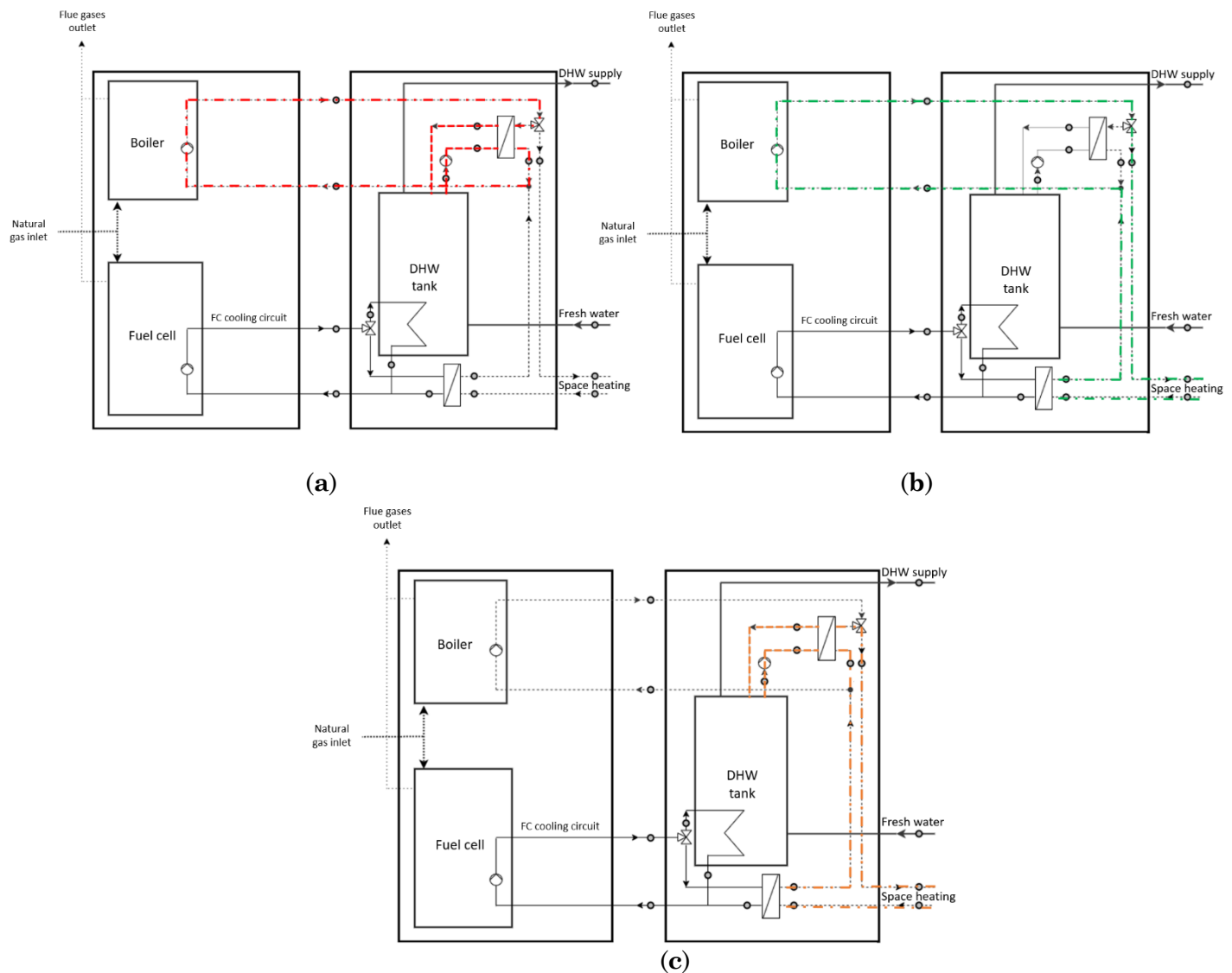
#### 5.1.4.1 Hydraulic flowchart of the complete hybrid system

Gas boiler hydraulic configuration possibilities are detailed in Figure 73. More specifically, the gas boiler DHW production and space heating modes are respectively illustrated in Figure 73 (a) and Figure 73 (b). The three-way valve called 'DHW priority valve' in Figure 68 allows for switching from one mode to the other. A third possible mode has been reported in Figure 73 (c) where the space heating uses the heat stored in the upper part

of the DHW tank (if its temperature is sufficient). This would have been a way for the system to use the tank as a heat storage for space heating and could have been useful to avoid having to start the gas condensing boiler if high temperature was needed in the space heating. However, this mode is unlikely for three main reasons:

- The ‘DHW priority valve’, as it is called in Figure 68, most likely consists of a ‘T-port’ three-way valve [533] with three positions: one for filling and draining the unit (all ports open), one for DHW production and one for space heating production [534]. Even if technically possible, there is no mention in the manufacturer documentation [534] of a fourth position of the ‘DHW priority valve’ that would only connect the DHW priority heat exchanger to the space heating and close the port towards the boiler, as in Figure 73 (c);
- This would only empty the heat stored in the upper part of the tank and this could be seen as going against the traditional DHW priority philosophy [535];
- This would require an additional external circulator to supply space heating, which would no longer be connected to the internal circulator of the boiler. Plus, this would lead to unrecommended hydraulic configurations when the gas boiler of the system is turned on for space heating. The two circulators would indeed be placed in series, which constitutes a risk of over or under feeding one of the circulators [536].

Hydraulic configurations of the PEMFC within the system have not been highlighted because they can trivially be deduced. Indeed, it has been observed (by looking inside the machine) that the three-way valve called ‘PEMFC valve for cooling circuit option’ in Figure 68 is the same as the ‘DHW priority valve’ described above. It is thus supposed that, when the fuel cell runs and needs to dissipate its heat, this valve also prioritizes heating the tank and implements the DHW priority philosophy [535]. Subsequently, it is considered that its only other operating position is obtained by switching to space heating pre-heating, when the tank is thermally loaded and the fuel cell return temperature becomes too high. In fact, as mentioned in *Section 4.1.2 - Applications and the different versions of the tested system*, if the return temperature to the fuel cell reaches 50°C (with the DHW tank thermally loaded and a space heating demand not sufficient), it has been reported by the OEM that the PEMFC stops running (and providing power) for safety reasons [537]. For the same three reasons stated here above for the ‘DHW priority valve’ that dictates the gas boiler hydraulic configurations, it is therefore again assumed unlikely that the valve called ‘PEMFC valve for cooling circuit option’ in Figure 68 enables the DHW tank to act as a heat storage for space heating. For information, this unlikely hydraulic configuration would have been obtained by closing the cooling circuit of the fuel cell and by permitting the flow from the bottom of the DHW tank to the heat exchanger that allows for pre-heating the space heating circuit, as it can be deduced from Figure 68.

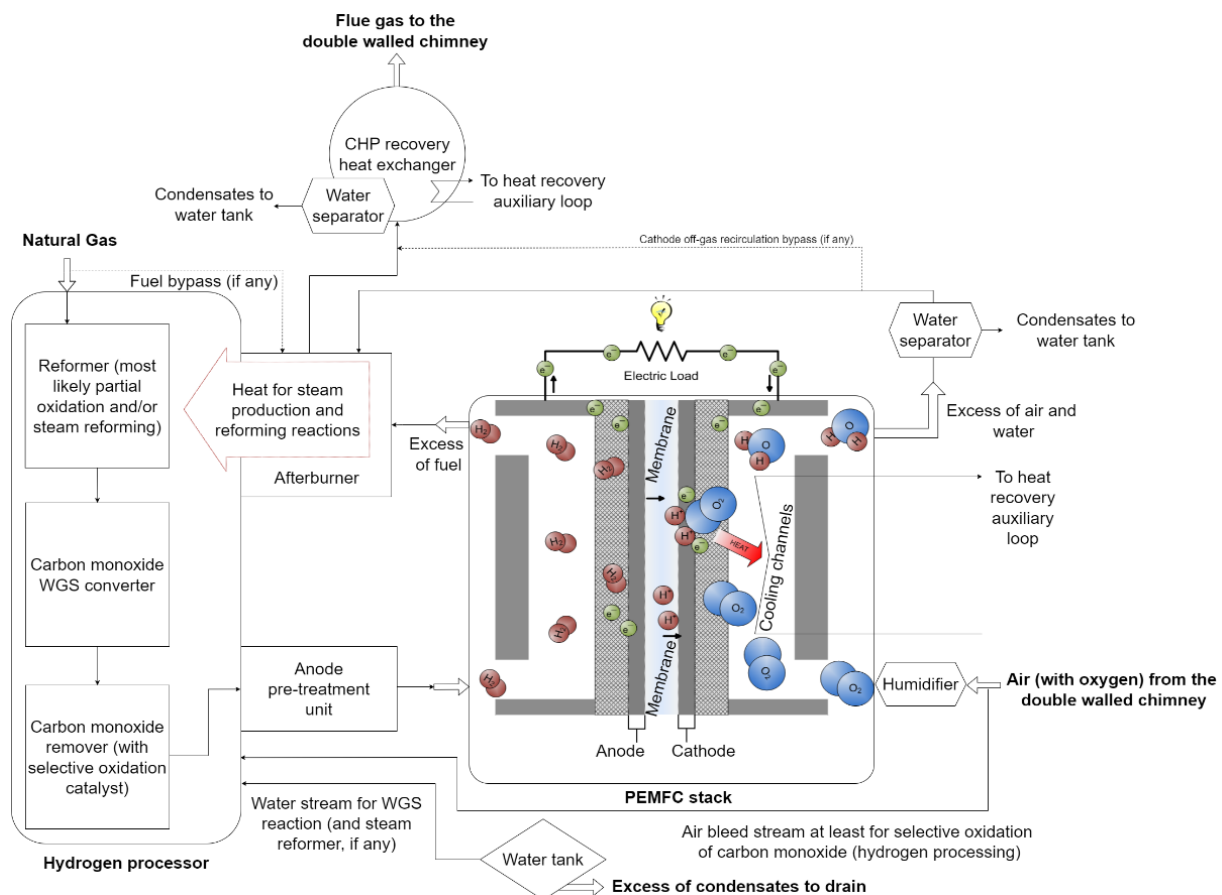


**Figure 73.** (a) Hydraulic configuration of the system in DHW production; (b) Hydraulic configuration of the system in space heating production by the boiler; (c) Unlikely hydraulic configuration where the DHW tank acts as a heat storage for the space heating circuit.

#### 5.1.4.2 PEMFC module internal configuration

The assumed flow-sheet scheme of the PEMFC module, composed of the hydrogen processor along with its integration to the PEMFC stack, is presented in Figure 74. Contrary to Figure 68, it does not involve the gas condensing boiler and DHW tank which the PEMFC module is hybridized to. This PEMFC module scheme has other particularities that should be mentioned, especially concerning how the different reactants are processed.

The PEMFC module has three inlets and three outlets. First, there is one inlet for each reactant (natural gas for hydrogen production and air as oxygen source). Similarly, there is one outlet for the flue gases (for both anode and cathode exhausts), as well as one outlet for the excess of condensates recovered in the system [524,534], that is not internally used for the WGS reaction or, if any, the steam, tri- or autothermal reforming process, as explained in *Section 5.1.1.2 - Hydrogen processor and reforming processes*. Outside air is supplied through the outer pipe of a double walled chimney [443]. This inlet air is also slightly heated all-along this chimney by the flue gases, which flow through the inner pipe.



**Figure 74.** Assumed basic scheme of the PEMFC module with its hydrogen processor. The water tank only consists of processed water (from the humid streams, such as the flue gases or the water produced by the stack and recuperated at the cathode exhaust) and should not be confused with the DHW tank illustrated in Figure 68. Several elements have not been illustrated : the scheme does not involve any pump or compressor to ensure flowing directions and appropriate pressure levels. It does not involve auxiliaries (such as safety valves, check valves, purging system, reactant filters, additional water recovery in humid streams such as at the anode outlet [509], potential natural gas desulfurizer, *etc*). Mostly, it does not illustrate internal heat management : each component has its own operating temperature and multiple internal heat exchanges are implemented to optimize accordingly the inlet gaseous streams temperatures [267] (the heat recovered from the cathode exhaust dehumidification, i.e. from its water recovery, is not shown, for example). Potential anode off-gases recirculation (to the anode inlet, to increase fuel efficiency [538]) is not shown. The air bleed stream could also serve other purposes such as the main reforming process (if it involves the methane partial oxidation reaction) or the potential carbon monoxide mitigation (see *APPENDIX 14: Literature review on PEMFC degradation mechanisms* for more details).

The last inlet and outlet are used in a close-loop auxiliary heat recovery circuit. This circuit recovers heat from the flue gases (allowing them to condense to participate in the internal water recovery) and also, through cooling channels in the stack, from the fuel cell reaction [524]. This heat recovery circuit is directly (or indirectly, through a potential additional heat exchanger) connected to the 'FC cooling circuit' observable in Figure 68. It thus allows for the running fuel cell to dissipate its heat either for DHW preparation or for a potential space heating demand from the dwelling. The exact configuration of this close-loop cooling circuit (that recovers heat from the PEMFC module, i.e. from the stack and from the flue gases) is unknown but it is supposed that cooling the stack is prioritized. It has indeed already been stated that the return temperature to the fuel cell stack shall not reach or overcome  $50^{\circ}\text{C}$  for the PEMFC not to be promptly stopped for safety reasons [537]. So, the heat recovery exchange with the flue gases might be optional and bypassed (if the heat

demand to the system for DHW or space heating are not sufficient to dissipate the heat from the running PEMFC).

As mentioned in Table 7 and described in more details in *APPENDIX 14: Literature review on PEMFC degradation mechanisms*, water management is crucial in PEMFC systems. Indeed, performance (conductivity), stability, and durability of a PEMFC stack depend on the membrane humidification [539] so humidity levels of reactant gases (at the anode and at the cathode) are usually controlled with dedicated continuous humidification processes [540]. This explains why Figure 74 includes both the ‘Humidifier’ at the cathode inlet and the ‘Anode pre-treatment’ unit at the anode inlet, which also implies other pre-treatment processes of the anode reactant. Indeed, as it is explained in details in *APPENDIX 14: Literature review on PEMFC degradation mechanisms*, the ‘Anode pre-treatment’ unit is also believed to involve an ‘ammonia remover’ apparatus. It is noteworthy that ammonia poisoning can occur from the high temperature of the reforming processes associated to the nitrogen compounds from ambient air (used in the CO remover and/or the potential partial oxidation reforming reaction). However, this ‘ammonia remover’ is placed downstream of the fuel processor and some of its catalysts still happen to be poisoned by ammonia (it is indeed the case for the oxidation catalyst of the CO remover, which can be deactivated and no longer fulfill its purpose). As explained in *APPENDIX 14: Literature review on PEMFC degradation mechanisms*, this is why, with this system, the 2.5-hour offline regeneration phase is executed after 45.5 hours of PEMFC functioning. Indeed, it is believed that a ‘reductive atmosphere’ is implemented (with high hydrogen and low air proportions) to remove the absorbed ammonia on the catalyst of the CO remover and hereby regenerate it.

As explained in *Section 5.1.4.2 - PEMFC module internal configuration*, the PEMFC module is not connected to the water mains (or to the DHW tank). It uses processed water only for humidification and steam production purposes (for the WGS reactor and potential steam reforming processes). As reported in literature [509], it surely recovers water from the humid streams, such as from the flue gases condensation (allowed by the heat recovery feature described above and shown in Figure 74) or from the water produced by the fuel cell stack reaction and recuperated at the cathode exhaust.

Also, as stated, the (potential) partial oxidation process in the carbon monoxide remover requires oxygen through an air bleed, which can come from the cathode inlet or the cathode exhaust. Literature usually reports air bleeds from the cathode inlet [509], for the following potential reasons :

- Bleeding air from the cathode exhaust would imply increasing the air flow rate in the stack. Therefore, this would increase nitrogen crossover from the cathode to the anode [541], which creates buildups and impedes the anode reaction by blocking the catalytic sites (as described in more details in *APPENDIX 14: Literature review on PEMFC degradation mechanisms*);
- The concentration of oxygen is lower at the cathode outlet than in fresh air, while the concentration of nitrogen is higher. Therefore, for the same number of oxygen atoms required in the carbon monoxide remover, more air (and thus more nitrogen) must be drawn from the cathode outlet than it would have been needed from fresh air. In addition to the already explained increased nitrogen crossover risk, this dilutes the hydrogen entering the anode (reduces its partial pressure), which in turn reduces the current density of the fuel cell [511]. It has also already been reported that a more diluted hydrogen stream leads to a reduction in the carbon monoxide tolerance of the fuel cell, which can lead to severe performance losses [512];
- Similarly, air bleeding from the cathode exhaust implies higher concentration of carbon dioxide (than from ambient air), which might cause formation of carbon monoxide (harmful to the stack) via the reverse water gas shift reaction [542].

As generally seen in literature [543–546], the anode exhaust stream is most probably sent back to an afterburner associated to the hydrogen processor (which also requires additional fuel from the natural gas inlet). Indeed, the recycling of the anode exhaust gases (still containing unconverted methane but more specifically, unused hydrogen) is a valuable recovery of heat that can be used to generate steam for the reforming processes and to reach their tremendously high temperature requirements (around 1000 K, as described in the previous section) [547]. Furthermore, it avoids releasing methane, which would be called ‘methane slip’ (see *Section 2.3.3 - Methane slip in natural gas fed fuel cells*) or molecular hydrogen in the atmosphere, which might represent an environmental risk of not yet well-known impacts on the stratosphere, for the possibility of destruction of ozone [548]. Although the oxidant reactant (oxygen) required for the afterburner usually comes from fresh air [543–546], which is not excluded in this case, it has been reported in several applications [508,509,549] that it could come from the cathode exhaust as a way of saving energy from (fresh) air compression [509]. It is worth mentioning that the cathode off-gases excess might bypass the afterburner and directly go through the flue gases chimney.

### 5.1.5 Conclusions of the section

- Several versions of the studied PEMFC system exist and existed. The tested one, i.e. the ‘P\*2, is hybridized internally to a gas condensing boiler and a DHW tank. Based on the same fuel cell stack, it now exists as a standalone PEMFC system (also fed by natural gas) under the name ‘P\*2’.
- The tested system offers an electrical power output of 750 W<sub>el</sub> that cannot be modulated (the PEMFC is either on or off). Its announced fuel cell LHV electrical and thermal efficiency are respectively 37% and 55% (at return temperatures of 30°C). The heat recovery is internally implemented and controlled in the system (to dissipate the fuel cell heat either in the space heating or the DHW embodied tank)
- A DC/AC inverter is already embodied in the system for residential applications.
- PEMFCs, such as the one studied in this chapter, require a high purity hydrogen fuel. This necessitates a complete fuel processing system that can involve reforming processes such as steam reforming and/or partial oxidation reactions. It also involves one or several ‘water-gas shift’ (WGS) reactor to increase the hydrogen purity from the main reforming processes.
- CO being an absolute poison of (LT-)PEMFC stack, such as the one used in the studied system, a CO remover apparatus must be included in the fuel processing system.
- CO remover and (potential) partial oxidation reforming reactions require an air bleed (usually from the cathode inlet, i.e. from ambient air).
- The PEMFC can function continuously for a maximum of 45.5 hours. Then a 2.5-hour regeneration phase is required. This work (in *APPENDIX 14: Literature review on PEMFC degradation mechanisms*) has demonstrated that this regeneration phase is most likely required to remove the ammonia poisoning of the oxidation catalyst of the carbon monoxide remover in the fuel processing system. Indeed, ammonia poisoning can occur from the high temperature of the reforming processes associated to the nitrogen compounds from ambient air (used in the CO remover and/or the potential partial oxidation reforming reaction).
- Anode recirculation to increase fuel efficiency cannot be excluded.
- Water is recuperated from the flue gases and most likely from the off-cathode gases. It is probably stored in an internal storage tank, to be used for the WGS reaction (and the potential steam reforming reaction). Excess of water is evacuated through a drain.
- An afterburner is used to generate the required heat for the reforming processes. It uses the off-anode gases as main fuel source and off-cathode gases as oxidizing agent. It is not excluded that it is also partially directly fed from the natural gas inlet.

- 
- Reforming processes (and their required additional heat) explain the relatively lower electrical efficiency of PEMFCs fed by hydrocarbons (compared to other fuel cell technologies, such as SOFCs).
  - Reactants are most likely humidified to ensure the proper proton conductivity of the membrane electrolyte (as already stated in *Chapter 3 - Fuel cell technologies and their residential applications*).
  - The heat of the fuel cell is recovered from the stack itself and most likely from the afterburner exhaust gases (enabling it to work as a CHP).

Most of the content of *Section 5.2 - Laboratory tests* was published in the *proceedings of the 19<sup>th</sup> International Refrigeration and Air Conditioning Conference (Herrick 2022)* [550]. This is the only part of this thesis for which I was not in charge and for which I was not the main author. The experimental work reported in this section was mainly performed by Camila Dávila Valdebenito, a dearest colleague of ULiege laboratory, who I thank again for her fruitful and interesting collaboration. Since I am not the main author, the content of this section was kept to the work I have contributed to as a co-author. It is therefore close to the minimum information required to understand the rest of this work.

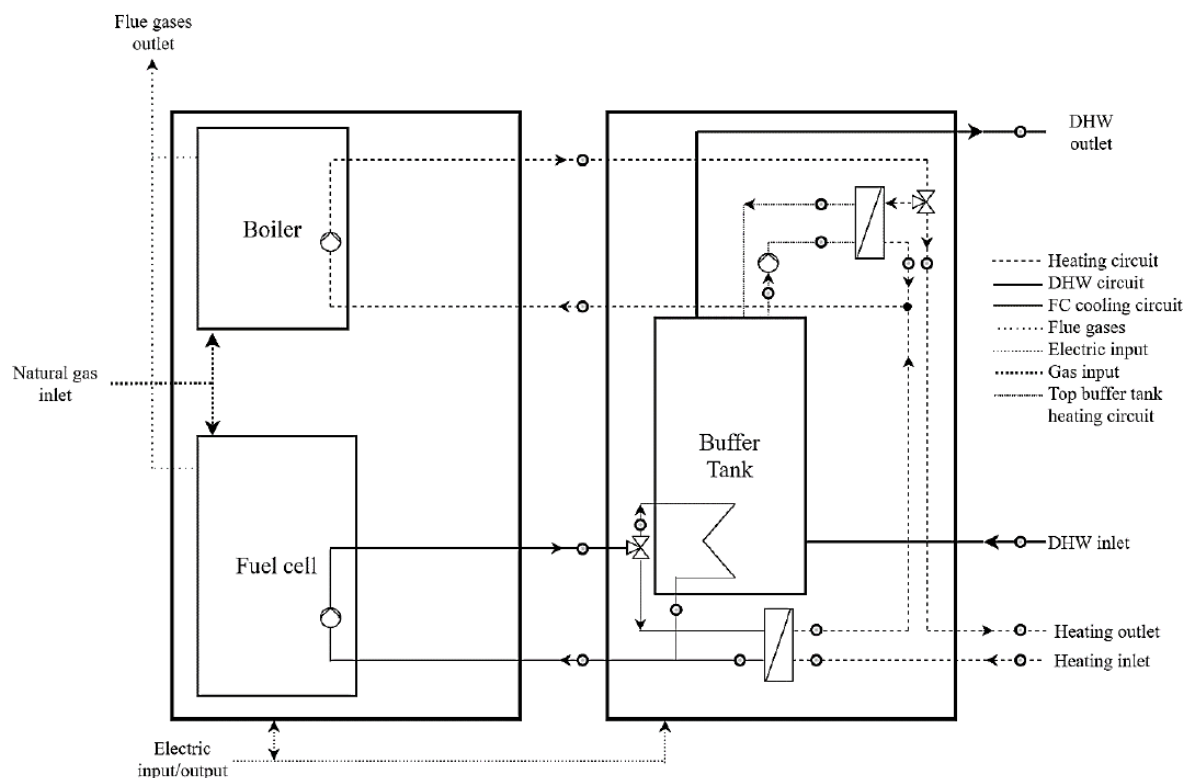
Tests have been carried out in the laboratory to characterize the behavior of the global system and its components under different demand requirements. To do so, an emulator of space heating (SH) and Domestic Hot Water (DHW) has been installed and measurements of gas consumption, heat production, and electricity consumption/generation have been collected.

A test campaign based on the requirements of the EN 50465 is proposed and performed this section, where the base requirements are extended to a wider range of depart temperatures for SH and DHW; also, the effect of the imposed load over the system global performance is studied. Afterwards, both boiler and fuel cell are tested separately to characterize their contribution to the global system.

## 5.2 Laboratory tests

### 5.2.1 Description of the test bench

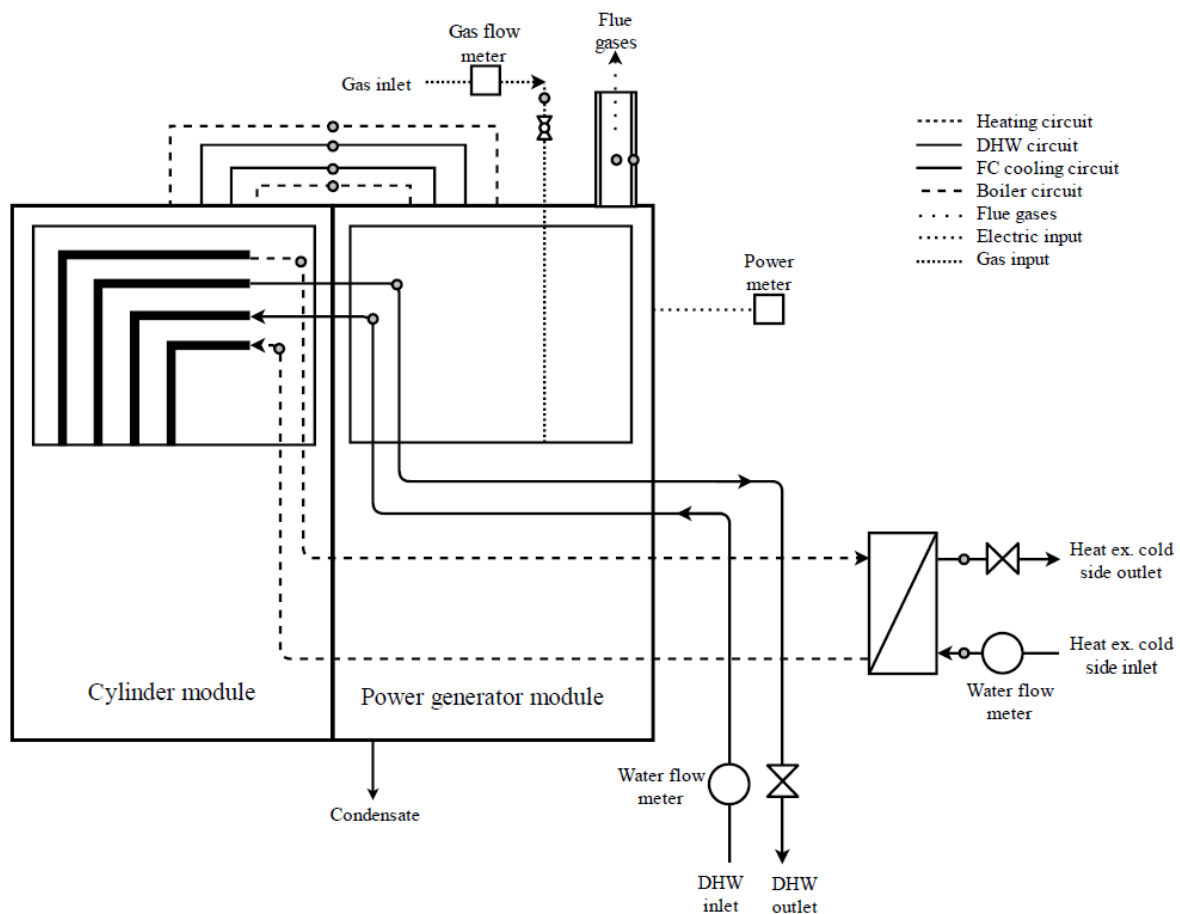
With the intention not to influence the performance of the machine, the sensors used to collect measurements inside the modules should not be invasive; this implies that, in terms of temperature measurements, only surface thermocouples are installed on the pipes of the cylinder module and on the connections with the fuel cell module, represented by circles, in the disposition shown in Figure 39.



**Figure 75.** Location of surface thermocouples (grey circles) in the P\*2 test bench.



A rear-view scheme of the test bench is shown in Figure 41. The different sensors and their locations are given as well; the same symbology is used regarding thermocouples, with the difference that, except for the connecting tubes between both modules that use surface thermocouples, immersion sleeves are used.



**Figure 76.** P\*2 test bench scheme rear-view.

The system is integrated to the rest of the test bench by 4 connections, including the supply and return flows intended for SH (Space Heating) and DHW (Domestic Hot Water). The SH demand is emulated by a heat exchanger, the capacity of which is controlled by a valve that regulates the water flow rate on the cold side. In the same way, the demand of DHW is controlled by adjusting the opening of a valve at the outlet. Both the heat exchanger and the water pipes are insulated and close to the system to avoid heat losses. The measurements of gas and electricity are realized on the supply lines of the system. The bidirectional electrical power meter shows both, the net electrical energy consumed and generated; the generated power exported to the grid is reduced by the power consumed by the operation of the PEMFC itself.

### 5.2.2 Measurement devices

In Table 26, the type of sensors, their accuracy, the amount of measuring points and the acquisition frequency are given. These sensors allow for collecting measurements of temperatures, water flows, gas consumption and electricity consumption/production.

The assembly configurations of the thermocouples is shown in Figure 44. As it was mentioned earlier, the temperature measurements inside the machine are recorded with surface thermocouples. For the flow temperatures of both SH and DHW, the thermocouples are installed in immersion sleeves in the elbows of the pipes. These sleeves

are positioned in such a way that their tips are facing the flow. On these two previous applications, the thermocouples are isolated after installation to ensure that the collected data correspond to the desired measurements and to avoid the influence of radiation or convection with other sources. In the case of the air inlet and flue gases, a thermocouple in the center of the cross section is installed.

Sensor	Type	Accuracy	Number of measure points
Thermocouples	T	$\pm 0.3$ K	24
Water meter	Volumetric	$\pm 2\%$ $Q_n$ ; $\pm 5\%$ $Q_{min}$	4
Gas meter	Diaphragm	$\pm 0.5\%$	1
Power meter	Multifunctional	$\pm 0.5\%$	1

**Table 26.** P\*2 test measurement devices.



**Figure 77.** Thermocouples assembly configurations: surface, elbow and air thermocouples (in the system's chimney).

The electrical and gas meters are presented in Figure 78. They are identical to the one used for the laboratory test campaigns of the studied SOFC system reported in *Section 4.2.2 - Measurement devices* (sensors that were already there in ULiege facilities).



**Figure 78.** Gas and electrical installations.

### 5.2.3 Test procedure

In a typical startup phase from ambient temperature, the heating process of the DHW tank is carried out by both the boiler and the fuel cell, and it always ends up in the same way, when the buffer tank is heated up to 50-52°C.

During this heating cycle, first, the boiler starts and heats the upper part of the buffer tank to the target temperature; this process is fast due to the large heat rate of the boiler (up to 30.8 kW<sub>th</sub> for the system tested in the laboratory). In the meantime, the fuel cell enters on *Startup Phase* before getting into *Power and heat generation Phase*; once this stage is reached, the fuel cell starts producing heat and electricity gradually until it reaches its maximum thermal and electrical capacity of 1.1 kW<sub>th</sub> and 0.75 kW<sub>el</sub>, respectively. The heat produced by the fuel cell is rejected to the bottom part of the buffer tank and since its thermal capacity is small compared to the boiler, raising the temperature of this part of the buffer tank is a quite slow process.

If a heat demand is imposed on the system, the stored energy from the buffer (DHW) tank is used from the top to the bottom following the temperature gradient generated by stratification; the temperature decrease will depend on the water flow demand and how long it is maintained. If the demand stops, the tank will be heated back again; on the contrary, if heat is still requested, the system will be forced to deliver the produced heat immediately to the circuit that requires it. This second scenario is favourable to avoid the storage effect of the buffer tank on the performance estimation since the amount of energy stored is hard to quantify with the sensors that are used.

Having said that, the tests are forced to start once the buffer tank at its minimum temperature (typically around 17°C) and the behavior of the appliance (i.e. both the fuel cell and the boiler) is steady. The steady-state operating conditions varies from one test to another and depend on factors such as the flow demand (high or low) and the defined setpoint temperatures (for both DHW or SH demands).

### 5.2.4 Test matrix

In order to achieve the characterization of the system performance, the test campaign is based on the European Standard EN 50465. In terms of DHW, a step of 5 K is proposed until a minimum of 30 ( $\pm 2$ ) K for delivery temperature; for SH, a step of 10 K is proposed with a minimum  $\Delta T^\circ$  of 20 ( $\pm 1$ ) K between the depart and return flows. In terms of load, two different water flow rates are imposed (low and high) thanks to their respective controlling valves, with the aim of visualizing their effect on efficiency. In terms of mode, tests are carried out with DHW or SH production separately. The performed test campaign is shown in Table 27.

DHW			SH		
60 $\pm$ 2 °C	Low flow demand (Valve 50%)	High flow demand (Valve 100%)	$\Delta 20$ ( $\pm 1$ ) K	Low flow demand (Valve 50%)	High flow demand (Valve 100%)
55 $\pm$ 2 °C			$\Delta 30$ ( $\pm 1$ ) K		
50 $\pm$ 2 °C			$\Delta 40$ ( $\pm 1$ ) K		
45 $\pm$ 2 °C			$\Delta 50$ ( $\pm 1$ ) K		
40 $\pm$ 2 °C			$\Delta 60$ ( $\pm 1$ ) K		
35 $\pm$ 2 °C					
30 $\pm$ 2 °C					

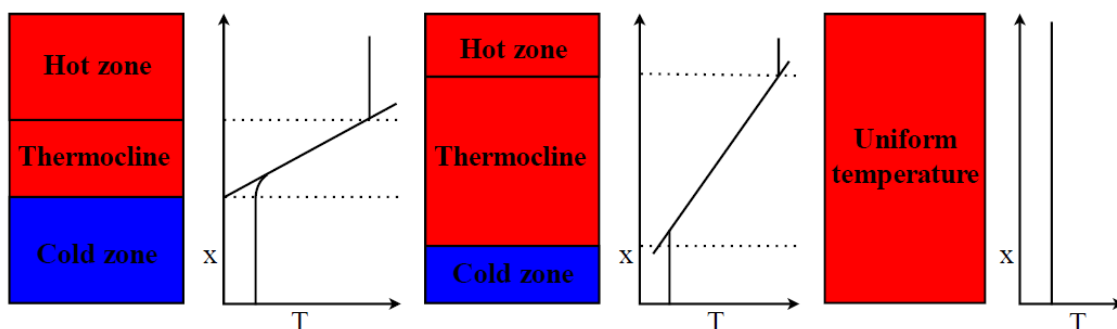
**Table 27.** P\*2 performed test campaigns.

The results of these tests give a first impression of the performance of the system, but they are not conclusive to perform a complete description of the appliance. To do so, it has been decided to characterize each component, fuel cell and boiler, separately.

Through the control panel display of the appliance, it is possible to turn off the fuel cell and work just with the boiler; then, the characterization of the boiler can be done. Unfortunately, it is not possible to turn off the boiler and use exclusively the fuel cell heat and electrical power, so in an attempt to characterize the fuel cell stack, an alternative to bypass the control of the system and perform tests just with the fuel cell is proposed. This consists in disconnecting the ignition wire of the boiler to cause a failure and disable the operation of the latter. By doing so, the whole production and consumption of the system depend on the fuel cell only.

As shown in Figure 39, the fuel cell stack rejects the heat to the buffer tank by means of a heat exchanger. The water flow rate of this loop is unknown but is estimated to be very small due to the nominal thermal output of the fuel cell; therefore, since it is not possible to estimate directly the fuel cell efficiency, a different method is applied.

The previous tests were conceived to avoid the effect of the storage of the buffer tank; now, the thermal and electrical efficiencies of the fuel cell are estimated based on the heat released to the buffer and the time required to increase its top and bottom temperatures from an initial to a final state. This, however, adds a new challenge since the available information does not allow to know *a priori* where the temperatures are being measured, i.e. where the thermocline is located as exemplified in Figure 79. Top and bottom temperatures are indeed given by the machine's display (not measured through dedicated laboratory instrumentation).

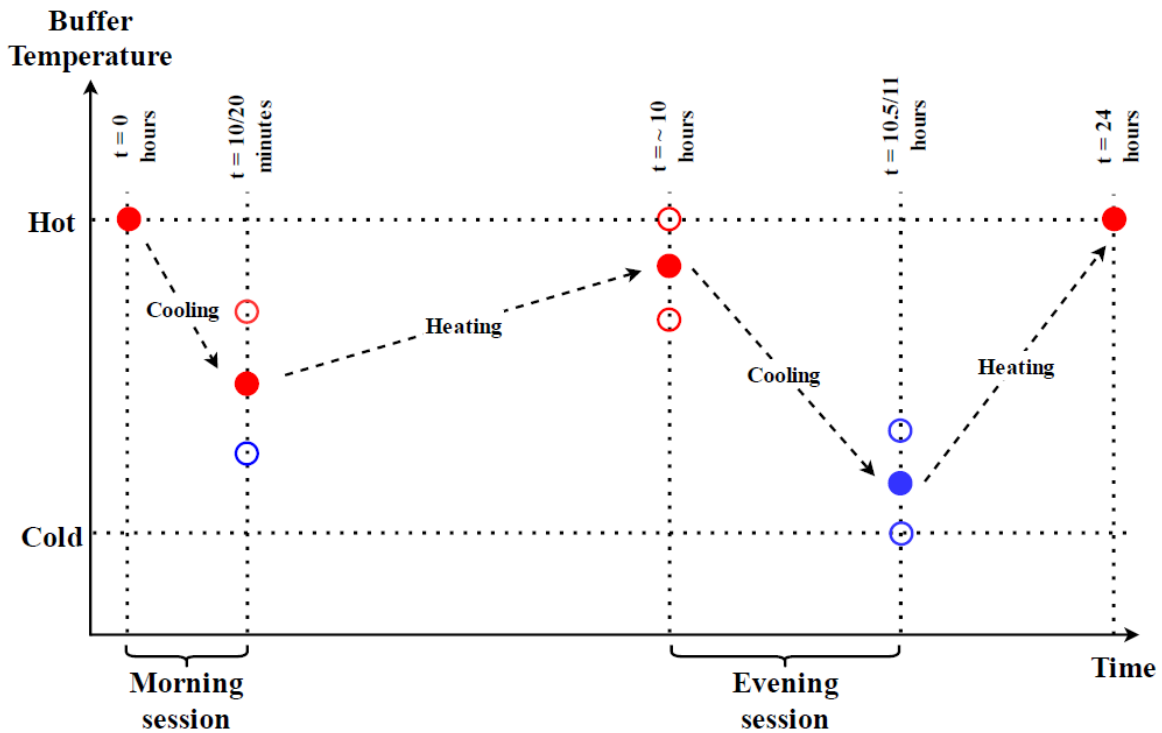


**Figure 79.** Graphical representation of the thermocline in the buffer tank.

Daily tests divided into morning and evening are proposed based on different adaptations of load profiles recommended by the official journal of the European Union as shown in Table 28. These profiles differ in the requested water flow and the duration of the demand imposed, following a daily cycle as shown in Figure 80.

	Profile		
	A	B	C
<b>Morning</b>	1 shower 10 minutes 6 L/min	2 showers 20 minutes 10 l/min	1 shower 10 minutes 8 l/min
<b>Evening</b>	2 showers 30 minutes 6 L/min	3 showers 60 minutes 10 L/min	2 showers 20 minutes 8 L/min

**Table 28.** Daily tests profiles description to estimate the fuel cell efficiency, morning and evening sessions.



**Figure 80.** Daily tests 24-hour cycle evolution for fuel cell-only performance estimation.

The tests start in the morning with a homogeneous hot buffer tank. Then, a demand is imposed for the mentioned duration depending on the selected profile (see Table 28), cooling down the buffer till a certain level. This triggers the fuel cell module that starts heating the buffer till the beginning of the evening session when the second load is imposed. Once this session is ended, the fuel cell module heats up the buffer till the next day, arriving at the same initial point and closing the cycle.

### 5.2.5 Experimental results and data analysis

Data related to the appliance's consumption of natural gas, water flow, and temperatures associated with each test performed are collected and shown in Table 29. For every test the electricity production was  $0.75 \text{ kW}_{\text{el}}$ , as expected (see Table 25). The laboratory indoor conditions were between  $20\text{-}25 \text{ }^\circ\text{C}$  for the temperature and 1 bar for the atmospheric pressure. The steady-state data collecting period was 45 minutes per test.

	DHW High flow demand (Valve 100%)				DHW Low flow demand (Valve 50%)			
	Gas Consumption [m3]	Water Consumption [m3]	Mean $\Delta T$ [K]	Test duration [s]	Gas Consumption [m3]	Water Consumption [m3]	Mean $\Delta T$ [K]	Tests duration [s]
60±2°C	2.353	0.809	22.913	2718	2.001	0.414	38.253	2728
55±2°C	2.399	0.827	23.173	2772	1.924	0.420	36.459	2739
50±2°C	2.249	0.801	22.476	2682	1.612	0.394	32.680	2627
45±2°C	1.936	0.809	19.316	2713	1.536	0.434	28.088	2834
40±2°C	1.593	0.808	16.013	2705	1.207	0.412	23.909	2695
35±2°C	1.245	0.800	12.770	2688	0.959	0.415	19.281	2725
30±2°C	0.915	0.788	9.487	2653	0.754	0.414	14.727	2726
	SH High flow demand (Valve 100%)				SH Low flow demand (Valve 50%)			
	Gas Consumption [m3]	Water Consumption [m3]	Mean $\Delta T$ [K]	Test duration [s]	Gas Consumption [m3]	Water Consumption [m3]	Mean $\Delta T$ [K]	Test duration [s]
60±1°C	2.429	1.128	17.205	2693	2.386	0.662	29.204	2678
50±1°C	2.010	1.123	14.650	2696	2.001	0.668	24.432	2677
40±1°C	1.640	1.125	12.055	2676	1.653	0.675	20.066	2665
30±1°C	1.208	1.137	8.756	2711	1.192	0.678	14.433	2698
20±1°C	0.844	1.144	5.958	2705	0.828	0.680	9.809	2693
Test performed	DHW 100%		DHW 50%		SH 100%		SH 50%	
HHV [kWh/Nm <sup>3</sup> ]	11.6003		11.5730		11.4588		11.3016	

**Table 29.** Experimental data collected through the test campaigns of the P\*2 PEMFC system.

The electrical, thermal and total efficiency of the system for each test was respectively established as shown in Equation (40), Equation (41) and Equation (42).

$$\eta_{el} = \frac{\dot{m} \times c_p \times \Delta T + 0.001 \times \dot{W}_{el}}{\dot{V}_{gas} \times HHV} \quad (40)$$

$$\eta_{th} = \frac{\dot{m} \times c_p \times \Delta T}{\dot{V}_{gas} \times HHV} \quad (41)$$

$$\eta_{syst} = \eta_{th} + \eta_{el} \quad (42)$$

Using these equations, the results of electrical, thermal and global efficiencies can be computed for each test. The high and low water flow demands are 0.298 [kg/s] and 0.152 [kg/s] respectively. The results are shown in Table 30 and Table 31.

	High flow demand			Low flow demand		
	$\eta_{syst}$	$\eta_{th}$	$\eta_{el}$	$\eta_{syst}$	$\eta_{th}$	$\eta_{el}$
DHW 60°C	0.807	0.790	0.018	0.821	0.796	0.024
DHW 55°C	0.818	0.800	0.018	0.826	0.799	0.026
DHW 50°C	0.821	0.802	0.019	0.834	0.803	0.030
DHW 45°C	0.832	0.809	0.023	0.829	0.797	0.032
DHW 40°C	0.841	0.814	0.028	0.860	0.820	0.041
DHW 35°C	0.858	0.822	0.035	0.889	0.838	0.051
DHW 30°C	0.867	0.819	0.048	0.877	0.812	0.065

**Table 30.** Electrical, thermal and global efficiencies of the system for DHW tests.

The results for the boiler only efficiency are given in Table 32 (PEMFC not producing). In this case, the hydraulic connections shown in Figure 39 allow a direct efficiency estimation using Equation (41) and Equation (42), where the system is now considered only as the boiler and for which the electrical consumption penalizes the efficiency of the system.

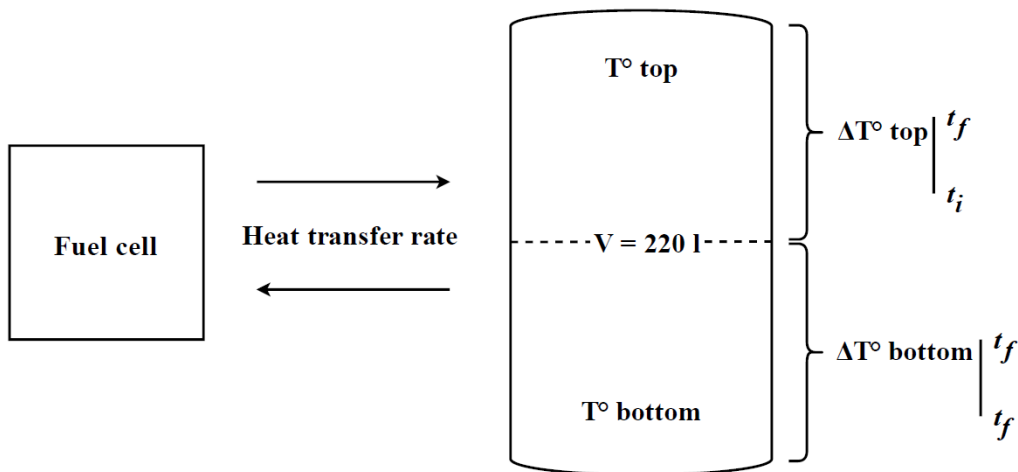
	High flow demand			Low flow demand		
	$\eta_{\text{syst}}$	$\eta_{\text{th}}$	$\eta_{\text{el}}$	$\eta_{\text{syst}}$	$\eta_{\text{th}}$	$\eta_{\text{el}}$
$\Delta T$ 60 K	0.831	0.811	0.020	0.855	0.834	0.021
$\Delta T$ 50 K	0.855	0.831	0.025	0.864	0.839	0.025
$\Delta T$ 40 K	0.869	0.839	0.030	0.874	0.843	0.030
$\Delta T$ 30 K	0.877	0.836	0.041	0.887	0.845	0.042
$\Delta T$ 20 K	0.878	0.820	0.058	0.889	0.829	0.060

**Table 31.** Electrical, thermal, and global efficiencies of the system for SH tests.

Profile		A	B	C
Morning	Thermal energy out. [kWh]	3.227	9.219	4.176
	Gas energy cons. [kWh]	3.614	10.510	4.321
	Electrical energy cons. [kWh]	0.019	0.047	0.024
	$\eta_{\text{th}}$	0.893	0.877	0.966
	$\eta_{\text{syst}}$	0.888	0.873	0.961
Evening	Thermal energy out. [kWh]	9.620	28.179	8.430
	Gas energy cons. [kWh]	11.837	34.618	10.492
	Electrical energy cons. [kWh]	0.065	0.140	0.047
	$\eta_{\text{th}}$	0.813	0.814	0.804
	$\eta_{\text{syst}}$	0.808	0.811	0.800

**Table 32.** Boiler efficiency results obtained during boiler-only operation.

The tests to estimate the fuel cell efficiency are performed several times each to minimize the error associated with the temperature measurement (and location) uncertainty in the buffer tank. To estimate the thermal efficiency, only the heating periods are considered, where it is assumed that half of the buffer tank is at  $T^\circ \text{ top}$  and half at  $T^\circ \text{ bottom}$ , leading to the definition of a  $\Delta T^\circ \text{ top}$  and  $\Delta T^\circ \text{ bottom}$  evaluated between the initial and final time of a heating period as shown in Figure 81. For example, this means that, for the morning (or evening) heating period, initial and final top and bottom temperatures are considered for the buffer tank, giving rise to a morning (or evening)  $\Delta T^\circ \text{ top}$  and a morning (or evening)  $\Delta T^\circ \text{ bottom}$ . This principle is applied as shown in Equation (43) for a daily estimation and the results are summarized in Table 33.



**Figure 81.** Buffer tank temperatures definition for fuel cell efficiency estimation.

$$\eta_{th,PEMFC} = \frac{0.5 \times V_w \times \rho_w \times cp_w \times (\Delta T_{top,m} + \Delta T_{bottom,m} + \Delta T_{top,e} + \Delta T_{bottom,e})}{3600000 \times V_{gas} \times HHV} \quad (43)$$

Profile		A	B	B	C	C	C
Start Morning	T° top	55	58	54	59	59	58
	T° bottom	55	58	54	59	59	58
End Morning	T° top	55	23	21	58	58	57
	T° bottom	49	20	20	44	48	44
Start Evening	T° top	58	51	50	57	50	57
	T° bottom	58	51	50	57	50	57
End Evening	T° top	25	18	19	27	24	27
	T° bottom	21	18	18	21	21	22
	Heat Rate [kW]	0.442	0.690	0.722	0.439	0.344	0.441
	Electrical eff.	0.301	0.319	0.295	0.295	0.328	0.292
	Thermal eff.	0.179	0.308	0.290	0.175	0.152	0.173
	Global eff.	0.480	0.626	0.585	0.470	0.480	0.465

**Table 33.** HHV efficiency estimation of the P\*2 fuel cell from experimental results.

## 5.2.6 Troubleshooting

The description and analysis of troubleshooting is certainly interesting to improve the performance and reliability of the system. Four main interventions have been performed on the following dates:

- May 2019
- October 2020
- November 2020
- January 2021

More detail and information about each intervention can be found in *APPENDIX 13: P\*2 – Laboratory troubleshooting description*. All of those interventions have been reported by my colleague, Camila Dávila Valdebenito, who I hereby thank again.

## 5.2.7 Conclusions of the section

In this work, the experimental characterization of the P\*2, i.e. a natural gas-driven micro-CHP PEMFC-based unit, has been performed. The tests were carried to characterize the behavior of the global system and its components, i.e. both the boiler and the fuel cell, separately, to study their contribution to the global system performance under different requirements.

The results obtained for the overall HHV efficiency of the complete system (boiler included) in steady-state, avoiding the thermal buffer effect, show that it is mainly composed of the thermal output, the electrical part being a small fraction of the total. A maximum value of about 89% for the global efficiency of the system was reached, where the electrical contribution did not exceed 6% of the total. The trends indicate that the lower the water outlet temperature, the higher the efficiency, as expected.

The results obtained for the boiler HHV efficiency are between those announced by the manufacturer, reaching about 96% (maximum value obtained in the laboratory tests).

For the PEMFC only, the results varied due to the complexity of the system. The thermocline inside the buffer and the lack of information regarding the cooling fluid mass flow rate and its temperatures certainly lead to an undervalued maximum global HHV



efficiency value of about 63%, obtained with the proposed estimation method. In that figure, 32 percentage points correspond to the electrical contribution and 31 percentage points to the thermal contribution. 32% of HHV electrical efficiency gives about 35.5% of LHV electrical efficiency (considering a HHV to LHV ratio of 1.1085 [132]), which is quite close to, although a little below, the 37% LHV electrical efficiency announced by the manufacturer (see Table 25). That difference of efficiency is however in the order of the propagated uncertainty from the measurements and HHV calculations. Indeed, as an example, the propagated uncertainties on the electrical efficiency established in details for the field-test systems of both the studied SOFC (as seen in *Section 4.3.5 - Uncertainty analyses*) and the PEMFC (as it will be seen in *Section 5.3.5 - Uncertainty analyses*) is in the order of 1 percentage points (uncertainty that can be considered also valid for the laboratory tests reported in this section).

Nevertheless, having about 30% as the maximum obtained value for thermal efficiency is unexpectedly low. Subsequently, this leads to a global efficiency far from the manufacturer's announced data (see Table 25). As stated, the significant difference is probably due to the lack of information regarding the water flow in the cooling circuit of the fuel cell loop. Although innovative, it can be considered that the method performed in this work to estimate the thermal efficiency of the PEMFC only (based on considering the DHW tank as composed of two identical volumes of water of homogenous temperatures) only is not sufficiently accurate and should therefore surely still be improved.

The content of *Section 4.3 - In-situ monitoring*, which mainly aims to report the energy performance of the field-tested systems in terms of natural gas consumption, net electricity production, as well as thermal and electrical efficiencies was published almost as-is in the *proceedings of the 35<sup>th</sup> International Conference On Efficiency, Cost, Optimization, Simulation and Environmental Impact of Energy Systems (ECOS2022)* [15]. Energetic performance and grid-matching figures reported in this section have also been published in the *proceedings of the 14th REHVA HVAC World Congress (CLIMA2022)* [477].

## 5.3 In-situ monitoring

### 5.3.1 Description of the buildings

As stated in the introduction of this chapter, the first house is located in Huy (South-East Belgium) whereas the other one is located in Oostmalle (North of Belgium). From a climatic point of view, one can state that the three houses are located in the same region. The location of the monitoring sites has been presented in Figure 52.



**Figure 52.** Location of the PEMFC monitoring sites.

The first monitored building (Huy) is a semi-detached house of the early 20<sup>th</sup> century but significant insulation work of walls and roofs has been conducted. Single-glazing windows have been replaced by double-glazing windows and a balanced ventilation has been installed. However, terminal units still consist of high temperature cast-iron radiators. The family that lives there consists of 2 active adults and 3 children under the age of 10.

The second monitored building (Oostmalle) is a full detached house from the 70<sup>s</sup> but tremendous renovation just took place before the study. Insulation has been increased of course, but the whole space heating architecture has also been revisited with the implementation of floor heating for the ground floor. On the first floor, terminal units consist of high temperature radiators as in the former house. The family consists of a young active couple with one child of a small age.

It must be reminded that the gas boiler of the P\*2 has to be chosen between four rated power versions from 11.4 to 30.8 kW<sub>th</sub> (see *Section 5.1 - Description of the machine*). Gas boiler rated thermal power within the machine is 11.4 kW<sub>th</sub> in Oostmalle whereas it is 24.5 kW<sub>th</sub> in Huy.

As stated in *Section 5.1 - Description of the machine*, none of the machines has been linked to a dedicated electrical energy meter that establishes the building's demand (for proper parametrization of the 'economy' or 'ecological' operating mode). In addition, neither economical nor ecological parameters have been set or modified by the users, at least according to them. It is thus assumed that each system functions according to the 'heat driven' operating mode (called 'thermoregulated'), which is explained in *Section 5.1 - Description of the machine*. However, it is not possible to absolutely ensure that the occupants (or their installers) have not changed the operating mode of the system after the commissioning of this field-test project. At least, the occupants have declared not to have altered those parameters.

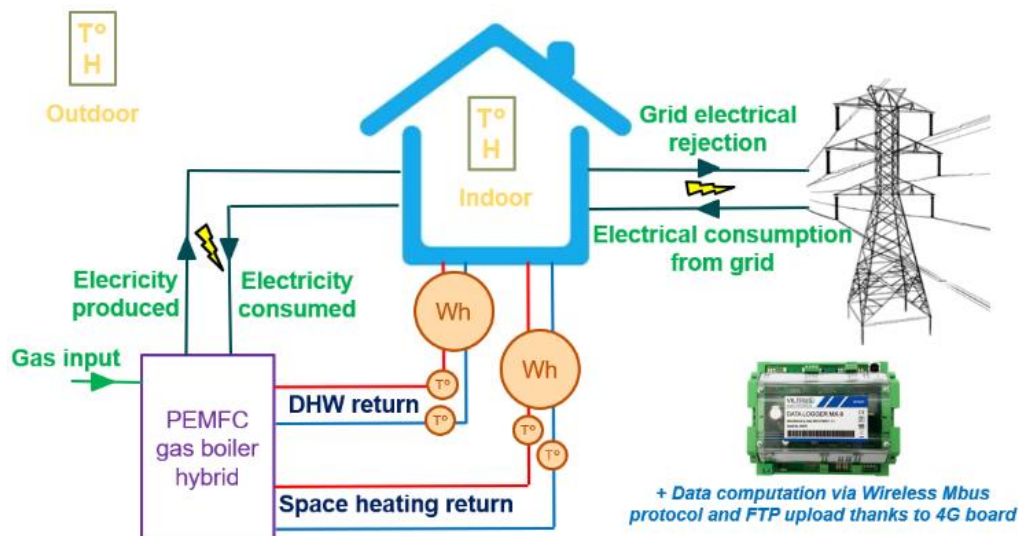
More details on the houses and the occupants are provided in *APPENDIX 11: Satisfactory Survey of the house in Huy* and *APPENDIX 12: Satisfactory Survey of the house in Oostmalle*. Those surveys contain identical questions than the ones reported for the studied SOFC system in the previous chapter. Therefore, they have also been designed, collected and analysed during this thesis as a way of gathering potential useful information about the households (and their occupants) that are not provided through the monitoring installation only. Those surveys aimed to answer such questions as :

- Why did the owners invest in such emergent technologies the first place ?
- Are they experiencing any inconvenience with the system in its everyday use ?
- How are they feeling about the user experience ?
- How are they feeling with the system's performance compared to their expectations ?
- *Etc*

Because of the small sample size (only two installations included in this study), it was not intended with this survey to perform statistical analyses on the answers. The surveys were mainly conceived at the early stage of the field-test study to establish an official communication mean with the owners and felicitate troubleshooting reporting. In addition, for confidentiality purposes, in the Appendices of this work, those surveys have been limited to the backup information that is actually referred to in this thesis.

### 5.3.2 Measurement devices

Both houses are equally monitored. Sensors are identical and are placed at the same spots, according to the simplified scheme of Figure 53. Sensor reference, precision and resolution of the acquired data are presented in Table 34. As the sensors are pretty much the same as in the SOFC laboratory study (see *Section 4.2.5 - Experimental results and data analysis*), most of them have already been partially validated by correlation with the corresponding laboratory sensors that have been used in that study (in a laboratory environment).



**Figure 83.** Monitored sensors configuration of the P\*2 field-test sites (a more detailed schematics can be found in *APPENDIX 9: Detailed schematics of the monitoring sensors configuration of the P\*2 field-test sites*).

Sensors	Reference	Resolution (data logger included)	Accuracy
Outdoor temperature and <u>humidity</u>	Weptech Munia [467]	0,1 K   <u>0,1 %</u>	± 0,3 K   <u>± 2 %</u>
Indoor temperature and <u>humidity</u>	Weptech Munia [467]	0,1 K   <u>0,1 %</u>	± 0,3 K   <u>± 2 %</u>
DHW and space heating heat counters	Qalcosonic E1 Qn2,5 $q_i=0.025m^3/h$   L=130mm [455]	1 kWh   1 L   0,1 K	Accuracy Class 2 [457]
Machine 2-ways electrical energy counter	Iskraemeco MT174-D2A42-V12G22-M3K0 [453]	10 Wh	Accuracy Class 1 [468]
House 2-ways electrical energy counter	Iskraemeco MT174-D2A42-V12G22-M3K0 [453]	10 Wh	Accuracy Class 1 [468]
Gas volume counter	BK-G4T DN25 Qmax 6 m <sup>3</sup> /h [452]	10 L	<0.5%
Data logger (cloud connection)	Viltrus MX-9 [469]	NA	NA

**Table 34.** Reference of the monitoring sensors and acquisition system for the P\*2 field-test sites. The sensors are the same as in the corresponding SOFC study conducted in the previous chapter except for the fact that the P\*2 field-test sites require an additional heat meter (of the same reference), as the system as not only one (as in the BI\*\*\*G\*N SOFC system) but two thermal outputs (for space heating and DHW).

Last very important parameter not shown in Table 34 is the sampling rate, the frequency of the acquisition, of the measurements. It has been set to a 2-minute time step for the house in Huy and a 5-minute one in Oostmalle. As stated in the previous chapter, with this data logger and its 'T2' communication mode [466], it is impossible to set a time step smaller than 2 minutes due to the fact that it must establish a successful Wireless M-bus (Meter-bus) connection with every sensor, one after the other, and that takes time (a few seconds for each connection) [466]. The reason not to have the same sampling rate for all houses is that the faster the rate is, the quicker the battery inside the sensors will be empty. Therefore, reducing the time step to 2 minutes required extra power supply, which was not possible to provide for the second house. Furthermore, for such thermal monitoring applications, a time step of 5 minutes is way enough for the majority of the analyses that is needed.

As in the previous chapter, this latter statement implies that the field-test monitoring measurements are not completely synchronous and this tends to impede transient behaviour analysis of the systems. Through those monitoring signals, systems

performance is thus preferably analysed over enlarged timeframes, typically 24 hours or more.

Since the sensors are the same as in the SOFC field-test study conducted in the previous chapter, the corresponding explanations detailed in *Section 4.3.2 - Measurement devices* also apply here, especially regarding how the total electrical demand of the dwelling can be computed thanks to Equation (17). It is worth mentioning that, compared to the Bl\*\*\*G\*N SOFC system studied in the previous chapter that has an external circulator, the space heating circulator is embodied to the P\*2. Therefore, its electrical consumption is already deduced from the electrical production of the system (as other internal auxiliaries, such as fans, electronic boards, *etc*).

### 5.3.3 Methodology

This monitoring section is based on data collected during the whole years 2020 and 2021. The year 2022 has not been extensively studied for those systems as it has been observed that it did not bring results and outcomes sufficiently different than the ones reported in this work for the years 2020 and 2021.

#### 5.3.3.1 Energetical performance

Electrical efficiencies have been computed considering the monitored electrical consumption of the system at the nominator (as a negative contributor). Only the equivalent energy of the consumed gas has been considered at the denominator of the efficiency calculations. It is worth mentioning that a consumption signal at the system's output can only be seen if the machine is not producing electricity. Indeed, the system provides electricity to its own auxiliaries in running mode and only the net electrical production is measured.

The energetical performance of the systems is therefore defined by their electrical and thermal efficiency, defined similarly as in the P\*2 laboratory study thanks to Equation (40) and Equation (41). The only differences are that heat meters directly provide the thermal output at the numerator (addition of the DHW and space heating measured heat) and that the measured electrical consumption of the system over a given timeframe (being measured when the fuel cell is not producing) has to be deduced from its electrical net production over the same timeframe (being measured when the fuel cell is producing).

#### 5.3.3.2 Economical and ecological performance

The chosen methodology for establishing performance indicators is the same as in the previous chapter (see *Section 4.3.3.2 - Economical and ecological performance*).

In order to compute the economical indicators, i.e. the utilization cost savings, one has considered the following assumptions for the year 2020: 0.2425€/kWh<sub>el</sub> for electrical energy and 0.041€/kWh<sub>HHV</sub> for natural gas [473]. Those prices are considered constant, which might be an assumption that is relevant for the whole year 2020 (the year of this performance study) but that could be criticized for further projections (as demonstrated by the energy crisis of 2021 [472]).

For 2021, as in the previous chapter, only the second semester average prices have been considered and applied to the whole monitoring data of the year, in order to partially consider the impact of the energy crisis [472] on the economical performance of the machine. The energy prices, again considered constant for the whole year, are thus 0.333€/kWh<sub>el</sub> for electrical energy and 0.093€/kWh<sub>HHV</sub> for natural gas [473]. It must be pointed out that European natural gas prices even rose by almost 70% after Russia invaded Ukraine in February 2022 [474] but that is not yet considered at this point.

Other important pricing assumption is that the electrical energy transport and distribution costs are rounded to 0.15€/kWh<sub>el</sub>, following the same assumptions as in the previous chapter.

Once again, the environmental indicators are based on the same method of comparison with reference systems as applied in the previous chapter (see *Section 4.3.3.2 - Economical and ecological performance*) and described in *Section 2.3 - Current emissions factors from heat and power generation*.

### 5.3.4 Results

One can observe in Table 35 and Table 36 the energy performance and key figures of both sites. HHV to LHV ratio has been once again assumed to be 1.1085 (according to the assumption of the Walloon energy regulator) [132].

Monitored data	Huy	Oostmalle	Monitored data	Huy	Oostmalle
HHV equivalent energy consumed (kWh) [465]	19515	32391	LHV Electrical efficiency (%)	10,8	10,1
Electrical production (kWh)	2175	3213	LHV Thermal efficiency (%)	70,3	80,3
Electrical consumption (kWh)	270	255	LHV Total efficiency (%)	81,1	90,4
DHW (kWh)	1599	1998	Space heating (kWh)	10779	21481
Utilization CO <sub>2eq</sub> savings (marginal emissions) – 1st dataset (kgCO <sub>2eq</sub> ) <sup>a</sup>	-97	566	Energy utilization cost savings (€) <sup>c</sup>	72	271
Utilization CO <sub>2eq</sub> savings – 2 <sup>nd</sup> dataset (kgCO <sub>2eq</sub> ) <sup>b</sup>	-746	-273			

<sup>a</sup> - 1<sup>st</sup> dataset emission factors : 251 gCO<sub>2eq</sub>/kWh for gas and 456 gCO<sub>2eq</sub>/kWh<sub>el</sub> for electricity (see Dataset 'A' from Table 4).

<sup>b</sup> - 2<sup>nd</sup> dataset emission factors : 254 gCO<sub>2eq</sub>/kWh for gas and hourly data from Belgian electrical consumption mix from [www.Electricitymap.org](http://www.Electricitymap.org) for electricity (see Dataset 'E1' from Table 4).

<sup>c</sup> - Electrical price: 0.2425€/kWh<sub>el</sub>. Gas price 0.041€/kWh<sub>HHV</sub>.

**Table 35.** 2020 field-test figures for both PEMFCs (1866 degree-days in 2020 [551], base 16.5°C [552]). Utilization savings indicators consider a gas condensing boiler of 90% constant LHV efficiency as reference for heat production.

The share of equivalent energy consumed by the fuel cell only can be estimated by dividing the electrical production by the announced 37% LHV efficiency of Table 25. It is however not trivial to estimate the share of thermal energy provided by the fuel cell only in the P\*2 hybrid system.

Only the total yearly efficiency in Oostmalle comes close to the declared optimal efficiencies of Table 25, mainly thanks to the higher thermal efficiency allowed by terminal units of lower temperature (floor heating).

Lower electrical efficiency in Oostmalle, due to higher heat demand, is balanced thanks this higher thermal efficiency. Electrical production in Oostmalle is greater, thanks to the higher heat demand and fuel cell increased capability of dissipating its heat in the space heating low temperature terminal units [477], but it is still about two times lower than the full PEMFC capacity (see Table 25). Actual PEMFC load factor [537] is therefore always below 50% (as it will also be demonstrated with Figure 86).

Key figures are similar for 2021 except that Oostmalle space heating demand has increased by 50%, which allowed for a prevalent use of the boiler within the system (at its nominal output), resulting in a better thermal (and total) efficiency. It is worth mentioning that the 16.5°C degree-days were increased by about 25% in 2021 compared to 2020. The reason for the lower (although quite similar) 2021 efficiencies in Huy (compared to 2020) is not yet established.

Efficiencies have been especially discretized monthly in Figure 84 for the year 2020. One can see that the Oostmalle house PEMFC has not been working in November and December (and that necessitated an intervention of the installer in January 2021). This timeframe is interesting because it points out that the system has a LHV efficiency close to 90% on its boiler only, which is consistent with the seasonal efficiency of conventional condensing boilers studied in similar field-test conditions [553]. This is also, as stated, the value considered as reference efficiency for gas condensing boilers by the local authority to compare space heating appliances [127].

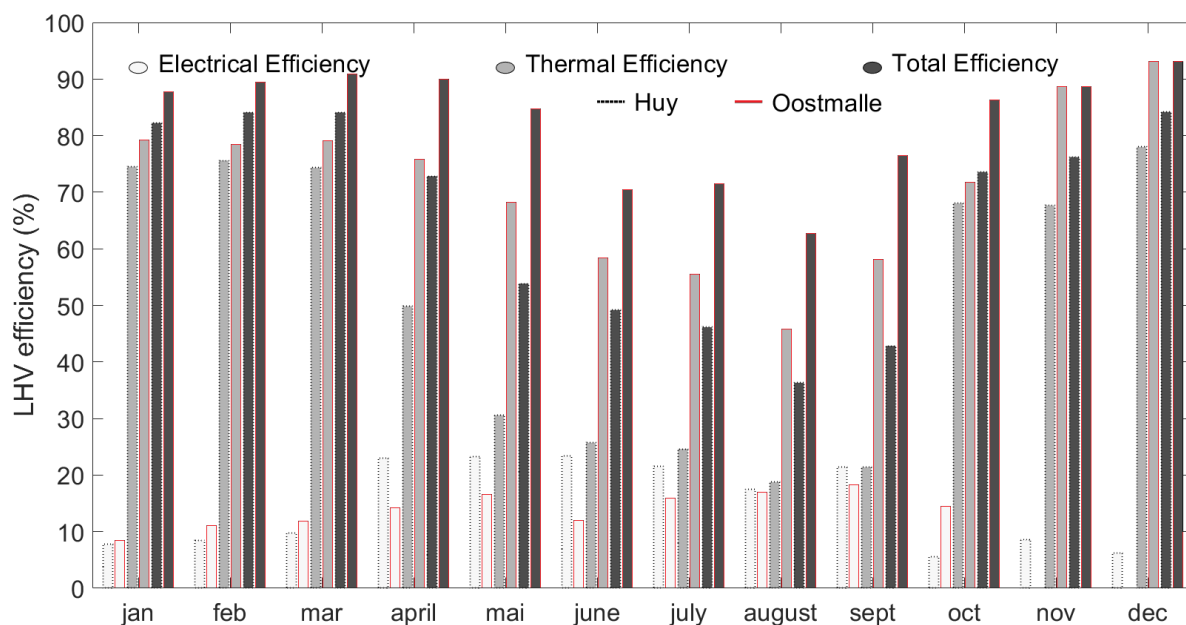
Monitored data	Huy	Oostmalle	Monitored data	Huy	Oostmalle
HHV equivalent energy consumed (kWh) [465]	20083	38243	LHV Electrical efficiency (%)	9,5	8,6
Electrical production (kWh)	2011	3222	LHV Thermal efficiency (%)	69,4	84,5
Electrical consumption (kWh)	298	258	LHV Total efficiency (%)	78,9	93,1
DHW (kWh)	1627	2095	Space heating (kWh)	10941	27061
Utilization CO <sub>2eq</sub> savings (marginal emissions) – 1st dataset (kgCO <sub>2eq</sub> ) <sup>a</sup>	-260	827	Energy utilization cost savings (€) <sup>c</sup>	-47	451
Utilization CO <sub>2eq</sub> savings – 2nd dataset (kgCO <sub>2eq</sub> ) <sup>b</sup>	-811	-144			

<sup>a</sup> - 1<sup>st</sup> dataset emission factors : 251 gCO<sub>2eq</sub>/kWh for gas and 456 gCO<sub>2eq</sub>/kWh<sub>el</sub> for electricity (see Dataset 'A' from Table 4).

<sup>b</sup> - 2<sup>nd</sup> dataset emission factors : 254 gCO<sub>2eq</sub>/kWh for gas and hourly data from Belgian electrical consumption mix from [www.Electricitymap.org](http://www.Electricitymap.org) for electricity (see Dataset 'E1' from Table 4).

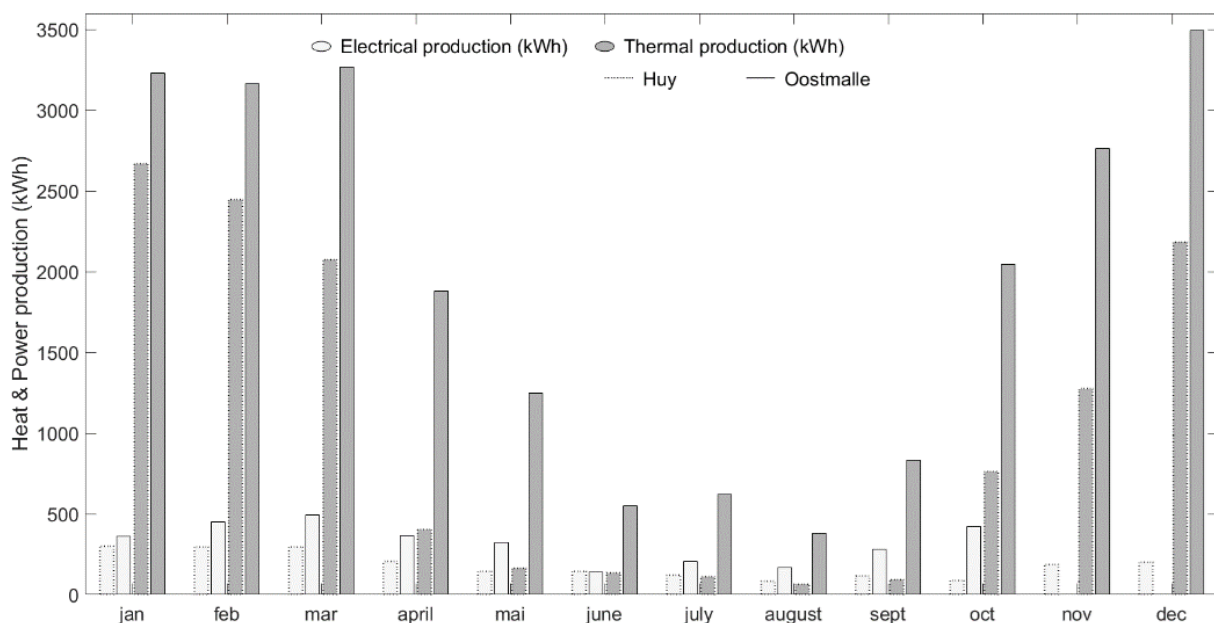
<sup>c</sup> - Electrical price: 0. 333€/kWh<sub>el</sub>. Gas price 0. 093€/kWh<sub>HHV</sub>.

**Table 36.** 2021 field-test figures for both PEMFCs (2286 degree-days in 2021 [554], base 16.5°C [552]). . Utilization savings indicators consider a gas condensing boiler of 90% constant LHV efficiency as reference for heat production.



**Figure 84.** Monthly LHV efficiencies for monitored P\*2 dwellings for the year 2020.

One can also see that in warmer seasons (less heat demand), the thermal and total efficiency drop whereas the electrical efficiency increases. This is especially seen in Huy because the Oostmalle house still uses its floor heating in the summer and in mid-season (newborn in the house). The main reason is that, in warmer seasons, there is nearly no need for space heating and the DHW is mainly provided by the PEMFC only through the storage tank. Therefore, electrical production of the machine becomes prevalent in the hybrid system (versus heat production), so as the standby losses of the heat tank. All this can be verified thanks to Figure 85 that even shows for the house in Huy that electrical production between June and September gets higher than thermal production. In fact, without much space heating demand, as the heat produced is stored for a certain duration in the DWH tank (before the DHW monitoring heat meter), the thermal (standby) losses become indeed significant. It must be remembered that the DHW heat meter only measures the energy when hot water is consumed and not when it is produced. Also, as it can be deduced from Table 25 or from Figure 84 and Figure 85, thermal (and total) efficiency of the PEMFC is not as high as the one of the boiler so the less this latter is used, the smaller the thermal (and total) efficiency will be.



**Figure 85.** Monthly heat and power production for both field-test P\*2 for the year 2020.

One can also see that thermal efficiency and total are greater for the Oostmalle house and it is mainly due to the transient peaks imposed on the system of Huy, as it will be explained later on in the modelling section of this chapter (see *Section 5.4 - Machine modelling*). It also comes once again from terminal units of lower temperature (Oostmalle has floor heating that favors efficient stationary operating conditions and lower working temperatures, which have been declared by the OEM to enhance thermal efficiency of the PEMFC, as shown in Figure 71). Even if it has been stated that the use of the PEMFC is prevalent in the system in warmer seasons, daily electrical production is lower during summer, as it can be deduced from Figure 85. Indeed, the absolute heat demand to the PEMFC is lower and it has to be shut down because the fuel cell is no longer able to dissipate the heat it generates.

It must be pointed out that comparing the performance of the SOFC systems reported in the previous chapter and the ones of the P\*2 systems is tricky. For example, the potential standby losses of the storage tank have not been considered for the SOFC systems, whereas they are trivially already taken into account at the outputs of the complete P\*2

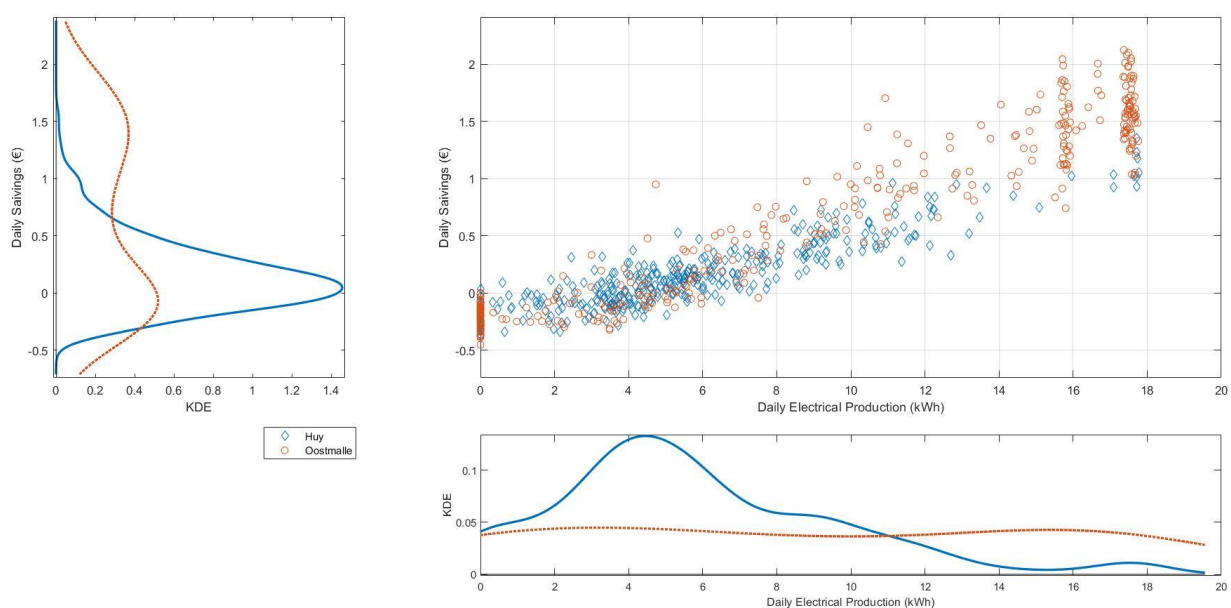


system (see Figure 68). In addition, as it has been seen in Equation (27), the economical performance are case-dependent as they are directly affected by the supply cover factor that is achieved by the specific and unique electrical load demanded by the occupants.

Regarding utilization cost savings, it can be observed that, thanks to its higher total efficiency, the system in Oostmalle is slightly more profitable. However, even if the system in Oostmalle is always profitable, the yearly savings are quite insufficient (between 100€ and 450€ of utilization costs savings a year). For instance, in order to achieve return on investments (ROI) times under 10 years, the system's capital costs shall not be higher than 1k€ to 4.5k€ compared to a classical gas condensing boiler, which seems unrealistic for the time being. Based on the results in Huy, if any, the system utilization costs savings are really insignificant compared to a gas condensing boiler. The 2021 indicators for Huy even show slightly negative profits probably because of the relatively higher gas price (compared to the 2020 prices) and because of the lower total efficiency of the system. Again, the fact that the PEMFC load factor is always below 50% has a great negative influence on utilization cost savings, as reported in Figure 86. This figures indeed shows that the house in Huy almost never reaches the maximal daily electrical production of the system (with the PEMFC always turned on), which lies around 17-18 kWh<sub>el</sub>. Instead, a statistical peak has been found around 4.25 kWh<sub>el</sub> accounting for a PEMFC load factor slightly below 25%.

One can observe from Figure 86 that the utilization cost savings (compared to a condensing boiler and grid electricity) evolve linearly to the daily electrical production, emphasizing the importance of the duration for which the PEMFC is actually on in the hybrid system.

For information, in Figure 86, the spectrum of the variables whose data is scattered in the main plot are represented. This is performed thanks to the Kernel density estimation (KDE). KDE is used in statistics as a non-parametric way to express the probability density function (or probability distribution) of a random variable [555]. It is basically a histogram for which the number of bins and their width is standardized (in order to avoid having to set and reset those parameters each time a new figure has to be drawn).



**Figure 86.** Daily Savings according to daily electrical production of the PEMFC machine (year 2020).

As demonstrated in Equation (18) through Equation (27) in the previous chapter (also applicable to this PEMFC system), the utilization cost savings depend on the supply cover factor (in addition to the energy prices).

The system of Huy has a yearly supply cover factor of 33.5 % in 2020 and 37.6% in 2021 whereas, for Oostmalle, it reaches 36.3% in 2020 and 34.1% in 2021, well below the 60% achieved by the owners with the SOFC reported in the previous chapter (partially explaining why the utilization costs savings are significantly lower in this case).

In early 2020, Oostmalle demand cover factor reaches almost 70%, which is quite a good performance and leads to the best daily savings seen in Figure 86. Unfortunately, this supply cover factor value could not be maintained over the whole year.

It is interesting to point out that this system does not allow the seasonal supply cover factor trend to go higher than 40% (even in the summer) whereas the Wallonia regulator, in its 'prosumer tariffication' for PV panels for households not equipped with 'smart' electrical meters, has assumed a referenced yearly supply cover factor of 37.76% (regulation currently applied) [556]. As established, the yearly values are even below this figure (but close to it). Even if the 'prosumer tariffication' assumption for the supply cover factor is not realistic (in order to keep encouraging people to invest in PV installations), it means that this PEMFC system will not be that favorized in Wallonia in terms of electrical rejection compared to PV installations. However, it is worth mentioning that prosumer households with 'smart' energy meters (which are mandatory for new electrical installations and which is encouraged for all installations) are not subjected to this 'prosumer tariffication' with the 37.46% assumption of supply cover factor (but they are billed exactly as considered in this work). A 'smart' energy meter is an electrical meter that measures both the building consumption and rejection on the grid and that is communicating its energy indexes in real-time to the electrical distribution administrator thanks to wireless communications.

For comparison purposes, in Belgium, for residential net zero-energy buildings (ZEBs, which represent a current standard as recommended by the EU directive 2010/31/EU on the energy performance of buildings) [477], (realistic) supply cover factors have been simulated to reach  $26\pm 4\%$  for different buildings [557], lower than the Walloon regulator assumption of 37.76% [556]. In that study, all systems have been assumed to be oriented directly South with an inclination of  $34^\circ$ , resulting in the highest annual electricity production [477], and the PV building's plant has been sized to match in size the yearly total electrical demand.

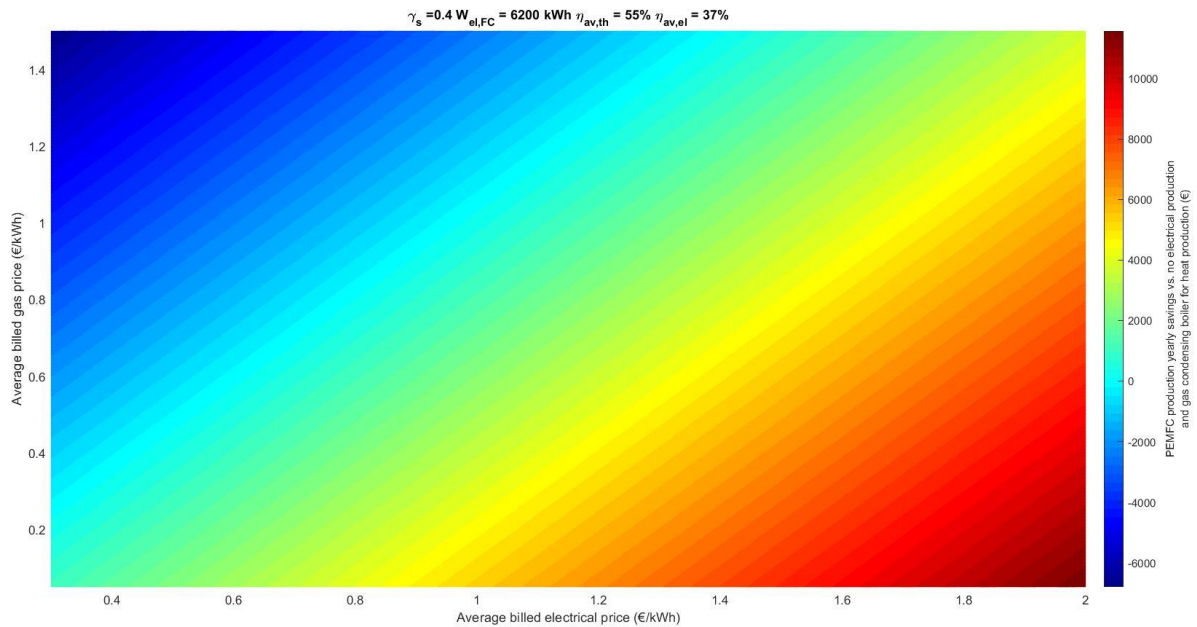
Similarly to Figure 57, established in the previous chapter for the studied SOFC, a sensitivity study of the utilization costs savings can be performed according to energy prices (with a fixed electrical production, electrical efficiency and supply cover factor). This has been done in Figure 87 for the studied PEMFC stack only (without the boiler, which can thus be assimilated to the PA\* system) based on its theoretical efficiencies (see *Section 5.1 - Description of the machine*). Figure 87 has directly been established from Equation (27). Whereas Figure 57 and the resulting Equation (28) and Equation (29) were built to demonstrate an example close to the 'worst case scenario' for the studied SOFC (minimal supply cover factor, minimal efficiencies) and highlighting the energy price zone for which a Return on Investment below 10 years would be ensured [481], in this case, Figure 87 adopts the opposite approach. Indeed, contrary to the exhibited low electrical production (and associated low load factor) of the PEMFC of the field-tested P\*2, Figure 87 considers a maximal electrical production (of 6200 kWh<sub>el</sub>). Thermal and electrical efficiencies are also maximized whereas the supply cover factor is slightly enhanced compared to the ones demonstrated in the field-test (injection prices still considered to 0.15 €/kWh, as in Figure 57).

It can be observed that about 2.5 k€ of savings (considered enough to guarantee ROI under 10 years, maintenance costs included) should be reached if energy prices respect Equation (44), also expressed as Equation (45), which have been established graphically (thanks to Figure 87):

$$\epsilon_g \leq \epsilon_e \times \frac{1.44}{1.25} - 0.58 \text{ [€/kWh]} \quad (44)$$

$$\epsilon_e \geq (\epsilon_g + 0.58 \text{ [€/kWh]}) \times \frac{1.25}{1.44} \quad (45)$$

For example, even in those quite optimal conditions, for the first semester of 2023, the difference between Belgian electricity and gas prices is still not sufficient for Equation (45) to be respected as electric and gas prices can respectively be considered equal to 0.425 €/kWh and 0.112 €/kWh [481]. However, the yearly savings would be yet around 1.5 k€ (Figure 87), which might still likely of offer a ROI under 10 years.



**Figure 87.** Sensitivity study of the energy utilization economic balance according to energy prices. Positive economic balances mean that the PEMFC system provide savings compared to the references (grid electricity consumption and gas condensing boiler).

Regarding ecological indicators, even when compared to the CCGT emission factor (Dataset 'A', corresponding to marginal emission factors in Belgium for the year 2020 and 2021, as explained in Section 2.3.1 - CO<sub>2</sub> and CO<sub>2eq</sub> emission factors), the system in Huy never seems to show better performance than the reference machines.

The only real savings that are observed are for Oostmalle and occur when compared to the CCGT emission factor (Dataset 'A'). They are of the same order of magnitude, although a little lower for the year 2020, as the corresponding yearly CO<sub>2</sub> savings observed for the SOFC systems studied in the previous chapter (see Table 18). However, it is tricky to compare the systems in their respective configurations and dwellings. Indeed, CO<sub>2</sub> utilization savings in Oostmalle might be only quite fictive as they are likely to be explained by the prevalent use of the boiler within the hybrid system that operates (for a long time) at a LHV thermal efficiency higher than the reference 90% boiler. In fact, the

reference of 90% is only a yearly average; it should be higher with high thermal demands (in the winter) and lower with low thermal demands (in the summer) [553].

In the particular case of Oostmalle, the thermal demand remains quite high in the summer and a classical boiler would still have quite a high thermal efficiency (close or higher than the reference 90% LHV). In fact, in a publication related to this work [15], the P\*2 of Oostmalle has been compared to a condensing gas boiler with an efficiency that is no longer constant (of 90%) but that is heat demand-dependent and it has been observed that the boiler within the system has worse performance than the heat-demand dependent gas boiler model. This could be demonstrated (for Oostmalle) in November and December 2020 where the PEMFC had broken down (see Figure 85). On the other hand, with the SOFC systems studied in the previous chapter that have been used only for DHW production, this might even be the opposite. Indeed, a corresponding heat demand-dependent gas boiler model would likely to exhibit LHV efficiency poorer than 90% (improving the ecological balance of the studied SOFCs).

It can be reminded that the previous chapter established with certainty that the studied SOFCs allow for actual utilization CO<sub>2</sub> savings compared to Combined Cycle Gas Turbines (CCGTs), even with 0% LHV thermal efficiency, as they intrinsically offer efficiencies higher than the one of CCGTs. Thus, those SOFC systems might therefore find their place in the energy transition (of countries such as Belgium that are still using a lot of CCGTs), especially since their electrical production is flexible. However, the same statements cannot be applied with the P\*2, simply by looking at the poor ecological performance of the machine in Huy. Nevertheless, if the PA\* (PEMFC of the P\*2 but as a standalone unit, see *Section 5.1 - Description of the machine*) is performing at its announced electrical efficiency of 37% LHV, it can be easily established with Dataset 'A' (of Table 4) that it would need a LHV thermal efficiency around 30% or more to start offering utilization CO<sub>2</sub> savings compared to CCGTs (of 55% LHV electrical efficiency) and to a 90% constant LHV efficiency gas condensing boiler. This level of thermal efficiency, although feasible, is yet to be demonstrated. In comparison, the field-tested SOFCs achieved LHV thermal efficiencies in the 10-15% range (Table 18) and the attempt of establishing the LHV thermal efficiency of the PEMFC only of the P\*2 gave figures no higher than 31% in laboratory investigations (Table 33). Even so, it would still to be unable to modulate, as it is possible with the studied SOFC.

It is worth mentioning that decentralized local electrical production avoids transportation and distribution losses (which can reach about 6-7% in EU [130] and is, to the knowledge of the author, not included in the considered emission factors). So, this could be considered in the ecological balances and they would actually be slightly improved, as performed in Table 37, build very similarly as Table 20 for the studied SOFC system. It should be pointed out that Table 37 only relies on the PEMFC (and not on the boiler); therefore, its actual LHV thermal efficiency (not known precisely either with the laboratory or the field-test investigations) has been assumed at its announced maximal value, i.e. 55% (deduced from Table 25). Thus, Table 37 is also applicable to the PA\* PEMFC system which is, as explained in *Section 4.1.2 - Applications and the different versions of the tested system*, basically a micro-CHP system based on the same fuel cell as in the studied P\*2 version but as a standalone unit (not embodied to a DHW tank and a boiler).

As stated for the studied SOFC in *Section 4.3.4 - Results*, a relevant extra gas network distance up to the dwellings could be considered in the 0.1-50 km range, given Belgian urbanization levels. This would still mean that the avoided GHG emissions allowed by the local electrical production of the PEMFC would at least be about ten times greater than the additional fugitive emissions. Therefore, the ecological balances of Table 36, i.e. the utilization CO<sub>2eq</sub> savings could be considered enhanced by about 25-31 kgCO<sub>2eq</sub>,

considering the figures reported in Table 37. The upper limit directly comes from Table 37 and the lower limits considers 50 km of extra gas network distance, considering PEMFC LHV electrical and thermal efficiencies respectively of 37% (same as in Table 37) and 40% as well as 6% of electrical network losses. Those kinds of corrections are considered negligible again, due to the low PEMFC load factor (and also, in this case, quite low electrical power output).

Yearly electrical production of the PEMFC - average of field-test figures of Table 36 [kWh <sub>el</sub> ]	'Ideal' electrical LHV efficiency of the PEMFC based on field-test figures of Table 25 [-]	Equivalent LHV energy contained in the gas consumed by the PEMFC [kWh]	'Ideal' thermal LHV efficiency of the PEMFC based on field-test figures of Table 25 [-]	'Ideal' yearly heat recovered by the PEMFC considering the 'ideal' thermal efficiency of this Table [kWh <sub>th</sub> ]	Equivalent LHV energy contained in the gas that would have been consumed by a condensing boiler of 90% of LHV efficiency [127] to match the heat recovered by the PEMFC [kWh]
2617	0,37	7072	0,55	3889,4	4322
Equivalent LHV energy contained in the gas consumed by the PEMFC for electrical production only, not considering the gas that would have been consumed for PEMFC heat production with a gas condensing boiler of 90% LHV efficiency [127] [kWh]	Average LHV of natural gas based on average 2021 field-test figures and a HHV to LHV ratio of 1.1085 [132] [kWh/m <sup>3</sup> ] <sup>a</sup>	Equivalent gas volume consumed by the PEMFC for electrical production only, not considering the gas that would have been consumed for PEMFC heat production with a gas condensing boiler of 90% LHV efficiency [127] [m <sup>3</sup> ]	Equivalent gas (CH <sub>4</sub> ) mass consumed by the PEMFC for electrical production only, not considering the gas that would have been consumed for PEMFC heat production with a gas condensing boiler of 90% LHV efficiency [127] <sup>b</sup> [kg]	Average CH <sub>4</sub> fugitive emissions in gas network [476] [kg CH <sub>4,fugitive</sub> / (km * kg CH <sub>4,consumed</sub> )]	Extra fugitive CH <sub>4</sub> emissions associated to the local electrical production only of the PEMFC [kg CH <sub>4,fugitive</sub> / km]
2750	9,85	279	235	5,40E-06	1,E-03
GWP-100 of CH <sub>4</sub> [15]. IPPC recommends the use of GWP-100 in CO <sub>2eq</sub> accounting of methane emissions [484].	CO <sub>2eq</sub> emissions related to the extra fugitive CH <sub>4</sub> emissions associated to the local electrical production only of the PEMFC [kg CO <sub>2eq</sub> / km]	Average emission factor of consumption electrical mix of Belgium in 2021 - data provided by <a href="http://Electricitymap.org">Electricitymap.org</a> [gCO <sub>2eq</sub> /kWh <sub>el</sub> ]	Average electrical energy network losses [130] [-]	CO <sub>2eq</sub> emissions avoided considering the local electrical production of the PEMFC, the average Belgian consumption emission factor of 2021 and the network losses [kg CO <sub>2eq</sub> ]	Maximum extra gas network distance that would lead to CO <sub>2eq</sub> emissions of fugitive natural gas that match the CO <sub>2eq</sub> saved from the avoided 7% electrical network losses thanks to decentralized power production [km]
28	0,035	167,7	0,07	31	866

<sup>a</sup> Average HHV for Huy = 11.49 kWh/m<sup>3</sup>. Average HHV for Oostmalle = 10.34 kWh/m<sup>3</sup>. Figures given hourly by the gas provider.

<sup>b</sup> Natural gas density = 0,84 kg/m<sup>3</sup>[485].

**Table 37.** CO<sub>2eq</sub> impact of avoided electrical network losses thanks to the decentralized electrical production of the PEMFC system and impact of extra fugitive natural gas emissions due to additional gas consumption at decentralized dwellings.

### 5.3.5 Uncertainty analyses

The method used for uncertainty propagations in this report is advised by the NIST (National Institute of Standards and Technology) [130] and to do so, the EES (Equation

Engineering Solver) software has been used, exactly as in *Section 4.3.5 - Uncertainty analyses* in the previous chapter.

The exact method previously described (*Section 4.3.5 - Uncertainty analyses*) gives an uncertainty on HHV figures of approximately  $\pm 235 \text{ Wh/m}^3$  for Huy and  $\pm 104 \text{ Wh/m}^3$  for Oostmalle. There is a need for separate uncertainty analyses between the sites because the gas type provided to the machine by the grid is different (see *APPENDIX 1: Energy content of natural gas in residential applications*). According to the gas provider, Oostmalle still has been provided with lean gas (called ‘type L’ in Belgium) whereas Huy already has rich gas (called ‘type H’ in Belgium). There is about a 10% difference in the given HHV figures between the two types of gas. Such a difference in the chemistry of the gas could indeed have a significant impact on the accuracy of the method used by the gas provider to establish HHV figures. It can be pointed out that this method is providing some safety on the uncertainty of the HVV measures established here. Indeed, the given figures on which the uncertainty is computed do not only account for accuracy only but they also involve the natural variation of the actual HHV due to variation in the gas mix.

Considering the accuracy of the monitoring sensors (Table 34), one obtains an uncertainty of about  $\pm 1\%$  for the electrical efficiency and of about  $\pm 4\%$  for the thermal and total efficiency for the site of Huy. The propagated uncertainty on the electrical efficiency is quite lower because of the intrinsic good accuracy of the electrical meter and the relatively lower electrical production.

Again similarly to *Section 4.3.5 - Uncertainty analyses*, in order to corroborate these calculations, one also can propagate uncertainties based directly on a yearly HHV energy consumption (and no longer based on daily observations). This is established thanks to a fictive fixed HHV figure (with the same uncertainties as before) and with the total volume of gas consumed in 2020 (given by the monitored gas indexes of January 1<sup>st</sup> and December 31<sup>st</sup>). One obtains greater uncertainties of only 1 percentage point:  $\pm 2\%$  for the electrical efficiency, the uncertainties for the thermal and total efficiency coming close to  $\pm 5\%$  (without exceeding the 5% range).

For the site of Oostmalle, both methods of propagating the uncertainties gave approximately similar results: close to  $\pm 1\%$  or  $\pm 2\%$  for the electrical efficiency depending on the method and  $\pm 4\%$  for the thermal and total efficiencies, without exceeding the 5% range.

Following the same methods for the economic and ecological indicators (utilization savings) given in Table 35 and Table 36, one also obtains about  $\pm 4\%$  of uncertainty, without exceeding the 5% range.

In conclusion, it is safe to consider that the propagated uncertainties for all the figures in this monitoring section are at a maximum of  $\pm 5\%$ . Of course, this is only based on the measured values and the intrinsic accuracy of the sensors. There is no estimation of the uncertainty induced by potential unoptimized installations of the sensors or unoptimized fluidic conditions, especially for the temperature probes of the heat flow meter (see *Section 4.3.5 - Uncertainty analyses*).

### 5.3.6 Troubleshooting

The house in Oostmalle is the only one that acknowledged major issues regarding the monitoring with the fuel cell being shut down for unknown reasons (with no explanation given by the manufacturer) from November 2020 to January 2021, as explained in *Section 5.3.4 - Results*. This has been resolved by the installer.

Some minor issues with the monitoring happened as well but since all sensors are providing indexes (that continue to measure even if communication is lost), the results presented here are secured.

As explained, P\*2 field-test performance is greatly impacted by the actual achievable PEMFC load factor, which is always under 50% for the two dwellings considered in this study. An extended study on the day-to-day behaviour of the systems has been established in order to find out the reasons of such low PEMFC load factors. It has been reported in *APPENDIX 10: P\*2 behavior and how it affects efficiency: zooming on representative days*.

This appendix exhibits OFF/ON behaviours of the boiler due to its inability to modulate as announced in the datasheet (when the PEMFC is turned on). Therefore, the space heating temperatures at the outputs of the system are not stable and they include overshoots (that may subsequently lead to return temperature above 50°C that, as explained in *Section 5.1 - Description of the machine*, lead to PEMFC shutdowns for safety reasons).

*APPENDIX 10: P\*2 behavior and how it affects efficiency: zooming on representative days* also reveals a potential design issue in the system's architecture for which the return line of the boiler is preheated by the fuel cell (when this latter is turned on). This might impede proper condensation of the boiler flue gases (reducing its efficiency) but it might also impede the proper modulation of the boiler's heat rate output, which could be the explanation for the unwanted fuel cell shutdowns (because of unstable temperatures at the output of the system that may reach 50°C or more).

In any case, it is believed that the low PEMFC load factor demonstrated in field-test is either due to highly transient heat demand induced by the occupants (in Huy), as deduced from *APPENDIX 11: Satisfactory Survey of the house in Huy*, or, in case of a smooth heat demand (such as in Oostmalle), due to the complexity of the hybridization with the boiler. It is indeed believed that the PEMFC and the boiler are integrated to such a high level that it prevents both systems to operate as optimally as they would have in standalone decoupled configurations. In addition, it is not easy to understand how such a complex hybrid system is controlled, which does not help in case of problem solving.

### 5.3.7 Conclusions of the section

The strongest limitation of the work reported in this section (as it was the case in the previous chapter) is that the resulting economical indicators are strongly case dependent and that considering only two machines does not allow for drawing statistical conclusions on the system's performance (especially the economical ones that are affected by the supply cover factors). The results developed here shall thus be considered as case studies. However, it should still be stated that the monitored systems exhibited poor yearly measured total LHV efficiencies that are lower or at least not sufficiently higher than the reference gas condensing boiler efficiency of 90% (as it is the efficiency assumption of nationally and internationally recognized organizations [127]). Also, the resulting economical balances are likely to impede achieving ROI under 10 years (only up to about 450 €/year of savings and even small losses for the house of Huy in 2021).

The utilization CO<sub>2</sub> savings of the P\*2 system are quite affected by the efficiency of the boiler within the system, which can in fact greatly vary from one household to the next, depending on the heat demands. Nevertheless, the utilization CO<sub>2</sub> savings of the monitored systems are still quite disappointing and, for one of the dwellings (in Huy), even worse than if the electricity was coming from a CCGT and the heat from a classical gas condensing boiler of 90% LHV thermal efficiency.

The poor exhibited PEMFC load factor (always under 50% for both houses) has a significant influence on the poor economical and ecological performance. There are some indications that points towards the complexity of the hybridization (and of its control) between the PEMFC and the gas boiler, which prevents them to operate in the optimized conditions they could have met as standalones units (see *APPENDIX 10: P\*2 behavior and*

*how it affects efficiency: zooming on representative days*). Indeed, one issue is that the architecture of the system (Figure 68) is showing that the PEMFC often pre-heats the boiler return (in space heating mode), which will have some more difficulties to condense [558] and which will decrease its efficiency. It also is assumed that it is preventing the boiler to properly modulate its thermal output, which can lead to temperature overshoots in the space heating circuits. As the PEMFC is shutdown with return temperatures of 50°C or more for safety reasons (see *Section 5.1 - Description of the machine*), this could be an explanation of the poor PEMFC load factors.

Since the monitored machines show such insignificant yearly savings and such poor ecological balances, it can already be stated that tremendous improvements are required for this system to play a role in the energy transition.

It might thus be preferable to consider the PA\* system, which consists only of the PEMFC of the P\*2 as a standalone unit (see *Section 5.1 - Description of the machine*). It could be simply integrated with an external storage tank. It would therefore be decoupled to the boiler (or the other space heating appliances) and would have its own simple control (based to the temperature of the storage tank). The configuration would thus be quite similar to the one of the SOFC BI\*\*\*G\*N systems studied in the previous chapter, which has, as stated, proven to be quite robust.

Based on announced optimal performance, it has been established that the PA\* PEMFC minimal LHV thermal efficiency to start offering utilization CO<sub>2</sub> savings (compared to a CCGT of 55% LHV electrical efficiency and a classical condensing boiler of 90% of LHV efficiency) should at least reach 30%. However, the PA\* system is still not able to modulate so it seems inappropriate to compare it to flexible CCGTs, which still offer electrical efficiencies almost 20 percentage points higher (and could implement heat recuperation as well). On the other hand, it would be very hard to offer ecological utilization CO<sub>2</sub> savings when compared to average grid electricity (with more and more renewables), as it was already the case for the studied SOFC (in the previous chapter). Even with high thermal LHV efficiencies (that should still be demonstrated in field-test applications), it can be considered a heat pump fed by low CO<sub>2</sub> electricity would always offer better performance (with the additional possibility of thermal storage to avoid the peak electricity demands that would maybe require the highly emitting CCGTs to be turned on).

As demonstrated in *Section 3.2.5 - Current and expected performance of micro-CHP systems based on a PEMFC or a SOFC*, the expected increase of performance of PEMFC systems (in terms of electrical efficiency) in the future is not actually that high compared to the current levels just considered here above. Thus, their interest as micro-CHP systems in the energy transition will keep being questionable as it has been established in this section that it is currently the case (even if they one day could modulate and become flexible). This is probably the reason why some fuel cell micro-CHP OEMs turned they back on the PEMFC technology to concentrate their efforts on the SOFC technology (as stated in *Section 3.2.2 - Status of commercialized HT-PEMFC-based micro-CHP systems*).



The content of *Section 5.4 - Machine modelling*, which aims to offer empirical models of the system suitable for simulation of such micro-CHP PEMFC installed in buildings, has been published almost as-is in *Energy Conversion and Management* under the name ‘*Field-test performance models of a residential micro-cogeneration system based on a proton exchange membrane fuel cell and a gas condensing boiler*’ [537].

Due to the complexity of modelling this hybrid PEMFC-gas condensing compared to a standalone fuel cell system such as the SOFC studied in the previous chapter and modelled in *Section 4.4 - Machine modelling*, this section is organized quite differently. However, its outputs are quite similar as both modelling sections provides thermal and electrical efficiency models (on LHV basis). An overview of the thermal and electrical efficiency models developed in this section will be shown in Figure 91.

It should be reminded that the models presented in this section intrinsically involve the internal DHW tank (and its standby losses), which was not the case for the tested SOFC system that works as a standalone unit (see *Section 4.4 - Machine modelling*).

## 5.4 Machine modelling

### 5.4.1 Introduction

All the models offered in this work rely on the field-test monitoring data (see *Section 4.3 - In-situ monitoring*) obtained for the two systems for the whole year 2020.

Contrary to models based on laboratory studies or on the datasheet figures, the main advantage of the models developed in this work is that they are based on real all year long field-test performance. Unoptimized operating conditions, that could potentially come from the way the owner uses the system or the way it has been installed in the building, are very likely to occur in real applications. Those sources of inefficiency are involved in the field-test data considered in the models of this work, making them therefore more realistic than a model solely based on laboratory testing in ideal conditions (which might have been applicable to systems working as standalone units, such as the SOFC studied in the previous chapter).

This section first offer two simple single-variable time-invariant [559] models that provide the daily (or monthly) thermal efficiency of the system with only one input : the total daily (or monthly) heat demand of the buildings, which thus considers the addition of the domestic hot water (DHW) demand and the space heating demand. The daily-based model is subsequently improved considering other parameters influencing the daily thermal efficiency. Firstly, the efficiency of space heating appliances is indeed known to be enhanced at lower operating temperatures [558]. Secondly, transient effect and unsmooth heat demand are known to lessen the thermal efficiency of space heating appliances [560]. Thanks to the monitoring data, both effects will be considered in the enhanced single-variable time-invariant models by implementing specifically defined correction factors. If a potential user of those models has an idea of the operating temperatures and/or of the smoothness of the heat demand that will occur in the building he is considering, he will have a more accurate estimation of the daily thermal efficiency of the system.

It has then been observed in *Section 4.3 - In-situ monitoring* that the daily electrical production of the system (which is part of the monitoring data), or more generally, the load factor of the PEMFC, has a significant influence on the thermal efficiency of the whole system. Therefore, two-variable models (daily heat demand and daily electrical production or daily PEMFC load factor) are thus also offered in this work. They provide the best estimate of the daily thermal efficiency of the system but the PEMFC load factor is unfortunately not easily estimated for potential users of those models.

At last, knowing the daily PEMFC load factor (or its daily electrical production), the daily electrical efficiency can also be computed for each of the models of this work.

## 5.4.2 Material and Methods

### 5.4.2.1 *Description of the system, monitored houses and measurement devices*

The description of the system has been detailed in *Section 5.1 - Description of the machine*; the monitored dwellings and the monitoring configuration has already been described in *Section 5.3.1 - Description of the buildings* and the measurements devices and acquisition system have been reported in *Section 0 - Because of the small sample size* (only two installations included in this study), it was not intended with this survey to perform statistical analyses on the answers. The surveys were mainly conceived at the early stage of the field-test study to establish an official communication mean with the owners and facilitate troubleshooting reporting. In addition, for confidentiality purposes, in the Appendices of this work, those surveys have been limited to the backup information that is actually referred to in this thesis.

Measurement devices.

### 5.4.2.2 *Black-box modelling instead of component modelling*

The whole internal control of the machine has trivially a significant impact on its performance and a theoretical model based on the different components within the system (seen in Figure 68) would unlikely reproduce it with accuracy. Indeed, even though those components are quite simple (heat exchangers, pumps, three-way valves, gas condensing boiler, DHW water tank, fuel cell as a heat and power generator), the way they are combined with each other and the way they are controlled is only known to the OEM.

Furthermore, the OEM's control, affecting the model, is likely to consider extra parameters that this study could not collect. For example, in the field-test, one is studying real machines installed in real homes, with real occupants, that can modify some control parameters anytime they want, such as ambient temperature setpoint, heating schedule and heating curve. Also, the machines are usually connected to the internet allowing the OEM to install updates in the control and any component modelling could instantaneously become obsolete.

Another difficulty of components modelling relies on the fact that no monitoring sensors could be placed within the machine due to occupant's warranty policies. Thus, there is no measure between the components so even deducing the control laws of one single component (such as one electrical three-way valve) would come with great uncertainties.

Therefore, it is preferable to build a performance model ('black-box' model) of the system based on empirical monitoring results that is robust to all those potential control strategies (and changes). The performance model will rely on the measurements of all incoming and outgoing energy flows as shown in Figure 83.

It is however expected that the variance of the resulting models and their goodness of fit will of course still be affected by potential difference in internal control, usage and parametrization of the system.

### 5.4.2.3 *The time bases of the models*

Modelling performance based on small timesteps (down to the minute or the second) is not relevant in this case for several reasons.

Firstly, as explained earlier, the monitoring sample time cannot be smaller than 2 minutes so the chosen modelling timestep must be (significantly) greater. Also, it is only an average sample time: the timeframe between two wireless communications from the sensor to the

data logger is not regular as the communication time itself is not regular with the Wireless M-bus protocol (see *Section 0 - Because of* the small sample size (only two installations included in this study), it was not intended with this survey to perform statistical analyses on the answers. The surveys were mainly conceived at the early stage of the field-test study to establish an official communication mean with the owners and felicitate troubleshooting reporting. In addition, for confidentiality purposes, in the Appendices of this work, those surveys have been limited to the backup information that is actually referred to in this thesis.

Measurement devices).

Secondly, information from the sensors is provided as energy indexes (with a resolution that is not sufficient for instantaneous calculations) and establishing the derivative of the signals provides too much noise.

Furthermore, it is worth remembering that the sensors are communicating with the data logger one at a time and that the signals are not sufficiently synchronous for analyses on quite small timesteps.

At last, it has been stated that no sensor could be placed inside the systems for warranty reasons and the heat stored in the tank is not monitored.

Therefore, one must analyze the performance of the system over a certain timeframe. It is assumed that the smallest timeframe is 24 hours as it corresponds to occupants natural (daily) cycles (DHW production scheduling, for example). However, even with a 24-hour timeframe, as it will be explained in this section, the effect of the storage tank (that could be heated one day and emptied the next one) can still cause significant dispersion and impede the goodness of fit of the daily models developed in this work. Therefore, in addition to daily-based models, a monthly-based model will also be reported in this section. Both time bases will be compared in terms of goodness of fit.

#### 5.4.2.4 *The modelling primary philosophy and its successive improvements*

As stated, this work's primary purpose is to build an empirical 'black-box' model that is estimating the daily (or monthly) electrical and thermal efficiency of the PEMFC – gas boiler hybrid system according to daily (or monthly) heat demands (DHW and space heating). As the heat demands can easily be measured, computed or estimated for any building, the primary model can be easily applicable.

The primary established daily-based model will then be enhanced by considering some other influencing factors that will bring increased accuracy and goodness of fit, but that will require extra data, not always available. Therefore, the methods used to enhance the model by considering working temperature and/or the ability of the machine to modulate its thermal output power might be more relevant than the resulting enhanced models themselves for potential other similar studies.

The first improvement will come by considering the working temperature: as expected from literature [160], the higher it is, the lower the thermal efficiency. This means that the system will perform better with low temperature terminal units such as floor heating. This can be explained by the increased ability of the system to condense and recover heat from its flue gases [160] and it applies both to the boiler and to the PEMFC of the system.

The second one will come by considering the behavior of the heat demand: highly transient and 'ON/OFF' heat demands will lower the thermal efficiency. As for the working temperature influencing factor, this second influencing factor can be partially linked to the terminal units as well. Indeed, for example, floor heating has greater inertia and thus requires longer and smoother heat productions.

At last, the daily-based model is even enhanced by considering as an input the PEMFC load factor, i.e. the achievable daily electrical production, i.e. its achievable operating time. Unfortunately, in reality, daily achievable electrical production is not exactly an 'input' such as the two 'influencing factors' previously cited and used for enhancing the models. However, the system is not electrically driven and is supposed to provide electricity as constantly as possible (which is desired for durability reasons [181]). Therefore, the PEMFC load factor is thus a consequence of the ability of the fuel cell to stay 'ON' and it depends on external factors, such as the thermal management of the fuel cell. Indeed, the PEMFC stops if it is no longer able to dissipate its heat either in the tank or in the space heating. In fact, the PEMFC thermal management is key to ensure its lifetime as literature reports that PEMFC could be stopped for improper thermal conditions (to ensure its integrity [181]) and this is probably why the OEM states the maximum internal return temperature to the fuel cell reaches 50 °C [15]. Unfortunately, that condition is very difficult to identify based on the collected data as it has been explained that the monitoring campaign could not include sensors inside the machine (and especially on the storage tank).

Since thermal conditions around the PEMFC are critical regarding the ability of the fuel cell to operate for long duration, the fuel cell load factor will depend the amount of heat that can be stored by the fuel cell in the storage tank (considering heat withdrawals including those that accounts for DHW) and/or the amount of heat that can be delivered to the space heating. In fact, this latter is partially dependent of the two previously cited influencing factors used to enhance the primary model (working temperature and heat demand behavior).

Thus, instead of considering the PEMFC load factor as a model input, further work might allow its modelling as a function of tangible influencing and predictable factors such as the heat demands of the building and occupants, their absolute daily values, their smoothness over the day, their average working temperature, *etc...*

In the meantime, for this work, the PEMFC load factor is taken into account for this modelling as an input as is. This input shall be considered as a daily indication of the adequation of the system (and its control) with the installation and with its occupants.

It should be noted that that the load factor is usually defined as the current power level relative to the maximum [182]. In this case, since the PEMFC is either turned 'OFF' or 'ON' at its nominal power, it is more relevant to use the load factor on a daily (energy) basis, i.e. the total daily electrical production divided by the maximum it could have produced (which is equal to 18 kWh<sub>el</sub>, considering a nominal output power of 0.75 kW<sub>el</sub> for 24 hours).

### 5.4.3 Modelling

#### 5.4.3.1 Key parameters – Electrical and thermal efficiencies both depend on heat demands

The most important contribution to such a 'black-box' model is to find key parameters on which the whole performance indicators can be deduced despite the specific parametrization, use and control.

Thanks to Figure 71, one can consider the electrical efficiency of the fuel cell only as constant. However, for the same duration of fuel cell utilization, the burner might not provide the same heating capacity: it can be shut down completely the whole day as well as it can be providing heat at nominal output rate. Therefore, the daily (or monthly) electrical efficiency will be affected by the heat production (and the way it is produced).

Furthermore, the gas boiler heat production has not only a direct impact on the electrical efficiency but it has also an indirect impact : indeed, the elevation of the return temperature due to the gas condensing boiler being turned ‘ON’ for space heating (especially with high temperature terminal units) could prevent the fuel cell from dissipating enough of its heat and force its temporarily shut down.

Figure 71 (b) also shows that thermal efficiency of the running fuel cell only cannot be assumed constant and depend on the working temperature conditions, which are themselves particularly affected by the heat demands of the house and the state of possible other heating appliances. For example, if the gas condensing boiler has to be turned ‘ON’ to meet the heat demand, it will likely elevate the return temperature to the fuel cell and decrease the efficiency of the heat transfer.

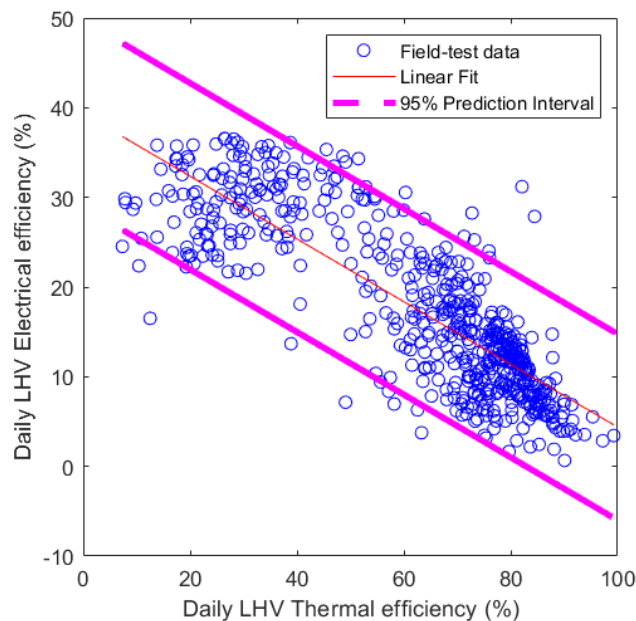
Thus, both the electrical and thermal daily efficiencies depend on the heat demands of the house and one can even link them together. Indeed, there is even a gross linear trend between the daily thermal and electrical efficiencies, as shown on Figure 88.

Based on Figure 88, a linear relation between LHV daily electrical efficiency  $\eta_{el}$  and LHV daily thermal efficiency  $\eta_{th}$  can be defined by Equation (46) :

$$\eta_{el}(\%) = 39.34 - 0.35 \eta_{th} \quad (46)$$

As a first approach, with Equation (46), one can therefore establish that modelling only the daily thermal efficiency of the unit would suffice to model the whole system daily performance. It should be considered that Equation (46) is not valid for low LHV thermal efficiencies (under about 10%) because electrical LHV efficiency of the PEMFC only cannot be higher than 37% (Table 25). A very similar linear relation to Equation (46), with coefficients (and confidence intervals) almost identical, can also be established between electrical and thermal efficiency on a monthly-basis instead than on a daily-basis.

It should be noted that the electrical consumption of the system (that is measured when the fuel cell is not running) is neglected in the efficiency calculations. The denominators of the established efficiencies consist only of the consumed gas expressed in LHV (thanks to a HHV to LHV assumed ratio of 1.1085 [132]).



**Figure 88.** Linear fit of the field-test daily electrical efficiency according to the daily thermal efficiency. The 95% confidence interval is however quite large as it defines a  $\pm 10$  percentage points zone around the fit for the daily electrical efficiency.

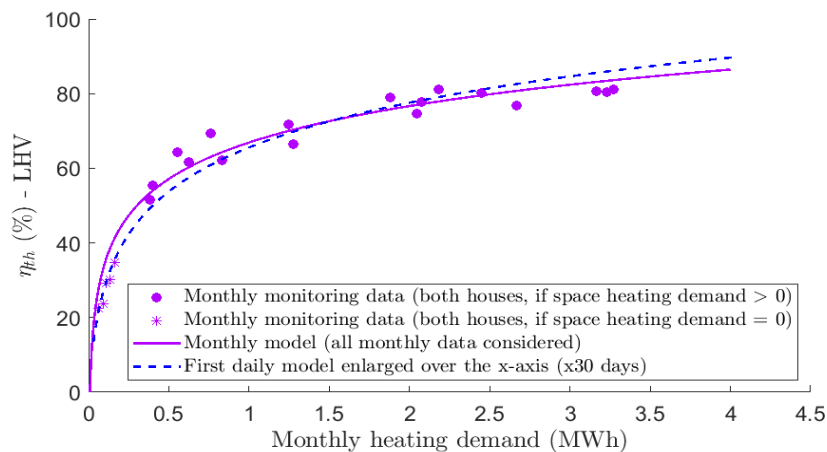
### 5.4.3.2 Simple single-variable time-invariant thermal efficiency models

Literature on monitoring gas condensing boilers combined with DHW storage tanks [183] has studied the relation between monthly LHV thermal efficiency and heat demand. The results show that a clear logarithmic trend can be deduced with an asymptotic limit as heat demand increases.

The same kind of results has been computed for the two systems of this work both on a daily and a monthly-basis. Also, based on those results, logarithmic simple model relations have been optimized automatically thanks to the Matlab software. The logarithmic models have as general equation the relation dictated by Equation (47), where  $\eta_{th}$  is the daily (or monthly) thermal LHV efficiency (expressed in %),  $Q_{SH}$  and  $Q_{DHW}$  are respectively the daily (or monthly) space heating demand and the DHW demand (expressed in kWh) and  $C_1$ ,  $C_2$ ,  $C_3$  are the constants that have been set automatically to optimize goodness of fit compared to empirical results (values given in Table 38).

$$\eta_{th} (\%) = C_1 + C_2 \log[(Q_{SH} + Q_{DHW}) + C_3] \quad (47)$$

Graphical results and coefficients of the monthly model based on Equation (47) are respectively reported in Figure 89 and Table 38. Goodness of fit can be studied easily with the Matlab software as RMSE (Root Mean Square Error) and R-square values (chosen indicators for this study) have been established in Table 38. The explanations regarding those features have been provided by the Matlab Software support [184] and have already been explained for the studied SOFC system in *Section 4.4 - Machine modelling*.



**Figure 89.** Comparison between the monthly and the first daily model defined by Equation (47) and whose coefficients are given in Table 38. To allow the comparison, the daily heat demand from the first daily model has been multiplied by the average number of days contained within a month, i.e. 30. As deduced from *APPENDIX 11: Satisfactory Survey of the house in Huy*, in the summer, it is likely that the house in Huy has completely shut down its space heating (high temperature terminal units controlled manually on demand) and that its system was only used for DHW. These monthly data were separated from the others monthly data to show that the models are relevant no matter if the system is used for DHW only or also for space heating.

Graphical results of the daily model based on Equation (47) are reported at the top of Figure 90. Again, Table 38 reports the coefficients from Equation (47) but also its goodness of fit indicators.

In this case, after removing some inconstant data mainly originated from monitoring signals losses (only for the daily models), R-square values for all of the single-variable daily models proposed in this work are always close to 89.5%, meaning that even the simplest model explains already about 90% of the total variation in the data about the average, which is quite significant already. In fact, the further single-variable daily models do not improve the R-square value.

Thus, the goodness of fit of the first daily model is sufficient whereas it is extremely satisfying with the monthly model. In fact, the difference in the goodness of fit indicators between the monthly and the (first) daily model(s) can mostly be explained by the effect of the internal DHW storage tank that causes significant dispersions on the daily performance. Indeed, as mentioned in *Section 5.4.2.3 - The time bases of the models*, with daily timeframes, the DWH tank could be heated one day (worsening the thermal efficiency of that day) and emptied the next one (improving the thermal efficiency of that following day).

For example, based on the tank capacity of 220 L of water that is considered as empty with an average temperature of 30 °C and loaded with an average temperature of 60 °C, the total energy considered to be stored is 7.67 kWh. Knowing that the average observed daily DHW consumption of both systems in the whole year 2020 is about 5 kWh, one can in fact imagine the ‘worst case’ impact that the storage could have on the variance of the thermal efficiency, especially in summer where space heating is null or minimum. However, DHW production is usually scheduled daily in those systems (with a function called ‘DHW priority’) [185], as standby heat losses prevent the temperature to stay sufficiently high to ensure DHW for the following day (even if there were no DHW consumption).

Comfort is not the only requirement to regularly keep the temperature of the tank quite high as Legionella prevention also advises it [186]. Therefore, DHW production variance fortunately does not reach the ‘worst case’ stated here above and only an uncertain smaller proportion of the tank is actually used on the following day rather than on the actual day. Still, this reflects on the R-square value of the single-variable daily models as this work considers the machine as a whole (gas condensing boiler + fuel cell + storage tank) without modelling the storage effect individually. Unfortunately, as it has already been stated, one could not monitor the state of the internal tank by lack of internal sensors (for warranty reasons).

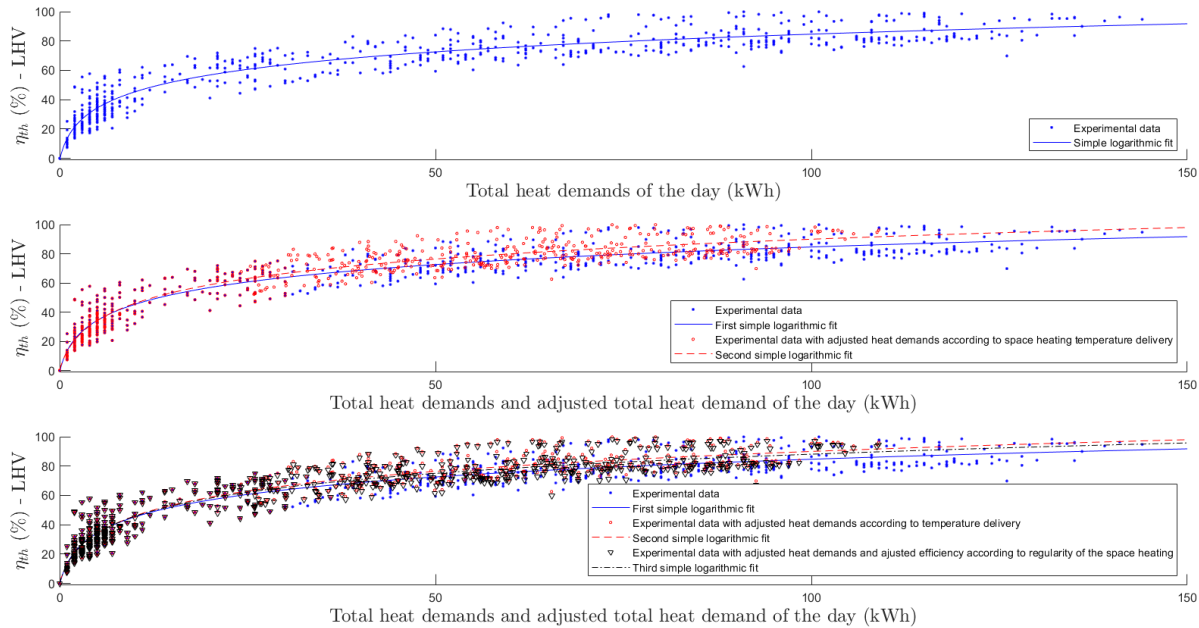
It would be expected that the kind of daily dispersion caused by the DHW storage tank leads to a distribution of residuals that is spread quite equivalently around the prediction of the daily model. This is actually confirmed by the fact that Figure 89 indicates that, on the same time base, the daily model is validated by its similarity with the monthly model (that shows amazing goodness of fit indicators). Therefore, both models can be considered as quite equivalent and relevant for the application (despite of the daily dispersion of the performance due to the DHW tank).

Still, it is possible to improve the single-variable daily model by considering other sources of performance dispersion occurring with the field-test systems. Unfortunately, the intrinsic errors due to the accuracy of the sensors (Table 34) unfortunately cannot be easily compensated in the models. However, the performance of space heating appliances are generally still affected by their operating temperature [160] and their dynamic behavior [161] regarding the heat demands profiles, which can be quite erratic or stable. Those effects are not considered in the first daily model and, as it will be seen in the following section, this is the purpose of the second and third daily models.

It is worth mentioning that only the two-variable daily models in the next section will also allow a significantly better goodness of fit indicators compared to the single-variable daily models.

Parameters & fit results	Monthly model ( $m$ )	First daily model ( $d$ )	Second daily model ( $d$ )	Third daily model ( $d$ )
$C_{1m}   C_{1d}   C'_{1d}   C''_{1d}$	-127.9	3.491	-2.035	-0.06732
$C_{2m}   C_{2d}   C'_{2d}   C''_{2d}$	14.1	17.59	19.93	19.1
$C_{3m}   C_{3d}   C'_{3d}   C''_{3d}$	$-3.3e^{-4}$	0.7636	1.13	0.9973
R-Square	0.9721	0.8974	0.8984	0.8937
RMSE	3.6020	7.9003	7.8621	7.8225

**Table 38.** Values for the parameters of the logarithmic models and goodness of fit indicators.



**Figure 90.** Step by step improvement of the primary logarithmic empirical model defined by Equation (2) to account for key effects on thermal efficiency.

#### 5.4.3.3 Improved daily thermal efficiency models

##### • **Operating temperature**

Literature on gas condensing boilers has stated that operating temperature (mainly return temperature for condensation reasons) can have a significant effect on thermal efficiency, even outside the ensured condensing mode zone (because of increased ambient losses) [160]. Also, for the PEMFC, the OEM has also reported in Figure 71 a thermal efficiency decrease with increased operating temperatures. Therefore, one might improve the first model by taking into account the working temperature of the machine (by considering the return temperature). There are several ways to account for this but one shall look at the return line temperature (inlet line for the machine), as it is done in literature [160]. In this case, one shall also preferably look at the space heating circuit for four main reasons:

- DHW can be assumed to be delivered at approximately the same temperature (for comfort and Legionella reasons [535]). Plus, inlet sanitary water comes from the water mains and will also be measured at approximately the same temperature (ambient or slightly lower).
- DHW daily production (with the boiler) is usually short in time and is represented by highly transient operating conditions. This would thus be very hard to distinguish the performance decrease due to the transient effects and the one due to the temperature levels.



- In this case, DHW production mainly goes into the storage tank and is not measured by the monitoring sensors.
- At last, over the whole monitored year, space heating use is far more prevalent than DHW production. For example, for the house in Huy, annual space heating demand is 12.5 times higher than DHW demand and this ratio goes up to 16.5 for the house in Oostmalle.

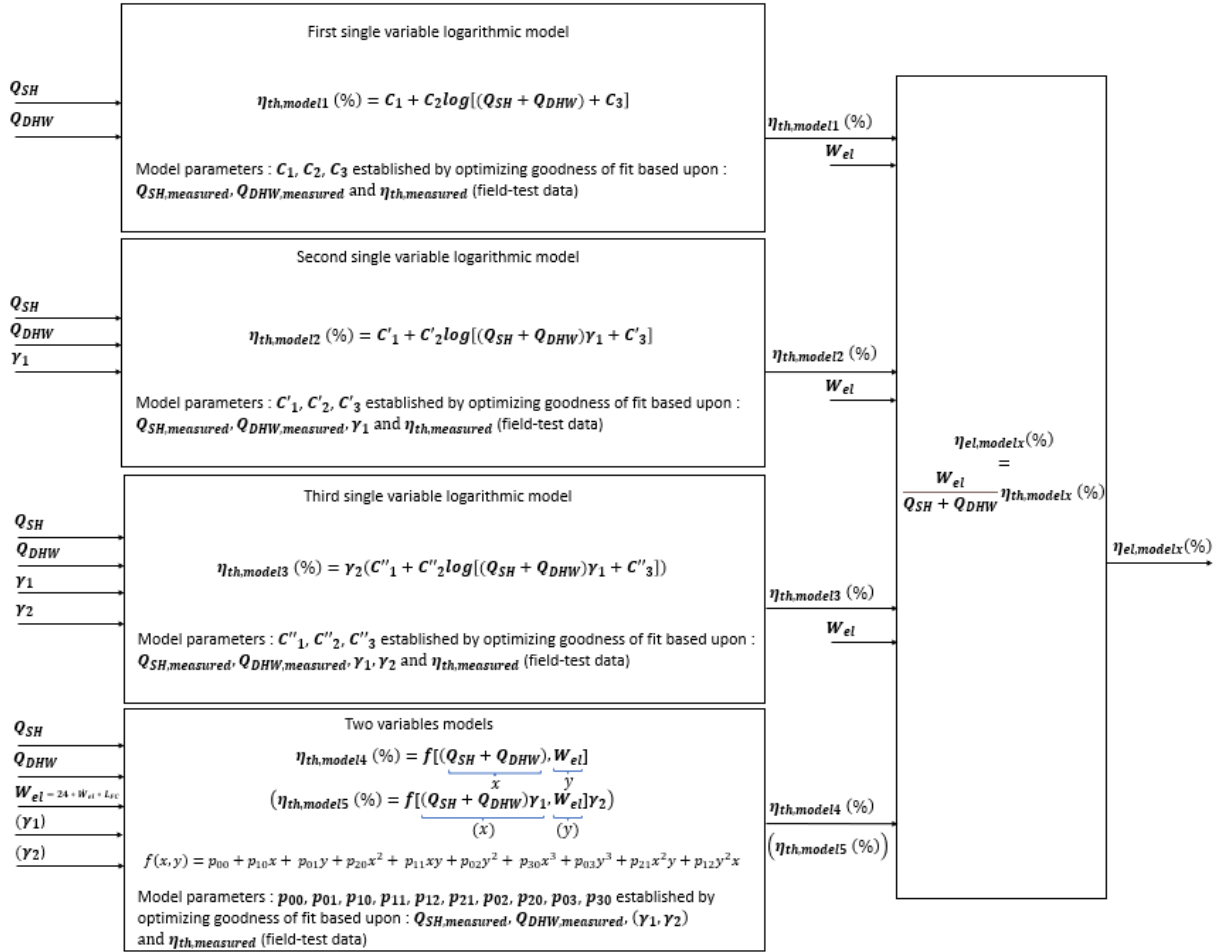
Since one is studying daily efficiency figures, it is wanted to build one single daily indicator that will represent the working temperature of the whole day. The problem is that the machine does not work in steady-state operations for the whole day. Looking only at the maximum temperature of the day in the return line would therefore not be representative of the whole day and might account for one single (very high) transient effect. Looking at the average temperature of the whole day is not ideal as well because a very erratic and high temperature space heating demand could result in the same average temperature as the one of a 24-hour long low temperature demand (typical of floor heating).

Therefore, it has been chosen in this work to look at the 4-hour gliding average of the return temperature and keep its maximum value of the day  $\overline{T_{R,4h}}$ .

The correction factor  $\gamma_1$  for space heating working temperature is applied on the horizontal axis (total heat demands:  $Q_{SH} + Q_{DHW}$ ) by adjusting the heat demands according to Equation (48).

$$(Q_{SH} + Q_{DHW})_{aj} = (Q_{SH} + Q_{DHW}) * \gamma_1 \quad (48)$$

This operation is presented in a flowchart in Figure 91 which also shows the impact of this correction factor on the generic logarithmic equation of the model defined by Equation (47).



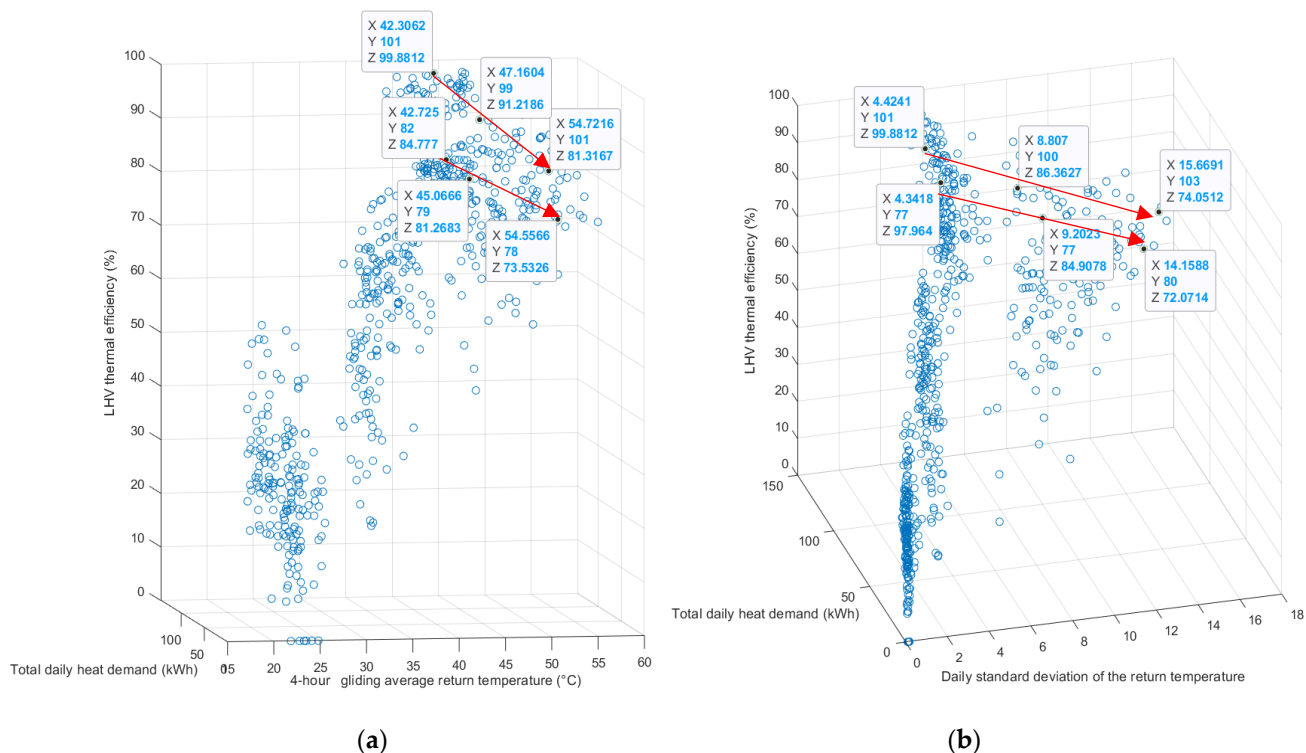
**Figure 91.** Flowchart of the daily models developed in this field-test study.

For low heat demands (warmer seasons), this adjustment shall not be applied as the system is mainly (and sometimes only) used for DHW and not for space heating. In this work, the limit to apply the correction factor has been set manually (to minimize RMSE) to 30 kWh. Although space heating is usually always seen with total heat demands over 10 kWh, the rather high proportion of the DHW demand in the 0-30 kWh total heat demands window prevents the fit to be improved that way. Over the 30-kWh limit, the DHW part in the total heat demands becomes sufficiently low for the correction factor to be applied. In this applicable window, the relation between thermal efficiency of the day and total heat demands has been considered as linear (see the top of Figure 90). As a first approach, for the same total heat demands, the relation between thermal efficiency and the maximum 4-hour gliding average temperature of the day on the return line  $\overline{T_{R,4h}}$  can also be considered as linear.

In fact, as it can be seen in Figure 92 (a), higher the total heat demand, higher the decrease in efficiency according to operating temperatures (maximum 4-hour gliding average temperature of the day on the return line). This validates the application of  $\gamma_1$  in Equation (48) as a correction factor applied relative to the total heat demand of the day.  $\gamma_1$  is defined according to Equation (49),  $\overline{T_{R,4h}}$  having been explained here above and  $Max_{\overline{T_{R,4h}}}$  being the maximum value of the daily  $\overline{T_{R,4h}}$  values of the dataset for the whole studied year (non-dimensionalization) :

$$\gamma_1 = 1 - \frac{\overline{T_{R,4h}}}{\text{Max}T_{R,4h}} * 0.3 \quad (49)$$

This data manipulation results in updated constants for the generic logarithmic model described by Equation (47) as well as small improvements of the RMSE and the R-Square value, as it can be deduced from Table 38. The resulting fit is presented in the middle graph of Figure 90. The weight of the correction implied by  $\gamma_1$  in Equation (49), i.e. the 0.3 value, has been optimized manually.



**Figure 92. (a)** Small decrease (considered linear) of thermal efficiency according to the operating temperature for identical total heat demands; **(b)** Small decrease (considered linear) of thermal efficiency according to the standard deviation of the return temperature for identical total heat demands. Six days have been highlighted per graph : X is either the 4-hour gliding average temperature or the daily standard deviation of the return temperature, Y is the total daily heat demand and Z is the LHV thermal efficiency.

- **Transient effects & power peaks**

As it is generally the case in engineering, it is better to operate a machine in steady-state conditions or as close as possible to those. In fact, one purpose of the storage tank of this system is indeed the increased thermal inertia it allows in order to smooth up the behavior as much as possible. Although, paradoxically, the tank accumulates heat and therefore intrinsically impedes steady-state conditions.

However, even with the tank, oversized space heating appliances and/or erratic demand set by the user can cause highly dynamic behaviors that induce decreased efficiencies.

This is also true with gas condensing boilers as it has been found in literature that improving their level of modulation, increasing the duration for which the machine operates in steady state conditions, can lead to an improved efficiency of about 4 percentage points [560].

This effect has also been studied in this work and integrated into the single-variable logarithmic model with a similar method as the ‘working temperature effect’ conducted in

the previous section. This is done by establishing a second correction factor  $\gamma_2$  as described by Equation (50) that is directly applied to the daily thermal efficiency (that becomes the adjusted daily thermal efficiency  $\eta_{th_{aj}}$ ).

$$\eta_{th_{aj}}(\%) = \eta_{th} * \gamma_2 \quad (50)$$

Again, this operation is presented in a flowchart in Figure 91 which also shows the impact of this correction factor on the generic logarithmic equation of the model.

To account for the effect of the erratic space heating demand and establish  $\gamma_2$ , it has been chosen again to observe the space heating return temperature and compute its standard deviation over the whole day ( $\sigma_{TR}$ ), which effect on the thermal efficiency is presented in Figure 92 (b). Again, it has been chosen not to affect the correction factor  $\gamma_2$  on the whole dataset. Indeed, smaller standard deviations in warmer seasons (with low or null space heating) can be explained mainly by the fact that the variance in the efficiency results comes mainly from the storage tank not modelled in this work, as explained earlier.

In addition, since standard deviation of the ambient temperature, where the sensor is placed, can also account for part of the standard deviation of the return temperature, it has been chosen to limit the application of the second correction factor  $\gamma_2$  on the daily data that have standard deviation above 3.25. Therefore, there is no need to set another application window on the total heat demands figures as it has been done in the previous method.

Thus,  $\gamma_2$  is established by Equation (51),  $\sigma_{TR}$  having been explained here above and  $Max_{\sigma_{TR}}$  being the maximum value of the daily  $\sigma_{TR}$  values of the dataset of the whole studied year (non-dimensionalization) :

$$\gamma_2 = 1 - \frac{\sigma_{TR}}{Max_{\sigma_{TR}}} * 0.05 \quad (51)$$

However, there is a significant difference with the ‘working temperature’ correction method established in the previous section: it is visible in the lower part of Figure 90 that the correction factor is applied on the vertical axis this time. It is indeed applied directly on the thermal efficiency as induced by Equation (50).

The  $\gamma_2$  correction factor means that erratic behavior of the machine can lead up to a 5% decrease in efficiency (based on data already adjusted by the previous method to account for working temperatures). This has been optimized manually and is relevant with consulted literature as it close to the 4-percentage points decrease cited earlier [560].

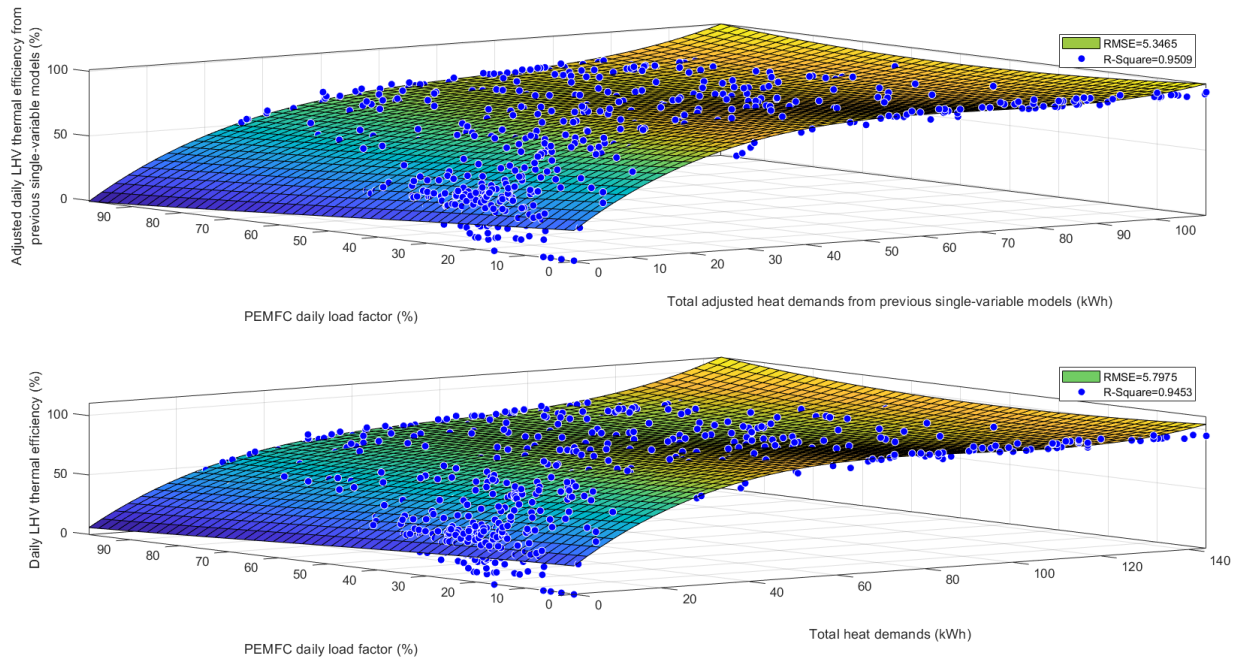
This second correction leads to the third and last of the single-variable models presented in this work, shown in the bottom of Figure 90 and whose goodness of fit is established in Table 38.

- **Two-variables models**

The fact that the PEMFC has intrinsically a worsen thermal efficiency than the boiler, as seen in Table 25, implies that the PEMFC daily electrical production affects the daily thermal efficiency of the system.

This comes in addition to the fact that most of the heat from the fuel cell goes in the tank and is thus subject to standby losses. Indeed, in winter, the heat demand is too high and the boiler needs to provide thermal energy directly to the hydraulically circuits of the house and in summer, mainly DHW from the tank is needed.

Up till now, the single-variable models developed in this work that fitted the data sufficiently already have not considered this effect, particularly significant in warmer seasons. This can be studied further by extending the models with an additional dimension, simply being the PEMFC daily load factor  $L_{FC}$  (defined earlier as the daily electrical production over the maximum value it can reach, i.e. 18 kWh<sub>el</sub>). The resulting two-variables models have been plotted in Figure 93.



**Figure 93.** Final two-variable models of this work. The first one includes the corrections made in the previous single-variable models (according to working temperatures and modulation smoothness) and provides a better fit. The data of the second one has not been postprocessed.

The first model considers the adjusted data from the last single-variable model developed in the previous section to account for the working temperature effect as well as the smoothness of the modulation of thermal energy. The second model is not considering those effects and it provides a sufficient but slightly worsen goodness of fit.

For both two-variable models, one can directly see a significantly better goodness of fit compared to previous single-variable models (even with R-square values). Both models are polynomial regressions of the third order on both dimensions performed thanks to the *Matlab* software with robust least squares fitting option called 'bisquare', which consists of minimizing a weighted sum of squares, where the weight given to each data point depends on how far the point is from the fitted curve. The resulting models are defined by Equation (52) ( $x$  being the total heat demands or the adjusted total heat demands and  $y$  being the daily electrical production deduced from the PEMFC load factor its nominal electrical output power).

$$f(x, y) = p_{00} + p_{10}x + p_{01}y + p_{20}x^2 + p_{11}xy + p_{02}y^2 + p_{30}x^3 + p_{03}y^3 + p_{21}x^2y + p_{12}y^2x \quad (52)$$

The values of the constants for both models are given in Table 39.

Main remaining errors of both models come again from very low total heat demands, again due to the prevalent effect of the storage tank. As explained, the tank can deliver thermal energy stored the day before and causes great variance in the results, which is visible on the bottom part of each graph of Figure 93). Part of the remaining error can also come from the potential difference in parametrization of the system by the installer or the user

and from the intrinsic uncertainties due the accuracy range of the sensors reported in Table 34.

These models have also been presented in the flowchart of Figure 91.

Models	$p_{00}$	$p_{01}$	$p_{10}$	$p_{02}$	$p_{11}$	$p_{20}$	$p_{03}$	$p_{12}$	$p_{21}$	$p_{30}$
1. with adjusted data	24.27	-1.648	3.024	0.01102	-0.01704	-0.04291	7.329e-5	6.384e-4	1.597e-4	1.976e-4
2. without adjusted data	24.76	-0.9458	2.494	-0.01896	-0.02719	-0.02819	5.325e-4	7.05e-4	1.642e-4	1.02e-4

**Table 39.** Values for the parameters of the two-variables models with and without adjusted data.

It shall be mentioned that the two-variables model defined by Equation (52) and which coefficient are given in the first row of Table 39 has been compared to steady-state laboratory experiments on the same CHP system [550] and correlation could be demonstrated [564].

#### 5.4.3.4 Electrical efficiency

In this work, the priority has been put on the thermal efficiency for several reasons:

- It is the main contributor of the total efficiency as it can be deduced from Figure 71 or Figure 88.
- As a first approach, there is a simple linear trend between thermal and electrical efficiency, as shown in Figure 88, and Equation (46) can easily be used to estimate it.

If one wants to go further than this not very accurate linear trend and if the PEMFC daily load factor  $L_{FC}$  is known (which should be the case for the two-variables models to be implemented), the daily electrical efficiency  $\eta_{el}$  could be calculated with Equation (53) :

$$\eta_{el} = \frac{W_{el}}{Q_{g,LHV}} = \frac{L_{FC} * 24 * \dot{W}_{el}}{Q_{g,LHV}} \quad (53)$$

Where  $W_{el}$  is the daily electrical production calculated based on  $\dot{W}_{el}$ , the nominal PEMFC output electrical power (0.75 kW<sub>el</sub> in this case).  $Q_{g,LHV}$  has been linked to the thermal efficiency in Equation (54) and corresponds to the LHV content of the gas consumed by the machine on the day. It could be grossly considered equal to the volume of gas consumed times the LHV figure established by gas provider. However, it has been demonstrated in an earlier study that it is more accurate to implement a correction factor to the monitored gas volume to account for the pressure and temperature measurement difference between the measuring conditions (in the gas pipe upstream the system) and the standard conditions at which the LHV are defined by the gas provider [465].

$$Q_{g,LHV} = \frac{Q_{SH} + Q_{DHW}}{\eta_{th}} \quad (54)$$

$Q_{SH}$ ,  $Q_{DHW}$  and  $\eta_{th}$  have already been explained earlier and are either inputs or outputs of the models established in this work.

So, one obtains Equation (55) :

$$\eta_{el}(\%) = \frac{L_{FC} * 24 * \dot{W}_{el}}{Q_{SH} + Q_{DHW}} \eta_{th} \quad (55)$$

This can even be detailed thanks to the equation of  $\eta_{th}$  given by the single-variable models of this work. For example, the use of Equation (47) relative to the first and most simple daily model developed in this work leads to ( $C_{1d}, C_{2d}, C_{3d}$  values given in Table 38) :

$$\eta_{el} = \frac{W_{el}}{Q_{SH} + Q_{DHW}} (C_1 + C_2 \log[(Q_{SH} + Q_{DHW}) + C_3]) \quad (56)$$

The other models of this work that provide  $\eta_{th}$  could also similarly be used. However, with the single-variable monthly model (see *Section 5.4.3.2 - Simple single-variable time-invariant thermal efficiency models*), it is important to consider in Equation (54) and Equation (56) the monthly load factor of the fuel cell instead of its daily load factor, in addition to replace the 24 coefficient by 720 (=24×30).

#### 5.4.4 Modelling limitations & further work

The fact that one might have been studying unoptimized controlled machines and/or unoptimized installations may constitute a limitation to the results of this study but it can in fact be considered that it is the whole point of the monitoring study to take into account those potential unoptimized real conditions in the performance review rather than study controllable optimized laboratory conditions.

Main drawback though is that one may argue that the number of tested machines in this study is far from being enough to statistically be representative. However, obtaining such qualitative correlations between the two machines although the houses they are placed into hold that much difference tend to indicate that the data might in fact be sufficiently representative. In fact, this is also an indication that the installation and the utilization of the machine is consistent with one another.

By design, mainly for durability reasons [561], the heat storage allows the PEMFC to run as long as possible with its small output power. Indeed, it can be assumed that the gas boiler provides heat directly to the outputs (supposably only, when necessary, for very high sudden DHW demand and for space heating), without much heat going through the tank and being subjected to standby losses. Therefore, another key variable not yet studied directly here is the effect caused by the proportion of DHW in the total heat demand of the day. Indeed, as explained, the tank acts as an energy storage, subjected to non negligible standby losses proportional to the duration of which all the heat will remain in the tank, before finally being measured by the sensors as the house draws DHW.

However, this effect of higher DHW part in the heat demands is already partially considered in the two-variables final models of this work since DHW prevalence in the total daily heat demand occurs in warmer seasons and coincides with lower PEMFC load factor (induced by the fact that the PEMFC is less often able to dissipate its heat in the space heating). Also, Figure 89 has indicated that the first single-variable models developed in this work (and by extension, their improvement) relevantly predict the system no matter if it produces only DHW or both DHW and space heating. Therefore, the possible improvement of considering the proportion of DHW in the total heat demand of the day/month is not expected to be significant.

Nevertheless, it is assumed that the one evident way to further improve the models would be by considering the internal tank (and its thermal state which would request DHW consumption modelling as well). This would indeed account for a lot of the variance in the data, especially for low total heat demands and daily time bases, as a higher part of the heat stored one day can be released the day after, greatly affecting thermal efficiency. Since it is not possible to place sensors inside the system, a state observer model for the tank might seem relevant. It should be noted that Figure 89 has indicated that the distribution of residuals due variance of the daily thermal efficiency data due the DHW

storage tank is spread quite equivalently around the prediction of the daily model (see *Section 5.4.3.2 - Simple single-variable time-invariant thermal efficiency models*). In other words, although a state observer model of the tank will enhance the goodness of fit indicators of the daily models, it would most likely not improve the monthly performance model developed in this work.

At last, the probable best improvement that could be performed to enhance the daily models of this work would be by modelling the PEMFC daily load factor  $L_{FC}$  by considering tangible influencing and predictable factors such as the heat demands of the building, their absolute daily values, their smoothness over the day, their average working temperature, the need for fuel cell mandatory regeneration phase [496], etc... Indeed, for the moment, the load factor is used as an input in the best daily thermal efficiency models developed in this work (the two-variable daily models) or is simply used to establish the electrical efficiency accurately thanks to any thermal efficiency model of this work. It is in fact considered as an input indicating the ability of the PEMFC to produce electricity and is therefore an indicator of the adequation between the system, the building and the occupants.

### 5.4.5 Conclusions of the section

This section has developed simple single-variable logarithmic and two-variable regression daily performance models for a PEMFC-gas condensing boiler hybrid system. A monthly single-variable logarithmic performance model has also been established.

As a first approach, electrical efficiency has been assumed to be linearly inversely proportional to the thermal efficiency so the whole system efficiencies could be modelled simply by modelling the thermal efficiency.

All the models of this work require the total daily (or monthly) heat demand of the house, which is the addition of DHW and space heating demands. This is even the single required input for the first simple logarithmic (daily and monthly) models developed in this study, which are defined thanks to Equation (47) and Table 38. This therefore facilitates the applicability of those models since space heating demands can be easily approximated with any building simulation and DHW load profiles may be assessed by well-known standards [565].

For example, the applicability of the interpolation models developed in this section can be extended to every homeowner that has an energy performance certificate as it is mandatory in Europe for any building or building unit which is constructed, sold or rented out to a new tenant [566]. Indeed, those usually involve energy performance indicators expressed in kWh/m<sup>2</sup> per year that could directly help to compute the heat demands used in this work.

This modelling work will thus help evaluating economical and environmental interests of that system in the much-needed energy transition towards a cleaner future.

The monthly performance model exhibits a tremendous goodness of fit. Regarding the daily models, their goodness of fit is inevitably affected by the variance due to the storage effect of the DHW, that can be heated one day and emptied the next one. However, all the daily models of this work still provide sufficient goodness of fit. In fact, the best daily model has been established considering both an adjusted daily total heat demand of the house (adjusted data to account for efficiency decreases related to unoptimized use of the system) and the daily PEMFC load factor (which in this case, must be established).

The adjusted data to compute the best daily model of this work considers two correction factors ( $\gamma_1$  and  $\gamma_2$ ), inspired by gas condensing boiler literature. The first one accounts for the decrease of thermal efficiency related to increased working temperatures. This first correction factor has been established by computing the maximum 4-hour gliding average



---

space heating temperature of each day. The second one accounts for the decrease of efficiency related to unsmooth heat demands. This second correction factor has been established by computing the daily standard variation of the space return temperature.

Eventually, the applicability of the daily models of this work based on the correction factors ( $\gamma_1$  and  $\gamma_2$ ) might be considered as limited to this particular study (and to its corresponding monitoring configuration). However, the methods used to improve them by accounting for nonoptimal uses of domestic heating appliances can easily be reproduced by implementing similar correction factors. Those methods might even be effective with other potential nonoptimal uses of heating systems than the ones reported in this work, which only considers the impact of operating temperatures and the ability of the system to modulate its heating capacity.

As it is based on the field-test data quite exhaustively analysed in the previous section, the models offered here do not bring significantly newer information on the system's performance.

This correlation work is based on the comparison of the best field-test empirical efficiency model developed in *Section 5.4 - Machine modelling* with the steady-state laboratory performance reported in *Section 5.2 - Laboratory tests*. However, those are very different than real field-test applications because the in-situ operating conditions are specific to the installation, the (local) climate and the occupant's behavior. Despite that, this section demonstrates how a correlation can still be conducted, mainly by implementing a primary energy penalty on the steady-state nonrealistic laboratory results. This correlation constitutes a validation both the experimental results and the field-test model developed in the previous section. This section was published almost as-is in the *proceedings of the 30<sup>th</sup> Congrès Annuel de la Société Française de Thermique (SFT 2022)* [564].

## 5.5 Comparison of laboratory and in-situ measurements

### 5.5.1 Field-test chosen model

The field-test model chosen for the correlation is simply the one developed in the previous section that is offering the best goodness of fit: it is the one presented at the top of Figure 93, defined by Equation (52), which parameters are given in Table 39 (with adjusted data).

It takes as inputs the daily total heat demand and the daily electrical production of the unit (or its daily load factor [537]). It also implements two correction factors ( $\gamma_1$  and  $\gamma_2$ ) in order to take into account two physical sensitivities that have an impact on the resulting efficiency (and therefore provides a better fit). The first effect that is taken into account (thanks to the  $\gamma_1$  parameter) is that higher working temperatures decrease the thermal efficiency (for identical heat demands) [558]. The second effect the chosen model is considering is that possible erratic behavior (highly transient) tends to decrease the thermal efficiency, as seen in literature [560]. The chosen model establishes a second correction factor  $\gamma_2$  to that end (see *Section 5.4 - Machine modelling*) but it will not be used in this section because the laboratory results used for the correlation have been reported for steady-state only [550].

### 5.5.2 Steady-state laboratory results

The laboratory tests chosen for the correlation are the one based on the EN 50465 (see *Section 5.2 - Laboratory tests*). Thus, four main test campaigns were performed: one with only the DHW valve fully opened, one with only the DHW valve 50% opened (the space heating valve being fully closed for both), one with only the space heating valve fully opened and at last one with only the space heating valve 50% opened (the DHW valve being fully closed for both) [550].

The results of those campaigns have already been reported in Table 29 and are reproduced in Table 40 and Table 41. Measured thermal energy assumes a constant calorific value  $cp$  of 4184 J/kg-K (assumption similar to initial work [550]). Thermal LHV efficiency can thus be trivially obtained. Electrical efficiency is not shown because the output electrical power has been verified to be quite constant and equal to the targeted 750 W (of Table 25) [537].

### 5.5.3 Correlation

It is clear that the best way to operate a correlation would have been to reproduce one typical day seen on the field-test in a laboratory but this could not be done. Laboratory operating conditions and field-test are thus difficult to correlate because the whole field-test analyses have been established based on daily values (not close at all from the laboratory steady-state operating conditions). In addition, the laboratory tests have been conducted for about 45 minutes only and do not include the warming up of the tank. Also, there is pretty much no standby losses in those laboratory tests as the heat demand is

always there and the 3-way valves (see Figure 68) are mainly switched to bypass the tank so the heat is directly measured by the sensors at the outlets. For DHW tests, the tank is not bypassed but there is still pretty much no storage effect as the enthalpy flow that comes in also comes out (so the standby losses of the DHW tank are also insignificant).

On the other hand, in the field-test, standby losses are not negligible, especially in low heat demand days (which account for similar heating demands as the 45-min laboratory tests, i.e. lower than 25 kWh as seen in Table 40 and Table 41). Therefore, a compensation parameter shall be applied on the laboratory results to ensure relevancy with the field-test model.

It is performed by considering a fictive extra primary energy consumption (or primary energy penalty)  $\varphi_0$  at the denominator of the 'adjusted' efficiency formula of the laboratory tests, presented in Equation (57).

$$\text{Adjusted } \eta_{th} = \frac{\int \dot{m} \times cp \times \Delta T \times dt}{\varphi_0 + \int \dot{V}_{gas} \times LHV \times dt} \quad (57)$$

$\int \dot{V}_{gas}$  is the gas consumption;  $\int \dot{m}$  is the mass of water heated during the test (relative density assumed to 1);  $\Delta T$  is the thermal difference between the depart and return to the system. All those measurements are given in Table 40 and Table 41. All the terms shall be expressed in kWh (and based on LHV). Optimized penalty  $\varphi_0$  to be applied to laboratory tests has been set to 10 kWh for fitting reasons (fitting performed manually). This value happens to be equal to the amount of energy that can be considered to be stored in the 220L DHW tank of the unit (thermally loaded temperature of 60°C compared to 20°C of rest temperature). As a first approach, this lump sum value of 10 kWh can be considered as the daily stand-by losses that are occurring onsite. Since DHW scheduling occurs pretty much every day (up to about 60°C as well), the daily standby losses with this system can be actually considered to approximate the total energy that can be stored in the tank. It is worth mentioning that the 'Adjusted  $\eta_{th}$ ' of the laboratory results has only been computed for correlation purposes and shall not be considered relevant as-is (one reason is that, with that equation, higher the working temperature, higher the efficiency, which is against what has previously been stated).

On the other hand, a proper use of the field-test model of Equation (52) requires two inputs:  $x$  and  $y$ .  $y$ , the electrical production of the day, can be considered as a first approach as the multiplication of the net power of the PEMFC (observed to be constant and equal to 750 W<sub>el</sub>) by the duration of the test, given in Table 40 and Table 41.  $x$ , the adjusted total heat demand of the day, is obtained by multiplying the measured thermal energy (the heat demand, that can directly come from Table 40 and Table 41) to the  $\gamma_1$  correction factor, as described by Equation (49) in the previous section.

For the laboratory results,  $\gamma_1$  can be expressed as a function of a second fitting parameter ( $C_\gamma$ ). Indeed,  $\gamma_1$  accounts for the fact that higher working temperatures tend to decrease the thermal efficiency. Unfortunately, the laboratory data cannot reuse Equation (50), defined in the previous section, as it is designed to be established based on the temperature data of one whole day. However, one can still establish  $\gamma_1$  manually in a similar way compared to Equation (50). Indeed, this equation gives a linear decrease of  $\gamma_1$  with higher working temperature and this kind of linear behavior can be reproduced for the laboratory tests. The maximum value of  $\gamma_1$  (which is 1, i.e. no correction) is assumed to be of application with the lowest temperature delivery, which is 20°C (as it can be seen in Table 40 and Table 41). This is coherent because in real operating conditions, heating temperatures shall rarely be lower than 20°C. Maximum operating conditions of 60°C (from Table 40 and Table 41) lead to a minimum value of the  $\gamma_1$  correction factor, called  $C_\gamma$  (optimized manually to 0.8 for fitting reasons). In fact, by looking at Equation (50),  $\gamma_1$  could

reach smaller values (down to 0.7) but it is not advised to assume that the maximum temperature operating conditions of the laboratory tests requires this absolute  $\gamma_1$  minimum value. Indeed, Equation (50) is only valid for the field-test and daily dataset that allows establishing the maximum 4h gliding average of the return temperature. This does not correspond to the laboratory tests operating conditions. Intermediate  $\gamma_1$  values are subsequently set linearly between 1 and 0.8 ( $C_\gamma$ ) according to the working temperature of Table 40 and Table 41.

There is no need to make a difference between the space heating only and the DHW only operating conditions because it has been stated that standby losses and storage effect could be neglected for both laboratory campaigns studied in this work. It can thus be assumed that they can be treated the same way, with the same correction factor (only depending on temperature).

#### 5.5.4 Results and conclusions of the section

The correlation method between the chosen field-test model and the laboratory steady-state results for this PEMFC-gas condensing boiler hybrid can be resumed with two main steps.

Firstly, on the one hand, to account for stand-by losses that have not occurred in the laboratory steady-state tests, one must apply a primary energy penalty  $\varphi_0$  on the laboratory results. It has been set equal to 10 kWh, which is approximately equivalent to the amount of thermal energy that can be stored in the 220 L tank of the system. This is an indication of the daily stand-by losses with this system in real applications (with daily DHW scheduling). Thus, one obtains the 'Adjusted' LHV thermal efficiency from Equation (57), that will be compared to the field-test model.

Secondly, on the other hand, the field-test model of Equation (52) intrinsically uses as an input the total heat demand, adjusted (multiplied) with the  $\gamma_1$  correction factor to account for the effect of the working temperatures on the thermal efficiency of the system. The laboratory measured thermal energy cannot thus be used as-is in Equation (52) because it has to be multiplied by  $\gamma_1$ , which should therefore be established beforehand. Unfortunately, the method used in the field-test model study to define  $\gamma_1$  [537] is not applicable for the laboratory results, but it can be established quite similarly, through optimizing only one fitting parameter, i.e.  $C_\gamma$  (which is the second fitting parameter after  $\varphi_0$ ).

All those manipulations are recorded in Table 40 and Table 41. One can see that the difference between the 'adjusted' laboratory efficiency (with the  $\varphi_0$  penalty) and the field-test model comes down to about 2 percentage point, which is way within the error margin, that can be deduced from the accuracy of the sensors presented in Table 26 (for the laboratory results) and in Table 34 (for the field-test model). For the field-test data, the propagated uncertainty can indeed be established to about  $\pm 5\%$  (as mentioned in *Section 5.3.5 - Uncertainty analyses*).

Even if the two fitting parameters ( $C_\gamma$ , used to establish  $\gamma_1$  and  $\varphi_0$  used for adjusting the laboratory results) have manually been optimized, they have still physical meanings. On one hand,  $C_\gamma$  (=0.8) is close to the minimum value allowable for  $\gamma_1$  of the chosen field-test model (as deduced from Equation (49) the minimum  $\gamma_1$  is 0.7 [537]). On the other hand,  $\varphi_0$  has already been stated close to the amount of thermal energy storable in the DHW tank of the system.

Such a correlation for all the laboratory data presented in Table 40 and Table 41 is quite amazing. Therefore, it highlights the relevance of the laboratory study [550] but even more significantly of the modelling work [537] that provided Equation (52), which was actually the main (achieved) purpose of this section. This has been performed despite of the

intrinsic differences between laboratory and field-test configurations (for example, despite the big differences in the hydraulic integration and in the sensors that have been used).

Space Heating 100% - DHW 0%													
	Gas Consumption [m3]	Water Consumption [m3]	Mean $\Delta T^\circ$ [°C]	Test duration [s]	HHV [kWh/m <sup>3</sup> ]	LHV equivalent gas energy [kWh]	Measured Thermal Energy [kWh]	$\gamma_1$ [-]	Adjusted Thermal Energy [kWh]	Electrical Energy [kWh]	Adjusted $\eta_{th}$ [-]	$\eta_{th}$ from field-test model [-]	difference between $\eta_{th}$ [percentage points]
60±1°C	2,4290	1,128	17,205	2693	11,4588	23,628	22,556	0,85	19,172	0,561	0,67	0,67	0,27
50±1°C	2,0100	1,123	14,650	2696	11,4588	19,552	19,121	0,8875	16,970	0,562	0,65	0,63	1,56
40±1°C	1,6400	1,125	12,055	2676	11,4588	15,953	15,762	0,925	14,580	0,558	0,61	0,59	1,91
30±1°C	1,2080	1,137	8,756	2711	11,4588	11,751	11,571	0,9625	11,137	0,565	0,53	0,52	1,32
20±1°C	0,8440	1,144	5,958	2705	11,4588	8,210	7,922	1	7,922	0,564	0,44	0,45	1,13
DHW Heating 100% - Space Heating 0%													
	Gas Consumption [m3]	Water Consumption [m3]	Mean $\Delta T^\circ$ [°C]	Test duration [s]	HHV [kWh/m <sup>3</sup> ]	LHV equivalent gas energy [kWh]	Measured Thermal Energy [kWh]	$\gamma_1$ [-]	Adjusted Thermal Energy [kWh]	Electrical Energy [kWh]	Adjusted $\eta_{th}$ [-]	$\eta_{th}$ from field-test model [-]	difference between $\eta_{th}$ [percentage points]
60±2°C	2,3530	0,809	22,913	2718	11,6003	23,171	21,544	0,85	18,312	0,566	0,65	0,65	0,45
55±2°C	2,3990	0,827	23,173	2772	11,6003	23,624	22,273	0,8688	19,350	0,578	0,66	0,67	0,81
50±2°C	2,2490	0,801	22,476	2682	11,6003	22,147	20,924	0,8875	18,570	0,559	0,65	0,66	0,75
45±2°C	1,9360	0,809	19,316	2713	11,6003	19,065	18,162	0,9063	16,459	0,565	0,62	0,62	0,25
40±2°C	1,5930	0,808	16,013	2705	11,6003	15,687	15,037	0,925	13,910	0,564	0,59	0,58	1,02
35±2°C	1,2450	0,800	12,770	2688	11,6003	12,260	11,873	0,9438	11,205	0,560	0,53	0,52	1,31
30±2°C	0,9150	0,788	9,487	2653	11,6003	9,011	8,688	0,9625	8,363	0,553	0,46	0,46	0,01
<b>Max difference :</b>												<b>1,91</b>	

**Table 40:** Laboratory results [550] (with adjustments) for comparison to field-test model (based on adjusted heat demands with correction factor  $\gamma_1$  and electrical production) – fully opened heat demand valves.

Space Heating 50% - DHW 0%													
	Gas Consumption [m3]	Water Consumption [m3]	Mean $\Delta T^\circ$ [°C]	Test duration [s]	HHV [kWh/m <sup>3</sup> ]	LHV equivalent gas energy [kWh]	Measured Thermal Energy [kWh]	$\gamma_1$ [-]	Adjusted Thermal Energy [kWh]	Electrical Energy [kWh]	Adjusted $\eta_{th}$ [-]	$\eta_{th}$ from field-test model [-]	difference between $\eta_{th}$ [percentage points]
60±1°C	2,3860	0,662	29,204	2678	11,3016	22,891	22,469	0,85	19,099	0,558	0,68	0,67	1,63
50±1°C	2,0010	0,668	24,432	2677	11,3016	19,198	18,968	0,8875	16,834	0,558	0,65	0,63	2,05
40±1°C	1,6530	0,675	20,066	2665	11,3016	15,859	15,742	0,925	14,561	0,555	0,61	0,59	2,09
30±1°C	1,1920	0,678	14,433	2698	11,3016	11,436	11,373	0,9625	10,947	0,562	0,53	0,51	1,58
20±1°C	0,8280	0,68	9,809	2693	11,3016	7,944	7,752	1	7,752	0,561	0,43	0,44	1,04
DHW Heating 50% - Space Heating 0%													
	Gas Consumption [m3]	Water Consumption [m3]	Mean $\Delta T^\circ$ [°C]	Test duration [s]	HHV [kWh/m <sup>3</sup> ]	LHV equivalent gas energy [kWh]	Measured Thermal Energy [kWh]	$\gamma_1$ [-]	Adjusted Thermal Energy [kWh]	Electrical Energy [kWh]	Adjusted $\eta_{th}$ [-]	$\eta_{th}$ from field-test model [-]	difference between $\eta_{th}$ [percentage points]
60±2°C	2,0010	0,414	38,253	2728	11,5730	19,659	18,406	0,85	15,645	0,568	0,62	0,61	1,28
55±2°C	1,9240	0,420	36,459	2739	11,5730	18,902	17,797	0,8688	15,461	0,571	0,62	0,60	1,14
50±2°C	1,6120	0,394	32,680	2627	11,5730	15,837	14,965	0,8875	13,281	0,547	0,58	0,56	1,60
45±2°C	1,5360	0,434	28,088	2834	11,5730	15,090	14,168	0,9063	12,839	0,590	0,56	0,55	1,11
40±2°C	1,2070	0,412	23,909	2695	11,5730	11,858	11,448	0,925	10,590	0,561	0,52	0,51	1,67
35±2°C	0,9590	0,415	19,281	2725	11,5730	9,422	9,300	0,9438	8,777	0,568	0,48	0,47	1,25
30±2°C	0,7540	0,414	14,727	2726	11,5730	7,408	7,086	0,9625	6,820	0,568	0,41	0,42	1,26
<b>Max difference :</b>												<b>2,09</b>	

**Table 41.** Laboratory results [550] (with adjustments) for comparison to field-test model (based on adjusted heat demands with correction factor  $\gamma_1$  and electrical production) – fully opened heat demand valves.

As it was the case for the studied SOFC in the previous chapter, besides the energy performance, it is important to assess the environmental performance of the system in terms of non-CO<sub>2</sub> pollutants, as introduced in *Section 2.3 - Current emissions factors from heat and power generation* (CO<sub>2</sub> utilization performance of those systems being already investigated in *Section 5.3 - In-situ monitoring*). Thus, CO, NO<sub>x</sub> and SO<sub>2</sub> are the pollutants specifically studied in *Section 5.6 - Non-CO<sub>2</sub> pollutant emissions*. The particular matters (PM) have not been tested as the available sensor was not sensitive enough to measure them (see Figure 64 in the previous chapter).

Most of the content of this section has been published in the *proceedings of the 36<sup>th</sup> International Conference On Efficiency, Cost, Optimization, Simulation and Environmental Impact of Energy Systems (ECOS2023)* [121], accepted for publication in the *Journal of Environmental Management* [122], and has been reproduced in *APPENDIX 8: Pollutant testing (NO<sub>x</sub>, SO<sub>2</sub> and CO) of commercialized micro-combined heat and power (mCHP) fuel cells*.

Although these reported publications (see *APPENDIX 8: Pollutant testing (NO<sub>x</sub>, SO<sub>2</sub> and CO) of commercialized micro-combined heat and power (mCHP) fuel cells*) report the main results of this section, this latter has the main advantage of containing meaningful graphs and figures related to the pollutant emissions of the studied PEMFC system that have not yet been published.

It is worth mentioning that the SO<sub>x</sub> and NO<sub>x</sub> emissions measurements from this section, in ppm, can be compared to the other space heating appliances SO<sub>x</sub> and NO<sub>x</sub> results from literature introduced in Table 5 and Table 6, through the conversion Equation (68) and Equation (67) specifically published and reported in details in *APPENDIX 8: Pollutant testing (NO<sub>x</sub>, SO<sub>2</sub> and CO) of commercialized micro-combined heat and power (mCHP) fuel cells*.

At last, potential methane emissions (methane slip) have already been considered negligible and have therefore not been measured, as explained in *Section 2.3.3 - Methane slip in natural gas fed fuel cells*.

## 5.6 Non-CO<sub>2</sub> pollutant emissions

### 5.6.1 Measurement devices

The pollutant sensors were already described in the previous chapter (see *Section 4.6.1 - Measurement devices*).

The pollutant emissions were exclusively taken on the field-test sites.

### 5.6.2 Measurements analysis

When monitoring pollutants onsite, the operating conditions that can be tested are limited. Indeed, total control of the machine in the owner's house is not possible. However, in this case, it was possible to conduct two quite exhaustive test campaigns at the field-test site of Huy and one in Oostmalle.

#### 5.6.2.1 Pollutant measurements in Huy

The first test in Huy had the system completely off, then the boiler (only) was turned on by opening the radiator valves and increasing the thermostat. About 30 minutes later, the radiator valves were shut down as well as the thermostat, allowing for recording the boiler turning down. The sensor was placed just above the machine in the chimney. This sensor was subsequently also placed in the chimney on the rooftop in this first test campaign (without turning down neither the machine nor the sensors). For the second test, fortunately, the PEMFC 'ON' mode occurred (without the boiler), providing the

opportunity to analyze the emissions of the PEMFC alone (but not of its startup nor of its shutdown as the PEMFC cannot be controlled). However, it must be pointed out that, for an unknown reason, the boiler started and automatically shut itself down, which resulted in evident pollutant peaks (that can be seen in Figure 99). In this case, the sensor was placed only in the chimney above the machine, as in the laboratory tests (i.e. not on the rooftop).

The results of the first campaign (boiler only) are presented in Figure 94, Figure 95 and Figure 96. One can infer the following statements from the first campaign:

- No difference between outside and inside the chimney if the boiler is not turned on (as expected).
- O<sub>2</sub> % drops from 21% (logical value for ambient air) to about 6 % (with small overshoot) once the boiler is on.
- Onsite, it is difficult to modulate the power of the boiler. The main reason is that one cannot alter the comfort of the occupants and bother them for so long. The onsite visits for pollution analyses were singular and short in time. Basically, only 'ON/OFF' thermal demands could be tested (closing and opening the valves of the terminal units). Therefore, no conclusion could be made onsite relatively to the modulation of the system regarding the pollutants emissions.
- Transient effect (turning on the boiler, warming up) is seen on almost all signals. This is explained by the close relation between temperatures and pollutants (in their formation, in their degradation, in their reaction), as stated in *Section 2.3.2 - SO<sub>2</sub> and NO<sub>x</sub> emission factors*.
- As expected, no significant difference between the measurements performed at the top of chimney (15cm above machine) and at the top of machine.
- No SO<sub>2</sub> measured for all the tests (as expected as the system involves a desulphurizer in the embodiment and also as natural gas is industrially desulphurized before being injected in the grid [496]).
- NO is only appearing with the boiler warming up (and it is expected for the NO to quickly convert into NO<sub>2</sub>, as stated in *Section 2.3.2 - SO<sub>2</sub> and NO<sub>x</sub> emission factors*). However, NO<sub>2</sub> is not increasing as NO reduces. Indeed, it reaches its stationary value quite quickly without overshooting. This could be due to chemical cells of the NO<sub>2</sub> sensor that might have delays and/or lower resolution. Timestep within the sensor might be too small for this chemical reaction to be properly observed.

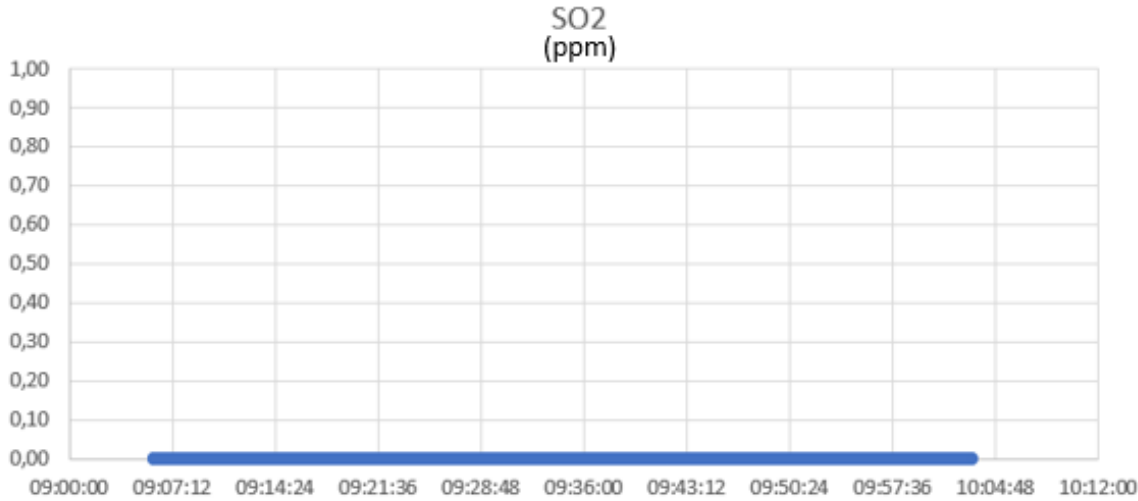


Figure 94. Field-test pollutant emissions in Huy - boiler only (part 1/3).





Figure 95. Field-test pollutant emissions in Huy - boiler only (part 2/3).

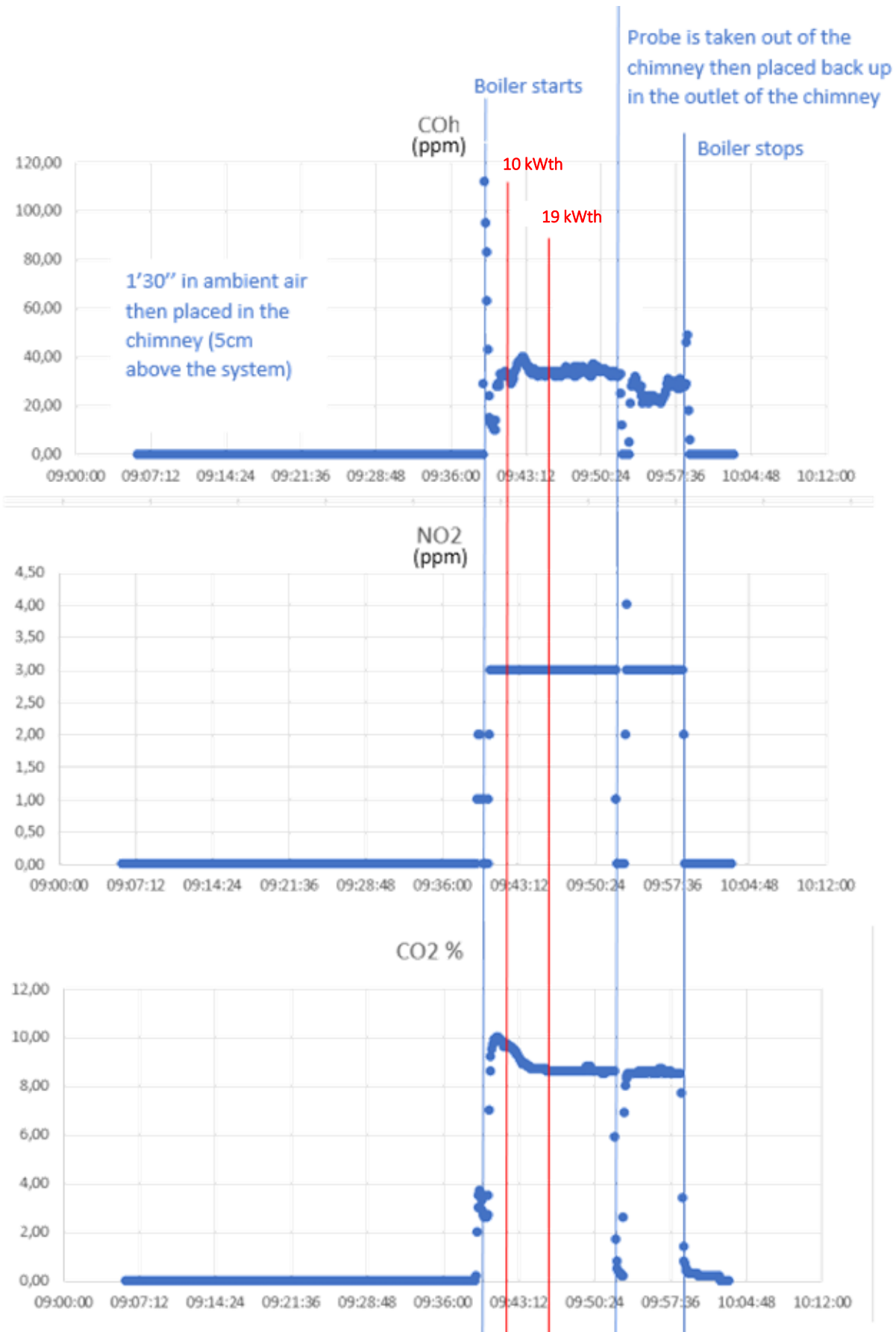
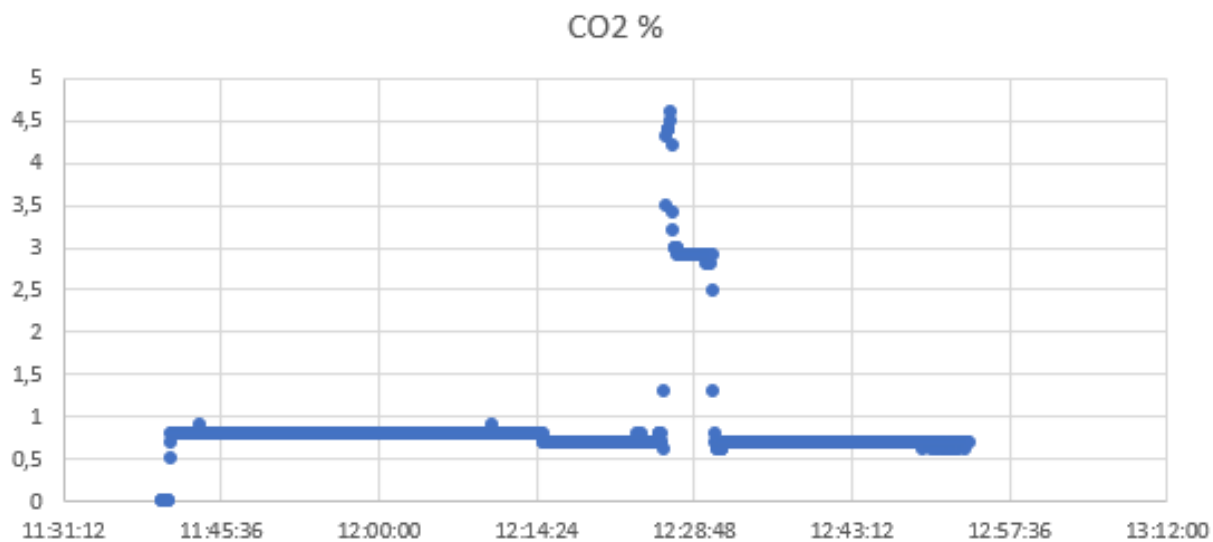


Figure 96. Field-test pollutant emissions in Huy - boiler only (part 3/3).

The results of the second campaign (PEMFC only) are presented in Figure 97, Figure 98 and Figure 99. One can infer the following statements from the second campaign in Huy:

- No NO<sub>x</sub> or SO<sub>2</sub> measured with the PEMFC only.
- O<sub>2</sub>% and CO<sub>2</sub>% measured at constant values (close to ambient values) .
- Inexplicable CO peak can be seen. Indeed, there is no indication on the monitored signals from the data logger to explain it (thermal heat rates, electrical powers, gas consumption), as shown in Figure 100.



**Figure 97.** Field-test pollutant emissions in Huy - PEMFC only (part 1/3).

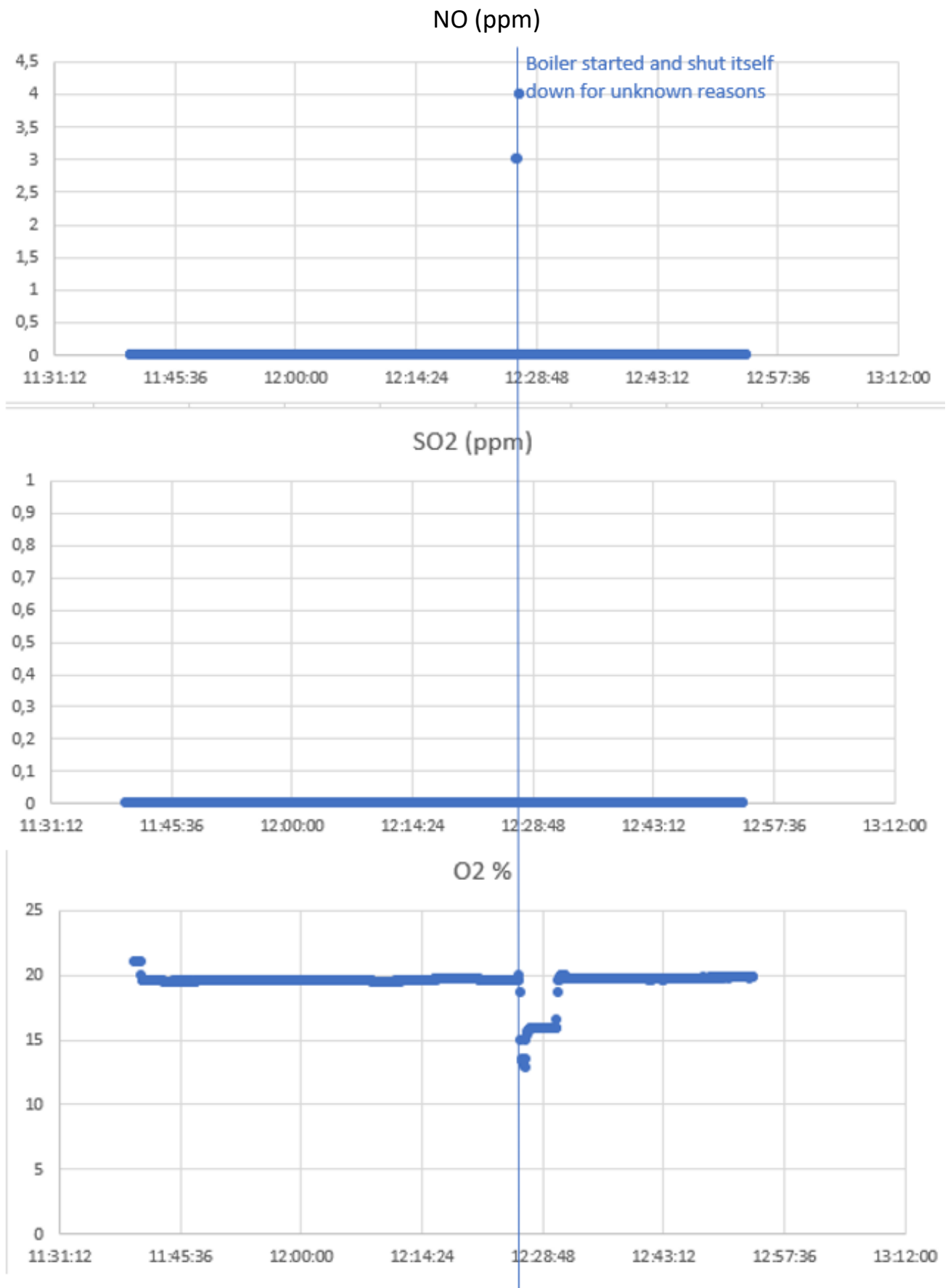


Figure 98. Field-test pollutant emissions in Huy - PEMFC only (part 2/3).

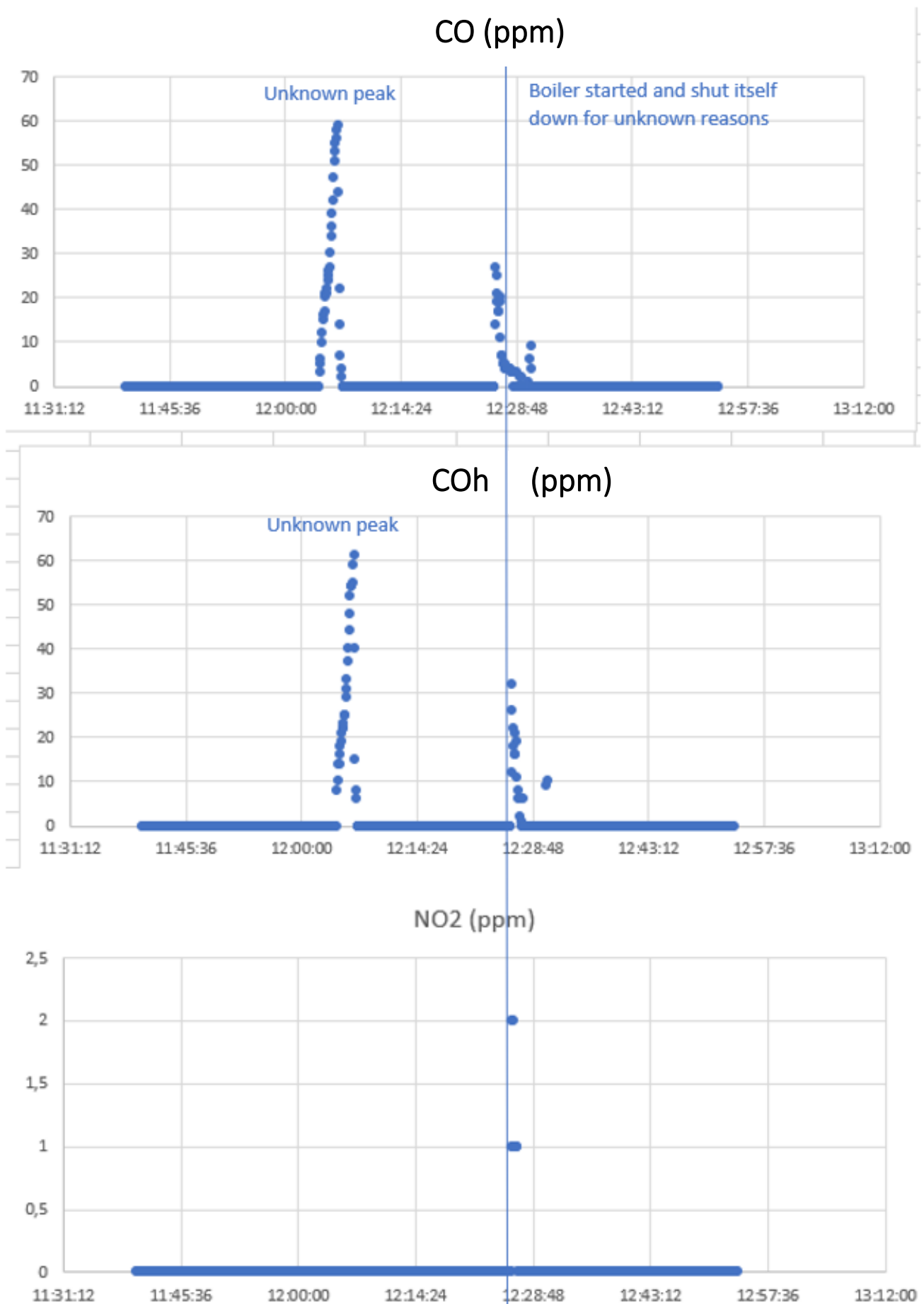
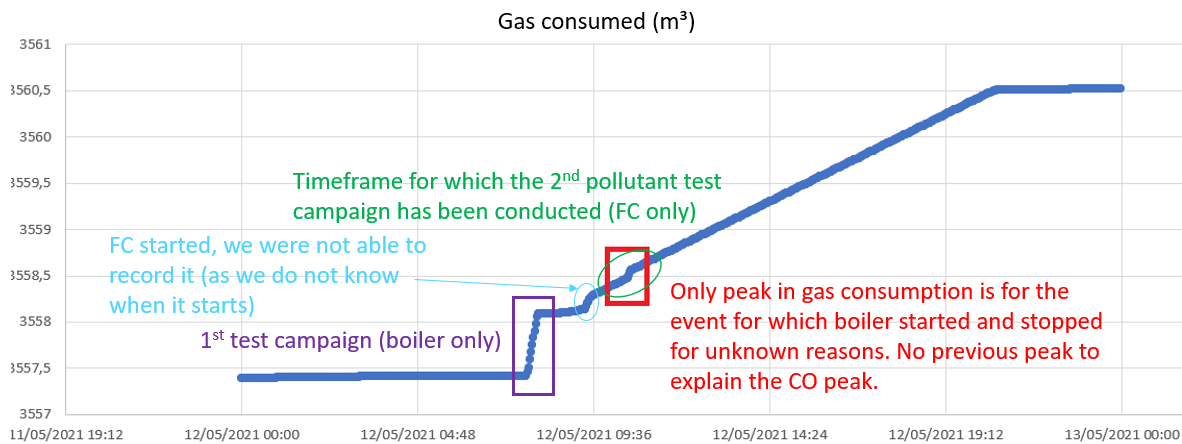


Figure 99. Field-test pollutant emissions in Huy - PEMFC only (part 3/3).



Time : clock of the data logger is offset compared to the clock of pollutant sensor

**Figure 100.** What happened on the monitored gas consumption during the field-test pollutant emissions (Huy).

### 5.6.2.2 Pollutant measurements in Oostmalle

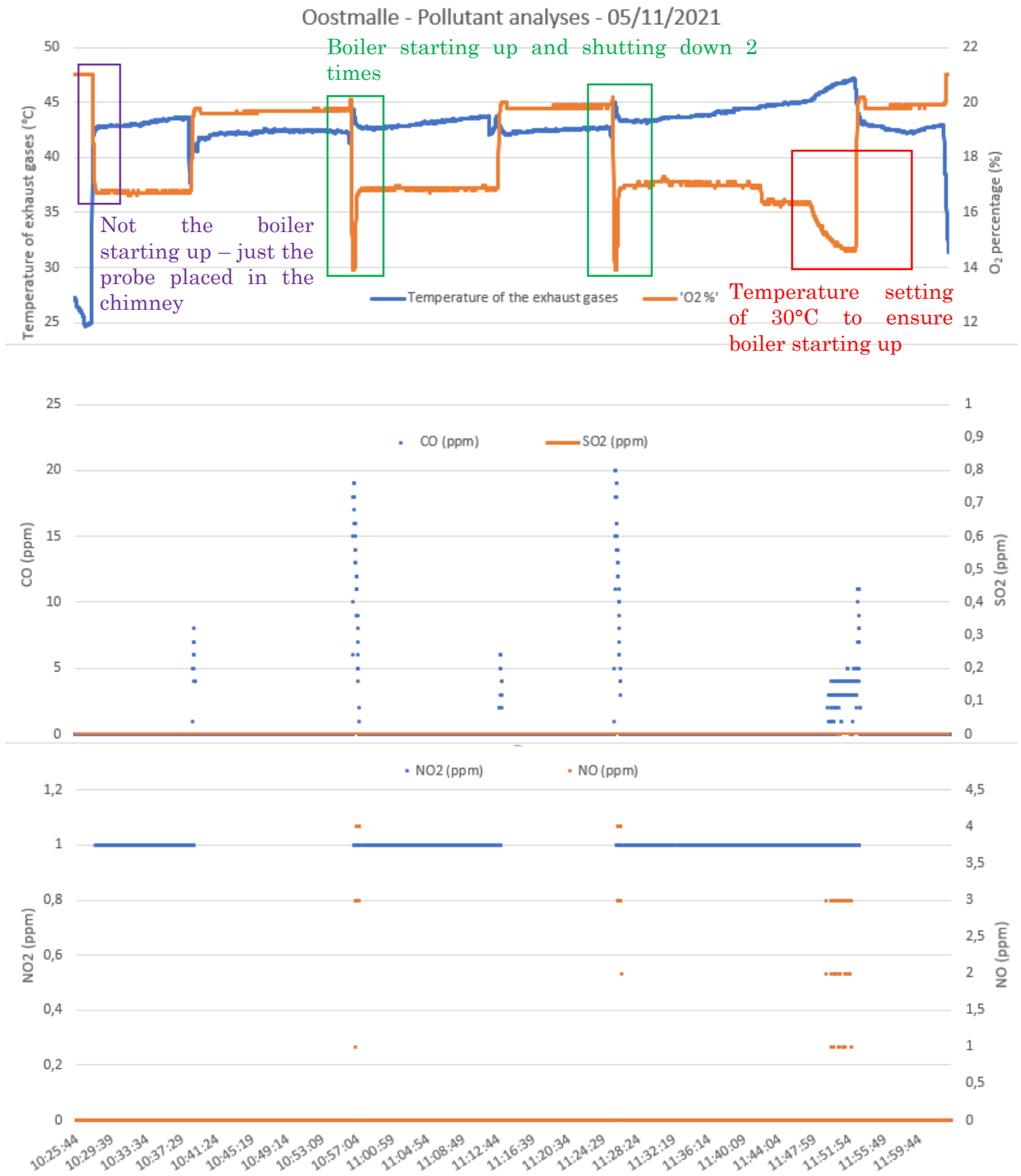
One could not access to the roof in Oostmalle for safety reasons and the probe has been installed just at the output of the system (in the chimney). The resulting graphs are presented in Figure 101. Only one test campaign could have been performed. At the beginning of the test, the PEMFC was running. During the test, the boiler happened to be turned on a few times (and the PEMFC remained always 'ON'). This 'ON/OFF' behavior of the boiler has been discussed in *Section 5.3.6 - Troubleshooting* and *APPENDIX 13: P\*2 - Laboratory troubleshooting description* (with the example of Figure 111). Towards the end of the test, the room temperature setting was increased to 30°C in order to ensure having the boiler 'ON' and ensure it reaches its nominal power.

The PEMFC only sequences (or the sequences when the boiler stopped) are easy to distinguish as the O<sub>2</sub> percentage is equal to about 20%, as it was the case for the house in Huy (Figure 98). Also, as in Huy (Figure 99), each time the boiler starts, CO peaks are visible. An interesting fact is that CO peaks are also visible when the boiler shuts down. As in Huy (Figure 99), NO peaks are visible when the boiler starts. NO<sub>2</sub> occurs only when the boiler is 'ON' (only 1 ppm in this case with both the PEMFC and the boiler turned on, whereas they were measured at 3 ppm in Huy, as shown in Figure 96). The NO<sub>2</sub> concentration with both the PEMFC and the boiler 'ON' is therefore lower than with the boiler only and that is certainly due to a higher air flow rate provided to the system (more dilution).

Again, as in all the previous pollutant tests, no SO<sub>2</sub> could be measured.

An interesting fact is that once the temperature setting has been set to 30°C in the end of the test (to ensure that the boiler reached its peak power), it can be noticed that the pollutant signals are adopting a specific behavior (different from for the other boilers starts that were not imposed to the system through the 30°C thermostat setting). This is visible for the red-boxed sequence of Figure 101 that is quite different from the green-boxed sequences.

The main assumption is that setting to the system such a high temperature demand has a significant impact on the temperature of the exhaust gases (and of the exhaust pipes), which also has a strong influence on pollutant degradation. For example, temperature is indeed a key parameter in NO conversion (see *Section 2.3.2 - SO<sub>2</sub> and NO<sub>x</sub> emission factors*).



**Figure 101.** Field-test pollutant emissions in Oostmalle. Test sequence has been detailed in the upper part of the figure.

However, literature states that CO emissions do not depend on temperature but rather on the excess of air [567]. In this case, it is likely that each change in the boiler operating conditions (internally or externally imposed) comes with a change in the signal that commands the fan of the system (and the air flow rate). It is probable that the response of the burner (combustion) does not have the same speed as the response of the inlet air flow rate (supposed to be slower) so that the ‘excess of air’ is not sufficient for a short amount of time when the boiler starts or when a prompt additional power demand is imposed. For that latter case, it is also possible that the fan is undersized for the maximum power of the system so that incomplete combustion occurs. Indeed, the red-boxed sequence with CO emissions lasts a few minutes (not only a few seconds) so that speed of response of the fan might not be the issue, as it probably was for the previous green-boxed boiler starts.

To sum up, the behavior of the Oostmalle machine regarding pollutant emissions is quite consistent with the with the one of the machine in Huy.

## 5.7 Conclusions of the chapter

Conclusions related to *Section 5.1 - Description of the machine*, *Section 5.2 - Laboratory tests*, *Section 5.3 - In-situ monitoring*, *Section 5.4 - Machine modelling* and *Section 5.5 - Comparison of laboratory and in-situ measurements* have been reported for each section in specific explicit ‘Conclusions of the section’ paragraphs.

In addition, the key contributions and findings of *Section 5.6 - Non-CO<sub>2</sub> pollutant emissions* have been summarized here below :

- CO, NO, NO<sub>2</sub> or SO<sub>2</sub> pollutants have been tested with the available sensors (see *Section 4.6.1 - Measurement devices*).
- For NO, SO<sub>2</sub>, NO<sub>2</sub>, the values are so low that they are in the lowest part of the measuring scale. Therefore, the effect of the accuracy of the sensor can be relatively important. However, one can ensure the fact that those pollutant levels are low.
- None of those pollutants were measured when only the PEMFC was running (and quite low pollution levels were observed with the boiler).
- However, an inexplicable CO peak can still occur with only the PEMFC running.
- The only main difference with the studied SOFC system (see *Section 4.6 - Non-CO<sub>2</sub> pollutant emissions*) is that this latter exhibited a few CO emissions, which is not the case for the studied PEMFC. This is probably due to the fact that the tested PEMFC was likely to involve a CO removing apparatus upstream of the fuel cell stack in the natural gas processing system (to avoid critical CO poisoning of the PEMFC) [496], as already introduced in Table 7 and confirmed in *Section 5.1.1.2 - Hydrogen processor and reforming processes*



# CHAPTER 6 RESIDENTIAL FUEL CELLS' CARBON FOOTPRINT MITIGATION POTENTIAL

In *Chapter 2 - Collective and individual GHG mitigation pathways*, *Section 2.1 - Confronting IPCC's carbon budgets to climate policies* explained how the global carbon budget from IPCC's work, expressed in CO<sub>2</sub>-only, could be established at the national or regional scale. Then, *Section 2.2 - Establishing individual carbon footprint pathways based on IPCC's carbon budgets*, pushed this further by demonstrating how those regional carbon budgets, also expressed in CO<sub>2</sub>-only, could be translated to individualized carbon footprint budgets and mitigation pathways, this time expressed in all-GHG emissions.

Aside from studying fuel cell residential CHP systems as performed in *Chapter 4 - Study of the B1\*\*\*G\*N SOFC system* and *Chapter 5 - Study of the P\*2 PEMFC system*, the aim of this thesis (and of this chapter) is to investigate their carbon footprint mitigation potential on a single individual (or household) basis. In order to do so, the individual carbon footprint calculator of the Climate and Air Walloon Agency (<https://calculateurs.awac.be/>), particularly relevant at the regional scale in Wallonia, has been used to compute an example of a typical current individual carbon footprint and evaluate the potential benefits that fuel cell micro-CHP systems could bring with their current and expected performances (as they have also been investigated in *Chapter 3 - Fuel cell technologies*). Most of the content of this section is currently under review in the *Progress in Energy* journal [328].

## 6.1 Carbon footprint calculators

The chosen individual carbon footprint calculator for this demonstration is the one from AwAC, i.e. the Climate and Air Walloon Agency (<https://calculateurs.awac.be/>). The main reason of this choice is that it has been developed by an official local agency. However, every carbon footprint calculator has its own accuracy, advantages and limitations. Usually, the more complex and long their associated survey is, the more accurate they will be, but this could be prohibitive to the many.

For example, the calculator that has been used does not consider the impact of pet animals or the fresh water consumption. Likewise, the impact of 'public services', i.e. the carbon footprint of collective public infrastructures and services (that, in a given country/region, are equivalently shared for all citizen of that country/region) is also not considered in the chosen calculator. It is noteworthy that this 'public services' footprint is the only category that is not directly related to the individual and that he cannot directly act on. The responsibility of mitigating this category of emissions purely lies with the administration and its political choices.

It is therefore advised for individuals to compute their carbon footprint with several calculators to better evaluate their sensitivity. Thus, a list of other well-known individual carbon footprint calculators has been reported here below. All those links have verified in August 2023.

<https://datagir.ademe.fr/apps/nos-gestes-climat/>

<https://www.goodplanet.org/fr/calculateurs-carbone/particulier/>

<https://www.rtbf.be/article/mobilite-energie-conso-a-combien-selevent-vos-emissions-de-co2-faites-le-test-avec-notre-calculateur-11074811>

<https://www.wwf.ch/fr/vie-durable/calculateur-d-empreinte-ecologique>

or

<https://footprint.wwf.org.uk/>

<https://www.footprintcalculator.org/home/en>

<https://www.reforestation.com/en/carbon-calculator>

<https://coolclimate.berkeley.edu/calculator>

<https://climate.selectra.com/fr/empreinte-carbone/calculer>

Users should pay specific attention to where the calculator comes from, as the assumptions behind them may depend on geography (such as the emission factors of grid electricity, for example). Similarly, the tool should preferably have been recently created or updated. Also, even if most calculators express the carbon footprint per capita in terms of all-GHG emissions (CO<sub>2eq</sub>), users should consider that it is not always the case (some calculators may express their results in CO<sub>2</sub>-only, for example).

It must also be reminded that such calculators only offer indicators and not accurate measured values. Indeed, the absolute value that results from those calculators is not exactly important. However, it is critical to monitor individual carbon footprints (regularly) as ‘raising awareness’ is the first step towards behavioral change and carbon footprint mitigation actions. For example, it has indeed been proven that energy motoring (performed regularly by the occupants) allows for the energy consumption of dwellings to be directly and significantly reduced through behavioral change [568].

In other words, the main goal of such calculators is to provide rough order of magnitudes of one’s carbon footprint and more importantly to guide users towards the most effective actions they could implement at their own individual levels to mitigate it.

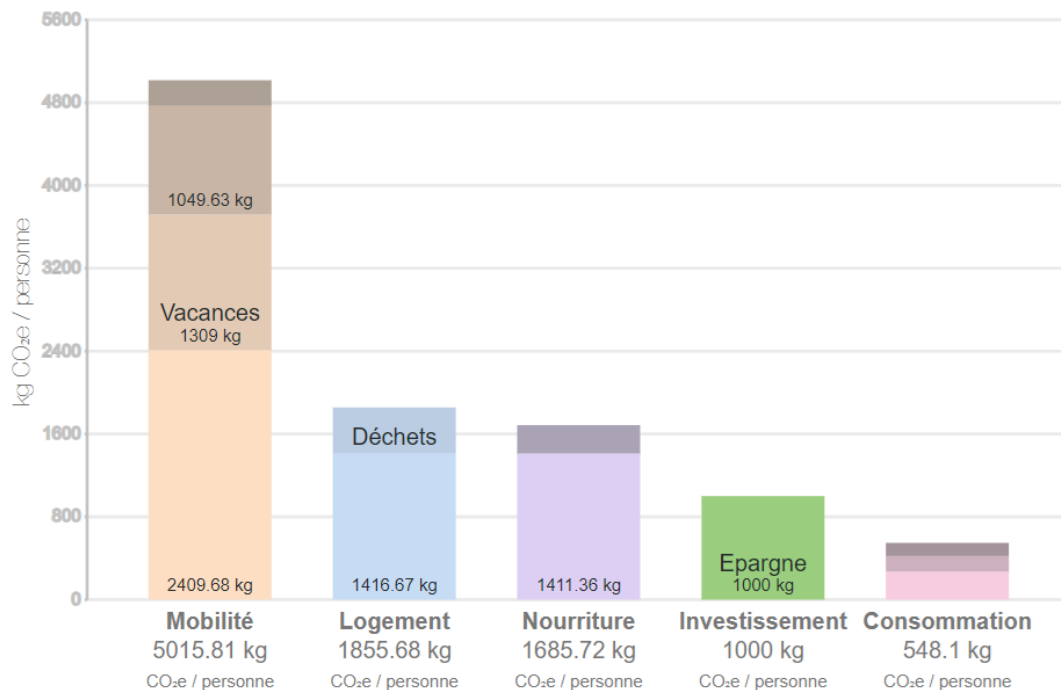
## 6.2 Individual carbon footprint example without energy uses

The main assumptions related to the chosen example of individual carbon footprint calculations are listed here below (and have been used for the simulation with the chosen calculator). Those case-dependent assumptions have been reported for reproducibility and to give examples of the level of details involved in the chosen carbon footprint calculator.

- Detached house of 200m<sup>2</sup>, 2 adults (children not considered)
- About 2.5 average garbage bags a week, including papers and cardboard, not including organic trashes
- Organic trashes thrown in an individual compost
- One small petrol car, bought second hand in 2020 and supposedly used until 2030
  - 8000 km/year for professional activities
  - 6000 km/year for personal activities
- Distance travelled by plane :
  - 7000 km for professional activities
  - 7000 km for personal vacation
- 14 meals/week (breakfasts not included): 2 red meat-based meals, 3 white meat-based meals, 1 fish-based meals, 5 vegetarian meals, 3 bread-based meat (with cheese)
- 10 drinks/week (that are not tap water)
- Groceries not specifically local but exhibiting bio labels, not frozen, packed (not bulk food), not specifically aligned with the seasons

- The dwelling possesses 2 computers, 2 smartphones (second handed, changed every 24 months), 2 TVs, 1 fridge, 1 freezer, 1 dishwasher, 1 dryer, 1 washing machine
- 20 h of HD streaming / week
- 5 pieces of new clothes / year
- 1000 € on a generic saving account

All those assumptions and the carbon footprint calculations are related to the year 2023. They are partially based upon the habits and uses of the author of this thesis. Those assumptions can be perceived as ‘average’ in the sense that they are not describing extreme cases, such as a fully vegan regime and only light-mobility uses or a fully red-meat regime along with long distances travelled with a heavy diesel car. However, it should be mentioned that those assumptions have not intended to represent the case the average Walloon, Belgian or European citizen, although it will be seen in Figure 102 and Table 42 that the resulting carbon footprint figure obtained with those assumptions (13 tCO<sub>2eq</sub>/year per capita) lies between the current average individual carbon footprint of France and Belgium, established in *Chapter 2 - Collective and individual GHG mitigation pathways* respectively to 9.2 tCO<sub>2eq</sub>/year and 16 tCO<sub>2eq</sub>/year.



**Figure 102.** Chosen example of individual carbon footprint without any energy uses considered for the dwelling (gas/electricity consumptions). The resulting total carbon footprint (without the energy uses of the dwelling) is close to 10 tCO<sub>2eq</sub>/year, way above of the 2050 individual target defined in *Chapter 2 - Collective and individual GHG mitigation pathways*. Implementing or not implementing a residential fuel cell (fed by natural gas, biogas or other climate neutral fuel) will not affect that remaining carbon footprint, so other actions should be taken to reach the 2050 carbon footprint target of 1 tCO<sub>2eq</sub>/year per capita established in *Chapter 2 - Collective and individual GHG mitigation pathways*. Indeed, for example, feeding habits and savings accounts have still have significant impacts that shall also be mitigated.

Up to this point, there was no consideration to any energy uses for the dwelling (gas/electricity consumption). Therefore, the resulting individual carbon footprint, which is given in Figure 102, is not related to the choice of the space heating appliance or the use of any cogeneration system (fuel cell-based or otherwise). In other words, it can already and trivially be stated that implementing fuel cell micro-CHPs, even fed with 100% efficiency and 100% biogas (or other climate neutral fuel) will be far from being sufficient. Other actions must be taken.

It is worth mentioning that the remaining CO<sub>2eq</sub> emissions reported for the dwelling in Figure 102 are related to the GHG emissions embodied to its construction (and that are vented onto the building's life).

### 6.3 Carbon footprint of energy uses

It has been decided to compute the carbon footprint of the average Belgian dwelling. According to the Belgian regulator [481], it corresponds to 17000 kWh<sub>th</sub> of natural gas consumption and 3500 kWh<sub>el</sub> of electrical consumption per year. With the emissions factors from Dataset 'A' and Dataset 'D1' established in Table 4 in *Chapter 2 - Collective and individual GHG mitigation pathways*, this respectively corresponds to a carbon footprint of energy uses of 5.8 tCO<sub>2eq</sub>/year and 4.9 tCO<sub>2eq</sub>/year, to be added in proportion to the number of occupants in the dwelling to the individual carbon footprint established in the previous section (and in Figure 102). This can be seen at the top of Table 42 and is from here onwards reported as the 'base scenario'. It is noteworthy that a gas condensing boiler of 90% of LHV thermal efficiency is assumed in the 'base scenario' (as it has been a common assumption all along this work).

Divided by the amount of occupants previously considered (i.e. two), those energy uses figures accounts for only about 25% of the total individual carbon footprint chosen example.

Table 42 also evaluates the carbon footprint of several 'ideal' fuel cell micro-CHP systems that would corresponds to an electrical production that would match the electrical production of the average Belgian dwelling (3500 kWh<sub>el</sub>). It also establishes the carbon footprint savings allowed by those fuel cells compared to the 'base scenario' established above. For simplicity, in all the 'ideal' cases considered in Table 42, the SOFC has been assumed fully flexible in its electrical production (to match exactly the dwelling's electrical load). This is not yet realistic as current SOFC systems have long startup times (see Table 7) so they cannot exactly be shut down (or modulated down to 0%). Nevertheless, as seen in *Chapter 4 - Study of the Bl\*\*\*G\*N SOFC system*, the modulation range of current SOFC systems is already quite large (about 33%-100%) and it could be hoped that it will even be extended in the future.

The efficiencies of the considered fuel cell systems are based on the work reported in the previous chapters of this thesis, as indicated here below :

- First case (1) : 60% and 25% LHV electrical and thermal efficiency for the current achieved performance of the SOFC technology (see Table 11 in *Chapter 4 - Study of the Bl\*\*\*G\*N SOFC system*).
- Second case (2) : 75% of expected LHV electrical efficiency for the SOFC technology seems realistic as inferred by *Section 3.2.5 - Current and expected performance of micro-CHP systems based on a PEMFC or a SOFC*. It has been assumed that this increased electrical efficiency would cause a decrease of the thermal efficiency of 5 percentage points.
- Third case (3) : same SOFC as in the second case but entirely fed by biogas (with assumed nil emission factors). The remaining heat demand of the dwelling, which should also be reduced thanks to better insulation levels (even if that is not considered in Table 42), is in any case also assumed to be provided with 'green energy' (with assumed nil emission factors).
- Fourth case (4) : similar assumptions than in the third case with a SOFC exhibiting slightly increased performance but this time, the SOFC is fed with solid biomass, i.e. dry biochar such as pinewood biochar (also with assumed nil emission factors). It would therefore be a DC-SOFC which, as explained in *Chapter 3 - Fuel cell technologies*, exhibits pure CO<sub>2</sub> at the anode exhaust and thus offers the capability of CO<sub>2</sub> capture

(and negative emissions). The maturity of DC-SOFC is however too low (see Table 7) to hope for the introduction of such systems within the timeframe of the needed energy transition. Nevertheless, its negative emissions capability might still be helpful later on no matter when the technology will emerge, as it will be demonstrated later on in this section. 80% LHV electrical efficiency is the average figure for DC-SOFC given in Table 7 (in *Chapter 3 - Fuel cell technologies*) but it is also a realistic efficiency figure often considered in the other reviewed literature [569]. For information, another reference [414] also states that the theoretical DC LHV efficiency of the electrochemical oxidation of solid carbon is close to 100% (which is, as stated in *Chapter 3 - Fuel cell technologies*, a similar theoretical figure as for methane-fed SOFCs [413]). As stated in *Chapter 3 - Fuel cell technologies*, DFAFCs (fed by formic acid) also exhibit pure CO<sub>2</sub> anode exhaust but they have not been considered in this chapter for simplicity reasons and because of their lower efficiencies (see Table 7).

Due to the poor environmental performance and the inflexible electrical production exhibited by the studied PEMFC system (see *Chapter 5 - Study of the P\*2 PEMFC system*), Table 42 does not consider the PEMFC technology. Aside simplification purposes, another reason for this lies in the low expected electrical efficiency increase of future PEMFCs compared to current values (see *Section 3.2.5 - Current and expected performance of micro-CHP systems based on a PEMFC or a SOFC*). This might be the reason why some OEMs concluded that the future of fuel cells in domestic built environment applications lies with SOFCs and have stopped PEMFC development [356], as stated in *Chapter 3 - Fuel cell technologies*. Table 42 could however be very easily reproduced for potential future flexible PEMFC systems as it only requires constant assumptions for LHV electrical and thermal efficiencies as inputs.

As in *Chapter 4 - Study of the Bl\*\*\*G\*N SOFC system*, Table 42 again shows actual carbon footprint savings of about compared to the 'base scenario' (positive values) when marginal emissions are considered. As explained in *Section 2.3.1 - CO<sub>2</sub> and CO<sub>2eq</sub> emission factors*, in Belgium in 2020 and 2021, there has always been a natural gas power plant that was functioning for electricity production. This has led to a high constant marginal emission factor of 456 gCO<sub>2eq</sub>/kWh<sub>el</sub> (i.e. Dataset 'A' in Table 4). However, compared to average grid electricity, the impact of fuel cells fed by natural gas is again prejudicial compared to the 'base scenario'. With CCGTs hopefully used less and less in the future, this again highlights the importance of flexible electrical production for future fuel cell micro-CHP systems (fortunately already partially achieved with the SOFC technology, as demonstrated in *Chapter 4 - Study of the Bl\*\*\*G\*N SOFC system*).

The carbon footprint savings due to the implementation of the ideal fuel cell micro-CHP systems on the average Belgian dwelling established in Table 42 have been reproduced graphically in Figure 103. This has been performed considering two occupants in the given dwelling, as reported in the previous section. Actually, in an average Belgian dwelling such as the one represented by the energy consumptions considered in this section, there might also be some children, but it has been chosen to report the established carbon footprint of the dwelling only on its (two) adults occupants. Figure 103 is in fact based on Figure 10 (from *Section 2.2 - Establishing individual carbon footprint pathways based on IPCC's carbon budgets*), which exhibited two pathways of mitigation of the average individual carbon footprint in Wallonia acceptable regarding IPCC's +2°C carbon budget recommendations. The initial carbon footprint chosen example (dot 'O' in Figure 103, i.e. about 13 tCO<sub>2eq</sub>/year per capita) is actually lower than the Wallonia's assumed current average individual carbon footprint, which is expected, depending on the mitigation scenario, to reach this value at least between 2025 and 2028 (see *Section 2.2.2 - Results for Wallonia : examples of sigmoidal GHG mitigation pathways*). In other words, this means that the assumptions implemented to the chosen carbon footprint calculator could

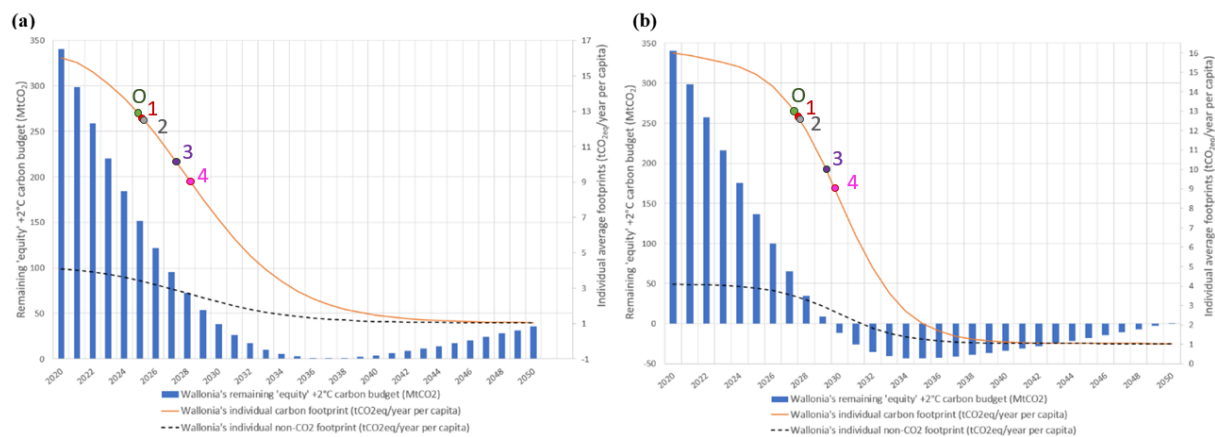
actually be considered to be a few years ahead on the GHG mitigation pathway compared to the average Belgian individual carbon footprint.

	Gas consumption emission factor (gCO <sub>2eq</sub> /kWh)	Electricity consumption emission factor (gCO <sub>2eq</sub> /kWh <sub>el</sub> )	Average gas consumption of the dwelling (kWh/year)	Average electricity consumption of the dwelling (kWh <sub>el</sub> /year)	Carbon footprint (tCO <sub>2eq</sub> /year)
Dataset 'A'	251	456	17000	3500	5,86
Dataset 'E1'	254	167	17000	3500	4,90
	Best 'current SOFC', 60% LHV electrical efficiency, 25% LHV thermal efficiency, fully flexible (1)	Best 'future SOFC', 75% LHV electrical efficiency, 20% LHV thermal efficiency, fully flexible (2)	Best 'future SOFC', 75% LHV electrical efficiency, 20% LHV thermal efficiency, fully flexible, 100% biogas (3)	Best 'future DC-SOFC', 80% LHV electrical efficiency, 15% LHV thermal efficiency, fully flexible, 100% biochar with CO <sub>2</sub> capture (4)	
FC electrical production (kWh <sub>el</sub> /year)	3500	3500	3500	3500	
Gas consumption related to the fuel cell electrical production (kWh/year)	5833	4667	4667	0	
Fuel cell heat production (kWh <sub>th</sub> /year)	1458	933	933	656	
Remaining heat demand, supposedly provided by a 90% LHV efficient gas boiler (kWh <sub>th</sub> /year)	13842	14367	14367	14644	
Total gas consumption, fuel cell and gas boiler (kWh/year)	21213	20630	20630	0	
Carbon footprint related to the gas consumption - Dataset 'A' (tCO <sub>2eq</sub> /year) - marginal emissions	5,32	5,18	0,00	0,00	
Carbon footprint related to the gas consumption - Dataset 'E1' (tCO <sub>2eq</sub> /year)	5,39	5,24	0,00	0,00	
Negative carbon footprint from CO <sub>2</sub> capture at the anode exhaust, with the assumption of 403 gCO <sub>2</sub> /kWh <sub>fuel</sub> (tCO <sub>2</sub> /year or tCO <sub>2eq</sub> /year in this case) <sup>a</sup>	N/A	N/A	N/A	1,76	
Carbon footprint savings - Dataset 'A' (tCO <sub>2eq</sub> /year) - marginal emissions	0,54	0,68	5,86 <sup>b</sup>	7,63 <sup>b</sup>	
Carbon footprint savings - Dataset 'E1' (tCO <sub>2eq</sub> /year)	-0,49	-0,34	4,90 <sup>b</sup>	6,67 <sup>b</sup>	

<sup>a</sup> Emission factor calculated for dry pinewood biochar (HHV = LHV = 24.49 MJ/kg, 59,86 % of carbon content, DC-SOFC, i.e. Direct Carbon Solid Oxide Fuel Cell, with 80% of electrical efficiency [569]).

<sup>b</sup> The carbon footprint savings are established compared to the base scenario (with current values of natural gas and electricity emissions factors). In other words, biogas introduction is only considered for the fuel cell and neither for the boiler, nor for electricity grid production (such as in CCGT power plants). The goal is to compare potential carbon footprint savings to actual levels (and not to future scenario involving greener grid gas and greener grid electricity).

**Table 42.** Yearly carbon footprint calculations of several SOFC micro-CHP systems energy uses corresponding to an average Belgian dwelling of 17000 kWh<sub>th</sub> and 3500 kWh<sub>el</sub> of gas and electricity consumption. The different cases are based on current and expected/hoped performance of fuel cell micro-CHPs. Those calculations are related to an average dwelling and are not expressed 'per capita'.



**Figure 103.** Impact of the implementation of the ideal fuel cell micro-CHP systems reported in Table 42 (for an average Belgian dwelling) on the individual carbon footprint pathways previously established in Figure 10 for Wallonia that allows for respecting IPCC's +2°C equity carbon budget. Only marginal emissions have been considered (Dataset 'A' from Table 42). Dataset 'E1' (also from Table 42) has not been used because there is no carbon footprint savings for natural gas fed fuel cells occur when average grid electricity is considered. The 'O' dot corresponds to the chosen example of initial carbon footprint, i.e. the addition of the carbon footprint without energy uses reported in Figure 102 with the carbon footprint of energy uses of the average Belgian dwelling established at the top of Table 42 divided by the number of adults occupants in the dwelling (i.e. two in this case).

Figure 103 actually again highlights the fact that, even when comparing to the electrical production of Combined Cycle Gas Turbines (CCGTs) with a high emission factor of 456  $\text{gCO}_{2\text{eq}}/\text{kWh}_{\text{el}}$ , even when considering with highly efficient future natural gas SOFCs (from dot 'O', i.e. the base scenario, to dot '1', then to dot '2', with an even more efficient future SOFC), the carbon footprint savings per capita are pretty insignificant for an average dwelling. However, carbon savings might become non negligible when 100% biogas (or other climate neutral fuel) is introduced (down to dot '3'), but that would also be the case for CCGTs (used as reference) so the benefits could actually be considered lower.

At last, negative emissions allowed by a potential efficient future DC-SOFC are not that significant compared to actual average individual carbon footprints but also not negligible, especially considering the magnitude future individual carbon footprints targets. It should be mentioning that electrification of mobility (and other uses) is likely to increase the average electricity demand of the average dwelling. Therefore, the ideal fuel cell electrical demand will likely increase far above the 3500  $\text{kWh}_{\text{el}}$  considered here, also increasing the potential negative emissions. For example, 20000 km annual distance travelled by a 20  $\text{kWh}_{\text{el}}/100 \text{ km}$  electric car would represent an additional demand to the fuel cell of 4000  $\text{kWh}_{\text{el}}$ . Added to the initial domestic demand of 3500  $\text{kWh}_{\text{el}}$ , this would lead to a 7500  $\text{kWh}_{\text{el}}$  annual electric demand to the fuel cell. Considering the DC-SOFC of the fourth scenario of Table 42 (with 80% of LHV electrical efficiency), negative emissions could reach values slightly lower than 4  $\text{tCO}_{2\text{eq}}/\text{year}$  for the dwelling (i.e. about 3.8  $\text{tCO}_{2\text{eq}}/\text{year}$ ). This corresponds to about 2  $\text{tCO}_{2\text{eq}}/\text{year}$  per capita when considering the number of adults occupants in the household or slightly higher than 1  $\text{tCO}_{2\text{eq}}/\text{year}$  per capita when considering also the current average fertility rate in Europe, i.e. 1.6 [570].

The potential negative emissions allowed by electrical production from biomass-fed DC-SOFCs can therefore be easily even higher than the recommended 2050 individual carbon footprint, which is also of about 1  $\text{tCO}_{2\text{eq}}/\text{year}$  per capita, as seen established in *Chapter 2 - Collective and individual GHG mitigation pathways*. As seen in *Section 2.1 - Confronting IPCC's carbon budgets to climate policies*, this 1  $\text{tCO}_{2\text{eq}}/\text{year}$  per capita target correspond to non- $\text{CO}_{2}$  emissions that could never be fully mitigated and achieving climate neutrality will imply similar level of (natural or technological) carbon absorption.

Technical negative emissions (with DC-SOFC fuel cells for example) will indeed be crucial in the future if natural territorial absorption levels are not sufficiently increased. Indeed, for example, achieving such level of carbon absorption with natural sinks only will be very challenging for Wallonia or France (respectively +300% and +370% increase of carbon sinks are needed vs. current levels), as reported in *Section 2.2 - Establishing individual carbon footprint pathways based on IPCC's carbon budgets*. Fortunately, it has just been demonstrated that the potential of CO<sub>2</sub> absorption of biomass-fed DC-SOFC micro-CHPs might be in that order of magnitude.

It is important to mention that those potential negative emissions would be added to the trivial benefits from the avoided fossil fuels allowed by electrification of society uses. For instance, in the case of the individual carbon footprint example demonstrated in Figure 102, the 'green' electrification of the personal petrol car represents an important GHG mitigation step of about 2.5 tCO<sub>2eq</sub>/year (thanks to avoided fossil fuels use).

Similarly to previous calculations see (*Section 4.3 - In-situ monitoring*), the electrical transportation and distribution losses (which can reach about 6-7% in EU [130]) that are avoided with decentralized electrical production from micro-CHP systems have not considered in this chapter.

## 6.4 Conclusion of the chapter

This chapter has shown that the environmental benefits of natural gas-fed fuel cell micro-CHPs compared to the total average individual carbon footprint is at best quite limited for an average Belgian dwelling, even with 'ideal' future efficiencies. Carbon footprint savings of about 0.5 tCO<sub>2eq</sub>/year have indeed been established in this chapter for an average dwelling (compared to a current average individual carbon footprint that is way higher, i.e. to about 16.5 tCO<sub>2eq</sub>/year, as considered in *Section 2.2 - Establishing individual carbon footprint pathways based on IPCC's carbon budgets*). Those savings only occur when comparing to current electricity marginal emissions (with a quite high emission factor of 456 tCO<sub>2eq</sub>/kWh<sub>el</sub>, corresponding to CCGT power plants). Although this marginal emission factor assumption is valid in Belgium for the whole years 2020 and 2021 (see *Section 2.3.1 - CO<sub>2</sub> and CO<sub>2eq</sub> emission factors*), it is likely to be reduced from at some point in the future with less and less CCGT utilization on the grid (for the sake of the energy transition). This would even reduce the already small carbon footprint savings of natural gas-fed micro-CHPs.

In addition, as already demonstrated in *Chapter 4 - Study of the Bl\*\*\*G\*N SOFC system* and *Chapter 5 - Study of the P\*2 PEMFC system*, it has again been shown in this chapter that even 'ideal' fuel cell micro-CHPs cannot compete environmentally with current grid electricity. Furthermore, this average grid electricity should also even become greener every day.

Therefore, other GHG mitigation measures shall absolutely be taken. For example, 100% biogas (and/or other fully green energies), with the potential help of increased insulation levels, would increase the carbon footprint savings to about 5 tCO<sub>2eq</sub>/year for the average dwelling, i.e. 10 times higher than the ones allowed by the implementation of natural gas fed 'ideal' SOFC micro-CHPs reported just here above. The electrification of personal cars have also a tremendous potential evaluated to 2.5 tCO<sub>2eq</sub>/year for the chosen example (additional savings allowed by reduction of fossil fuel use). Again, this will still not be enough and (non-technological) behaviour changes are mandatory: for instance, as demonstrated in the carbon footprint example of Figure 102, feeding habits and saving accounts have also significant impacts that shall also be mitigated.

However, fuel cell CHP technologies can offer the capability of easy CO<sub>2</sub> capture at the anode exhaust. Indeed, as stated in *Chapter 3 - Fuel cell technologies*, pure CO<sub>2</sub> is the only



---

fuel cell reaction product at the anode of DFAFCs (fed by formic acid, preferably used as a 'green' 'e-fuel') and at the anode of the more efficient DC-SOFCs (fed by solid carbon, preferably biomass). Therefore, negative emissions have been considered in this chapter for the example of such (efficient) future DC-SOFC micro-CHPs sized based upon the electric demand of the average Belgian dwelling. Oversizing the DC-SOFC to also meet future electrification needs (increased electrical production and increased negative emissions potential), it has been demonstrated that those negative emissions can easily reach about 4 tCO<sub>2eq</sub>/year for an average Belgian dwelling including only one electric car, which corresponds to slightly more than 2 tCO<sub>2eq</sub>/year per capita for the considered dwelling with two (adults) occupants and the average current fertility rate in Europe. That exact level of negative emissions per capita will in fact always be the minimum needed for climate neutrality to be reached, as established in *Chapter 2 - Collective and individual GHG mitigation pathways*. Even if that should preferably be performed through natural sinks, exceeding the carbon budget recommended by IPCC's (see *Section 2.1.1 - Carbon budgets background information*) is a risk that cannot be taken and the negative emissions potential of such fuel cell micro-CHPs offer much hope in that regard.

## CHAPTER 7 PERSPECTIVES

### 7.1 Summary of key findings and contributions

Key findings and contributions have been specified according to the chapter they are related to in the following list. Aside from key results and findings, main contributions have been written in **bold characters**.

#### 7.1.1 Chapter 1 – Introduction

N/A

#### 7.1.2 Chapter 2 – Collective and individual GHG mitigation pathways

- Some of the **main limitations of current Nationally Determined Contributions (NDCs)** for France and Wallonia climate strategies **have been established**, which are likely to be applicable to similar NDCs of other countries (unrealistic linear GHG mitigation pathways are assumed, mainly long term GHG reduction targets, difficulty for the population to relate to objectives set at the community level, no target on imported emissions, no direct link with IPCC's carbon budgets).
- Even the projected territorial emissions only will exceed IPCC +1.5°C AR6 2020 equity carbon budgets (according to France and Wallonia current NDCs).
- France can respect IPCC's +2°C equity carbon budget if the GHG reduction effort to be made on imported emissions reach at least the same extent as the one projected on the territorial emissions (according to the current NDC). Projected territorial emissions in Wallonia according to their current NDC leave absolutely no room for imported emissions in the +2°C equity carbon budget so it must commit to more ambitious GHG reduction targets (both territorially and, as there is currently none, regarding imported emissions).
- The **method established** in this work **to evaluate the compatibility of the studied NDCs with IPCC's carbon budgets** can also be easily reproduced for other regions/nations.
- To solve some of the common NDC issues reported here above, **an innovative method** then has been established **to set individual carbon footprint pathways compatible with IPCC's carbon budgets**. The difficulty lied in **linking IPCC's carbon budgets, expressed in CO<sub>2</sub>-only**, i.e. expressed only in terms of long-lived climate pollutants, **to all-GHG carbon footprint, expressed in CO<sub>2eq</sub>**, i.e. expressed in both long and short-lived climate pollutants.
- One of the advantages of this method is that **individual carbon footprint calculators can thus be used** to verify if one's carbon footprint is correctly following the targeted pathway and, if necessary, to easily reset new compatible objective pathways. Through those individualized objectives, it is hoped that individuals could better relate to IPCC's global carbon budgets.
- The **proposed pathway** (which can be changed) is **based on an 'S-curve' pattern**, that **allows for considering 'inertia' and 'asymptotic' effects in the implementation of new (renewable) technologies**.
- At net-zero CO<sub>2</sub> emissions levels, some non-CO<sub>2</sub> GHG will not be completely mitigated and will account for about 1 tCO<sub>2eq</sub>/year per capita, which this work has thus considered as the 2050 individual carbon footprint target.

- Carbon neutrality implies thus at least a territorial absorption (naturally and/or technologically-based) at least equivalent to that 1 tCO<sub>2eq</sub>/year per capita carbon footprint. For France and Wallonia, this represents respectively +370% and +300% increases compared to current (natural) carbon sinks assumed levels. Considering technological carbon absorption too risky at this stage, it has been demonstrated that such levels of natural sinks could only be reached by rethinking land-use in every single area of the territory (intensive urban vegetation such as green roofs, alternative agricultural techniques such as permaculture, intensification of the vegetation on residential lawns, *etc*).
- For Wallonia, unlike France, the initial (current) carbon footprint is so high that the carbon emissions budget is ‘consumed’ very early in the 2020-2050 timeframe. Therefore, scenarios compatible with IPCC’s +2°C carbon budget show that, even with strong and rapid GHG reduction, CO<sub>2</sub> neutrality would have to be reached at least 10 years before the 2050 climate-neutral European Green Deal commitment. This emphasizes the significance of the effort that will have to be made.
- A **literature review on emissions factors for energy consumption** has also been reported (for CO<sub>2</sub>, CO<sub>2eq</sub>, NO<sub>x</sub>, SO<sub>x</sub>), mainly for Belgium.
- It has been reported that methane slip (i.e. methane emissions) from PEMFCs and SOFCs fed by natural gas can be considered negligible.
- **CO, NO<sub>x</sub> and SO<sub>x</sub> harmful effects on human health and environments** have also been reported from a review of literature.

### 7.1.3 Chapter 3 – Fuel cell technologies and residential applications

- Electrochemical oxidation of species other than hydrogen are common in fuel cells, such as carbon in DC-SOFCs, CH<sub>4</sub> and/or CO in methane-fed SOFCs, ammonia in DAFCs, *etc*... Partly because of the many types of fuel that can be processed (directly or indirectly) by fuel cells, a tremendous amount of **fuel cell types** exists and most of them have been reported in an **innovative identification key** proposed in this work (Figure 18), which is based on the charge carrier. In that identification key as well as in most relevant literature, the ‘Direct’ appellation in the fuel cell acronym means a ‘direct’ utilization of the fuel at the anode of the stack, i.e. not processed indirectly, prior to the fuel cell stack (either inside or outside of the fuel cell embodiment). This fuel can either participate directly in the electrochemical oxidation occurring in the fuel cell or it can also be decomposed onto the anode in another fuel type (that participates in the fuel cell electrochemical reaction). In fact, the proposed identification key does not consider indirect decomposition of fuels (only direct utilization or decomposition, as it has just been defined here above).
- An **extensive review of the main fuel cell types has been performed to their characteristics could be compared** (see Table 7). It highlighted that DC-SOFCs and DAFCs are fuel cell types that exhibit a potential pure CO<sub>2</sub> off-anode stream that could facilitate CO<sub>2</sub> capture and offer the possibility of negative emissions (if fed by carbon neutral fuels).
- Although attempts have been numerous, a **dedicated literature review on HT-PEMFCs CHP manufacturers** performed in this work has reported that there is still no successful commercial applications of this technology on the market.
- Another **dedicated review on future expected performance of fuel cells** indicates that the maximum expected LHV electrical efficiency of methane-fed LT-PEMFCs and HT-PEMFCs is respectively about 40% and 45%, which are quite close figures compared to current performance. On the other hand, methane-fed SOFCs already exist with up to 65% LHV electrical efficiency (AC) or 75% LHV electrical gross efficiency (DC). Theoretical electrochemical oxidation of methane or carbon in a SOFC

is close to 100% so is not unrealistic to hope for SOFC-based micro-CHP systems with LHV electrical efficiencies of 70%-80% (AC) or even more in a mid-term future.

#### 7.1.4 Chapter 4 – Study of the BI\*\*\*G\*N SOFC system

- **Reverse engineering and SOFC literature reviews** have allowed for establishing the most probable **internal scheme and working principle of the system** (see Figure 31). The main difference compared to schematics reported in literature is that water impurities (from the water main connection required for steam reforming purposes) are processed through several filters involving reverse osmosis. It is believed that, at a certain point, the water impurities concentration in the inlet water volume becomes too high compared to the pressure used for the reverse osmosis. Thus, the remaining inlet water (with high levels of impurities) has to be thrown away through a specific water outlet, for another periodical grid fresh water withdrawal from the mains to take place (and to be submitted to the reverse osmosis filter).
- **A simplified, cheap and reproducible space heating appliance test bench** that allows for controlling (varying) and stabilizing both the return temperature and the space heating flow rate has been **designed, built and reported**. It is mainly based on a thermostatic three-way valve that partially bypass a high-capacity dissipating heat exchanger.
- Laboratory tests of the tested SOFC resulted in electrical power outputs tremendously stable and corresponding to the output power settings. This leads to very stable electrical efficiencies.
- The electrical efficiency (and power output) has been found not altered at all by changes in working temperature of the heat recovery circuit (nor by change in heat recovery flow rate). Thermal efficiency is almost not altered by the heat recovery flow rate in the tested range but is affected quite linearly by the working temperature of the heat recovery circuit. Thermal efficiency decreases as working temperature increases.
- It has been found that modulating the electrical power output in the 66-100% range gives similar electrical and total efficiency results. However, lowering the electrical power output down to its lowest, i.e. 33%, reduces mainly the electrical efficiency, which is not balanced by the increase of the thermal efficiency, meaning that the total efficiency is decreased.
- Based on experimental results, **non-dimensional simple polynomial and exponential performance models** (exhibiting sufficient goodness of fit) are **proposed respectively for thermal and electrical efficiency of such SOFC systems**. They could easily be used in building performance simulation and/or energy planning tools.
- The 2021 field-test monitoring study has demonstrated the announced 60% LHV electrical efficiency of the tested residential SOFC micro-CHP system in a real application (at least for one of the two field-tested SOFCs, the other coming close to that figure probably because of ageing, because of the intrinsic variance between manufactured products and because it has been functioning at partial load on the studied timeframe).
- Demonstrated LHV thermal efficiency in the field-test is not higher than 12-15%, mainly because the heat recovery is mostly used for DHW production (at high delivery temperature). However, the amount of heat still recovered has been proven to be quite significant and sufficient, for example, to cover DHW demand of the average USA household (backup heating appliance is still advised to ensure sufficient delivery temperature at all times).
- Field-test yearly resulting energy utilization costs savings (not considering the impact of the Ukraine-Russia conflict on the energy prices) are significant and at about 1.3 -

1.4 k€/year (for 2021 Belgian energy prices assumptions). This figure has been achieved thanks to a quite high monitored supply cover factor of about 60% for each household (mainly allowed thanks to one electric car). Potential dynamic day-ahead tariffication could even improve those energy utilization cost savings.

- From an environmental point of view, two considerations could be made: compared to the actual Belgian consumption mix, the CO<sub>2eq</sub> balance is way negative because of the intrinsic use of natural gas (that remains a fossil fuel). However, the system has intrinsically better efficiencies than CCGT power plants and its power output can be modulated from distance. Therefore, it can partially be considered that this system allows for decreasing the electrical demand on centralized CCGT power plants. This marginal emissions consideration changes totally the CO<sub>2eq</sub> balances that become highly beneficial. This has been thoroughly demonstrated through the field-test study.
- All the results of the laboratory and field-test studies performed in this work are consistent with the manufacturer announced targets and correlate. This allows for assuming that, even in real field-test applications, the system is robust and behave as intended.
- CO, NO, NO<sub>2</sub> or SO<sub>2</sub> pollutants have been tested with the available sensors (see *Section 4.6.1 - Measurement devices*). CO is the only pollutant that could be measured. It has been found that the max CO concentration is obtained at intermediate output electrical power (1000 W<sub>el</sub>) and is about 11 ppm (still a quite low value).
- Since CO can act as a fuel for SOFC, this fact even leaves room for improvement of the electrical efficiency of the system, which might therefore get closer the expected performance of SOFC technologies (reported earlier, in *Chapter 3 - Fuel cell technologies and their residential applications*).
- At last, it has been found that the optional heat recovery circuit (and its working temperature) has no influence on the pollutant emissions.

### 7.1.5 Chapter 5 – Study the P\*2 PEMFC system

- **Reverse engineering and PEMFC literature reviews** have allowed for establishing the most probable **internal scheme and working principle of the system** (see Figure 74). The main difference compared to schematics reported in literature lies in the ‘anode pre-treatment unit’, shown in Figure 74, that most likely includes an ammonia remover (to prevent ammonia poisoning of the stack). However, most likely for simplicity, this ammonia remover is placed after the fuel processor (hydrogen production processes) and it does not prevent ammonia poisoning of some of its catalysts. Concurrently, this literature review has also **allowed for explaining the most probable reason for the shutdown 2.5-hour shutdown regeneration phase required for the studied PEMFC** system every 48 hours of PEMFC functioning. In fact, it has been established that it is most likely implemented to create a ‘reductive atmosphere’ (with high hydrogen and low air proportions) and remove this ammonia poisoning of the hydrogen processor’s catalyst(s). *APPENDIX 14: Literature review on PEMFC degradation mechanisms* contains additional details about this process.
- Due to the complexity of the hybridization of the studied PEMFC with its embodied gas condensing boiler and DHW buffer tank, it has not been easy to isolate the thermal performance of the fuel cell only. By modelling the DHW tank quite simply with only two temperature measurements (one at the top and one at the bottom), **an innovative method has been proposed to reduce the uncertainty level induced by the unknown state of the DHW tank**. However, it has been considered **not sufficiently accurate** as resulting PEMFC thermal efficiencies were almost 25 percentage points lower than the manufacturer’s announced values. The significant difference is probably due to the lack of information regarding the water flow in the cooling circuit

of the fuel cell loop. The proposed method can surely be improved, as it will be reported in the following section.

- The field-test systems exhibited poor yearly measured total LHV efficiencies that are lower or at least not sufficiently higher than the reference gas condensing boiler efficiency of 90% (as it is the efficiency assumption of nationally and internationally recognized organizations).
- Field-test resulting economical balances are likely to impede achieving ROI under 10 years (only up to about 450 €/year of savings and even small losses for one field-test house over one of the monitoring years).
- The utilization CO<sub>2</sub> savings of the field-tested machines are quite affected by the efficiency of the boiler within the system, which can in fact greatly vary from one household to the next, depending on the heat demands. Nevertheless, the utilization CO<sub>2</sub> savings of the monitored systems are at best quite insignificant and, for one of the monitored dwellings, negatives, even when compared to current marginal emissions in Belgium (represented by a constant use of highly emitting CCGTs).
- The poor exhibited PEMFC load factor (always under 50% for both field-tested houses) has a significant influence on the poor economical and ecological performance. **This work has reported some indications that points towards the complexity of the hybridization** (and of its control) between the PEMFC and the gas boiler, which **prevents them to operate in the optimized conditions they could have met as standalones units** (return temperature of the system suddenly too high and the PEMFC has to be shut down for safety reasons). *APPENDIX 12: P\*2 behavior and how it affects efficiency: zooming on representative days* contains additional details about the potential unoptimized operating conditions occurring when both the gas boiler and the PEMFC system are turned on in the studied micro-CHP embodiment. This allows for assuming that the current system is not sufficiently robust and does not behave as intended in certain real field-test applications.
- Based on announced optimal electrical performance, it has been established that the same PEMFC stack as the one studied, but working as a standalone unit, should exhibit a LHV thermal efficiency at least of 30% to start being environmentally beneficial when compared to current Belgian marginal emissions (represented by a constant use of highly emitting CCGTs). However, again compared to CCGTs, it would still not be able to modulate its power output and would still offer electrical efficiencies almost 20 percentage points lower. Even with high thermal LHV efficiencies (that should still be demonstrated in field-test applications), it can be considered that a heat pump fed by future low CO<sub>2</sub> electricity would always offer better performance (with the additional possibility of thermal storage to avoid the peak electricity demands that would maybe still require the highly emitting CCGTs).
- Based on experimental results, **non-dimensional simple polynomial and exponential daily and monthly performance models** (exhibiting sufficient goodness of fit) are **proposed respectively for thermal and electrical efficiency of such PEMFC-gas boiler hybrid systems**. They could easily be used in building performance simulation and/or energy planning tools.
- To compute the most accurate of those performance models, **an innovative and reproducible modelling method considering two correction factors ( $\gamma_1$  and  $\gamma_2$ )**, inspired by gas condensing boiler literature, **has been established and reported**. The first one accounts for the decrease of thermal efficiency related to increased working temperatures. This first correction factor has been established by computing the maximum 4-hour gliding average space heating temperature of each day. The second one accounts for the decrease of efficiency related to unsmooth heat demands. This second correction factor has been established by computing the daily standard variation of the space return temperature.

- As a first approach, electrical efficiency has been assumed to be linearly inversely proportional to the thermal efficiency so the whole system efficiencies could be estimated simply by modelling the thermal efficiency.
- A correlation between the field-test models and the laboratory steady-state results for this PEMFC-gas condensing boiler hybrid is proposed and demonstrated. It has mainly exhibited that a penalty of about 10 kWh, which is equivalent to the amount of thermal energy that can be stored in the 220 L tank of the system, should be applied on the steady-state laboratory results to account for its unconsidered standby thermal losses. This 10 kWh is an indication of the daily stand-by losses with this system in real applications (with daily DHW scheduling).
- CO, NO, NO<sub>2</sub> or SO<sub>2</sub> pollutants have been tested with the available sensors (see *Section 4.6.1 - Measurement devices*). For NO, SO<sub>2</sub>, NO<sub>2</sub>, the values are so low or even nil that they are in the lowest part of the measuring scale. So, one can ensure the fact that those pollutant levels are very low. For the PEMFC only, none the tested pollutants were measured (except for an inexplicable CO sudden peak) which constitutes a small difference compared to the previously tested SOFC system (that exhibited small constant CO emissions. This is probably due to the fact that LT-PEMFCs require a CO remover in their fuel processor.

#### 7.1.6 Chapter 6 – Residential fuel cells’ carbon footprint mitigation potential

- This chapter answers the main research questions of this thesis. It has shown that the environmental benefits of natural gas-fed fuel cell micro-CHPs compared to the total average individual carbon footprint is at best quite limited for an average Belgian dwelling, even with ‘ideal’ future fuel cell efficiencies, even when compared to current Belgian marginal emissions (represented by a constant use of highly emitting CCGTs). Even if their fuel is decarbonized, their mitigation potential would still be way insufficient, and other actions, including behavioural changes would still have to be implemented.
- However, since some fuel cell technologies, such as Direct Carbon Solid Oxide Fuel Cells (DC-SOFCs) or Direct Formic Acid Fuel Cells (DFAFCs) offer the capability of facilitating pure CO<sub>2</sub> capture at their anode exhaust, they could allow for potential negative emissions. With the case study of an average Belgian dwelling’s electrical demand and the use of an electric car (for about 20000 km/year) provided by a DC-SOFC with an electrical LHV efficiency of 80% fed by biomass, **this thesis demonstrated that the negative emissions potential of such fuel cell systems could be up to about 4 MtCO<sub>2eq</sub>/year (for the considered dwelling)**. This figure is in the same order of magnitude as the minimal carbon absorption level implied by the carbon neutrality target (reported in earlier, in *Chapter 2 - Collective and individual GHG mitigation pathways*), even with gross greenhouse gases emissions mitigated to their minimum (which will never reach zero according to IPCC’s AR6). Since this carbon absorption will unlikely rely only on natural sinks in populated western countries (as also reported earlier, in Chapter 2), **this thesis infers that those kinds of negative emissions potential of such fuel cell systems shall absolutely be further developed and implemented.**

#### 7.1.7 Chapter 7 – Perspectives and further works

N/A

## 7.1.8 Chapter 8 – Conclusions

N/A

## 7.1.9 Appendixes

- **An innovative method for converting natural gas HHV provided in standard conditions of pressure and temperature to real onsite conditions** has been established and reported in *APPENDIX 1*.
- **Conversion equations from ppm to mg/kWh of SO<sub>x</sub>, NO<sub>x</sub> and CO pollutant emissions from natural gas appliances** have been reported from a **dedicated literature review** in *APPENDIX 8*.
- **A literature review on PEMFC reversible degradations mechanisms and corresponding recovery methods** has been reported in *APPENDIX 14*.



## 7.2 Discussion, limitations & further works

- Carbon budgets are reduced continuously as long as GHG emissions are not stopped. Therefore, some inferences conducted in *Chapter 2 - Collective and individual GHG mitigation pathways* (such as the proposed GHG mitigation pathways) have a limited period of validity close to the year 2020 (year of reference for IPCC's carbon budget). For example, in 2030 (or even sooner), updated (lower) carbon budgets and updated NDCs will have to be analysed, probably leading to other required GHG reduction pathway (that would surely be even more constraining if the emissions are not reduced expectedly in the years to come). Fortunately, the methods developed in this work are easily reproducible.
- Although individualized carbon footprint pathways (relevant with IPCC's carbon budgets) developed in this work are compatible with carbon footprint calculators, this remains to be implemented. Alternatively, a new carbon footprint calculator featuring such carbon footprint pathways could be developed. Additionally, the use of forcing-equivalent potential of GHG varying over time (to consider the future warming impact of short-lived climate pollutants, i.e. SLCPs) instead of traditional 'absolute' GWP in carbon budgets and carbon footprints would be more accurate and constitutes an opportunity that could directly be implemented at the carbon footprint calculator level.
- The proposed individual carbon footprint pathways are not perfect, mainly because one's capability of mitigating its GHG emissions can be quite different to one another's and because there is no scientific consensus on the method of calculating carbon footprint. However, one of the aims of this work is for everyone to relate to the order of magnitude that individual carbon footprint shall reach both on short-term and long-term basis and the goal is not to focus on absolute (and uncertain) carbon footprint values.
- The fuel used for the experimental investigation was always natural gas from the grid (with a quite constant composition). 'Future' fuels, such as biogas or syngas (with varying hydrogen proportions), have not been tested, which constitutes potential future works related to this thesis.
- The tested SOFC has been reported to be flexible. Although its modulated electrical production has been studied, its response time to varying electrical demand has not and this constitutes another improvement to this work.
- As stated in the previous section, although innovative, the method established in the laboratory to evaluate the thermal efficiency of the PEMFC only in the tested hybrid system though the modelling of the DHW thanks to two temperatures measurements was not sufficiently accurate. Those tests could have been performed with the 'PA\*' system, which involved the same PEMFC as the tested hybrid system but working as a standalone unit. Alternately, an attempt could be performed in modelling the water flow in the cooling circuit of the fuel cell loop and/or improving the DHW tank model (and not only divide the tank in two equal volumes each represented by an homogenous temperature). For example, time varying thermocline of the DHW tank could be modelled as well as its standby thermal losses.
- The strongest limitation of the field-test work (and even of the laboratory tests) reported in the thesis is that it is highly case dependent. Indeed, considering only two/three machines of each studied systems does not allow for drawing statistical conclusions on the system's performance (especially for the economical ones, that are affected by the supply cover factor specific to the household). The results developed here shall thus mainly be considered as case studies and caution should specifically be exercised if generalization of the results obtained for those tested machines were to be applied to other similar systems or technologies. This should particularly be considered when the monitored systems exhibit poor performance, far from their announced

targets (as it is the case for the field-tested PEMFCs studied in this work). This is why this thesis has also investigated the performance of ideal PEMFC micro-CHP systems (such as the one constituted by the same PEMFC stack as the tested hybrid system, but working as a standalone unit).

- The whole LCA of the respective fuel cells could be included in the performed ecological balances (thus not only considering the CO<sub>2</sub>/CO<sub>2eq</sub> utilization savings). Therefore, the emissions associated to their manufacturing and disposal shall be investigated and more information about their life expectancy shall be gathered.
- Utilization costs savings established in this work are mainly valid for current residential energy tariffications in Belgium. Firstly, others countries do not necessarily adopt the same energy pricing strategies and secondly, even in Belgium, those evolve in time. For example, with smart meters progressively included on the market, fixed tariffs are bound to disappear to lead people to change their consumption behaviour according to the availability of renewables on the grid. This highlights the importance of flexible modulating fuel cell micro-CHP systems (such as the tested SOFC).
- Internal components modelling of the tested systems has not been attempted. It could be interesting to do so and compare them to the 'black-box' performance models developed in this work. This could offer the possibility of validating the proposed most probable schematics (and working principles) reported in this work and understand better how they are controlled and how they might be improved.
- This study only demonstrates the high potential of negative emissions represented by DC-SOFC (which exhibit a significantly higher potential in terms of electrical efficiency than DFAFCs) technologies as micro-CHP systems but it does not investigate in details the remaining challenges that prevent those to be implemented on the market. Also, for these DC-SOFCs, those potential negative emissions have been related to an average Belgian household and to one type of biochar fuel, i.e. dried pinewood. Therefore, this potential is not applicable to any household nor any other biochar fuel as-is. However, **the method developed** in this work to **estimate the negative emission potential of the fuel cell micro-CHP system** is easily **reproducible**.
- Concurrently, generalizing this negative emission potential to a large number of households should be exercised with caution. For example, discarding the possible prohibitive costs of the technology, it should beforehand be verified that the capacity in terms of manufacturing materials and fuel availability will be sufficient. In addition, complete LCA (again) but also social and biodiversity studies of those systems shall be investigated to be sure not to generate other problems by focusing only on climate change mitigation.
- Another possibly interesting feature of fuel cell systems lies in their potential reversibility. Associated with high level of highly fluctuating renewables, some fuel cells technologies can also be used as electrolyzers and could consume the extra electricity available on the grid to create a 'decarbonized' 'e-fuel'. This study has not considered this additional potential that is surely worth investigating.
- Hybridization of fuel cell micro-CHPs with other appliances, such as heat pumps, have not been considered in this work. Yet, using the electrical production of the fuel cell to generate extra heat with a modulating heat pump could be a versatile and efficient way to provide various electrical and thermal efficiencies, that could optimally be modulated according to the considered application (or to the varying weather conditions).
- At last, several building performance simulation and energy planning tools exist that could easily use the performance models developed in this thesis (or dedicated derivative models of biofueled DC-SOFCs or DFAFCs with negative emissions capabilities). For example, in Wallonia alone, several of those tools have been

developed by other teams of researchers, such as *ProCEBaR* or *Energyscope* ('*TD*' or '*Pathway*').

*ProCEBaR* is tool developed by the Thermodynamic laboratory of ULiege that models the whole Belgian building stock and evaluates its energy demands. It has been designed to evaluate the impact of implementing new energy production appliances in buildings (that are also modelled). It exists in different version as it has been associated with buildings renovation rate (more insulation and lower heat demands over time), global warming (higher cooling demands and, again, lower heat demands over time), *etc...* Depending on the constraints that are set, the tool can establish the maximum penetration rate of a technology. For example, not all buildings are suitable for the implementation of a natural gas-fed CHP system as all buildings are not connected to the natural gas grid. Provided with emission factors, it can also establish the associated CO<sub>2</sub> emissions of the whole studied building stock. This tool can indeed be particularly useful to evaluate the potential CO<sub>2</sub> savings that fuel cell micro-CHPs could bring to the whole representative Belgian building stock. This tool is not yet equipped with constraints relative to energy storage, investments costs or mitigation pathways (such as an imposed carbon budget over a certain timeframe). The amounts of emissions are indeed an output of the tool and not an input. Also, oppositely to energy planning tools, it does not provide information about which power plant shall be activated and when to meet the daily demand profiles (even though those demands can be established with the tool on a quarter-hourly basis). At last, it does not consider other energy uses (such as mobility). Examples of studies using the *ProCEBaR* tool are numerous [571–573].

*Energyscope TD* is an energy planning tool developed by the University of Louvain (UCL) that models regional various energy uses (including heating, electricity and mobility). It initially existed as *Energyscope TD (Typical Days)*, which provides the cost optimisation of multi-sector and multi-carrier of a target single future year, with constraints expressed in terms of renewable primary energy share (for the studied year), and without much constraints on 'the path to get there'. Indeed, it does not prevent any sharp shift of technologies between simulations performed on different future years (it could advise totally different energy systems solutions if you impose a 50% renewable energy share in 2035 and then a 55% renewable energy share in 2036). However, this tool provides information about which energy carriers shall be activated, when, and to what extent, to meet the demands of the studied future year. It is able to size and simulate energy storage systems. As for the previous tool, the GHG emissions are also an output of the tool. In its soon to be published version, i.e. *Energyscope Pathway*, constraints shall be applied on the whole pathway to get to the studied year, providing more consistent (and realistic) results. The cost optimization will be realized on the whole period and unrealistic sharp technological shift could be avoided. The total GHG emissions on the studied timeframe will remain an output but could be compared to IPCC's 'equity' carbon budgets reported in this work (and if necessary, more constraining renewable share could be imposed to the tool). This could provide useful information such as, considering technology costs (unlike the previous tool), the amount of CCGT production that should be replaced by fuel cell technologies. Examples of studies using *Energyscope* tools are also numerus [574–576].

## CHAPTER 8 CONCLUSIONS

Through theoretical, simulation and experimental work conducted both in a laboratory environment and in real field-test applications, this thesis demonstrated that the role of fuel cell micro-CHP system fed with fossil fuel in society's decarbonisation is at best limited. Although this work demonstrated that they do not emit any NO<sub>x</sub> (nor SO<sub>x</sub> emissions) and, at worst, a little CO emission (only with the tested SOFC system), they cannot really compete with the average grid electricity from an environmental point of view, which, in addition, becomes greener and greener every day.

However, as electrical grids will require reinforced flexible production means, they often include CCGT plants to achieve peak demands. Compared to these marginal centralized combustion-based power plants, fuel cell micro-CHP can offer reduced GHG emissions. Indeed, their decentralized production prevent transport and distributions losses, which have been evaluated to 6-7% in the EU. Also, commercial fuel cell systems already achieve LHV electrical efficiencies up to 60% (demonstrated experimentally in this work with the tested SOFC) or to 65% (with another SOFC launched on the market in 2023), i.e. higher than the conventional 55% LHV efficiency usually considered for CCGTs. At last, as decentralized solutions, they offer a cheaper and easier way of recovering their heat (and increase their total efficiency) than with CCGTs. This consideration can only be valid for flexible modulating systems, which is the case of the studied SOFC system, but which is not the case of the studied-PEMFC system. In addition, because of its reformer and hydrogen processor, it has been demonstrated in this work that the maximum expected electrical efficiency of the PEMFC technology when fed with hydrocarbons is around 40%, i.e. significantly lower than CCGTs. Concurrently, for residential applications, hydrogen is currently not considered suitable for safety and practical reasons. This explains why several fuel cell CHP OEMs concluded that the future of fuel cells in domestic built environment applications lies with SOFCs and have stopped PEMFC development

Regrettably, since the dwelling's energy demands are just a part of the average carbon footprint, even with highly efficient SOFCs fed with climate neutral fuels, their GHG mitigation potential will still not be sufficient enough to ensure proper decarbonization. Other mitigation efforts and behaviour changes must thus be implemented.

Nevertheless, some fuel cell technologies, like Direct Carbon Solid Oxide Fuel Cells (DC-SOFCs) or Direct Formic Acid Fuel Cells (DFAFCs), have the unique capability of enabling pure CO<sub>2</sub> capture at their anode exhaust, thus possibly facilitating negative emissions (when fed with decarbonized fuels). A case study involving an average Belgian household's electricity demand and the use of an electric car (for approximately 20000 km/year) powered by a biomass-fed DC-SOFC, boasting an electrical LHV efficiency of 80%, suggests that these fuel cells could potentially generate negative emissions of up to about 4 MtCO<sub>2eq</sub>/year (for the studied dwelling and all its occupants).

Considering the minimal carbon absorption level required to reach the carbon neutrality targets, reported in this work to about 1 tCO<sub>2eq</sub>/year per capita, it becomes crucial to further develop and implement such fuel cell systems to unlock their significant negative emissions potential. Indeed, in densely populated western countries such as France and Wallonia, reliance solely on natural sinks is unlikely to suffice as they would require respectively +370% and +300% increases compared to current levels. LCA, social and biodiversity impacts, manufacturing capacity, biofuels and materials availability have not been considered in this work and remain to be thoroughly investigated.

Otherwise, the previous section has singled out this work's specific scientific contributions.

---

# APPENDIX 1: ENERGY CONTENT OF NATURAL GAS IN RESIDENTIAL APPLICATIONS

The content of this Appendix was published almost as-is in the *proceedings of the 8th Conference of the Sustainable Solutions for Energy and Environment (EENVIRO 2022)* [465]. The aims of this appendix is to describe the method that has been used in *Chapter 4 - Study of the Bl\*\*\*G\*N SOFC system* and *Chapter 5 - Study of the P\*2 PEMFC system* to establish the energy content of natural gas residential consumption. Indeed, multiplying the metered gas volume consumed by the LHV of natural gas, if this latter is known, can lead to significant imprecisions. Actually, this gas volume, and the equivalent energy level that it contains and that is required for efficiency calculations, is affected by the atmospheric pressure and the temperature at the field-test site, as well as by the always varying natural gas composition.

## Introduction

Targets of temperature increase compared to pre-industrial levels have scientifically been linked to remaining carbon budgets of future Greenhouse Gases (GHG) emissions allowed for all humanity [8]. Actually, in its Sixth Assessment Report (AR6) released in early 2022, Intergovernmental Panel on Climate Change's Working Group III (IPCC WGIII) has reported that if humanity does not exceed 890 GtCO<sub>2</sub> of emissions from January 1st 2020, it will have 2 out of 3 chances of not exceeding the +2°C maximum limit set in the 'Paris Agreement' back in 2015 [3]. Mitigating GHG emissions is generally associated to the 'low carbon transition' [577], i.e. to the 'energy transition'.

Beside lowering the energy demand, i.e. the 'energy sobriety principle' [578], and increasing territorial carbon absorption [579], it is usually considered that one main pillar of the much-needed energy transition lies in the 'energy efficiency' [578]. Efficiency is always crucial at all levels, both in case of fossil fuel and renewable energy use. For heating appliances at residential scale, energy efficiency establishment and enhancement often require field-test monitoring of energy consumptions. Although the electrical consumption of electrical appliances (such as electrical heat pumps) is quite trivially measured and monitored (an example of electrical energy meter has been shown in Figure 1), the energy consumption of gas-fed appliances is not that easily established.

Indeed, as the energy content of natural gas depends on its varying chemical composition (which requires specific and expensive laboratory hardware, such as chromatographs), it is unrealistic to measure (continuously) it at every residential monitoring field-test sites.

Therefore, in most applications, the only sensor placed on residential gas inlet pipe is a simple diaphragm gas volume meter (such as the one shown in Figure 2), which can also serve as a base for billing purposes.



**Figure 1.** Example of residential field-test electrical energy meter ('MT174' by Iskraemeco)



**Figure 2.** Example of residential gas (volume) consumption meter ('BKG4-T' by Elster)

Gas consumed volume is converted into energy content either thanks to the gas High Heating Value (HHV), usually used when water vapour contained in the gas is able (or should be able) to condense, or thanks to the Low Heating Value (LHV). Nowadays, most applications use the HHV as reference because gas appliances technologies have been improved to recover the latent energy in the gas water vapour.

As it will be seen the following section, HHV are measured (by the gas provider) and provided in 'reference conditions' of pressure and temperature. Those figures are usually available freely on the local gas provider website (or they also can usually be requested over emails). Unfortunately, the 'reference conditions' of temperature and pressure are not the ones that occur at the field-test delivery sites. Therefore, the conversion of the field-test measured gas volume into energy content thanks to the HHV (provided by the gas provider) is not trivial and requires to establish some conversion factors. The aim of this work is to report a documented method for this to be performed.

It is worth mentioning that, with the upcoming of 'power to gas' technologies (such as biomethanation) [580] or biomethanization [581], the method described in this work is not only relevant with conventional (fossil) natural gas appliances, but also with biogas (renewable) appliances.

This exact method has been used for several field-test monitoring studies, on several gas-fed residential space heating appliances, such as Solid Oxide Fuel Cells (SOFC) [427], Proton Exchange Membrane Fuel Cells [15,537,564] or absorption heat pumps [582].

### Establishing the HHV of the consumed gas at the field-test delivery conditions

As stated, HHV are established by the gas provider from regular samples on the high or medium-pressure pipes (and not on the low-pressure pipes at the delivery points of the field-test studies). They usually are performing this hourly according to the composition of the gas (usually measured thanks to a chromatograph) and their combustion enthalpy at 25 °C and 1 atm [583]. The volume of the gas mixture sample from high or medium-pressure pipes is measured as well by the gas provider and converted to a ‘normalized’ volume at 0 °C and 1 atm (reference conditions) according to Equation (58), which corresponds to the real gases equation of state [584]:

$$V_N = V_B \frac{P_L T_N Z_N}{P_N T_L Z_L} \quad (58)$$

Where  $V_N$  is the normalized volume at 0 °C, i.e. 273.15 K ( $T_N$ ) and 1 atm, i.e. 101325 Pa ( $P_N$ ),  $V_B$  is the measured volume of the gas sample whose composition is established thanks to a chromatograph at  $T_L$  and  $P_L$  (also measured on the high or medium-pressure pipes by the gas provider).  $Z_N$  and  $Z_L$  are the compressibility factors of the natural gas mixture and can also be established according to the composition, the temperature (either  $T_N$  or  $T_L$ , explained above) and the pressure (either  $P_N$  or  $P_L$ , explained above) [585]. Similarly, the method of establishing the compressibility factor of natural gas mixtures can be applied according to other inputs (such as the density) and is well documented as the SGERG-88 method [586].

Therefore, the HHV are provided in ‘reference conditions’ for the ‘metered volume’ ( $T_N$  and  $P_N$ ), but the reference for the combustion is different (25 °C, i.e. 298.15 K, from here onwards called  $T_{r,C}$  and  $P_N$ ). However, those are different from the delivery conditions so a relation similar to Equation (58) must be implemented to convert the monitored gas volume  $V_M$  adequately according to the HHV reference conditions. So, one obtains  $V_{M,N}$  :

$$V_{M,N} = V_M \frac{P_D T_N Z_N}{P_N T_D Z_D} \quad (59)$$

Where  $P_D$ ,  $T_D$  and  $Z_D$  are respectively the pressure, temperature and compressibility factors at the delivery point of the field-test study, which are unfortunately not measured.

Nevertheless, delivery temperature  $T_D$  can usually be assumed at 15 °C, i.e. 288.15 K, because gas meter used in field-test studies are often said to ensure temperature compensation via ‘a bimetallic element’, which is the case for the ‘BK-G4T’ shown in Figure 2 [452]. Indeed, the error curve for similar uncompensated meters (called ‘BK-G4’) is supposed to be null at 15 °C, which can be therefore considered as their metering reference. Thanks to temperature compensation, the accuracy range of the sensor can be extended from -10 °C to 40 °C and since the only additional feature is the ‘bimetallic element’ for temperature compensation, the 15 °C reference is assumed to remain. This means that the field-test volume given by the gas meter, whatever the temperature changes between -10 °C and 40 °C, is the same as if the temperature had stayed constantly to 15 °C.

Unfortunately, pressure is usually not compensated in any way with conventional gas meters and since it is not measured in the low-pressure pipes at the field-test monitoring sites (as opposed to the high or medium-pressure pipes where the HHV are established), assumptions must be made. The delivery pressure  $P_D$  is affected by the barometric

pressure at sea level (meteorologic variable), by the altitude of the delivery point and of course by the main gas distribution pressure regulator setting (and its well-known imperfections such as boost and droop [587]). This pressure regulator aims to control the operational pressure and flow of the gas [588]. It is placed upstream of the gas meter (mostly for metering accuracy [589]). In most countries (such as in Belgium), it is used to reduce the pressure from the high or medium-pressure gas distribution pipes to 21 mbar to meet the requirements of residential standard gas appliances [590] (and this pressure requirement is also specified in official industrial standards [591]). However, in Belgium, natural gas comes from different sources, which implies different gas compositions and different HHV, which leads to the appellations ‘lean’ and ‘rich’ gas, respectively for the natural gas source providing the lower and the higher HHV [592].

Lean gas, also called ‘type L’ gas, is supposed to be progressively replaced (in Belgium) by 2030 by rich gas, also called ‘type H’ gas [593]. The existence of lean gas on part of the Belgian market subsequently leads to some changes in the recommended pressure regulator setting (25 mbar instead of the usual 21 mbar for ‘type H’ gas) [594].

Barometric pressures at sea level  $P_M$  constitute data that can easily and freely be gathered. For example, in Belgium, it is measured in Uccle and provided hourly by the Royal Meteorological Institute of Belgium (RMI). Uccle, near Brussels, is considered as the reference climatology Belgian station [595].

Altitude of the monitoring field-test sites can also be gathered easily. For example, in Belgium, it can be established based on the coordinates of the field-test sites thanks to the CalcMaps website ([www.calcmaps.com/fr/map-elevation/](http://www.calcmaps.com/fr/map-elevation/)). This has been reported in

Field-test sites	Altitude
ULiege laboratory (for SOFC and PEMFC tests)	237 m
Riemst (SOFC)	114 m
Duffel (SOFC)	7 m
Huy (PEMFC)	72 m
Oostmalle (PEMFC)	24 m

**Table 43.** Altitude of the field-test sites.

The relationship between altitude  $h$  (m) and its corresponding atmospheric pressure  $P_h$  (Pa) can be established thanks to Equation (60) [596] :

$$P_h = P_0 \left( 1 - 0.0065 \frac{h}{T_0} \right)^{5.2561} \quad (60)$$

Where  $P_0$  and  $T_0$  are defined as the International Standard Atmosphere (ISA) conditions at Mean Sea Level (MSL) [597]. For information,  $T_0$  is equal to  $T_D$ , i.e. 288.15 K whereas  $P_0$  is equal to  $P_N$ , i.e. 101325 Pa.

Thanks to the actual RMI barometric pressure data at sea level  $P_M$  (Pa), thanks to the actual external temperature monitored onsite  $T_M$  (K) and knowing that temperature decreases with altitude at constant rate of -6.5 K per km up to the tropopause according to ISA assumptions [598], one can replace  $P_0$  and  $T_0$  in Equation (60) to achieve better accuracy for modelling the onsite atmospheric pressure  $P_{h,M}$  (Pa). One thus obtains Equation (61):

$$P_{h,M} = P_M \left( 1 - 0.0065 \frac{h}{T_M + 6.5 \frac{h}{1000}} \right)^{5.2561} \quad (61)$$



Pressure at the delivery point  $P_D$  is thus equal to the onsite modelled atmospheric pressure  $P_{h,M}$  added to the pressure regulator setting  $P_{reg}$  :

$$P_D = P_{h,M} + P_{reg} \quad (62)$$

Where, in Belgium,  $P_{reg}$  is equal to 21 mbar for ‘type H’ gas or to 25 mbar for ‘type L’ gas, as explained. Since the actual pressure regulator devices of the field-test are not known, their potential imprecision (such as the well-known boost and droop [587]) can only be neglected.

The compressibility factors at the delivery conditions  $Z_D$  and in reference conditions  $Z_N$  cannot be established based upon the available data stated above (the gas provider does not usually disclose the composition of the gas nor its density in order to be able to implement the SGERG88 model [586]). It is worth mentioning that the SGERG88 model is considered as too complex to be solutioned by hand so, even if the relevant data were available, one would still need the proprietary software to run it.

However, even if  $Z_N$  has not been provided, one can assume that it has been established by the gas provider in reference conditions  $T_N$  and  $P_N$ . Similarly,  $Z_D$  would have been calculated at the assumed temperature  $T_D$  and pressure  $P_D$  (that have been previously established). Fortunately, Equation (59) only requires the ratio of the compressibility factors and not their absolute values, and this ratio can be estimated thanks to acknowledge relevant conversion factors [487] :

$$\frac{Z_{0^\circ\text{C},1\text{atm}}}{Z_{15^\circ\text{C},1\text{atm}}} = 0.9996 \quad (63)$$

Equation (63) assumes a reference composition of the natural gas mixture (surely different from the real one). By assuming that the real composition of the natural gas used in the field-test sites during the whole study would only affect the absolute value of the compressibility factor and not its ratio over a given (small) temperature range, by assuming that the slight pressure difference between  $P_D$  and 1 atm, i.e. the reference pressure of Equation (63), does not affect the ratio of compressibility factors over the given temperature range either, one obtains Equation (64):

$$\frac{Z_N}{Z_D} = \frac{Z_{0^\circ\text{C},1\text{atm}}}{Z_{15^\circ\text{C},1\text{atm}}} = 0.9996 \quad (64)$$

Provided that the gas provider has measured the HHV in ‘reference conditions’ hourly as it is generally the case, Equation (59) can thus be fully implemented and the equivalent HHV energy contained in the consumed gas  $Q_{HHV}$  for a given duration of  $n$  hours is defined by Equation (65):

$$Q_{HHV} = \sum_{i=0}^{i=n} (V_{M,N_i} \times HHV_i) \quad (65)$$

Where  $i$  is the index associated one single hour included in the studied given duration of  $n$  hours,  $HHV_i$  is the HHV established by the gas provider in references conditions ( $T_N$  and  $P_N$ ) for the hour  $i$ , and  $V_{M,N_i}$  is the monitored gas volume consumed over the hour  $i$ , adjusted to the references conditions ( $T_N$  and  $P_N$ ) thanks to Equation (59) and its subsequent assumptions.

It is worth mentioning that the reference temperature of combustion  $T_{r,C}$  used in the definition of the HHV, i.e. 25 °C, has not been altered or converted in any way. This means consumed gas HHV energy  $\Delta_{E,g}$  and the resulting efficiencies that can be subsequently calculated shall normally highlight the reference temperature of combustion for HHV

establishment, and that is not often the case. Indeed, for example, considering that the combustion of a reference natural gas mixture occurs at 0 °C instead of 25 °C (at 1 atm in both cases) would increase the HHV value by a factor 1.0026 [487], which is small but not that insignificant.

## Discussions and conclusions

For space heating combustion appliances, keeping the reference temperature at 25 °C, slightly above air comfort temperature and therefore the return temperature to the space heating appliance, seems relevant. However, in practice, the combustion reactants are not heated up to the reference temperature of combustion of 25 °C by thermal exchange with ambiance upstream of the appliance. For example, the natural gas mixture had flowed a significant amount of time in the ground gas network and its resulting temperature before entering the heating system often cannot reasonably be assumed over 15 °C. Same kind of assumptions can be made on the incoming air also required as reactant for any combustion to take place (or combustion-like reactions, such as in residential fuel cells).

Therefore, even with a perfect heating system and combustion, the HHV efficiency could never reach 100% as some energy from the combustion is drawn to heat up the reactants from their actual delivery temperature (not measured) to the fictive reference combustion temperature (25 °C). Thus, the resulting HHV efficiency (specifying the reference temperature of combustion) is not more than the best reproduceable indicator that could be thought of and remains a partially biased image of the real achievable efficiency of the system.

Alternatively, considering a reference temperature of combustion closer to the one of the reactants (for example, 15 °C) is not preferable because this time, some energy from the combustion would similarly be required to heat up the products of the combustion. Indeed, it is not reasonable to consider that the combustion products can exhaust the system at a temperature below a realistic comfort air temperature or even below usual space heating return temperatures (which can be assumed, at no less than 25 °C for low temperature terminal units).

Despite this clarification on the HHV definition, the impact of reducing the calorific value by considering the heating up of the reactant on a temperature range such as 10 K remains very low (compared to monitoring measurement uncertainties that, for instance, can reach about 5% with usual Class 2 heat meters [457], required to monitor the heat rate produced by the space heat appliance). This can be demonstrated thanks to the CoolProp open-source library ([www.coolprop.org](http://www.coolprop.org)) in the following example :

By considering natural gas as pure methane at 1 atm, the energy required to elevate its temperature from 15 °C to 25 °C is 22.2 kJ/kg;

On the other hand, considering an arbitrary based HHV of 11 kWh/Nm<sup>3</sup> used only for the sake of this example (in reference conditions, 1 atm and 0 °C) accounts for about 55.2 MJ/kg (in the same reference conditions, for the same assumed reactant);

Therefore, it could be considered that the energy required to elevate the temperature of the fuel reduces its reference HHV of about 0.04 %.

Considering that air, assimilated as a mixture of 21% of oxygen and 79% of nitrogen, also has to be heated from 15 °C to 25 °C (at 1 atm); considering a complete stoichiometric reaction for the combustion of methane with that air, would require an additional energy taken out of the reference HHV of 48.3 kJ per kg of methane.

Therefore, it could be considered that the energy required to elevate the temperature of the air reduce the reference HHV of about 0.087 %.

---

Thus, the total reduction impact of heating up the reactants on the reference HHV approaches 0.13%. This is without considering a combustion in excess of air, which is usually the case for gas condensing boilers (in the 1.05 – 1.4 excess of air range) as an optimum choice between thermal efficiency and Nitrogen Oxides (NO<sub>x</sub>) emissions has to be made [599]. Indeed, increasing excess of air is known to lessen the flame temperature, and therefore the NO<sub>x</sub> emissions [600], but also the efficiency, by reducing the sensible heat transfer [599]. It is worth mentioning that excess of air also lessens thermal efficiency by reducing the latent heat recovery [599], as it dilutes water vapor contained in the flue gases (lower specific humidity and therefore lower dewpoint to achieve with the latent heat recovery heat exchanger of the gas condensing boiler).

Considering excess of air would even increase the HHV reduction impact (up to about 0.16 % for the worst 1.4 excess of air assumption).

# APPENDIX 2: DOCUMENT PROPERTIES OF THE PREVIOUS BL\*\*\*G\*N MODEL INSTALLATION'S MANUAL



Manuel/Handleiding/Handbuch - BlueGEN Manuel d'installation / Installatiehandleiding / Installationshandbuch

## Propriétés du document

Nom du document: BlueGEN Manuel d'installation / Installatiehandleiding / Installationshandbuch  
 Type de document: Manuel/Handleiding/Handbuch  
 Réf. du document: 002-MC-12086  
 Numéro de révision: 4  
 Date de création: Novembre 2015

## Droits d'auteur et confidentialité

Droits d'auteur © SOLIDpower GmbH 2015.

SOLIDpower GmbH [SP] a préparé le présent document à l'usage du personnel ou des sous-traitants autorisés SP. Les informations contenues dans le présent guide sont exclusives et confidentielles et sont communiquées au destinataire à la condition expresse d'en respecter la confidentialité et de les utiliser aux seules fins d'installation et d'utilisation des produits SP. Les informations du présent document ne doivent pas être transmises à des tiers sans autorisation écrite de SP. Cet avertissement doit être reproduit sur toutes les copies.

## Clause de non garantie

SP a préparé le présent document en bonne foi et a tout mis en œuvre pour s'assurer de l'exactitude des informations qu'il contient. Cependant, de nombreux paramètres non connus actuellement par SP et au-delà de son contrôle peuvent affecter l'utilisation ou le fonctionnement des produits SP. SP n'offre aucune garantie que le document est exempt d'erreurs ou d'omissions.

Dans la plus large mesure possible, SP refuse de manière expresse d'offrir une garantie explicite ou implicite quant à l'état, à la valeur marchande ou à la pertinence de ces documents et limite sa responsabilité pour la perte directe ou indirecte liée à la disposition de SP à réviser le document ou au coût de sa correction.

Comme tout produit électrique ou à gaz, les produits SP doivent être installés et utilisés de manière appropriée. Vous devez vous assurer que vous lisez, comprenez et suivez les directives de SP – ainsi que toutes les lois locales et les normes de sécurité – et prenez tout le soin raisonnable lors de l'installation ou de l'utilisation des produits SP.

Si vous ne comprenez pas les instructions ou les informations fournies dans ce document, veuillez contacter SP à l'adresse ci-dessous pour obtenir une assistance.

## Commentaire

Pour tout commentaire ou question à propos de ce document, veuillez contacter SP :

SOLIDpower GmbH  
 Boos-Fremery-Straße 62  
 D-52525, Heinsberg, Germany  
 Technique: +49 (0)2452 15 3701  
 Sales: +49 (0)2452 15 3758  
 Facsimile: +49 (0)2452 15 3755  
 Enquiries: info@solidpower.com



# APPENDIX 3: USER MANUAL OF THE TESTED BL\*\*\*G\*N SOFC SYSTEM



BlueGen Manuel d'Information Utilisateur /  
Informatiehandleiding Eindgebruiker

**BlueGEN**

*Modèle / Model B-B-F-B-B-B*

Manuel/Handleiding





### Propriétés du document

Nom du document : BlueGen Manuel d'Information Utilisateur / Informatiehandleiding Eindgebruiker  
Type de document : Manuel/Handleiding  
Réf. du document : 400-MA-999468  
Numéro de révision : 03  
Date de création : Novembre 2019

### Droits d'auteur

Droits d'auteur © SOLIDpower GmbH 2019.

SOLIDpower GmbH a préparé le présent document à l'usage du personnel ou des sous-traitants autorisés SP. Les informations contenues dans le présent guide sont exclusives et confidentielles et sont communiquées au destinataire à la condition expresse d'en respecter la confidentialité et de les utiliser aux seules fins d'installation et d'utilisation des produits SP. Les informations du présent document ne doivent pas être transmises à des tiers sans autorisation écrite de SP. Cet avertissement doit être reproduit sur toutes les copies.

### Clause de non garantie

SP a préparé le présent document en bonne foi et a tout mis en œuvre pour s'assurer de l'exactitude des informations qu'il contient. Cependant, de nombreux paramètres non connus actuellement par SP et au-delà de son contrôle peuvent affecter l'utilisation ou le fonctionnement des produits SP. SP n'offre aucune garantie que le document est exempt d'erreurs ou d'omissions.

Dans la plus large mesure possible, SP refuse de manière expresse d'offrir une garantie explicite ou implicite quant à l'état, à la valeur marchande ou à la pertinence de ces documents et limite sa responsabilité pour la perte directe ou indirecte liée à la disposition de SP à réviser le document ou au coût de sa correction.

Comme tout produit électrique ou à gaz, les produits SP doivent être installés et utilisés de manière appropriée. Vous devez vous assurer que vous lisez, comprenez et suivez les directives de SP – ainsi que toutes les lois locales et les normes de sécurité – et prenez tout le soin raisonnable lors de l'installation ou de l'utilisation des produits SP.

Si vous ne comprenez pas les instructions ou les informations fournies dans ce document, veuillez contacter SP à l'adresse ci-dessous pour obtenir une assistance.

### Commentaire

Pour tout commentaire ou question à propos de ce document, veuillez contacter SP en se référant aux coordonnées à la fin de ce document.





### Document properties

Naam van het document: BlueGen Manuel d'Information Utilisateur / Informatiehandleiding Eindgebruiker  
Soort document: Manuel/Handleiding  
Document ID: 400-MA-999468  
Revisie Nummer: 03  
Revisie Datum: November 2019

### Copyright & confidentialiteit

Copyright © SOLIDpower GmbH 2019.

SOLIDpower GmbH heeft dit document aangemaakt voor gebruik door personeel of gemachtigde aannemers van SP. De informatie in dit document is eigendom van SP, vertrouwelijk en is verstrekt onder de belofte van de ontvanger om deze informatie vertrouwelijk te houden en alleen te gebruiken voor de installatie of het gebruik van producten van SP. De informatie in dit document mag niet worden verstrekt aan derden zonder schriftelijke toestemming van SP. Deze kennisgeving moet worden weergegeven op alle kopieën.

### Disclaimer

SP heeft dit document te goeder trouw opgemaakt en heeft getracht ervoor te zorgen dat de informatie in dit document correct is. Er kunnen echter vele factoren meespelen buiten de huidige kennis of controle van SP die een invloed kunnen uitoefenen op het gebruik of de exploitatie van de producten van SP door de gebruiker. SP kan niet garanderen of maakt geen bewering dat dit document vrij is van fouten of weglatingen.

Hierbij sluit SP uitdrukkelijk alle expliciete of impliciete garantie uit met betrekking tot de conditie, verkoopbaarheid of geschiktheid van dit document en beperkt haar aansprakelijkheid voor directe of gevolgschade, naar keuze van SP, om het document opnieuw aan te leveren of de kosten van het corrigeren van het document te vergoeden.

Net als alle elektrische of gasproducten, moeten de producten van SP correct worden geïnstalleerd en bediend. U moet ervoor zorgen dat u de instructies van SP - en alle lokale wetten of veiligheidsnormen - leest, begrijpt en opvolgt en redelijke zorg besteed bij het installeren of het gebruik van de producten van SP producten.

Als u de instructies of informatie in dit document niet begrijpt, neem dan contact op met SP op het onderstaande adres voor verdere hulp.

### Feedback

Voor opmerkingen of vragen betreffende dit document, gelieve contact op te nemen met SP. Contactinformatie is te vinden op de laatste bladzijde van dit document.



0063



Manuel/Handleiding - BlueGen Manuel d'Information Utilisateur / Informatiehandleiding Eindgebruiker

## SOMMAIRE / INHOUD / INHALT

<b>1. INTRODUCTION</b> .....	<b>1</b>
1.1. OBJET.....	1
1.2. LEGENDE.....	1
1.3. CONTEXTE.....	2
<b>2. MESURES DE SECURITE A OBSERVER PENDANT LE FONCTIONNEMENT</b> .....	<b>3</b>
2.1. EXIGENCES EN MATIERE DE SECURITE.....	3
2.2. PROCEDURES D'ARRET D'URGENCE.....	4
<b>3. INSTALLATION</b> .....	<b>6</b>
3.1. EXIGENCES.....	6
3.2. PLAQUE SIGNALÉTIQUE DU BLUEGEN.....	7
<b>4. PRESENTATION DU BLUEGEN</b> .....	<b>8</b>
4.1. DIMENSIONS DE L'APPAREIL.....	8
<b>5. FONCTIONNEMENT</b> .....	<b>11</b>
5.1. PRESENTATION GENERALE.....	11
5.2. EXIGENCES OPERATIONNELLES.....	11
5.3. DEMARRAGE ET ARRET.....	12
5.4. OPTIMISATION DES PERFORMANCES DU SYSTEME.....	12
5.5. DEFAUTS DE FONCTIONNEMENT.....	13
<b>6. MAINTENANCE</b> .....	<b>14</b>
6.1. PRESENTATION GENERALE.....	14
6.2. INTERVALLES DE MAINTENANCE.....	14
6.3. NETTOYAGE.....	15
<b>7. INSTRUCTIONS D'UTILISATION DU LOGICIEL BLUEGEN-NET</b> .....	<b>16</b>
7.1. PRESENTATION GENERALE.....	16
7.2. ACCES AU BLUEGEN-NET.....	16
7.3. ÉCRAN DE PRESENTATION DE DONNEES DE BLUEGEN-NET.....	17
7.4. AMÉLIORATIONS ULTÉRIEURES.....	18
7.5. GESTION DES LICENCES INTÉGRÉES.....	18
<b>8. INLEIDING</b> .....	<b>19</b>
8.1. DOEL.....	19
8.2. LEGENDE.....	19
8.3. ACHTERGROND.....	20
<b>9. VEILIGHEIDSMATREGELEN TIJDENS HET GEBRUIK</b> .....	<b>21</b>
9.1. VEILIGHEIDSVEREISTEN.....	21
9.2. PROCEDURE NOODUITSCHAKELING.....	22
<b>10. INSTALLATIE</b> .....	<b>24</b>
10.1. VEREISTEN.....	24
10.2. BLUEGEN TYPEPLAATJE.....	25
<b>11. BLUEGEN APPARAAT OVERZICHT</b> .....	<b>26</b>
11.1. APPARAAT AFMETINGEN.....	26





Manuel/Handleiding - BlueGen Manuel d'Information Utilisateur / Informatiehandleiding Eindgebruiker

<b>12. WERKING</b> .....	<b>29</b>
12.1. OVERZICHT .....	29
12.2. OPERATIONELE VEREISTEN .....	29
12.3. STARTEN EN STOPPEN .....	30
12.4. OPTIMALISERING VAN SYSTEEMPRESTATIES .....	30
12.5. OPERATIONELE GEBREKEN .....	31
<b>13. ONDERHOUD</b> .....	<b>32</b>
13.1. OVERZICHT .....	32
13.2. ONDERHOUDSINTERVALLEN .....	32
13.3. REINIGING .....	33
<b>14. BLUEGEN-NET SOFTWARE INSTRUCTIES</b> .....	<b>34</b>
14.1. OVERZICHT .....	34
14.2. TOEGANG TOT BLUEGEN-NET .....	34
14.3. BLUEGEN-NET RAPPORTAGESCHERM .....	35
14.4. TOEKOMSTIGE UITBREIDING .....	36
14.5. BLUEGEN GEÏNTEGREERDE SOFTWARE LICENTIE .....	36
<b>APPENDIX A CARACTERISTIQUES / SPECIFICATIES</b> .....	<b>37</b>
<b>APPENDIX B LICENCES DES LOGICIELS GRATUIT INTEGRES / BLUEGEN TOEGELATEN VRIJE SOFTWARE</b> .....	<b>43</b>



## 1. INTRODUCTION

### 1.1. Objet

Ce manuel présente de manière générale la conception et le fonctionnement de l'appareil BlueGEN et décrit les mesures de sécurité à respecter après l'installation et la mise en service de l'appareil.

Par ailleurs, le présent manuel contient des instructions permettant d'accéder aux données de performance de l'appareil BlueGEN via le service Web sécurisé de présentation des données : BlueGEN-net.

Veuillez lire soigneusement les informations fournies dans le présent manuel et le conserver dans un lieu sûr pour toute consultation ultérieure.





Le présent manuel d'utilisateur final n'inclut pas les instructions concernant les points suivants:

- installation du BlueGEN et raccordements aux alimentations — vous référer au manuel d'installation du BlueGEN.
- installation du cœur de pile à combustible dans le module HotBoP de pile à combustible (également nommé "balance-of-plant" ou BoP).
- Installation de l'onduleur externe.
- maintenance courante du BlueGEN
- fonctionnement du BlueGEN.

Toutes ces activités répertoriées ci-dessus doivent être réalisées exclusivement par un personnel qualifié.

### 1.2. Légende

Voici les symboles utilisés dans le présent guide :

Symbole	Description
	<b>Attention</b> Le fait d'ignorer ces avertissements peut endommager le BlueGEN ou causer la mort ou entraîner des blessures graves.
	<b>Risque d'incendie</b> Indique un risque d'incendie ou des mesures de sécurité à prendre en cas d'incendie.
	<b>Référence à des informations supplémentaires</b> Détaille toutes les étapes à suivre et les informations utiles à prendre en compte avant d'entreprendre les tâches d'installation et d'entretien décrites.
	<b>Déclaration Européenne de conformité</b> Certifie que ce produit répond aux exigences de l'Union Européenne en matière de sécurité. L'appareil a été conçu et construit pour fonctionner sans risque et ne présenter aucun danger pour les personnes, animaux domestiques ou biens dans le cadre d'une utilisation normale, telle que définie par l'article 1 de la règlement (EU) 2016/426 sur les appareils à gaz.



### 1.3. Contexte

Les piles à combustible sont de plus en plus reconnues pour leurs avantages écologiques et pour leur potentiel dans les systèmes distribués de génération d'énergie à haut rendement. Dans le monde entier, les installations d'énergie sont confrontées à de sérieux problèmes dont la hausse de la demande, la limitation des centrales traditionnelles, les pénuries de carburant et des contraintes d'émission des gaz à effet de serre.

SP a mis au point un système de pile à combustible à usage domestique, le BlueGEN, conçu pour fournir une électricité de charge de base, sécurisée, fiable et à haut rendement.

BlueGEN représente l'innovation en termes de technologie SOFC et fonctionne comme un générateur électrique connecté au réseau et peut faire varier le niveau d'électricité produite pour différents niveaux de besoins en matière de production d'électricité.

Le BlueGEN fonctionne au gaz naturel et à l'eau approvisionnés par les réseaux de distribution respectifs. Grâce à une réaction électrochimique, le BlueGEN fournit à la fois de l'électricité et de la chaleur pouvant être utilisée pour chauffer l'eau.

L'appareil BlueGEN fournit de l'énergie électrique en courant continu (@400VDC) : pour une connexion correcte au réseau électrique, un onduleur externe spécifique doit être connecté. Les deux unités séparées sont spécifiquement configurées pour fonctionner à l'état nominal et maximiser la production d'énergie.

Les principales caractéristiques du BlueGEN / onduleur externe sont:

- 0 à 1,5 kW de puissance électrique nette en courant continu en fonctionnement sur gaz naturel.
- un rendement électrique élevé : jusqu'à 60% nets.
- une conversion du combustible d'entrée en énergie électrique avec niveaux de bruit, de vibration et d'émissions négligeables.
- une modulation de la production d'électricité entre 0 et 100 %, permettant un fonctionnement flexible pour différentes situations et installations.
- un module HotBoP de pile à combustible, se composant d'un générateur électrique intégrant un cœur de pile à combustible, ayant pour résultat une conception compacte et à haut rendement thermique.
- un échangeur de chaleur intégré (unité de récupération de la chaleur résiduelle) pour récupérer la chaleur du module de pile à combustible permettant au BlueGEN d'être installé soit en tant que système générateur électrique soit en tant que système de cogénération.
- un accès à distance aux données via Ethernet pour la surveillance et le contrôle.

SP a développé le BlueGEN pour fonctionner d'une façon sûre et fiable. Pour ce faire, il est fondamental d'observer certaines précautions lors de son fonctionnement.



## 2. MESURES DE SECURITE A OBSERVER PENDANT LE FONCTIONNEMENT

### 2.1. Exigences en matière de sécurité

Afin de prévenir tout risque de blessures et d'éviter d'éventuels dommages matériels, veuillez respecter ce qui suit :

- Dans l'éventualité peu probable où l'appareil émet une odeur inhabituelle (produits de combustion ou odeur de gaz naturel par exemple), n'allumez ni n'éteignez aucun appareil ou dispositif électrique situé à proximité. Contactez directement votre installateur ou SP.
- Les portes de coffret du BlueGEN doivent rester fermées et verrouillées en permanence pendant son fonctionnement. Pour votre propre sécurité, n'ouvrez pas le coffret de l'appareil. L'utilisateur ne doit intervenir sur aucune pièce interne de l'appareil.
- Assurez-vous que le commutateur d'arrêt d'urgence ainsi que les vannes d'isolement de gaz naturel et d'eau sont facilement accessibles en permanence.
- N'insérez ni vos doigts, ni aucun autre objet dans le BlueGEN.
- Ne pas stocker et utiliser de liquides ou vapeurs inflammables à proximité du BlueGEN.
- Ne pas enlever et ne pas réinstaller de raccordement au BlueGEN, y compris les raccordements du système de conduit de fumées, les raccordements d'alimentation (gaz, électricité et eau), l'évacuation et les connexions de communication.
- N'installez aucun appareil qui utilise l'air en provenance d'un bâtiment (par exemple un système de chauffage, de refroidissement, de ventilation) près de la sortie du conduit de fumées, ce dernier pouvant contenir des produits de combustion, y compris des gaz toxiques (par exemple du monoxyde de carbone).
- Ne placez aucun objet sur, contre ou à proximité immédiate du BlueGEN. Pour faciliter la maintenance, veuillez vous assurer qu'il existe un espace libre approprié autour du BlueGEN tel qu'indiqué dans la section 11.1.2.
- N'utilisez aucun liquide ou poudre pour nettoyer le BlueGEN, ne pulvérisez aucun liquide sur l'appareil.
- Les enfants et les personnes présentant une infirmité ne doivent pas avoir accès au BlueGEN ni à ses installations (tuyauterie, conduit de fumées, vannes et commutateurs des lignes d'alimentation).
- Cet appareil peut être utilisé par des enfants âgés de 8 ans et plus ou par des personnes ayant des capacités physiques, sensorielles ou mentales réduites ou encore sans expérience et connaissances à condition d'être supervisés ou instruits quand à l'utilisation de l'appareil en toute sécurité et après avoir été informé des dangers en cas d'usage incorrect de l'appareil.
- Les enfants ne doivent pas jouer avec l'appareil
- Le nettoyage et la maintenance de l'appareil ne doivent pas être effectués par des enfants sans surveillance.



Manuel/Handleiding - BlueGen Manuel d'Information Utilisateur / Informatiehandleiding Eindgebruiker



#### Attention

Ignorer ces avertissements peut causer des dégâts au BlueGEN ou la mort ou des blessures graves, en plus d'annuler toutes les garanties.

## 2.2. Procédures d'arrêt d'urgence

Le BlueGEN est équipé d'un système de commande de sécurité gaz certifié CE. Dans le cadre d'un fonctionnement de l'appareil en dehors de ses paramètres normaux, le système de sécurité est conçu pour isoler l'alimentation interne en gaz et pour couper sans risque le système.



Manuel/Handleiding - BlueGen Manuel d'information Utilisateur / Informatiehandleiding Eindgebruiker

### 2.2.1. Fuite de gaz

En cas d'urgence, le gaz naturel, l'électricité et l'alimentation en eau du BlueGEN doivent être isolés mais seulement si cela peut être fait en toute sécurité (voir la section 0).

Le BlueGEN produit du gaz naturel désodorisé via le désulfuriseur. Si une fuite interne se produisait, en aval du désulfuriseur, elle ne serait pas perceptible par l'odeur. Il est important que l'appareil soit mis en route et entretenu par un personnel autorisé uniquement, selon les procédures de sécurité approuvées.



#### Attention

Le BlueGEN doit uniquement fonctionner avec les portes fermées et verrouillées en permanence pour empêcher toute fuite de monoxyde de carbone ou du gaz naturel vers l'environnement externe en cas de fuite interne.

### 2.2.2. Arrêt d'urgence

En cas d'urgence, lorsque des vies ou des biens sont menacés par le fonctionnement continu du BlueGEN, tous les services comprenant le gaz naturel, l'électricité et l'alimentation en eau du BlueGEN doivent être isolés mais uniquement si cela peut-être fait en toute sécurité.

Ceci doit être fait à l'aide des commutateurs et des vannes d'isolement correspondants. Ces commutateurs et vannes doivent être installés sur le site, à proximité immédiate du BlueGEN, et conformément aux codes d'installation appropriés.

En cas d'arrêt d'urgence du BlueGEN, il y a un risque sérieux de dommages ou de défaillance du cœur de la pile à combustible. Cependant, ceci ne devrait jamais influencer la décision d'arrêter le BlueGEN en situation d'urgence.



#### Attention

Le BlueGEN peut produire une source interne de courant électrique. L'isolement des alimentations électriques ne supprimera pas les risques à l'intérieur du BlueGEN.

Si une fuite de gaz est suspectée dans la zone autour de l'appareil BlueGEN, isoler uniquement l'alimentation principale du gaz en entrée.

### 2.2.3. Sécurité contre l'incendie

Si des vies ou des biens sont menacés, contactez immédiatement les services de secours.



#### Risque d'incendie

En cas d'incendie au cours de l'utilisation du BlueGEN, utilisez un extincteur au CO2 ou à poudre sèche, si cela peut-être fait en toute sécurité.



## 3. INSTALLATION

### 3.1. Exigences



#### Attention

Cet appareil doit être installé exclusivement par un personnel suffisamment qualifié. L'installation doit satisfaire toute la législation applicable aux appareils à gaz domestique avant leur utilisation dans le pays concerné. Une installation incorrecte annulera la garantie.



#### Attention

Pour une installation de Type B33 (pour laquelle l'air est pris directement dans la pièce où l'appareil est installé): aucun produit chimique (par exemple aérosol, peinture, solvant) ne doit être utilisé ou stocké à proximité du BlueGEN



#### Référence à des informations supplémentaires

Les installateurs doivent suivre les instructions fournies dans le manuel d'installation du BlueGEN.

L'installateur a l'obligation d'avoir achevé les tâches suivantes:

- vous avoir fourni une copie de ces instructions et les instructions pour l'onduleur externe.
- vous avoir formé sur le fonctionnement et l'emplacement des vannes d'isolement du gaz naturel et de l'eau ainsi que du commutateur électrique d'arrêt d'urgence (à côté de l'appareil et dans le tableau de contrôle). Il est de la responsabilité de l'utilisateur de s'assurer qu'ils sont tous facilement accessibles à tout moment. veiller à ce que toutes les alimentations (gaz, eau et électricité) et le système de conduit de fumées aient été installés de manière correcte et conformément aux réglementations locales du pays concerné.
- avoir veillé à ce que votre alimentation en eau et l'évacuation aient été installées de manière correcte.
- s'être assuré que votre évacuation n'a pas été modifiée après l'installation de l'appareil puisque ceci pourrait causer le refoulement vers l'appareil, pouvant éventuellement provoquer la défaillance du système.
- avoir veillé à ce que votre circuit de chauffage ait été installé correctement (le cas échéant).
- avoir veillé à ce que le type et la pression de gaz indiqués sur la plaque signalétique de l'appareil correspondent au gaz fourni.
- avoir veillé à ce que votre alimentation électrique ait été installée selon les normes locales. Puisque l'appareil peut exporter de l'électricité, votre fournisseur d'électricité doit avoir été contacté et avoir donné son accord préalable avant l'utilisation de l'appareil.
- avoir veillé à ce que la protection anti-îlotage du l'onduleur externe corresponde aux normes locales.
- avoir veillé à ce que la connexion internet locale ait été installée correctement. Le trafic mensuel des données d'une connexion internet peut classiquement atteindre 4 MB en téléchargement montant et 2



Manuel/Handleiding - BlueGEN Manuel d'information Utilisateur / Informatiehandleiding Eindgebruiker

MB en téléchargement descendant, selon les circonstances. Le débit minimal en téléchargement montant doit être supérieur à 560 kBit/s. Les coûts liés au transfert des données sont supportés par l'utilisateur final.

- avoir veillé à ce que vous disposiez de l'accès à BlueGEN-net (le cas échéant) pour consulter les données de performance.

### 3.2. Plaque signalétique du BlueGEN

La plaque signalétique du BlueGEN est représentée par la Figure 1.



  <b>0063/19</b> 0063CL3210	<b>BlueGEN</b> PWM = 10 bar IP20 T <sub>ambiant max</sub> = 45°C		100000026598	BG2000	B-B-F-B-B-B
	NL 25mbar DE 20mbar FR; BE 20/25mbar CH; GB; IT 20mbar	P <sub>th</sub> = 0,6kW (30/36°C) Q <sub>(HS)</sub> = 3,6kW PMS = 3bar T <sub>max</sub> = 80°C	P <sub>elmax</sub> = 2,0kW Output: 390-400V / = P <sub>elin</sub> = 0,2kW input: 230V / ~ 50Hz	P <sub>elin</sub> = 1,55kW I2N; I2EK B33, C43(x), C13(x), C33(x), C53(x), C63(x) I2N; I2ELL B33, C43(x), C13(x), C33(x), C53(x), C63(x), C93(x) I2N B33, C43(x), C13(x), C33(x), C53(x), C63(x) I2N; I2H B33, C43(x), C13(x), C33(x), C53(x), C63(x)	

Figure 1: plaque signalétique du BlueGEN

Terminologie	Définition
P <sub>elin</sub>	Alimentation électrique
P <sub>th</sub>	puissance thermique
P <sub>elin</sub>	Charge électrique connectée
T <sub>max</sub>	Circuit thermique à température maximale
PMS	Pression d'eau maximale cycle thermique
Q <sub>(HS)</sub>	Puissance raccordée au gaz (pouvoir calorifique supérieur)
T <sub>ambiant max</sub>	Température ambiante maximale pendant le fonctionnement

Tableau 1: légende de la plaque signalétique de l'appareil

La plaque signalétique du BlueGEN contient les informations suivantes :

- Le raccordement au secteur est réservé au fonctionnement monophasé en courant continu. L'unité est conçue pour fonctionner avec un onduleur externe afin de répondre aux exigences des installations domestiques. La puissance nominale de sortie est de 1,55 kW.
- La puissance thermique maximale du BlueGEN est de 0,6 kW. La quantité réelle fournie dépend des facteurs liés à l'état opérationnel du BlueGEN. L'utilisation de la chaleur dégagée du BlueGEN est facultative et dépend de la présence d'un circuit de récupération de chaleur connecté au système.
- L'unité utilise un faible débit de gaz naturel. L'installateur aura installé le système conformément à vos conditions locales avant le démarrage.

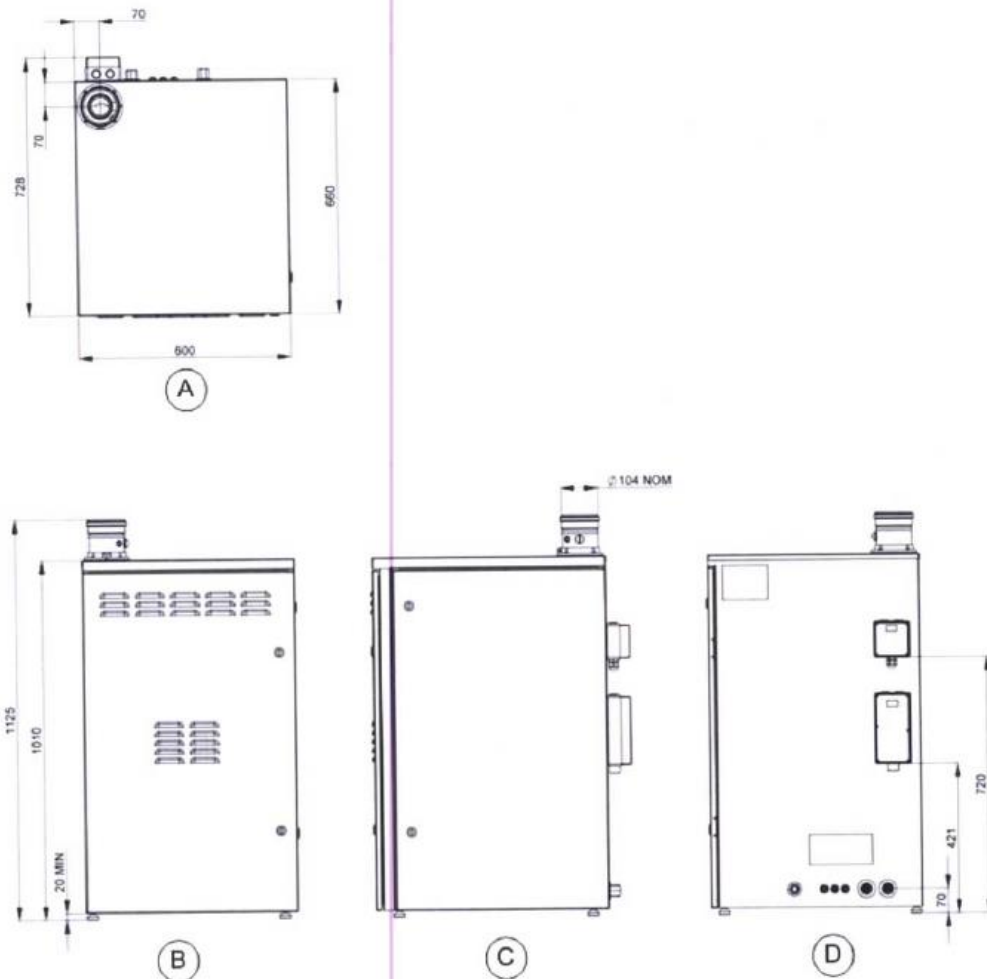




## 4. PRESENTATION DU BLUEGEN

### 4.1. Dimensions de l'appareil

La Figure 2 représente le BlueGEN tel qu'il est fourni au client. Les interfaces de raccordement sont fournies avec l'appareil.



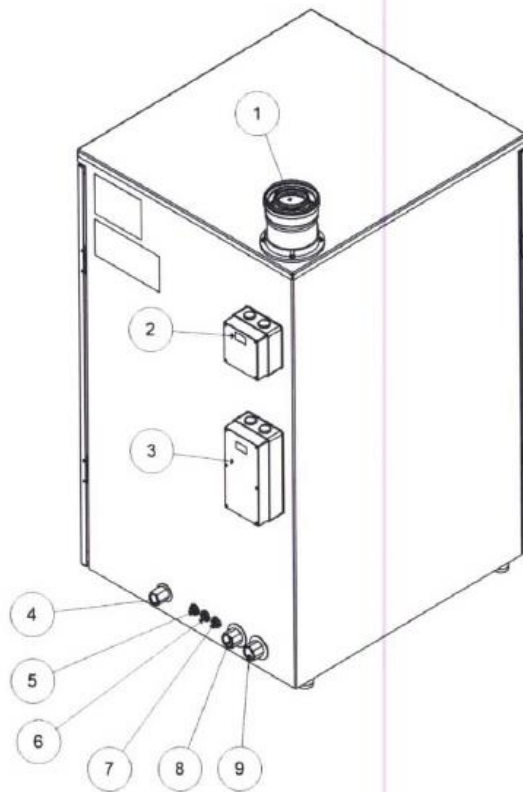
- A. Vue de dessus
- B. Vue de face
- C. Vue de côté
- D. Vue arrière (raccordements des alimentations)

Figure 2: dimensions de l'appareil (mm)



#### 4.1.1. Raccordement aux alimentations

La Figure 3 indique les emplacements des raccords.



1. Évacuation des gaz de combustion avec interface concentrique standard de diamètre 60/100 mm
2. Raccordement Ethernet
3. Boîtier électrique
4. Arrivée de gaz naturel (½" gaz femelle)
5. Arrivée d'eau (raccord rapide ¼" « John Guest »)
6. Evacuation d'eau osmose inverse (raccord rapide ¼" « John Guest »)
7. Ecoulement ou de trop-plein (raccord rapide ¼" « John Guest »)
8. Départ de récupération de la chaleur résiduelle (raccord femelle BSPP ¼")
9. Retour de récupération de la chaleur résiduelle (raccord femelle BSPP ¼")

Figure 3: raccords du BlueGEN



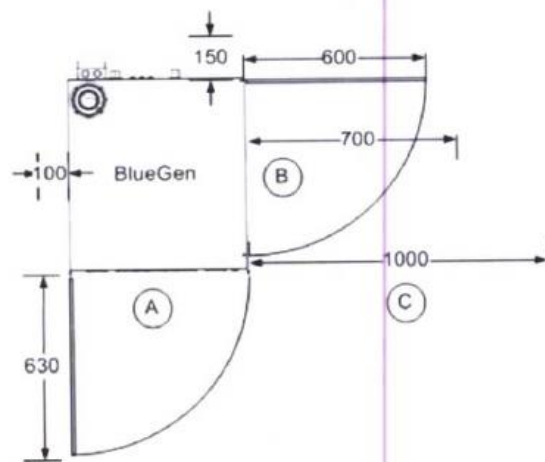
#### 4.1.2. Exigences de dégagement minimum

Un espace suffisant pour l'accès et les opérations de maintenance est nécessaire. Cela sera pris en compte par votre installateur au moment de l'installation du BlueGEN. La Figure 4 spécifie les caractéristiques de dégagement minimum.

Le BlueGEN a été conçu pour disposer d'un accès de maintenance à partir de deux côtés. Il faut assez d'espace sur ces côtés pour permettre aux portes d'être ouvertes pendant les opérations de maintenance.

Sur le côté droit de l'appareil, un mètre de sol stable et horizontal est requis pour permettre l'installation du module HotBoP de pile à combustible. Aucune obstruction permanente ne doit exister dans cet espace. Il est important qu'aucune obstruction permanente ou provisoire ne soit placée devant l'appareil car ceci pourrait réduire la circulation d'air refroidissant les composants électriques de l'appareil.

Les dégagements des autres côtés de l'appareil sont des dégagements minima absolus. Un grand soin doit être pris pour assurer un accès facile aux raccords du BlueGEN et, le cas échéant, aux raccords du ballon.



- A. Avant
- B. Droite
- C. Dégagement horizontal de 1000 mm minimum pour l'accès de maintenance

Figure 4: dégagements autour de l'appareil (mm)



## 5. FONCTIONNEMENT



### Attention

Le BlueGEN ne peut être utilisé qu'après le raccordement de toutes les alimentations (l'eau, le gaz, l'électricité) et du système de conduit de fumées et après l'actionnement des commutateurs et l'ouverture des vannes d'isolement.

Seul un personnel suffisamment qualifié est autorisé à actionner la vanne d'isolement pour l'eau et l'alimentation en gaz, ainsi que le commutateur d'urgence de l'alimentation électrique.

### 5.1. Présentation générale

Le BlueGEN est conçu pour une utilisation sûre et fiable. Pour la présentation des données la maintenance et les diagnostics avancés, la surveillance du BlueGEN se fait à distance via Internet.

Le système de contrôle du BlueGEN commande automatiquement tous les aspects du fonctionnement – du démarrage jusqu'à la production d'électricité, la maintenance et l'arrêt du système.

Les phases de fonctionnement de base sont :

#### Montée en température

Pendant cette phase, l'appareil chauffe de la température ambiante à la température de fonctionnement d'une façon régulière et contrôlée. Le procédé montée en température peut prendre jusqu'à 30 heures avant que l'appareil ne produise de l'électricité. Le BlueGEN est alimenté par le secteur pendant cette phase.

#### Autosuffisance

L'appareil se trouve en phase Autosuffisance une fois qu'il a atteint la température de fonctionnement et qu'il génère une puissance électrique permettant de compenser les charges parasites mais sans exporter de la puissance sur le réseau.

#### Production d'électricité

Pendant cette phase, l'appareil est totalement opérationnel et exporte l'électricité. La puissance électrique produite peut être modulée entre 0 et 100 %.

#### Refroidissement

L'appareil est en phase Refroidissement quand il ne produit plus de puissance électrique et est alimenté par le secteur pour s'arrêter d'une manière contrôlée. Le processus de refroidissement peut durer jusqu'à 30 heures avant que l'appareil atteigne la température ambiante.

### 5.2. Exigences opérationnelles

Pendant le fonctionnement, votre appareil BlueGEN a besoin de :

- Un approvisionnement continu et permanent en gaz. Veuillez informer votre installateur ou votre représentant SP si une interruption de l'alimentation de gaz peut survenir dans votre zone.
- Une alimentation continue et permanente en eau. Veuillez informer votre installateur ou votre représentant SP si une interruption de l'alimentation d'eau peut survenir dans votre zone. Le BlueGEN peut utiliser maximale jusqu'à 36 litres d'eau par jour (à 1,55 kW puissance électrique).



- Une alimentation électrique continue pendant les phases de montée en température et de refroidissement quand le BlueGEN n'est pas en mode Autosuffisance. Veuillez informer votre installateur ou votre représentant SP si une interruption de l'alimentation électrique peut survenir dans votre zone.
- Une connexion Internet permanente pour la surveillance et la gestion du BlueGEN. Veuillez informer votre installateur ou votre représentant SP si une interruption de l'alimentation électrique peut survenir dans votre zone.

### 5.3. Démarrage et arrêt



#### Attention

Le BlueGEN doit être utilisé exclusivement par un personnel autorisé, y compris pour les opérations de démarrage et d'arrêt.

Le BlueGEN peut fonctionner pendant de longues périodes sans interruption. Les processus de démarrage et d'arrêt de l'appareil prennent un temps significatif et doivent être programmés.

Veuillez contacter votre installateur ou votre représentant SP pour obtenir des informations détaillées sur la planification d'un démarrage ou d'un arrêt du système.



#### Référence à des informations supplémentaires

Voir la section 9.2 pour des informations sur l'arrêt du BlueGEN en situation d'urgence.

### 5.4. Optimisation des performances du système

Pour un fonctionnement sûr et fiable, SP recommande que vous observiez les directives suivantes pendant l'utilisation du BlueGEN :

- Assurer l'alimentation continue en gaz, en eau et en électricité de l'appareil. Un arrêt intempestif provoqué par une absence d'eau, de gaz ou d'électricité peut endommager le BlueGEN.
- Libérer les alentours de l'appareil, pour permettre un accès facile en cas de besoin de maintenance.
- Ne pas obstruer les prises d'air de refroidissement et les événements du BlueGEN (laisser au moins un mètre entre les grilles et tout autre élément pour empêcher la recirculation de l'air).
- Ne pas emmêler les raccordements des alimentations (gaz, eau, gaz de combustion, électricité), et ne placer aucun objet derrière l'appareil.
- Maintenir la température ambiante entre 1°C et 45°C. Une température ambiante de 20°C est recommandée. En aucun cas la température ne doit descendre au-dessous de 0°C car l'appareil n'est pas protégé contre le gel.
- Utiliser la chaleur produite par le BlueGEN (système de récupération de chaleur) si possible. Ceci permet au BlueGEN de réduire sensiblement sa consommation d'eau et prolonge la vie des filtres d'eau.
- Veiller à ce que le système de conduit de fumées soit correctement entretenu (par un personnel suffisamment qualifié) et libre de toute obstruction.



- Assurer une communication Internet fiable. Ceci permet à SP de répondre rapidement à un problème potentiel lié à l'appareil.
- La question de l'optimisation du rendement électrique du BlueGEN doit être abordée avec votre représentant SP. Notez que la production thermique du système est un sous-produit de la production électrique et de la performance de la pile à combustible et elle n'est pas réglable.

## 5.5. Défauts de fonctionnement

Si le BlueGEN présente un défaut au cours de son fonctionnement, l'appareil émettra une demande d'assistance à distance via BlueGEN-net. Notez que le BlueGEN-net nécessite une connexion Internet opérationnelle et permanente.

Ces défauts seront résolus soit via le BlueGEN-net, soit sur site par le personnel de maintenance.

Dans l'éventualité peu probable d'un problème veuillez consulter le tableau ci-dessous.

Problème	Action
L'appareil émet une odeur inhabituelle (par exemple de produit de combustion, ou une odeur de gaz naturel)	Contactez votre installateur ou votre représentant SP.
L'appareil produit des bruits inhabituels	Contactez votre installateur ou votre représentant SP.
De l'eau coule de l'appareil	Contactez votre installateur ou votre représentant SP.

Tableau 2: guide de résolution des problèmes



## 6. MAINTENANCE

### 6.1. Présentation générale

Le BlueGEN a été conçu avec un système interne de diagnostic pour permettre un entretien préventif et optimiser son fonctionnement continu.

Le système de surveillance et d'assistance BlueGEN-net informe SP de toutes les tâches d'entretien imminentes. En outre, la surveillance continue de la performance par BlueGEN-net permet aux alertes d'être également envoyées si l'entretien d'un élément est devenu nécessaire en dehors du programme normal.

Dans l'éventualité peu probable d'un problème, SP sera automatiquement averti et répondra en conséquence, probablement avant même que vous ne vous rendiez compte de la présence d'un problème.

Le BlueGEN, via BlueGEN-net, s'ajuste automatiquement aux conditions locales. Puisque le gaz naturel utilisé par le BlueGEN subit une conversion chimique lors de son utilisation dans la pile à combustible, aucun réglage de gaz ou réglage de combustion n'est exigé au cours de la vie de l'appareil.

L'utilisateur ne doit intervenir sur aucune pièce interne du système. Les portes de coffret du BlueGEN doivent rester fermées et verrouillées en permanence pendant son fonctionnement. Pour votre propre sécurité, n'ouvrez pas le coffret de l'appareil.



#### Attention

Seul un personnel suffisamment qualifié est autorisé à assurer l'entretien du BlueGEN.

### 6.2. Intervalles de maintenance

Le programme suivant détaille les éléments typiques de l'entretien et les intervalles d'intervention. En fonction du lieu de l'installation, des conditions locales et de l'utilisation du BlueGEN, certains intervalles peuvent être plus courts ou plus longs par rapport à la liste ci-dessous.

Ces éléments peuvent être maintenus ou remplacés exclusivement par votre agent local SP qualifié.

Élément	Description	Durée de vie
Filtre à air	Filtre l'air de la combustion <sup>1</sup>	12 mois
Système de récupération du condensat	Filtres à eau <sup>2</sup>	6 mois
Système de traitement de l'eau	Diverses membranes de filtres et d'osmose inverse <sup>2</sup>	0,5 à 3 ans
Désulfuriseur	Retient le soufre contenu dans le gaz fourni <sup>1</sup>	1 à 2 ans

1. Fonction de la qualité du gaz/air du site.

2. Fonction du type de filtre et de la qualité de l'eau.

Tableau 3: éléments de maintenance



### 6.3. Nettoyage

Les parois externes du BlueGEN peuvent être nettoyées à l'aide d'un pinceau doux, ou essuyées avec un tissu humidifié d'un mélange de détergent non corrosif et d'eau. Ne laissez pas l'eau s'infiltrer par les prises d'air de refroidissement des composants électroniques.

Ne pulvérisez l'eau sur aucune prise d'air, n'utilisez pas de jets d'eau pour nettoyer l'appareil.

Le nettoyage ne doit pas être effectué par des enfants sans surveillance.





## 7. INSTRUCTIONS D'UTILISATION DU LOGICIEL BLUEGEN-NET

### 7.1. Présentation générale

Le cas échéant, les utilisateurs peuvent surveiller et visualiser leur BlueGEN à distance via BlueGEN-net.

BlueGEN-net est un outil de télésurveillance et de présentation des performances qui permet aux utilisateurs de visualiser des tableaux et des graphiques de données de performance et de télécharger un historique des données.

### 7.2. Accès au BlueGEN-net

Les utilisateurs inscrits peuvent accéder au BlueGEN-net en saisissant l'adresse [www.BlueGEN.net](http://www.BlueGEN.net) dans un navigateur Internet et en saisissant leurs paramètres de connexion. L'application BlueGEN-net est compatible avec la majorité des navigateurs Internet.

Pour accéder au BlueGEN-net :

- A. Indiquez votre nom d'utilisateur (User) et votre mot de passe (Password) dans la fenêtre d'ouverture de session (Login) de la page d'accueil de BlueGEN-net ([www.BlueGEN.net](http://www.BlueGEN.net)) :

The image shows a login form with the following elements:

- Title: Login
- User field: A text input box with a person icon to its left.
- Password field: A text input box with a key icon to its left.
- Login button: A blue button with the text 'Login'.
- Forgot Password? link: A text link below the login button.

- B. Cliquez sur le bouton Login.
- C. Lisez et acceptez l'accord de licence d'utilisateur (end user license agreement).



### 7.3. Écran de présentation de données de BlueGEN-net

Une fois la session ouverte, l'écran principal de présentation des données apparaît (voir Figure 5)

Figure 5: écran principal de présentation des données

L'écran principal de présentation des données donne un aperçu du BlueGEN sélectionné et comprend les sections suivantes :

#### Unité sélectionnée [Unit selected] (le cas échéant)

Pour les utilisateurs qui ont plus d'un appareil, cette fonctionnalité affiche les données du BlueGEN concerné.

#### Informations [Information]

Fournit des données sur l'emplacement physique de l'appareil, le statut actuel du fonctionnement et le mode d'exportation de l'électricité.

#### Instantané [Snapshot]

Rapporte le rendement électrique réel du BlueGEN sélectionné, ainsi que la puissance gaz consommée (en watts) et la puissance électrique exportée par l'appareil (en watts).

#### Téléchargement [Download]

Un historique des données de performance peut être téléchargé pour le BlueGEN sélectionné et être utilisé dans un logiciel tiers (par exemple Microsoft Excel).

#### Section sur les tableaux et les graphiques [Table – Graph]

C'est un outil interactif de présentation de données qui permet aux utilisateurs de visualiser un historique des données dans un format de tableau ou de graphique selon les critères définis.

---

Manuel/Handleiding - BlueGen Manuel d'Information Utilisateur / Informatiehandleiding Eindgebruiker

Pour plus d'informations, cliquez sur 'help' en haut à droite de l'écran:

Welcome CHCL Demo (CHCL) | Edit Preferences | Help | **Help**

### 7.4. Améliorations ultérieures

Comme avec tous les développements technologiques, et particulièrement les développements de logiciel, BlueGEN-*net* sera mis à jour pour intégrer les fonctionnalités les plus récentes.

### 7.5. Gestion des licences intégrées

Le BlueGEN utilise un logiciel propriétaire pour son fonctionnement et son contrôle qui a été développé par SP, en plus d'un autre logiciel de conception indépendante publié avec des licences « gratuites ». Conformément aux clauses des licences des logiciels gratuits, SP a l'obligation de révéler les termes des accords de licence applicables.

Ces licences permettent à ce logiciel libre d'être intégré aux produits propriétaires tels que BlueGEN. Pour plus de détails sur les licences des logiciels intégrés, veuillez vous référer à Annexe B.

Le code source de ces programmes libres et une liste complète des droits d'auteur peuvent être obtenus sur demande auprès de SP.

---

© SOLIDpower GmbH 2019

18

## APPENDIX 4: INSTALLATION MANUAL OF THE (TESTED) BL\*\*\*G\*N (FRONT PAGE AND DOCUMENT PROPERTIES)





Manual/Handleiding - BlueGEN Manuel d'installation / Installatiehandleiding

### Propriétés du document

Nom du document: BlueGEN Manuel d'installation / Installatiehandleiding  
Type de document: Manuel/Handleiding  
Réf. du document: 400-MA-999473  
Numéro de révision: 03  
Date de création: Janvier 2020

### Droits d'auteur

Droits d'auteur © SOLIDpower GmbH 2020.

SOLIDpower GmbH [SP] a préparé le présent document à l'usage du personnel ou des sous-traitants autorisés SP. Les informations contenues dans le présent guide sont exclusives et confidentielles et sont communiquées au destinataire à la condition expresse d'en respecter la confidentialité et de les utiliser aux seules fins d'installation et d'utilisation des produits SP. Les informations du présent document ne doivent pas être transmises à des tiers sans autorisation écrite de SP. Cet avertissement doit être reproduit sur toutes les copies.

### Clause de non garantie

SP a préparé le présent document en bonne foi et a tout mis en œuvre pour s'assurer de l'exactitude des informations qu'il contient. Cependant, de nombreux paramètres non connus actuellement par SP et au-delà de son contrôle peuvent affecter l'utilisation ou le fonctionnement des produits SP, SP n'offre aucune garantie que le document est exempt d'erreurs ou d'omissions.

Dans la plus large mesure possible, SP refuse de manière expresse d'offrir une garantie explicite ou implicite quant à l'état, à la valeur marchande ou à la pertinence de ces documents et limite sa responsabilité pour la perte directe ou indirecte liée à la disposition de SP à réviser le document ou au coût de sa correction.

Comme tout produit électrique ou à gaz, les produits SP doivent être installés et utilisés de manière appropriée. Vous devez vous assurer que vous lisez, comprenez et suivez les directives de SP – ainsi que toutes les lois locales et les normes de sécurité – et prenez tout le soin raisonnable lors de l'installation ou de l'utilisation des produits SP.

Si vous ne comprenez pas les instructions ou les informations fournies dans ce document, veuillez contacter SP à l'adresse ci-dessous pour obtenir une assistance.

### Commentaire

Pour tout commentaire ou question à propos de ce document, veuillez contacter SP :

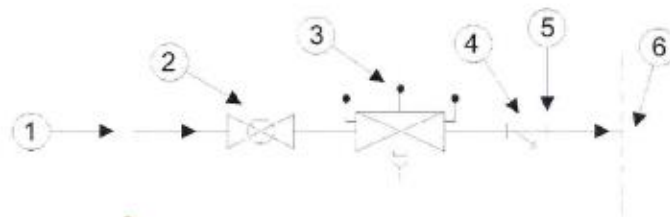
#### SOLIDpower GmbH

Borsigstrasse 80  
D-52525, Heinsberg, Germany  
Technique: +49 (0)2452 15 3701  
Sales: +49 (0)2452 15 3758  
Facsimile: +49 (0)2452 15 3755  
Enquiries: info@solidpower.com



# APPENDIX 5: INSTALLATION MANUAL OF THE (TESTED) BL\*\*\*G\*N (REVERSE OSMOSIS PAGE)

Manuel/Handleiding - BlueGEN Manuel d'installation / Installatiehandleiding



1. Réseau de distribution d'eau
2. Vanne d'isolement de l'alimentation d'eau
3. Disconnecteur type BA
4. Tamis filtrant (en option)
5. Adaptateur 3/8" vers 1/4" John Guest
6. Interface du BlueGEN : raccord rapide 1/4" « John Guest »

Figure 16: configuration recommandée pour le raccordement de l'alimentation en eau

## 5.5.2 Eau usagée d'osmose inverse

Le raccord utilisé pour l'eau usagée de l'osmose inverse (RO) sur le BlueGEN est un raccord rapide 1/4" « John Guest ».

Un clip de verrouillage 1/4" « John Guest » doit être fixé sur tous les raccords rapides prévus pour la ligne d'osmose inverse du BlueGEN vers l'écoulement des eaux usagées.

L'eau usagée est évacuée sous pression (entre 0 et 1 bar ou entre 0 et 100 kPa).

Approximativement, les deux-tiers de l'eau fournie sont rejetés comme eau usagée de l'osmose inverse lorsque le BlueGEN effectue un remplissage à partir de l'alimentation du réseau uniquement. La quantité totale d'eau évacuée peut atteindre 27 litres par jour avec une puissance électrique de 1,5 kW.

Si l'évacuation du trop-plein doit se trouver à l'extérieur (exposé à des températures négatives), le diamètre choisi doit garantir que l'évacuation ne peut se bloquer en cas de gel. Un diamètre minimal d'un pouce est recommandé.



### Attention

L'extrémité du tuyau d'eau usagée d'osmose inverse ne doit en aucun cas être immergée, comme dans une trappe d'égout par exemple. Dans ce cas, de l'eau contaminée serait aspirée dans le réservoir de stockage d'eau du BlueGEN causant des problèmes de fonctionnement.



### Attention

Si l'évacuation d'eau usagée doit se trouver à l'extérieur (exposée à des températures négatives), le diamètre choisi doit garantir que l'évacuation ne peut se bloquer en cas de gel. Un diamètre minimal d'un pouce est recommandé.

# APPENDIX 6: CALIBRATION PRINCIPLES OF THE SOFC TEST BENCH

## SOFC – Test bench calibration



Water meter → graduated container (circuit had to be converted in open-loop) → flow rate about 200 L/h → total 10 L poured → error not perceptible with calibration method → assumption that sensor is within its intrinsic accuracy range

Gas meters → not calibrated as is → assumption that their calibration comes from the fact that their signals are consistent over several days. A verification has been performed with the main gas meter of the whole building (since this was the only gas appliance on the building's grid at the time).

Electrical meters → not calibrated as is → assumption that their calibration comes from the fact that their signals are consistent (max difference under 0,5%) over several days (+ consistency with power on on the inverter's screen, which indeed is displaying the electrical power output of the SOFC)

Thermocouples → plunged in ice and boiling water

PT500 → not calibrated as is → assumption that their calibration comes from the fact that their signals are consistent with thermocouples at ambient temperature (+ clear consistency in the tests)

Heat meter → not calibrated as is → consistency with first thermodynamics law ( $\dot{m} * c_p * \Delta T$ ) demonstrated in all the tests (consistent with water meter and thermocouples)

---

# APPENDIX 7: SOFC LABORATORY

## MEASUREMENTS PROCEDURE

The following procedure has been applied to ensure the validity of non-synchronous measurements described in *Section 4.2.4 - Test procedure* (and also, ensure the correlation between all the sensors that have been used).

1. For each stationary condition (having waited sufficiently, as described in *Section 4.2.4 - Test procedure*), mark the time and date
2. Manually mark the flow rate, power, return & depart temperature thanks to the Qalcosonic E1 heat meter (its measurements are instantaneous but constant). The correlation with the water meter and thermocouples can be performed (see step 6).
3. Manually mark the electrical power from the A2000 electrical power meter (its measurement is instantaneous but constant). The correlation with the MT174 electrical energy counter is possible (see step 6).
4. Mark the temperature return and depart from the thermocouples. Also mark the water flow rate measured from the frequency of the pulses provided by the DHV1300 water meter. This is performed with LabVIEW software (measurements are instantaneous but constant). The correlation with the heat meter is possible (see step 6).
5. Manually take the time of  $0,01\text{m}^3$  of gas consumption on the gas meter display, at least 3 times consecutively to avoid potential human timing error. Perform this with the two gas meters for correlation. This is the only measurement that does not include a direct power measurement display. Longer duration of acquisition (between two gas meter logs), with quantities of gas consumed higher than  $0,01\text{m}^3$ , has not been considered for two reasons. Firstly, the chosen quantity of  $0,01\text{m}^3$  corresponds already to 10 times the resolution of the gas meter. Secondly, as it is seen in the results of Table 7, Table 8 and Table 9, the logged duration is very highly repeatable even when compared to other operating conditions (temperature and flow rates), which indicates a very repeatable gas consumption (according to the chosen electrical output power) and corresponding power equivalent contained in the gas. Therefore, increasing the acquisition time would not change the resulting (average) equivalent power contained in the gas (and the resulting established efficiencies).
6. Perform the correlation between laboratory sensors (A2000 electrical power meter, depart and return thermocouples, DHV1300 water meter of the heat recovery circuit, BKG4T gas meter) and additional field-test sensors (Qalcosonic E1 heat meter, BKG4T gas meter, MT174 electrical meter). The correlation between the DHV1300 water meter associated to the depart and return thermocouples and the Qalcosonic E1 heat meter is direct as the Qalcosonic provides both temperature signals and counts the 'volume' of water that has passed through the sensor, exactly as the water meter. The correlation between the two gas meters BKG4T is also quite direct as well as their both have a gas volume display (both correlates if both indexes evolves similarly). The correlation between the A2000 electrical power meter and the MT174 (not associated to a frequency meter and LabVIEW) can be performed by establishing the electrical power related to the electrical energy measures/pulses of the MT174. This can be performed by measuring the duration associated to 10 Wh, i.e. 10 pulses, i.e. 10 blinks of the MT174 red led and deducing the corresponding electrical power to compare it to the A2000 display.



7. Repeat operations 2 to 4. If measures are not consistent, a reading error has surely occurred (or steady-state conditions are not occurring), so all the sequence has to be conducted again.

# APPENDIX 8: POLLUTANT TESTING (NO<sub>x</sub>, SO<sub>2</sub> AND CO) OF COMMERCIALIZED MICRO-COMBINED HEAT AND POWER (MCHP) FUEL CELLS

This appendix has been published as-is in the proceedings of the *36th International Conference On Efficiency, Cost, Optimization, Simulation and Environmental Impact of Energy Systems (ECOS2023)* [121] and accepted for publication in the *Journal of Environmental Management* [122]. Mainly, it aims to offer a more generalist approach than in the respective *Chapter 4 - Study of the Bl\*\*\*G\*N SOFC system* and *Chapter 5 - Study of the P\*2 PEMFC system* (more precisely in *Section 4.6 - Non-CO<sub>2</sub> pollutant emissions* and *Section 5.6 - Non-CO<sub>2</sub> pollutant emissions*) that focus on one technology at a time. Here, comparisons with other typical combustion appliances such as gas condensing boilers and Euro 6 diesel vehicle are presented. In addition, to enable suitable comparison with literature results, conversion equations of pollutant measurements from ppm to mg/kWh have been reported.

## Introduction

In its latest Sixth Assessment Report in April 2022, the Intergovernmental Panel on Climate Change has reported a maximum carbon budget of 890 GtCO<sub>2</sub> that humanity can emit from January 1<sup>st</sup> 2020 in order for global warming to likely remain under the +2 °C widely acknowledged limit compared to preindustrial temperature levels [3]. Even at residential scales, this much-needed GreenHouse Gases (GHG) mitigation brings focus on cleaner power sources and on combined heat and power (CHP) systems, such as fuel cells [550]. The two primary technologies that have already been commercialized are the Proton Exchange Membrane Fuel Cells (PEMFCs) and the Solid Oxide Fuel Cells (SOFCs), which are compared in Table 44. GHG emissions (in terms of CO<sub>2</sub> or CO<sub>2eq</sub>) of such systems have already been addressed [15,427] but another key element in assessing the environmental impacts of those technologies lies in the other common air pollutants : the emissions of nitrogen oxides (NO<sub>x</sub>), sulphur dioxide (SO<sub>2</sub>), and carbon monoxide (CO).

The novelty of this study lies within the evaluation of SO<sub>2</sub>, NO<sub>x</sub> and CO emissions of fuel cell technologies commercialized for residential applications in both laboratory and field-test configurations (in real dwellings in Belgium). This has been performed on several machines of different ages, for one PEMFC-based and one SOFC-based technology, thanks to a combustion analyser portable meter. This study compares the emission levels of those pollutants measured for the studied fuel cell systems with other combustion technologies, such as a recent Euro 6 diesel automotive vehicle and classical gas condensing boilers. To facilitate comparison with relevant literature, a method of converting the concentration of pollutants (measured in ppm) detected by the sensors into pollutant intensity per unit of energy (in g/kWh) has been documented and reported, which has never been the case in

an academic work to the knowledge of the authors. This approach enables the assessment of pollutant emissions levels across different studies, including those conducted using alternative measuring sensors.

Fuel cell type & Charge carrier	Typical electrolyte	Major contaminants	Stack operating temperature (°C)	Specific advantages	Specific disadvantages	LHV Electrical efficiency (%)
PEMFC & H+	Solid Nafion®, a polymer	Carbon monoxide (CO) <sup>a</sup> Hydrogen sulfide (H <sub>2</sub> S) <sup>a</sup>	60–80 (only low-temperature PEMFC are currently commercialized [261])	Highly modular for most applications	Complex water and thermal management <sup>a</sup> Low-grade heat High sensitivity to contaminants <sup>d</sup> Expensive catalyst Expensive Nafion® membrane [260]	40-60 (with H <sub>2</sub> ) (Currently limited to 38.5 with CH <sub>4</sub> as some fuel needs to be burned to provide heat to a methane reformer [259])
				High power density Compact structure Rapid start-up due to low temperature operation Excellent dynamic response		
SOFC & O <sup>2-</sup>	Solid yttria-stabilized zirconia, i.e. YSZ, a ceramic	Sulfides	800-1000	High electrical efficiencies	Slow start-up Low power density Strict material requirements High thermal stresses Sealing issues Durability issues	55-65 (with H <sub>2</sub> ) (Currently limited to 60%-65% with CH <sub>4</sub> [261,410], i.e. still high thanks to the SOFC fuel flexibility)
				High-grade heat High tolerance to contaminants Possibility of internal reforming Fuel flexibility Inexpensive catalyst Simpler water management (SOFC can work at a perfect drying state [274])		

<sup>a</sup> Contaminants, thermal and water management of PEMFC stacks have been discussed more deeply in another work [496].

**Table 44.** Comparison between PEMFCs and SOFCs. Reproduced and adapted from reference [205].

## Material and methods

### Tested systems

#### PEMFC hybridized to a gas condensing boiler

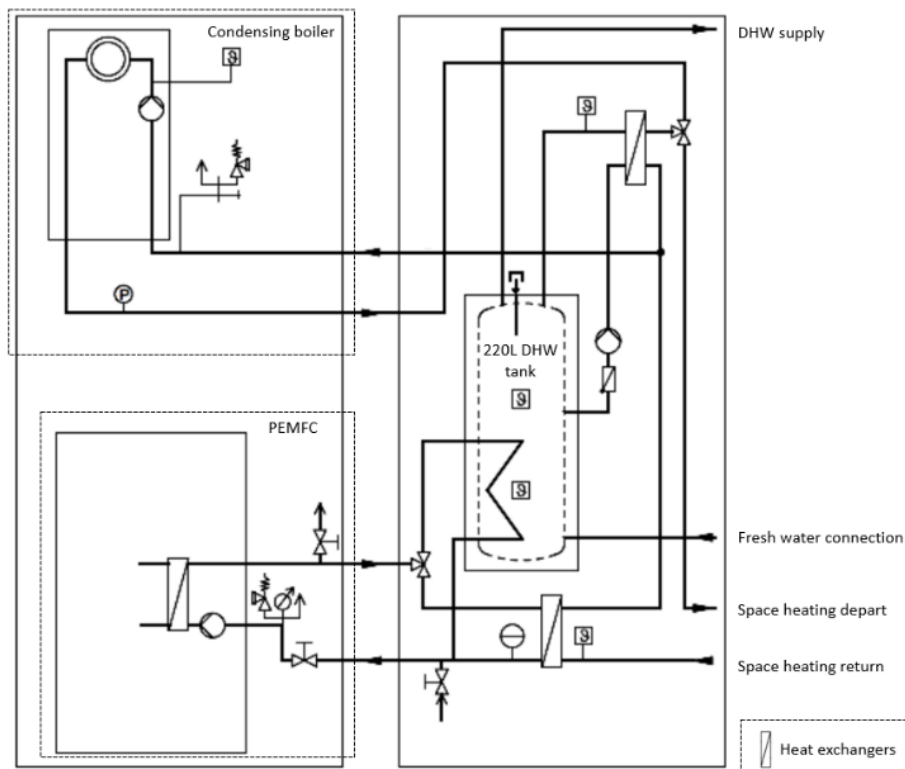
The PEMFC is not a standalone unit. It is hybridized to a gas condensing boiler and to a Domestic Hot Water (DHW) tank. It is fed by natural gas and is designed to cover all the heat demands, including DHW, of residential houses and to participate locally in the electrical production. This particular system exists in several versions all based upon the same PEMFC module of nominal constant power of 0.75kW<sub>el</sub> (and 1.1kW<sub>th</sub>) and the same 220L DHW tank. The only module that may vary is the gas boiler that is supposed to ensure peak heat demands. Indeed, it exists in four rated power versions from 11.4 to 30.8kW<sub>th</sub>, depending on thermal needs [523]. The heat rate output of the field-test system considered in this study is rated to 24.5 kW<sub>th</sub> and is located in Huy, in Belgium. System's architecture is presented in Figure 104, which does not show the double walled chimney used for both the air inlet and flue gases exhaust [443]. Main datasheet characteristics are presented in Table 45.

The complete system’s behaviour is heat driven. Its PEMFC has not been designed to be driven by the electrical demand and it is preferable that it runs as long as possible. It includes a methane reforming apparatus to feed the fuel cell stack with clean hydrogen and requires an automated fuel cell shutdown recovery procedure of 2.5 hours at least every two days to handle some reversible ageing processes [496]. For further information, this system has been quite exhaustively studied in other publications [15,477,496,537,550,564].

Datasheet figures	Values
Maximum electrical production a year	6200kWh <sub>el</sub>
Fuel cell rated electrical and thermal power as defined by EN 50465 [550]	0.75kW <sub>el</sub> & 1.1kW <sub>th</sub>
Electrical fuel cell efficiency	37% (LHV)
Max global Fuel cell efficiency	92% (LHV)
Max boiler efficiency (at rated power) <sup>a</sup>	108.6% (LHV)
NO <sub>x</sub> , class 6 [493]	7.2 mg/kWh
Size without chimney (Hight x Width x Depth)	1800 mm x 595 mm x 600 mm

<sup>a</sup> Considering High Heating Value (HHV) to Low Heating Value (LHV) ratio of 1.1085 [132]

**Table 45.** PEMFC gas boiler hybrid expected targets (data published by manufacturer) [523].



**Figure 104.** PEMFC system’s architecture, including two heat exchangers, several 3-way valves, several circulators, the gas condensing boiler and the DHW tank [15].

**SOFC**

The studied SOFC is also fed by natural gas. It is designed to provide 1.5 kW<sub>el</sub> of nominal output power with a high announced LHV electrical efficiency of 60%, along with a heat recovery of 0.6 kW<sub>th</sub> representing a LHV thermal efficiency up to 25% [427]. The output power can be modulated down remotely (by the manufacturer, upon the owner’s request) as wanted in the 0.5 - 1.5 W<sub>el</sub> range, affecting those announced efficiencies. It is not advised to completely shut it down because thermal cycles affect its durability and because start-up operations are long and have been reported in the user manual to last up to 30 hours [448].

Discarding its chimney, the system has approximately the same size as a dishwasher, as it can be seen in Figure 105. Its internal schematics has not been disclosed but has been discussed in a previous publication [427], based on observations of the system and cogeneration SOFC literature. Amongst other particularities, the reforming process of the inlet natural gas (into hydrogen) is not only internal, i.e. directly at the anode onto the stack (allowed with high operating temperatures occurring with that fuel cell technology [181]), but it also uses an external steam reformer upstream of the stack (called ‘preformer’ [427]). For information, the newer version of this system is stated by the manufacturer as belonging to class 6 in terms of NO<sub>x</sub> [492] (according to EN 15502-1 [493]) but the exact emission levels have not been reported, to the knowledge of the author.



**Figure 105.** Tested micro-CHP SOFC in the laboratory facilities of the University of Liege [447].

### Gas condensing boiler

The tested mural gas condensing boiler dates from 2005 and is quite classical. Its identification name is ‘Buderus Logamax plus GB142-45’ and it can provide up to 45 kW<sub>th</sub> (that can be modulated down to 30%). It is able to provide heat to an optional DHW tank but cannot provide instantaneous DHW directly as it has only one hydraulic inlet and one hydraulic outlet (used in close circuit configurations). The emissions of CO and NO<sub>x</sub> are reported by the manufacturer respectively to 15 mg/kWh and 20 mg/kWh [601].

### Euro 6 diesel vehicle

The tested vehicle is a 4-year BMW X1 sDrive18d that is proper maintenance and had 111210 kilometers on the odometer at the moment of the test. Its four-stroke engine has four cylinders and represents a displacement of 1995cm<sup>3</sup>. Net power is 100 kW at 4000 rpm. The certificate of conformity presents average emissions on the New European Driving Cycle (NEDC) for CO and NO<sub>x</sub> respectively of 86.8 mg/km and 19.2 mg/km. Maximum Real Driving Emissions (RDE) NO<sub>x</sub> emissions are reported to be equal to 168 mg/km. Considering an effective consumption of 6L per 100 km (according to the dashboard of the vehicle), considering a diesel LHV of 43.51 MJ/kg and a density of 827 kg/m<sup>3</sup> [602], those emissions correspond respectively to 145 mg/kWh (average CO emissions on the NEDC), 32 mg/kWh (average NO<sub>x</sub> emissions on the NEDC) and 280 mg/kWh (maximum Real Driving Emissions NO<sub>x</sub>). They are relative to the diesel LHV input to the engine.

## Measurement device

To perform the pollutants emissions analyses of the tested systems, the same portable combustion analyser meter has been used. It is called 'Multilyzer STx' and is shown in Figure 63 whereas its specifications are shown in Table 23.

It measures CO, NO, NO<sub>2</sub> and SO<sub>2</sub> in ppm, whereas O<sub>2</sub> and CO<sub>2</sub> concentration levels are expressed in percentage (by volume). Carbon monoxide sensors have generally a significant cross-sensitivity to hydrogen, meaning that the real carbon monoxide concentration can be overestimated if hydrogen is present as well in the tested gas sample [603]. Therefore, as presented in Table 23, the 'Multilyzer STx' combustion analyser portable meter has implemented a hydrogen compensation for its carbon monoxide measurements.



**Figure 106.** 'Multilyzer STx' combustion analyser portable meter.

Sensor	Range	Accuracy	Resolution
NO	0 - 5000 ppm	± 5 ppm (< 50 ppm) ± 5% reading (> 50 ppm)	1 ppm
NO <sub>2</sub>	0 - 500 ppm	± 10 ppm (< 50 ppm) ± 10% reading (> 50 ppm)	1 ppm
SO <sub>2</sub>	0 - 5000 ppm	± 10 ppm (< 200 ppm) ± 5% reading (> 200 ppm)	1 ppm
CO (hydrogen compensated)	0 - 10000 ppm	± 5 ppm (< 50 ppm) ± 5% reading (> 50 ppm)	1 ppm
O <sub>2</sub>	0 - 21 % vol.	± 0,2% vol.	0,1% vol.
CO <sub>2</sub> (calculated from O <sub>2</sub> level)	0 % vol. up to (CO <sub>2</sub> ) <sub>N</sub> which depends on fuel type, see Equation (66)	± 0,2% vol.	0,1% vol.
Gas temperature	0 - 1150 °C	± 1 °C (0 - 300°C) ± 1% reading (> 300°C)	0,1 °C

**Table 46.** Specifications of the 'Multilyzer STx' combustion analyser portable meter [494].

## Conversion of ppm to mg/kWh

Literature on space heating appliances pollution levels is quite rare and pollutant emissions are regularly reported in terms of concentration (in ppm [604]) or in terms of intensity (in mg/kWh [180]). However, it is quite rare for both pieces of information to be provided. In this case, the pollutant emissions measurements are provided by the metering device in ppm (see Table 23) whereas, for comparison purposes, it would be more

meaningful to express them in terms of mg/kWh. Indeed, Table 6 for example reports from literature the NO<sub>x</sub> emission levels of several space heating appliances in mg/kWh. In addition, as it has been seen earlier, the datasheets of the tested space heating appliances only express the emissions in terms of mg/kWh. Therefore, to use those figures as references for this study, the emission measures performed in this work must be converted from ppm to mg/kWh.

For natural gas appliances, this can be performed for carbon monoxide emissions thanks to Equation (66) [493]:

$$CO_{(mg/kWh)} = 1.074 \times CO_{(ppm)} \times \frac{(CO_2)_N}{(CO_2)_M} \quad (66)$$

Where  $CO_{(mg/kWh)}$  is the carbon monoxide emissions level per unit of energy (kWh) that must be established for the studied combustion test;  $CO_{(ppm)}$  is the measured carbon monoxide concentration at the exhaust of the system during the combustion test (in ppm);  $(CO_2)_M$  is the measured carbon dioxide concentration at the exhaust of the system during the combustion test (in %) and  $(CO_2)_N$  is the maximum carbon dioxide concentration of the dry, air-free, combustion products (in %), which depends only on the natural gas type that is fed to the studied system during the combustion.  $(CO_2)_N$  is equal to 11.7% for G20 natural gas and 11.5% for G25 natural gas [493].

Indeed, in Belgium [465] (as in France or Germany [605]), natural gas comes from different sources, which implies different gas compositions and different HHV and leads to the appellations 'lean' and 'rich' gas, respectively for the natural gas source providing the lower and the higher HHV [592]. Lean gas is also called 'L-gas' [593], 'type L' gas [465] or G25 [605] whereas rich gas is also called 'H-gas' [593], 'type H' gas [465] or G20 [605]. The type of gas provided on the grid only depends on the localization of the delivery point. All lean gas deliveries are supposed to be progressively replaced (in Belgium) by 2030 by rich gas deliveries [593].

As reported in the previous section,  $(CO_2)_M$  and  $CO_{(ppm)}$  are provided by the meter used in this work. Also, in Equation (66), the 1.074 constant is the unit conversion coefficient related to CO emissions from natural gas appliances [606].

Space-heating appliance	NOx range (source from 1998 : Electrabel-SPE – combustion only) mg/kWh <sub>LHV</sub>	NOx (source from 2007 : Fondation Rurale de Wallonie - combustion only) mg/kWh <sub>th</sub>	NOx (source accessed in 2007: Gemis 4.5 - complete LCA cycle) mg/kWh <sub>th</sub>
Old oil-fired boiler	up to 200	Unavailable	Unavailable
Non-Low NOx oil-fired boiler	150 – 180	144	244
Low NOx oil-fired boiler	90 – 120	Unavailable	Unavailable
Old gas boiler	150 – 200	Unavailable	Unavailable
Atmospheric gas boiler	100 – 180	Unavailable	Unavailable
Modulating gas condensing boiler	20 – 90	144	140
Old log wood boiler	Unavailable	180	Unavailable
Modern log wood boiler	Unavailable	151	235
Wood chip boiler (wood chips)	Unavailable	162	Unavailable
Condensing wood boiler (pellets)	Unavailable	Unavailable	344

**Table 47.** Combustion only and Life Cycle Assessment (LCA) NO<sub>x</sub> emission level reported from Energie+ [180] (website developed by the University of Louvain-la-Neuve and the Energy department of the Walloon Region, in Belgium).

Similarly, ppm to mg/kWh conversion for NOx emissions of natural gas appliances is obtained thanks to Equation (67) :

$$NOx_{(mg/kWh)} = \frac{\left( C_g \times NOx_{(ppm)} \times \frac{(CO_2)_N}{(CO_2)_M} \right) - 0.85(20 - T_m) + \frac{0.34(h_m - 10)}{1 - 0.02(h_m - 10)}}{\left( 1 + \frac{0.02(h_m - 10)}{1 - 0.02(h_m - 10)} \right)} \quad (67)$$

Where  $NOx_{(mg/kWh)}$  is the nitrogen oxide emissions level per unit of energy (kWh) that must be established for the studied combustion test;  $C_g$  is the unit conversion coefficient related to NOx emissions from natural gas appliances [607] and is equal to 1.764 for G20 (rich gas) or 1.767 for G25 (lean gas) [493];  $NOx_{(ppm)}$  is the sum of the measured nitrogen dioxide and nitric oxide concentrations at the exhaust of the system during the combustion test (in ppm);  $(CO_2)_N$  and  $(CO_2)_M$  have already been described for Equation (66);  $T_m$  is the temperature of the outdoor air used for the combustion (in °C) and  $h_m$  is the absolute humidity of the outdoor air used for the combustion (in g of water per kg of dry air).  $h_m$  is the only variable of Equation (67) that is not provided by the combustion analyser meter (see Table 23). By assimilating inlet air to humid air of relative humidity between 40 and 80%, at atmospheric pressure and at the  $T_m$  temperature,  $h_m$  can be approximated with the Engineering Equation Solver (EES) software. It is worth mentioning for Equation (67) that the allowable ranges for  $T_m$ ,  $h_m$ ,  $NOx_{(mg/kWh)}$  and are respectively 15 - 25 °C, 5 - 15 g of water per kg of dry air, and 50-300 mg/kWh. However, industrial partners in this work advise to use Equation (67) anyway even if some parameters are out of those ranges.

The European standard from which Equation (66) and Equation (67) are deduced [493] unfortunately does not provide any information about SO<sub>2</sub> emissions conversion. Fortunately, another reference [608] provided Equation (68), which has been reported to be relevant not only for SO<sub>2</sub> but also for CO and NOx emissions, giving similar conversion results respectively to Equation (66) and Equation (67) (in its allowable range).

$$PEI_{(mg/kWh)} = F \times PEC_{(ppm)} \times \frac{20.9}{20.9 - (O_2)_M} \quad (68)$$

Where  $PEI_{(mg/kWh)}$  is the pollutant emissions intensity, i.e. the emission level per unit of energy (kWh) that must be established for the studied combustion test;  $F$  is an emission rate conversion factor that depends on the pollutant (and the type of fuel) and that is given in Table 48,  $PEC_{(ppm)}$  is the measured pollutant emissions concentration at the exhaust of the system during the combustion test (in ppm) and  $(O_2)_M$  is the measured oxygen concentration at the exhaust of the system during the combustion test (in %). Equation (68) has the particularity to consider O<sub>2</sub> concentration (in %) in the exhaust whereas Equation (66) and Equation (67) rely on CO<sub>2</sub> concentration (in %).

Similar conversion equations for diesel engines have not been reported in this work but can also be found in literature [609].

Pollutant	$F$ mg/(kWh-ppm)
CO	0.974313
NOx	1.608389
SO <sub>2</sub>	2.242466

**Table 48.** Natural gas  $F$  coefficients for Equation (68) depending on the pollutant type [608].



## Testing procedure and results

The end of the probe of the 'Multilyzer STx' must be placed at the centre of the exhaust gas chimney (or tailpipe) and the probe axis can either be oriented in the perpendicular plane of this chimney (or tailpipe) or parallel to it (if the measurements are conducted at the exit of the chimney/tailpipe). The probe disposes of a conical adjustable mechanical stop to ensure the correct probe depth to the centre of the chimney (see Figure 63).

The studied PEMFC system, which is composed of a PEMFC stack hybridized to a gas condensing boiler (see the tested systems described above), has the advantage of being equipped by design with a small, sealable access hole, fitted with a cap, directly at the exhaust of the system (in the first 5 cm of the chimney). There is thus no need with the PEMFC system to place the combustion analyser meter at the exit of the chimney, which access is very often difficult and potentially risky if it figures on the roof of the building. However, some measurements have still been taken at the exit of the chimney for comparison purposes (with the probe fully inserted in the chimney). Indeed, temperature (which varies all along the double walled chimney that cools down the flue gases and heats up the inlet air from outdoors) is not only known to influence the NO<sub>x</sub> formation but also the NO-NO<sub>2</sub> equilibrium. This is especially the case in the near-post-flame zone [610] (close to the outlet of the system), but also in the atmosphere in the presence of Volatile Organic Compounds (close to the exit of the chimney) [140], which can be co-emitted in hydrocarbons combustion [610]. The PEMFC hybrid system was tested in two separate modes : with only the PEMFC turned on and with only the gas condensing boiler turned on. This system, installed in 2019, was tested in a field-test application (in a real house) in Huy (in Belgium). At the moment of the tests, the whole machine has been functioning for about 15000 hours but its integrated fuel cell has only been producing electricity for about 5500 hours. It is worth mentioning that another machine of this system, which was perfectly new, was tested in a laboratory environment (see Figure 107).

The studied micro-CHP SOFC system does not involve any hole in its chimney by design. However, since one machine of this system was tested in laboratory facilities, a hole was manufactured at a chimney height of 50 cm (above the system flue gases outlet). This particular machine was used for two pollutant test campaigns (conducted at minimum and intermediate electrical power output, i.e. 500 W<sub>el</sub> and 1000 W<sub>el</sub>). This machine, installed in 2021, had already been functioning for about 6000 hours before being tested. In the laboratory facilities, the return temperature of the heat recovery circuit could be controlled [448] (which affects the exhaust gas temperature). For the other pollutant test campaign (at full rated electrical power output, i.e. 1500 W<sub>el</sub>), the combustion analyser meter was placed in another configuration. It was indeed positioned at the exit of the chimney (and fully inserted in it) since this campaign was performed on another SOFC machine (with the same reference) in a field-test application in Riemst (Belgium). At the moment of the pollutant measurements, this second machine, installed in 2017, has already been functioning for about 45000 hours.

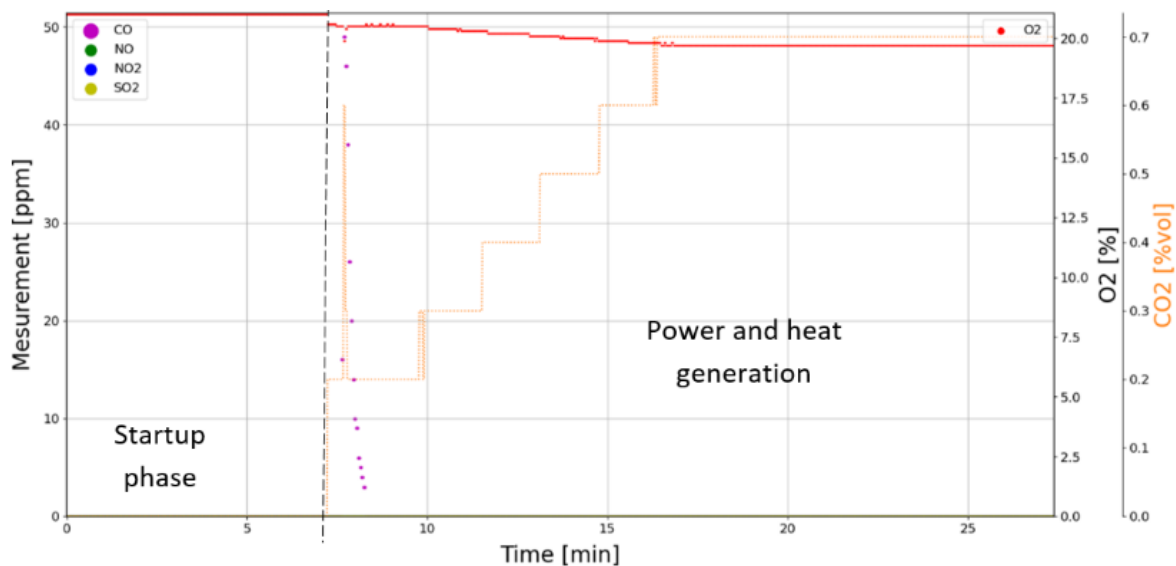
As mentioned, another classical gas condensing boiler has been tested (only at the exit of its chimney, with the probe fully inserted in it). This system was tested in a field-test application in Riemst (Belgium).

At last, the Euro 6 diesel vehicle was tested at the exit of both of its tailpipes. The probe of the sensor could be oriented parallel to the tailpipe so it has either been fully inserted in the tailpipe (about 35 cm before its exit) or only inserted over about 15 cm. The purpose was to see the changes in the exhaust gas temperature and their impact on the pollutant measurements. It is worth mentioning that the car engine was tested at idle ( $\pm 850$  rpm) and at 1500 rpm but the clutch was always disengaged.

All the tests include a purge with clean air before starting the measurements. It is indeed a mandatory step requested by the 'Multilyzer STx' combustion analyser meter. At last, the sample time was always of one second.

All the tests have other specificities in the way they have been conducted and those are reported accordingly in Table 49 along with the pollutant emissions results.

In addition, for information, a graphical example of such similar pollutant tests (performed with the same sensor) is given in Figure 107 for the studied PEMFC system in its startup phase (with the boiler turned off). In that test, no NO<sub>x</sub> nor SO<sub>2</sub> could be measured. Startup phase (duration between the machine's startup initiated thanks to a thermal demand and the moment when the fuel cell starts producing electricity) takes about 7 min whereas the total duration to reach steady-state is about 15-20 min (gradually from 0 W<sub>el</sub> to its nominal output power of 750 W<sub>el</sub>). A CO peak of about 2 minutes, with a maximum at 55 ppm, can be noticed at the beginning of the power and heat generation phase, probably due to transient behaviours of the internal reformer required for this PEMFC fed by natural gas [496]. The stepped behaviour of the CO<sub>2</sub> percentage measurement is explained by the resolution of the sensor and the fact that it is not directly measured but established by the combustion analyser from O<sub>2</sub> measurements (Table 23). However, the CO<sub>2</sub> sudden peak is probably an outlier as it could not be explained.



**Figure 107.** Pollutant measurements of the fuel cell (only) startup phase of the PEMFC-gas condensing boiler hybrid system (performed in a laboratory environment).

Test and conditions	NO <sup>a</sup>	NO <sub>2</sub> <sup>a</sup>	CO <sup>a</sup>	Remarks
PEMFC hybrid system ( <b>PEMFC only mode</b> ) Measured on the field-test site in Huy without control on the return temperature (or on the exhaust gas temperature)	0	0	- Startup : short peak up to 55 ppm for 2 min (in total). Also measured in the laboratory (Figure 107). - Steady state : 0 but an unexplainable short peak similar to fuel cell startup has been measured while the PEMFC was running	- Boiler turned down by closing the radiator valves in the house - No difference in the pollutant measurement between the exit of the chimney (on the roof) and the exit of the system
PEMFC hybrid system ( <b>condensing gas boiler only mode</b> ) Measured on the field-test site in Huy without control on the return temperature (or on the exhaust gas temperature)	- Startup : peak up to 7 ppm for 5 min (in total) - Steady state : 0	- Startup : 3 ppm - Steady state : 3 ppm, i.e. 6.7 mg/kWh	- Startup : short peak up to 80 ppm for 30 sec (in total) - Steady state : 30 ppm, i.e. 40.7 mg/kWh	- Boiler turned on by opening the radiator valves in the house and setting a high temperature setpoint on the thermostat (the PEMFC happened to be turned off, probably conducting a regeneration procedure [496])
SOFC – 500 and 1000 W <sub>el</sub> output Tested in laboratory with different heat recovery temperatures, i.e. different exhaust gases temperature (from 45°C to 25°C)	0	0	5 ppm (at 500 W <sub>el</sub> ), i.e. 28.3 mg/kWh 11 ppm (at 1000 W <sub>el</sub> ), i.e. 41.5 mg/kWh	- Return temperature of the heat recovery circuit has no influence on the pollutant measurements - Only steady state data (the system in supposed to be turned on continuously and the startup test was not conducted)
SOFC - 1500 W <sub>el</sub> output Measured on the field-test site in Riemst with only one heat recovery temperature corresponding to 60°C of exhaust gases temperature	0	0	8 ppm, i.e. 17.0 mg/kWh	- Same reference but a different system as the previous row) - Only steady state data (the system in supposed to be turned on continuously and the startup test was not conducted)
Classical gas condensing boiler - high DHW load (exhaust gases temperature of about 65°C at the exit of the chimney) Measured on the field-test site in Riemst	- Startup : peak up to 8 ppm for 2 min (in total) - Steady state : 5 ppm, i.e. 10.1 mg/kWh	- Startup : peak up to 4 ppm for 2,5 min (in total) - Steady state : 2 ppm, i.e. 4.1 mg/kWh	- Startup : peak up to 50 ppm for 2 min (in total) - Steady state : 10 ppm, i.e. 12.3 mg/kWh	- No remark
Classical gas condensing boiler - low temperature space heating load (exhaust gases temperature of about 30°C at the exit of the chimney) Measured on the field-test site in Riemst	- Startup : Untested - Steady state : 0 ppm	- Startup : Untested - Steady state : 0 ppm	- Startup : Untested - Steady state : 8 ppm, i.e. 10.7 mg/kWh	- No remark
Euro 6 Diesel Engine at idle, i.e. ±850 rpm (car in neutral)	- Startup : continuous increase for about 20 min up to 60 ppm - Steady state : 55 ppm, i.e. 238 mg/kWh [609]	0	- Startup : rapid increase for about 3 min to the 200-300 ppm range - Steady state : 200-300 ppm, i.e. 800-1200 mg/kWh [609]	- The probe must be fully inserted in the tailpipe to record pollutant emissions - There is no difference between the left and right tailpipes
Euro 6 Diesel Engine at 1500 rpm	- Startup : unavailable (engine already warmed up) Steady state : 40 ppm, i.e. 173 mg/kWh [609]	0	- Startup : unavailable (engine already warmed up) Steady state : 850 ppm, i.e. 3430 mg/kWh [609]	- The probe must be fully inserted in the tailpipe to record pollutant emissions - There is no difference between the left and right tailpipes

<sup>a</sup> Equation (68) has been used to convert ppm measurement into mg/kWh for steady-state measurements only (of natural gas appliances). The similar conversion law for diesel engines comes from literature [609]. Peaks and startups have highly transient dynamic behaviours both on the pollutant concentration and the O<sub>2</sub> percentage signal, making the ppm to mg/kWh conversion hazardous.

**Table 49.** Pollutant emissions measurements results (in all tests, the sensor indicated 0 ppm of SO<sub>2</sub> emissions).

## Discussion and conclusion

None of the tested systems (PEMFC, SOFC, gas condensing boilers and Euro 6 diesel engine) showed any SO<sub>2</sub> emissions. This is either an indication of an issue with the SO<sub>2</sub> sensor or it proves the efficiency of the desulphurization treatment implemented in the natural gas process before it enters the grid [496]. In addition, both fuel cell systems include a desulphurizer in their respective fuel processors according to the consulted manufacturer's documentation. Regarding the diesel vehicle, the lack of SO<sub>2</sub> emissions could be explained by low sulphur content of diesel in the EU, limited to 10 ppm according to the EN 590:2009 regulation [611]. It could also be explained by the oxidation of SO<sub>2</sub> into SO<sub>3</sub> (not measured by the sensor) in the selective catalytic converter used in the exhaust of the engine to reduce NO<sub>x</sub> emissions [612].

Both fuel cell systems (PEMFC and SOFC) do not show any NO<sub>x</sub> emissions even if they involve high temperature reforming processes [427,496]. Oppositely NO<sub>x</sub> emissions of gas boilers (in steady state) were measured between 3 and 7 ppm, which is rather low. Using Equation (68) and thus considering the O<sub>2</sub> percentage measurement (not shown in Table 49), those figures can be converted in the 6.7-14.2 mg/kWh range, which is slightly better than literature provided (see Table 6). The lower part of that range, i.e. 6.7 mg/kWh, corresponds to the gas boiler of the PEMFC hybrid system, and it is indeed under the 7.2 mg/kWh figure announced by the manufacturer. For the other classical gas condensing boiler, it is also under the announced value of 20 mg/kWh. In comparison, the diesel Euro 6 engine showed NO<sub>x</sub> concentration of 55 ppm in neutral and 40 ppm at 1500 rpm (without any load since the clutch was not engaged). Considering another conversion equation from ppm to mg/kWh provided by literature for diesel engines [609] (Equation (68) and the coefficients of Table 48 being only relevant for natural gas appliances) and a molar mass of NO of 30, these NO<sub>x</sub> emission concentrations corresponds to the 173-238 mg/kWh range, i.e. under but close to the maximum NO<sub>x</sub> Real Driving Emissions announced at about 280 mg/kWh, assuming an average consumption of 6L per 100 km. It also approximately corresponds to the emissions of an old oil-fired boiler (Table 6).

For all tested systems, the NO<sub>2</sub> emissions are either nil or quite low compared to NO emissions, which was expected as NO has been reported to be the predominant nitrogen oxide emitted by combustion devices [610].

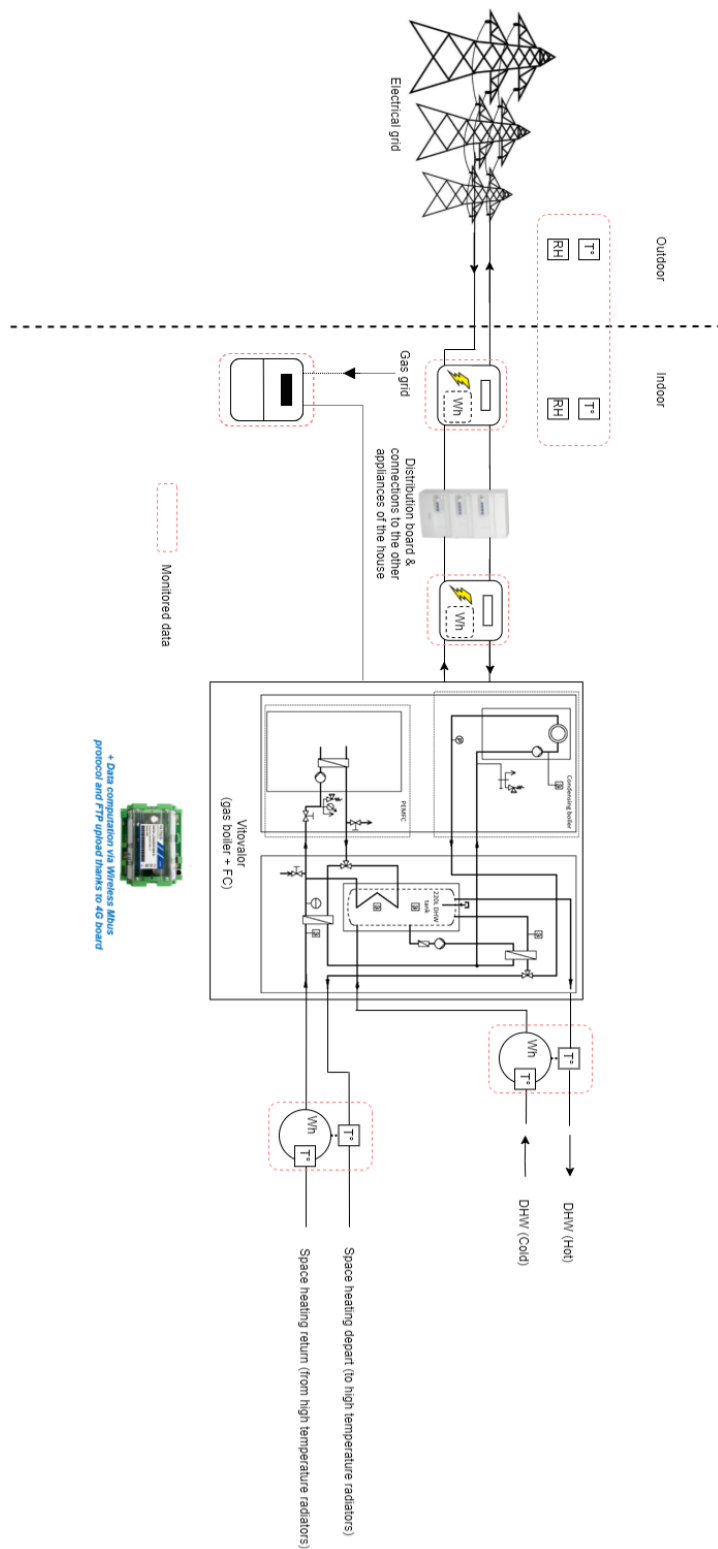
There were no CO emissions regarding the steady state operating conditions of the PEMFC system (other than an explicable peak that is similar to the transient CO peak that occurs at the PEMFC startup, as seen in Figure 107). This was expected since CO is a major pollutant of PEMFC stacks and since it has been reported that the system is equipped with a CO removing apparatus in the fuel (natural gas) processing system (prior to the stack) [496]. Transient CO peaks are surely not caused by the fuel cell stack but by the fuel processor of the PEMFC system. For example, it could happen when the reforming processes start and is not yet at its steady state temperature levels, impeding the CO remover to operate efficiently. During these transients for which CO can occur, the PEMFC stack must indeed surely be bypassed [496]. Also, it has been reported that the PEMFC system involves an afterburner for reforming purposes (because methane reforming requires temperatures much higher than the one occurring in the PEMFC stack) [496]. In addition to burning the stack exhaust gases when the PEMFC is running (the anode exhaust still contains unused hydrogen and the cathode contains an excess of air, which is at a higher temperature than the ambient air), this afterburner also requires a direct feed from the natural gas supply to ensure enough heat for the reforming processes [496]. The inexplicable CO peak while the PEMFC was running is likely to be related to this afterburner (after the stack) and it can once again be assumed that no CO has gone through the PEMFC stack.

Oppositely, the SOFC system (two different machines of the same reference tested) showed slight CO emissions (5 ppm, 11 ppm and 8 ppm respectively at 500  $W_{el}$ , 1000  $W_{el}$  and 1500  $W_{el}$  of power output) with no dependence on the thermal output or on the exhaust gases temperature (driven by the return temperature of the heat recovery system). Through Equation (68), these CO concentrations respectively correspond to 28.3 mg/kWh, 41.5 mg/kWh and 17.0 mg/kWh. It is worth mentioning that the PEMFC system was mainly tested in field-test real applications so the return temperature (and the exhaust gas temperature) could not be controlled, although it is not believed to affect the pollutant emissions in steady state (which were nil).

CO emissions peak (between 50 and 60 ppm) at gas condensing boilers startup is probably due to the momentary incomplete combustion in this highly transient starting process. In steady-state, the tested machines showed 8 to 30 ppm of CO emissions, corresponding to 10.7 mg/kWh to 40.7 mg/kWh using Equation (68) (very similar to the CO emissions range of the SOFC). The gas condensing boilers were tested in field-test applications so the return temperature (and therefore the exhaust gases temperature) could not be controlled. Regarding the diesel engine, the steady state CO emissions were much higher, between 200 and 300 ppm at idle and up to 850 ppm at 1500 rpm. Equation (68) and the coefficients of Table 48 can only be used with natural gas. Therefore, another conversion law has been found in literature [609], which leads to the 800-1200 mg/kWh range at idle and to about 3430 mg/kWh for the 1500 rpm test. Those levels of CO emissions are far greater than the one announced on the certificate of conformity for the average NEDC (calculated in this work to about 145 mg/kWh). This is another proof of the inadequacy of the NEDC to account for pollutant emissions [613] but it also should be reminded that maintaining the engine at 1500 rpm while keeping the vehicle stationary is also not exactly representative of real driving conditions (although it provides interesting results for comparisons).

As a final conclusion, both tested residential fuel cell technologies fed by natural gas can be considered clean in terms of SO<sub>2</sub> and NO<sub>x</sub> emissions. In addition, the CO emissions can be considered quite low for the tested SOFC and even nil for the tested PEMFC. Those statements apply even with machines that have already been running for up to 45000 hours. Therefore, the biggest issue of natural gas fuel cell technologies still lies in the CO<sub>2</sub> emissions associated with the fossil fuel they consume.

# APPENDIX 9: DETAILED SCHEMATICS OF THE MONITORING SENSORS CONFIGURATION OF THE P\*2 FIELD-TEST SITES



# APPENDIX 10 : P\*2 BEHAVIOR AND HOW IT AFFECTS EFFICIENCY: ZOOMING ON REPRESENTATIVE DAYS

In order to illustrate the efficiency difference seen on yearly performance stated above, one ‘typical’ week has been identified in the data. By ‘typical’, one has tried to identify some repeatable days in order for the behavior of the system and of the occupants (and the difference in behavior) to be highlighted. The focus is thus brought on the seven first days of October 2020 for both houses (Oostmalle and Huy).

Table 50 presents the main monitoring data for that focus week. Since the goal of this section is to illustrate the efficiency difference between the two houses (and show how they relate to the behavior), the main criterion to consider those days as ‘repeatable’ is that they show similar efficiencies. Indeed, one can see in Table 50 that the hardness of the climate is not the same along the focus week. This has an influence on the space heating demand as one can see the direct influence for the Oostmalle house. However, it is not as clear for the house in Huy that shows a greater variance in the heat demand. This is mainly due to the fact that the Huy house uses high temperature terminal units and the heat demand is strongly dependent on the building occupancy, as deduced from *APPENDIX 11: Satisfactory Survey of the house in Huy* (whereas the Oostmalle house has floor heating that implies very smooth almost constant heat demands). Therefore, it is assumed that the Huy occupants have a bigger interaction with the terminal units (they manually open and close the radiator valves) and the resulting heat demand is more linked to the amount of time the valves are opened than to the hardness of the climate. This has been verified by questioning the occupants as it can be read in *APPENDIX 11: Satisfactory Survey of the house in Huy*.

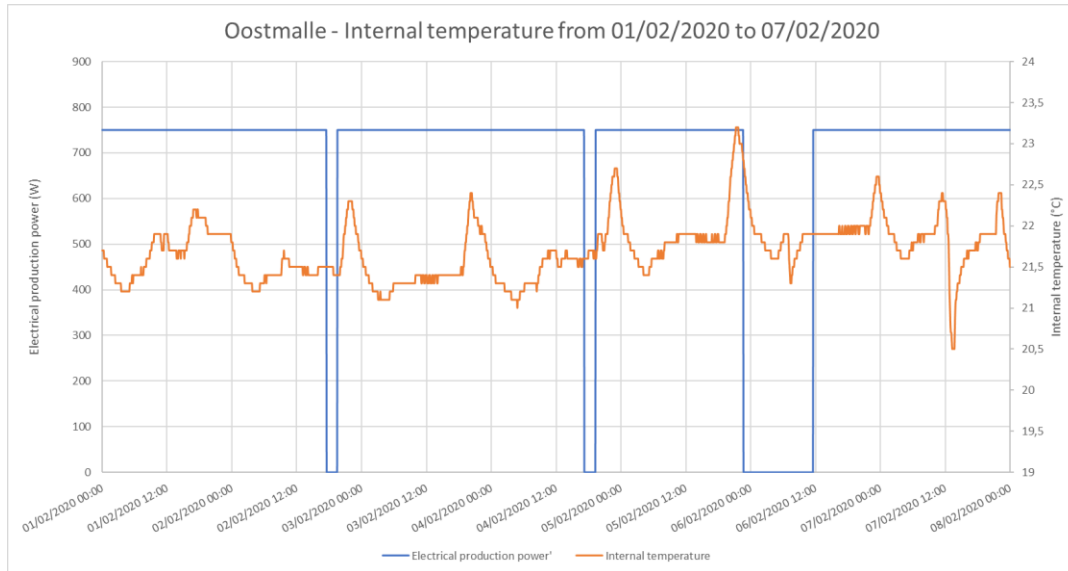
	External temperature (°C)	DHW production (kWh)		Space heating production (kWh)		Electrical production (kWh)		HHV energy consumed in the gas (kWh)		LHV daily thermal efficiency* (%)		LHV daily electrical efficiency* (%)		LHV daily total efficiency* (%)		
		Huy	Oostmalle	Huy	Oostmalle	Huy	Oostmalle	Huy	Oostmalle	Huy	Oostmalle	Huy	Oostmalle	Huy	Oostmalle	
Saturday	01/02/2020	11,3	3	9	84	77	8,12	17,57	122,67	129,1	77,20	73,84	7,21	15,08	84,41	88,92
Sunday	02/02/2020	10,2	6	11	50	85	8,92	15,87	83,16	135,43	72,45	78,32	11,54	12,95	83,99	91,27
Monday	03/02/2020	10,4	7	9	45	86	7,18	17,49	75,106	138,68	74,57	75,93	10,30	13,98	84,87	89,91
Tuesday	04/02/2020	5,4	7	6	73	101	8,57	15,7	111,16	150,86	78,30	78,38	8,39	11,50	86,69	89,88
Wednesday	05/02/2020	5,3	6	3	91	104	9,1	16,41	133,6	153,74	79,22	76,98	7,43	11,81	86,65	88,79
Thursday	06/02/2020	3,3	7	10	75	107	9,59	8,81	113,48	143,09	78,71	89,21	9,21	6,72	87,92	95,93
Friday	07/02/2020	2,6	3	9	68	107	9,69	17,337	109,06	166,65	71,37	77,16	9,74	11,55	81,11	88,71
Average		6,9	5,6	8,1	69,4	95,3	8,7	15,6	106,9	145,4	76,0	78,5	9,1	11,9	85,1	90,5

\*HHV to LHV ratio assumed to be equal to 1,1085.

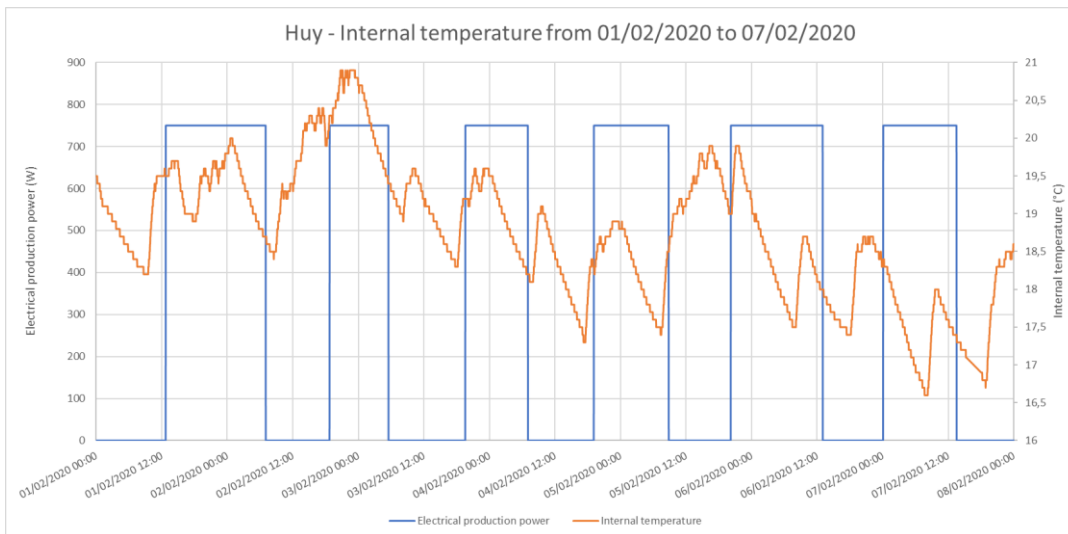
**Table 50.** Field-test data for a repeatable week (7 repeatable days) for the two monitored houses. Main differences have been highlighted.

The total efficiency difference between the two houses is clear and is equal to about 5 percentage points on the chosen period. Also, it can be seen that even if the Oostmalle house is more recent and a priori more insulated than the house in Huy, the space heating production is about 50% higher. This can be partially explained by Figure 108 and Figure 109 where one can see that the indoor temperature setpoint of Oostmalle is about 22 °C whereas it is only about 18.5°C in Huy. In addition, the higher variance in indoor temperature in Huy (Figure 109) confirms the assumption of a strong interaction with the terminal units (the occupants only open the radiator valves for short periods of time and that partially decorrelates heat demand and climate hardness, as explained above). At

last, the electrical production of the Oostmalle house is about two times greater than in Huy (and is close to the  $17 \text{ kWh}_{\text{el}}$  claimed maximum of Table 25). This is also shown in Figure 108 and Figure 109 : the PEMFC manages to stay 'ON' way longer in Oostmalle. As the PEMFC has not the same thermal efficiency as the boiler, a difference in daily electrical production will not only have an influence on the daily electrical efficiency but also on the daily thermal (and total) efficiency. This influence has been demonstrated in detail in *Section 5.4 - Machine modelling*.



**Figure 108.** Indoor temperature in the Oostmalle house for the focus week.



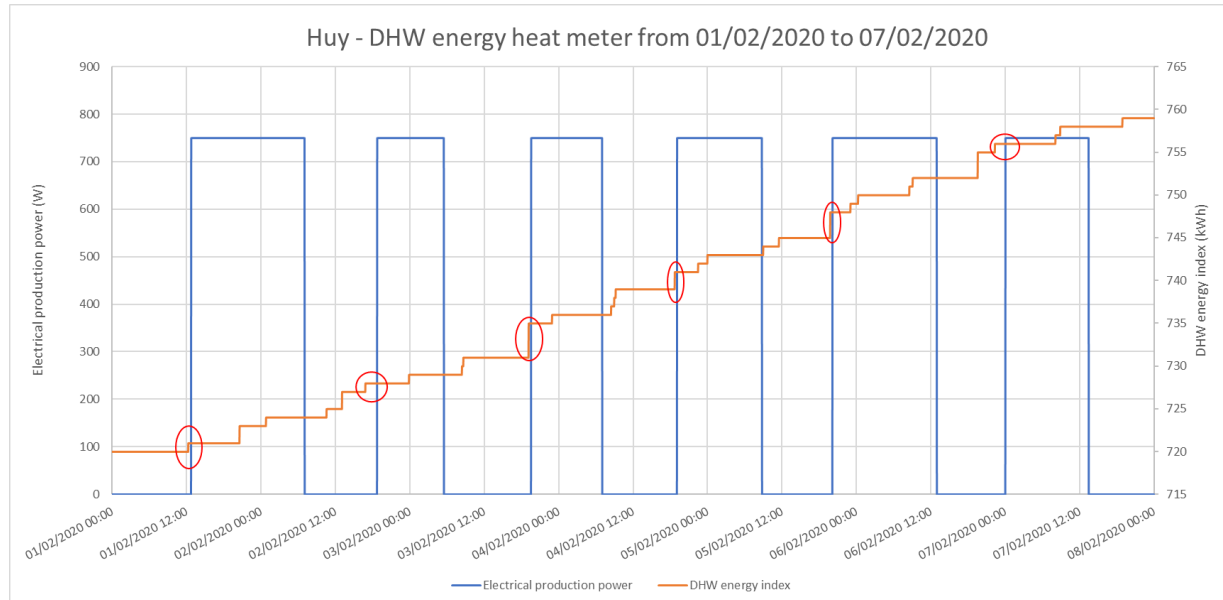
**Figure 109.** Indoor temperature in the Huy house for the focus week.

For both houses, a periodicity is clearly visible on the indoor temperature signal. The Oostmalle house has a lower regime at night (temperature decreases significantly each time after midnight). In addition, the only other significant decrease in temperature is a minimal sudden peak visible on February 7<sup>th</sup> just after noon (this has not been explained yet but the assumption is that a door was not properly closed). In Huy, the frequency of significant decreases in temperature is higher: it is about twice a day, which corresponds to the already established assumption of manual openings and closing of the radiator valves (in the morning and in the evening).

As expected, (by looking in the datasheet of the system [523]), the electrical power is indeed constant.



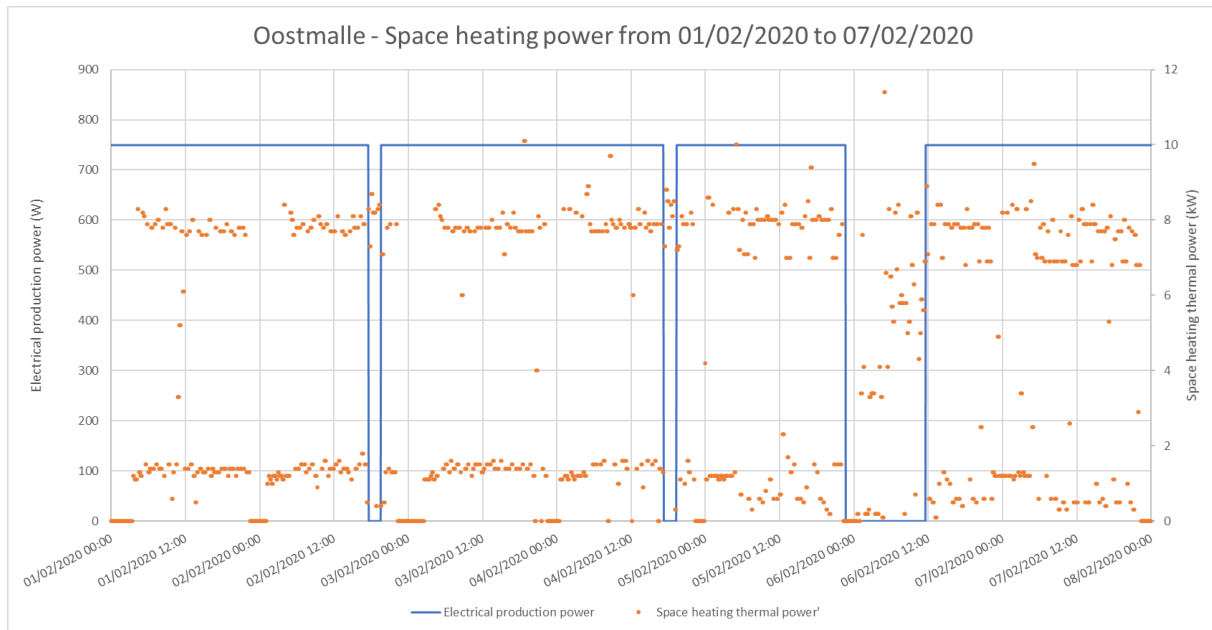
Another interesting fact is the regularity, the periodicity for which the PEMFC is started. It is also something that the occupant noticed (in *APPENDIX 11: Satisfactory Survey of the house in Huy*). The resident is saying that he can hear ‘the fuel cell starting after the bath of the children’. This can be verified with **Figure 110**. On February 2<sup>nd</sup> and February 6<sup>th</sup>, it seems that the PEMFC launch is not as direct as in the other days. This is probably due to the fact that the DHW draw has not allowed a sufficient decrease in the tank temperature. For those days, it is believed that the remaining temperature decrease of the tank has been achieved by stand-by losses.



**Figure 110.** DHW energy index in the Huy house for the focus week. Red circles are showing that the PEMFC starts when (sufficient) DHW is drawn.

In Oostmalle, this DHW draws dependency cannot be seen because the PEMFC is able to work most of the time (supposably thanks to the low temperature smooth space heating demand allowed by floor heating).

Space heating thermal power in Oostmalle shows quite an odd and inexplicable behavior, as illustrated in Figure 111. Indeed, thermal power varies so much between about 8 kW<sub>th</sub> and 1 kW<sub>th</sub> that a solid line between the dots could not be drawn (as it has been done for the Huy house in Figure 112). This thermal signal is dropping to 0 kW<sub>th</sub> only a few times along the focus week. This highly variant behavior is not a sensor issue because this signal frequency can also be seen on the depart and return temperature signal and most importantly on the gas consumption signal, which leads to believe that the boiler is constantly turned ‘ON’ and ‘OFF’. The occurrence of this frequency on the gas consumption signal is an indication that it does not come from the DHW potential priority (and the 3-way valve switching from space heating to the upper DHW tank as shown in Figure 68). In addition, this assumption is reinforced by the fact that this kind of variation could not be seen on the flow rate signal of the heat meter, which remains very smooth.

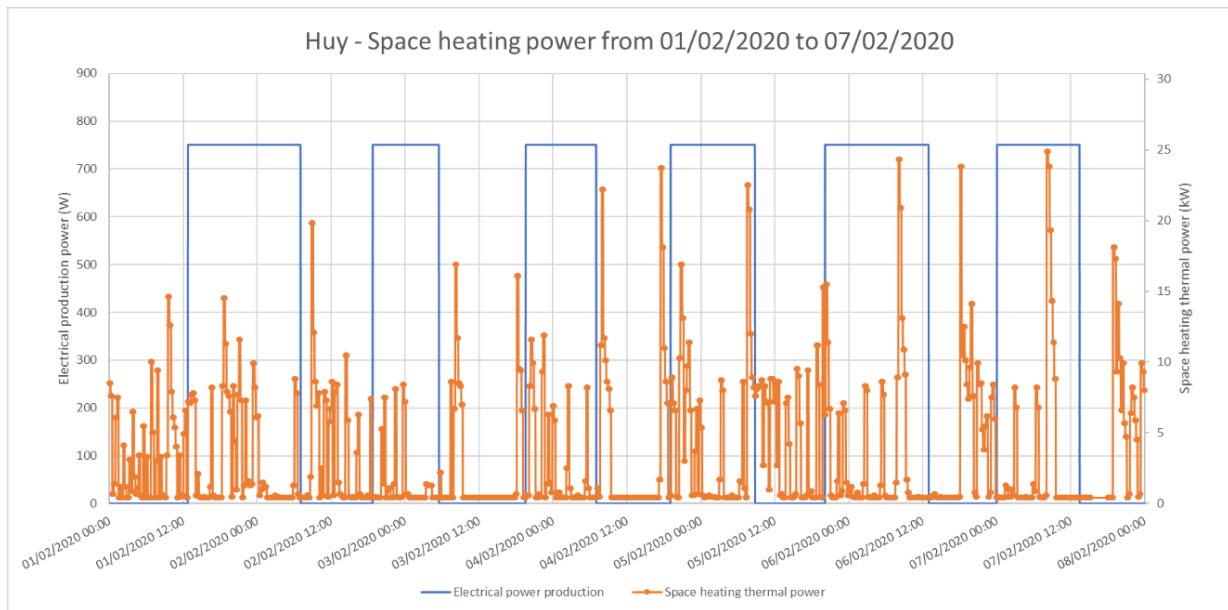


**Figure 111.** Space heating thermal power in the Oostmalle house for the focus week.

It is worth mentioning that the  $8 \text{ kW}_{\text{th}}$  of thermal power corresponds to partial load for this particular system and that the lower level of about  $1.1 \text{ kW}_{\text{th}}$  corresponds to the thermal power capacity of the PEMFC (see Table 25). Indeed, when the PEMFC is off (or that its heat is provided to the DHW tank rather than to the space heating), the lower-level thermal power signal is dropping from  $1.1$  to  $0 \text{ kW}_{\text{th}}$ . Also, on February 6<sup>th</sup>, for unknown reasons, when the PEMFC is off, the thermal power seems to achieve intermediate values (not only varies from an upper to a lower level).

For the house in Huy (Figure 112), the behavior is not as ‘discretized’ in levels and certainly does not vary as much (even if, as stated, the sample rate is even smaller). For example, on February 1<sup>st</sup>, one gets about one peak in the power signal per hour (followed by a ‘shutdown’). However, the behavior cannot at all be considered as smooth, probably again because of the boiler. The periods for which it is visible that the thermal power remains to  $0 \text{ kW}_{\text{th}}$  corresponds to the ones when the indoor temperature significantly decreases (Figure 109), so the sensors partially correlate. However, when the system provides heat, it is doing so quite erratically.

This highly transient behavior is expected to have an effect on overall efficiency as shown in literature [560]. It is surely one of the reasons that the LHV efficiencies shown in Table 50 ( $85 - 90 \%$ ) are about 20 to 25 percentage points lower than the targeted efficiency of Table 25, which is said to be equal to  $98 \%$  HHV (this figure corresponds to a LHV efficiency of about  $108.5 \%$ , considering the usual HHV to LHV ratio of  $1.1085$  considered in this work).

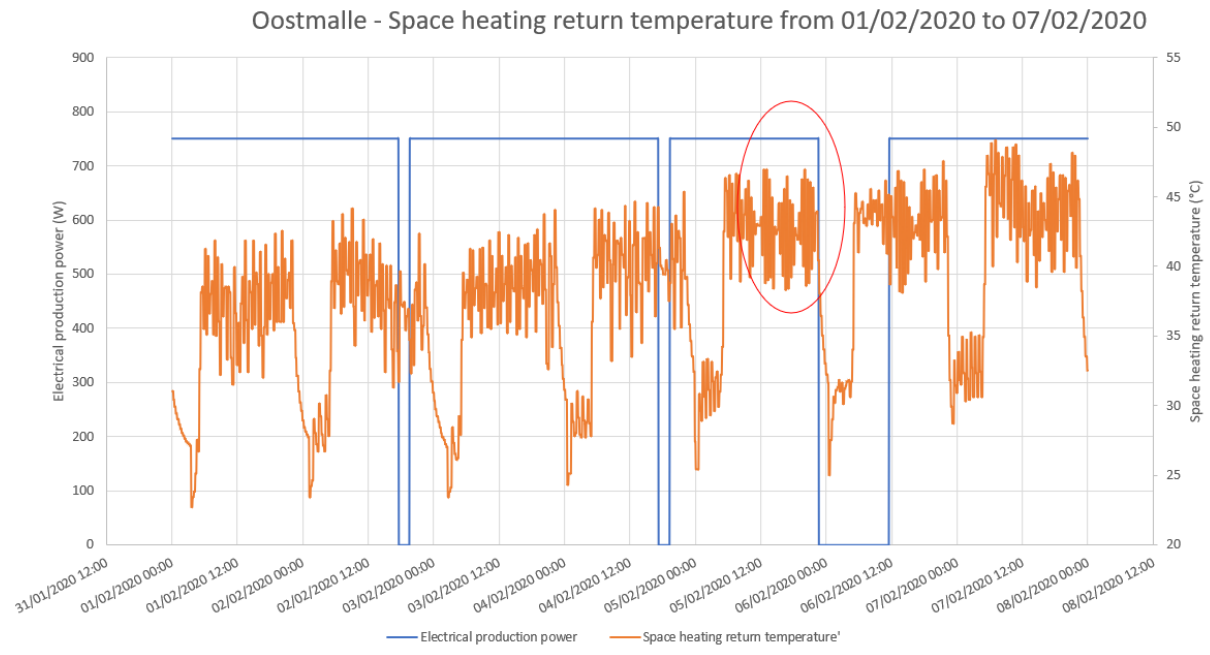


**Figure 112.** Space heating thermal power in the Huy house for the focus week.

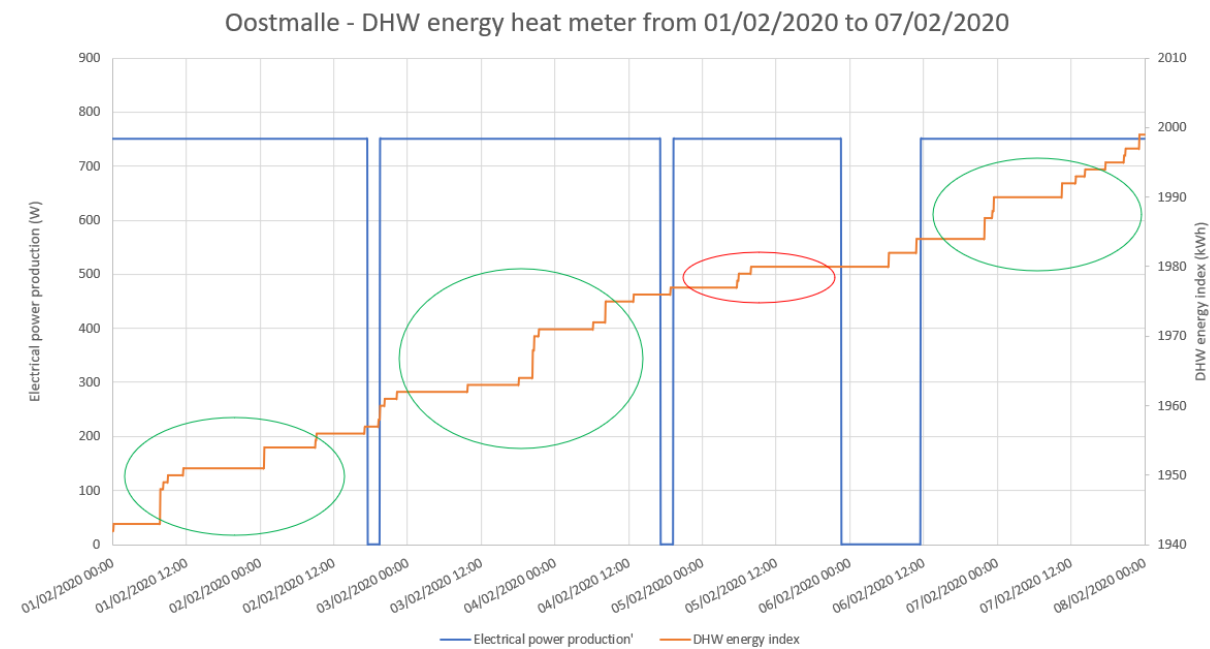
#### A. Why does the PEMFC stop? – Oostmalle

It is clear thanks to the electrical power signal that the PEMFC in Oostmalle manages to stay on pretty much as designed. Indeed, in *Section 5.1 - Description of the machine*, one has explained that the PEMFC shall produce electricity for no more than 45.5 h, followed by 2.5 h of ‘regeneration’ and that behavior is visible except on February 5<sup>th</sup> around 11 pm, for which the Oostmalle PEMFC is actually shutting down. In Figure 113, that is also showing the return temperature of the space heating, this stop has been circled in red. As it has been said *Section 5.1 - Description of the machine*, the PEMFC is stopping with high return temperature (50°C is supposed to be the limit). In this case, the limit is not exceeded but the signal is getting closer than it was for the previous days. It is an indication that it becomes harder and harder for the PEMFC to release its heat in the space heating circuit. Also, the temperature changes seem to increase in frequency compared to the previous days. As explained, the temperature variance is caused by the gas boiler that shows an ‘ON/OFF’ behavior (which frequency increases just before the undesired, red-circled stop). The main assumption for this increased frequency behavior and increased return temperature is that it is due to potential improper weather compensation (programmed in the system) because the climate was becoming harder and harder around those days (see Table 50).

Since the higher return temperature and frequency remain for the last days and this still allows for the PEMFC to produce electricity, there is another reason for the undesired, red-circled stop of the PEMFC. An interesting fact is that just before the undesired red-circle PEMFC stop, the indoor temperature (Figure 108) has probably exceeded the setpoint (assumed to be 23°C). Therefore, this has probably mainly contributed to the fact that the PEMFC could no longer dissipate its heat in the space heating circuits (thermostatic valves are closing with higher room temperature and there is no more heat demand). Also, it is assumed that the DHW tank was also fully charged and has not been discharged sufficiently in the previous hours. This is confirmed by Figure 114.

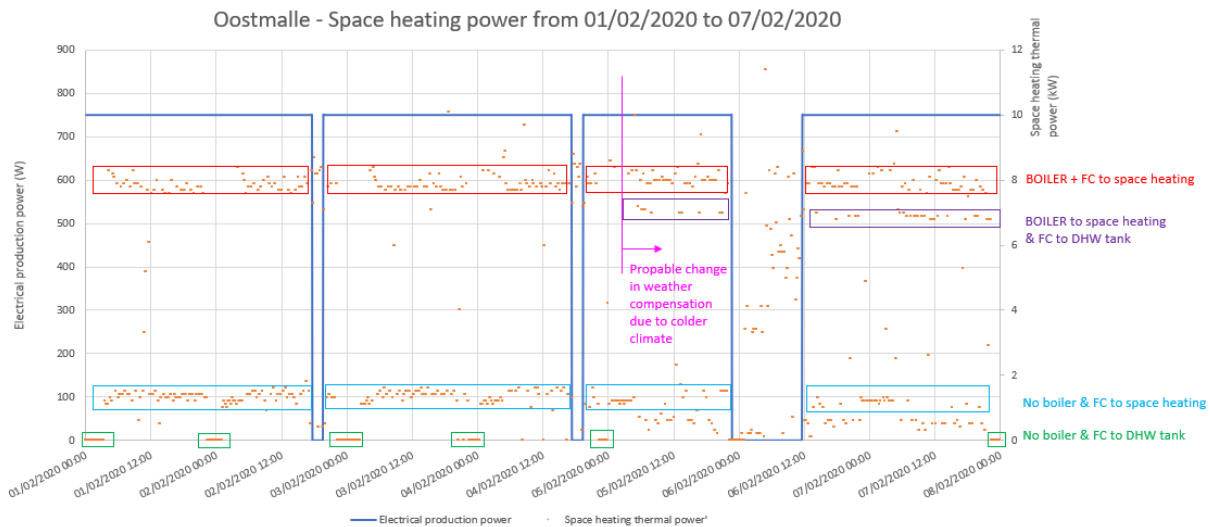


**Figure 113.** Space heating return temperature in the Huy house for the focus week. The red circle highlights the moment when the PEMFC is breaking its designed cycle (and is not shut down only for ‘regeneration’).



**Figure 114.** DHW energy index in the Oostmalle house for the focus week. Green circles are highlighting sufficient DHW draws for the PEMFC to keep running whereas the red circle is highlighting a probable insufficient DHW draw.

Figure 111 also points towards these assumptions as since February 5<sup>th</sup> around 6 am (a few hours before the undesired red-circled stop), another thermal power level is achieved in the space heating circuit when the PEMFC is running (around 6.9 kW<sub>th</sub>). It corresponds to the upper level of 8 kW<sub>th</sub> already explained minus the 1.1 kW<sub>th</sub> of the PEMFC, which is provided to the DHW (until it is fully charged and the PEMFC is stopped). It means that the 6.9 kW<sub>th</sub> level is achieved on the space heating by the gas condensing boiler only. This is summarized in Figure 115.



**Figure 115.** Detailed behavior of the system for Oostmalle on the focus week according to the space heating thermal power signal.

In the previous days when the PEMFC is behaving as designed, the return temperature of the space heating allowed for the PEMFC to dissipate its heat in it (thermal power of space heating of 8 kW<sub>th</sub>) and periodically, it switches to the tank (each day around midnight). It is probably due to DHW scheduling and not because of DHW draws because on February 1<sup>st</sup> around 6 am, there is an important demand (Figure 114) and the 3-way valve of the PEMFC only switches to the DHW tank about 18 hours later at midnight.

To sum up the Oostmalle behavior:

- Two different behaviors can be visible on the focus week, probably depending on the hardness of the climate (and weather compensation programmed rules).
- With both supposed behaviors, highly transient behavior of the boiler is seen. It does not modulate; it is working in 'ON/OFF' mode (between 6.9 kW<sub>th</sub> and 0 kW<sub>th</sub>). This was not expected, it is still not explained and will have an effect on the performance [560].
- The first days (with warmer climate), both the boiler and the PEMFC provide heat to the space heating circuit except on DHW scheduling. Based on the 'colder days period' (discussed below), even if it has not been seen over the 'warmer days period', it is assumed that if the return temperature limit of 50°C or if the indoor temperature setpoint are exceeded, space heating circuit are shut down and the PEMFC thermal power is switched to the DHW tank, if it is not fully charged already (in that case, it has to shut down). Over that period, the PEMFC is producing electricity as expected and is only stopping for the 2.5 h of 'regeneration' (*Section 5.1 - Description of the machine*).
- The last few days (with colder climate), the working temperatures are increasing (and the 50°C return temperature limit is getting closer). The 'ON/OFF' frequency of the boiler is also increasing, probably because working temperature is lowering faster once the boiler is off and the system's regulation makes it restart faster as well. With that mode, the PEMFC no longer only provides heat to the space heating and produces DHW only on schedule (it dissipates its heat in the DHW tank). The assumption is that with increased working temperature for the space heating circuit, the 3-way valve has to switch to the DHW tank from time to time. This is consistent with the assumptions stated for the 'warmer days period' explained here above which are also confirmed by the PEMFC electrical production promptly stop that is occurring when the indoor temperature setting is supposedly exceeded while the DHW tank is supposedly fully thermally charged.

- It is assumed that the undesired stop in the electrical production could have been prevented if the boiler was able to modulate properly (because then, with lower modulated thermal power provided by the boiler, the PEMFC could have still dissipated its heat in the space heating circuit).
- Looking at Figure 68, it can be deduced that once the PEMFC and the boiler are providing heat to the space heating which is mostly the case over the chosen analyzed period, the return to the boiler is preheated by the PEMFC. Since the space heating temperature is already quite high (between 35°C and 48°C), if it is preheated before the boiler, the latter will have poorer performance [558]. This will especially be the case if condensation is prevented by higher return temperature as literature advises remaining under 49°C to 54°C [614]. Ensuring condensation might be a reason why the boiler is promptly stopped again and again ('ON/OFF' behavior seen here) and/or a reason why the 3-way valve controlling the PEMFC thermal power is switching from the space heating circuit to the DHW tank. This could be solved with another internal architecture of the system.

#### B. Why does the PEMFC stop ? – Huy

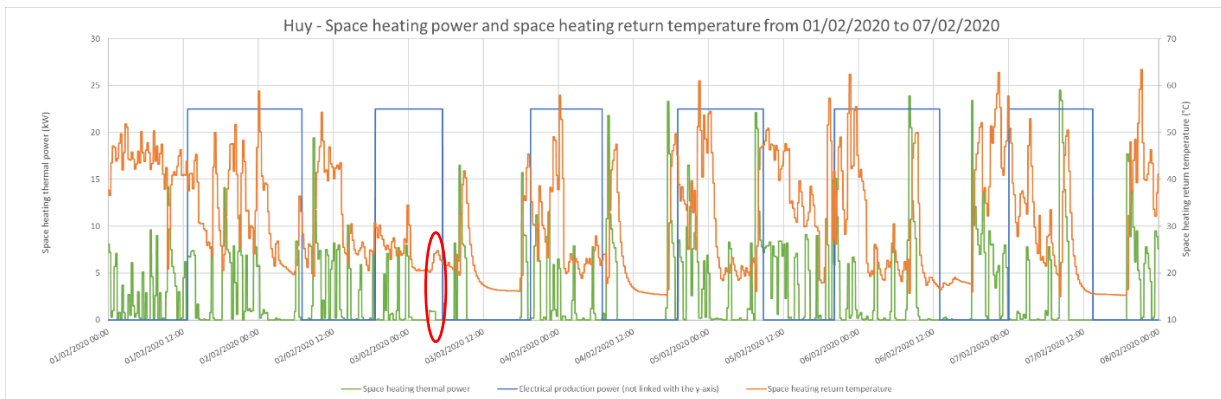
Regarding the house in Huy, the behavior stated here above (for Oostmalle) cannot be certainly confirmed nor disproved. Indeed, the main difficulty for the analyses lies in the fact that space heating thermal power has no preferential distinctive levels (Figure 112). For example, in Figure 116, when the return temperature is exceeding the PEMFC limit of 50°C and the fuel cell is on, it is not possible to establish the switching of the 3-way valve from the space heating to the DHW tank. However, it seems that subsequently to peak temperature above 50°C in the return, even the boiler is shut down (probably to ensure that it is condensing). Again, this might explain the highly transient behavior of the boiler. It can be therefore assumed that for that house, the higher working temperature and very prompt space heating demands created by occupant interaction with the radiator valves (see *APPENDIX 11: Satisfactory Survey of the house in Huy*) are making the PEMFC to only (or at least mostly) dissipate its heat in the DHW tank. This is consistent with the earlier statement that big DHW draws ('children's bath') allows for the PEMFC to start. Supposably, it stops when the DHW tank is fully thermally loaded. It is not excluded that the system includes some kind of machine learning so it has established in time that the space heating thermal demand is so short in time and so high that it is not appropriate for the PEMFC (too many switching of valves, too many thermal cycles that have been proven to reduce lifetime [528]). However, on February 3<sup>rd</sup> at around 3 am (red box in Figure 116), thermal power achieves only about 1 kW<sub>th</sub> (for a quite low space heating temperature) which still rather point towards PEMFC heat dissipation than gas boiler modulation (which minimum is announced in the datasheet at 2 kW<sub>th</sub> [523]).

Therefore, it can be assumed that once the system is switched towards heat dissipation in the DHW tank (for the Huy house, it is the case as soon as the PEMFC starts, because of the large DHW draws for the 'children's bath' explained earlier), it does not switch towards heat dissipation in the space heating circuit until the DHW is fully thermally loaded. Once this is done, for the house in Huy and its punctual (two times a day) openings of the radiator valves and thus of space heating heat demands, it rarely has the opportunity to switch towards heat dissipation in the space heating circuits and therefore has to shut down.

Nevertheless, the assumptions made for the site of Huy are way harder to confirm than for the ones made for the house of Oostmalle (due to the absence of distinctive levels in the space heating thermal power, mainly due to the punctual openings of the radiator valves).

At last, it is worth mentioning that on working days, one can see several peaks of space heating demand (not only one, as believed by reading *APPENDIX 11: Satisfactory Survey of the house in Huy*). That must be because the residents do not open all the radiator valves at once but as soon as one occupant gets up early, he is warming one main living room (the boiler starts, heats up the room and shuts down) and only later on, the other radiators (in other rooms) are opened.

At last, *APPENDIX 11: Satisfactory Survey of the house in Huy* is also very interesting because the occupants have declared that they have no room thermostat and that for comfort reasons, they have set to the machine a non-rationally higher temperature setpoint. Indeed, because one room thermostat in the living room could not ensure reaching and maintaining the desired temperature in all the rooms (for example, in the bathroom), they are using local radiator thermostatic valves to regulate temperature setpoints. This particular occupant behavior in addition to the frequent openings and closings of the radiator valves are likely to account for the highly transient behavior of the boiler (and thus to a lowered efficiency [558] than the one presented in the datasheet). Again, even if it is probably not the case in Huy (as explained, the PEMFC mainly dissipates its heat in the DHW tank), this is also added to the fact that the internal architecture is allowing gas condensing boiler return line preheating by the PEMFC, which also can lead to eventual boiler prompt shutdowns.



**Figure 116.** Space heating thermal power and space heating return temperature in the Huy house for the focus week. The red box highlights a possible heat dissipation of the PEMFC in the space heating circuits.

# APPENDIX 11 : SATISFACTORY SURVEY OF THE HOUSE IN HUY

Comments of the ULiege engineering team are shown in red

Responses of the occupants are highlighted in yellow

Merci de lire le questionnaire jusqu'au bout avant de commencer à y répondre !

## Questionnaire de satisfaction relatifs à votre système de chauffage

Nom :

Prénom :

Adresse :

Taille du ménage : 5 (2 adultes et 3 enfants de moins de 8 ans)

Surface chauffée (approximation) : 207 m<sup>2</sup>

- Les questions soulignées ne sont pas à remplir s'il s'agit de votre 1er système de chauffage.
- Échelle : 0 → Très mauvais / Pas familier / Pas importante / ...  
10 → Très bon / Très familier / Très importante / ...

### Le profil de votre ménage

<b>Composition de votre ménage</b>	Nombre : 5	Sexes : <b>M x 4</b> <b>F x 1</b>	Âges : <b>M : 2, 5, 8, 39</b> <b>F : 35</b>	
<b>Occupation de votre maison</b>	100%	<b>Hors horaire de travail/école</b>	Presque jamais	Uniquement la nuit



<b>Votre consommation d'eau chaude sanitaire</b>	Nombre de bains par semaine : <b>7</b>	Nombre de douches par semaine : <b>14</b>
--	--	---

**Pourriez-vous approfondir vos réponses en citant quelques inconvénients/ avantages/ problèmes en termes de confort ? Classer par ordre d'importance (0 → 10)**

Avantages	Inconvénients	Fréquence d'apparition	Exemples/ Problèmes
			<p><i>J'ai déjà expérimenté plusieurs courtes périodes où seule la pile à combustible tournait (sans l'appoint du brûleur) et la puissance de chauffage semblait insuffisante pour chauffer certaines pièces.</i></p> <p><i>La maison est composée d'un logis central et d'un corps annexé. Le logis central est bien isolée (façade par l'intérieur et autres murs par l'extérieur). Le corps annexé et moins bien isolée et comporte la salle de bain ce qui crée un certain inconfort. La cage d'escalier est relativement froide également.</i></p>

**Votre interaction avec votre installation de chauffage**

<b>Votre installation comprend-elle un thermostat d'ambiance ? Où ?</b>	Oui	<b>Non</b>	Je ne sais pas
	Où ? :		

<p>Vos émetteurs de chaleur (radiateurs) comportent-ils des vannes thermostatiques ?</p>	<p>Oui</p>	<p>Non</p>	<p>Je ne sais pas</p>	<p>Sans objet</p>
<p>À quelle fréquence vous modifier les réglages de ces vannes ?</p>	<p>Jamais</p>	<p>Plusieurs fois par an</p>	<p><u>Tous les jours</u>  <i>La demande de chaleur est pilotée pièce par pièce au moyen des vannes (ouverture sur 3 (et sur 5 dans salle de bain) et fermeture en fonction des périodes d'occupation). Une consigne fort élevée a été imposée sur le système de production de chaleur afin de rendre la production de chaleur tout le temps disponible (éviter par exemple de ne pas pouvoir chauffer la salle de bain si le confort est atteint dans la salle à manger).</i></p>	

Ajustez-vous régulièrement certains réglages de votre installation de chauffage ? Quoi ?	Oui	Non	Je ne sais pas	Sans objet
	Quoi ? :			

### Votre interaction avec votre système de production de chaleur

Vous arrive-t-il de modifier les réglages de votre système de production de chaleur ?	Plusieurs fois par an	Tous les mois	Toutes les semaines	Jamais
Dans quel but modifiez-vous les réglages ?	Changer les températures de consigne de l'eau chaude sanitaire/ chauffage  <i>Modification de la loi d'eau afin de tenir compte des pertes de chaleur sur le circuit de distribution en caves.</i>	Changer les programmes de chauffe	Tenter d'améliorer la performance de votre système	

Pourriez-vous approfondir vos réponses en citant quelques inconvénients/ avantages/ problèmes en termes d'économie d'énergie ? Classer par ordre d'importance (0 → 10)

Avantages	Inconvénients	Fréquence d'apparition	Exemples/ Problèmes
-----------	---------------	------------------------	---------------------

<p><i>Régulation interne de la machine efficace</i></p> <p>The occupant means that he thinks the circulator is correctly automatically shutting down when he closes its radiator valves.</p>	<p><i>Absence de thermostat d'ambiance ou de vannes thermostatiques pilotables électroniquement pièce par pièce</i></p> <p><i>Chauffage à trop haute température et trop intermittent (le chauffage est coupé la nuit et dans les pièces non occupées) pour permettre une utilisation prolongée de la production électrique.</i></p>		
--	--	--	--

**Performances énergétiques du système de chauffage**

<p>Si votre système produit également de l'électricité (cogénération), suivez-vous votre autoconsommation électrique grâce aux index des compteurs?</p>	<p><u>Oui</u></p> <p>Vous prenez des actions pour augmenter l'autoconsommation ? :</p> <p><i>Oui, pendant près de deux ans j'ai mesuré mon autoconsommation journalière (par de la production électrique instantanément autoconsommée) et mon épouse et moi avons pris l'habitude de faire tourner les gros électroménagers (lave-vaisselle, machine à laver et sèche-linge) lorsque la pile produit de l'électricité (ce qu'on peut entendre en « tendant l'oreille »). Le régime de la pile est assez régulier, elle s'enclenche généralement en tout début de soirée après avoir donnée les bains.</i></p>	<p>Non</p>
---	---	------------

---

## **APPENDIX 12 : SATISFACTORY SURVEY OF THE HOUSE IN OOSTMALLE**

No backup information from the survey is used and referred to in the thesis manuscript. This survey has therefore not been disclosed in this document for confidentiality purposes.

# APPENDIX 13 : P\*2 – LABORATORY

## TROUBLESHOOTING DESCRIPTION

### May 2019

Once the test bench has been set in the laboratory, the protocols for the Start-Up of the system indicated on the Installation Manual were followed.

After a couple of days and with the system on Stand-by mode for DHW and heating, an error appeared on the display. The description of this error is shown in Table 51.

N°	Text	Subscriber	Help
F475	42F1	94	Notify heating contractor

**Table 51.** Display error description.

According to this, the support service was contacted and a commissioning visit by a technician (from the manufacturer) was scheduled on Tuesday 7/05/2019.

The conclusion of this visit was that air bubbles on the system caused the error. The system was successfully commissioned and installation was approved by a technician from the manufacturer. Remarks regarding the low water flow indicated on the display system as 'Flow sensor' were made; his conclusion was that this could be caused by the water flow meters installed on the heating circuit or due to the high pressure drop on the heat exchanger. During the visit it was also discussed that the control of the whole system is really complex; it was mentioned that trying to predict the behavior of the system is really hard and that sometimes for the same operational conditions the response is not the same.

Problems with 2 of the 4 initially installed water meters were detected. These two meters are part of the boiler and heating circuits and were placed at the systems heating and boiler inlet. Here, the obtained reading of the water flow rate is minimum or null even though there is a flow imposed, probably related to the low flow indicated by the technician.

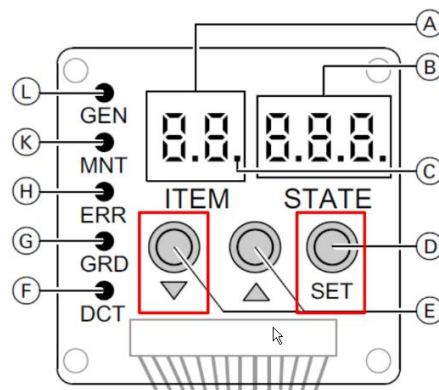
Based on this, it has been decided to replace water meters with new meters and eliminate the one placed on the return heating line of the system to achieve the expected water flow on the boiler circuit and decrease the pressure drop. The objective is to ensure the functioning of the system as it would be in a typical application and not compromise the results of further tests. To do this, the system was put into 'Maintenance mode', the circuit was drained, and the meters removed and replaced. Afterwards, a new commissioning was requested to the manufacturer.

Following these modifications, the installations were finally approved and now the flow shown on the display appeared to be the expected one for the system. Tests were made by the technician to guarantee the good response of the system to common problems that could arise (mainly, a gas supply cut). As a result, the error that appeared on the display related to a gas cut did not have the description expected; this meant, the alert was 'no gas' but the description associated to the situation imposed was slightly different to what it should be. This could be related to an error in programming or in the control of the system. Even though, it is not something directly related to the daily operation (it is an exceptional condition), it must be mentioned.

## October 2020

The fuel cell did not turn on during the weekend, even when the 'Energy manager OFF' mode was selected, heating and DHW production were set ON. The following process was tried successfully, based on the recommendations made by the manufacturer, described on the test campaign timeline.

Reset of the fuel cell: on the fuel cell keyboard (Figure 117), go to Item 52 with the arrows. Push the SET button till '52 CL' appears on the screen, then cut the fuel cell current during 5 seconds. If there is a production demand for heating or DHW, the fuel cell restarts working after 90 minutes approximately,



**Figure 117.** Fuel cell keyboard.

On the following day a burner fault was shown on the display in the afternoon. A reset of the burner was made successfully. The day after no messages or faults were displayed on the screen, but an abnormal behavior was observed; a low flow rate was detected by the flow sensor (around 200 l/h during boiler operation, normally around 600 l/h) which led to several boiler startups to heat up the top of the buffer tank. With normal flow, this process takes around 5 minutes, while with low flow after 30 minutes the target temperature was not reached. Also, the depart boiler temperature exceeded 100°C. A intervention from the manufacturer was requested.

## November 2020. Interventions summary and previous visits

During the first and second manufacturer visits, the technician tried many things as follows:

- Look up for obstructions in every pipe
- Check the 3-way valve functioning
- Check the heat exchangers
- Check the circulation pumps

He checked also the water meter on the boiler loop. He did not find any big obstruction on the grill (a little bit of rust, not enough to generate the problem according to him) and the water meter worked properly (tested by him). At the end, he replaced the heat exchanger and circulation pump associated to the previously mentioned DHW heating loop. He did not succeed on the troubleshooting; a third visit was set.

Then, they removed a water meter and closed the installation as shown in Figure 118. Without any meter installed, they arrived at a 'normal' water flow (around 800 l/h during boiler operation). Tests were performed, and now the top of the buffer tank was heated normally.

Here it should be pointed that the installation worked fine with the mentioned meter and was approved since the beginning by the manufacturer. To be more specific, the original

test bench was approved by the manufacturer including the water flow meter on the mentioned location. It is normal, and expected, that after removing the meter of the circuit the flow increases (less pressure drops), but at the end, they did not manage to fix the system based on the original installation. It is possible that the problem is still not solved and linked to the boiler circulation pump (that was tested, but not changed), the flow sensor or the control of the system.

Since the mentioned pressure drops are linked to the heating circuit, after the intervention, some of the tests of the test campaign were made to see their impact on the system efficiency.



**Figure 118.** Boiler return line after removing the installed water meter.

### January 2021

On the last week of December 2020, the system was put on standby to avoid any problems during the holidays, i.e. the DHW and heating production were 'OFF' and the fuel cell is in 'Power generation off' mode. The 4<sup>th</sup> of January, the message shown in Figure 119 is on the display.

Fault list				
Time	No.	Text	Subscriber	Help
08:07 02.01.21	F.415	Communication error, M-Bus gateway	1	?
08:08 02.01.21	F.13	Lead break, outside temperature sensor	1	?
08:08 02.01.21	F.196	13F0	94	?

**Figure 119.** January 2021 fault message.

This fault was new and not described on the user manual. Thus, the question was made to the manufacturer and received the following answer:



---

*'If the fuel cell shows the fault 13F0 (detection of flammable gas in the fuel cell), a technical intervention is necessary'*

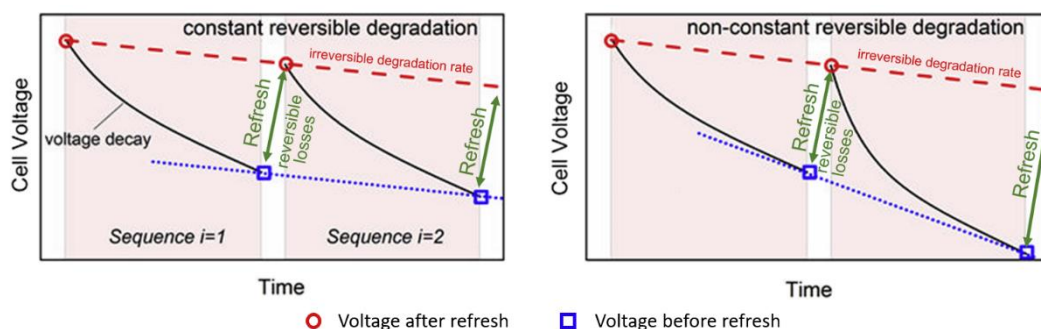
This fault was due to the fact that the gas detection probe of the fuel cell found 'unburned gas'. This probe detects CH<sub>4</sub>, but also hydrogen or combustion gases coming back from the chimney. When this happens, the fuel cell stops for caution. The sensor was replaced and a software update was performed.

# APPENDIX 14 : LITERATURE REVIEW ON PEMFC DEGRADATION MECHANISMS

The content of this appendix is meant to be included in a full paper and submitted to the *Journal of Power Sources* [496] along with most of the content of *Section 5.1.1.2 - Hydrogen processor and reforming processes* and *Section 5.1.4 - Probable internal schemes*. That paper has already been reviewed by the co-authors. Its main purpose is to investigate through deep literature and patent reviews why the fuel cell of the studied PEMFC system has to be stopped for a 2.5-hour regeneration phase every 48 hours (see *Section 5.1 - Description of the machine*).

## Reversible and irreversible degradation of PEMFCs

The discrimination between reversible and irreversible is not as trivial as one may have thought, especially from a characterization point of view. Although it is pretty clear that ‘irreversible degradation includes irreversible changes to the fuel cell materials’ [615] and ‘reversible degradation is often a result of transient processes where the loss in voltage may be reversed’ [615], there is no recognized consensus in the scientific community for evaluating the performance losses attributed to reversible or irreversible degradation phenomena [616]. For example, as shown in Figure 120, irreversible performance losses can be established after or before recovery steps (which imply reversible/recoverable degradation) [616]. Figure 120 illustrates that it is more relevant to characterize the irreversible and reversible losses after the recovery steps rather than before because the transient processes that account for reversible losses are likely to differ between recovery cycles in real applications (with operating conditions that are also likely to differ as well). It is worth mentioning that the expression ‘reversible degradation’ is disputed and the expressions ‘reversible phenomena’ or ‘reversible mechanism’ are sometimes preferred [617].



**Figure 120.** Characterization of reversible and irreversible losses in PEMFCs. Since PEMFC operating conditions can vary with time, reversible degradation (voltage loss) might not occur at a constant rate. Therefore, irreversible losses are more relevantly established after the recovery procedures than before. Figure reproduced and adapted with permission [616].

In more general terms, PEMFC degradation (reversible or irreversible) leads to performances losses, which can be expressed in terms of power losses with a constant current profile [617]. In practice, a very commonly method used for stack lifetime testing

consists in operating Open Circuit Voltage (OCV) conditions (no electric loading applied) [618]. Indeed, the OCV, i.e. the theoretical difference between the equilibrium potentials (i.e. Nernst potentials) of oxygen reduction reaction (ORR) and hydrogen oxidation reaction (HOR) [619], decreases with fuel cell operating time [620] and therefore fuel cell aging. To that end, voltage is measured at zero current density and, in addition to fuel cell degradation (ageing), it depends on temperature levels, reactants and products partial pressures (which are controlled) [618].

OCV operating conditions can also simply be used to induce PEMFC ageing as an easily reproducible process, and the performance losses are thus determined with other diagnostical methods [620]. Unfortunately, there is again no recognized consensus in the scientific community regarding durability diagnostical methodologies as well. Indeed, literature usually reports methods such as:

Polarization curves, which establish fuel cell voltage against current density generally in steady-states conditions [621];

Electrochemical impedance spectroscopy (EIS), which consists in applying a small sinusoidal current (or potential) as a perturbation to the PEMFC and measuring the potential (or current) response to establish impedance plots [622];

Several kinds of voltammetry techniques [623]. The most common one is cyclic voltammetry (CV) [624], which consists in applying a triangular waveform scanning voltage onto the fuel cell and measure the current response [624]. The scan rate is constant and usually in the 1-1000 mV s<sup>-1</sup> range [624], so the frequency of the triangular waveform is in a range starting at a few mHz up to a few Hz, way lower than the frequency generally used for the EIS method that can go up to 100 kHz [622,625]. Cycling the voltage applied to the PEMFC lead to the successive oxidation and reduction of electroactive substances in solution or attached to the electrode surface. Those reactions can be identified by the peaks that are occurring on the current response [624]. Linear sweep voltammetry (LSV) is very similar to CV for which the voltage waveform is not triangular; it is not continuously reversed when it reaches its maximum value, it is discontinued and the next wave is simply started by switching directly to its minimal value again [626].

Therefore, the underlying degradations mechanisms (such as potential electrode contamination) can be identified with voltammetry techniques, similarly to EIS. Indeed, dynamic responses provide diagnostic information about a wide range of electrochemical phenomena depending on the frequency stimuli, including charge transfer reaction at the interface electrode/electrolyte, reaction mechanisms, electrode material properties, state of health of fuel cells and so on [625]. This is not the case with solely with OCV measurements or polarization curves, because the contributions of different degradation processes overlap in the overall performance losses that can be measured [622].

However, OCV diagnostical studies, which give similar outputs as shown in Figure 120, have the advantage to be performed with normal fuel cell operating methods (so as the polarization curves) [618,627], which is not the case of the EIS or the voltammetry techniques, that must be conducted offline (with a potentiostat) [628].

## **General literature review of PEMFC degradations and corresponding recovery procedures**

Unfortunately, one cannot state with certainty the reversible processes that are occurring in the short 2.5-hour recovery phase of the studied PEMFC system (see *Section 5.1 - Description of the machine*). Furthermore, studies usually focus on unrecoverable losses [629]. Nevertheless, several voltage losses and their corresponding recovery methods have been identified (not exhaustively) in literature, with a particular focus on methods executed periodically (and if possible, at fuel cell shutdown).

### Lack of humidity and gas crossover

Lack of humidity at the membrane surface tends to expand micro cracks and allows increased gas crossover [630]. On the one hand, hydrogen crossover (instead of protons) leads to a loss of reactant and reduces efficiency [631]. On the other hand, oxygen permeating through the membrane (oxygen crossover) reacts with hydrogen to form water at the anode side (and not at the cathode), which also constitutes a loss of reactant and reduces efficiency by impeding the hydrogen from reaching the catalyst [631] (see *Section Water accumulation* in this Appendix). Oxygen crossover has been reported to cause several other problems related to the durability of PEMFC such as the risk of hydrogen peroxide formation that damages the membrane or the risk of increased cathode potential that may induce its corrosion [632] (oxidation of the carbon used in the cathode catalyst layer [633]). Similarly to oxygen crossover, with air as reactant, nitrogen crossover from the cathode to the anode has been reported, also leading to buildups and reduced performance (again, by blocking the catalytic sites) [634].

Membrane deep drying is quite irreversible as it leads to rapid failures [635] but, up to some extent, the pinholes induced by lack of humidity may fortunately be shrunk or even filled and sealed by liquid water by rehumidification, which has been reported to eliminate the gas crossover [636]. Membrane drying may thus be limited to reversible performance decays, with corresponding recovery phases that consist in rehydrating the membrane; this, for example, has been conducted periodically in literature at PEMFC rest mode at high humidity levels [629]. However, as shown in Figure 74, it is likely that the humidity levels of reactant gases (at the anode and at the cathode) are controlled with dedicated continuous humification processes during fuel cell stack operation for performance purposes (as humidity facilitates proton transport mechanism through the membrane) [540]. Therefore, one can assume that membrane drying is simply continuously mitigated with those required humidifiers and it is thus not likely to occur with this studied commercial PEMFC system .

### Water accumulation

As it has been reported in the previous section, oxygen crossover can lead to water buildup (accumulation, flooding) at the anode side [631]. Water can also directly permeate through the membrane to the anode side (water crossover [637,638], also called ‘diffusion’ [639]), which can lead to an excessive accumulation of water that lowers the hydrogen concentration and deteriorates the fuel cell performance [637,640]. Indeed, water accumulation, possibly at both electrodes, is known to impede the reactant flows to the catalysts [637,640]. Water flooding induces other unwanted effects such as the corrosion of the carbon used in the anodic and cathodic catalyst layers [641]. Purging by flushing dry gases can be conducted as an efficient recovery method [616].

Amongst other existing methods (such as increasing the gas temperature), water at the cathode is usually removed through evaporation and advection by periodical momentarily high flow rate air flushes or simply by a continuous increase of the air flow rate above stoichiometric levels in the operating conditions [640]. However, with its continuous aspect, the latter constitutes more of a mitigation method than a recovery method. Moreover, periodical cathode purges have been reported to achieve higher stack power densities with less wasted fuel [642] and, for increased power stability and efficiency, they can even be performed on a group of cells only at a time (and not on the all stack) [643]. To the knowledge of the authors, cathode water management is usually simple enough to be performed in use (online) and does not require the fuel cell to be shut down (as it is the case for the studied system and its offline 2.5-hour recovery procedure).

At the anode, hydrogen periodical purges are usually implemented [644] but this comes with unavoidable fuel losses and decreased efficiency [645]. Thus, those periodical purges

(also called ‘flushes’) have to be adapted to the operating conditions (optimizing the purge cycle, i.e. the period and purge duration [644]) in order to obtain a compromise between fuel saving and stack performance [646]. This is usually done in use, for the whole stack, but it can lead to voltage instabilities [647] and purging only a group of cells at a time within the stack might be preferable. However, some purge strategies are still preferably executed in open circuit state [648] as it could be the case in this application.

It is worth mentioning that anode purging strategies also allow for removal of nitrogen built-up, which comes from unavoidable gas crossover from the cathode (see *Section Lack of humidity and gas crossover* in this Appendix). Indeed, nitrogen can accumulate (especially if anode recirculation and/or dead-end anode operations are implemented to increase fuel efficiency), and impedes hydrogen from reaching cell reaction sites effectively [538,649].

Periodic purges of the anode are not the only way for removing the water (or nitrogen) accumulation. Indeed, if anode recirculation is implemented (to increase fuel efficiency), those buildups can be moderated below an acceptable concentration if the recirculation is kept moderate [538], i.e. if a part of the anode off-gasses is not recirculated to the anode inlet (and, in case of PEMFCs fed by natural gas goes directly to the afterburner of the reformer, as illustrated in Figure 74). Again, this constitutes more of a mitigation than a recovery method and it can be assumed that it is simple enough to have been online (in use) for the studied commercialized system.

### Carbon monoxide poisoning

As explained, carbon monoxide contamination (poisoning) of the anodic catalyst results in the reduction of surface-active sites available for hydrogen (protons) adsorption and oxidation [650]. Indeed, carbon monoxide is an unavoidable impurity coming from the reforming processes of hydrocarbons into hydrogen and is documented to bind easily with platinum catalysts [651]. In this case, carbon monoxide is a direct by-product of the partial oxidation or steam reforming processes respectively defined by Equation (34) and Equation (37), but it can also come from reverse water gas shift reaction (carbon dioxide originated from the fuel reacts in-situ with hydrogen) [652]. As mentioned, this justifies the presence of the carbon monoxide remover based on a preferential/selective oxidation catalyst in the hydrogen processor, as shown in Figure 74. However, it has been reported that, even after a preferential oxidation reactor (carbon monoxide remover), the outlet carbon monoxide content is about 50 ppm [653], i.e. ten times the already reported acceptable concentration [517]. Indeed, even 10 ppm of carbon monoxide in the fuel stream has been reported to deteriorate the stack [654] so PEMFC system fed by hydrocarbons must include additional features (in addition to the carbon monoxide remover unit).

One well-known solution consists in anode air/oxygen bleeding (or oxidant-bleeding in more general terms [655]) techniques, which consist in blending low levels of an oxidant such as air or oxygen into the anode fuel stream [655]. This allows for increasing the carbon monoxide tolerance of the stack based on its oxidation to form carbon dioxide [656]. Since the gas phase oxidation of carbon monoxide by oxygen is assumed to be negligible at the low operating temperature of the PEM fuel cell, the oxidation of carbon monoxide is considered heterogenous, meaning that carbon monoxide is absorbed onto the anodic catalyst layer and then oxidized [657].

The air bleed usually comes from the cathode inlet and not from the cathode exhaust, as for the bleed air required for the carbon monoxide selective oxidation in the carbon monoxide remover of the hydrogen processor (as in Figure 74). The reasons are basically identical (see *Section 5.1.1.2 - Hydrogen processor and reforming processes*) : lower nitrogen crossover in the stack with lower cathode stoichiometry [541], more oxygen in the fresh air stream which allows for less dilution of the hydrogen fuel (so less current density

loss [511] and higher carbon monoxide tolerance of the stack [512]) and lower carbon dioxide content in fresh air so less risk of carbon monoxide formation by the reverse water gas shift reaction [542]. However, it should be mentioned that internal air bleeding also exists (from the air crossover from the cathode to the anode, with intentionally thin membrane,) but it involves major drawback such as the difficulty of optimizing it for different carbon monoxide concentrations and the fact that air may not cross the membrane uniformly, which does not prevent severe local poisoning of the catalyst [658]. Therefore, from here onwards, 'air bleeding' only refers to 'external air bleeding', such as shown in Figure 74.

Air bleeding (~0.5-1% oxygen concentration by volume is sufficient [657]) is usually operated in fuel cell use continuously (online) [659,660], which should then be classified as a mitigation method rather than a recovery method. However, air bleeding techniques performed intermittently (air bleed pulses) have also been reported in fuel cell use (online) [656,661] or offline, at fuel cell shutdown [662], which constitutes more of a recovery phase.

Unfortunately, a loss in fuel conversion to electricity is involved with air bleeding techniques, especially with the continuous ones [657]. Indeed, oxygen also heterogeneously reacts with the absorbed hydrogen to form water (highly exothermic reaction) on the anode catalyst instead of at the cathode (again, phase oxidation is assumed negligible at PEMFC temperature levels) [657]. In fact, it has been reported that continuous oxidant bleeding is not really efficient, as only 1 out of every 400 oxygen molecules participates in the oxidation of carbon monoxide [663]. It is indeed very difficult to control, especially if the PEMFC fuel feed composition is not fixed [659], which is the case with natural gas from the grid (so it is harder to establish the ideal bleed rate). Therefore, the loss in fuel conversion to electricity can reach a few percents [518], i.e. the same order of magnitude as the continuous bleed rate. In contrast, intermittent air bleeding pulses (shorter injection timings) have been reported to reduce hydrogen losses (and air bleeding compression work) by offering more chance for oxygen to be adsorbed on the catalyst surface and increasing the reaction rate of absorbed carbon monoxide oxidation [656]. For example, 10 seconds air bleed pulses every 10 seconds, with a bleed rate of 4% (~1% oxygen concentration) allows for increasing the carbon monoxide tolerance to about 50 ppm [656], i.e. the approximative concentration at the outlet of the selective oxidation carbon remover [653]. Other studies with intermittent 5% air (~1% oxygen concentration) bleeds in the anode fuel stream show about 90% recovery in only about 10 minutes [660] or even in about 1 minute [664].

Nevertheless, hydrogen losses are not the only drawback of bleeding techniques. Indeed, they have been reported to increase the complexity and cost of the system, they may lead to overheating if the air bleed is not mixed properly, they may cause hydrogen peroxide formation which can lead to membrane degradation [665]. Furthermore, the unwanted highly exothermic hydrogen oxygen reaction (to form water) at the anode may even initiate catalyst sintering [666]. Some additional risks of having oxygen at the anode side have also already been stated in *Section Lack of humidity and gas crossover* in this Appendix and the oxygen bleed at the anode must thus be implemented at very low concentrations, specifically tuned based on targeted carbon monoxide poisoning levels [666].

Although offline air bleeding techniques, that are supposed simpler and less risky, cannot be excluded in the 2.5-hour recovery phase implemented for this application at fuel cell shut-down (or in a part of it), there are still quite unlikely. Indeed, temperature is expected to decrease with PEMFC shut-down whereas it should remain quite high for thermal oxidation (by oxygen) of carbon monoxide into carbon dioxide, even with catalysts [502]. Water (or steam), conveniently produced by the fuel cell reaction or by the necessary humidification of the reactants (Figure 74), has similarly been reported as an oxidizing reagent [667] for carbon monoxide desorption (oxidation), but it also requires heat [668].

Furthermore, consulted literature only mentions once the anode carbon monoxide removal with air bleeding at fuel cell shutdown. And it is preceded by fuel recirculation at the anode while still providing air to the cathode [662]. Subsequently, this basically consists in fuel starvation, which is an independent recovery method for carbon monoxide removal that aims at increasing the anode potential [516] and that could easily be implemented in the investigated offline 2.5-hour recovery procedure.

Indeed, increasing the anode potential has been established to induce carbon monoxide electro-oxidation thanks to the 'reactant pair mechanism' (into carbon dioxide thanks to oxygen or water) [669]. As it might be the case for the studied commercial system, this can be performed very simply by purging the anode with air at fuel cell shutdown [616] (because it does not necessarily require the high temperature levels mentioned earlier for thermal degradation of carbon monoxide). It is usually mentioned that voltage shall reach at least levels between 0.6 to 0.7 V vs. Normal Hydrogen Electrode (vs. NHE) [655]. It is indeed also around those voltage levels that carbon monoxide poisoning seems to disappear using another offline recovery method known as anode potential cycling (or anode potential sweep) [662,670], which simply consist in applying a cycling voltammetry technique to the anode (see *Section Reversible and irreversible degradation of PEMFCs* in this Appendix). This however would require an unlikely potentiostat embodied in the PEMFC commercial system.

Similarly, an online recovery method for carbon monoxide contamination consists in potential holding (for about 2 hours, keeping a cell voltage of 0.6 V) [671] but the study reports the use of a pure hydrogen feed, which it is not likely to be the case in this residential application since the system only operates with reformat fuel.

Reaching anode over-potentials can also be achieved with other in use (online) methods thanks to high current pulsed techniques [672], also reported as 'pulsed oxidation' [673]. This technique consists in periodically demanding positive increases in current from the fuel cell in order to elevate the anode potential sufficiently for electro-oxidation of carbon monoxide to take place (up to about 600 mV) [673]. The main parameters to optimize associated with this technique are the pulse length and amplitude [663] but more importantly the pulse period [674] (in regard of the carbon monoxide contamination level of the fuel feed). Although it is not mentioned in the consulted literature, it could be imagined for this technique to be used as an offline procedure in the studied commercial system.

Likewise, negative voltage pulses have also been mentioned in literature in order to induce the electrolysis of the water [675] (which, as mentioned earlier, is present at the anode through water crossover [637,638]). This is performed at fuel cell rest by applying directly a negative voltage onto the fuel cell electrodes (i.e. by applying a sufficient voltage of opposite polarity to the fuel cell) [675]. The required voltage for electrolysis to take place (achieved by means of an external voltage source) has been reported to be down to -2.3 V (whereas, in comparison, the maximum operating cell voltage in pure hydrogen conditions has been reported to approach +800 mV) [675]. Water electrolysis allows for the formation of oxidizing agents (oxygen atoms) that will react with carbon monoxide to form carbon dioxide, but this requires a significant amount of power [516]. Indeed, a power of about 130 W for one single cell has been reported [675]. Negative voltage pulses are not to be mistaken with heating pulses which are used in another online recovery method that offered interesting experimental results (by ensuring high temperature in the catalyst layer for the carbon monoxide oxidation by water or by oxygen to take place) [676]. This is performed without causing overheating to the neighboring PEMFC membrane thanks to a thin-film-type micro-heating device embedded in the electrolyte membrane, close to the anode side surface) [676].

It is worth mentioning that gas crossover can move carbon monoxide through the membrane and affect the cathode even more than the anode [510]. Indeed, carbon monoxide poisoning, which is also an airborne pollutant [677], has a similar effect on the cathode that it has on the anode, as it reduces the catalyst activity by blocking the access of the reactant to the reactive sites. Therefore, one can assume that many mitigation and recovery strategies specifically listed for the anode might be also applicable for the cathode.

Cathode carbon monoxide poisoning must not be confused with cathode carbon corrosion, that comes directly from the oxidation of the support of the gas diffusion layer and/or the catalyst layer, usually both involving electrically and thermally conductive carbon particles [633]. Although anode carbon monoxide poisoning can come from the corrosion/oxidation of the anode carbon support (and therefore from the formation of carbon monoxide molecules onto the anode) [662], this particular process has not been reported at the cathode side in the consulted literature.

### Oxidation, dissolution and sintering of the platinum catalysts

Another widely studied degradation mechanism of PEMFCs is the lowered oxygen reduction reaction kinetics at the cathode usually caused by oxidation, dissolution [678] and sintering (redeposition mechanism of crystallite growth) [679] of the platinum catalyst, commonly used to enhance the rate of the reduction reaction [680]. It is worth mentioning that the formation of platinum oxides at the anode has also been reported as a PEMFC poisoning mechanism, but at a much slower rate than at the cathode [681].

Based on an analysis of equilibrium potentials, platinum oxidation is the principal degradative process [682] but (irreversible) dissolution and sintering of platinum oxides also occurs once they are formed [683].

Fortunately, cathode potential below 0.65 V vs. the reversible hydrogen electrode (RHE) is known to allow the reduction of the platinum oxides [616], but this is not in the usual operational range of PEMFCs [684]. Therefore, reducing cathode potential is assumed to be preferably conducted at fuel cell shutdown.

This can be done by purging the cathode with nitrogen (while feeding fuel to the anode) [616] or with potential cycling methods [685]. It can be assumed that the studied commercial system unlikely implements any method based on pure nitrogen purge but potential cycling methods remain highly conceivable. These latter processes are basically composed of voltage steps applied onto the cell (by controlling an external load): for example, a recovery procedure consisting in cycling the cell voltage between OCV and 0.2 V with steps of 0.1 V has been reported [686]. At each step, the voltage is maintained for 5 min and the current is monitored. This procedure is repeated several cycles until the cell performance has no apparent change and it has been reported that it could take up to 10 cycles to complete the entire recovery process [686]. Potential cycling (voltage steps recovery procedure) has been reported quite effective as 2.25 hours (90 cycles of three voltage steps of 30 seconds at 0.6 V, 0.3 V, and open-circuit) even suffices to remove platinum oxides from the catalyst layer [685]. The voltage steps method has even been simplified to one single periodical step of holding up the cell voltage at 0.3 V during only 2 hours (without much details on the rest of the recovering protocol) [687]. With an electrical variable resistance as a dummy load, such a potential cycling recovery method is possibly implemented in the investigated 2.5-hour regeneration phase implemented for this commercial application at fuel cell shut-down.

Both methods of platinum oxide reduction (hydrogen to the anode with non-oxidant nitrogen to the cathode and potential cycling) are often combined. For example, one particular recovery procedure consists in 4 hours of gas flushes (nitrogen and hydrogen),



with the cell load turned off, followed by 12 hours of current (re)conditioning [688]. In fact, a conditioning process is generally required for newly manufactured PEMFCs to be activated. It is indeed assumed that the number of active catalytic sites increases especially with the progressive humidification of the polymer in the membrane and in the catalyst layer [689]. Current conditioning also named ‘current control’ is indeed a classical conditioning method (as well as voltage or potential conditioning) and consists in applying and maintaining current or voltage steps onto the stack [690]. Conditioning processes are thus similarly to the potential cycling method described here above as a recovery method for platinum oxides stripping from the catalyst layer. The duration of initial current conditioning is quite high and can reach up to 25 [691] or even 50 hours [692]. It can also be shorter as one auxiliary study on cathode catalyst layers mentions a current conditioning method of 6 hours [693].

It must be stressed that the platinum oxides removal studies reported in this work, based on potential cycling (or potential holding) and/or cathode purge with nitrogen, use pure hydrogen as fuel at the anode (even though pure hydrogen has not been reported as necessary for the platinum oxides recovery to take place). Therefore, it is assumed that these procedures not only allowed the PEMFC to recover from platinum oxidation degradation because the gas flushes might also have allowed the removal of excess water [688] (see *Section Water accumulation* in this Appendix) and the potential holding under pure hydrogen use might have allowed the removal of carbon monoxide poisoning [671] (see *Section Carbon monoxide poisoning* in this Appendix). Thus, it is quite difficult to isolate the recoverable losses attributed to one single contamination, i.e. the platinum oxidation in this case.

It is worth mentioning that, in laboratory environment (with external electrodes), at fuel cell shutdown, linear sweep voltammetry (usually used as a diagnostical method, see *Section Reversible and irreversible degradation of PEMFCs* in this Appendix) has also been reported as a recovery method for platinum oxides stripping from the catalyst layer [694]. As it is the case with other voltammetry techniques, this method could only have been implemented in the studied commercial application with the unlikely use of an embodied potentiostat.

### Sulfur contamination

Contamination by sulfur compounds (sulfur oxide, carbonyl sulfide but mostly hydrogen sulfide [695]) is not considered in this work as relevant for this application from the fuel supply point of view. Although hydrogen sulfide is even more harmful than carbon monoxide poisoning [696] as even 1 ppm significantly reduces PEMFC performance [188], adsorptive desulfurizer in the hydrogen processor of the PEMFC module are commonly mentioned in patents about PEMFCs fed by natural gas [697].

Furthermore, even without desulfurizer included in the PEMFC system, natural gas is referred as ‘a clean fuel’ that contributes to ‘zero sulfur oxide emissions’ [698]. This is emphasized by the fact that the Belgian local energy regulator has stated that biogas must be desulfurized in order to make it compatible with the gas network [699], which implies that the latter does not contain any sulfur species. Decentralized desulfurization has indeed been stated in literature as ‘a very important step in utilization of natural gas resources, not only in terms of preventing the formation of sulfur oxide after combustion, but also to avoid catalyst poisoning in subsequent processing steps’ [168]. In practice, most natural gas markets require less than 4 ppm of (all) sulfur-containing compounds in the gas [167], which is in indeed very low. So, if there is no desulfurizer in the hydrogen processor and the PEMFC system, one can assume that the resulting even lower hydrogen sulfide concentration in natural gas is sufficiently low prevent particular damage to PEMFCs.

It is worth mentioning that, even with fuel desulfurizers, airborne sulfur species can still occur if air is used as the oxidizing agent, which is common in commercial applications. Those species are easily adsorbed by platinum particles and modify reaction sites for oxygen reduction [700]. Therefore, recovering methods still exist (mainly based on ozone offline treatment [701], high humidity gases cathode flushing [702] or again repetitive offline cycling voltammetry, performed with an external potentiostat [188]).

## **Dedicated review of similar commercialized applications by patent research**

It is likely that the 2.5-hour offline recovery phase performed every two days does not target only one of those main known issues of recoverable ageing. Indeed, the U.S. Department Of Energy has suggested a performance recovery protocol of similar duration to be performed quite regularly (every 24 hours). The latter is indeed supposed to handle ‘various degradation mechanisms’ [703]. Therefore, it is likely that the stack OEM has also implemented such a multi-aim recovery procedure based on know-how and empirical feedback in order to optimize PEMFC durability. This is confirmed by the number of patents that have been published regarding contaminants and reversible ageing of PEMFCs. For example, recently, an offline procedure that combined gas management (including nitrogen flushes), cyclic voltammetry (with an external potentiostat) and potential cycling has stated to tackle platinum oxidation as well as poisoning by carbon monoxide and sulfur contaminants [704].

In such an industrialized application, dedicated researches of patents published by the manufacturer prior to the commercialization could indeed narrow down the possibilities of targeted degradation mechanisms. However, it is even quite the opposite since patents also point towards regeneration procedures not only of the fuel cell stack but also of the catalysts contained in the fuel processor (reforming processes), as described in the following sections.

### Carbon deposition on the reforming catalyst

It is well known that temperatures above 875 K in reformers can induce unwanted side reactions involving carbon deposition on the reforming catalyst, which leads to its deactivation [705]. Such a risk must therefore be considered here since it has been established in *Section 5.1.1.2 - Hydrogen processor and reforming processes* that the reformer is assumed to operate around 1000 K, as required by the partial oxidation of methane reaction reported in Equation (34) or the steam reforming reported in Equation (37) and Equation (12).

For example, carbon deposition issues can be solved by periodical 2-hour regeneration steps for which the reformer is shutdown (and its catalyst is fed with hydrogen for carbon methanation) [706]. Another study suggests oxidation of carbon deposits for silica-supported catalysts (thanks to a heated oxygen flow) [707]. This tends to generate metal oxides on the catalyst layer, which is why the oxidation phase is reported to be followed by a reduction reaction using a heated hydrogen flow (to remove oxygen atoms from the catalyst) [707]. This represents overall a 2,5-hour recovery phase [707]. A similar heated ambient air carbon oxidation technique followed by hydrogen reduction has been used as regeneration procedure for a ruthenium catalyst supported on the magnesium aluminate spinel [708]. Other gases have also been reported for the regeneration of the reforming catalyst deactivated by coke (carbon deposits) buildup, e.g. carbon dioxide and even nitrogen [709]. Carbon dioxide has been reported effective as it directly reacts with the carbon deposits to form carbon monoxide, but carbon deposits gasification with inert nitrogen proceeded at much slower rate [710]. Indeed, nitrogen does not directly react with carbon at the temperature levels used in reforming processes and this suggests that it only

acts at a gasification agent, providing heat, and that the catalyst surface contains other adsorbed species which reacted with carbon when thermally activated [710]. In fact, that study suggests the presence of hydroxyl species [710], that are reported to react with the coke on the surface of the catalyst to form carbon monoxide and hydrogen [711], similarly to another reforming catalyst coke removal method based on steam [712].

This carbon deposition problem is emphasized by the fact that PEMFC applications fed by natural gas require further catalytic processes prior to the stack as shown in Figure 74. Indeed, the WGS (Water-gas shift) reactor and the carbon monoxide remover, used to limit the carbon monoxide concentration in the stack supply around 5 ppm, as stated in *Section 5.1.1.2 - Hydrogen processor and reforming processes*, have their own catalysts also potentially subjected to carbon deposition problems.

However, even if carbon deposition occurs with every reforming process [713], some coking-resistant catalysts have long been known, both for partial oxidation [714] or for steam reforming [715]. Since partial oxidation, which has even been reported 'not often susceptible to catalyst deactivation via carbon deposition' [716], and steam reforming are the most probable reforming processes involved in this application (see *Section 5.1.1.2 - Hydrogen processor and reforming processes*), it is thus assumed that the risk of carbon deposition falls down onto the catalysts of the following reforming units used to further eliminate carbon monoxide (left by the main reforming process), i.e. the WGS reactor and the carbon monoxide remover.

Nevertheless, since the temperature limit for carbon deposition depends on the metal used in the catalyst (about 400 to 500 °C for ruthenium and about 300 to 400 °C for nickel), proper thermal management can be implemented to prevent it [697]. Indeed, the WGS conversion and the carbon monoxide removing processes are respectively reported to occur at about 350 to 200 °C and about 200 to 100 °C in the natural gas processing system of patented PEMFC fuel production systems [513,697], i.e. below the coke deposition temperature levels.

Similarly, coke deposition is never a problem within the PEMFC stack. Indeed, even high-temperature PEMFC operates below 200 °C [717], whereas coke deposits only occurs several hundred degrees over that temperature [697,705].

Therefore, it is assumed that the 2.5-hour offline recovery phase performed every two days for this commercialized PEMFC cogeneration unit unlikely involves coke removal processes of any kind.

#### Ammonia poisoning of the oxidation catalyst of the carbon monoxide remover

In addition to the carbon deposit risk, patent researches have highlighted ammonia poisoning as an even more relevant hazard for hydrogen production systems of PEMFCs fed by natural gas, along with its proper offline recovery procedure. In fact, ammonia is known to be harmful to the fuel cell stack in several ways. On the one hand, ammonium ions tend to decrease the conductivity of the membrane and of the electrode ionomer. On the other hand, possible adsorption of ammonia onto the anode catalyst and, after crossover, onto the cathode catalyst affects the kinetic of both the oxidation and the reduction reactions [718]. Unfortunately, high-temperature reforming of natural gas, that usually contains nitrogen, induces the formation of a few hundred ppm of ammonia that poisons the PEMFC stack and requires specific hardware to be removed from the reformat [719]. Nitrogen has indeed been reported to react at high temperature levels with the hydrogen generated by the reformer to produce ammonia [720]. For information, if ammonia poisoning (of the anode) were too severe, it often can be recovered thanks to specific very slow recovery steps that mainly consists in operating the fuel cell in pure hydrogen [721] or with ammonium sulfide solution (dissolution into product water) [722].

Ammonia poisoning of the fuel cell anode is not as investigated as the other degradation mechanisms previously discussed [723] and this is certainly because ammonium ions can act as proton carriers through the membrane. Since they can be oxidized at the cathode back into nitrogen (and water), this allows for lower performance losses (and slower performance decay) [724]. Industrially, it seems that the OEMs implement an ammonia remover device disposed upstream from the fuel cell stack [725]. The ammonia remover basically consists in ammonia absorption by water drops, which are subsequently moved to an electro dialysis chamber that is generating hypochlorite anions (from chlorine anions in a water solution). As described by Equation (69), hypochlorite anions react with the ammonia captured in the water to form nitrogen, water, and back again, the chlorine anions for the recirculation towards the electro dialysis chamber [720]. Water has indeed an ability to absorb a very large quantity of ammonia vapor [726] and water pulverization is a common way of capturing it [727].



This ammonia remover is placed just before the stack, in the ‘Anode pre-treatment unit’ of Figure 74. Therefore, it does not prevent prior ammonia poisoning of the catalysts used in the upstream hydrogen processor, i.e. the reformer, the carbon monoxide WGS converter and the carbon monoxide remover as illustrated in Figure 74.

In fact, the selective oxidation catalyst used in the carbon monoxide remover usually involve ruthenium because it is relatively inexpensive compared with other noble metals and it presents high selective oxidation performance over a wide temperature range [728]. Unfortunately, ruthenium-based catalysts durability against trace amounts of ammonia is an important issue [728]. This very common other type of ammonia poisoning (of the oxidation catalyst of the carbon remover prior to the stack and not of the stack itself), said to be caused by nitrosyl formation from ammonia and oxygen (nitric oxide bonded to the metal catalyst), subsequently leads to ineffective carbon monoxide removal in the reformatted fuel [729], already stated as very critical for the fuel cell performance and lifespan (see *Section Carbon monoxide poisoning* in this Appendix). Also, disposing the ammonia remover within the hydrogen processor (prior to the carbon monoxide remover) has been reported too complex and expensive for commercial applications [725]

Therefore, industrialists have determined the maximum cumulative amount of ammonia supplied to the carbon monoxide remover and they have established a maximum operating duration threshold that triggers a fuel cell shutdown and a specific oxidation catalyst regeneration method [725]. This catalyst reactivation needs to be conducted in a reductive atmosphere that mainly consists of hydrogen [730] obtained by reducing the amount of air to the carbon monoxide remover (compared to the fuel cell operating period) but still providing natural gas to the reformer (and steam to the WGS reactor) [725]. Temperature (tested in the 115-185 °C range [731], i.e. exactly in the operating range of the carbon monoxide remover [513,697]) is said to help the reduction of absorbed nitrosyl compounds back to ammonia vapor [731]. It is worth mentioning that this ammonia vapor contained in the hydrogen reductive atmosphere and produced in this offline recovery process is not subsequently removed in the ammonia remover described here above (used continuously in fuel cell operating mode). Indeed, it has been reported as ‘post-processing’ that the hydrogen gas containing ammonia it is simply burned by the heater of reformer [725], i.e. the afterburner shown in Figure 74. In addition to simplicity, ensuring the safety of the stack (from high carbon monoxide concentration in the fuel stream during the carbon monoxide remover recovery phase) is the most probable reason. This would require an additional feature on the schematics of the PEMFC module (not shown in Figure 74) : the anode of the PEMFC stack shall be bypassed (only during this so called ‘post-processing’ procedure) with an internal pipe that starts between the carbon monoxide remover

---

(hydrogen processor) and the ammonia remover and ends at the anode exhaust (before the entering the afterburner).

In the patent search, the maximum PEMFC operating time has been set to 40 hours, followed by a fuel cell shutdown of 5 hours (which includes the stopping process, the regeneration of the oxidation catalyst, the described 'post-processing' that burns the resulting ammonia vapor, and the following start-up process) [725]. Those durations have probably been progressively optimized by the OEM to 45.5 hours of operating time and 2.5 hours of shutdown time, as it the case for the commercialized PEMFC cogeneration system concerned by this work. One can therefore assume that this ammonia poisoning of the carbon monoxide remover catalyst (that loses its ability to prevent carbon monoxide poisoning of the stack) is the main degradation mechanism targeted by the 2.5-hour offline recovery procedure occurring for the studied commercialized fuel cell system.

---

## REFERENCES

- [1] Brännlund R, Ghalwash T, Nordström J. Increased energy efficiency and the rebound effect: Effects on consumption and emissions. *Energy Econ* 2007;29:1–17. <https://doi.org/10.1016/j.eneco.2005.09.003>.
- [2] Foxon TJ. Technological lock-in and the role of innovation. *Handbook of Sustainable Development*, Edward Elgar Publishing; 2014. <https://doi.org/10.4337/9781782544708.00031>.
- [3] Paulus N. Confronting Nationally Determined Contributions (NDCs) to IPCC's +2°C carbon budgets through the analyses of France and Wallonia climate policies. *Journal of Ecological Engineering* 2023;24. <https://doi.org/10.12911/22998993/162984>.
- [4] United Nations. FCCC/CP/2015/L.9/Rev.1 - Adoption of the Paris Agreement. Paris: 2015.
- [5] High Ambition Coalition. High Ambition Coalition COP 26 Leaders' Statement. Glasgow: 2021.
- [6] High Ambition Coalition. Energy growing behind ambitious Glasgow Package. Glasgow: 2021.
- [7] IPCC WGI. Global Warming of 1.5°C. An IPCC Special Report on the impacts of global warming of 1.5°C above pre-industrial levels and related global greenhouse gas emission pathways, in the context of strengthening the global response to the threat of climate change, sustainable development, and efforts to eradicate poverty. IPCC - Working Group I Technical Support Unit 2018. <https://doi.org/10.1017/9781009157940>.
- [8] Rogelj J, Forster PM, Kriegler E, Smith J. Estimating and tracking the remaining carbon budget for stringent climate targets. *Nature* 2019;571. <https://doi.org/10.1038/s41586-019-1368-z>.
- [9] IPCC WGI. Climate Change 2021: The Physical Science Basis - Summary for Policymakers. IPCC - Working Group I Technical Support Unit 2021.
- [10] IPCC WGIII. Climate Change 2022 Mitigation of Climate Change - Summary for Policymakers. IPCC - Working Group III Technical Support Unit 2022. <https://doi.org/10.1017/9781009157926.001>.
- [11] Gignac R, Matthews HD. Allocating a 2 °C cumulative carbon budget to countries. *Environmental Research Letters* 2015;10. <https://doi.org/10.1088/1748-9326/10/7/075004>.
- [12] IPCC WGI. Climate Change 2013: The Physical Science Basis. IPCC - Working Group I Technical Support Unit 2013.
- [13] Smith SM, Lowe JA, Bowerman NHA, Gohar LK, Huntingford C, Allen MR. Equivalence of greenhouse-gas emissions for peak temperature limits. *Nat Clim Chang* 2012;2:535–8. <https://doi.org/10.1038/nclimate1496>.
- [14] Rogelj J, Meinshausen M, Schaeffer M, Knutti R, Riahi K. Impact of short-lived non-CO2 mitigation on carbon budgets for stabilizing global warming. *Environmental Research Letters* 2015;10. <https://doi.org/10.1088/1748-9326/10/7/075001>.
- [15] Paulus N, Dávila C, Lemort V. Field-test economic and ecological performance of Proton Exchange Membrane Fuel Cells (PEMFC) used in micro-combined heat and

- power residential applications (micro-CHP). Proceedings of the 35th International Conference On Efficiency, Cost, Optimization, Simulation and Environmental Impact of Energy Systems (ECOS2022) 2022. <https://doi.org/10.11581/dtu.00000267>.
- [16] Gernaat DEHJ, Calvin K, Lucas PL, Luderer G, Otto SAC, Rao S, et al. Understanding the contribution of non-carbon dioxide gases in deep mitigation scenarios. *Global Environmental Change* 2015;33. <https://doi.org/10.1016/j.gloenvcha.2015.04.010>.
- [17] Ehlert D, Zickfeld K. What determines the warming commitment after cessation of CO<sub>2</sub> emissions? *Environmental Research Letters* 2017;12. <https://doi.org/10.1088/1748-9326/aa564a>.
- [18] Steffen W, Rockström J, Richardson K, Lenton TM, Folke C, Liverman D, et al. Trajectories of the Earth System in the Anthropocene. *Proc Natl Acad Sci U S A* 2018;115. <https://doi.org/10.1073/pnas.1810141115>.
- [19] Lowe JA, Bernie D. The impact of Earth system feedbacks on carbon budgets and climate response. *Philos Trans A Math Phys Eng Sci* 2018;376. <https://doi.org/10.1098/rsta.2017.0263>.
- [20] Maris G, Flouros F. The Green Deal, National Energy and Climate Plans in Europe: Member States' Compliance and Strategies. *Adm Sci* 2021;11. <https://doi.org/10.3390/admsci11030075>.
- [21] Ministère de la transition écologique. Stratégie nationale bas-carbone révisée - NOR : TRER2010109P. 2020.
- [22] Ministère de la transition écologique. Stratégie nationale bas-carbone - DICOM-DGEC/PLA/19092. CAIRN; 2020.
- [23] Gouvernement Wallon. Plan Air Climat Energie (PACE) 2030. 2023.
- [24] Gouvernement Wallon. Contribution de la Wallonie au Plan National Energie Climat 2030 (PNEC 2030). 2019.
- [25] Service Public de Wallonie. 20 FEVRIER 2014. - Décret "Climat." 2014.
- [26] AwAC. Avis du Comité wallon d'experts sur le climat - Ambition générale du projet de Plan Wallon Energie Climat 2030. 2019.
- [27] Gouvernement Wallon. Stratégie à long terme pour la Wallonie (SLT 2050): "Vers une Wallonie climatiquement neutre en 2050." 2019.
- [28] Vandevyvere H, Nevens F. Lost in Transition or Geared for the S-Curve? An Analysis of Flemish Transition Trajectories with a Focus on Energy Use and Buildings. *Sustainability* 2015;7:2415–36. <https://doi.org/10.3390/su7032415>.
- [29] Lombardi M, Laiola E, Tricase C, Rana R. Assessing the urban carbon footprint: An overview. *Environ Impact Assess Rev* 2017;66. <https://doi.org/10.1016/j.eiar.2017.06.005>.
- [30] Feng K, Hubacek K, Sun L, Liu Z. Consumption-based CO<sub>2</sub> accounting of China's megacities: The case of Beijing, Tianjin, Shanghai and Chongqing. *Ecol Indic* 2014;47. <https://doi.org/10.1016/j.ecolind.2014.04.045>.
- [31] Klemeš JJ, Liu X, Petar S, Varbanova. Virtual Greenhouse Gas and Water Footprints Reduction: Emissions, Effluents and Water Flows Embodied in International Trade. *Chem Eng Trans* 2017;56. <https://doi.org/10.3303/CET1756010>.
- [32] Haut Conseil pour le Climat. Maîtriser l'empreinte carbone de la France - Réponse à la saisine du gouvernement. 2020.

- [33] Yellishetty M, Ranjith PG, Tharumarajah A. Iron ore and steel production trends and material flows in the world: Is this really sustainable? *Resour Conserv Recycl* 2010;54. <https://doi.org/10.1016/j.resconrec.2010.03.003>.
- [34] Hambÿe C, Hertveldt B, Michel B. Does consistency with detailed national data matter for calculating carbon footprints with global multi-regional input–output tables? A comparative analysis for Belgium based on a structural decomposition. *J Econ Struct* 2018;7. <https://doi.org/10.1186/s40008-018-0110-6>.
- [35] Towa E, Zeller V, Merciai S, Schmidt J, Achten WMJ. Toward the development of subnational hybrid input–output tables in a multiregional framework. *J Ind Ecol* 2022;26. <https://doi.org/10.1111/jieec.13085>.
- [36] Hertwich EG, Peters GP. Carbon Footprint of Nations: A Global, Trade-Linked Analysis. *Environ Sci Technol* 2009;43. <https://doi.org/10.1021/es803496a>.
- [37] Lamb WF, Mattioli G, Levi S, Timmons Roberts J, Capstick S, Creutzig F, et al. Discourses of climate delay. *Global Sustainability* 2020;3. <https://doi.org/10.1017/SUS.2020.13>.
- [38] Petrova MA. “NIMBYism” revisited: public acceptance of wind energy in the United States. *WIREs Climate Change* 2013;4. <https://doi.org/10.1002/wcc.250>.
- [39] Semenza JC, Hall DE, Wilson DJ, Bontempo BD, Sailor DJ, George LA. Public Perception of Climate Change: Voluntary Mitigation and Barriers to Behavior Change. *Am J Prev Med* 2008;35:479–87. <https://doi.org/10.1016/J.AMEPRE.2008.08.020>.
- [40] Moser SC. Communicating climate change: history, challenges, process and future directions. *Wiley Interdiscip Rev Clim Change* 2010;1:31–53. <https://doi.org/10.1002/WCC.11>.
- [41] Pandey D, Agrawal M, Pandey JS. Carbon footprint: current methods of estimation. *Environ Monit Assess* 2010;178. <https://doi.org/10.1007/s10661-010-1678-y>.
- [42] Bureau du Plan. Perspectives démographiques 2019-2070 : Population et ménages. 2020.
- [43] PRB. 2020 World Population Data sheet - Booklet. 2020.
- [44] van Nimwegen N, van der Erf R. Europe at the Crossroads: Demographic Challenges and International Migration. *J Ethn Migr Stud* 2010;36. <https://doi.org/10.1080/1369183x.2010.515132>.
- [45] McLaren D. A comparative global assessment of potential negative emissions technologies. *Process Safety and Environmental Protection* 2012;90. <https://doi.org/10.1016/j.psep.2012.10.005>.
- [46] Allen MR, Shine KP, Fuglestvedt JS, Millar RJ, Cain M, Frame DJ, et al. A solution to the misrepresentations of CO<sub>2</sub>-equivalent emissions of short-lived climate pollutants under ambitious mitigation. *NPJ Clim Atmos Sci* 2018;1. <https://doi.org/10.1038/s41612-018-0026-8>.
- [47] Iweps. Emissions de gaz à effet de serre (GES) - Fiche A006-REDUC.GES - dernières données régionales disponibles au 01/06/2022. 2022.
- [48] CITEPA. Rapport National d'Inventaire pour la France au titre de la Convention cadre des Nations Unies sur les Changements Climatiques et du Protocole de Kyoto. 2022.
- [49] Blujdea VNB, Viñas RA, Federici S, Grassi G. The EU greenhouse gas inventory for the LULUCF sector: I. Overview and comparative analysis of methods used by EU



- member states. Carbon Manag 2016;6:247–59. <https://doi.org/10.1080/17583004.2016.1151504>.
- [50] Kumar A, Singh P, Raizada P, Hussain CM. Impact of COVID-19 on greenhouse gases emissions: A critical review. *Sci Total Environ* 2022;806. <https://doi.org/10.1016/j.scitotenv.2021.150349>.
- [51] Nataly Echevarria Huaman R, Xiu Jun T. Energy related CO2 emissions and the progress on CCS projects: A review. *Renewable and Sustainable Energy Reviews* 2014;31:368–85. <https://doi.org/10.1016/j.rser.2013.12.002>.
- [52] McQueen N, Gomes KV, McCormick C, Blumanthal K, Pisciotta M, Wilcox J. A review of direct air capture (DAC): scaling up commercial technologies and innovating for the future. *Progress in Energy* 2021;3. <https://doi.org/10.1088/2516-1083/ABF1CE>.
- [53] Yamano N, Joaquim G. CO2 emissions embodied in international trade and domestic final demand. *OECD Science, Technology and Industry Working Papers* 2020;11. <https://doi.org/10.1787/8f2963b8-en>.
- [54] Paulus N. Developing individual carbon footprint reduction pathways from carbon budgets: examples with Wallonia and France. *Renewable and Sustainable Energy Reviews* 2024;In Press.
- [55] Auger C, Hilloulin B, Boisserie B, Thomas M, Guignard Q, Rozière E. Open-Source Carbon Footprint Estimator: Development and University Declination. *Sustainability* 2021;13. <https://doi.org/10.3390/su13084315>.
- [56] Matthews HD, Wynes S. Current global efforts are insufficient to limit warming to 1.5°C. *Science (1979)* 2022;376:1404–9. <https://doi.org/10.1126/SCIENCE.ABO3378>.
- [57] Martin MA, Sendra OA, Bastos A, Bauer N, Bertram C, Blenckner T, et al. Ten new insights in climate science 2021: a horizon scan. *Global Sustainability* 2021;4. <https://doi.org/10.1017/SUS.2021.25>.
- [58] Liu Z, Deng Z, Davis SJ, Giron C, Ciais P. Monitoring global carbon emissions in 2021. *Nat Rev Earth Environ* 2022;3:217–9. <https://doi.org/10.1038/s43017-022-00285-w>.
- [59] Peters GP. Beyond carbon budgets. *Nat Geosci* 2018;11:378–80. <https://doi.org/10.1038/s41561-018-0142-4>.
- [60] Raupach MR, Davis SJ, Peters GP, Andrew RM, Canadell JG, Ciais P, et al. Sharing a quota on cumulative carbon emissions. *Nat Clim Chang* 2014;4:873–9. <https://doi.org/10.1038/NCLIMATE2384>.
- [61] Dooley K, Holz C, Kartha S, Klinsky S, Roberts JT, Shue H, et al. Ethical choices behind quantifications of fair contributions under the Paris Agreement. *Nat Clim Chang* 2021;11:300–5. <https://doi.org/10.1038/S41558-021-01015-8>.
- [62] van der Ploeg F. The safe carbon budget. *Clim Change* 2018;147:47–59. <https://doi.org/10.1007/s10584-017-2132-8>.
- [63] Mills-Novoa M, Liverman DM. Nationally Determined Contributions: Material climate commitments and discursive positioning in the NDCs. *Wiley Interdiscip Rev Clim Change* 2019;10. <https://doi.org/10.1002/WCC.589>.
- [64] Hausfather Z, Moore FC. Climate science Commitments could limit warming to below 2 oC. *Nature* 2022;604. <https://doi.org/10.1038/d41586-022-00874-1>.
- [65] Kriegler E, Bertram C, Kuramochi T, Jakob M, Pehl M, Stevanović M, et al. Short term policies to keep the door open for Paris climate goals. *Environmental Research Letters* 2018;13. <https://doi.org/10.1088/1748-9326/AAC4F1>.

- [66] Riahi K, Kriegler E, Johnson N, Bertram C, den Elzen M, Eom J, et al. Locked into Copenhagen pledges - Implications of short-term emission targets for the cost and feasibility of long-term climate goals. *Technol Forecast Soc Change* 2015;90:8–23. <https://doi.org/10.1016/J.TECHFORE.2013.09.016>.
- [67] van Vuuren DP, Stehfest E, Gernaat DEHJ, Doelman JC, van den Berg M, Harmsen M, et al. Energy, land-use and greenhouse gas emissions trajectories under a green growth paradigm. *Global Environmental Change* 2017;42:237–50. <https://doi.org/10.1016/J.GLOENVCHA.2016.05.008>.
- [68] Gambhir A, George M, McJeon H, Arnell NW, Bernie D, Mittal S, et al. Near-term transition and longer-term physical climate risks of greenhouse gas emissions pathways. *Nat Clim Chang* 2021;12:88–96. <https://doi.org/10.1038/s41558-021-01236-x>.
- [69] Grant N. The Paris Agreement’s ratcheting mechanism needs strengthening 4-fold to keep 1.5°C alive. *Joule* 2022;6:703–8. <https://doi.org/10.1016/j.joule.2022.02.017>.
- [70] Stockwell C, Geiges A, Ramalope D, Gidden M, Hare B, de Villafranca Casas MJ, et al. Glasgow’s 2030 credibility gap: net zero’s lip service to climate action. *Climate Action Tracker*, <https://ClimateactiontrackerOrg> 2021.
- [71] Williamson K, Satre-Meloy A, Velasco K, Green K. *Climate Change Needs Behavior Change: Making the Case for Behavioral Solutions to Reduce Global Warming*. Rare 2018.
- [72] Allen MR, Fuglestvedt JS, Shine KP, Reisinger A, Pierrehumbert RT, Forster PM. New use of global warming potentials to compare cumulative and short-lived climate pollutants. *Nat Clim Chang* 2016;6:773–6. <https://doi.org/10.1038/nclimate2998>.
- [73] Kucharavy D, De Guio R. Application of S-shaped curves. *Procedia Eng* 2011;9:559–72. <https://doi.org/10.1016/J.PROENG.2011.03.142>.
- [74] Berkson J. Tables for the Maximum Likelihood Estimate of the Logistic Function. *Biometrics* 1957;13:28. <https://doi.org/10.2307/3001900>.
- [75] Ren J, McIsaac KA, Patel R V., Peters TM. A potential field model using generalized sigmoid functions. *IEEE Transactions on Systems, Man, and Cybernetics, Part B: Cybernetics* 2007;37:477–84. <https://doi.org/10.1109/TSMCB.2006.883866>.
- [76] Klimstra M, Zehr EP. A sigmoid function is the best fit for the ascending limb of the Hoffmann reflex recruitment curve. *Exp Brain Res* 2008;186:93–105. <https://doi.org/10.1007/S00221-007-1207-6>.
- [77] Matthews HD, Tokarska KB, Nicholls ZRJ, Rogelj J, Canadell JG, Friedlingstein P, et al. Opportunities and challenges in using remaining carbon budgets to guide climate policy. *Nature Geoscience* 2020 2020;13:769–79. <https://doi.org/10.1038/s41561-020-00663-3>.
- [78] Bowerman NHA, Frame DJ, Huntingford C, Lowe JA, Smith SM, Allen MR. The role of short-lived climate pollutants in meeting temperature goals. *Nat Clim Chang* 2013;3:1021–4. <https://doi.org/10.1038/NCLIMATE2034>.
- [79] Salzmann M. Global warming without global mean precipitation increase’. *Sci Adv* 2016;2. <https://doi.org/10.1126/SCIADV.1501572>.
- [80] Allen RJ, Horowitz LW, Naik V, Oshima N, O’Connor FM, Turnock S, et al. Significant climate benefits from near-term climate forcer mitigation in spite of aerosol reductions. *Environmental Research Letters* 2021;16. <https://doi.org/10.1088/1748-9326/ABE06B>.
- [81] Dreyfus GB, Xu Y, Shindell DT, Zaelke D, Ramanathan V. Mitigating climate disruption in time: A self-consistent approach for avoiding both near-term and long-

- term global warming. *Proc Natl Acad Sci U S A* 2022;119. <https://doi.org/10.1073/PNAS.2123536119>.
- [82] Lund MT, Myhre G, Samset BH. Anthropogenic aerosol forcing under the Shared Socioeconomic Pathways. *Atmos Chem Phys* 2019;19:13827–39. <https://doi.org/10.5194/ACP-19-13827-2019>.
- [83] Ou Y, Roney C, Alsalam J, Calvin K, Creason J, Edmonds J, et al. Deep mitigation of CO<sub>2</sub> and non-CO<sub>2</sub> greenhouse gases toward 1.5 °C and 2 °C futures. *Nat Commun* 2021;12:1–9. <https://doi.org/10.1038/s41467-021-26509-z>.
- [84] Folini D, Kubler F, Malova A, Scheidegger S. The Climate in Climate Economics. Proceedings of the 19th European Geosciences Union General Assembly (EGU22) 2022. <https://doi.org/10.5194/egusphere-egu22-2607>.
- [85] Jenkins S, Millar RJ, Leach N, Allen MR. Framing Climate Goals in Terms of Cumulative CO<sub>2</sub>-Forcing-Equivalent Emissions. *Geophys Res Lett* 2018;45:2795–804. <https://doi.org/10.1002/2017GL076173>.
- [86] Mengis N, Matthews HD. Non-CO<sub>2</sub> forcing changes will likely decrease the remaining carbon budget for 1.5 °C. *NPJ Clim Atmos Sci* 2020;3:1–7. <https://doi.org/10.1038/s41612-020-0123-3>.
- [87] Leach NJ, Millar RJ, Haustein K, Jenkins S, Graham E, Allen MR. Current level and rate of warming determine emissions budgets under ambitious mitigation. *Nat Geosci* 2018;11. <https://doi.org/10.1038/s41561-018-0156-y>.
- [88] Jenkins S, Cain M, Friedlingstein P, Gillett N, Walsh T, Allen MR. Quantifying non-CO<sub>2</sub> contributions to remaining carbon budgets. *NPJ Clim Atmos Sci* 2021;4:1–10. <https://doi.org/10.1038/s41612-021-00203-9>.
- [89] Reay DS, Davidson EA, Smith KA, Smith P, Melillo JM, Dentener F, et al. Global agriculture and nitrous oxide emissions. *Nat Clim Chang* 2012;2:410–6. <https://doi.org/10.1038/NCLIMATE1458>.
- [90] Lannelongue L, Grealey J, Inouye M. Green Algorithms: Quantifying the Carbon Footprint of Computation. *Advanced Science* 2021;8. <https://doi.org/10.1002/ADVS.202100707>.
- [91] Smith MA, Cain M, Allen MR. Further improvement of warming-equivalent emissions calculation. *NPJ Clim Atmos Sci* 2021;4:1–3. <https://doi.org/10.1038/s41612-021-00169-8>.
- [92] Lynch J, Cain M, Pierrehumbert R, Allen M. Demonstrating GWP\*: a means of reporting warming-equivalent emissions that captures the contrasting impacts of short- and long-lived climate pollutants. *Environmental Research Letters* 2020;15. <https://doi.org/10.1088/1748-9326/AB6D7E>.
- [93] Cain M, Lynch J, Allen MR, Fuglestvedt JS, Frame DJ, Macey AH. Improved calculation of warming-equivalent emissions for short-lived climate pollutants. *NPJ Clim Atmos Sci* 2019;2:1–7. <https://doi.org/10.1038/s41612-019-0086-4>.
- [94] Meinshausen M, Nicholls Z. GWP\* is a model, not a metric. *Environmental Research Letters* 2022;17. <https://doi.org/10.1088/1748-9326/AC5930>.
- [95] Turbat V, Gribble R, Zeng W. Population, Burden of Disease, and Health Services 2022:59–77. [https://doi.org/10.1007/978-3-031-02040-7\\_4](https://doi.org/10.1007/978-3-031-02040-7_4).
- [96] Bureau du Plan. Population par région et âge, au 1er janvier. Perspectives de Population 2021-2070 2022. [https://www.plan.be/databases/data-35-fr-perspectives\\_de\\_population\\_2021\\_2070](https://www.plan.be/databases/data-35-fr-perspectives_de_population_2021_2070) (accessed July 8, 2022).

- [97] Dumont G-F. L'Ukraine face à la guerre : géopolitique et population. *Population & Avenir* 2022;758:17–9. <https://doi.org/10.3917/POPAV.758.0017>.
- [98] Keller DP, Lenton A, Littleton EW, Oschlies A, Scott V, Vaughan NE. The Effects of Carbon Dioxide Removal on the Carbon Cycle. *Curr Clim Change Rep* 2018;4:250–65. <https://doi.org/10.1007/S40641-018-0104-3>.
- [99] Matthews HD, Zickfeld K, Dickau M, MacIsaac AJ, Mathesius S, Nzotungicimpaye C-M, et al. Temporary nature-based carbon removal can lower peak warming in a well-below 2°C scenario. *Commun Earth Environ* 2022;3:1–8. <https://doi.org/10.1038/s43247-022-00391-z>.
- [100] Batres M, Wang FM, Buck H, Kapila R, Kosar U, Licker R, et al. Environmental and climate justice and technological carbon removal. *The Electricity Journal* 2021;34:107002. <https://doi.org/10.1016/J.TEJ.2021.107002>.
- [101] Lenzi D. The ethics of negative emissions. *Global Sustainability* 2018;1:1–8. <https://doi.org/10.1017/SUS.2018.5>.
- [102] Perrin D, Temmerman M, Laitat E. Calculation on the impacts of forestation, afforestation and reforestation on the C-sequestration potential in Belgian forests ecosystems. *Biotechnologie, Agronomie, Société et Environnement* 2000;4.
- [103] Hathaway MD. Agroecology and permaculture: addressing key ecological problems by rethinking and redesigning agricultural systems. *J Environ Stud Sci* 2016;6:239–50. <https://doi.org/10.1007/S13412-015-0254-8>.
- [104] Neumann M, Smith P. Carbon uptake by European agricultural land is variable, and in many regions could be increased: Evidence from remote sensing, yield statistics and models of potential productivity. *Science of The Total Environment* 2018;643:902–11. <https://doi.org/10.1016/J.SCITOTENV.2018.06.268>.
- [105] Jyoti Nath A, Lal R, Kumar Das A. Fired Bricks: CO2 Emission and Food Insecurity. *Global Challenges* 2018;2. <https://doi.org/10.1002/GCH2.201700115>.
- [106] Smith P, Andrén O, Karlsson T, Perälä P, Regina K, Rounsevell M, et al. Carbon sequestration potential in European croplands has been overestimated. *Glob Chang Biol* 2005;11:2153–63. <https://doi.org/10.1111/J.1365-2486.2005.01052.X>.
- [107] Viglizzo EF, Ricard MF, Taboada MA, Vázquez-Amábile G. Reassessing the role of grazing lands in carbon-balance estimations: Meta-analysis and review. *Science of The Total Environment* 2019;661:531–42. <https://doi.org/10.1016/J.SCITOTENV.2019.01.130>.
- [108] Delescaille L-M. Nature conservation and pastoralism in Wallonia. *Pasture Landscapes and Nature Conservation* 2002:39–52. [https://doi.org/10.1007/978-3-642-55953-2\\_3](https://doi.org/10.1007/978-3-642-55953-2_3).
- [109] Seto KC, Churkina G, Hsu A, Keller M, Newman PWG, Qin B, et al. From Low- to Net-Zero Carbon Cities: The Next Global Agenda. *Annu Rev Environ Resour* 2021;46. <https://doi.org/10.1146/annurev-environ-050120-113117>.
- [110] Alderweireld M, Rondeux J, Latte N, Hébert J, Lecomte H. Chapter 8 - Belgium (Wallonia). *National Forest Inventories Assessment of Wood Availability and Use*. Springer, 2016, p. 159–79. [https://doi.org/10.1007/978-3-319-44015-6\\_8](https://doi.org/10.1007/978-3-319-44015-6_8).
- [111] Kuittinen M, Hautamäki R, Tuhkanen EM, Riikonen A, Ariluoma M. Environmental Product Declarations for plants and soils: how to quantify carbon uptake in landscape design and construction? *International Journal of Life Cycle Assessment* 2021;26:1100–16. <https://doi.org/10.1007/S11367-021-01926-W>.
- [112] Carnicer J, Alegria A, Giannakopoulos C, Di Giuseppe F, Karali A, Koutsias N, et al. Global warming is shifting the relationships between fire weather and realized fire-

- induced CO<sub>2</sub> emissions in Europe. *Scientific Reports* 2022 12:1 2022;12:1–6. <https://doi.org/10.1038/s41598-022-14480-8>.
- [113] Cox PM, Betts RA, Jones CD, Spall SA, Totterdell IJ. Acceleration of global warming due to carbon-cycle feedbacks in a coupled climate model. *Nature* 2000;408:184–7. <https://doi.org/10.1038/35041539>.
- [114] Haut Conseil pour le Climat. Dépasser les constats. Mettre en oeuvre les solutions. 2022.
- [115] Fawcett T, Hvelplund F, Meyer NI. Making It Personal. Generating Electricity in a Carbon-Constrained World, Elsevier; 2010, p. 87–107. <https://doi.org/10.1016/B978-1-85617-655-2.00004-3>.
- [116] INSEE. Résultats détaillés des projections de population 2021-2070 pour la France – Scénario central. Projections de Population 2021-2070 2021. <https://www.insee.fr/fr/statistiques/5894083?sommaire=5760764> (accessed November 23, 2023).
- [117] INSEE. Évolution de la population. Tableaux de l'économie Française - Édition 2020 2020. <https://www.insee.fr/fr/statistiques/4277615?sommaire=4318291> (accessed November 26, 2023).
- [118] Ikhlassé H, Benjamin D, Vincent C, Hicham M. Environmental impacts of pre/during and post-lockdown periods on prominent air pollutants in France. *Environ Dev Sustain* 2021;23. <https://doi.org/10.1007/S10668-021-01241-2>.
- [119] Bourgeois A, Lafrogne-Joussier R, Lequien M, Ralle P. Un tiers de l'empreinte carbone de l'Union européenne est dû à ses importations. *Insee Analyses* 2022;74.
- [120] Pandey D, Agrawal M, Jai ; Pandey S, Pandey D, Agrawal · M, et al. Carbon footprint: current methods of estimation. *Environ Monit Assess* 2011;178:135–60. <https://doi.org/10.1007/S10661-010-1678-Y>.
- [121] Paulus N, Lemort V. Pollutant testing (NO<sub>x</sub>, SO<sub>2</sub> and CO) of commercialized micro-combined heat and power (mCHP) fuel cells. Proceedings of the 36th International Conference On Efficiency, Cost, Optimization, Simulation and Environmental Impact of Energy Systems (ECOS2023) 2023. <https://doi.org/10.52202/069564-0104>.
- [122] Paulus N, Lemort V. Experimental assessment of pollutant emissions from residential fuel cells and comparative benchmark analysis. *J Environ Manage* 2024;In Press.
- [123] International Energy Agency. CO<sub>2</sub> intensity of power - Belgium. *Energy Transition Indicators* n.d. <https://www.iea.org/countries/belgium> (accessed April 17, 2023).
- [124] International Energy Agency. CO<sub>2</sub> Emissions From Fuel Combustion - Highlights 2013. [https://doi.org/10.1787/co2\\_fuel-2013-en](https://doi.org/10.1787/co2_fuel-2013-en).
- [125] IPCC WGIII. Climate Change 2014: Mitigation of Climate Change. IPCC - Working Group III Technical Support Unit 2014.
- [126] Koffi B, Cerutti A, Duerr M, Iancu A, Kona A, Janssens-Maenhout G. Covenant of Mayors for Climate and Energy: default emission factors for local emission inventories : version 2017. Publications Office; 2017. <https://doi.org/doi/10.2760/290197>.
- [127] CWaPE. Décision CD-5j18-CWaPE relative à “la définition des rendements annuels d'exploitation des installations modernes de référence, ...” 2005.
- [128] IPCC WGI. Climate Change 1995: The Science of Climate Change. IPCC - Working Group I Technical Support Unit 1995.

- [129] IPCC WGI. Climate Change 2021: The Physical Science Basis. IPCC - Working Group I Technical Support Unit 2021.
- [130] Psomopoulos CS, Skoula I, Karras C, Chatzimpiros A, Chionidis M. Electricity savings and CO<sub>2</sub> emissions reduction in buildings sector: How important the network losses are in the calculation? *Energy* 2010;35:485–90. <https://doi.org/10.1016/j.energy.2009.10.016>.
- [131] Gouvernement Wallon. Arrêté ministériel déterminant les procédures et le Code de comptage de l'électricité produite à partir de sources d'énergie renouvelables et/ou de cogénération. 2007.
- [132] Daoud I. Installer une Cogénération dans votre Etablissement. Ministère de La Région Wallonne Direction Générale Des Technologies, de La Recherche et de l'Energie (GGTRE) 2003.
- [133] Sovacool BK. Valuing the greenhouse gas emissions from nuclear power: A critical survey. *Energy Policy* 2008;36:2950–63. <https://doi.org/10.1016/J.ENPOL.2008.04.017>.
- [134] Chae Y, Kim M, Yoo SH. Does natural gas fuel price cause system marginal price, vice-versa, or neither? A causality analysis. *Energy* 2012;47:199–204. <https://doi.org/10.1016/J.ENERGY.2012.09.047>.
- [135] Siler-Evans K, Azevedo IL, Morgan MG. Marginal Emissions Factors for the U.S. Electricity System. *Environ Sci Technol* 2012;46:4742–8. <https://doi.org/10.1021/es300145v>.
- [136] ELIA. Grid constraints backbone Antwerp & Liège region. 2023.
- [137] Larsen E, van Ackere A. Importing from? Capacity adequacy in a European context. *The Electricity Journal* 2023;36:107236. <https://doi.org/10.1016/j.tej.2023.107236>.
- [138] Tranberg B, Corradi O, Lajoie B, Gibon T, Staffell I, Andresen GB. Real-time carbon accounting method for the European electricity markets. *Energy Strategy Reviews* 2019;26:100367. <https://doi.org/10.1016/J.ESR.2019.100367>.
- [139] Cheremisinoff NP. Introduction to Air Quality. *Handbook of Air Pollution Prevention and Control*, Elsevier; 2002, p. 1–52. <https://doi.org/10.1016/B978-075067499-7/50002-X>.
- [140] Cheremisinoff PN, Young RA. *Air pollution control and design handbook*. Part II. New York: Marcel Dekker; 1977.
- [141] Gupta P. *Environmental and ecotoxicology. Illustrated Toxicology*, Elsevier; 2018, p. 373–425. <https://doi.org/10.1016/B978-0-12-813213-5.00014-6>.
- [142] Galloway JN, Leach AM, Bleeker A, Erisman JW. A chronology of human understanding of the nitrogen cycle. *Philosophical Transactions of the Royal Society B: Biological Sciences* 2013;368:20130120. <https://doi.org/10.1098/rstb.2013.0120>.
- [143] Cao Y-L, Yu M-X, Jiang J, Cao N-N, Zhao M, Wang C, et al. Effects of simulated acid rain on soil N<sub>2</sub>O emission from typical forest in subtropical southern China. *J Appl Ecol* 2021;32. <https://doi.org/10.13287/j.1001-9332.202104.007>.
- [144] Thomson AJ, Giannopoulos G, Pretty J, Baggs EM, Richardson DJ. Biological sources and sinks of nitrous oxide and strategies to mitigate emissions. *Philosophical Transactions of the Royal Society B: Biological Sciences* 2012;367:1157–68. <https://doi.org/10.1098/rstb.2011.0415>.
- [145] Muret J, Fernandes TD, Gerlach H, Imberger G, Jörnvall H, Lawson C, et al. Environmental impacts of nitrous oxide: no laughing matter! Comment on Br J

- Anaesth 2019; 122: 587–604. Br J Anaesth 2019;123:e481–2. <https://doi.org/10.1016/j.bja.2019.06.013>.
- [146] Portmann RW, Daniel JS, Ravishankara AR. Stratospheric ozone depletion due to nitrous oxide: influences of other gases. *Philosophical Transactions of the Royal Society B: Biological Sciences* 2012;367:1256–64. <https://doi.org/10.1098/rstb.2011.0377>.
- [147] Lammel G, Graßl H. Greenhouse effect of NOX. *Environmental Science and Pollution Research* 1995;2:40–5. <https://doi.org/10.1007/BF02987512>.
- [148] Kuo Y-M, Zhao E, Li M-J, Yu H, Qin J. Ambient Precursor Gaseous Pollutants and Meteorological Conditions Controlling Variations of Particulate Matter Concentrations. *Clean (Weinh)* 2017;45:1600655. <https://doi.org/10.1002/clen.201600655>.
- [149] Peng RD. Coarse Particulate Matter Air Pollution and Hospital Admissions for Cardiovascular and Respiratory Diseases Among Medicare Patients. *JAMA* 2008;299:2172. <https://doi.org/10.1001/jama.299.18.2172>.
- [150] Hamra GB, Guha N, Cohen A, Laden F, Raaschou-Nielsen O, Samet JM, et al. Outdoor Particulate Matter Exposure and Lung Cancer: A Systematic Review and Meta-Analysis. *Environ Health Perspect* 2014;122:906–11. <https://doi.org/10.1289/ehp/1408092>.
- [151] Brook RD, Rajagopalan S, Pope CA, Brook JR, Bhatnagar A, Diez-Roux A V., et al. Particulate Matter Air Pollution and Cardiovascular Disease. *Circulation* 2010;121:2331–78. <https://doi.org/10.1161/CIR.0b013e3181d8e3e1>.
- [152] Sher E. Environmental Aspects of Air Pollution. *Handbook of Air Pollution From Internal Combustion Engines*, Elsevier; 1998, p. 27–41. <https://doi.org/10.1016/B978-012639855-7/50041-7>.
- [153] Sillman S. Tropospheric Ozone and Photochemical Smog. *Treatise on Geochemistry*, Elsevier; 2003, p. 407–31. <https://doi.org/10.1016/B0-08-043751-6/09053-8>.
- [154] Raza W, Saeed S, Saulat H, Gul H, Sarfraz M, Sonne C, et al. A review on the deteriorating situation of smog and its preventive measures in Pakistan. *J Clean Prod* 2021;279:123676. <https://doi.org/10.1016/j.jclepro.2020.123676>.
- [155] Jiang L, Hiltunen E, He X, Zhu L. A Questionnaire Case Study to Investigate Public Awareness of Smog Pollution in China's Rural Areas. *Sustainability* 2016;8:1111. <https://doi.org/10.3390/su8111111>.
- [156] Zhou B, Cui T, Li D. Climate Monitoring and Formation Mechanism of Smog Pollution in China. *Chinese Journal of Urban and Environmental Studies* 2015;03. <https://doi.org/10.1142/S234574811550013X>.
- [157] Grzywa-Celińska A, Krusiński A, Milanowski J. 'Smogging kills' – Effects of air pollution on human respiratory system. *Annals of Agricultural and Environmental Medicine* 2020;27:1–5. <https://doi.org/10.26444/aaem/110477>.
- [158] Geddes JA, Murphy JG. The science of smog: a chemical understanding of ground level ozone and fine particulate matter. *Metropolitan Sustainability*, Elsevier; 2012, p. 205–30. <https://doi.org/10.1533/9780857096463.3.205>.
- [159] Hanrahan G. Air Pollutants and Associated Chemical and Photochemical Processes. *Key Concepts in Environmental Chemistry*, Elsevier; 2012, p. 215–42. <https://doi.org/10.1016/B978-0-12-374993-2.10007-X>.
- [160] Rypdal K, Rive N, Berntsen T, Fagerli H, Klimont Z, Mideksa TK, et al. Climate and air quality-driven scenarios of ozone and aerosol precursor abatement. *Environ Sci Policy* 2009;12:855–69. <https://doi.org/10.1016/j.envsci.2009.08.002>.

- [161] Graedel TE. Sulfur dioxide, sulfate aerosol, and urban ozone. *Geophys Res Lett* 1976;3:181–4. <https://doi.org/10.1029/GL003i003p00181>.
- [162] Varma DR, Mulay S, Chemtob S. Carbon Monoxide. *Handbook of Toxicology of Chemical Warfare Agents*, Elsevier; 2015, p. 267–86. <https://doi.org/10.1016/B978-0-12-800159-2.00021-X>.
- [163] Eichhorn L, Thudium M, Jüttner B. The Diagnosis and Treatment of Carbon Monoxide Poisoning. *Dtsch Arztebl Int* 2018. <https://doi.org/10.3238/arztebl.2018.0863>.
- [164] Chameides WL, Fehsenfeld F, Rodgers MO, Cardelino C, Martinez J, Parrish D, et al. Ozone precursor relationships in the ambient atmosphere. *J Geophys Res* 1992;97:6037. <https://doi.org/10.1029/91JD03014>.
- [165] Rotmans J, Den Elzen MGJ. A model-based approach to the calculation of global warming potentials (GWP). *International Journal of Climatology* 1992;12:865–74. <https://doi.org/10.1002/joc.3370120809>.
- [166] Johnson CE, Derwent RG. Relative radiative forcing consequences of global emissions of hydrocarbons, carbon monoxide and NO<sub>x</sub> from human activities estimated with a zonally-averaged two-dimensional model. *Clim Change* 1996;34:439–62. <https://doi.org/10.1007/BF00139301>.
- [167] Speight JG. Energy security and the environment. *Natural Gas: A Basic Handbook*, Gulf Professional Publishing; 2019, p. 361–90. <https://doi.org/10.1016/B978-0-12-809570-6.00010-2>.
- [168] Xu S, Deng Y, Webb K, Wright H, Dimick PS, Cremaschi S, et al. Sour Gas Sweetening Technologies for Distributed Resources – A Process Simulation Study. *Computer Aided Chemical Engineering* 2020;48:1483–8. <https://doi.org/10.1016/B978-0-12-823377-1.50248-2>.
- [169] Papadopoulo M, Kaddouh S, Pacitto P, Prieur-Vernat A. Life Cycle Assessment of the European Natural Gas Chain focused on three environmental impact indicators. Brussels: 2011.
- [170] Proszak-Miasik D, Rabczak S. Methods for reducing low emissions from heating devices in single- family housing. *E3S Web of Conferences* 2018;45:00069. <https://doi.org/10.1051/E3SCONF/20184500069>.
- [171] Fuentes E, Arce L, Salom J. A review of domestic hot water consumption profiles for application in systems and buildings energy performance analysis. *Renewable and Sustainable Energy Reviews* 2018;81:1530–47. <https://doi.org/10.1016/J.RSER.2017.05.229>.
- [172] de Gouw JA, Parrish DD, Frost GJ, Trainer M. Reduced emissions of CO<sub>2</sub>, NO<sub>x</sub>, and SO<sub>2</sub> from U.S. power plants owing to switch from coal to natural gas with combined cycle technology. *Earths Future* 2014;2:75–82. <https://doi.org/10.1002/2013EF000196>.
- [173] Turconi R, Boldrin A, Astrup T. Life cycle assessment (LCA) of electricity generation technologies: Overview, comparability and limitations. *Renewable and Sustainable Energy Reviews* 2013;28:555–65. <https://doi.org/10.1016/J.RSER.2013.08.013>.
- [174] Asiaban S, Kayedpour N, Samani AE, Bozalakov D, De Kooning JDM, Crevecoeur G, et al. Wind and Solar Intermittency and the Associated Integration Challenges: A Comprehensive Review Including the Status in the Belgian Power System. *Energies (Basel)* 2021;14. <https://doi.org/10.3390/EN14092630>.
- [175] ELIA. Belgium’s 2022 electricity mix: the increase in renewable energy and availability of nuclear power plants kept exports high. Brussels: 2023.



- [176] Fritsche U, Rausch L. Life Cycle Analysis of GHG and Air Pollutant Emissions from Renewable and Conventional Electricity, Heating, and Transport Fuel Options in the EU until 2030 - ETC/ACC Technical Paper 2009/18. Bilthoven: 2009.
- [177] Chen D, Christensen TH. Life-cycle assessment (EASEWASTE) of two municipal solid waste incineration technologies in China. *Waste Management & Research* 2010;28:508–19. <https://doi.org/10.1177/0734242X10361761>.
- [178] Psomopoulos CS, Kaminaris SD, Ioannidis GCh, Themelis NJ. Contribution of WTE plants in EU's targets for renewables. A review until 2014. Proceedings of the 5th International Conference on Sustainable Solid Waste Management (ATHEN 2017) 2017.
- [179] Belgian Waste-To-Energy. Foire aux questions - FAQ n.d. <http://www.bw2e.be/fr/foire-aux-questions-faq/> (accessed April 18, 2023).
- [180] Energie+. Emissions de polluants liée à la consommation énergétique 2007. <https://energieplus-lesite.be/theories/consommation-energetique/les-emissions-de-polluants-liee-a-la-consommation-energetique/> (accessed April 17, 2023).
- [181] Aguiar P, Chadwick D, Kershenbaum L. Effect of methane slippage on an indirect internal reforming solid oxide fuel cell. *Chem Eng Sci* 2004;59:87–97. <https://doi.org/10.1016/j.ces.2003.09.022>.
- [182] Kee RJ, Zhu H, Sukeshini AM, Jackson GS. Solid Oxide Fuel Cells: Operating Principles, Current Challenges, and the Role of Syngas. *Combustion Science and Technology* 2008;180:1207–44. <https://doi.org/10.1080/00102200801963458>.
- [183] Chartrand R. Intergovernmental Advanced Stationary PEM Fuel Cell System Demonstration Final Report. US Department of Energy 2011. <https://doi.org/10.2172/1038683>.
- [184] Payne R, Love J, Kah M. Generating Electricity at 60% Electrical Efficiency from 1 - 2 kWe SOFC Products. *ECS Trans* 2009;25:231–9. <https://doi.org/10.1149/1.3205530>.
- [185] Wagner AL, Wagner JP, Krause TR, Carter JD. Autothermal Reforming Catalyst Development for Fuel Cell Applications. *Journal of Engines* 2002.
- [186] Baldi F, Moret S, Tammi K, Maréchal F. The role of solid oxide fuel cells in future ship energy systems. *Energy* 2020;194:116811. <https://doi.org/10.1016/j.energy.2019.116811>.
- [187] Kistner L, Schubert FL, Minke C, Bensmann A, Hanke-Rauschenbach R. Techno-economic and Environmental Comparison of Internal Combustion Engines and Solid Oxide Fuel Cells for Ship Applications. *J Power Sources* 2021;508:230328. <https://doi.org/10.1016/j.jpowsour.2021.230328>.
- [188] Urdampilleta I, Uribe F, Rockward T, Brosha EL, Pivovar B, Garzon FH. PEMFC Poisoning with H<sub>2</sub>S: Dependence on Operating Conditions. *ECS Trans* 2007;11:831–42. <https://doi.org/10.1149/1.2780996>.
- [189] Bang E-S, Kim M-H, Park S-K. Options for Methane Fuel Processing in PEMFC System with Potential Maritime Applications. *Energies (Basel)* 2022;15:8604. <https://doi.org/10.3390/en15228604>.
- [190] Rabiou AM, Dlangamandla N, Ulleberg Ø. Novel Heat Integration in a Methane Reformer and High Temperature PEM Fuel Cell-based mCHP System. *APCBEE Procedia* 2012;3:17–22. <https://doi.org/10.1016/j.apcbee.2012.06.039>.
- [191] Minei Y, Okajima K, Yasuda M, Ube R. PEMFC System for Utilization of Exhaust Gas from Bright Heat Treatment furnace. Proceedings of the 12th International Conference on Applied Energy (ICAE2020) 2020. <https://doi.org/10.46855/energy-proceedings-7263>.

- [192] Schumann P, Graf C, Friedrich KA. Modeling and Simulation of a PEM Fuel Cell System for Aircraft Applications. *ECS Trans* 2008;12:651–61. <https://doi.org/10.1149/1.2921590>.
- [193] Paulus N. Comprehensive assessment of fuel cell types: A novel fuel cell classification system. Submitted in *Journal of Power Sources* 2024. <https://doi.org/10.2139/ssrn.4800979>.
- [194] Dan Milici L, Milici M, Pentiu R, Pohoata S, Cirdei D. Study of the Energetic Regime for a Fuel Cell Discharge Sorin Pohoata Study of the Energetic Regime for a Fuel Cell Discharge. *Proceedings of the 2nd International Conference on Modern Power Systems (MPS 2008)* 2008.
- [195] Tawalbeh M, Murtaza SZM, Al-Othman A, Alami AH, Singh K, Olabi AG. Ammonia: A versatile candidate for the use in energy storage systems. *Renew Energy* 2022;194:955–77. <https://doi.org/10.1016/J.RENENE.2022.06.015>.
- [196] Yi Q, Chu H, Tang M, Zhang Y, Liu X, Zhou Z, et al. A Novel Membraneless Direct Hydrazine/Air Fuel Cell. *Fuel Cells* 2014;14:827–33. <https://doi.org/10.1002/FUCE.201400098>.
- [197] Wei GL, Luo JL, Sanger AR, Chuang KT, Zhong L. Li<sub>2</sub>SO<sub>4</sub>-based proton-conducting membrane for H<sub>2</sub>S–air fuel cell. *J Power Sources* 2005;145:1–9. <https://doi.org/10.1016/J.JPOWSOUR.2004.12.015>.
- [198] Choudhury NA, Raman RK, Sampath S, Shukla AK. An alkaline direct borohydride fuel cell with hydrogen peroxide as oxidant. *J Power Sources* 2005;143:1–8. <https://doi.org/10.1016/J.JPOWSOUR.2004.08.059>.
- [199] Sanli AE, Aytac A. Response to Disselkamp: Direct peroxide/peroxide fuel cell as a novel type fuel cell. *Int J Hydrogen Energy* 2011;36:869–75. <https://doi.org/10.1016/J.IJHYDENE.2010.09.038>.
- [200] Lindorfer J, Rosenfeld DC, Böhm H. 23 - Fuel Cells: Energy Conversion Technology. *Future Energy: Improved, Sustainable and Clean Options for Our Planet*, Elsevier; 2020, p. 495–517. <https://doi.org/10.1016/B978-0-08-102886-5.00023-2>.
- [201] Molaeimanesh GR, Torabi F. Chapter 1 - Fuel cell fundamentals. *Fuel Cell Modeling and Simulation*, Elsevier; 2023, p. 1–56. <https://doi.org/10.1016/B978-0-32-385762-8.00005-1>.
- [202] Corbo P, Migliardini F, Veneri O. Fuel Cells for Automotive Applications. *Hydrogen Fuel Cells for Road Vehicles*, vol. 11, Springer Verlag; 2011, p. 71–102. [https://doi.org/10.1007/978-0-85729-136-3\\_3/FIGURES/9](https://doi.org/10.1007/978-0-85729-136-3_3/FIGURES/9).
- [203] Hanif MA, Nadeem F, Tariq R, Rashid U. Chapter 10 - Hydrogen and fuel cells. *Renewable and Alternative Energy Resources*, Academic Press; 2022, p. 605–57. <https://doi.org/10.1016/B978-0-12-818150-8.00010-1>.
- [204] Lucia U. Overview on fuel cells. *Renewable and Sustainable Energy Reviews* 2014;30:164–9. <https://doi.org/10.1016/J.RSER.2013.09.025>.
- [205] Sharaf OZ, Orhan MF. An overview of fuel cell technology: Fundamentals and applications. *Renewable and Sustainable Energy Reviews* 2014;32:810–53. <https://doi.org/10.1016/J.RSER.2014.01.012>.
- [206] Brett DJL, Brandon NP, Hawkes AD, Staffell I. Fuel cell systems for small and micro combined heat and power (CHP) applications. *Small and Micro Combined Heat and Power (CHP) Systems*, Elsevier; 2011, p. 233–61. <https://doi.org/10.1533/9780857092755.2.233>.

- [207] Das S, Dutta K, Nessim GD, Kader MA. Introduction to direct methanol fuel cells. *Direct Methanol Fuel Cell Technology*, Elsevier; 2020, p. 1–12. <https://doi.org/10.1016/B978-0-12-819158-3.00001-X>.
- [208] Narayan S, Valdez TI, Narayanan SR, Chun W. Hydrogen Peroxide Oxidant Fuel Cell Systems for Ultra-Portable Applications. Jet Propulsion Laboratory (California Institute of Technology) 2001.
- [209] Kim K, Kim T, Lee K, Kwon S. Fuel cell system with sodium borohydride as hydrogen source for unmanned aerial vehicles. *J Power Sources* 2011;196:9069–75. <https://doi.org/10.1016/J.JPOWSOUR.2011.01.038>.
- [210] Jenkins B, Mullinger P. Chapter 2 - The combustion process. *Industrial and Process Furnaces*, Butterworth-Heinemann; 2023, p. 31–63. <https://doi.org/10.1016/B978-0-323-91629-5.00011-2>.
- [211] Ren R, Wang X, Chen H, Miller HA, Salam I, Varcoe JR, et al. Reshaping the Cathodic Catalyst Layer for Anion Exchange Membrane Fuel Cells: From Heterogeneous Catalysis to Homogeneous Catalysis. *Angewandte Chemie International Edition* 2021;60:4049–54. <https://doi.org/10.1002/ANIE.202012547>.
- [212] Kim J, Yu J, Lee S, Tahmasebi A, Jeon CH, Lucas J. Advances in catalytic hydrogen combustion research: Catalysts, mechanism, kinetics, and reactor designs. *Int J Hydrogen Energy* 2021;46:40073–104. <https://doi.org/10.1016/J.IJHYDENE.2021.09.236>.
- [213] Mahapatra MK, Singh P. Chapter 24 - Fuel Cells: Energy Conversion Technology. *Future Energy: Improved, Sustainable and Clean Options for our Planet*, Elsevier; 2014, p. 511–47. <https://doi.org/10.1016/B978-0-08-099424-6.00024-7>.
- [214] Marimuthu S, Grace AN. Ceramics for solid oxide fuel cells. *Advanced Ceramics for Energy Storage, Thermoelectrics and Photonics*, Elsevier; 2023, p. 185–208. <https://doi.org/10.1016/B978-0-323-90761-3.00006-1>.
- [215] Dincer I, Rosen MA. Exergy analyses of fuel cell systems. *Exergy*, Elsevier; 2021, p. 479–514. <https://doi.org/10.1016/B978-0-12-824372-5.00018-X>.
- [216] Sudhakar YN, Selvakumar M, Bhat DK. Biopolymer Electrolytes for Fuel Cell Applications. *Biopolymer Electrolytes*, Elsevier; 2018, p. 151–66. <https://doi.org/10.1016/B978-0-12-813447-4.00005-4>.
- [217] Breeze P. Direct Methanol Fuel Cell. *Fuel Cells*, Elsevier; 2017, p. 75–82. <https://doi.org/10.1016/B978-0-08-101039-6.00008-X>.
- [218] Rejal SZ, Masdar MS, Kamarudin SK. A parametric study of the direct formic acid fuel cell (DFAFC) performance and fuel crossover. *Int J Hydrogen Energy* 2014;39:10267–74. <https://doi.org/10.1016/j.ijhydene.2014.04.149>.
- [219] Mahapatra MK, Singh P. Chapter 24 - Fuel Cells: Energy Conversion Technology. *Future Energy: Improved, Sustainable and Clean Options for our Planet*, Elsevier; 2014, p. 511–47. <https://doi.org/10.1016/B978-0-08-099424-6.00024-7>.
- [220] Hamouda RA, El-Naggar NEA. Chapter 14 - Cyanobacteria-based microbial cell factories for production of industrial products. *Microbial Cell Factories Engineering for Production of Biomolecules*, Academic Press; 2021, p. 277–302. <https://doi.org/10.1016/B978-0-12-821477-0.00007-6>.
- [221] Leech D, Kavanagh P, Schuhmann W. Enzymatic fuel cells: Recent progress. *Electrochim Acta* 2012;84:223–34. <https://doi.org/10.1016/j.electacta.2012.02.087>.
- [222] Karim NA, Kamarudin SK. Chapter 2 - Introduction to direct alcohol fuel cells (DAFCs). *Direct Liquid Fuel Cells*, Elsevier; 2021, p. 49–70. <https://doi.org/10.1016/B978-0-12-818624-4.00002-9>.

- [223] Dincer I, Zamfirescu C. Chapter 4 - Hydrogen and Fuel Cell Systems. *Advanced Power Generation Systems*, Elsevier; 2014, p. 143–98. <https://doi.org/10.1016/B978-0-12-383860-5.00004-3>.
- [224] Demin A. Thermodynamic analysis of a methane fed SOFC system based on a protonic conductor. *Solid State Ion* 2002;152–153:555–60. [https://doi.org/10.1016/S0167-2738\(02\)00363-6](https://doi.org/10.1016/S0167-2738(02)00363-6).
- [225] Liu F, Duan C. Direct-Hydrocarbon Proton-Conducting Solid Oxide Fuel Cells. *Sustainability* 2021;13. <https://doi.org/10.3390/su13094736>.
- [226] Sumi H, Shimada H, Yamaguchi Y, Mizutani Y, Okuyama Y, Amezawa K. Comparison of electrochemical impedance spectra for electrolyte-supported solid oxide fuel cells (SOFCs) and protonic ceramic fuel cells (PCFCs). *Sci Rep* 2021;11:10622. <https://doi.org/10.1038/s41598-021-90211-9>.
- [227] Basbus J, Arce M, Troiani H, Su Q, Wang H, Caneiro A, et al. Study of BaCe<sub>0.4</sub>Zr<sub>0.4</sub>Y<sub>0.2</sub>O<sub>3-δ</sub>/BaCe<sub>0.8</sub>Pr<sub>0.2</sub>O<sub>3-δ</sub> (BCZY/BCP) bilayer membrane for Protonic Conductor Solid Oxide Fuel Cells (PC-SOFC). *Int J Hydrogen Energy* 2020;45:5481–90. <https://doi.org/10.1016/j.ijhydene.2019.06.164>.
- [228] Shi H, Su C, Ran R, Cao J, Shao Z. Electrolyte materials for intermediate-temperature solid oxide fuel cells. *Progress in Natural Science: Materials International* 2020;30:764–74. <https://doi.org/10.1016/j.pnsc.2020.09.003>.
- [229] Rashid NLRM, Samat AA, Jais AA, Somalu MR, Muchtar A, Baharuddin NA, et al. Review on zirconate-cerate-based electrolytes for proton-conducting solid oxide fuel cell. *Ceram Int* 2019;45. <https://doi.org/10.1016/j.ceramint.2019.01.045>.
- [230] Dong Y, Xing L, Li X, Gao Y, Cao Z, Liu J. A membrane-less molten hydroxide direct carbon fuel cell with fuel continuously supplied at low temperatures: A modeling and experimental study. *Appl Energy* 2022;324:119585. <https://doi.org/10.1016/j.apenergy.2022.119585>.
- [231] Li S, Yang X, Zhu H, Chen Y, Liu Y. Investigation of amorphous CoB alloy as the anode catalyst for a direct borohydride fuel cell. *J Power Sources* 2011;196. <https://doi.org/10.1016/j.jpowsour.2011.02.016>.
- [232] Ma J, Choudhury NA, Sahai Y. A comprehensive review of direct borohydride fuel cells. *Renewable and Sustainable Energy Reviews* 2010;14:183–99. <https://doi.org/10.1016/j.rser.2009.08.002>.
- [233] Sahoo PC, Kim K, Lee JH, Han J-I, Oh Y-K. Biomimetically Synthesized Hierarchical TiO<sub>2</sub>-Graphitic Carbon as Anodic Catalysts for Direct Alkaline Sulfide Fuel Cell. *ACS Sustain Chem Eng* 2015;3:1764–70. <https://doi.org/10.1021/acssuschemeng.5b00277>.
- [234] Li Y, Feng Y, Xianda S+, He Y, Li [ Y S, Feng Y, et al. A Sodium-Ion-Conducting Direct Formate Fuel Cell: Generating Electricity and Producing Base. *Angewandte Chemie* 2017;129:5828–31. <https://doi.org/10.1002/ANGE.201701816>.
- [235] Shin DW, Guiver MD, Lee YM. Hydrocarbon-Based Polymer Electrolyte Membranes: Importance of Morphology on Ion Transport and Membrane Stability. *Chem Rev* 2017;117. <https://doi.org/10.1021/acs.chemrev.6b00586>.
- [236] Bidault F, Middleton PH. 4.07 - Alkaline Fuel Cells: Theory and Application. *Comprehensive Renewable Energy*, Elsevier; 2012, p. 179–202. <https://doi.org/10.1016/B978-0-08-087872-0.00405-4>.
- [237] Ferriday TB, Middleton PH. Alkaline fuel cell technology - A review. *Int J Hydrogen Energy* 2021;46:18489–510. <https://doi.org/10.1016/J.IJHYDENE.2021.02.203>.

- [238] Couture G, Alaaeddine A, Boschet F, Ameduri B. Polymeric materials as anion-exchange membranes for alkaline fuel cells. *Prog Polym Sci* 2011;36:1521–57. <https://doi.org/10.1016/j.progpolymsci.2011.04.004>.
- [239] Samsudin AM, Bodner M, Hacker V. A Brief Review of Poly(Vinyl Alcohol)-Based Anion Exchange Membranes for Alkaline Fuel Cells. *Polymers* 2022, Vol 14, Page 3565 2022;14. <https://doi.org/10.3390/POLYM14173565>.
- [240] Lan R, Tao S. Ammonia Carbonate Fuel Cells Based on a Mixed  $\text{NH}_4^+/\text{H}^+$  Ion Conducting Electrolyte. *ECS Electrochemistry Letters* 2013;2:F37–40. <https://doi.org/10.1149/2.007305eel>.
- [241] Thompson ST, Peterson D, Ho D, Papageorgopoulos D. Perspective—The Next Decade of AEMFCs: Near-Term Targets to Accelerate Applied R&D. *J Electrochem Soc* 2020;167:084514. <https://doi.org/10.1149/1945-7111/ab8c88>.
- [242] Khaodee W, Wongsakulphasatch S, Kiatkittipong W, Arpornwichanop A, Laosiripojana N, Assabumrungrat S. Selection of appropriate primary fuel for hydrogen production for different fuel cell types: Comparison between decomposition and steam reforming. *Int J Hydrogen Energy* 2011;36:7696–706. <https://doi.org/10.1016/J.IJHYDENE.2011.03.123>.
- [243] Lamy C, Coutanceau C, Leger JM. Chapter 1 - The Direct Ethanol Fuel Cell: a Challenge to Convert Bioethanol Cleanly into Electric Energy. *Catalysis for Sustainable Energy Production*, John Wiley & Sons, Ltd; 2009, p. 1–46. <https://doi.org/10.1002/9783527625413.CH1>.
- [244] Rathore SS, Biswas S, Fini D, Kulkarni AP, Giddey S. Direct ammonia solid-oxide fuel cells: A review of progress and prospects. *Int J Hydrogen Energy* 2021;46. <https://doi.org/10.1016/j.ijhydene.2021.08.092>.
- [245] Sgroi M, Zedde F, Barbera O, Stassi A, Sebastián D, Lufrano F, et al. Cost Analysis of Direct Methanol Fuel Cell Stacks for Mass Production. *Energies (Basel)* 2016;9. <https://doi.org/10.3390/en9121008>.
- [246] Qiu P, Sun S, Yang X, Chen F, Xiong C, Jia L, et al. A review on anode on-cell catalyst reforming layer for direct methane solid oxide fuel cells. *Int J Hydrogen Energy* 2021;46. <https://doi.org/10.1016/j.ijhydene.2021.05.040>.
- [247] Ideris A, Croiset E, Pritzker M, Amin A. Direct-methane solid oxide fuel cell (SOFC) with Ni-SDC anode-supported cell. *Int J Hydrogen Energy* 2017;42. <https://doi.org/10.1016/j.ijhydene.2017.07.117>.
- [248] Murray EP, Tsai T, Barnett SA. A direct-methane fuel cell with a ceria-based anode. *Nature* 1999;400:649–51. <https://doi.org/10.1038/23220>.
- [249] Zhang B, Wang L, Li R. Chapter 10 - Bioconversion and Chemical Conversion of Biogas for Fuel Production. *Advanced Bioprocessing for Alternative Fuels, Biobased Chemicals, and Bioproducts: Technologies and Approaches for Scale-Up and Commercialization*, Woodhead Publishing; 2019, p. 187–205. <https://doi.org/10.1016/B978-0-12-817941-3.00010-3>.
- [250] Kalmula B, Kondapuram VR. Fuel processor – fuel cell integration: Systemic issues and challenges. *Renewable and Sustainable Energy Reviews* 2015;45:409–18. <https://doi.org/10.1016/j.rser.2015.01.034>.
- [251] Dicks AL. Hydrogen generation from natural gas for the fuel cell systems of tomorrow. *J Power Sources* 1996;61:113–24. [https://doi.org/10.1016/S0378-7753\(96\)02347-6](https://doi.org/10.1016/S0378-7753(96)02347-6).

- [252] Zohuri B, McDaniel P. Chapter 9 - Energy insight: an energy essential guide. *Introduction to Energy Essentials*, Academic Press; 2021, p. 321–70. <https://doi.org/10.1016/B978-0-323-90152-9.00009-8>.
- [253] Dincer I, Ishaq H. Chapter 1 - Introduction. *Renewable Hydrogen Production*, Elsevier; 2022, p. 1–33. <https://doi.org/10.1016/B978-0-323-85176-3.00001-9>.
- [254] Konwar D, Nguyen NTQ, Yoon HH. Evaluation of BaZr<sub>0.1</sub>Ce<sub>0.7</sub>Y<sub>0.2</sub>O<sub>3</sub>- electrolyte prepared by carbonate precipitation for a mixed ion-conducting SOFC. *Int J Hydrogen Energy* 2015;40:11651–8. <https://doi.org/10.1016/j.ijhydene.2015.05.056>.
- [255] Shirbhate SC, Singh K, Acharya SA, Yadav AK. Review on local structural properties of ceria-based electrolytes for IT-SOFC. *Ionics (Kiel)* 2017;23:1049–57. <https://doi.org/10.1007/s11581-016-1893-9>.
- [256] Venkataramana K, Madhuri C, Reddy CV. Triple-doped Ceria–Carbonate (Ce<sub>0.82</sub>La<sub>0.06</sub>Sm<sub>0.06</sub>Gd<sub>0.06</sub>O<sub>2-δ</sub> – (Li–Na)<sub>2</sub>CO<sub>3</sub>) nanocomposite solid electrolyte materials for LT–SOFC applications. *Ceram Int* 2020;46:27584–94. <https://doi.org/10.1016/j.ceramint.2020.07.252>.
- [257] de Leon CP, Walsh FC, Pletcher D, Browning DJ, Lakeman JB. Direct borohydride fuel cells. *J Power Sources* 2006;155:172–81. <https://doi.org/10.1016/j.jpowsour.2006.01.011>.
- [258] Kim K, Son J, Han J-I. Metal sulfides as anode catalysts in direct alkaline sulfide fuel cell. *Int J Hydrogen Energy* 2014;39:10493–7. <https://doi.org/10.1016/j.ijhydene.2014.04.208>.
- [259] Perna A, Minutillo M. Residential cogeneration and trigeneration with fuel cells. *Current Trends and Future Developments on (Bio-) Membranes*, Elsevier; 2020, p. 197–239. <https://doi.org/10.1016/B978-0-12-817807-2.00009-5>.
- [260] Park JO, Hong S-G. Design and Optimization of HT-PEMFC MEAs. *High Temperature Polymer Electrolyte Membrane Fuel Cells*, Cham: Springer International Publishing; 2016, p. 331–52. [https://doi.org/10.1007/978-3-319-17082-4\\_16](https://doi.org/10.1007/978-3-319-17082-4_16).
- [261] Element Energy. D1.7 - Summary report on specifications for newest model deployment in PACE. *PACE - Pathway to a Competitive European Fuel Cell Micro-CHP Market* 2021.
- [262] Cong S, Wang J, Wang Z, Liu X. Polybenzimidazole (PBI) and benzimidazole-linked polymer (BILP) membranes. *Green Chemical Engineering* 2021;2:44–56. <https://doi.org/10.1016/j.gce.2020.11.007>.
- [263] Ramani V, Kunz HR, Fenton JM. Investigation of Nafion®/HPA composite membranes for high temperature/low relative humidity PEMFC operation. *J Memb Sci* 2004;232:31–44. <https://doi.org/10.1016/j.memsci.2003.11.016>.
- [264] Mack F, Heissler S, Laukenmann R, Zeis R. Phosphoric acid distribution and its impact on the performance of polybenzimidazole membranes. *J Power Sources* 2014;270:627–33. <https://doi.org/10.1016/j.jpowsour.2014.06.171>.
- [265] Schonvogel D, Büsselmann J, Wagner P, Kraus H, Misz U, Langnickel H, et al. Effect of air contamination by sulfur dioxide on the high temperature PEM fuel cell. *Int J Hydrogen Energy* 2021;46:6751–61. <https://doi.org/10.1016/j.ijhydene.2020.11.136>.
- [266] Ellamla HR, Staffell I, Bujlo P, Pollet BG, Pasupathi S. Current status of fuel cell based combined heat and power systems for residential sector. *J Power Sources* 2015;293:312–28. <https://doi.org/10.1016/J.JPOWSOUR.2015.05.050>.

- [267] Arsalis A. A comprehensive review of fuel cell-based micro-combined-heat-and-power systems. *Renewable and Sustainable Energy Reviews* 2019;105:391–414. <https://doi.org/10.1016/j.rser.2019.02.013>.
- [268] Meyer Q, Yang C, Cheng Y, Zhao C. Overcoming the Electrode Challenges of High-Temperature Proton Exchange Membrane Fuel Cells. *Electrochemical Energy Reviews* 2023;6:16. <https://doi.org/10.1007/s41918-023-00180-y>.
- [269] Weaver. *Fuel Cell Technology Review*. World Fuel Cells, Elsevier; 2002, p. 81–96. <https://doi.org/10.1016/B978-185617397-1/50005-8>.
- [270] Zha S, Cheng Z, Liu M. Gd<sub>2</sub>Ti<sub>2</sub>-XMoXO<sub>7</sub>-Based Anode Materials for H<sub>2</sub>S-Air Solid Oxide Fuel Cells. *ECS Trans* 2006;1:293–302. <https://doi.org/10.1149/1.2215563>.
- [271] Samavati M, Raza R, Zhu B. Design of a 5-kW advanced fuel cell polygeneration system. *Wiley Interdiscip Rev Energy Environ* 2012;1:173–80. <https://doi.org/10.1002/wene.6>.
- [272] Raza R, Wang X, Ma Y, Zhu B. Study on calcium and samarium co-doped ceria based nanocomposite electrolytes. *J Power Sources* 2010;195:6491–5. <https://doi.org/10.1016/j.jpowsour.2010.04.031>.
- [273] Faghri A, Guo Z. Challenges and opportunities of thermal management issues related to fuel cell technology and modeling. *Int J Heat Mass Transf* 2005;48:3891–920. <https://doi.org/10.1016/j.ijheatmasstransfer.2005.04.014>.
- [274] Wen T. Material research for planar SOFC stack. *Solid State Ion* 2002;148:513–9. [https://doi.org/10.1016/S0167-2738\(02\)00098-X](https://doi.org/10.1016/S0167-2738(02)00098-X).
- [275] Kuterbekov KA, Nikonov A V., Bekmyrza KZh, Pavzderin NB, Kabyshev AM, Kubenova MM, et al. Classification of Solid Oxide Fuel Cells. *Nanomaterials* 2022;12. <https://doi.org/10.3390/nano12071059>.
- [276] Patcharavorachot Y, Brandon NP, Paengjuntuek W, Assabumrungrat S, Arpornwichanop A. Analysis of planar solid oxide fuel cells based on proton-conducting electrolyte. *Solid State Ion* 2010;181:1568–76. <https://doi.org/10.1016/j.ssi.2010.09.002>.
- [277] Wang B, Li T, Gong F, Othman MHD, Xiao R. Ammonia as a green energy carrier: Electrochemical synthesis and direct ammonia fuel cell - a comprehensive review. *Fuel Processing Technology* 2022;235:107380. <https://doi.org/10.1016/j.fuproc.2022.107380>.
- [278] Afif A, Radenahmad N, Rahman SMH, Torino N, Saqib M, Hossain S, et al. Ceramic fuel cells using novel proton-conducting BaCe<sub>0.5</sub>Zr<sub>0.3</sub>Y<sub>0.1</sub>Yb<sub>0.05</sub>Zn<sub>0.05</sub>O<sub>3-δ</sub> electrolyte. *Journal of Solid State Electrochemistry* 2022;26:111–20. <https://doi.org/10.1007/s10008-021-05062-1>.
- [279] Sun S, Awadallah O, Cheng Z. Poisoning of Ni-Based anode for proton conducting SOFC by H<sub>2</sub>S, CO<sub>2</sub>, and H<sub>2</sub>O as fuel contaminants. *J Power Sources* 2018;378:255–63. <https://doi.org/10.1016/j.jpowsour.2017.12.056>.
- [280] Lee K-C, Choi M-B, Lim D-K, Singh B, Song S-J. Effect of humidification on the performance of intermediate-temperature proton conducting ceramic fuel cells with ceramic composite cathodes. *J Power Sources* 2013;232:224–33. <https://doi.org/10.1016/j.jpowsour.2013.01.001>.
- [281] Wang W, Medvedev D, Shao Z. Gas Humidification Impact on the Properties and Performance of Perovskite-Type Functional Materials in Proton-Conducting Solid Oxide Cells. *Adv Funct Mater* 2018;28:1802592. <https://doi.org/10.1002/adfm.201802592>.

- [282] Lei L, Keels JM, Tao Z, Zhang J, Chen F. Thermodynamic and experimental assessment of proton conducting solid oxide fuel cells with internal methane steam reforming. *Appl Energy* 2018;224:280–8. <https://doi.org/10.1016/j.apenergy.2018.04.062>.
- [283] Guo Y, Lin Y, Ran R, Shao Z. Zirconium doping effect on the performance of proton-conducting BaZryCe<sub>0.8-y</sub>Y<sub>0.2</sub>O<sub>3-δ</sub> (0.0 ≤ y ≤ 0.8) for fuel cell applications. *J Power Sources* 2009;193:400–7. <https://doi.org/10.1016/j.jpowsour.2009.03.044>.
- [284] Fabbri E, Bi L, Pergolesi D, Traversa E. Towards the Next Generation of Solid Oxide Fuel Cells Operating Below 600 °C with Chemically Stable Proton-Conducting Electrolytes. *Advanced Materials* 2012;24:195–208. <https://doi.org/10.1002/adma.201103102>.
- [285] Chen X, Zhang H, Li Y, Xing J, Zhang Z, Ding X, et al. Fabrication and performance of anode-supported proton conducting solid oxide fuel cells based on BaZr<sub>0.1</sub>Ce<sub>0.7</sub>Y<sub>0.1</sub>Yb<sub>0.1</sub>O<sub>3-δ</sub> electrolyte by multi-layer aqueous-based co-tape casting. *J Power Sources* 2021;506:229922. <https://doi.org/10.1016/j.jpowsour.2021.229922>.
- [286] Hossain S, Abdalla AM, Jamain SNB, Zaini JH, Azad AK. A review on proton conducting electrolytes for clean energy and intermediate temperature-solid oxide fuel cells. *Renewable and Sustainable Energy Reviews* 2017;79:750–64. <https://doi.org/10.1016/j.rser.2017.05.147>.
- [287] Mojaver P, Chitsaz A, Sadeghi M, Khalilarya S. Comprehensive comparison of SOFCs with proton-conducting electrolyte and oxygen ion-conducting electrolyte: Thermo-economic analysis and multi-objective optimization. *Energy Convers Manag* 2020;205:112455. <https://doi.org/10.1016/j.enconman.2019.112455>.
- [288] Sadeghi M, Jafari M, Hajimolana YS, Woudstra T, Aravind PV. Size and exergy assessment of solid oxide fuel cell-based H<sub>2</sub>-fed power generation system with alternative electrolytes: A comparative study. *Energy Convers Manag* 2021;228:113681. <https://doi.org/10.1016/j.enconman.2020.113681>.
- [289] Liu J, Jin Z, Miao L, Ding J, Tang H, Gong Z, et al. A novel anions and cations co-doped strategy for developing high-performance cobalt-free cathode for intermediate-temperature proton-conducting solid oxide fuel cells. *Int J Hydrogen Energy* 2019;44:11079–87. <https://doi.org/10.1016/j.ijhydene.2019.03.001>.
- [290] Demin A. Thermodynamic analysis of a hydrogen fed solid oxide fuel cell based on a proton conductor. *Int J Hydrogen Energy* 2001;26:1103–8. [https://doi.org/10.1016/S0360-3199\(01\)00043-X](https://doi.org/10.1016/S0360-3199(01)00043-X).
- [291] Jamsak W, Assabumrungrat S, Douglas PL, Laosiripojana N, Charojrochkul S. Theoretical performance analysis of ethanol-fuelled solid oxide fuel cells with different electrolytes. *Chemical Engineering Journal* 2006;119:11–8. <https://doi.org/10.1016/j.cej.2006.03.001>.
- [292] Ni M, Leung DYC, Leung MKH. Thermodynamic analysis of ammonia fed solid oxide fuel cells: Comparison between proton-conducting electrolyte and oxygen ion-conducting electrolyte. *J Power Sources* 2008;183:682–6. <https://doi.org/10.1016/j.jpowsour.2008.05.022>.
- [293] Assabumrungrat S, Sangtongkitcharoen W, Laosiripojana N, Arpornwichanop A, Charojrochkul S, Praserttham P. Effects of electrolyte type and flow pattern on performance of methanol-fuelled solid oxide fuel cells. *J Power Sources* 2005;148:18–23. <https://doi.org/10.1016/j.jpowsour.2005.01.034>.
- [294] Saebea D, Arpornwichanop A, Patcharavorachot Y. Thermodynamic analysis of a proton conducting SOFC integrated system fuelled by different renewable fuels. *Int*



- J Hydrogen Energy 2021;46:11445–57. <https://doi.org/10.1016/j.ijhydene.2020.07.264>.
- [295] Eapen DE, Suseendiran SR, Rengaswamy R. Phosphoric acid fuel cells. *Compendium of Hydrogen Energy*, Elsevier; 2016, p. 57–70. <https://doi.org/10.1016/B978-1-78242-363-8.00002-5>.
- [296] Ebrahimi M. Fuel cell power plants. *Power Generation Technologies*, Elsevier; 2023, p. 533–74. <https://doi.org/10.1016/B978-0-323-95370-2.00013-2>.
- [297] Okada O, Yokoyama K. Development of Polymer Electrolyte Fuel Cell Cogeneration Systems for Residential Applications. *Fuel Cells* 2001;1:72–7. [https://doi.org/10.1002/1615-6854\(200105\)1:1<72::AID-FUCE72>3.0.CO;2-P](https://doi.org/10.1002/1615-6854(200105)1:1<72::AID-FUCE72>3.0.CO;2-P).
- [298] Kazeroonian FK, Rahimpour MR. Application of syngas in fuel cell. *Advances in Synthesis Gas : Methods, Technologies and Applications*, Elsevier; 2023, p. 337–67. <https://doi.org/10.1016/B978-0-323-91878-7.00021-6>.
- [299] Sammes NM, Boersma R. Small-scale fuel cells for residential applications. *J Power Sources* 2000;86:98–110. [https://doi.org/10.1016/S0378-7753\(99\)00415-2](https://doi.org/10.1016/S0378-7753(99)00415-2).
- [300] Li Y, Zhang X, Yuan W, Zhang Y, Liu X. A novel CO<sub>2</sub> gas removal design for a micro passive direct methanol fuel cell. *Energy* 2018;157:599–607. <https://doi.org/10.1016/j.energy.2018.05.159>.
- [301] Fadzillah DM, Kamarudin SK, Zainoodin MA, Masdar MS. Critical challenges in the system development of direct alcohol fuel cells as portable power supplies: An overview. *Int J Hydrogen Energy* 2019;44:3031–54. <https://doi.org/10.1016/j.ijhydene.2018.11.089>.
- [302] Campanari S, Guandalini G. Fuel cells: opportunities and challenges, 2020, p. 335–58. <https://doi.org/10.1016/B978-0-444-64337-7.00018-5>.
- [303] Agrahari R, Agarwal P, Rani R. Microbial fuel cell for simultaneous wastewater treatment and bioelectricity generation. *Bio-Based Materials and Waste for Energy Generation and Resource Management*, Elsevier; 2023, p. 77–102. <https://doi.org/10.1016/B978-0-323-91149-8.00012-0>.
- [304] Squadrito G, Cristiani P. Microbial and enzymatic fuel cells. *Compendium of Hydrogen Energy*, Elsevier; 2016, p. 147–73. <https://doi.org/10.1016/B978-1-78242-363-8.00006-2>.
- [305] Huang L, Chai X, Cheng S, Chen G. Evaluation of carbon-based materials in tubular biocathode microbial fuel cells in terms of hexavalent chromium reduction and electricity generation. *Chemical Engineering Journal* 2011;166:652–61. <https://doi.org/10.1016/j.cej.2010.11.042>.
- [306] Delaney GM, Bennetto HP, Mason JR, Roller SD, Stirling JL, Thurston CF. Electron-transfer coupling in microbial fuel cells. 2. performance of fuel cells containing selected microorganism-mediator-substrate combinations. *Journal of Chemical Technology and Biotechnology* 2008;34:13–27. <https://doi.org/10.1002/jctb.280340104>.
- [307] Rani G, Jaswal V, Yogalakshmi KN. Anode modification: An approach to improve power generation in microbial fuel cells (MFCs). *Development in Wastewater Treatment Research and Processes*, Elsevier; 2023, p. 133–52. <https://doi.org/10.1016/B978-0-323-88505-8.00015-2>.
- [308] Korkut Uru S, Kilic MS, Yetiren F. Sustainable and renewable electric energy generation with continuous flow enzymatic fuel cell. *Environ Prog Sustain Energy* 2022;41. <https://doi.org/10.1002/ep.13910>.

- [309] Yu S, Myung N V. Recent Advances in the Direct Electron Transfer-Enabled Enzymatic Fuel Cells. *Front Chem* 2021;8. <https://doi.org/10.3389/fchem.2020.620153>.
- [310] Wang F, Deng S, Zhang H, Wang J, Zhao J, Miao H, et al. A comprehensive review on high-temperature fuel cells with carbon capture. *Appl Energy* 2020;275:115342. <https://doi.org/10.1016/j.apenergy.2020.115342>.
- [311] Carmo M, Doubek G, Sekol RC, Linardi M, Taylor AD. Development and electrochemical studies of membrane electrode assemblies for polymer electrolyte alkaline fuel cells using FAA membrane and ionomer. *J Power Sources* 2013;230:169–75. <https://doi.org/10.1016/j.jpowsour.2012.12.015>.
- [312] Swider-Lyons K, Garsany Y, Hjelm RME. Comparison of Direct Sodium Borohydride Fuel Cells with Cation and Anion Exchange Membranes. *ECS Meeting Abstracts* 2019;MA2019-02:1699–1699. <https://doi.org/10.1149/MA2019-02/36/1699>.
- [313] Merino-Jiménez I, Ponce de León C, Shah AA, Walsh FC. Developments in direct borohydride fuel cells and remaining challenges. *J Power Sources* 2012;219:339–57. <https://doi.org/10.1016/j.jpowsour.2012.06.091>.
- [314] Demirci UB. Direct liquid-feed fuel cells: Thermodynamic and environmental concerns. *J Power Sources* 2007;169:239–46. <https://doi.org/10.1016/j.jpowsour.2007.03.050>.
- [315] Hong P, Liao S-J, Zeng J-H, Zhong Y-L, Liang Z-X. A miniature passive direct formic acid fuel cell based twin-cell stack with highly stable and reproducible long-term discharge performance. *J Power Sources* 2011;196:1107–11. <https://doi.org/10.1016/j.jpowsour.2010.08.111>.
- [316] Yu X, Pickup PG. Recent advances in direct formic acid fuel cells (DFAFC). *J Power Sources* 2008;182:124–32. <https://doi.org/10.1016/j.jpowsour.2008.03.075>.
- [317] Ma Z, Legrand U, Pahija E, Tavares JR, Boffito DC. From CO<sub>2</sub> to Formic Acid Fuel Cells. *Ind Eng Chem Res* 2021;60:803–15. <https://doi.org/10.1021/acs.iecr.0c04711>.
- [318] Fang B, Kim M, Yu J-S. Hollow core/mesoporous shell carbon as a highly efficient catalyst support in direct formic acid fuel cell. *Appl Catal B* 2008;84:100–5. <https://doi.org/10.1016/j.apcatb.2008.03.005>.
- [319] Jung WS, Han J, Ha S. Analysis of palladium-based anode electrode using electrochemical impedance spectra in direct formic acid fuel cells. *J Power Sources* 2007;173:53–9. <https://doi.org/10.1016/j.jpowsour.2007.08.023>.
- [320] Watanabe K, Araki T, Inoue G, Mochizuki R, Tsujiguchi T. The Effect of CO<sub>2</sub> Bubble Distribution on Power Generation Performance of a Direct Formic Acid Fuel Cell. *ECS Trans* 2019;92:335–40. <https://doi.org/10.1149/09208.0335ecst>.
- [321] Prakash S, Mustain WE, Kohl PA. Chapter 1 - Electrolytes for Long-Life, Ultra Low-Power Direct Methanol Fuel Cells. *Micro Fuel Cells: Principles and Applications*, Academic Press; 2009, p. 1–50. <https://doi.org/10.1016/B978-0-12-374713-6.00001-9>.
- [322] Busca G. Chapter Three - Structural, Surface, and Catalytic Properties of Aluminas. In: Academic Press, editor. *Advances in Catalysis*, vol. 57, 2014, p. 319–404. <https://doi.org/10.1016/B978-0-12-800127-1.00003-5>.
- [323] Wu J, Yuan X-Z, Martin JJ, Wang H. Fuel cells – Proton-Exchange Membrane Fuel Cells | Life-Limiting Considerations. *Encyclopedia of Electrochemical Power Sources*, Elsevier; 2009, p. 848–67. <https://doi.org/10.1016/B978-044452745-5.00894-7>.
- [324] Rahimnejad M. Microbiological concepts of MFCs. *Biological Fuel Cells*, Elsevier; 2023, p. 29–65. <https://doi.org/10.1016/B978-0-323-85711-6.00010-2>.

- [325] Viridis B, Rabaey K, Yuan Z, Rozendal RA, Keller J. Electron Fluxes in a Microbial Fuel Cell Performing Carbon and Nitrogen Removal. *Environ Sci Technol* 2009;43:5144–9. <https://doi.org/10.1021/es8036302>.
- [326] Laheäär A, Przygocki P, Abbas Q, Béguin F. Appropriate methods for evaluating the efficiency and capacitive behavior of different types of supercapacitors. *Electrochem Commun* 2015;60:21–5. <https://doi.org/10.1016/j.elecom.2015.07.022>.
- [327] Valøen LO, Shoesmith MI. The effect of PHEV and HEV duty cycles on battery and battery pack performance. *Proceedings of the 1st Plug-in Hybrid and Electric Vehicles Conference (PHEV07) 2007*.
- [328] Paulus N. Decarbonization potentials of fuel cell technologies in micro-cogeneration application. *Progress in Energy* 2024;Under Review.
- [329] Martinez S, Michaux G, Salagnac P, Bouvier J-L. Micro-combined heat and power systems (micro-CHP) based on renewable energy sources. *Energy Convers Manag* 2017;154:262–85. <https://doi.org/10.1016/j.enconman.2017.10.035>.
- [330] Hinnells M. Combined heat and power in industry and buildings. *Energy Policy* 2008;36:4522–6. <https://doi.org/10.1016/j.enpol.2008.09.018>.
- [331] De Paepe M, D’Herdt P, Mertens D. Micro-CHP systems for residential applications. *Energy Convers Manag* 2006;47:3435–46. <https://doi.org/10.1016/j.enconman.2005.12.024>.
- [332] COGEN Europe. Fuel Cell Combined Heat and Power for Specialised Trade - Training Documents : Module 1: Basics. PACE - Pathway to a Competitive European Fuel Cell Micro-CHP Market 2020.
- [333] Verhaert I, Mulder G, De Paepe M. Evaluation of an alkaline fuel cell system as a micro-CHP. *Energy Convers Manag* 2016;126:434–45. <https://doi.org/10.1016/j.enconman.2016.07.058>.
- [334] Ghouse M, Abaoud H, Al-Boeiz A. Operational experience of a 1 kW PAFC stack. *Appl Energy* 2000;65:303–14. [https://doi.org/10.1016/S0306-2619\(99\)00112-9](https://doi.org/10.1016/S0306-2619(99)00112-9).
- [335] Cigolotti V, Genovese M, Fragiaco P. Comprehensive Review on Fuel Cell Technology for Stationary Applications as Sustainable and Efficient Poly-Generation Energy Systems. *Energies (Basel)* 2021;14:4963. <https://doi.org/10.3390/en14164963>.
- [336] Staffell I, Green R. The cost of domestic fuel cell micro-CHP systems. *Int J Hydrogen Energy* 2013;38:1088–102. <https://doi.org/10.1016/j.ijhydene.2012.10.090>.
- [337] Staffell I, Ingram A. Life cycle assessment of an alkaline fuel cell CHP system. *Int J Hydrogen Energy* 2010;35:2491–505. <https://doi.org/10.1016/j.ijhydene.2009.12.135>.
- [338] Gallucci F, van Sint Annaland M, Roses L, Manzolini G. Using palladium membrane-based fuel reformers for combined heat and power (CHP) plants. *Palladium Membrane Technology for Hydrogen Production, Carbon Capture and Other Applications*, Elsevier; 2015, p. 319–44. <https://doi.org/10.1533/9781782422419.2.319>.
- [339] Ramakrishnan S, Ramya K, Rajalakshmi N. High-temperature proton exchange membrane—an insight. *PEM Fuel Cells*, Elsevier; 2022, p. 223–42. <https://doi.org/10.1016/B978-0-12-823708-3.00003-1>.
- [340] Herdem MS, Sinaki MY, Farhad S, Hamdullahpur F. An overview of the methanol reforming process: Comparison of fuels, catalysts, reformers, and systems. *Int J Energy Res* 2019;43:5076–105. <https://doi.org/10.1002/er.4440>.

- [341] Lehnert W, Lüke L, Samsun RC. High Temperature Polymer Electrolyte Fuel Cells. Fuel Cells : Data, Facts and Figures, Weinheim, Germany: Wiley-VCH Verlag GmbH & Co. KGaA.; 2016, p. 235–47. <https://doi.org/10.1002/9783527693924.ch24>.
- [342] Syah R, Isola LA, Guerrero JWG, Suksatan W, Sunarsi D, Elveny M, et al. Optimal parameters estimation of the PEMFC using a balanced version of Water Strider Algorithm. Energy Reports 2021;7:6876–86. <https://doi.org/10.1016/j.egy.2021.10.057>.
- [343] Molle M, Schmidt TJ, Benicewicz BC. Polybenzimidazole Fuel Cell Technology. Fuel Cells, New York, NY: Springer New York; 2013, p. 391–431. [https://doi.org/10.1007/978-1-4614-5785-5\\_13](https://doi.org/10.1007/978-1-4614-5785-5_13).
- [344] McConnell VP. High-temperature PEM fuel cells: Hotter, simpler, cheaper. Fuel Cells Bulletin 2009;2009:12–6. [https://doi.org/10.1016/S1464-2859\(09\)70411-0](https://doi.org/10.1016/S1464-2859(09)70411-0).
- [345] E.ON partners with Efficiency to bring Elcore fuel cell systems to German residential market. Fuel Cells Bulletin 2017;2017:1. [https://doi.org/10.1016/S1464-2859\(17\)30241-9](https://doi.org/10.1016/S1464-2859(17)30241-9).
- [346] Schenk A, Gamper S, Grimmer C, Pichler BE, Bodner M, Weinberger S, et al. Development of Low Cost High-Temperature Polymer Electrolyte Fuel Cell Membrane-Electrode-Assemblies for Combined Heat and Power Plants in Single Family Homes. ECS Trans 2016;75:435–41. <https://doi.org/10.1149/07514.0435ecst>.
- [347] Nielsen ER, Prag CB, Bachmann TM, Carnicelli F, Boyd E, Walker I, et al. Status on Demonstration of Fuel Cell Based Micro-CHP Units in Europe. Fuel Cells 2019;fu.201800189. <https://doi.org/10.1002/fuce.201800189>.
- [348] Bednarek T, Davies J, Malkow T, Weidner E. Historical Analysis of FCH 2 JU Stationary Fuel Cell Projects: Progress of Key Performance Indicators against the State of the Art. JRC Technical Report 2021. <https://doi.org/10.2760/527879>.
- [349] Freudenberg Group. 2019 Annual Report. 2020.
- [350] BHKW Forum 2019. <https://www.bhkw-forum.de/diskussion/thread/8843-etliche-elcore-2400-komplett-ab-450-aus-insolvenzmasse/?pageNo=1> (accessed May 25, 2023).
- [351] Wei M, Smith SJ, Sohn MD. Experience curve development and cost reduction disaggregation for fuel cell markets in Japan and the US. Appl Energy 2017;191:346–57. <https://doi.org/10.1016/j.apenergy.2017.01.056>.
- [352] Doosan. PureCell® Model 400. 2018.
- [353] Kanuri S V. UTC Power and the PureCell Model 400 fuel cell power plant finding wide application. Fuel Cells Bulletin 2012;2012:12–5. [https://doi.org/10.1016/S1464-2859\(12\)70056-1](https://doi.org/10.1016/S1464-2859(12)70056-1).
- [354] Jo A, Oh K, Lee J, Han D, Kim D, Kim J, et al. Modeling and analysis of a 5 kWe HT-PEMFC system for residential heat and power generation. Int J Hydrogen Energy 2017;42:1698–714. <https://doi.org/10.1016/j.ijhydene.2016.10.152>.
- [355] Olabi AG, Wilberforce T, Sayed ET, Elsaid K, Abdelkareem MA. Prospects of Fuel Cell Combined Heat and Power Systems. Energies (Basel) 2020;13:4104. <https://doi.org/10.3390/en13164104>.
- [356] Elmer T, Worall M, Wu S, Riffat SB. Fuel cell technology for domestic built environment applications: State of-the-art review. Renewable and Sustainable Energy Reviews 2015;42:913–31. <https://doi.org/10.1016/j.rser.2014.10.080>.
- [357] Petrecky J, Ashley CJ. CHP Fuel Cell Durability Demonstration - Final Report. Plug Power 2014. <https://doi.org/10.2172/1160148>.

- [358] Pasupathi S, Calderon Gomez JC, Su H, Reddy H, Bujlo P, Sita C. Stationary HT-PEMFC-Based Systems—Combined Heat and Power Generation. *Recent Advances in High-Temperature PEM Fuel Cells*, Elsevier; 2016, p. 55–77. <https://doi.org/10.1016/B978-0-12-809989-6.00005-0>.
- [359] Cumalioglu I. GenSys Blue: Fuel Cell Heating Appliance. *Plug Power* 2009.
- [360] Vogel J, Marcinkoski J. Highly Efficient, 5 kW CHP Fuel Cells Demonstrating Durability and Economic Value in Residential and Light Commercial Applications. DOE Hydrogen Program FY 2010 Annual Progress Report 2010.
- [361] Hubert C-E, Achard P, Metkemeijer R. Study of a small heat and power PEM fuel cell system generator. *J Power Sources* 2006;156:64–70. <https://doi.org/10.1016/j.jpowsour.2005.08.022>.
- [362] Plug Power restructures to focus on materials handling market. *Fuel Cells Bulletin* 2010;2010:8. [https://doi.org/10.1016/S1464-2859\(10\)70186-3](https://doi.org/10.1016/S1464-2859(10)70186-3).
- [363] Feitelberg AS, Stathopoulos J, Qi Z, Smith C, Elter JF. Reliability of Plug Power GenSys™ fuel cell systems. *J Power Sources* 2005;147:203–7. <https://doi.org/10.1016/j.jpowsour.2005.01.012>.
- [364] Arsalis A, Nielsen MP, Kær SK. Modeling and off-design performance of a 1kWe HT-PEMFC (high temperature-proton exchange membrane fuel cell)-based residential micro-CHP (combined-heat-and-power) system for Danish single-family households. *Energy* 2011;36:993–1002. <https://doi.org/10.1016/j.energy.2010.12.009>.
- [365] De Castro ES, Kaye I, Chen R, Pavlik T. (Invited) Compact Design of HT Pefmc Stacks with Advanced Cooling. *ECS Meeting Abstracts* 2022;MA2022-02:1466–1466. <https://doi.org/10.1149/MA2022-02401466mtgabs>.
- [366] Serenergy. Fuel Cell Stack Module - Serenus 166/390 Air C - Datasheet v2.5-0210. n.d.
- [367] Araya SS, Zhou F, Liso V, Sahlin SL, Vang JR, Thomas S, et al. A comprehensive review of PBI-based high temperature PEM fuel cells. *Int J Hydrogen Energy* 2016;41:21310–44. <https://doi.org/10.1016/j.ijhydene.2016.09.024>.
- [368] Staffell I, Scamman D, Velazquez Abad A, Balcombe P, Dodds PE, Ekins P, et al. The role of hydrogen and fuel cells in the global energy system. *Energy Environ Sci* 2019;12:463–91. <https://doi.org/10.1039/C8EE01157E>.
- [369] Kopasz J, Dolan C, Gangi J, Homann Q. 2020 Hydrogen and Fuel Cell Technologies Market Report. The Fuel Cell and Hydrogen Energy Association 2022. <https://doi.org/10.2172/1859747>.
- [370] Dodds PE, Staffell I, Hawkes AD, Li F, Grünewald P, McDowall W, et al. Hydrogen and fuel cell technologies for heating: A review. *Int J Hydrogen Energy* 2015;40:2065–83. <https://doi.org/10.1016/j.ijhydene.2014.11.059>.
- [371] Nazir H, Muthuswamy N, Louis C, Jose S, Prakash J, Buan MEM, et al. Is the H2 economy realizable in the foreseeable future? Part III: H2 usage technologies, applications, and challenges and opportunities. *Int J Hydrogen Energy* 2020;45:28217–39. <https://doi.org/10.1016/j.ijhydene.2020.07.256>.
- [372] Intralink. The Hydrogen Economy South Korea Market Intelligence Report. 2021.
- [373] Park C. Green Hydrogen Economy Roadmap: A Korean Perspective. 37th European Photovoltaic Solar Energy Conference and Exhibition (EU PVSEC 2020) 2020.
- [374] Stangarone T. South Korean efforts to transition to a hydrogen economy. *Clean Technol Environ Policy* 2021;23:509–16. <https://doi.org/10.1007/s10098-020-01936-6>.

- [375] Bozorgmehri S, Heidary H, Salimi M. Market diffusion strategies for the PEM fuel cell-based micro-CHP systems in the residential sector: scenario analysis. *Int J Hydrogen Energy* 2023;48:3287–98. <https://doi.org/10.1016/j.ijhydene.2022.10.159>.
- [376] Code 2 - Cogeneration Observatory and Dissemination Europe. Micro-CHP potential analysis European level report. Intelligent Energy Europe 2014.
- [377] Aguilo-Rullan A. Fuel Cells and Hydrogen Joint Undertaking - EU policy & micro-CHP. *Journée Micro-Mini Cogénérations* 2017.
- [378] Atanasiu M. Clean Heat and Power with Hydrogen. *Clean Hydrogen Joint Undertaking* 2023.
- [379] Parra D, Valverde L, Pino FJ, Patel MK. A review on the role, cost and value of hydrogen energy systems for deep decarbonisation. *Renewable and Sustainable Energy Reviews* 2019;101:279–94. <https://doi.org/10.1016/j.rser.2018.11.010>.
- [380] Fuel Cells and Hydrogen 2 Joint Undertaking (FCH 2 JU). Addendum to the Multi - Annual Work Plan 2014 - 2020 2018.
- [381] Whiston MM, Lima Azevedo IM, Litster S, Samaras C, Whitefoot KS, Whitacre JF. Paths to market for stationary solid oxide fuel cells: Expert elicitation and a cost of electricity model. *Appl Energy* 2021;304:117641. <https://doi.org/10.1016/j.apenergy.2021.117641>.
- [382] Löbberding L, Madlener R. Techno-economic analysis of micro fuel cell cogeneration and storage in Germany. *Appl Energy* 2019;235:1603–13. <https://doi.org/10.1016/j.apenergy.2018.11.023>.
- [383] Hedman B. Integration of MicroCHP in the United States. National Institute of Standards and Technology 2010.
- [384] SOLIDpower agrees German distribution with Bosch's Buderus. *Fuel Cells Bulletin* 2018;2018:12–12. [https://doi.org/10.1016/S1464-2859\(18\)30259-1](https://doi.org/10.1016/S1464-2859(18)30259-1).
- [385] New fuel cell products for residential use. *Fuel Cells Bulletin* 2018;2018:2–3. [https://doi.org/10.1016/S1464-2859\(18\)30190-1](https://doi.org/10.1016/S1464-2859(18)30190-1).
- [386] Brennstoffzellen-Heizgeräte : Vi\*ov\*\*r P\*2 - Vi\*ov\*\*r P\*2. Doc N°9441 906 - 8 DE 2021.
- [387] mPower takes over Hexis. *Fuel Cells Bulletin* 2020;2020:13–13. [https://doi.org/10.1016/S1464-2859\(20\)30310-2](https://doi.org/10.1016/S1464-2859(20)30310-2).
- [388] Into SOFC developer Hexis, links with Panasonic. *Fuel Cells Bulletin* 2012;2012:3–4. [https://doi.org/10.1016/S1464-2859\(12\)70311-5](https://doi.org/10.1016/S1464-2859(12)70311-5).
- [389] Mai A, Grolig JG, Sarda V, Dold M, Schuler A. Status of HEXIS' SOFC Module Development. *Proceedings of the 14th European SOFC & SOE Forum (EFCF 2020)* 2020. <https://doi.org/10.5281/zenodo.5115820>.
- [390] Hexis. Leonardo Fuel Cell CHP For residential and commercial applications. 2022.
- [391] Schuh S, Dragosits S, Seidl C, Grimm S. Brennstoffzellen für den Endkundenbereich. *Internationale Energiewirtschaftstagung an Der TU-Wien (IEWT 2021)* 2021.
- [392] inhouse engineering. Specification of the Fuel Cell System inhouse5000+. 2020.
- [393] Kaul I. Trial Overview & Customer Insights. *Element Energy* 2023.
- [394] Tomasi A, Concina M, Grossoni M, Caracino P, Blanchard J. Field Applications: Fuel Cells as Backup Power for Italian Telecommunication Sites. *28th International Telecommunications Energy Conference (INTELEC 06)*, IEEE; 2006, p. 1–8. <https://doi.org/10.1109/INTLEEC.2006.251666>.

- [395] Plug Power acquires ReliOn for PEM stack tech. *Fuel Cells Bulletin* 2014;2014:1. [https://doi.org/10.1016/S1464-2859\(14\)70094-X](https://doi.org/10.1016/S1464-2859(14)70094-X).
- [396] Convion. Convion C60 - datasheet 2021.
- [397] New FCH JU project PACE will deploy 2650 micro CHP units. *Fuel Cells Bulletin* 2016;2016:5. [https://doi.org/10.1016/S1464-2859\(16\)30140-7](https://doi.org/10.1016/S1464-2859(16)30140-7).
- [398] Penny C. Heatstack Programme Review Days 2018. *Fuel Cells and Hydrogen Joint Undertaking* 2018.
- [399] New enerday becomes Sunfire Fuel Cells, targeting micro CHP. *Fuel Cells Bulletin* 2019;2019:11–11. [https://doi.org/10.1016/S1464-2859\(19\)30115-4](https://doi.org/10.1016/S1464-2859(19)30115-4).
- [400] Ruth M. 1–10 kW Stationary Combined Heat and Power Systems Status and Technical Potential: Independent Review. US Department of Energy Hydrogen and Fuel Cells Program 2012.
- [401] Pasdag O, Kvasnicka A, Steffen M, Heinzl A. Highly Integrated Steam Reforming Fuel Processor with Condensing Burner Technology for Maximised Electrical Efficiency of CHP-PEMFC Systems. *Energy Procedia* 2012;28:57–65. <https://doi.org/10.1016/j.egypro.2012.08.040>.
- [402] Di Marcoberardino G, Manzolini G. Investigation of a 5 kW micro-CHP PEM fuel cell based system integrated with membrane reactor under diverse EU natural gas quality. *Int J Hydrogen Energy* 2017;42:13988–4002. <https://doi.org/10.1016/j.ijhydene.2017.02.016>.
- [403] Korsgaard A, Nielsen M, Kaer S. Part one: A novel model of HTPeM-based micro-combined heat and power fuel cell system. *Int J Hydrogen Energy* 2008;33:1909–20. <https://doi.org/10.1016/j.ijhydene.2008.01.009>.
- [404] Haider R, Wen Y, Ma Z-F, Wilkinson DP, Zhang L, Yuan X, et al. High temperature proton exchange membrane fuel cells: progress in advanced materials and key technologies. *Chem Soc Rev* 2021;50:1138–87. <https://doi.org/10.1039/D0CS00296H>.
- [405] Cigolotti V, Genovese M. Stationary Fuel Cell Applications - Current and future technologies - Cost, performances, and potential. *Technology Collaboration Programme by IEA* 2021.
- [406] International Energy Agency. *Technology Roadmap Hydrogen and Fuel Cells*. 2015.
- [407] Fan L, Tu Z, Chan SH. Recent development of hydrogen and fuel cell technologies: A review. *Energy Reports* 2021;7:8421–46. <https://doi.org/10.1016/j.egy.2021.08.003>.
- [408] Andersson M, Froitzheim J. *Technology review - Solid Oxide Cells* 2019. *Energiforsk* 2019.
- [409] Wachsman ED, Marlowe CA, Lee KT. Role of solid oxide fuel cells in a balanced energy strategy. *Energy Environ Sci* 2012;5:5498–509. <https://doi.org/10.1039/C1EE02445K>.
- [410] Bloom Energy. *The Bloom Energy Server 5.5. Data Sheet* 2023. <https://www.bloomenergy.com/wp-content/uploads/bloom-energy-server-datasheet-2023.pdf> (accessed May 29, 2023).
- [411] Mendonça C, Ferreira A, Santos DMF. Towards the Commercialization of Solid Oxide Fuel Cells: Recent Advances in Materials and Integration Strategies. *Fuels* 2021;2:393–419. <https://doi.org/10.3390/FUELS2040023>.
- [412] Liu J, Tang Q, Su Y, Li T, Wang Y, Zhu M. Economic Analysis of Solid Oxide Fuel Cell and Its Role in Carbon Peak, Carbon Neutralization Process. 4th International Conference on Energy, Electrical and Power Engineering (CEEPE 2021), IEEE; 2021, p. 115–9. <https://doi.org/10.1109/CEEPE51765.2021.9475688>.

- [413] Boldrin P, Brandon NP. Progress and outlook for solid oxide fuel cells for transportation applications. *Nat Catal* 2019;2:571–7. <https://doi.org/10.1038/s41929-019-0310-y>.
- [414] Li X, Zhu Z, De Marco R, Bradley J, Dicks A. Modification of Coal as a Fuel for the Direct Carbon Fuel Cell. *J Phys Chem A* 2010;114:3855–62. <https://doi.org/10.1021/jp9062719>.
- [415] Stambouli AB, Traversa E. Solid oxide fuel cells (SOFCs): a review of an environmentally clean and efficient source of energy. *Renewable and Sustainable Energy Reviews* 2002;6:433–55. [https://doi.org/10.1016/S1364-0321\(02\)00014-X](https://doi.org/10.1016/S1364-0321(02)00014-X).
- [416] Zeng Z, Qian Y, Zhang Y, Hao C, Dan D, Zhuge W. A review of heat transfer and thermal management methods for temperature gradient reduction in solid oxide fuel cell (SOFC) stacks. *Appl Energy* 2020;280:115899. <https://doi.org/10.1016/j.apenergy.2020.115899>.
- [417] Ferguson K, Dubois A, Albrecht K, Braun RJ. High performance protonic ceramic fuel cell systems for distributed power generation. *Energy Convers Manag* 2021;248:114763. <https://doi.org/10.1016/j.enconman.2021.114763>.
- [418] Leah RT, Bone A, Hammer E, Selcuk A, Rahman M, Clare A, et al. Development of High Efficiency Steel Cell Technology for Multiple Applications. *ECS Trans* 2017;78:2005–14. <https://doi.org/10.1149/07801.2005ecst>.
- [419] Weeber K, Horstmann P, Miersch J. Changes in Power Generation and Distribution and the role of SOFC. *Proceedings of the 13th European SOFC & SOE Forum (EFCF 2018)* 2018.
- [420] Leah RT, Bone A, Selcuk A, Rahman M, Clare A, Lankin M, et al. Latest Results and Commercialization of the Ceres Power SteelCell® Technology Platform. *ECS Trans* 2019;91:51–61. <https://doi.org/10.1149/09101.0051ecst>.
- [421] Noponen M, Göös J, Torri P, Chade D, Vähä-Piikkiö H, Hallanoro P. Status of Elcogen unit cell and stack development. *Proceedings of the 12th European SOFC & SOE Forum (EFCF 2016)* 2016.
- [422] Beale SB, Andersson M, Boigues-Muñoz C, Frandsen HL, Lin Z, McPhail SJ, et al. Continuum scale modelling and complementary experimentation of solid oxide cells. *Prog Energy Combust Sci* 2021;85:100902. <https://doi.org/10.1016/j.pecs.2020.100902>.
- [423] Noponen M, Göös J, Torri P, Chade D, Vähä-Piikkiö H, Hallanoro P. Performance Characteristics of Elcogen Solid Oxide Fuel Cell Stacks. *Proceedings of the 12th European SOFC & SOE Forum (EFCF 2016)* 2016.
- [424] Bertoldi M, Bucheli O, Ravagni A V. Development and Manufacturing of SOFC-Based Products at SOFCpower SpA. *Proceedings of the 11th European SOFC & SOE Forum (EFCF 2014)* 2014.
- [425] Bertoldi M, Bucheli O, Ravagnia A V. High-efficiency cogenerators from SOLIDpower SpA. *Proceedings of the 12th European SOFC & SOE Forum (EFCF 2016)* 2016.
- [426] Halinen M, Rautanen M, Saarinen J, Pennanen J, Pohjoranta A, Kiviaho J, et al. Performance of a 10 kW SOFC Demonstration Unit. *ECS Trans* 2011;35:113–20. <https://doi.org/10.1149/1.3569985>.
- [427] Paulus N, Lemort V. Field-test performance of Solid Oxide Fuel Cells (SOFC) for residential cogeneration applications. *Proceedings of the 7th International High Performance Buildings Conference at Purdue (Herrick 2022)* 2022.



- [428] Sinha V, Mondal S. Recent development on performance modelling and fault diagnosis of fuel cell systems. *Int J Dyn Control* 2018;6:511–28. <https://doi.org/10.1007/s40435-017-0328-4>.
- [429] Hauch A, Hagen A, Hjelm J, Ramos T. Sulfur Poisoning of SOFC Anodes: Effect of Overpotential on Long-Term Degradation. *J Electrochem Soc* 2014;161:F734–43. <https://doi.org/10.1149/2.080406jes>.
- [430] Sui S, Xiu GH. Fuels and fuel processing in SOFC applications. *High-Temperature Solid Oxide Fuel Cells for the 21st Century*, Elsevier; 2016, p. 461–95. <https://doi.org/10.1016/B978-0-12-410453-2.00014-2>.
- [431] Fernandes MD, de P. Andrade ST, Bistrizki VN, Fonseca RM, Zacarias LG, Gonçalves HNC, et al. SOFC-APU systems for aircraft: A review. *Int J Hydrogen Energy* 2018;43:16311–33. <https://doi.org/10.1016/j.ijhydene.2018.07.004>.
- [432] Peng J, Huang J, Wu X, Xu Y, Chen H, Li X. Solid oxide fuel cell (SOFC) performance evaluation, fault diagnosis and health control: A review. *J Power Sources* 2021;505:230058. <https://doi.org/10.1016/j.jpowsour.2021.230058>.
- [433] Buderus. Heizsysteme mit zukunft - Brennstoffzellentechnologie - Bl\*\*\*G\*N BG-\*\*. 2020.
- [434] Linhart A, Bekebrok H, Zobel M, Dyck A, Optenhostert T, Spieker C, et al. Overview of the developments and results of the Design 2 Service project. *Proceedings of the 8th European Fuel Cell Technology & Applications Piero Lunghi Conference (EFC 19) 2019*.
- [435] Dikwal CM, Bujalski W, Kendall K. The effect of temperature gradients on thermal cycling and isothermal ageing of micro-tubular solid oxide fuel cells. *J Power Sources* 2009;193:241–8. <https://doi.org/10.1016/j.jpowsour.2009.01.097>.
- [436] Nakajo A, Mueller F, Brouwer J, Van herle J, Favrat D. Mechanical reliability and durability of SOFC stacks. Part II: Modelling of mechanical failures during ageing and cycling. *Int J Hydrogen Energy* 2012;37:9269–86. <https://doi.org/10.1016/j.ijhydene.2012.03.023>.
- [437] KATEK Memmingen GmbH. Steca coolcept fleX - StecaGrid 1511 | 2011 | 2511 | 3011 | 3011\_2 | 3611 | 3611\_2 | 4611\_2. 2019.
- [438] Shao Z, Haile SM, Ahn J, Ronney PD, Zhan Z, Barnett SA. A thermally self-sustained micro solid-oxide fuel-cell stack with high power density. *Nature* 2005;435:795–8. <https://doi.org/10.1038/nature03673>.
- [439] Schmidt-Rohr K. Why Combustions Are Always Exothermic, Yielding About 418 kJ per Mole of O<sub>2</sub>. *J Chem Educ* 2015;92:2094–9. <https://doi.org/10.1021/acs.jchemed.5b00333>.
- [440] Braun RJ, Klein SA, Reindl DT. Evaluation of system configurations for solid oxide fuel cell-based micro-combined heat and power generators in residential applications. *J Power Sources* 2006;158:1290–305. <https://doi.org/10.1016/j.jpowsour.2005.10.064>.
- [441] Wagner PH. Integrated Design, Optimization, and Experimental Realization of a Steam-Driven Micro Recirculation Fan for Solid Oxide Fuel Cell Systems. *Ecole Polytechnique de Lausanne* 2019. <https://doi.org/10.5075/epfl-thesis-9337>.
- [442] Zhang T, Zhao H, Du H, Wang H. Thermodynamic performance study of a novel cogeneration system combining solid oxide fuel cell, gas turbine, organic Rankine cycle with compressed air energy storage. *Energy Convers Manag* 2021;249:114837. <https://doi.org/10.1016/j.enconman.2021.114837>.

- [443] Lichtenegger K, Hebenstreit B, Pointner C, Schmidl C, Höftberger E. The role of leak air in a double-wall chimney. *Heat and Mass Transfer* 2015;51:787–94. <https://doi.org/10.1007/s00231-014-1454-6>.
- [444] Chen KK, Han Y, Tong Z, Gasda M, Ho WSW. Membrane processes for CO<sub>2</sub> removal and fuel utilization enhancement for solid oxide fuel cells. *J Memb Sci* 2021;620:118846. <https://doi.org/10.1016/j.memsci.2020.118846>.
- [445] Fritzmann C, Löwenberg J, Wintgens T, Melin T. State-of-the-art of reverse osmosis desalination. *Desalination* 2007;216:1–76. <https://doi.org/10.1016/j.desal.2006.12.009>.
- [446] Lv X, Ding X, Weng Y. Effect of fuel composition fluctuation on the safety performance of an IT-SOFC/GT hybrid system. *Energy* 2019;174:45–53. <https://doi.org/10.1016/j.energy.2019.02.083>.
- [447] Paulus N, Lemort V. Simplified test bench for experimental investigations of space heating appliances. *IOP Conf Ser Earth Environ Sci* 2023;1185:012014. <https://doi.org/10.1088/1755-1315/1185/1/012014>.
- [448] Paulus N, Lemort V. Experimental investigation of a Solid Oxide Fuel Cell (SOFC) used in residential cogeneration applications. *Proceedings of the 36th International Conference On Efficiency, Cost, Optimization, Simulation and Environmental Impact of Energy Systems (ECOS2023)* 2023. <https://doi.org/10.52202/069564-0056>.
- [449] Paulus N, Lemort V. Experimental investigation of a Solid Oxide Fuel Cell (SOFC) used in residential cogeneration applications. *Entropie* 2024;Under Review.
- [450] ESBE. Vanne thermostatique - SÉRIES VTA370, VTA570. 2019.
- [451] Wilo. Yonos PARA - The new standard in High Efficiency. 2012.
- [452] Elster. BK-G4 and BK-G4T - High quality residential diaphragm gas meters. 2012.
- [453] Iskraemeco. BASIC MT174 - Polyphase multi-tariff meter. 2021.
- [454] Gossen Metrawatt. A2000 Multifunctional Power Meter. 2015.
- [455] Axioma. Ultrasonic heating/cooling meter - Qalcosonic E1. 2019.
- [456] Metering EUROPE. DHV1300. 2022.
- [457] International Organization of Legal Metrology. OIML R 75-1: 2002 (E): Heat meters Part 1: General requirements Compteurs d'énergie thermique Partie 1: Exigences générales. 2002.
- [458] Tegeler E, Heyer D, Siebert BerndRL. Uncertainty of the Calibration of Paired Temperature Sensors for Heat Meters. *Int J Thermophys* 2008;29:1174–83. <https://doi.org/10.1007/s10765-008-0416-y>.
- [459] International Electrotechnical Commission. IEC 60751: Industrial platinum resistance thermometers and platinum temperature sensors. 2022.
- [460] Liso V, Olesen AC, Nielsen MP, Kær SK. Performance comparison between partial oxidation and methane steam reforming processes for solid oxide fuel cell (SOFC) micro combined heat and power (CHP) system. *Energy* 2011;36:4216–26. <https://doi.org/10.1016/j.energy.2011.04.022>.
- [461] Verhaert I, Van Riet F, Baetens R, De Pauw M, Van Erdeweghe M. Performance evaluation of different micro-CHP configurations in real life conditions and the influence of part load behaviour. *E3S Web of Conferences* 2019;111:01084. <https://doi.org/10.1051/e3sconf/201911101084>.
- [462] Föger Australia Other K, Rowe T. Ceramic Fuel Cells LTD Residential Generator - Ultra-efficient distributed power generation in Smart Grid Environment.

- Proceedings of the 2nd International Gas Union Research Conference (IGRC 2011) 2011.
- [463] Staffell I. Zero carbon infinite COP heat from fuel cell CHP. *Appl Energy* 2015;147:373–85. <https://doi.org/10.1016/j.apenergy.2015.02.089>.
- [464] Staffell I, Baker P, Barton JP, Bergman N, Blanchard R, Brandon NP, et al. UK microgeneration. Part II: technology overviews. *Proceedings of the Institution of Civil Engineers - Energy* 2010;163:143–65. <https://doi.org/10.1680/ener.2010.163.4.143>.
- [465] Paulus N, Lemort V. Establishing the energy content of natural gas residential consumption: example with Belgian field-test applications. *IOP Conf Ser Earth Environ Sci* 2023;1185:012013. <https://doi.org/10.1088/1755-1315/1185/1/012013>.
- [466] European Commission. EN 13757-4 - Communication systems for meters and remote reading of meters - Part 4: Wireless meter readout (Radio meter reading for operation in SRD bands). 2013.
- [467] WEPTECH elektronik. wM-Bus humidity & temperature sensor MUNIA. 2021.
- [468] International Electrotechnical Commission. IEC 62053-21: Electricity metering equipment (a.c.) – Particular requirements. Part 21 : Static meters for active energy (classes 1 and 2). 2003.
- [469] Viltrus Electronics. MX-9 Wireless M-Bus Data Logger 433MHz/868MHz. 2022.
- [470] Butler D, Abela A, Martin C. Heat meter accuracy testing. UK Government - Department for Business, Energy & Industrial Strategy 2016.
- [471] European Parliament. DIRECTIVE 2012/27/EU on energy efficiency, amending Directives 2009/125/EC and 2010/30/EU and repealing Directives 2004/8/EC and 2006/32/EC. 2012.
- [472] Batlle C, Tim S, Christopher R. K. Power Price Crisis in the EU: Unveiling Current Policy Responses and Proposing a Balanced Regulatory Remedy. MIT Center for Energy and Environmental Policy Research 2022.
- [473] CREG. Analyse semestrielle de l'évolution des prix de l'énergie – 2ème semestre 2021. 2022.
- [474] Emerald Expert Briefings. Ukraine crisis will bring heavy costs for Europe. Oxford Analytica 2022.
- [475] CWaPE. Communication FAQ-Tarif Prosumer. 2020.
- [476] Skone TJ, Littlefield J, Marriott J. Life Cycle Greenhouse Gas Inventory of Natural Gas Extraction, Delivery and Electricity Production. US Department of Energy 2011. <https://doi.org/10.2172/1515238>.
- [477] Paulus N, Lemort V. Grid-impact factors of field-tested residential Proton Exchange Membrane Fuel Cell systems. *Proceedings of the 14th REHVA HVAC World Congress (CLIMA2022)* 2022. <https://doi.org/10.34641/CLIMA.2022.176>.
- [478] Näsäkkälä E, Fleten S-E. Flexibility and technology choice in gas fired power plant investments. *Review of Financial Economics* 2005;14:371–93. <https://doi.org/10.1016/j.rfe.2005.01.001>.
- [479] Napoli R, Gandiglio M, Lanzini A, Santarelli M. Techno-economic analysis of PEMFC and SOFC micro-CHP fuel cell systems for the residential sector. *Energy Build* 2015;103:131–46. <https://doi.org/10.1016/j.enbuild.2015.06.052>.
- [480] Felice A, Rakocevic L, Peeters L, Messagie M, Coosemans T, Ramirez Camargo L. Renewable energy communities: Do they have a business case in Flanders? *Appl Energy* 2022;322:119419. <https://doi.org/10.1016/j.apenergy.2022.119419>.

- [481] CREG. Analyse semestrielle de l'évolution des prix de l'énergie – 2ème semestre 2023. 2023.
- [482] Adams T, Mac Dowell N. Off-design point modelling of a 420 MW CCGT power plant integrated with an amine-based post-combustion CO<sub>2</sub> capture and compression process. *Appl Energy* 2016;178:681–702. <https://doi.org/10.1016/j.apenergy.2016.06.087>.
- [483] Huisman R, Huurman C, Mahieu R. Hourly electricity prices in day-ahead markets. *Energy Econ* 2007;29:240–8. <https://doi.org/10.1016/j.eneco.2006.08.005>.
- [484] Burnham A, Han J, Clark CE, Wang M, Dunn JB, Palou-Rivera I. Life-Cycle Greenhouse Gas Emissions of Shale Gas, Natural Gas, Coal, and Petroleum. *Environ Sci Technol* 2012;46:619–27. <https://doi.org/10.1021/es201942m>.
- [485] Grubert EA, Brandt AR. Three considerations for modeling natural gas system methane emissions in life cycle assessment. *J Clean Prod* 2019;222:760–7. <https://doi.org/10.1016/j.jclepro.2019.03.096>.
- [486] Taylor BN, Kuyatt CE. Guidelines for Evaluating and Expressing the Uncertainty of NIST Measurement Results - 1994 edition. National Institute of Standards and Technology 1994.
- [487] International Organization for Standardization. ISO 13443 - Natural gas - Standard reference conditions. 1996.
- [488] American Society of Mechanical Engineers (ASME). Thermowells Performance Test Codes - ASME PTC 19.3 TW-2010. 2010.
- [489] Klason P, Kok GJ, Pelevic N, Holmsten M, Ljungblad S, Lau P. Measuring Temperature in Pipe Flow with Non-Homogeneous Temperature Distribution. *Int J Thermophys* 2014;35:712–24. <https://doi.org/10.1007/s10765-014-1579-3>.
- [490] Kolpatzik SJ, Hilgenstock A, Dietrich H, Nath B. The location of temperature sensors in pipe flows for determining the mean gas temperature in flow metering applications. *Flow Measurement and Instrumentation* 1998;9:43–57. [https://doi.org/10.1016/S0955-5986\(98\)00009-0](https://doi.org/10.1016/S0955-5986(98)00009-0).
- [491] MathWorks. Matlab R2023a - Curve Fitting Toolbox User's guide. 2023.
- [492] D2SERVICE. WP4: Design changes required for an easier and more competitive service of SP's µCHP appliance - D4.4: Service manual (prescriptions and instructions to installer). 2019. <https://doi.org/10.3030/671473>.
- [493] European Commission. EN 15502-1 - Gas-fired heating boilers - Part 1: General requirements and tests. 2021.
- [494] AFRISO-EURO-INDEX Group. MULTILYZER® STx - Analyseur de service. FR19001 2019.
- [495] Systronik, AFRISO-EURO-INDEX Group. STM 225 Dust monitor. FR 18001 2018.
- [496] Paulus N, Job N, Lemort V. Investigation of degradation mechanisms and corresponding recovery procedures of a field-tested residential cogeneration Polymer Electrolyte Membrane fuel cell. To Be Submitted 2024.
- [497] Sundén B, Fu J. Fuel Cells. Heat Transfer in Aerospace Applications, Elsevier; 2017, p. 145–53. <https://doi.org/10.1016/B978-0-12-809760-1.00008-9>.
- [498] Ghenciu AF. Review of fuel processing catalysts for hydrogen production in PEM fuel cell systems. *Curr Opin Solid State Mater Sci* 2002;6:389–99. [https://doi.org/10.1016/S1359-0286\(02\)00108-0](https://doi.org/10.1016/S1359-0286(02)00108-0).
- [499] Dolci F, Thomas D, Hilliard S, Guerra CF, Hancke R, Ito H, et al. Incentives and legal barriers for power-to-hydrogen pathways: An international snapshot. *Int J*

- Hydrogen Energy 2019;44:11394–401.  
<https://doi.org/10.1016/J.IJHYDENE.2019.03.045>.
- [500] Verduyn L. Vi\*ov\*\*r 3\*\*-P. 2017.
- [501] Vernon PDF, Green MLH, Cheetham AK, Ashcroft AT. Partial oxidation of methane to synthesis gas. *Catal Letters* 1990;6:181–6. <https://doi.org/10.1007/bf00774718>.
- [502] Golodets GI. Chapter X: The Oxidation of Carbon Monoxide. *Stud Surf Sci Catal*, vol. 15, Elsevier; 1983, p. 280–311. [https://doi.org/10.1016/S0167-2991\(08\)64835-1](https://doi.org/10.1016/S0167-2991(08)64835-1).
- [503] Heinzl A, Vogel B, Hübner P. Reforming of natural gas—hydrogen generation for small scale stationary fuel cell systems. *J Power Sources* 2002;105:202–7. [https://doi.org/10.1016/s0378-7753\(01\)00940-5](https://doi.org/10.1016/s0378-7753(01)00940-5).
- [504] Song C, Pan W. Tri-reforming of methane: a novel concept for catalytic production of industrially useful synthesis gas with desired H<sub>2</sub>/CO ratios. *Catal Today* 2004;98:463–84. <https://doi.org/10.1016/j.cattod.2004.09.054>.
- [505] Abdullah B, Abd Ghani NA, Vo D-VN. Recent advances in dry reforming of methane over Ni-based catalysts. *J Clean Prod* 2017;162:170–85. <https://doi.org/10.1016/j.jclepro.2017.05.176>.
- [506] Asencios YJO, Assaf EM. Combination of dry reforming and partial oxidation of methane on NiO–MgO–ZrO<sub>2</sub> catalyst: Effect of nickel content. *Fuel Processing Technology* 2013;106:247–52. <https://doi.org/10.1016/j.fuproc.2012.08.004>.
- [507] Li B, Xu X, Zhang S. Synthesis gas production in the combined CO<sub>2</sub> reforming with partial oxidation of methane over Ce-promoted Ni/SiO<sub>2</sub> catalysts. *Int J Hydrogen Energy* 2013;38:890–900. <https://doi.org/10.1016/j.ijhydene.2012.10.103>.
- [508] Authayanun S, Wiyaratn W, Assabumrungrat S, Arpornwichanop A. Theoretical analysis of a glycerol reforming and high-temperature PEMFC integrated system: Hydrogen production and system efficiency. *Fuel* 2013;105:345–52. <https://doi.org/10.1016/j.fuel.2012.07.036>.
- [509] Ercolino G, Ashraf MA, Specchia V, Specchia S. Performance evaluation and comparison of fuel processors integrated with PEM fuel cell based on steam or autothermal reforming and on CO preferential oxidation or selective methanation. *Appl Energy* 2015;143:138–53. <https://doi.org/10.1016/j.apenergy.2014.12.088>.
- [510] Qi Z. Effect of CO in the anode fuel on the performance of PEM fuel cell cathode. *J Power Sources* 2002;111:239–47. [https://doi.org/10.1016/s0378-7753\(02\)00300-2](https://doi.org/10.1016/s0378-7753(02)00300-2).
- [511] Zhou S, Chen F. Chapter 4 - PEMFC System Modeling and Control. *Advances in Chemical Engineering*, vol. 41, Academic Press; 2012, p. 197–263. <https://doi.org/10.1016/B978-0-12-386874-9.00007-5>.
- [512] Chen C-Y, Huang K-P. Performance and transient behavior of the kW-grade PEMFC stack with the Pt Ru catalyst under CO-contained diluted hydrogen. *Int J Hydrogen Energy* 2017;42:22250–8. <https://doi.org/10.1016/j.ijhydene.2017.06.037>.
- [513] Koichi K. Method of shutdown of reforming apparatus. US8202333B2, 2012.
- [514] Umeda T, Sugawara Y, Shibata S, Nakayama A, Nakamura A. Fuel Cell Power Generation System And Method For Operating The Same. EP2475038B1, 2014. <https://doi.org/10.1016/J.JPOWSOUR>.
- [515] Welaya YMA, El Gohary MM, Ammar NR. Steam and partial oxidation reforming options for hydrogen production from fossil fuels for PEM fuel cells. *Alexandria Engineering Journal* 2012;51:69–75. <https://doi.org/10.1016/j.aej.2012.03.001>.

- [516] Valdés-López VF, Mason T, Shearing PR, Brett DJL. Carbon monoxide poisoning and mitigation strategies for polymer electrolyte membrane fuel cells – A review. *Prog Energy Combust Sci* 2020;79:100842. <https://doi.org/10.1016/J.PECS.2020.100842>.
- [517] Adams WA, Blair J, Bullock KR, Gardner CL. Enhancement of the performance and reliability of CO poisoned PEM fuel cells. *J Power Sources* 2005;145:55–61. <https://doi.org/10.1016/j.jpowsour.2004.12.049>.
- [518] Gottesfeld S, Pafford J. A New Approach to the Problem of Carbon Monoxide Poisoning in Fuel Cells Operating at Low Temperatures. *J Electrochem Soc* 1988;135:2651–2. <https://doi.org/10.1149/1.2095401>.
- [519] Korotkikh O, Farrauto R. Selective catalytic oxidation of CO in H<sub>2</sub>: fuel cell applications. *Catal Today* 2000;62:249–54. [https://doi.org/10.1016/S0920-5861\(00\)00426-0](https://doi.org/10.1016/S0920-5861(00)00426-0).
- [520] Arpornwichanop A, Authayanun S. Recent Trends in the Development of Proton Exchange Membrane Fuel Cell Systems. *Alternative Energy and Shale Gas Encyclopedia*, Hoboken, NJ, USA: John Wiley & Sons, Inc.; 2016, p. 509–25. <https://doi.org/10.1002/9781119066354.ch50>.
- [521] Vi\*ov\*\*r P\*2 (génération C). 2019.
- [522] Vi\*ov\*\*r 3\*\* - P - Notice pour l'étude. Doc N°5790 433 B/f 2017.
- [523] Vi\*ov\*\*r P\*2 - Notice pour l'étude. Doc N°5790433 BE 2021.
- [524] Vi\*ov\*\*r PA\* - Feuille technique. Doc N°6153237 BE 2020.
- [525] Yu Y, Li H, Wang H, Yuan X-Z, Wang G, Pan M. A review on performance degradation of proton exchange membrane fuel cells during startup and shutdown processes: Causes, consequences, and mitigation strategies. *J Power Sources* 2012;205:10–23. <https://doi.org/10.1016/j.jpowsour.2012.01.059>.
- [526] Wang Y, Sauer DU, Koehne S, Ersoez A. Dynamic modeling of high temperature PEM fuel cell start-up process. *Int J Hydrogen Energy* 2014;39:19067–78. <https://doi.org/10.1016/j.ijhydene.2014.09.095>.
- [527] Zhang T, Wang P, Chen H, Pei P. A review of automotive proton exchange membrane fuel cell degradation under start-stop operating condition. *Appl Energy* 2018;223:249–62. <https://doi.org/10.1016/j.apenergy.2018.04.049>.
- [528] Borup R, Meyers J, Pivovar B, Kim YS, Mukundan R, Garland N, et al. Scientific aspects of polymer electrolyte fuel cell durability and degradation. *Chem Rev* 2007;107. <https://doi.org/10.1021/cr050182l>.
- [529] Barbir F, Balasubramanian B, Neutzler J. Trade-Off Design Analysis of Operating Pressure and Temperature in PEM Fuel Cell Systems. *Advanced Energy Systems*, American Society of Mechanical Engineers; 1999, p. 305–15. <https://doi.org/10.1115/IMECE1999-0840>.
- [530] Rivarolo M, Rattazzi D, Lamberti T, Magistri L. Clean energy production by PEM fuel cells on tourist ships: A time-dependent analysis. *Int J Hydrogen Energy* 2020;45:25747–57. <https://doi.org/10.1016/j.ijhydene.2019.12.086>.
- [531] Sarma U, Ganguly S. Design optimisation for component sizing using multi-objective particle swarm optimisation and control of PEM fuel cell-battery hybrid energy system for locomotive application. *IET Electrical Systems in Transportation* 2020;10:52–61. <https://doi.org/10.1049/iet-est.2018.5053>.
- [532] Vi\*ov\*\*r P\*2 - Notice d'utilisation pour l'utilisateur. Doc N°5835792 BE 2018.
- [533] Williams SC. Three-Way Ball Valve Flow Patterns-T-Port and L-Port. *Industrial Specialties Mfg & IS MED Specialties* 2018.

- [534] Installation and service instructions for contractors - Vi\*ov\*\*r P\*2 Type E11T, E19T, E25T, E32T, 0.9 to 30.8 kW. Fuel cell based micro CHP unit with integral gas condensing boiler and adjacent cylinder module. Natural gas version. Doc N°5835783 GB 2019.
- [535] Zhang L, Xia J, Thorsen JE, Gudmundsson O, Li H, Svendsen S. Technical, economic and environmental investigation of using district heating to prepare domestic hot water in Chinese multi-storey buildings. *Energy* 2016;116:281–92. <https://doi.org/10.1016/J.ENERGY.2016.09.019>.
- [536] GAMBICA, BEAMA, BPMA. Variable speed driven pumps - Best practise guide - Second Edition 2016.
- [537] Paulus N, Lemort V. Field-test performance models of a residential micro-cogeneration system based on the hybridization of a proton exchange membrane fuel cell and a gas condensing boiler. *Energy Convers Manag* 2023;295:117634. <https://doi.org/10.1016/j.enconman.2023.117634>.
- [538] Hou J, Yang M, Zhang J. Active and passive fuel recirculation for solid oxide and proton exchange membrane fuel cells. *Renew Energy* 2020;155:1355–71. <https://doi.org/10.1016/j.renene.2020.04.002>.
- [539] Kim S, Hong I. Effects of humidity and temperature on a proton exchange membrane fuel cell (PEMFC) stack. *Journal of Industrial and Engineering Chemistry* 2008;14:357–64. <https://doi.org/10.1016/j.jiec.2008.01.007>.
- [540] Daud WRW, Rosli RE, Majlan EH, Hamid SAA, Mohamed R, Husaini T. PEM fuel cell system control: A review. *Renew Energy* 2017;113:620–38. <https://doi.org/10.1016/j.renene.2017.06.027>.
- [541] Ahluwalia RK, Wang X. Buildup of nitrogen in direct hydrogen polymer-electrolyte fuel cell stacks. *J Power Sources* 2007;171:63–71. <https://doi.org/10.1016/j.jpowsour.2007.01.032>.
- [542] R. Lattner J. Comparison of conventional and membrane reactor fuel processors for hydrocarbon-based PEM fuel cell systems. *Int J Hydrogen Energy* 2004;29:393–417. <https://doi.org/10.1016/j.ijhydene.2003.10.013>.
- [543] Dicks A, Connor T, Bradley J, Lashtabeg A. Impact of Australian natural gas and coal bed methane composition on PEM fuel cell performance. *Int J Hydrogen Energy* 2009;34:8892–904. <https://doi.org/10.1016/j.ijhydene.2009.08.019>.
- [544] Najafi B, Haghghat Mamaghani A, Rinaldi F, Casalegno A. Long-term performance analysis of an HT-PEM fuel cell based micro-CHP system: Operational strategies. *Appl Energy* 2015;147:582–92. <https://doi.org/10.1016/j.apenergy.2015.03.043>.
- [545] Jannelli E, Minutillo M, Perna A. Analyzing microcogeneration systems based on LT-PEMFC and HT-PEMFC by energy balances. *Appl Energy* 2013;108:82–91. <https://doi.org/10.1016/j.apenergy.2013.02.067>.
- [546] Boait PJ, Greenough R. Can fuel cell micro-CHP justify the hydrogen gas grid? Operating experience from a UK domestic retrofit. *Energy Build* 2019;194:75–84. <https://doi.org/10.1016/J.ENBUILD.2019.04.021>.
- [547] Avcı AK, Trimm DL, Önsan ZI. Quantitative investigation of catalytic natural gas conversion for hydrogen fuel cell applications. *Chemical Engineering Journal* 2002;90:77–87. [https://doi.org/10.1016/s1385-8947\(02\)00069-4](https://doi.org/10.1016/s1385-8947(02)00069-4).
- [548] Kikuchi R. Penetration of hydrogen-based energy system and its potential for causing global environmental change: Scoping risk analysis based on life cycle thinking. *Environ Impact Assess Rev* 2006;26:206–18. <https://doi.org/10.1016/j.eiar.2005.07.014>.

- [549] Liu Z, Mao Z, Xu J, Hess-Mohr N, Schmidt VM. Modelling of a PEM Fuel Cell System with Propane ATR Reforming. *Fuel Cells* 2006;6:376–86. <https://doi.org/10.1002/fuce.200500104>.
- [550] Dávila C, Paulus N, Lemort V. Experimental investigation of a Micro-CHP unit driven by natural gas for residential buildings. *Proceedings of the 19th International Refrigeration and Air Conditioning Conference (Herrick 2022)* 2022.
- [551] Gas.be. Historique des degrés-jours à partir de 1961. 2020.
- [552] The Chartered Institution of Building Services Engineers. Degree-days: theory and application (TM41: 2006). 2006.
- [553] Orr G, Lelyveld T, Burton S. Final Report: In-situ monitoring of efficiencies of condensing boilers and use of secondary heating. Energy Saving Trust 2009.
- [554] Gas.be. Historique des degrés-jours à partir de 1961. 2021.
- [555] Kim J, Scott CD. Robust Kernel Density Estimation. *Journal of Machine Learning Research* 2012;13. <https://doi.org/10.48550/arXiv.1107.3133>.
- [556] CWaPE. Tarification Prosumers - AVIS CD-19k29-CWaPE-1853. 2019.
- [557] Baetens R, De Coninck R, Van Roy J, Verbruggen B, Driesen J, Helsen L, et al. Assessing electrical bottlenecks at feeder level for residential net zero-energy buildings by integrated system simulation. *Appl Energy* 2012;96:74–83. <https://doi.org/10.1016/j.apenergy.2011.12.098>.
- [558] Baldi S, Quang T Le, Holub O, Endel P. Real-time monitoring energy efficiency and performance degradation of condensing boilers. *Energy Convers Manag* 2017;136:329–39. <https://doi.org/10.1016/j.enconman.2017.01.016>.
- [559] Hoskins RF. Chapter 4 - Time-invariant Linear Systems. *Delta Functions*, Woodhead Publishing; 2011, p. 76–98. <https://doi.org/10.1533/9780857099358.76>.
- [560] Bennett G, Elwell C. Effect of boiler oversizing on efficiency: a dynamic simulation study. *Building Services Engineering Research & Technology* 2020;41:709. <https://doi.org/10.1177/0143624420927352>.
- [561] De Bruijn FA, Dam VAT, Janssen GJM. Review: Durability and Degradation Issues of PEM Fuel Cell Components. *Fuel Cells* 2008;8:3–22. <https://doi.org/10.1002/FUCE.200700053>.
- [562] Staffell I, Green R, Kendall K. Cost targets for domestic fuel cell CHP. *J Power Sources* 2008;181:339–49. <https://doi.org/10.1016/J.JPOWSOUR.2007.11.068>.
- [563] Van Kenhove E, Dinne K, Janssens A, Laverge J. Overview and comparison of Legionella regulations worldwide. *Am J Infect Control* 2019;47:968–78. <https://doi.org/10.1016/J.AJIC.2018.10.006>.
- [564] Paulus N, Dávila C, Lemort V. Correlation between field-test and laboratory results for a Proton Exchange Membrane Fuel Cell (PEMFC) used as a residential cogeneration system. *Proceeding of the 30th “Congrès Annuel de La Société Française de Thermique” (SFT 2022)* 2022. <https://doi.org/10.25855/SFT2022-119>.
- [565] European Commission. Commission Delegated Regulation No 811/2013 of 18 February 2013 with regard to the energy labelling of space heaters, ... *Official Journal of the European Union* 2013.
- [566] European Parliament. DIRECTIVE 2010/31/EU on the energy performance of buildings. *Official Journal of the European Union* 2010.
- [567] Cardu M, Baica M. Regarding the relation between the NO<sub>x</sub> content and CO content in thermo power plants flue gases. *Energy Convers Manag* 2005;46:47–59. <https://doi.org/10.1016/j.enconman.2004.02.009>.



- [568] van Dam SS, Bakker CA, van Hal JDM. Home energy monitors: impact over the medium-term. *Building Research & Information* 2010;38:458–69. <https://doi.org/10.1080/09613218.2010.494832>.
- [569] Jafri N, Wong WY, Doshi V, Yoon LW, Cheah KH. A review on production and characterization of biochars for application in direct carbon fuel cells. *Process Safety and Environmental Protection* 2018;118:152–66. <https://doi.org/10.1016/j.psep.2018.06.036>.
- [570] Leridon H. Population mondiale : vers une explosion ou une implosion ? *Population & Sociétés* 2020;N° 573:1–4. <https://doi.org/10.3917/popsoc.573.0001>.
- [571] Elnagar E, Davila C, Lemort V. Impact of integration of electric and gas heat pumps on the final energy consumption of Belgian residential building stock. *Proceedings of the 14th REHVA HVAC World Congress (CLIMA2022)* 2022. <https://doi.org/10.34641/clima.2022.102>.
- [572] Elnagar E, Doutreloup S, Lemort V. Modeling the impact of Climate Change on Future Heating Demand in Different Types of Buildings in the Belgian residential building stock, 2021. <https://doi.org/10.26868/25222708.2021.30851>.
- [573] Lemort V, Georges E, Gendebien S, Garsoux P. Evolution of the energy load profiles of the Belgian residential building stock with new heating technologies for demand side management. *Proceedings of the 1st Seminar on Demand Response of the Belgian Energy Research Alliance (BERA 2016)* 2016.
- [574] Limpens G, Rixhon X, Contino F, Jeanmart H. Energyscope Pathway: An Open-Source Model to Optimise the Energy Transition Pathways of a Regional Whole-Energy System. Preprint 2023. <https://doi.org/10.2139/ssrn.4512873>.
- [575] Rixhon X, Limpens G, Coppitters D, Jeanmart H, Contino F. The Role of Electrofuels under Uncertainties for the Belgian Energy Transition. *Energies (Basel)* 2021;14:4027. <https://doi.org/10.3390/en14134027>.
- [576] Limpens G, Moret S, Jeanmart H, Maréchal F. EnergyScope TD: A novel open-source model for regional energy systems. *Appl Energy* 2019;255:113729. <https://doi.org/10.1016/j.apenergy.2019.113729>.
- [577] Wimbadi RW, Djalante R. From decarbonization to low carbon development and transition: A systematic literature review of the conceptualization of moving toward net-zero carbon dioxide emission (1995–2019). *J Clean Prod* 2020;256:120307. <https://doi.org/10.1016/J.JCLEPRO.2020.120307>.
- [578] Campos I, Marín-González E. People in transitions: Energy citizenship, prosumerism and social movements in Europe. *Energy Res Soc Sci* 2020;69:101718. <https://doi.org/10.1016/J.ERSS.2020.101718>.
- [579] Paulus N. From “equity” carbon budget to individual carbon footprint mitigation pathways : examples for Wallonia and France. To Be Submitted 2023.
- [580] Collet P, Flottes E, Favre A, Raynal L, Pierre H, Capela S, et al. Techno-economic and Life Cycle Assessment of methane production via biogas upgrading and power to gas technology. *Appl Energy* 2017;192:282–95. <https://doi.org/10.1016/J.APENERGY.2016.08.181>.
- [581] Kumara Behera B, Varma A. Biomethanization. *Microbial Resources for Sustainable Energy*, Springer, Cham; 2016, p. 35–122. [https://doi.org/10.1007/978-3-319-33778-4\\_2](https://doi.org/10.1007/978-3-319-33778-4_2).
- [582] Dávila C, Paulus N, Lemort V. Experimental Investigation of a Gas Driven Absorption Heat Pump and In-Situ Monitoring. *Proceedings of the 9th Heat Powered Cycles International Conference (HPC 2021)* 2022.

- [583] International Organization for Standardization. ISO 6976 - Natural gas - Calculation of calorific values, density, relative density and Wobbe index from composition. 1995.
- [584] Simpson DA. Chapter Zero - Introduction. Practical Onshore Gas Field Engineering, Gulf Professional Publishing; 2017, p. 1–43. <https://doi.org/10.1016/B978-0-12-813022-3.00021-3>.
- [585] International Organization for Standardization. ISO 12213-3 - Natural gas - Calculation of compression factor - Part 3: Calculation using physical properties. 2006.
- [586] Jaeschke S, Humprheys A. GERG Technical Monograph 5 (TM5) - Standard GERG Virial Equation for Field Use. 1991.
- [587] Shaw K. Fundamental Principles of Pressure Regulators. Proceedings of the 38th American School of Gas Measurement Technology (ASGMT 2003) 2003.
- [588] Patil MG, Barjibhe RB. Flow Analysis of Gas Pressure Regulator by Numerical & Experimental Method. International Research Journal of Engineering and Technology 2018;5.
- [589] Squire Energy. Gas Pressures - FAQ's. 2017.
- [590] Ozturk M, Dincer I. Development of renewable energy system integrated with hydrogen and natural gas subsystems for cleaner combustion. J Nat Gas Sci Eng 2020;83:103583. <https://doi.org/10.1016/J.JNGSE.2020.103583>.
- [591] Institution of Gas Engineers and Managers. IGEM/GM/PRS/41 - Low pressure meter installation kits. 2019.
- [592] Haeseldonckx D, D'haeseleer W. The use of the natural-gas pipeline infrastructure for hydrogen transport in a changing market structure. Int J Hydrogen Energy 2007;32:1381–6. <https://doi.org/10.1016/J.IJHYDENE.2006.10.018>.
- [593] CREG. (F)1736 - Study on the cost-effectiveness of natural gas (CNG or compressed natural gas) used as fuel in cars. Commission de Régulation de l'Electricité et Du Gaz 2018.
- [594] fvb ffc constructiv. Manuel modulaire chauffage central : Module 7 - Installations au gaz - Volume 3 - Annexes (D/2012/1698/15). Fonds de Formation Professionnelle de La Construction 2012.
- [595] Dury M, Ginion S, Erpicum M. Estimation de la transparence de l'atmosphère par ciel clair à la Station scientifique des Hautes-Fagnes (SSHF), Mont Rigi, Belgique. Comparaison avec la Station d'Uccle-Bruxelles (IRM). Bulletin de La Société Géographique de Liège 2008;51.
- [596] Cavcar M. The International Standard Atmosphere (ISA). 2000.
- [597] International Civil Aviation Organization. ICAO 7488 - Manual of the ICAO Standard Atmosphere. 1993.
- [598] Daidzic NE. On Atmospheric Lapse Rates. International Journal of Aviation, Aeronautics, and Aerospace 2019;6:2. <https://doi.org/10.15394/ijaaa.2019.1374>.
- [599] Liu F, Zheng L, Zhang R. Emissions and thermal efficiency for premixed burners in a condensing gas boiler. Energy 2020;202:117449. <https://doi.org/10.1016/J.ENERGY.2020.117449>.
- [600] Habib MA, Elshafei M, Dajani M. Influence of combustion parameters on NOx production in an industrial boiler. Comput Fluids 2008;37:12–23. <https://doi.org/10.1016/J.COMPFLUID.2007.04.006>.
- [601] Buderus. Installation instructions - Condensing gas boiler - Logamax plus GB142-24/30/45/60. 7215 0200 (11/2011) US/CA 2011.

- [602] Parravicini M, Barro C, Boulouchos K. Compensation for the differences in LHV of diesel-OME blends by using injector nozzles with different number of holes: Emissions and combustion. *Fuel* 2020;259:116166. <https://doi.org/10.1016/j.fuel.2019.116166>.
- [603] Hall JE, Hooker P, Jeffrey KE. Gas detection of hydrogen/natural gas blends in the gas industry. *Int J Hydrogen Energy* 2021;46:12555–65. <https://doi.org/10.1016/j.ijhydene.2020.08.200>.
- [604] McDonald R. Evaluation of Gas, Oil and Wood Pellet Fueled Residential Heating System Emissions Characteristics. Upton, NY (United States): 2009. <https://doi.org/10.2172/1015127>.
- [605] Bruijstens AJ, Beuman WPH, Molen MVD, Rijke JD, Cloudt RPM, Kadijk G, et al. Biogas Composition and Engine Performance, Including Database and Biogas Property Model. *BiogasMax* 2008.
- [606] Zlateva P, Penkova N, Krumov K. Analysis of combustion efficiency at boilers operating on different fuels. 2020 7th International Conference on Energy Efficiency and Agricultural Engineering (EE&AE), IEEE; 2020, p. 1–4. <https://doi.org/10.1109/EEAE49144.2020.9278784>.
- [607] Bălănescu D-T, Homutescu V-M. Experimental Study on the Combustion System Optimization in the Case of a 36 kW Condensing Boiler. *Procedia Eng* 2017;181:706–11. <https://doi.org/10.1016/j.proeng.2017.02.453>.
- [608] TSI Incorporated. An Overview of Measurements, Methods and Calculations Used in Combustion Analysis. 2004.
- [609] Pilusa TJ, Mollagee MM, Muzenda E. Reduction of Vehicle Exhaust Emissions from Diesel Engines Using the Whale Concept Filter. *Aerosol Air Qual Res* 2012;12:994–1006. <https://doi.org/10.4209/aaqr.2012.04.0100>.
- [610] Bowman CT. Kinetics of pollutant formation and destruction in combustion. *Prog Energy Combust Sci* 1975;1:33–45. [https://doi.org/10.1016/0360-1285\(75\)90005-2](https://doi.org/10.1016/0360-1285(75)90005-2).
- [611] European Commission. EN 590:2009 - Automotive fuels - Diesel - Requirements and test methods. 2009.
- [612] Wade J, Farrauto RJ. Controlling emissions of pollutants in urban areas. *Metropolitan Sustainability*, Elsevier; 2012, p. 260–91. <https://doi.org/10.1533/9780857096463.3.260>.
- [613] Pavlovic J, Tansini A, Fontaras G, Ciuffo B, Garcia Otura M, Trentadue G, et al. The Impact of WLTP on the Official Fuel Consumption and Electric Range of Plug-in Hybrid Electric Vehicles in Europe, 2017. <https://doi.org/10.4271/2017-24-0133>.
- [614] Vanwormer C, Grassl D. Best Practices for Condensing Boilers. *ASHRAE J* 2018.
- [615] Kundu S, Fowler M, Simon LC, Abouatallah R. Reversible and irreversible degradation in fuel cells during Open Circuit Voltage durability testing. *J Power Sources* 2008;182:254–8. <https://doi.org/10.1016/j.jpowsour.2008.04.009>.
- [616] Gazdzick P, Mitzel J, Garcia Sanchez D, Schulze M, Friedrich KA. Evaluation of reversible and irreversible degradation rates of polymer electrolyte membrane fuel cells tested in automotive conditions. *J Power Sources* 2016;327:86–95. <https://doi.org/10.1016/j.jpowsour.2016.07.049>.
- [617] Jouin M, Gouriveau R, Hissel D, Péra M-C, Zerhouni N. Degradations analysis and aging modeling for health assessment and prognostics of PEMFC. *Reliability Engineering & System Safety* 2016;148:78–95. <https://doi.org/10.1016/j.res.2015.12.003>.

- [618] Zhang J, Zhang H, Wu J, Zhang J. Chapter 7 - Fuel Cell Open Circuit Voltage. *Pem Fuel Cell Testing and Diagnosis*, Elsevier; 2013, p. 187–200. <https://doi.org/10.1016/B978-0-444-53688-4.00007-3>.
- [619] Yousfi-Steiner N, Moçotéguy Ph, Candusso D, Hissel D, Hernandez A, Aslanides A. A review on PEM voltage degradation associated with water management: Impacts, influent factors and characterization. *J Power Sources* 2008;183:260–74. <https://doi.org/10.1016/j.jpowsour.2008.04.037>.
- [620] Rohendi D, Majlan EH, Mohamad AB, Daud WRW, Kadhum AAH, Shyuan LK. Effects of temperature and backpressure on the performance degradation of MEA in PEMFC. *Int J Hydrogen Energy* 2015;40:10960–8. <https://doi.org/10.1016/j.ijhydene.2015.06.161>.
- [621] Bharti A, Natarajan R. Chapter 7 - Proton exchange membrane testing and diagnostics. *PEM Fuel Cells: Fundamentals, Advanced Technologies, and Practical Application*, Elsevier; 2022, p. 137–71. <https://doi.org/10.1016/B978-0-12-823708-3.00007-9>.
- [622] Yuan X, Wang H, Colinsun J, Zhang J. AC impedance technique in PEM fuel cell diagnosis—A review. *Int J Hydrogen Energy* 2007;32:4365–80. <https://doi.org/10.1016/j.ijhydene.2007.05.036>.
- [623] Climent V, Feliu JM. Cyclic Voltammetry. *Encyclopedia of Interfacial Chemistry: Surface Science and Electrochemistry*, Elsevier; 2018, p. 48–74. <https://doi.org/10.1016/B978-0-12-409547-2.10764-4>.
- [624] Forster RJ, Walsh D, Adamson K, Spain E. Voltammetry | Overview. *Encyclopedia of Analytical Science (Third Edition)*, Academic Press; 2019, p. 209–17. <https://doi.org/10.1016/B978-0-12-409547-2.14562-7>.
- [625] Wagner N. Electrochemical Impedance Spectroscopy. *PEM Fuel Cell Diagnostic Tools*, Routledge Handbooks Online; 2011, p. 37–70. <https://doi.org/10.1201/B11100-5>.
- [626] Pletcher D, Greff R, Peat R, Peter LM, Robinson J. Potential sweep techniques and cyclic voltammetry. *Instrumental Methods in Electrochemistry*, Woodhead Publishing; 2010, p. 178–228. <https://doi.org/10.1533/9781782420545.178>.
- [627] Saleh FS, Easton EB. Diagnosing Degradation within PEM Fuel Cell Catalyst Layers Using Electrochemical Impedance Spectroscopy. *J Electrochem Soc* 2012;159:B546–53. <https://doi.org/10.1149/2.098205jes>.
- [628] Bezmalinovic D, Simic B, Barbir F. Characterization of PEM fuel cell degradation by polarization change curves. *J Power Sources* 2015;294:82–7. <https://doi.org/10.1016/j.jpowsour.2015.06.047>.
- [629] Wang F, Yang D, Li B, Zhang H, Hao C, Chang F, et al. Investigation of the recoverable degradation of PEM fuel cell operated under drive cycle and different humidities. *Int J Hydrogen Energy* 2014;39:14441–7. <https://doi.org/10.1016/j.ijhydene.2014.02.023>.
- [630] Kreitmeier S, Schuler GA, Wokaun A, Büchi FN. Investigation of membrane degradation in polymer electrolyte fuel cells using local gas permeation analysis. *J Power Sources* 2012;212:139–47. <https://doi.org/10.1016/j.jpowsour.2012.03.071>.
- [631] Schalenbach M, Hoefner T, Paciok P, Carmo M, Lueke W, Stolten D. Gas Permeation through Nafion. Part 1: Measurements. *The Journal of Physical Chemistry C* 2015;119:25145–55. <https://doi.org/10.1021/acs.jpcc.5b04155>.

- [632] Baik KD, Hong BK, Kim MS. Novel technique for measuring oxygen crossover through the membrane in polymer electrolyte membrane fuel cells. *Int J Hydrogen Energy* 2013;38:8927–33. <https://doi.org/10.1016/j.ijhydene.2013.04.142>.
- [633] Young AP, Stumper J, Gyenge E. Characterizing the Structural Degradation in a PEMFC Cathode Catalyst Layer: Carbon Corrosion. *J Electrochem Soc* 2009;156:B913. <https://doi.org/10.1149/1.3139963>.
- [634] Baik KD, Kim MS. Characterization of nitrogen gas crossover through the membrane in proton-exchange membrane fuel cells. *Int J Hydrogen Energy* 2011;36:732–9. <https://doi.org/10.1016/j.ijhydene.2010.09.046>.
- [635] Huang X, Solasi R, Zou Y, Feshler M, Reifsnider K, Condit D, et al. Mechanical endurance of polymer electrolyte membrane and PEM fuel cell durability. *J Polym Sci B Polym Phys* 2006;44:2346–57. <https://doi.org/10.1002/polb.20863>.
- [636] Kreitmeier S, Michiardi M, Wokaun A, Büchi FN. Factors determining the gas crossover through pinholes in polymer electrolyte fuel cell membranes. *Electrochim Acta* 2012;80:240–7. <https://doi.org/10.1016/j.electacta.2012.07.013>.
- [637] Izhan Noor Azam AM, Choon PM, Masdar MS, Zainoodin AM, Husaini T. Performance and water transport behaviour in Polymer Electrolyte Membrane fuel cells. *Int J Hydrogen Energy* 2022;47:40803–13. <https://doi.org/10.1016/j.ijhydene.2021.12.146>.
- [638] Santangelo PE, Tartarini P. Effects of load variation and purge cycles on the efficiency of Polymer Electrolyte Membrane Fuel Cells for stationary applications. *Journal of Renewable and Sustainable Energy* 2018;10:014301. <https://doi.org/10.1063/1.5000936>.
- [639] Zhao J, Jian Q, Huang Z. Experimental and theoretical study on improving the operating characteristics of an open-cathode PEMFC stack by generating periodic disturbances at anode. *Energy Convers Manag* 2019;196:1433–44. <https://doi.org/10.1016/j.enconman.2019.06.034>.
- [640] Li H, Tang Y, Wang Z, Shi Z, Wu S, Song D, et al. A review of water flooding issues in the proton exchange membrane fuel cell. *J Power Sources* 2008;178:103–17. <https://doi.org/10.1016/j.jpowsour.2007.12.068>.
- [641] Zhao J, Tu Z, Chan SH. Carbon corrosion mechanism and mitigation strategies in a proton exchange membrane fuel cell (PEMFC): A review. *J Power Sources* 2021;488:229434. <https://doi.org/10.1016/j.jpowsour.2020.229434>.
- [642] Van Nguyen T, Knobbe MW. A liquid water management strategy for PEM fuel cell stacks. *J Power Sources* 2003;114:70–9. [https://doi.org/10.1016/s0378-7753\(02\)00591-8](https://doi.org/10.1016/s0378-7753(02)00591-8).
- [643] Knobbe MW, He W, Chong PY, Nguyen T V. Active gas management for PEM fuel cell stacks. *J Power Sources* 2004;138:94–100. <https://doi.org/10.1016/j.jpowsour.2004.06.029>.
- [644] Nikiforow K, Karimäki H, Keränen TM, Ihonen J. Optimization study of purge cycle in proton exchange membrane fuel cell system. *J Power Sources* 2013;238:336–44. <https://doi.org/10.1016/j.jpowsour.2012.11.153>.
- [645] Wang B, Deng H, Jiao K. Purge strategy optimization of proton exchange membrane fuel cell with anode recirculation. *Appl Energy* 2018;225:1–13. <https://doi.org/10.1016/j.apenergy.2018.04.058>.
- [646] Dumercy L, Péra M-C, Glises R, Hissel D, Hamandi S, Badin F, et al. PEFC Stack Operating in Anodic Dead End Mode. *Fuel Cells* 2004;4:352–7. <https://doi.org/10.1002/fuce.200400053>.

- [647] Jian Q, Luo L, Huang B, Zhao J, Cao S, Huang Z. Experimental study on the purge process of a proton exchange membrane fuel cell stack with a dead-end anode. *Appl Therm Eng* 2018;142:203–14. <https://doi.org/10.1016/j.applthermaleng.2018.07.001>.
- [648] Yu X, Pingwen M, Ming H, Baolian Y, Shao Z-G. The critical pressure drop for the purge process in the anode of a fuel cell. *J Power Sources* 2009;188:163–9. <https://doi.org/10.1016/j.jpowsour.2008.11.105>.
- [649] Rabbani A, Rokni M. Effect of nitrogen crossover on purging strategy in PEM fuel cell systems. *Appl Energy* 2013;111:1061–70. <https://doi.org/10.1016/j.apenergy.2013.06.057>.
- [650] Baschuk JJ, Li X. Carbon monoxide poisoning of proton exchange membrane fuel cells. *Int J Energy Res* 2001;25:695–713. <https://doi.org/10.1002/er.713>.
- [651] Ham DJ, Kim YK, Han SH, Lee JS. Pt/WC as an anode catalyst for PEMFC: Activity and CO tolerance. *Catal Today* 2008;132:117–22. <https://doi.org/10.1016/j.cattod.2007.12.076>.
- [652] Gu T, Lee W-K, Zee JW Van. Quantifying the ‘reverse water gas shift’ reaction inside a PEM fuel cell. *Appl Catal B* 2005;56:43–50. <https://doi.org/10.1016/j.apcatb.2004.08.016>.
- [653] Jiménez S, Soler J, Valenzuela RX, Daza L. Assessment of the performance of a PEMFC in the presence of CO. *J Power Sources* 2005;151:69–73. <https://doi.org/10.1016/j.jpowsour.2005.02.049>.
- [654] Yim S-D, Sohn Y-J, Yoon Y-G, Um S, Kim C-S, Lee W-Y. Operating characteristics of 40W-class PEMFC stacks using reformed gas under low humidifying conditions. *J Power Sources* 2008;178:711–5. <https://doi.org/10.1016/j.jpowsour.2007.09.104>.
- [655] Cheng X, Shi Z, Glass N, Zhang L, Zhang J, Song D, et al. A review of PEM hydrogen fuel cell contamination: Impacts, mechanisms, and mitigation. *J Power Sources* 2007;165:739–56. <https://doi.org/10.1016/j.jpowsour.2006.12.012>.
- [656] Chen C-H, Chung C-C, Lin H-H, Yan Y-Y. Improvement of CO Tolerance of Proton Exchange Membrane Fuel Cell by an Air-Bleeding Technique. *J Fuel Cell Sci Technol* 2008;5. <https://doi.org/10.1115/1.2784278>.
- [657] Zamel N, Li X. Transient analysis of carbon monoxide poisoning and oxygen bleeding in a PEM fuel cell anode catalyst layer. *Int J Hydrogen Energy* 2008;33:1335–44. <https://doi.org/10.1016/j.ijhydene.2007.12.060>.
- [658] Pérez LC, Rajala T, Ihonen J, Koski P, Sousa JM, Mendes A. Development of a methodology to optimize the air bleed in PEMFC systems operating with low quality hydrogen. *Int J Hydrogen Energy* 2013;38:16286–99. <https://doi.org/10.1016/j.ijhydene.2013.10.037>.
- [659] Hedstrom L, Tingelof T, Alvfors P, Lindbergh G. Experimental results from a 5kW PEM fuel cell stack operated on simulated reformat from highly diluted hydrocarbon fuels: Efficiency, dilution, fuel utilisation, CO poisoning and design criteria. *Int J Hydrogen Energy* 2009;34:1508–14. <https://doi.org/10.1016/j.ijhydene.2008.11.079>.
- [660] Sung L-Y, Hwang B-J, Hsueh K-L, Su W-N, Yang C-C. Comprehensive study of an air bleeding technique on the performance of a proton-exchange membrane fuel cell subjected to CO poisoning. *J Power Sources* 2013;242:264–72. <https://doi.org/10.1016/j.jpowsour.2013.05.042>.
- [661] Tullius V, Zobel M, Dyck A. Development of a Heuristic Control Algorithm for Detection and Regeneration of CO Poisoned LT-PEMFC Stacks in Stationary Applications. *Energies (Basel)* 2020;13:4648. <https://doi.org/10.3390/en13184648>.

- [662] Decoopman B, Vincent R, Rosini S, Paganelli G, Thivel P-X. Proton exchange membrane fuel cell reversible performance loss induced by carbon monoxide produced during operation. *J Power Sources* 2016;324:492–8. <https://doi.org/10.1016/j.jpowsour.2016.05.113>.
- [663] Thomason AH, Lalk TR, Appleby AJ. Effect of current pulsing and “self-oxidation” on the CO tolerance of a PEM fuel cell. *J Power Sources* 2004;135:204–11. <https://doi.org/10.1016/j.jpowsour.2004.03.070>.
- [664] Sung L-Y, Hwang B-J, Hsueh K-L, Tsau F-H. Effects of anode air bleeding on the performance of CO-poisoned proton-exchange membrane fuel cells. *J Power Sources* 2010;195:1630–9. <https://doi.org/10.1016/j.jpowsour.2009.09.062>.
- [665] Farrell CG, Gardner CL, Ternan M. Experimental and modelling studies of CO poisoning in PEM fuel cells. *J Power Sources* 2007;171:282–93. <https://doi.org/10.1016/j.jpowsour.2007.07.006>.
- [666] Delgado S, Lagarteira T, Mendes A. Air Bleeding Strategies to Increase the Efficiency of Proton Exchange Membrane Fuel Cell Stationary Applications Fuelled with CO ppm-levels. *Int J Electrochem Sci* 2020;15:613–27. <https://doi.org/10.20964/2020.01.58>.
- [667] Iwase M. Optimized Co Tolerant Electrocatalysts for Polymer Electrolyte Fuel Cells. *ECS Proceedings Volumes* 1995;1995–23:12–23. <https://doi.org/10.1149/199523.0012PV>.
- [668] Das SK, Reis A, Berry KJ. Experimental evaluation of CO poisoning on the performance of a high temperature proton exchange membrane fuel cell. *J Power Sources* 2009;193:691–8. <https://doi.org/10.1016/j.jpowsour.2009.04.021>.
- [669] Gilman S. The Mechanism of Electrochemical Oxidation of Carbon Monoxide and Methanol on Platinum. II. The “Reactant-Pair” Mechanism for Electrochemical Oxidation of Carbon Monoxide and Methanol. *J Phys Chem* 1964;68:70–80. <https://doi.org/10.1021/j100783a013>.
- [670] Noda Z, Hirata K, Hayashi A, Taniguchi S, Nakazato N, Seo A, et al. PEFC-type impurity sensors for hydrogen fuels. *Int J Hydrogen Energy* 2012;37:16256–63. <https://doi.org/10.1016/j.ijhydene.2012.08.062>.
- [671] Bhatia KK, Wang C-Y. Transient carbon monoxide poisoning of a polymer electrolyte fuel cell operating on diluted hydrogen feed. *Electrochim Acta* 2004;49:2333–41. <https://doi.org/10.1016/j.electacta.2004.01.014>.
- [672] Ozdemir MO, Pasaogullari U. Modeling the oscillative behavior and carbon monoxide removal by current pulsing technique in H<sub>2</sub>/CO mixtures for Pt catalyst layer. *Int J Hydrogen Energy* 2016;41:10854–69. <https://doi.org/10.1016/j.ijhydene.2016.05.055>.
- [673] Sarma PJ, Gardner CL, Chugh S, Sharma A, Kjeang E. Strategic implementation of pulsed oxidation for mitigation of CO poisoning in polymer electrolyte fuel cells. *J Power Sources* 2020;468:228352. <https://doi.org/10.1016/j.jpowsour.2020.228352>.
- [674] Carrette LPL, Friedrich KA, Huber M, Stimming U. Improvement of CO tolerance of proton exchange membrane (PEM) fuel cells by a pulsing technique. *Physical Chemistry Chemical Physics* 2001;3:320–4. <https://doi.org/10.1039/b005843m>.
- [675] Wingelaar PJH, Geers MPA, Duarte JL, Hendrix MAM. CO-tolerant operation of platinum-loaded PEM fuel cells. *IEEE International Symposium on Industrial Electronics* 2007:2631–6. <https://doi.org/10.1109/ISIE.2007.4375023>.
- [676] Guo SM, Hasan ABM. Proton Exchange Membrane Fuel Cell High Carbon Monoxide Tolerance Operation Using Pulsed Heating and Pressure Swing. *J Fuel Cell Sci Technol* 2008;6. <https://doi.org/10.1115/1.2972163>.

- [677] Baturina OA, Dyatkin B, Reshetenko T V. Influence of air impurities on the performance of nanostructured PEMFC catalysts. *Nanostructured Materials for Next-Generation Energy Storage and Conversion: Fuel Cells*, Springer Berlin Heidelberg; 2018, p. 407–41. [https://doi.org/10.1007/978-3-662-56364-9\\_14/TABLES/2](https://doi.org/10.1007/978-3-662-56364-9_14/TABLES/2).
- [678] Zhang Y, Chen S, Wang Y, Ding W, Wu R, Li L, et al. Study of the degradation mechanisms of carbon-supported platinum fuel cells catalyst via different accelerated stress test. *J Power Sources* 2015;273:62–9. <https://doi.org/10.1016/J.JPOWSOUR.2014.09.012>.
- [679] Xie J, Wood DL, More KL, Atanassov P, Borup RL. Microstructural Changes of Membrane Electrode Assemblies during PEFC Durability Testing at High Humidity Conditions. *J Electrochem Soc* 2005;152:A1011. <https://doi.org/10.1149/1.1873492/XML>.
- [680] Darling RM, Meyers JP. Kinetic Model of Platinum Dissolution in PEMFCs. *J Electrochem Soc* 2003;150:A1523. <https://doi.org/10.1149/1.1613669/XML>.
- [681] Wang Z-B, Zuo P-J, Chu Y-Y, Shao Y-Y, Yin G-P. Durability studies on performance degradation of Pt/C catalysts of proton exchange membrane fuel cell. *Int J Hydrogen Energy* 2009;34:4387–94. <https://doi.org/10.1016/j.ijhydene.2009.03.045>.
- [682] Kim L, Chung CG, Sung YW, Chung JS. Dissolution and migration of platinum after long-term operation of a polymer electrolyte fuel cell under various conditions. *J Power Sources* 2008;183:524–32. <https://doi.org/10.1016/j.jpowsour.2008.05.062>.
- [683] Ren P, Pei P, Li Y, Wu Z, Chen D, Huang S. Degradation mechanisms of proton exchange membrane fuel cell under typical automotive operating conditions. *Prog Energy Combust Sci* 2020;80:100859. <https://doi.org/10.1016/j.pecs.2020.100859>.
- [684] Rinaldo SG, Lee W, Stumper J, Eikerling M. Mechanistic Principles of Platinum Oxide Formation and Reduction. *Electrocatalysis* 2014;5:262–72. <https://doi.org/10.1007/s12678-014-0189-y>.
- [685] Zhang S, Yuan X-Z, Hin JNC, Wang H, Wu J, Friedrich KA, et al. Effects of open-circuit operation on membrane and catalyst layer degradation in proton exchange membrane fuel cells. *J Power Sources* 2010;195:1142–8. <https://doi.org/10.1016/j.jpowsour.2009.08.070>.
- [686] Zhang X, Guo L, Liu H. Recovery mechanisms in proton exchange membrane fuel cells after accelerated stress tests. *J Power Sources* 2015;296:327–34. <https://doi.org/10.1016/j.jpowsour.2015.07.063>.
- [687] Owejan JP, Owejan JE, Gu W. Impact of Platinum Loading and Catalyst Layer Structure on PEMFC Performance. *J Electrochem Soc* 2013;160:F824–33. <https://doi.org/10.1149/2.072308jes>.
- [688] Dhanushkodi SR, Kundu S, Fowler MW, Pritzker MD. Study of the effect of temperature on Pt dissolution in polymer electrolyte membrane fuel cells via accelerated stress tests. *J Power Sources* 2014;245:1035–45. <https://doi.org/10.1016/j.jpowsour.2013.07.016>.
- [689] Bezmalinović D, Radošević J, Barbir F. Initial conditioning of Polymer Electrolyte Membrane fuel cell by temperature and potential cycling. *Acta Chim Slov* 2015;62. <https://doi.org/10.17344/acsi.2014.730>.
- [690] Yuan X-Z, Zhang S, Sun JC, Wang H. A review of accelerated conditioning for a polymer electrolyte membrane fuel cell. *J Power Sources* 2011;196:9097–106. <https://doi.org/10.1016/j.jpowsour.2011.06.098>.



- [691] Bi W, Gray GE, Fuller TF. PEM Fuel Cell Pt/C Dissolution and Deposition in Nafion Electrolyte. *Electrochemical and Solid-State Letters* 2007;10:B101. <https://doi.org/10.1149/1.2712796>.
- [692] Kim J-H, Lee H-I, Bae B, Yong Ha H, Shukla AK, Christensen PA, et al. Electrochemical Analysis of the Pre-Conditioning Effects on DMFC Performance. *Electrochim Acta* 1983;45.
- [693] Xie Z, Zhao X, Adachi M, Shi Z, Mashio T, Ohma A, et al. Fuel cell cathode catalyst layers from “green” catalyst inks. *Energy Environ Sci* 2008;1:184. <https://doi.org/10.1039/b808613n>.
- [694] Zago M, Baricci A, Bisello A, Jahnke T, Yu H, Maric R, et al. Experimental analysis of recoverable performance loss induced by platinum oxide formation at the polymer electrolyte membrane fuel cell cathode. *J Power Sources* 2020;455:227990. <https://doi.org/10.1016/j.jpowsour.2020.227990>.
- [695] Gould BD, Bender G, Bethune K, Dorn S, Baturina OA, Rocheleau R, et al. Operational Performance Recovery of SO<sub>2</sub>-Contaminated Proton Exchange Membrane Fuel Cells. *J Electrochem Soc* 2010;157:B1569. <https://doi.org/10.1149/1.3483108>.
- [696] Shi W, Yi B, Hou M, Shao Z. The effect of H<sub>2</sub>S and CO mixtures on PEMFC performance. *Int J Hydrogen Energy* 2007;32:4412–7. <https://doi.org/10.1016/j.ijhydene.2007.06.029>.
- [697] Kani Y, Wakita H, Fujihara S, Nakajima T. Fuel cell system and operation method for fuel cell system. WO2011036886A1, 2011.
- [698] Deng J, Wang X, Wei Z, Wang L, Wang C, Chen Z. A review of NO<sub>x</sub> and SO<sub>x</sub> emission reduction technologies for marine diesel engines and the potential evaluation of liquefied natural gas fuelled vessels. *Science of The Total Environment* 2021;766:144319. <https://doi.org/10.1016/j.scitotenv.2020.144319>.
- [699] CWaPE. Vade-mecum: Injection de biométhane dans le réseau de distribution. 2019.
- [700] Jayaraj P, Karthika P, Rajalakshmi N, Dhathathreyan KS. Mitigation studies of sulfur contaminated electrodes for PEMFC. *Int J Hydrogen Energy* 2014;39:12045–51. <https://doi.org/10.1016/j.ijhydene.2014.06.011>.
- [701] Kakati BK, Kucernak ARJ. Gas phase recovery of hydrogen sulfide contaminated polymer electrolyte membrane fuel cells. *J Power Sources* 2014;252:317–26. <https://doi.org/10.1016/j.jpowsour.2013.11.077>.
- [702] Nagahara Y, Sugawara S, Shinohara K. The impact of air contaminants on PEMFC performance and durability. *J Power Sources* 2008;182:422–8. <https://doi.org/10.1016/j.jpowsour.2007.12.091>.
- [703] Office of Energy Efficiency & Renewable Energy - Fuel Cell Technologies Office (FCTO). Multi-Year Research, Development, and Demonstration Plan - 3.4 Fuel Cells. US Department of Energy (DOE) 2016.
- [704] Gould B, Swider-Lyons K, Baturina OA. Performance recovery of a fuel cell. US10026981B2, 2018.
- [705] van Beurden P. On the catalytic aspects of steam-methane reforming. Energy Research Centre of the Netherlands (ECN) 2004.
- [706] Abdelsadek Z, Sehailia M, Halliche D, Gonzalez-Delacruz VM, Holgado JP, Bachari K, et al. In-situ hydrogasification/regeneration of NiAl-hydrotalcite derived catalyst in the reaction of CO<sub>2</sub> reforming of methane: A versatile approach to catalyst recycling. *Journal of CO<sub>2</sub> Utilization* 2016;14:98–105. <https://doi.org/10.1016/j.jcou.2016.03.004>.

- [707] Ferreira-Aparicio P, Guerrero-Ruiz A, Rodríguez-Ramos I. Comparative study at low and medium reaction temperatures of syngas production by methane reforming with carbon dioxide over silica and alumina supported catalysts. *Appl Catal A Gen* 1998;170:177–87. [https://doi.org/10.1016/s0926-860x\(98\)00048-9](https://doi.org/10.1016/s0926-860x(98)00048-9).
- [708] Zhang J-C, Ge B-H, Liu T-F, Yang Y-Z, Li B, Li W-Z. Robust Ruthenium-Saving Catalyst for High-Temperature Carbon Dioxide Reforming of Methane. *ACS Catal* 2019;10:783–91. <https://doi.org/10.1021/acscatal.9b03709>.
- [709] Spivey JJ. Chapter 10 - Deactivation of Reforming Catalysts. *Fuel Cells: Technologies for Fuel Processing*, Elsevier; 2011, p. 285–315. <https://doi.org/10.1016/B978-0-444-53563-4.10010-0>.
- [710] Alenazey F, Cooper CG, Dave CB, Elnashaie SSEH, Susu AA, Adesina AA. Coke removal from deactivated Co–Ni steam reforming catalyst using different gasifying agents: An analysis of the gas–solid reaction kinetics. *Catal Commun* 2009;10:406–11. <https://doi.org/10.1016/j.catcom.2008.10.010>.
- [711] Bu K, Kuboon S, Deng J, Li H, Yan T, Chen G, et al. Methane dry reforming over boron nitride interface-confined and LDHs-derived Ni catalysts. *Appl Catal B* 2019;252:86–97. <https://doi.org/10.1016/j.apcatb.2019.04.007>.
- [712] Zhou J, Zhao J, Zhang J, Zhang T, Ye M, Liu Z. Regeneration of catalysts deactivated by coke deposition: A review. *Chinese Journal of Catalysis* 2020;41:1048–61. [https://doi.org/10.1016/s1872-2067\(20\)63552-5](https://doi.org/10.1016/s1872-2067(20)63552-5).
- [713] Vogt C, Kranenborg J, Monai M, Weckhuysen BM. Structure Sensitivity in Steam and Dry Methane Reforming over Nickel: Activity and Carbon Formation. *ACS Catal* 2019;10:1428–38. <https://doi.org/10.1021/acscatal.9b04193>.
- [714] Chen P, Zhang H-B, Lin G-D, Tsai K-R. Development of coking-resistant Ni-based catalyst for partial oxidation and CO<sub>2</sub>-reforming of methane to syngas. *Appl Catal A Gen* 1998;166:343–50. [https://doi.org/10.1016/s0926-860x\(97\)00291-3](https://doi.org/10.1016/s0926-860x(97)00291-3).
- [715] Wang Y, Chin YH, Rozmiarek RT, Johnson BR, Gao Y, Watson J, et al. Highly active and stable Rh/MgOAl<sub>2</sub>O<sub>3</sub> catalysts for methane steam reforming. *Catal Today* 2004;98:575–81. <https://doi.org/10.1016/j.cattod.2004.09.011>.
- [716] Ayodele B V, Cheng CK. Process Modelling, Thermodynamic Analysis and Optimization of Dry Reforming, Partial Oxidation and Auto-Thermal Methane Reforming for Hydrogen and Syngas production. *Chemical Product and Process Modeling* 2015;10:211–20. <https://doi.org/10.1515/cppm-2015-0027>.
- [717] Chandan A, Hattenberger M, El-kharouf A, Du S, Dhir A, Self V, et al. High temperature (HT) polymer electrolyte membrane fuel cells (PEMFC) – A review. *J Power Sources* 2013;231:264–78. <https://doi.org/10.1016/j.jpowsour.2012.11.126>.
- [718] Mitzel J, Zhang Q, Gazdzicki P, Friedrich KA. Review on mechanisms and recovery procedures for reversible performance losses in polymer electrolyte membrane fuel cells. *J Power Sources* 2021;488:229375. <https://doi.org/10.1016/j.jpowsour.2020.229375>.
- [719] Fowles M, Carlsson M. Steam Reforming of Hydrocarbons for Synthesis Gas Production. *Top Catal* 2021;64:856–75. <https://doi.org/10.1007/s11244-021-01496-z>.
- [720] Kobayashi S, Fujishima S, Ono J, Kuwabara T, Yoshino Y. Ammonia removing method and ammonia removing device. JP2005317419A, 2005.
- [721] Halseid R, Vie PJS, Tunold R. Effect of ammonia on the performance of polymer electrolyte membrane fuel cells. *J Power Sources* 2006;154:343–50. <https://doi.org/10.1016/j.jpowsour.2005.10.011>.

- [722] Garzon F, Lopes T, Rockward T, Sansiñena J-M, Kienitz B, Mukundan R. The Impact of Impurities on Long-Term PEMFC Performance. *ECS Trans* 2009;25:1575–83. <https://doi.org/10.1149/1.3210713>.
- [723] Gomez YA, Oyarce A, Lindbergh G, Lagergren C. Ammonia Contamination of a Proton Exchange Membrane Fuel Cell. *J Electrochem Soc* 2018;165:F189–97. <https://doi.org/10.1149/2.0761803jes>.
- [724] Hongsirikarn K, Goodwin JG, Greenway S, Creager S. Effect of cations (Na<sup>+</sup>, Ca<sup>2+</sup>, Fe<sup>3+</sup>) on the conductivity of a Nafion membrane. *J Power Sources* 2010;195:7213–20. <https://doi.org/10.1016/j.jpowsour.2010.05.005>.
- [725] Wakita H, Kani Y, Fujihara S, Ukai K, Maenishi A. Hydrogen generator, fuel cell system and their operating methods. US8652224B2, 2014.
- [726] Raghuvanshi S, Maheshwari G. Analysis of Ammonia –Water (NH<sub>3</sub>-H<sub>2</sub>O) Vapor Absorption Refrigeration System based on First Law of Thermodynamics. *Int J Sci Eng Res* 2011;2.
- [727] Eremin AP, Kotov G V, Sidorovich T V, Fisenko SP. Absorption of ammonia by moving drops of water. *Journal of Engineering Physics and Thermophysics* 2007;80:461–8. <https://doi.org/10.1007/s10891-007-0061-5>.
- [728] Sato K, Zaitso S, Kitayama G, Yagi S, Kayada Y, Nishida Y, et al. Operando Spectroscopic Study of the Dynamics of Ru Catalyst during Preferential Oxidation of CO and the Prevention of Ammonia Poisoning by Pt. *JACS Au* 2022;2:1627–37. <https://doi.org/10.1021/jacsau.2c00195>.
- [729] Sato K, Yagi S, Zaitso S, Kitayama G, Kayada Y, Teramura K, et al. Inhibition of Ammonia Poisoning by Addition of Platinum to Ru/ $\alpha$ -Al<sub>2</sub>O<sub>3</sub> for Preferential CO Oxidation in Fuel Cells. *ChemSusChem* 2014;7:3264–7. <https://doi.org/10.1002/cssc.201402583>.
- [730] Wakita H, Ukai K, Takeguchi T, Ueda W. Deactivation of Ru/Al<sub>2</sub>O<sub>3</sub> Catalyst for Preferential CO Oxidation in the Presence of Low-concentration NH<sub>3</sub> by Nitrosyl Species. *Chem Lett* 2006;35:734–5. <https://doi.org/10.1246/CL.2006.734>.
- [731] Wakita H, Ukai K, Takeguchi T, Ueda W. Mechanistic Investigation of Deactivation of Ru/Al<sub>2</sub>O<sub>3</sub> Catalyst for Preferential CO Oxidation in the Presence of NH<sub>3</sub>. *The Journal of Physical Chemistry C* 2007;111:2205–11. <https://doi.org/10.1021/jp065497z>.
- [732] Karimaghloo A, Koo J, Kang H-S, Song SA, Shim JH, Lee MH. Nanoscale Surface and Interface Engineering of Solid Oxide Fuel Cells by Atomic Layer Deposition. *International Journal of Precision Engineering and Manufacturing-Green Technology* 2019;6:611–28. <https://doi.org/10.1007/s40684-019-00090-9>.
- [733] Yang BC, Koo J, Shin JW, Go D, Shim JH, An J. Direct Alcohol-Fueled Low-Temperature Solid Oxide Fuel Cells: A Review. *Energy Technology* 2019;7:5–19. <https://doi.org/10.1002/ente.201700777>.
- [734] Guo L, Calo JM, DiCocco E, Bain EJ. Development of a Low Temperature, Molten Hydroxide Direct Carbon Fuel Cell. *Energy & Fuels* 2013;27:1712–9. <https://doi.org/10.1021/ef302100h>.
- [735] Xie Y, Tang Y, Liu J. A verification of the reaction mechanism of direct carbon solid oxide fuel cells. *Journal of Solid State Electrochemistry* 2013;17:121–7. <https://doi.org/10.1007/s10008-012-1866-5>.
- [736] Aguilar L, Zha S, Cheng Z, Winnick J, Liu M. A solid oxide fuel cell operating on hydrogen sulfide (H<sub>2</sub>S) and sulfur-containing fuels. *J Power Sources* 2004;135:17–24. <https://doi.org/10.1016/j.jpowsour.2004.03.061>.

- [737] Dicks AL. Fuel cells – Molten Carbonate Fuel Cells | Overview. Encyclopedia of Electrochemical Power Sources, Elsevier; 2009, p. 446–53. <https://doi.org/10.1016/B978-044452745-5.00263-X>.
- [738] Kim K, Kim H-T, Han J-I. Compatibility of platinum with alkaline sulfide fuel: Effectiveness and stability of platinum as an anode catalyst in direct alkaline sulfide fuel cell. *Int J Hydrogen Energy* 2015;40:4141–5. <https://doi.org/10.1016/j.ijhydene.2015.01.160>.
- [739] Zhang H, Chen L, Zhang J, Chen J. Performance analysis of a direct carbon fuel cell with molten carbonate electrolyte. *Energy* 2014;68:292–300. <https://doi.org/10.1016/j.energy.2014.02.049>.
- [740] Yamada K. Investigation of PEM type direct hydrazine fuel cell. *J Power Sources* 2003;115:236–42. [https://doi.org/10.1016/S0378-7753\(03\)00008-9](https://doi.org/10.1016/S0378-7753(03)00008-9).
- [741] Yamada K, Yasuda K, Tanaka H, Miyazaki Y, Kobayashi T. Effect of anode electrocatalyst for direct hydrazine fuel cell using proton exchange membrane. *J Power Sources* 2003;122:132–7. [https://doi.org/10.1016/S0378-7753\(03\)00440-3](https://doi.org/10.1016/S0378-7753(03)00440-3).
- [742] Dzhafarov TD, Yuksel SA. Porous Silicon-Based Direct Hydrogen Sulphide Fuel Cells. *J Nanosci Nanotechnol* 2011;11:9012–5. <https://doi.org/10.1166/jnn.2011.3456>.
- [743] Schulze M, Gülzow E. Fuels Cells – Alkaline Fuel Cells | Overview Performance and Operational Conditions. Encyclopedia of Electrochemical Power Sources, Elsevier; 2009, p. 353–61. <https://doi.org/10.1016/B978-044452745-5.00285-9>.
- [744] An L, Chen R. Direct formate fuel cells: A review. *J Power Sources* 2016;320:127–39. <https://doi.org/10.1016/j.jpowsour.2016.04.082>.
- [745] Zhao J, Xu X, Zhou W, Blakey I, Liu S, Zhu Z. Proton-Conducting La-Doped Ceria-Based Internal Reforming Layer for Direct Methane Solid Oxide Fuel Cells. *ACS Appl Mater Interfaces* 2017;9:33758–65. <https://doi.org/10.1021/acsami.7b07938>.
- [746] Chen H, Xu Z, Peng C, Shi Z, Luo J-L, Sanger A, et al. Proton conductive YSZ-phosphate composite electrolyte for H<sub>2</sub>S SOFC. *Ceram Int* 2010;36:2163–7. <https://doi.org/10.1016/j.ceramint.2010.06.002>.
- [747] Jeong HJ, Kim JW, Bae K, Jung H, Shim JH. Platinum–Ruthenium Heterogeneous Catalytic Anodes Prepared by Atomic Layer Deposition for Use in Direct Methanol Solid Oxide Fuel Cells. *ACS Catal* 2015;5:1914–21. <https://doi.org/10.1021/cs502041d>.
- [748] Gorte RJ, Vohs JM. Novel SOFC anodes for the direct electrochemical oxidation of hydrocarbons. *J Catal* 2003;216:477–86. [https://doi.org/10.1016/S0021-9517\(02\)00121-5](https://doi.org/10.1016/S0021-9517(02)00121-5).
- [749] Fu X-Z, Lin J-Y, Xu S, Luo J-L, Chuang KT, Sanger AR, et al. CO<sub>2</sub> emission free co-generation of energy and ethylene in hydrocarbon SOFC reactors with a dehydrogenation anode. *Physical Chemistry Chemical Physics* 2011;13:19615. <https://doi.org/10.1039/c1cp22837d>.
- [750] Serov A, Kwak C. Direct hydrazine fuel cells: A review. *Appl Catal B* 2010;98:1–9. <https://doi.org/10.1016/j.apcatb.2010.05.005>.
- [751] Tamura K, Kahara T. Exhaust Gas Compositions and Fuel Efficiencies of Hydrazine-Air Fuel Cells. *J Electrochem Soc* 1976;123:776–80. <https://doi.org/10.1149/1.2132932>.